

**BER II  
EXPERIMENTAL  
REPORTS 2010**

# BER II EXPERIMENTAL REPORTS 2010



Lise Meitner and Otto Hahn

edited by

Andreas Rödig, Astrid Brandt  
and Thomas Gutberlet

User Coordination Neutrons

Helmholtz-Zentrum Berlin für Materialien und Energie GmbH

in der Helmholtz Gemeinschaft

July 2011

---

Berichte des Helmholtz-Zentrums Berlin

**HZB - B - 12**

ISSN 1868-5781

Picture on front cover:

Overview of the temperature dependence of the diffraction pattern along  $Q = (1,0,l)$  of the magnetic order parameters of the magnetoelectric hexaferrite  $Ba_{0.5}Sr_{1.5}Zn_{22}(Fe_{1-x}Al_x)_{12}O_{22}$  ( $x = 0.08$ ) measured at the diffractometer E5 at HZB by Jae-Ho Chung and co-workers of Korea University in Seoul, South Korea (report page 36).

The scans along  $(1,0,l)$  revealed that there are two different additional commensurate magnetic ordering wave vectors for the two temperature ranges, respectively. The additional magnetic intensities were observed at  $k_2 = (0,0,3/2)$  for 80 – 180 K, whereas the intensity of the nuclear Bragg peaks were enhanced below 80 K indicating  $k_0 = (0,0,0)$ .

Picture on back cover:

View of the “Technikum”, the infrastructure building hosting the components required for the power supply of the 25 to 30 Tesla high field magnet at neutron guide hall II. The building gives space to the electric power installations, water-cooling and water treatment facilities and the refrigerator supplying the super-conductive coil with cryogenic helium.

The cover was designed by *screenworks*, Leibnizstraße 59, 10629 Berlin, [www.screenworks.de](http://www.screenworks.de)

---

**Editorial:**

The Helmholtz-Zentrum Berlin für Materialien und Energie GmbH (HZB) is a member of the Helmholtz Association of German Research Centres. The HZB is operating the neutron source BER II at the Lise-Meitner-Campus in Berlin Wannsee and the 3<sup>rd</sup> generation synchrotron source BESSY II at the Wilhelm-Conrad-Röntgen-Campus in Berlin Adlershof.

The HZB User Coordination – with its outposts in Wannsee (HZB-Neutrons) and Adlershof (HZB-Photons) – assists scientists from all over the world with their application for beam time, organising their stay at the HZB and performing their experiments at the two large-scale user facilities BER II and BESSY II.

**Contact HZB Neutrons:**

HZB User Coordination - Neutrons  
Helmholtz-Zentrum Berlin  
für Materialien und Energie GmbH  
Lise-Meitner-Campus  
Hahn-Meitner-Platz 1  
14109 Berlin  
Germany

Phone: +49-30-8062 42778, - 42169, -42304, -43153  
FAX: +49-30-8062 42523  
Email: [neutrons@helmholtz-berlin.de](mailto:neutrons@helmholtz-berlin.de)  
Web: <http://www.helmholtz-berlin.de/user/neutrons>

## CONTENTS

<b>Introduction</b>	<b>IV</b>
<b>List of BER II Instruments</b>	<b>VII</b>
<b>How to apply for BER II Beam Time</b>	<b>XI</b>
<b>Acknowledgement for Support by the European Commission</b>	<b>XIII</b>
<b>List of Contributed Reports</b>	<b>XV</b>

### Part I: EXPERIMENTAL REPORTS 2010

<b>Development of Instruments and Methods</b>	<b>1</b>
<b>Magnetism</b>	<b>15</b>
<b>Structure</b>	<b>75</b>
<b>Biology &amp; Soft Matter</b>	<b>97</b>
<b>Material Science</b>	<b>135</b>
<b>Cultural Heritage</b>	<b>163</b>

### Part II: LIST OF BER II RELATED PUBLICATIONS

<b>Theses</b>	<b>171</b>
<b>Publications 2010</b>	<b>172</b>
<b>Author Index</b>	<b>181</b>

## Introduction

With the merger of the Hahn-Meitner-Institut and the Berlin synchrotron radiation source BESSY in 2009 to the new Helmholtz-Zentrum Berlin für Materialien und Energie GmbH (HZB) the synergistic use of neutron and synchrotron radiation has become a major focus of the new institute. Being one of the few centres worldwide that offers now the whole range of instruments for neutron and synchrotron radiation experiments in one laboratory structure users have the unique opportunity to exploit both probes within a single administrative unit. The common user entry point and the common Scientific Selection Panel dealing with the proposals for both facilities were established successfully in 2010 with two proposal rounds which reviewed 358 internal and external proposals asking for 2550 days of neutron beam time. The present “BER II Experimental Report”, now the second of its kind, gives an overview on the research with neutrons carried out at the HZB in 2010. The reactor BER II was shut down for the planned large upgrade of the cold source, beam guide systems in the neutron guide hall I and relocation and upgrade of instruments there in October 2010. Up to October the BER II delivered neutrons for experiments on 168 days. Fourteen instruments were fully scheduled for external user operation. The experiments performed are reviewed by 153 reports, 117 from external users and 36 from HZB scientists.

## User Service

The HZB neutron facility BER II is open to the national and international scientific community. About 70% of the available beam time at scheduled instruments is given to external users, 30% to in-house researchers. A fraction of the beam time for external users (up to 20% of the total beam time of an instrument) can be assigned to long-term collaborating groups from German universities and other national and international research institutions. The remaining time (at least 50% of the total beam time) is allocated to short term projects via a peer-review selection process.

The HZB has an outstanding tradition in providing sample environment for extreme conditions. Special emphasis is put on high magnetic fields and low and ultra-low temperatures. Sample environment for high pressures up to 10 kbar and high temperatures is as well available.

More recently, a further focus in sample environment was put on the development of equipment for neutron scattering experiments under controlled gas pressure to serve a growing user community from fields of material science and soft condensed matter. This new “Dedicated Environment for Combined Gas Adsorption and

Scattering Experiments” (DEGAS) includes humidity chambers for investigating biological samples as well as equipment for in-situ adsorption experiments on e.g. metal-organic framework systems.

For “off-beam” preliminary test experiments or additional investigations three specialised laboratories are also available for users. These are

- the MagLab equipped with four fully operating measurement systems for magnetic fields up to 14.5 T and temperatures down to 260 mK,
- the GasLab equipped with a whole suite of modular experimental set-ups for experiments under controlled gas pressures and
- the Biolab offering a broad range of laboratory-based equipment with a focus on methods in optical spectroscopy.

The access to these ancillary laboratories is mediated by the responsible instrument scientists. A detailed technical handbook describing the existent equipment has been published by the sample environment group of HZB and is continuously updated. This handbook as well as detailed descriptions of the neutron instruments is available on the internet under:

<http://www.helmholtz-berlin.de/user>

## Scientific Selection Panel

To strengthen the synergetic use of neutron and synchrotron radiation, HZB has implemented a common HZB Scientific Selection Panel reviewing all proposals for neutron and synchrotron radiation beam time at BER II and BESSY II in joint sessions. To this purpose, the HZB Scientific Selection Panel is organised in Scientific Colleges, which are grouped according to research fields in order to facilitate discussions on the scientific merit of the proposals. All users applying for either neutron or synchrotron radiation beam time are requested to choose the appropriate Scientific College for their proposal upon on-line submission. The current scientific colleges are:

- C1** – Soft Matter and Biology
- C2** – Macromolecular Crystallography
- C3** – Chemistry, Catalysis
- C4** – Electronic structures
- C5** – Magnetism and Superconductivity
- C6** – Material Science, Hard Condensed Matter

There are two proposal rounds per year. The regular deadlines for submission of proposals are 1 March and 1 September.

[http://www.helmholtz-berlin.de/user/neutrons/user-info/call-for-proposals\\_en.html](http://www.helmholtz-berlin.de/user/neutrons/user-info/call-for-proposals_en.html)

The proposals are allocated to the appropriate college as indicated by the proposer. Between 7 to 8 weeks after the deadlines the colleges of the Scientific Selection Panel meet at the HZB and discuss and evaluate the proposals in closed sessions. They provide a priority ranking of the proposals based on their scientific merit and give advice on the appropriate amount of beam time to be granted. Beam time conflicts between different colleges are discussed and usually settled in a meeting of the college speakers following the college sessions. The final decision is taken by the Scientific Director of the HZB based on the recommendations of the college speakers. The results of the selection process are communicated to the proposers by the user coordinator. Rejected applicants are supplied with a written comment explaining the reasons for the refusal. For more detailed information please see

<http://www.helmholtz-berlin.de/user/user-info/colleges>

### Support for European Access to BER II

HZB is a major partner in the European Access programme “*Integrated Infrastructure Initiative for Neutron Scattering and Muon Spectroscopy (NMI3)*”, under the 7<sup>th</sup> EU Framework Programme (FP7), Grant Agreement number 226507-NMI3-Integrating Activities. NMI3-FP7 includes 12 different access activities offering European users approximately 1400 beam days of access to more than 150 instruments at European neutron and muon facilities with support for travel and subsistence. The recent programme for access started in February 2009 and ends in January 2011. The HZB has committed itself to provide a minimum of 240 instrument days for European users over this period of two years.

In 2010, 61 projects of 53 different European groups using 418.5 instrument days have been supported by HZB. A total of 93 individual users out of 14 countries were involved. A list of the respective experimental reports included in this volume can be found on page XIII.

### Major Instrumental Upgrades

In 2010 the most time was spent with the user operation at the instruments running. Parallel the plans for the large upgrade projects in the neutron guide hall I were finalised and the work was started in October. The complete guide system from the source to the instruments was removed and started to be replaced by new supermirror coated guides. Replacement of the old cold source started to be ready for the installation of the new cold source with a focusing type moderator cell in the first months of 2011.

These activities are on-going to get finished in July 2011.

In parallel some of the highly demanded user instruments in neutron guide hall I are completely refurbished:

- The three-axes spectrometer V2/FLEX is relocated to an end position at its own dedicated neutron guide equipped with modern neutron optical devices as an elliptical mirror as beam focussing element and a special polarising device.
- The time-of-flight spectrometer V3/NEAT was completely dismantled and will be shifted out of the neutron guide hall I into an own new building. A new guide system will be installed and the chopper system and the whole secondary spectrometer of NEAT will be replaced.
- The tomography station V7/CONRAD is completely refurbished.
- A new detector system based on an arrangement of <sup>3</sup>He-filled position-sensitive tubes is installed at the small-angle scattering machine V4.

An overall increase of performance by an order of magnitude at the instruments can be expected by these upgrades.

The construction of two new instruments in the neutron guide hall I was continued in 2010. They are both designed by university groups and are funded by the German Ministry of Education and Research. These instruments are

- BioRef, a TOF reflectometer with a focus on the characterisation of bio-functional interfaces (University of Heidelberg in cooperation with HZB). The instrument had first users with successful experiments in 2010 and is now in user operation.
- PONTO, a tomography station with a focus on the use of polarised monochromatic neutrons (Beuth University of Applied Sciences Berlin in cooperation with HZB).

In the new neutron guide hall II the final two instruments designated for this hall have been built up: the extreme-environment diffractometer EXED and the high resolution SANS machine VSANS. Both instruments were in the commissioning phase in 2010.

## Special Events

### 31<sup>th</sup> Berlin Neutron School

The 31<sup>th</sup> Berlin Neutron School was held at HZB from 11 - 19 March 2010. It was attended by 30 students with backgrounds ranging from physics, materials science, engineering, chemistry, biology and soft matter. The majority were

PhD students, but there were also some diploma and master students as well as several post docs. Most of the participants came from European universities and research institutes, among them 12 from German institutions. The generous support by the European Union under its NMI3 Program is gratefully acknowledged. The school is part of the curriculum of the Faculty of Mathematics and Sciences of the Technical University Berlin.

As in the previous year the school was held on nine days with detailed lectures on all the techniques the students encountered in the experiments. The practical sessions consisted of seven experiments on the V2/FLEX triple-axis spectrometer, the powder diffractometer E9, the V3/NEAT time-of-flight spectrometer, the V7/CONRAD cold-neutron tomography station and the V5/SPAN neutron spin-echo spectrometer. Each practical lasted a half day, where the students were divided into groups of four people which rotated between the experiments over a period of three and a half days. The last day of the school consisted of lectures on how neutron scattering is used as a research tool in the areas of biology, chemistry, engineering and physics. The school was closed by an overview talk on the user service provided and the formalities to be observed when applying for beam time.

### **2<sup>nd</sup> Joint BER II and BESSY II User Meeting, 9. – 10.12.2010**

The 2<sup>nd</sup> Joint BER II and BESSY II User Meeting was held from 9 – 10 December 2010 at Berlin-Adlershof in the vicinity of the Wilhelm-Conrad-Röntgen Campus of the HZB. About 350 external users of both facilities attended this meeting. The meeting was accompanied by an industrial exhibition featuring 45 companies.

The scientific program of the meeting was focused on topics covered by College 3 (Chemistry/Catalysis) and College 6 (Material Science/Hard Condensed Matter) of the six colleges of the Scientific Selection Panel.

Starting with a key-note lecture on graphene given by T. Seyller (University of Erlangen-Nürnberg) the meeting continued by the first session on recent research results. After the lunch break, reports of the representatives of the German synchrotron community (U. Pietsch, chairman of the KFS), the German neutron community (G. Eckold, chairmen of the KFN) and the European Neutron Scattering Association (M. Steiner, chairman of the ENSA) were given and the Innovation Award on Synchrotron Radiation, the Ernst-Eckard-Koch prize, was bestowed. The day ended with the public lecture “Unveiling Secrets of Qumram”, given by I. Rabin (BAM Berlin) and with a poster session in the BESSY II Experimental Hall. In the evening,

all participants enjoyed a “Berliner Büffet”, which was sponsored by the exhibiting companies. The second day started with facility reports on BESSY II and BER II and the bestowal of the HZB poster prize. It was continued with the second session on research results.

### **SNI 2010, 24. - 26.02.2010**

The German meeting “Deutsche Tagung für Forschung mit Synchrotronstrahlung, Neutronen und Ionenstrahlen an Großgeräten” was held on 24 – 26 February 2010 at the Freie Universität Berlin. With 81 oral presentations, more than 500 posters and about 750 participants this meeting was an outstanding event hosted by the HZB for the German synchrotron and neutron community. In three parallel sessions, two intensive poster sessions and two evening lectures to the general audience the meeting demonstrated the broadness and the vitality of research with synchrotron radiation, neutrons and ion beams in Germany. The successful meeting was accompanied with an evening dinner for the participants and visits of the BER II and BESSY II facilities and the tumor therapy center ATT at HZB.

### **Innovative Instrumentierung zur Untersuchung nanostrukturierter, weicher und biologischer Materie, 6. - 7.05.2010**

The workshop on innovative instrumentation to investigate nanostructured soft and biological material was organized by the BMBF Kompetenzverbund NanoSOFT at the Lise-Meitner Campus of HZB on 6 – 7 May 2010. 16 presentations by German research groups were given on various aspects of structural investigations using neutron and x-ray reflectometry, neutron spin echo spectroscopy and IR spectroscopy. The options at the new BioRef neutron reflectometer at BER II for this research were discussed.

### **Neutrons for Geoscience, 8.12.2010**

The aim of the workshop, held as a satellite event to the Joint BER II and BESSY II User Meeting on 8 December 2010 was to bring together selected members of the geoscience scientific community and BER II scientists in order to estimate and discuss the necessary technical requirements for future successful geoscience experiments at BER II. Almost 30 scientists from Germany, Italy, Greece and Poland came together in Berlin to discuss trends

in geoscience and archaeology. Experts from the HZB presented the experimental options offered by HZB. A large amount of time was used for stimulating discussions of future projects, both scientifically and for developing new experimental options.

## List of BER II Instruments

### Instruments in the BER II Experiment Hall (thermal neutrons) *Telephone numbers: +49(0)30/8062-*

	<b>Instrument</b>	<b>ext.</b>	<b>Inst. Scientists</b>	<b>ext.</b>
<b>E1</b>	3-Axis Spectrometer with Polarisation Analysis <i>(limited access only in close co-operation with local staff members)</i>	43101	M. Mihalik A. Hoser	42793 42847
<b>E2</b>	Flat-Cone Single Crystal Diffractometer <i>(E2a: Crystal-Test Diffractometer)</i>	43102	J. Hoffmann I. Glavatskyi	42185 42673
<b>E3</b>	Residual Stress Analysis and Texture Diffractometer	43103	R. Wimpory M. Boin	43097 43097
<b>E4</b>	2-Axis-Diffractometer <i>(E4b: Position for Single Crystal Orientation)</i>	43104	K. Prokes S. Matas	42804 42804
<b>E5</b>	4-Circle Diffractometer	43104	M. Reehuis	42692
<b>E6</b>	Focusing Single Crystal Diffractometer	43105	A. Hoser T. Hofmann	42847 42793
<b>E7</b>	Residual Stress Analysis Diffractometer <i>(limited access only in close co-operation with local staff members)</i>	43107	R. Wimpory	43097
<b>E9</b>	Fine Resolution Powder Diffractometer (FIREPOD)	43106	S. Schorr M. Tovar	42317 42768
<b>E10</b>	HELIX, 3He-Diffractometer	43106	K. Siemensmeyer	42757

### Instruments in the BER II Cold Neutron Guide Halls

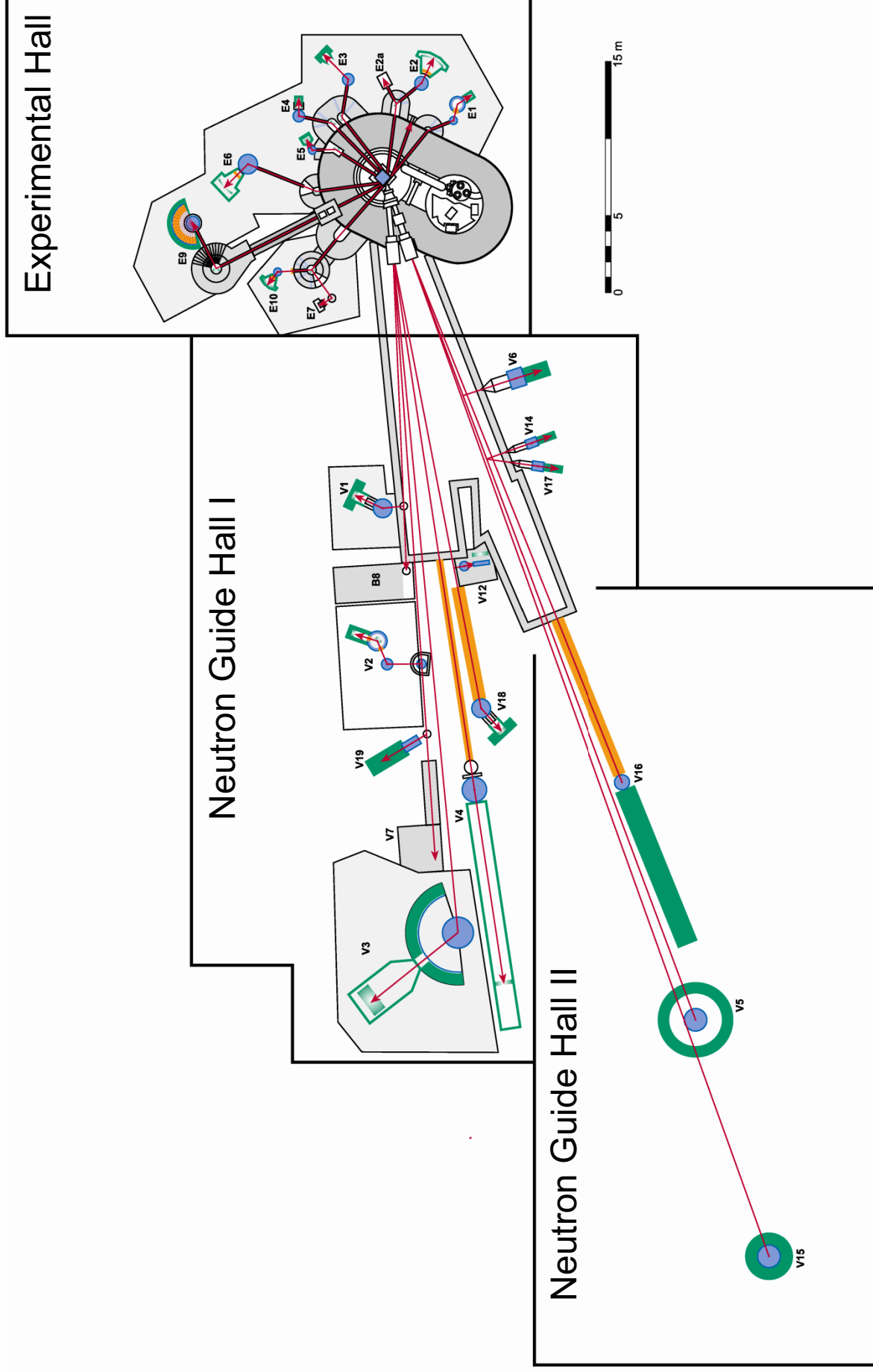
*Telephone numbers: +49(0)30/8062-*

	<b>Instrument</b>	<b>ext.</b>	<b>Inst. Scientists</b>	<b>ext.</b>
<b>V1</b>	Membrane Diffractometer <i>(upgrade in progress)</i>	43121	T. Hauß A. Becker	42071 43198
<b>V2</b>	I: 3-Axis Spectrometer (FLEX) II: FLEX with NRSE opt. <i>(upgrade in progress)</i>	43122	K. Habicht K. Rule M. Skoulatos D. Le	42807 43067 42171 42803
<b>V3</b>	Time-of-Flight Spectrometer (NEAT) <i>(upgrade in progress)</i>	43123	M. Russina	43159
<b>V4</b>	Small Angle Scattering Instrument (SANS)	43124	U. Keiderling S. Prévost V. Ryukhtin A. Brandt	42339 42339 43099 42169
<b>V5</b>	Spin-Echo Spectrometer with ToF Option (SPAN)	43125	B.-A. Brüning	42391
<b>V6</b>	Reflectometer	42806	R. Steitz R. Köhler A. Teichert	42149 43077 42044
<b>V7</b>	Cold Neutron Tomography and Radiography (CONRAD) <i>(upgrade in progress)</i>	43327	N. Kardjilov	42298
<b>B8</b>	Neutron-Autoradiography <i>(limited access only in close co-operation with local staff members)</i>	43121	A. Denker	43000
<b>V12a</b>	Bent-crystal Diffractometer (USANS) / Tomography <i>(upgrade in progress)</i>	43131	W. Treimer S. Seidel	42221 43298
<b>V14</b>	Mirror Test Device	42284	T. Krist	42045



	<b>Instrument</b>	<b>ext.</b>	<b>Inst. Scientists</b>	<b>ext.</b>
<b>V15</b>	Extreme Environment Diffractometer (EXED) <i>(commissioning)</i>	43283	O. Prokhnenko W.-D. Stein	43068 43079
<b>V16</b>	Very Small Angle Neutron Scattering (VSANS) <i>(commissioning)</i>	43281	D. Clemens K. Vogtt	42280 43022
<b>V17</b>	Detector Test Station	43284	T. Wilpert C. Schulz S. Alimov	42743 42675 42675
<b>V18</b>	Reflectometer for biological applications (BioRef) <i>(available for user experiments in 2011)</i>	****	M. Trapp M. Strobl	42161 42490
<b>V19</b>	Polarized Neutron Tomography (PONTO) <i>(under construction)</i>	****	W. Treimer O. Ebrahimi	42221 43076
<b>X2</b>	X-ray Reflectometer <i>(Sample preparation V6, only in close co-operation with local staff members)</i>	43112	H. Bleif	42758
<b>X3</b>	X-ray $\mu$ -CT <i>(complementary to V7, only in close cooperation with local staff members)</i>		N. Kardjilov A. Hilger	42298 42298

# Floor Plan of the Neutron Instruments at the BER II

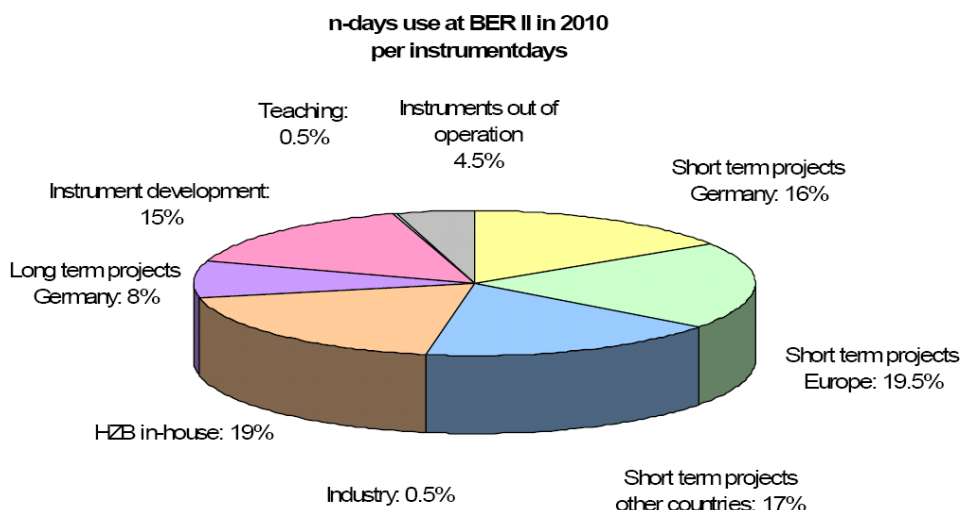


# Instrument Statistics 2010

Table: Detailed statistical data on the use of the scheduled instruments

Inst.	Inst. days	EXT (DE) in %	EXT (EU) in %	EXT (other) in %	LT in %	EF in %	Other use in %	Inst in %	OOO in %
E1	146	0	0	0	0	23	0	51	26
E2	146	17	14	27	0	34	0	9	0
E3	146	13	29	21	0	23	0	12	0
E4	146	4	14	48	0	29	0	4	0
E5	146	41	7	27	0	23	0	0	1
E6	146	20	34	11	0	26	0	9	0
E9	146	13	25	7	0	6	0	39	10
V1	141	44	7	10	13	14	0	11	0
V2	141	0	23	28	0	25	3	20	0
V3	141	2	28	23	0	28	0	19	0
V4	141	29	12	12	6	13	1	3	21
V5	141	9	41	10	11	0	0	19	11
V6	141	26	10	11	22	14	0	17	0
V7	141	19	22	16	7	22	0	14	0
V12	141	0	25	9	67	0	0	0	0

Note: The table gives detailed statistical data on the use of the scheduled instruments. The pie chart shows the statistical data given in the table, summarized over all instruments. The meaning of the individual entries is explained in the legend below. EXT (DE), EXT (EU) and EXT (other) refer to projects performed by external users from Germany, EU or other countries via accepted "normal" short-term proposals submitted to BER II. Please note that the long-term projects are also projects performed by external user groups, where instrument time is either given on the basis of an accepted long-term proposal or on the basis of a cooperation agreement with BER II.



<b>Inst.-days</b>	Neutron days per Instrument
<b>EXT (DE)</b>	German Universities, Research institutes
<b>EXT (EU)</b>	Universities and Research Institutes from the EU and associated states
<b>EXT (other)</b>	Non-EU Universities and Research Institutes
<b>LT</b>	Long term projects
<b>EF</b>	In-house projects
<b>other use</b>	e.g. industry, teaching (neutron school)
<b>Inst.</b>	Instrument time (tests, developments ...)
<b>OOO</b>	out of operation

## How to apply for beam time at BER II (HZB-Neutrons) and BESSY II (HZB-Photons)

The research reactor BER II is a major European neutron scattering facility with exceptional capabilities to conduct complex experiments under extreme conditions. Outstanding sample environment provides high static magnetic fields up to 17 T, high, low, and ultra-low temperatures and controlled gas pressures up to 10 kbar. The advanced and partly unique neutron scattering instrumentation and the quality of the user service attract researchers worldwide.

The storage ring BESSY II is a leading third-generation synchrotron-radiation source providing ultrabright photon beams from the long wavelength Terahertz region to hard X-rays with complete control of the polarization of the radiation and energy range. More than 50 beamlines offer a multi-faceted mixture of experimental opportunities at undulator, wiggler and dipole sources with excellent energy resolutions.

Details on the instrumentation at both sources are available on the WEB:

<http://www.helmholtz-berlin.de/user>

BER II and BESSY II are open to both the national and the international user community. The main fraction of the beam time is reserved for external short-term research proposals. All applications are reviewed by an international Scientific Selection Panel (SSP) twice a year. Beamtime is granted on the basis of scientific merit. To promote the synergetic use of neutron and synchrotron radiation, the Scientific Selection Panel is dealing with proposals for neutrons and synchrotron photons in joint sessions. To this purpose the Panel is divided in 6 sub-groups (colleges) each being focussed on a particular scientific field in order to facilitate in-depth discussions.

**Deadlines for the submission of proposals are**

**1 March and 1 September**

The instrument scientists of HZB are asked to advise potential users and comment on the technical feasibility of the proposed experiments. For these tasks this limited class of HZB-scientists has access to the submitted proposals.

Requests for urgent or confidential experiments (Director's Discretionary Time) and for industrial use may be submitted at any time.

Applications for HZB-Neutrons as well as HZB-Photons beam time should be made by using GATE, the common user entry point for both neutron and synchrotron radiation applications

[http://www.helmholtz-berlin.de/user/gate\\_en.html](http://www.helmholtz-berlin.de/user/gate_en.html)

Research projects for the complementary use of HZB-Neutrons and HZB-Photons are strongly encouraged.

For further information please contact:

### **Helmholtz-Zentrum Berlin für Materialien und Energie GmbH**

HZB User Office – Neutrons  
Lise Meitner Campus  
Hahn-Meitner Platz 1  
D-14109 Berlin (Wannsee)  
Germany

Phone: +49 - 30 - 8062 42304 / 43153  
Fax: +49 - 30 - 8062 42523  
Email: neutrons@helmholtz-berlin.de

HZB User Office – Photons  
Wilhelm-Conrad-Röntgen Campus  
Albert-Einstein-Str. 15  
D-12489 Berlin (Adlershof)  
Germany

Phone: +49 - 30 - 8062-12931  
Fax: +49 - 30 - 8062-14746  
Email: photons@helmholtz-berlin.de

The BER II Experimental Reports are intended as interim summaries. In view of the short time available between the termination of certain experiments and the deadline for this report, the results presented here have to be considered as preliminary. The inclusion of reports in this volume does not constitute a publication in the usual sense. Final results will be submitted for publication in regular scientific journals.

## Acknowledgement for Support by the European Commission

The access of users from European Community Member States and Associated States to the neutron facility BER II has been substantially supported in the past by the European Community under the Framework Programs FP5 and FP6. We gratefully acknowledge the continuation of this support under the Framework Program FP7: HZB is a partner in the EU supported network of European neutron facilities – the **Neutron and Muon Integrated Infrastructure Initiative (NMI3)** – and the access to the BER II is supported by the European Commission under the 7<sup>th</sup> Framework Program through the “Research Infrastructures” action of the “Capacities Program”, Contract No: CP-CSA\_INFRA-2008-1.1.1 Number 226507-NMI3. This access program started on 1 February 2009 and will be finished on 31 January 2011.

Results of EU supported groups are contained in 38 reports of this volume.

<i>NMI3-Nº.</i>	<i>Page</i>	<i>Authors</i>	<i>Affiliation</i>
1528	52	Sikolenko et al.	ETH Zürich and PSI, CH
1541	5	Wiedenmann et al.	ILL Grenoble, FR
1542	99	Bradshaw et al.	Univ. of Edinburgh, UK
1544	108	Saiani et al.	Univ. of Manchester, UK
1565	151	Paris et al.	MU Leoben, AT
1568	85	Remhof et al.	EMPA, CH
1569	59	Nikseresht et al.	EPFL Lausanne, CH
1570	44	Cermak et al.	CU Prague, CZ
1571	80	Pospisil et al.	CU Prague, CZ
1572	18	Freeman et al.	ILL Grenoble, FR
1573	143	Cerrado et al.	IPCMS, FR
1574	110	Fouquet et al.	ILL Grenoble, FR
1579	60	Ruegg et al.	UCL, UK
1582	118	Zarbakhsh et al.	QM UCL, UK
1585	145	O'Dowd et al.	Univ. of Limerick, IE
1586	111	Schiro et al.	UNIPA, IT
1591	46	Jaworska-Golab et al.	JU Krakow, PL
1593	95	Gondek et al.	AGH-UST Krakow, PL
1594	158	Gondek et al.	AGH-UST Krakow, PL
1595	55	Kabanov et al.	IJS Ljubljana, SI

<i>NMI3-Nº.</i>	<i>Page</i>	<i>Authors</i>	<i>Affiliation</i>
1596	45	Señaris-Rodríguez et al.	Univ. de A Coruña, ES
1596	56	Señaris-Rodríguez et al.	Univ. de A Coruña, ES
1597	147	Schöbel et al.	TU Wien, AT
1598	122	Zahn et al.	ETH Zürich, CH
1599	61	Hüvonen et al.	ETH Zürich, CH
1601	37	Marti et al.	CU Prague, CZ
1602	31	Kamarad et al.	ASCR IP, Prague, CZ
1605	105	Peters et al.	ILL Grenoble, FR
1608	148	Davies et al.	ICL, UK
1615	3	Raitman et al.	LAS Riga, LV
1615	10	Raitman et al.	LAS Riga, LV
1616	94	Kuzmin et al.	Univ. of Latvia, LV
1618	150	Gondek et al.	AGH-UST Krakow, PL
1619	96	Gondek et al.	AGH-UST Krakow, PL
1620	49	Baran et al.	JU Krakow, PL
1621	50	Budziak et al.	PAS IFJ Krakow, PL
1624	109	Bakandritsos et al.	Univ. of Patras, GR
1627	112	Falus et al.	ILL Grenoble, FR

Notice:

The quality of figures in the electronic versions, CD and WEB ([http://www.helmholtz-berlin.de/user/neutrons/reports\\_en.html](http://www.helmholtz-berlin.de/user/neutrons/reports_en.html)) – especially in colour presentation – is remarkably higher than in the print version.

## List of Contributed Experimental Reports

PAGE TITLE TEAM PROPOSAL

### *Development of Instruments and Methods*

<b>3</b>	<b>Neutron Bragg front and back-face scattering from the perfect and deformed Si single crystal excited with acoustic waves</b>	E. Raitman <sup>1</sup> V. Gavrilov <sup>1</sup> A. Hoser <sup>2</sup> T. Hofmann <sup>2</sup>	<sup>1</sup> LAS, Riga, LV <sup>2</sup> HZB	E6	<b>PHY-01-2882</b>
<b>4</b>	<b>Resolving dispersive mode doublets with the NRSE method</b>	K. Habicht <sup>1</sup> F. Groitl <sup>1</sup> K. Kiefer <sup>1</sup>	<sup>1</sup> HZB	V2	<b>PHY-02-750-EF</b>
<b>5</b>	<b>TISANE Investigations of Microsecond Dynamics in Magnetic Nanomaterials</b>	A. Wiedenmann <sup>1</sup> J. Kohlbrecher <sup>2</sup> U. Keiderling <sup>3</sup> V. Ryukhtin <sup>3</sup>	<sup>1</sup> ILL, Grenoble, FR <sup>2</sup> PSI, CH <sup>3</sup> HZB	V4	<b>PHY-04-1830</b>
<b>6</b>	<b>High pressure cell for neutron reflectivity measurements up to 2500 bar (1)</b>	R. Winter <sup>1</sup> Ch. Jeworrek <sup>1</sup> C. Czeslik <sup>1</sup> R. Steitz <sup>2</sup>	<sup>1</sup> TU Dortmund <sup>2</sup> HZB	V6	<b>EF</b>
<b>7</b>	<b>Trial for a new SANS method using dark-field tomography</b>	K. Taketani <sup>1</sup> A. Hilger <sup>2</sup> N. Kardjilov <sup>2</sup> I. Manke <sup>2</sup> M. Strobl <sup>2</sup>	<sup>1</sup> KEK, Tsukuba, JP <sup>2</sup> HZB	V7	<b>PHY-04-1946</b>
<b>8</b>	<b>2D-reconstruction on V12 (I)</b>	S.-O. Seidel <sup>1</sup> W. Treimer <sup>1</sup> O. Ebrahimi <sup>1</sup> N. Karakas <sup>1</sup>	<sup>1</sup> TFH, Berlin	V12a	<b>PHY-04-1849-LT</b>
<b>9</b>	<b>2D-reconstruction on V12 (II)</b>	S.-O. Seidel <sup>1</sup> W. Treimer <sup>1</sup> O. Ebrahimi <sup>1</sup> N. Karakas <sup>1</sup>	<sup>1</sup> TFH, Berlin	V12a	<b>PHY-04-1849-LT</b>
<b>10</b>	<b>Spatial distributions of neutrons scattered by vibrating Ge crystals (Laue geometry)</b>	E. Raitman <sup>1</sup> V. Gavrilov <sup>1</sup> S.-O. Seidel <sup>2</sup> M. Strobl <sup>2</sup>	<sup>1</sup> LAS, Riga, LV <sup>2</sup> HZB	V12a	<b>PHY-04-2014</b>
<b>11</b>	<b>Energy analysing by magnesium fluoride prisms</b>	R. Bartmann <sup>1</sup> J. Schulz <sup>1</sup> T. Krist <sup>1</sup>	<sup>1</sup> HZB	V14	<b>PHY-04-2017-EF</b>
<b>12</b>	<b>BioRef – testing operational modes</b>	M. Strobl <sup>1</sup> R. Steitz <sup>1</sup> M. Kreuzer <sup>2</sup> R. Dahint <sup>2</sup>	<sup>1</sup> HZB <sup>2</sup> Uni Heidelberg	V18	<b>EF</b>
<b>13</b>	<b>Visualization of the flux-pinning by polarized neutron radiography</b>	S.-O. Seidel <sup>1</sup> W. Treimer <sup>1</sup> O. Ebrahimi <sup>1</sup> N. Karakas <sup>1</sup>	<sup>1</sup> TFH, Berlin	V19	<b>EF</b>

### *Magnetism*

<b>17</b>	<b>Diffuse magnetic scattering of the pseudo-triangular antiferromagnet alpha-CaCr2O4</b>	B. Lake <sup>1</sup> S. Toth <sup>1</sup> S. Kimber <sup>1</sup> D. Argyriou <sup>1</sup> O. Pieper <sup>1</sup> N. Islam <sup>1</sup>	<sup>1</sup> HZB	E2	<b>PHY-01-2697-EF</b>
<b>18</b>	<b>Magnetic order of Incommensurately Charge-Stripe Ordered La(1.725)Sr(0.275)NiO(4)</b>	P. Freeman <sup>1</sup> I. Glavatskyi <sup>2</sup>	<sup>1</sup> ILL, Grenoble, FR <sup>2</sup> HZB	E2	<b>PHY-01-2702</b>



## List of Contributed Experimental Reports

PAGE	TITLE	TEAM	PROPOSAL
19	<b>Crystal and magnetic structure evolution of Ni-Mn-In and Ni-Co-Mn-In metamagnetic shape memory alloy</b>	Ch. Biswas <sup>1</sup> S. Singh <sup>1</sup> I. Glavatskyi <sup>2</sup> S. Gerischer <sup>2</sup>	<sup>1</sup> Bose Center, IN <sup>2</sup> HZB E2 <b>PHY-01-2704</b>
20	<b>Magnetic structure of Tm<sub>2</sub>AlB<sub>6</sub></b>	T. Mori <sup>1</sup> K. Siemensmeyer <sup>2</sup> I. Glavatskyi <sup>2</sup> S. Gerischer <sup>2</sup>	<sup>1</sup> NIMS, JP <sup>2</sup> HZB E2 <b>PHY-01-2705</b>
21	<b>Magnetic Structure of PrB6</b>	H.C. Walker <sup>1</sup> K.A. McEwen <sup>2</sup> M.D. Le <sup>3</sup> I. Glavatskyi <sup>3</sup>	<sup>1</sup> ESRF Grenoble, FR <sup>2</sup> UCL, UK <sup>3</sup> HZB E2 <b>PHY-01-2742-EF</b>
22	<b>Basal plane anisotropy of the antiferromagnetism in YbCo<sub>2</sub>Si<sub>2</sub></b>	O. Stockert <sup>1</sup> A. Haase <sup>1</sup> J.-U. Hoffmann <sup>2</sup>	<sup>1</sup> MPI, CPfS, Dresden <sup>2</sup> HZB E2 <b>PHY-01-2833</b>
23	<b>Magnetic order within subsystem of Cr atoms intercalated into transition metal dichalcogenides</b>	N. Baranov <sup>1</sup> A. Gubkin <sup>1</sup> E.M. Sherokalova <sup>2</sup> N.V. Selezneva <sup>2</sup> I. Glavatskyi <sup>3</sup>	<sup>1</sup> RAS IMP, RU <sup>2</sup> USU Ekaterinburg, RU <sup>3</sup> HZB E2 <b>PHY-01-2837</b>
24	<b>Low-Temperature Magnetic Structure of Frustrated Antiferromagnet SrYb<sub>2</sub>O<sub>4</sub></b>	D.L. Quintero Castro <sup>1</sup> B. Lake <sup>1</sup> M. Reehuis <sup>1</sup> N. Islam <sup>1</sup>	<sup>1</sup> HZB E4 E6 E9 <b>PHY-01-2615-EF</b> <b>PHY-01-2595-EF</b> <b>PHY-01-2626-EF</b>
25	<b>The neutron study of PrFe(CN)<sub>6</sub> nH<sub>2</sub>O</b>	S. Mat'as <sup>1</sup> K. Prokes <sup>1</sup> Z. Mitroova <sup>2</sup>	<sup>1</sup> HZB <sup>2</sup> SAS Kosice, SK E4 <b>PHY-01-2743-EF</b>
26	<b>Investigation of the low temperature and applied field phase diagram in azurite</b>	K.C. Rule <sup>1</sup> C. Gibson <sup>1</sup> Alan Tennant <sup>1</sup>	<sup>1</sup> HZB E4 <b>PHY-01-2747-EF</b>
27	<b>Magnetic ordering of the Er<sup>3+</sup>-ions in ErVO<sub>3</sub></b>	C. Ulrich <sup>1</sup> B. Keimer <sup>1</sup> S. Miyasaka <sup>2</sup> J. Fujioka <sup>2</sup> Y. Tokura <sup>2</sup> M. Reehuis <sup>3</sup> K. Prokes <sup>3</sup> S. Mat'as <sup>3</sup>	<sup>1</sup> MPI Stuttgart <sup>2</sup> Uni Tokyo, JP <sup>3</sup> HZB E4 <b>PHY-01-2750</b>
28	<b>Magnetic structure of pressure- and field- induced magnetically ordered phases in YbAgGe with a quasi-kagome lattice</b>	K. Umeo <sup>1</sup> T. Onimaru <sup>1</sup> H. Kubo <sup>1</sup> T. Takabatake <sup>1</sup> K. Prokes <sup>2</sup>	<sup>1</sup> Uni Hiroshima, JP <sup>2</sup> HZB E4 <b>PHY-01-2751</b>
29	<b>Magnetic structure of magnetoelectric hexaferrites under low field: planar or conical?</b>	J.-H. Chung <sup>1</sup> H. Lee <sup>1</sup> K. Prokes <sup>2</sup>	<sup>1</sup> Korea University, KR <sup>2</sup> HZB E4 <b>PHY-01-2752</b>
30	<b>Evolution of the magnetic order in Yb(Rh<sub>1-x</sub>Cox)<sub>2</sub>Si<sub>2</sub></b>	O. Stockert <sup>1</sup> A. Haase <sup>1</sup> S. Mat'as <sup>2</sup>	<sup>1</sup> MPI, CPfS, Dresden <sup>2</sup> HZB E4 <b>PHY-01-2873</b>
31	<b>Effect of uniaxial pressure on helimagnetic structures in Lu<sub>2</sub>Fe<sub>17</sub> and Y<sub>2</sub>Fe<sub>17</sub></b>	J. Kamarad <sup>1</sup> M. Misek <sup>1</sup> K. Prokes <sup>2</sup> S. Mat'as <sup>2</sup>	<sup>1</sup> ASCR IP Prague, CZ <sup>2</sup> HZB E4 <b>PHY-01-2874</b>
32	<b>Magnetic ordering in Tb<sub>0.3</sub>Er<sub>0.7</sub>Ni<sub>5</sub> single crystal with competitive anisotropies</b>	A. Pirogov <sup>1</sup> P. Terentev <sup>1</sup> K. Prokes <sup>2</sup> S. Mat'as <sup>2</sup>	<sup>1</sup> RAS, RU <sup>2</sup> HZB E4 <b>PHY-01-2875</b>

## List of Contributed Experimental Reports

PAGE	TITLE	TEAM	PROPOSAL
33	<b>Structural and magnetic properties of <math>\text{Sr}_3\text{Fe}_2\text{O}_{7-x}</math></b>	M. Reehuis <sup>1</sup> A. Maljuk <sup>1</sup> J. Kim <sup>2</sup> B. Keimer <sup>2</sup>	<sup>1</sup> HZB <sup>2</sup> MPI Stuttgart E5 <b>PHY-01-2784-LT</b>
34	<b>Magnetic structure determination of the pseudo-triangular antiferromagnet <math>\alpha\text{-CaCr}_2\text{O}_4</math></b>	B. Lake <sup>1</sup> S. Toth <sup>1</sup> S. Kimber <sup>1</sup> D. Argyriou <sup>1</sup> O. Pieper <sup>1</sup> N. Islam <sup>1</sup>	<sup>1</sup> HZB E5 <b>PHY-01-2786-EF</b>
35	<b>T-Dependence of the magnetic structure of <math>\text{YbVO}_3</math></b>	C. Ulrich <sup>1</sup> B. Keimer <sup>2</sup> M. Reehuis <sup>3</sup> J. Fujioka <sup>4</sup> S. Miyasaka <sup>4</sup> Y. Tokura <sup>4</sup>	<sup>1</sup> ANSTO, AU <sup>2</sup> MPI Stuttgart <sup>3</sup> HZB <sup>4</sup> Uni Tokyo, JP E5 <b>PHY-01-2789</b>
36	<b>Magnetic structure of magnetoelectric hexaferrites under low field: planar or conical?</b>	J.-H. Chung <sup>1</sup> H. Lee <sup>1</sup> M. Reehuis <sup>2</sup>	<sup>1</sup> Korea University, KR <sup>2</sup> HZB E5 <b>PHY-01-2791</b>
37	<b>Investigating the magnetic unit cell doubling in room temperature semiconductor <math>\text{LiMnAs}</math></b>	X. Marti <sup>1</sup> V. Holy <sup>1</sup> V. Novak <sup>2</sup> Th. Jungwirth <sup>2</sup> M. Reehuis <sup>3</sup>	<sup>1</sup> CU Prague, CZ <sup>2</sup> ASCR IP Prague, CZ <sup>3</sup> HZB E5 <b>MAT-01-2897</b>
38	<b>Structural properties of <math>\text{YbVO}_3</math></b>	C. Ulrich <sup>1</sup> B. Keimer <sup>2</sup> M. Reehuis <sup>3</sup> J. Fujioka <sup>4</sup> S. Miyasaka <sup>4</sup> Y. Tokura <sup>4</sup>	<sup>1</sup> ANSTO, AU <sup>2</sup> MPI Stuttgart <sup>3</sup> HZB <sup>4</sup> Uni Tokyo, JP E5 <b>PHY-01-2899</b>
39	<b>Determination of magnetic structures of complex transition metal chalcogenides</b>	W. Bensch <sup>1</sup> J. Opehy <sup>1</sup> B. Dietl <sup>1</sup> A. Arulraj <sup>2</sup>	<sup>1</sup> CAU Kiel <sup>2</sup> IGCAR, Kalpakkam, IN E6 <b>CHE-01-2133</b>
40	<b>Determination of magnetic structure of <math>\text{NpPdSn}</math></b>	K. Gofryk <sup>1+2</sup> R. Caciuffo <sup>1+2</sup> J.-Ch. Griveau <sup>2</sup> K. Prokes <sup>3</sup> D. Wallacher <sup>3</sup> S. Gerischer <sup>3</sup> T. Hoffman <sup>3</sup> N. Grimm <sup>3</sup>	<sup>1</sup> ITU Karlsruhe <sup>2</sup> LANL, US <sup>3</sup> HZB E6 <b>PHY-01-2511</b>
41	<b>Evolution of the magnetic structure of <math>\text{YbCo}_2\text{Si}_2</math> in magnetic field</b>	N. Mufti <sup>1</sup> O. Stockert <sup>1</sup> A. Hoser <sup>2</sup>	<sup>1</sup> MPI, CPfS, Dresden <sup>2</sup> HZB E6 <b>PHY-01-2629</b>
42	<b>Magnetic phase transition in <math>\text{NdIr}_2\text{Si}_2</math></b>	M. Mihalik <sup>1</sup> A. Hoser <sup>1</sup>	<sup>1</sup> HZB E6 <b>PHY-01-2758-EF</b>
43	<b>From 1D to 3D magnetism: spin chain with enhanced interchain coupling</b>	O. Stockert <sup>1</sup> A. Haase <sup>1</sup> A. Hoser <sup>2</sup>	<sup>1</sup> MPI, CPfS, Dresden <sup>2</sup> HZB E6 <b>PHY-01-2762</b>
44	<b>Frustrated magnetic structure of Y-substituted <math>\text{CePdAl}</math> studied by powder neutron diffraction</b>	P. Cermak <sup>1</sup> A. Hoser <sup>2</sup> T. Hofmann <sup>2</sup>	<sup>1</sup> CU Prague, CZ <sup>2</sup> HZB E6 <b>PHY-01-2764</b>
45	<b>Magnetic structure of <math>\text{Cs}_3\text{Mn}_2\text{O}_4</math></b>	M.A. Señaris-Rodríguez <sup>1</sup> M. Jansen <sup>2</sup> M. Reehuis <sup>3</sup> A. Hoser <sup>3</sup> T. Hofmann <sup>3</sup>	<sup>1</sup> Uni A Coruña, ES <sup>2</sup> MPI Stuttgart <sup>3</sup> HZB E6 <b>PHY-01-2765</b>

## List of Contributed Experimental Reports

PAGE	TITLE	TEAM	PROPOSAL
46	Temperature dependence of magnetic and crystal structure parameters of $\text{NdMn}_{2-x}\text{Cu}_x\text{Ge}_2$ and $\text{PrMn}_{2-x}\text{Fe}_x\text{Ge}_2$ ( $x=0.3$ )	T. Jaworska-Golab <sup>1</sup> S. Baran <sup>1</sup> A. Hoser <sup>2</sup> T. Hofmann <sup>2</sup>	<sup>1</sup> JU Krakow, PL <sup>2</sup> HZB E6 <b>PHY-01-2771</b>
47	Magneto-structural Studies on Intermetallics $\text{Tb}_5\text{Si}_3$ and $\text{Ho}_5\text{Ge}_4$ using Neutron Diffraction	S. Rayaprol <sup>1</sup> V. Siruguri <sup>1</sup> E.V. Sampathkumaran <sup>2</sup> A. Hoser <sup>3</sup>	<sup>1</sup> UGC-DAE CSR, IN <sup>2</sup> TIFR, IN <sup>3</sup> HZB E6 <b>PHY-01-2774</b>
48	Structural and Magnetic Properties of Solid Oxygen Confined into Oriented Mesopores of Anodized Aluminum	T. Hofmann <sup>1</sup> D. Wallacher <sup>1</sup>	<sup>1</sup> HZB E6 <b>PHY-01-2878-EF</b>
49	Investigation of magnetic structures in $\text{Tm}_3\text{Cu}_4\text{X}_4$ ( $X = \text{Ge}, \text{Sn}$ ) compounds	S. Baran <sup>1</sup> A. Gil <sup>2</sup> A. Hoser <sup>3</sup> T. Hofmann <sup>3</sup>	<sup>1</sup> JU Krakow, PL <sup>2</sup> JDU, PL <sup>3</sup> HZB E6 <b>PHY-01-2885</b>
50	Magnetic structure of hexagonal $\text{HoMn}_2\text{D}_{4.5}$ deuteride	A. Budziak <sup>1</sup> L. Gondek <sup>2</sup> A. Hoser <sup>3</sup>	<sup>1</sup> PAS IFJ Krakow, PL <sup>2</sup> AGH-UST, Krakow, PL <sup>3</sup> HZB E6 <b>PHY-01-2888</b>
51	Sublattice Magnetization in $\text{RbMnF}_3$	J. Klein <sup>1</sup> U. Köbler <sup>2</sup> A. Hoser <sup>3</sup>	<sup>1</sup> Univ. of Pennsylvania, US <sup>2</sup> FZ Jülich <sup>3</sup> HZB E6 <b>PHY-01-2889</b>
52	Neutron diffraction studies of the crystal and magnetic structure of $\text{Pr}_{0.5}\text{Sr}_x\text{La}_{1-x}\text{CoO}_3$	V. Sikolenko <sup>1</sup> V. Efimov <sup>2</sup>	<sup>1</sup> ETH Zürich, CH <sup>2</sup> PSI, CH E9 <b>PHY-01-2598</b>
53	Magnetic transitions in a frustrated triangular lattice compound $\text{Ca}_{0.5}\text{CrO}_2$	S. Toth <sup>1</sup> B. Lake <sup>1</sup> S. Kimber <sup>1</sup>	<sup>1</sup> HZB E9 <b>PHY-01-2605-DT</b>
54	Neutron diffraction studies $\text{Y}_2\text{Co}_2\text{O}_5+\delta$ doped with Fe	V. Sikolenko <sup>1+2</sup> V. Efimov <sup>3</sup>	<sup>1</sup> ETH Zürich, CH <sup>2</sup> PSI, CH <sup>3</sup> JINR Dubna, RU E9 <b>PHY-01-2726</b>
55	Neutron diffraction study of the crystal and magnetic structure transformation in $\text{Pr}_{0.5}\text{A}_{0.5}\text{FeO}_3$ -d perovskite	V. Kabanov <sup>1</sup> V. Sikolenko <sup>2</sup> V. Efimov <sup>3</sup>	<sup>1</sup> IJS, Ljubljana, SI <sup>2</sup> PSI, CH <sup>3</sup> JINR Dubna, RU E9 <b>PHY-01-2732</b>
56	Field-induced magnetic transitions in $\text{Cs}_3\text{Mn}_2\text{O}_4$	M. Señaris-Rodríguez <sup>1</sup> M. Reehuis <sup>2</sup> A. Hoser <sup>2</sup> M. Jansen <sup>3</sup>	<sup>1</sup> Uni A Coruña, ES <sup>2</sup> HZB <sup>3</sup> MPI Stuttgart E9 <b>PHY-01-2728</b>
57	Magnetic excitation Spectrum of the distorted triangular antiferromagnet $\alpha\text{-CaCr}_2\text{O}_4$	B. Lake <sup>1</sup> S. Toth <sup>1</sup> K. Rule <sup>1</sup>	<sup>1</sup> HZB V2 <b>PHY-02-736-EF</b>
58	Low-Temperature investigations of the Spin Waves on $\text{SrYb}_2\text{O}_4$	D. Quintero Castro <sup>1</sup> B. Lake <sup>1</sup> N. Islam <sup>1</sup>	<sup>1</sup> HZB V2 <b>PHY-02-751-EF</b>
59	Thermal and quantum critical scattering in the dipolar coupled planar antiferromagnet $\text{LiErF}_4$	N. Nikseresht <sup>1</sup> H. Ronnow <sup>1</sup> N. Tsyrlin <sup>1</sup> K. Rule <sup>2</sup>	<sup>1</sup> EPFL, CH <sup>2</sup> HZB V2 <b>PHY-02-753</b>
60	Spin Excitations and Bose-Einstein Condensation in the random bond spin ladder material $(\text{C}_5\text{D}_{12}\text{N})_2\text{CuBr}_4$ ( $1-x$ ) $\text{Cl}_{4x}$	Ch. Rüegg <sup>1</sup> S. Ward <sup>1</sup>	<sup>1</sup> UCL, UK V2 <b>PHY-02-754</b>

## List of Contributed Experimental Reports

PAGE	TITLE	TEAM	PROPOSAL
61	<b>Magnetic field dependence of Luttinger Parameter for a spin chain</b>	D. Huvonen <sup>1</sup> D. Le <sup>2</sup> K. Rule <sup>2</sup>	<sup>1</sup> ETH, Zürich, CH <sup>2</sup> HZB V2 <b>PHY-02-771</b>
62	<b>Magnetic Excitations of the Quantum Spin-Chain Compounds <math>\beta</math>-CuNb<sub>2</sub>O<sub>6</sub></b>	B. Lake <sup>1</sup> O. Pieper <sup>1</sup> N. Islam <sup>1</sup>	<sup>1</sup> HZB V3 <b>PHY-03-661-EF</b>
63	<b>Magnetic Excitations of the Quantum Spin-Chain Compounds <math>\beta</math>-CuNb<sub>2</sub>O<sub>6</sub></b>	B. Lake <sup>1</sup> O. Pieper <sup>1</sup> N. Islam <sup>1</sup>	<sup>1</sup> HZB V3 <b>PHY-03-686</b>
64	<b>Structural and magnetic properties of ortho-Sr<sub>2</sub>VO<sub>4</sub></b>	B. Lake <sup>1</sup> S. Toth <sup>1</sup> J. Deisenhofer <sup>2</sup> E. Giannini <sup>3</sup>	<sup>1</sup> HZB <sup>2</sup> Uni Augsburg <sup>3</sup> Uni Geneva, CH V3 <b>PHY-03-712-EF</b>
65	<b>Polarized SANS measurements on <math>\gamma</math>-Fe<sub>2</sub>O<sub>3</sub> nanoparticles</b>	U. Keiderling <sup>1</sup> E. Josten <sup>2</sup> P. Busch <sup>2</sup> S. Bedanta <sup>2</sup> S. Disch <sup>2</sup>	<sup>1</sup> HZB <sup>2</sup> FZ Jülich V4 <b>PHY-04-1651</b>
66	<b>Search for the FFLO phase in a heavy-fermion superconductor CeCoIn<sub>5</sub></b>	H. Furukawa <sup>1</sup> S. Kawamura <sup>1</sup> P. Das <sup>1</sup> A. Cameron <sup>3</sup> E.M. Forgan <sup>3</sup> U. Keiderling <sup>4</sup> S. Gerischer <sup>4</sup>	<sup>1</sup> OU Tokyo, JP <sup>2</sup> University of Notre Dame, US <sup>3</sup> Uni Birmingham, UK <sup>4</sup> HZB V4 <b>PHY-04-1672</b> <b>PHY-04-1673</b> <b>PHY-04-1841</b>
67	<b>The critical dynamic of the helix structure in YMn<sub>6</sub>Sn<sub>6</sub></b>	E. Moskvina <sup>1</sup> S. Grigoriev <sup>1</sup> V. Piyadov <sup>1</sup> S. Wellert <sup>2</sup>	<sup>1</sup> RAS PNPI Gatchina, RU <sup>2</sup> HZB V5 <b>PHY-03-679-LT</b>
68	<b>Magnetization reversal in exchange coupled system with a field perpendicular to the cooling field and the sample plane</b>	A. Paul <sup>1</sup>	<sup>1</sup> HZB V6 <b>PHY-04-1956-EF</b>
69	<b>PNR study of the magnetization reversal mechanism of the implanted Ni/NiO system</b>	J. Demeter <sup>1</sup> E. Menendez <sup>1</sup> A. Teichert <sup>1+2</sup>	<sup>1</sup> KU Leuven, BE <sup>2</sup> HZB V6 <b>PHY-04-1959-EF</b>
70	<b>PNR study of the proximity effect in a Nb/Fe/Nb superconductor/ferromagnet multilayer</b>	J. Demeter <sup>1</sup> S. Couet <sup>1</sup> A. Teichert <sup>1+2</sup>	<sup>1</sup> KU Leuven, BE <sup>2</sup> HZB V6 <b>PHY-04-1960-LT</b>
71	<b>Inverse proximity effects at the superconductor-ferromagnet interface revealed by polarized neutron</b>	Y. Khaydukova <sup>1</sup> B. Nagy <sup>2</sup> R. Steitz <sup>3</sup> A. Paul <sup>3</sup> D. Wallacher <sup>3</sup>	<sup>1</sup> FLNP JINR, RU <sup>2</sup> RMKI KFKI, RU <sup>3</sup> HZB V6 <b>PHY-04-1705</b>
72	<b>PNR and AMR measurement along the easy axis of a Co/CoO exchange bias system</b>	J. Demeter <sup>1</sup> E. Menendez <sup>1</sup> K. Kiefer <sup>2</sup> A. Teichert <sup>1+2</sup>	<sup>1</sup> KU Leuven, BE <sup>2</sup> HZB V6 <b>PHY-04-2045-LT</b>
73	<b>Investigation of vortex lattices by means of TOF-SANS</b>	V. Ryukhtin <sup>1</sup> O. Prokhnenko <sup>1</sup> W.D. Stein <sup>1</sup> U. Keiderling <sup>1</sup>	<sup>1</sup> HZB V15 <b>PHY-01-2926-EF</b>
74	<b>Visualization of the Meissner effect by polarized neutron radiography</b>	S.-O. Seidel <sup>1</sup> W. Treimer <sup>1+2</sup> O. Ebrahimi <sup>2</sup> N. Karakas <sup>2</sup>	<sup>1</sup> HZB <sup>2</sup> TFH, Berlin V19 <b>EF</b>

## List of Contributed Experimental Reports

PAGE	TITLE	TEAM	PROPOSAL
<b>Structure</b>			
77	Temperature evolution of nano-twinned martensitic structure in $\text{Ni}_{1.99}\text{Mn}_{1.14}\text{Ga}_{0.87}$ single crystal	N. Glavastka <sup>1</sup> I. Glavatskyi <sup>2</sup>	<sup>1</sup> IMP, UA <sup>2</sup> HZB E2 <b>PHY-01-2841</b>
78	Structure evolution of AgI in a restricted geometry	A. Naberezhnov <sup>1</sup> D. Kurdyukov <sup>1</sup> M. Tovar <sup>2</sup> I. Glavatskyi <sup>2</sup>	<sup>1</sup> Ioffe Institute, RU <sup>2</sup> HZB E2 E9 <b>PHY-01-2603</b> <b>PHY-01-2491</b>
79	The neutron feasibility study on $\text{PrFe}(\text{CN})6\text{nH}_2\text{O}$ and $\text{K}_3\text{Fe}(\text{CN})_6 \times \text{mH}_2\text{O}$	S. Mat'as <sup>1</sup> Z. Mitroova <sup>2</sup>	<sup>1</sup> HZB <sup>2</sup> SAS Kosice, SK E4 E6 <b>PHY-01-2757-EF</b>
80	The annealing process and high temperature phase transition of $\text{UCoGe}$	J. Pospisil <sup>1</sup> M. Kratochvilova <sup>1</sup> K. Prokes <sup>2</sup> M. Reehuis <sup>2</sup> M. Tovar <sup>2</sup>	<sup>1</sup> CU Prague, CZ <sup>2</sup> HZB E5 E9 <b>PHY-01-2788</b> <b>PHY-01-2727</b>
81	Crystal structure of $\text{SrYb}_2\text{O}_4$	B. Lake <sup>1</sup> D. Quintero Castro <sup>1</sup> M. Reehuis <sup>1</sup> N. Islam <sup>1</sup>	<sup>1</sup> HZB E5 <b>PHY-01-2781-EF</b>
82	Single-crystal neutron diffraction study of $\text{LiCuVO}_4$	H. Schier <sup>1</sup> R.K. Kremer <sup>1</sup> C. Kallfaß <sup>1</sup> M. Reehuis <sup>2</sup>	<sup>1</sup> MPI Stuttgart <sup>2</sup> HZB E5 <b>MAT-01-2894</b>
83	Polymorphism of $\text{REIr}_2\text{Si}_2$ : LT-HT and HT-LT structure transformations	X. Marti <sup>1</sup> M. Mihalik <sup>2</sup> T. Hofmann <sup>2</sup> A. Hoser <sup>2</sup>	<sup>1</sup> CU Prague, CZ <sup>2</sup> HZB E6 <b>PHY-01-2759-EF</b>
84	Solidified Deuterium in Silicon Nanchannels	D. Wallacher <sup>1</sup> T. Hofmann <sup>1</sup>	<sup>1</sup> HZB E6 <b>PHY-01-2761-EF</b>
85	Structure and thermal decomposition of $\text{LiZn}_2(\text{BD}_4)_5$	A. Remhof <sup>1</sup> O. Friedrichs <sup>1</sup> D. Wallacher <sup>2</sup>	<sup>1</sup> EMPA, CH <sup>2</sup> HZB E6 <b>MAT-01-2763</b>
86	In situ neutron diffraction investigation on the support effect of $\text{V}_2\text{O}_5$ containing catalyst systems	O. Görke <sup>1</sup> A. Berthold <sup>1</sup> A. Hoser <sup>2</sup> T. Hofmann <sup>2</sup> D. Wallacher <sup>2</sup>	<sup>1</sup> TU Berlin <sup>2</sup> HZB E6 <b>MAT-01-2880</b>
87	Neutron powder diffraction study of $\text{Sr}_3\text{Fe}_2\text{O}_{7-x}$	J. Kim <sup>1</sup> B. Keimer <sup>1</sup> M. Reehuis <sup>2</sup> A. Maljuk <sup>2</sup> A. Hoser <sup>2</sup> T. Hofmann <sup>2</sup>	<sup>1</sup> MPI Stuttgart <sup>2</sup> HZB E6 <b>PHY-01-2784-LT</b>
88	Order and disorder in kesterite ( $\text{Cu}_2\text{ZnSnS}_4$ )	S. Schorr <sup>1</sup> M. Tovar <sup>2</sup>	<sup>1</sup> FU Berlin <sup>2</sup> HZB E9 <b>PHY-01-2520</b>
89	Potential Neutron Powder Diffraction in $\text{La}_{2/3}\text{Ca}_{1/3}\text{AxMn}(1-x)\text{O}_3$ with $\text{A}=\text{Cr}(x=0.07 \text{ and } 0.08)$ , $\text{Fe}(x=0.03)$	O. Arnache <sup>1</sup> D. Girata <sup>1</sup> D. Quintero Castro <sup>2</sup>	<sup>1</sup> Uni Antioquia, CO <sup>2</sup> HZB E9 <b>PHY-01-2532</b>
90	Structural investigation of the kesterites $\text{Cu}_2\text{ZnSn}(\text{S}_{1-x}\text{Se}_x)_4$	S. Schorr <sup>1</sup> M. Berkes <sup>1</sup> M. Tovar <sup>2</sup>	<sup>1</sup> FU Berlin <sup>2</sup> HZB E9 <b>PHY-01-2596</b>
91	Investigations in the phase system $\text{Li-Zr-Y-Mg-O}$	U. Simon <sup>1</sup> O. Görke <sup>1</sup> M. Tovar <sup>2</sup> D. Wallacher <sup>2</sup> N. Holst <sup>2</sup>	<sup>1</sup> TU Berlin <sup>2</sup> HZB E9 <b>MAT-01-2723</b>

## List of Contributed Experimental Reports

PAGE	TITLE	TEAM	PROPOSAL
92	Neutron diffraction studies on Nd <sub>7</sub> Rh <sub>3</sub>	S. Rayaprol <sup>1</sup> V. Siruguri <sup>1</sup> E.V. Sampathkumaran <sup>2</sup> A. Hoser <sup>3</sup> P. Henry <sup>3</sup>	<sup>1</sup> UGC-DAE CSR, IN <sup>2</sup> TIFR, IN <sup>3</sup> HZB E9 <b>PHY-01-2734</b>
93	Determination of metal atom site distribution in complex transition metal chalcogenides	W. Bensch <sup>1</sup> K. Gerwien <sup>1</sup> P. Henry <sup>2</sup> M. Tovar <sup>2</sup>	<sup>1</sup> CAU Kiel <sup>2</sup> HZB E9 <b>CHE-01-2652</b>
94	Isothermal structural transition in Bi <sub>1-x</sub> La <sub>x</sub> FeO <sub>3</sub> system	A. Kuzmin <sup>1</sup> V. Sikolenko <sup>2+3</sup> V. Efimov <sup>4</sup>	<sup>1</sup> Uni Latvia, LV <sup>2</sup> ETH Zürich, CH <sup>3</sup> PSI, CH <sup>4</sup> JINR Dubna, RU E9 <b>PHY-01-2863</b>
95	Crystal electric field in PrT <sub>2</sub> Ge <sub>2</sub> (T = Ni, Rh) compounds	L. Gondek <sup>1</sup> J. Czub <sup>1</sup> Z. Izaola <sup>2</sup>	<sup>1</sup> AGH-UST, Krakow, PL <sup>2</sup> HZB V3 <b>PHY-03-692</b>
96	Changes of crystal field upon deuteration of RPdIn compounds	L. Gondek <sup>1</sup> J. Czub <sup>1</sup> N. Tsapatsaris <sup>2</sup>	<sup>1</sup> AGH-UST, Krakow, PL <sup>2</sup> HZB V3 <b>PHY-03-717</b>

### *Biology & Soft Matter*

99	Molecular actions of arginine, glucose and arginine-glucose MRP on DMPC bilayer	J. Bradshaw <sup>1</sup> L. Ke <sup>1</sup> F. Sa'adedin <sup>1</sup> Th. Hauß <sup>2</sup>	<sup>1</sup> Uni Edinburgh, UK <sup>2</sup> HZB V1 <b>BIO-01-2661</b>
100	Membrane disruption by NK-2	R. Willumeit <sup>1</sup> A. Rzeszutek <sup>1</sup> M. Golub <sup>1</sup>	<sup>1</sup> GKSS Geesthacht V1 <b>BIO-01-2799</b>
101	Investigation of the effects of penetration enhancers on the lipid assembly in stratum corneum lipid model membranes	T. Engelbrecht <sup>1</sup> B. Dobner <sup>1</sup> R. Neubert <sup>1</sup> A. Buchsteiner <sup>2</sup> Th. Hauß <sup>2</sup>	<sup>1</sup> MLU Halle/Saale <sup>2</sup> HZB V1 <b>BIO-01-2801</b>
102	Effects of oleic acid on the lipid assembly in stratum corneum lipid model membranes based on asymmetric ceramides	T. Engelbrecht <sup>1</sup> B. Dobner <sup>1</sup> R. Neubert <sup>1</sup> A. Buchsteiner <sup>2</sup> Th. Hauß <sup>2</sup>	<sup>1</sup> MLU Halle/Saale <sup>2</sup> HZB V1 <b>BIO-01-2904</b>
103	Molecular Structure of the Stratum corneum Lipid Membrane: A New Theoretical Model for the Lipid matrix	A. Schröter <sup>1</sup> T. Engelbrecht <sup>1</sup> R. Neubert <sup>1</sup> Th. Hauß <sup>2</sup>	<sup>1</sup> MLU Halle/Saale <sup>2</sup> HZB V1 <b>BIO-01-2905</b>
104	Structure of the model oral epithelial membranes based on ceramide-6	N. Ryabova <sup>1</sup> S. Sheverev <sup>1</sup> A. Buchsteiner <sup>2</sup> Th. Hauß <sup>2</sup>	<sup>1</sup> JINR, Dubna, RU <sup>2</sup> HZB V1 <b>BIO-01-2908</b>
105	Does specific protein mutation affect the myelin membrane dynamics?	J. Peters <sup>1</sup> W. Knoll <sup>1</sup> N. Tsapatsaris <sup>2</sup>	<sup>1</sup> ILL, Grenoble, FR <sup>2</sup> HZB V3 <b>BIO-03-715</b>
106	SANS study of temperature-stable colloidal structures in mixtures of ionic liquids	O. Zech <sup>1</sup> A. Harrar <sup>1</sup> D. Rengstl <sup>1</sup> W. Keiderling <sup>2</sup>	<sup>1</sup> Uni Regensburg <sup>2</sup> HZB V4 <b>CHE-04-1555</b>
107	Protein Interactions in Solution Containing Concentrated Electrolytes Studied by SANS	F. Schreiber <sup>1</sup> F. Zhang <sup>1</sup> M. Wolf <sup>1</sup> A. Sauter <sup>1</sup> U. Keiderling <sup>2</sup>	<sup>1</sup> Uni Tübingen <sup>2</sup> HZB V4 <b>PHY-04-1652</b>

## List of Contributed Experimental Reports

PAGE	TITLE	TEAM	PROPOSAL
108	<b>Self-assembly and gelation mechanism of ionic complementary peptides</b>	A. Saiani <sup>1</sup> J.-B. Guilhaud <sup>1</sup> D. Adams <sup>1</sup> S. Prevost <sup>2</sup>	<sup>1</sup> Uni Manchester, UK <sup>2</sup> HZB V4 <b>BIO-04-1835</b>
109	<b>Structural characterization of magnetic drug carriers</b>	A. Bakandritsos <sup>1</sup> K. Avgoustakis <sup>1</sup> A. Papagiannopoulos <sup>2</sup> S. Pispas <sup>2</sup> Th. Steriotis <sup>3</sup> F. Winnegeld <sup>4</sup> V. Ryukhtin <sup>5</sup>	<sup>1</sup> Uni Patras, GR <sup>2</sup> NHRF, Athens, GR <sup>3</sup> NCSR, Demokritos, GR <sup>4</sup> EMPA, Zürich, CH <sup>5</sup> HZB V4 <b>MAT-04-1905</b>
110	<b>Rotational and translational self-diffusion of benzene molecules on graphite</b>	P. Fouquet <sup>1</sup> I. Calvo-Almazan <sup>1</sup> S. Wellert <sup>2</sup> B. Bruening <sup>2</sup>	<sup>1</sup> ILL, Grenoble, FR <sup>2</sup> HZB V5 <b>PHY-03-703</b>
111	<b>How does supercooled water diffuse?</b>	G. Schiro <sup>1</sup> A. Cupane <sup>1</sup> M. Levantino <sup>1</sup> M. Cammarata <sup>2</sup>	<sup>1</sup> Uni Palermo, IT <sup>2</sup> Stanford University, US V5 <b>PHY-03-704</b>
112	<b>Effect of cholesterol on the collective bilayer undulations of phospholipid model membranes: Linking curvature and lateral compression modes</b>	P. Falus <sup>1</sup> B. Brüning <sup>2</sup> R. Stehle <sup>3</sup> C. Pappas <sup>4</sup>	<sup>1</sup> ILL, Grenoble, FR <sup>2</sup> HZB <sup>3</sup> Uni Bayreuth <sup>4</sup> TU Delft, NL V5 <b>PHY-03-721-IT</b>
113	<b>Binding and diffusion of Glutamate on PAH and PSS terminated polyelectrolyte multilayers</b>	A. Paul <sup>1</sup> N. Paul <sup>1</sup> M. Kreuzer <sup>1</sup>	<sup>1</sup> HZB V6 <b>PHY-04-1952-EF</b>
114	<b>Functional interfaces under load (hydrostatic pressure)</b>	R. Steitz <sup>1</sup> M. Reinhardt <sup>1</sup> M. Kreuzer <sup>2</sup>	<sup>1</sup> HZB <sup>2</sup> RKU, Heidelberg V6 <b>PHY-04-1953-EF</b>
115	<b>Temperature Dependent Unbinding of Lipid Multilayers</b>	R. Steitz <sup>1</sup> M. Kreuzer <sup>2</sup> R. Dahint <sup>2</sup>	<sup>1</sup> HZB <sup>2</sup> RKU, Heidelberg V6 <b>BIO-04-1958-EF</b>
116	<b>Measurements of solvent distribution in swollen lamella-forming block copolymer films</b>	L. Tsarkova <sup>1</sup> R. Krastev <sup>2</sup> R. Köhler <sup>3</sup>	<sup>1</sup> Uni Bayreuth <sup>2</sup> Uni Tübingen <sup>3</sup> HZB V6 <b>MAT-04-1962</b>
117	<b>Diffusion in Polyelectrolyte Multilayers</b>	C.A. Helm <sup>1</sup> O. Soltwedel <sup>1</sup> P. Nestler <sup>1</sup> R. Köhler <sup>2</sup>	<sup>1</sup> EMAU Greifswald <sup>2</sup> MPI V6 <b>MAT-04-1966</b>
118	<b>Critical and multilayer adsorption from alkane + perfluoroalkane mixtures to chemically modified silicon substrates</b>	A. Zorbakhsh <sup>1</sup> J. Webster <sup>2</sup> R. Steitz <sup>3</sup> A. Teichert <sup>3</sup>	<sup>1</sup> QM UCL, UK <sup>2</sup> RAL ISIS, UK <sup>3</sup> HZB V6 <b>PHY-04-1968</b>
119	<b>Tuning the hydrate water in polyelectrolyte multilayers by varying the preparation conditions</b>	C.A. Helm <sup>1</sup> O. Soltwedel <sup>1</sup> P. Nestler <sup>1</sup> R. Köhler <sup>2</sup>	<sup>1</sup> EMAU Greifswald <sup>2</sup> MPI V6 <b>MAT-04-1701</b>
120	<b>Structure of ionic liquids in thin films and at solid interfaces</b>	R. Köhler <sup>1</sup> R. Krastev <sup>2</sup> J. Restolho <sup>3</sup> B. Saramago <sup>3</sup>	<sup>1</sup> MPI <sup>2</sup> Uni Tübingen <sup>3</sup> IST, Lisbon, PT V6 <b>PHY-04-2042-LT</b> <b>PHY-04-1954-LT</b>
121	<b>Diffusion in the Outer Zone of Polyelectrolyte Multilayers</b>	C.A. Helm <sup>1</sup> O. Soltwedel <sup>1</sup> P. Nestler <sup>1</sup> R. Köhler <sup>2+3</sup>	<sup>1</sup> EMAU Greifswald <sup>2</sup> HZB <sup>3</sup> Stranski Lab, Berlin V6 <b>MAT-04-2054</b>
122	<b>Water Distribution in Electrochemically Swellable Polyelectrolyte Multilayers</b>	R. Zahn <sup>1</sup> J. Vörös <sup>1</sup> T. Zambelli <sup>1</sup> K. Bickel <sup>2</sup> R. Köhler <sup>3</sup>	<sup>1</sup> ETH, Zürich, CH <sup>2</sup> KIT <sup>3</sup> HZB V6 <b>CHE-04-2057</b>

## List of Contributed Experimental Reports

PAGE	TITLE	TEAM	PROPOSAL
123	<b>Neutron reflectivity from Silicon/EVA interface</b>	B. Röder <sup>1</sup> S. Jungwirth <sup>1</sup> R. Steitz <sup>2</sup> R. Köhler <sup>2</sup>	<sup>1</sup> HU Berlin <sup>2</sup> HZB V6 <b>PHY-04-1898</b>
124	<b>Internal Interfaces of Polyelectrolyte Multilayers</b>	C.A. Helm <sup>1</sup> O. Soltwedel <sup>1</sup> P. Nestler <sup>1</sup> O. Ivanova <sup>1</sup> M. Meyer <sup>1</sup>	<sup>1</sup> EMAU Greifswald V6 <b>PHY-04-1902</b>
125	<b>Evaluation of systematic Hofmeister effects on protein adsorption</b>	C. Czeslik <sup>1</sup> F. Evers <sup>1</sup> M. Tolan <sup>1</sup> Ch. Jeworrek <sup>1</sup> R. Steitz <sup>2</sup>	<sup>1</sup> TU Dortmund <sup>2</sup> HZB V6 <b>CHE-04-1963</b>
126	<b>Visualisation of plant root structure and water uptake from soil using neutron radiography and D<sub>2</sub>O</b>	S.E. Oswald <sup>1</sup> N. Rudolph <sup>1</sup> H.G. Esser <sup>1</sup> U. Matsushima <sup>2</sup> A. Carminati <sup>3</sup> A.B. Moradi <sup>3</sup> A. Hilger <sup>4</sup> N. Kardjilov <sup>4</sup>	<sup>1</sup> Uni Potsdam <sup>2</sup> Iwate University, JP <sup>3</sup> UFZ Leipzig <sup>4</sup> HZB V7 <b>BIO-04-1944</b>
127	<b>Combining neutron radiography and fluorescence imaging to simultaneously record dynamics of oxygen, pH and water</b>	N. Rudolph <sup>1</sup> S.E. Oswald <sup>1</sup> A.B. Moradi <sup>2</sup> N. Kardjilov <sup>3</sup> A. Hilger <sup>3</sup>	<sup>1</sup> Uni Potsdam <sup>2</sup> UFZ Leipzig <sup>3</sup> HZB V7 <b>BIO-04-2024</b>
128	<b>Structure of DNA films</b>	A. Becker <sup>1</sup> M. Strobl <sup>1</sup> R. Steitz <sup>1</sup> M. Reinhardt <sup>1</sup> M. Kreuzer <sup>2</sup>	<sup>1</sup> HZB <sup>2</sup> RKU, Heidelberg V18 <b>MAT-04-2041-EF</b>
129	<b>Phase transition of the lipid molecule DMPC in a combined Neutron Reflectivity and FTIR experiment</b>	M. Strobl <sup>1</sup> R. Steitz <sup>1</sup> M. Kreuzer <sup>2</sup> R. Dahint <sup>2</sup>	<sup>1</sup> HZB <sup>2</sup> RKU, Heidelberg V18 <b>EF</b>
130	<b>Instrument test: Grafted PMMA film in the low-grafting-density-regime</b>	B. Stühn <sup>1</sup> M. Müller <sup>1</sup> M. Appel <sup>1</sup> A. Weber <sup>1</sup> M. Strobl <sup>2</sup> M. Reinhardt <sup>2</sup>	<sup>1</sup> TU Darmstadt <sup>2</sup> HZB V18 <b>EF</b>
131	<b>Protein adsorption to charged polymer brushes</b>	R. Steitz <sup>1</sup> M. Reinhardt <sup>1</sup> M. Strobl <sup>1</sup> M. Kreuzer <sup>2</sup>	<sup>1</sup> HZB <sup>2</sup> RKU, Heidelberg V18 <b>EF</b>
132	<b>Interaction of lipid multilayers with the polysaccharide hyaluronic acid</b>	M. Strobl <sup>1</sup> R. Steitz <sup>1</sup> M. Kreuzer <sup>2</sup> R. Dahint <sup>2</sup>	<sup>1</sup> HZB <sup>2</sup> RKU, Heidelberg V18 <b>EF</b>
133	<b>Origins of swelling of a lipid multilayer system induced by the polysaccharide HA</b>	M. Strobl <sup>1</sup> R. Steitz <sup>1</sup> M. Reinhardt <sup>1</sup> M. Kreuzer <sup>2</sup> R. Dahint <sup>2</sup>	<sup>1</sup> HZB <sup>2</sup> RKU, Heidelberg V18 <b>EF</b>
134	<b>Lateral phase separation in oriented bylayers made from an unsaturated, a saturated and a hybrid lipid at fixed humidity</b>	Ch. Garvey <sup>1</sup> G. Bryant <sup>2</sup> T. Hunt <sup>2</sup> M. Kreuzer <sup>3</sup> M. Strobl <sup>3</sup>	<sup>1</sup> ANSTO, AU <sup>2</sup> RMIT University, AU <sup>3</sup> RKU, Heidelberg V18 <b>EF</b>



## List of Contributed Experimental Reports

PAGE TITLE TEAM PROPOSAL

### **Material Science**

<b>137 Phase transitions and crystal structure of Zr-Cu based high temperature shape memory alloys</b>	G. Firstov <sup>1</sup> I. Glavatskyi <sup>2</sup> D. Wallacher <sup>2</sup>	<sup>1</sup> IMP, Kiev, UA <sup>2</sup> HZB	E2	<b>PHY-01-2695-EF</b>
<b>138 Residual stress states in case hardened discs for the validation of simulation results</b>	J. Epp <sup>1</sup> Th. Hirsch <sup>1</sup> R.C. Wimpory <sup>2</sup>	<sup>1</sup> Uni Bremen <sup>2</sup> HZB	E3	<b>MAT-01-2496</b>
<b>139 Complementary surface measurements (using synchrotron, neutron and hole drilling methods)</b>	R. C. Wimpory <sup>1</sup> T. Fuß <sup>1</sup> Ch. Genzel <sup>1</sup> M. Klaus <sup>1</sup>	<sup>1</sup> HZB	E3	<b>MAT-01-2809-EF</b>
<b>140 Martensite Structure and Orientation of Polycrystalline Ni-Mn-Ga Foam</b>	M. Chmielus <sup>1</sup> R.C. Wimpory <sup>1</sup> R. Schneider <sup>2</sup> P. Müllner <sup>3</sup> D.C. Dunand <sup>4</sup>	<sup>1</sup> HZB <sup>2</sup> TFH, Berlin <sup>3</sup> BSU, US <sup>4</sup> NWU, US	E3	<b>MAT-01-2810-EF</b>
<b>141 Residual stress states in gears and shafts after different manufacturing steps</b>	J. Epp <sup>1</sup> Th. Hirsch <sup>1</sup> R.C. Wimpory <sup>2</sup>	<sup>1</sup> Uni Bremen <sup>2</sup> HZB	E3	<b>MAT-01-2813</b>
<b>142 Through-thickness residual stress determination in welded high strength steels with longitudinal stiffeners</b>	Th. Nitschke-Pagel <sup>1</sup> R.C. Wimpory <sup>2</sup>	<sup>1</sup> Uni Braunschweig <sup>2</sup> HZB	E3	<b>MAT-01-2814</b>
<b>143 Precision drawn tubes</b>	A. Carrado <sup>1</sup> Th. Pirling <sup>2</sup> R.C. Wimpory <sup>3</sup>	<sup>1</sup> IPCMS, Strasbourg, FR <sup>2</sup> ILL, Grenoble, FR <sup>3</sup> HZB	E3	<b>MAT-01-2816</b>
<b>144 Residual stresses in welded crenulated wide plates</b>	K. Nikbin <sup>1</sup> C.M. Davies <sup>1</sup> S.E. Eren <sup>1</sup> R.C. Wimpory <sup>2</sup>	<sup>1</sup> ICL, UK <sup>2</sup> HZB	E3	<b>MAT-01-2818</b>
<b>145 The effect of Residual stress Distribution on Creep Cracking Behaviour of Weld 316H Stainless Steel</b>	N.P. O'Dowd <sup>1</sup> H.N. Yazdani <sup>1</sup> C.M. Davies <sup>2</sup> R.C. Wimpory <sup>3</sup>	<sup>1</sup> Uni Limerick, IE <sup>2</sup> ICL, UK <sup>3</sup> HZB	E3	<b>MAT-01-2819</b>
<b>146 Residual Stress Analysis of Drawn 1045 Steel Bars</b>	A. da S. Rocha <sup>1</sup> R. Nunes <sup>1</sup> J. Dagnese <sup>1</sup> Th. Hirsch <sup>2</sup> R.C. Wimpory <sup>3</sup>	<sup>1</sup> UFRGS, DEMET, Porto Alegre, BR <sup>2</sup> Uni Bremen <sup>3</sup> HZB	E3	<b>MAT-01-2820</b>
<b>147 Residual stresses in large scale continuously cast steel slabs</b>	M. Schöble <sup>1</sup> J. Jonke <sup>1</sup> P. Degischer <sup>1</sup>	<sup>1</sup> TU Wien, AT	E3	<b>MAT-01-2917</b>
<b>148 Residual Stress in Creep Damaged Specimens and its influence on Fatigue and Fracture</b>	C.M. Davies <sup>1</sup> A.N. Mehmanparast <sup>1</sup> K.M. Nikbin <sup>1</sup>	<sup>1</sup> ICL, UK	E3	<b>MAT-01-2918</b>
<b>149 Testing fundamental understandings of evolution of lattice strains under in-situ multi-axial loading</b>	R. Woracek <sup>1</sup> D. Penumadu <sup>1</sup> J. Bunn <sup>1</sup> R.C. Wimpory <sup>2</sup> N. Kardjilov <sup>2</sup>	<sup>1</sup> UTK, US <sup>2</sup> HZB	E3	<b>MAT-01-2923</b>
<b>150 Structural characterisation of Ti-Zr-Ni nanoalloys and its deuterides</b>	L. Gondek <sup>1</sup> A. Zywczyk <sup>1</sup> A. Hoser <sup>2</sup>	<sup>1</sup> AGH-UST, Krakow, PL <sup>2</sup> HZB	E6	<b>MAT-01-2884</b>
<b>151 Freezing and melting of water in confinement</b>	O. Paris <sup>1</sup> M. Erko <sup>1</sup> Th. Hauß <sup>2</sup>	<sup>1</sup> MU Leoben, AT <sup>2</sup> HZB	V1	<b>PHY-01-2803</b>

## List of Contributed Experimental Reports

PAGE	TITLE	TEAM	PROPOSAL
152	Carbon dioxide adsorption to montmorillonite clay and nanoporous silica	G. Rother <sup>1</sup> D. Wallacher <sup>1</sup> N. Grimm <sup>2</sup>	<sup>1</sup> ORNL, US <sup>2</sup> HZB V1 <b>PHY-01-2804</b>
153	Investigation of pristine and SO <sub>3</sub> H modified benzene PMO by SANS with in situ nitrogen adsorption	M. Wark <sup>1</sup> M. Sharifi <sup>1</sup> D. Wallacher <sup>2</sup> Th. Hauß <sup>2</sup>	<sup>1</sup> Uni Hannover <sup>2</sup> HZB V1 <b>MAT-01-2906</b>
154	Temperature evolution of dynamics of lead nanoparticles	A. Naberezhnov <sup>1</sup> P. Parshin <sup>2</sup> Y. Kibalin <sup>3</sup> M. Russina <sup>4</sup>	<sup>1</sup> RAS Ioffe, RU <sup>2</sup> NRC KI, Moscow, RU <sup>3</sup> RAS PNPI, Gatchina, RU <sup>4</sup> HZB V3 <b>PHY-03-632</b>
155	Water Diffusion in Clay	L. Aldridge <sup>1</sup> W. Gates <sup>2</sup> R. Havenith <sup>3</sup> H. Nunes Bordallo <sup>4</sup>	<sup>1</sup> ANSTO, AU <sup>2</sup> Monash University, AU <sup>3</sup> Uni Groningen, NL <sup>4</sup> HZB V3 <b>MAT-03-693</b>
156	Deuterium absorption in Mg <sub>70</sub> Al <sub>30</sub> alloy thin films with bilayer catalysts	H. Fritzsche <sup>1</sup> E. Poirier <sup>1</sup> C. Harrower <sup>2</sup> A. Teichert <sup>3</sup> R. Steitz <sup>3</sup> D. Wallacher <sup>3</sup> N. Grimm <sup>3</sup>	<sup>1</sup> NRC-CNBC, CA <sup>2</sup> NRC-NINT, CA <sup>3</sup> HZB V6 <b>CHE-04-1970</b>
157	Martensite Structure, Grain Orientation and Cracks in Polycrystalline Ni-Mn-Ga Foams	M. Chmielus <sup>1</sup> A. Paulke <sup>1</sup> R. Schneider <sup>2</sup> P. Müllner <sup>3</sup> D.C. Dunand <sup>4</sup>	<sup>1</sup> HZB <sup>2</sup> TFH, Berlin <sup>3</sup> BSU, US <sup>4</sup> NWU, US V7 <b>MAT-04-1928-EF</b>
158	Hydrogen distribution in cylindrical-like hydrogen-metal based storage tanks by neutron imaging	L. Gondek <sup>1</sup> J. Czub <sup>1</sup> N. Kardjilov <sup>2</sup>	<sup>1</sup> AGH-UST, Krakow, PL <sup>2</sup> HZB V7 <b>MAT-04-1942</b>
159	Cold Neutron Imaging of a Humified PEM Ruel Cell Membrane	D. Penumadu <sup>1</sup> J. Bunn <sup>1</sup> R. Woracek <sup>1</sup> S. Williams <sup>2</sup> A. Hilger <sup>2</sup>	<sup>1</sup> UTK, US <sup>2</sup> HZB V7 <b>MAT-04-1947</b>
160	Multimodality of Partially Saturated Sand from High Resolution Neutron and X-ray Tomography	D. Penumadu <sup>1</sup> F. Kim <sup>1</sup> N. Kardjilov <sup>2</sup> A. Hilger <sup>2</sup> M. Dawson <sup>2</sup>	<sup>1</sup> UTK, US <sup>2</sup> HZB V7 <b>MAT-04-1947</b>
161	Carbon Fiber Polymer Composites and Environmental Degradation Using Neutron Tomography	D. Penumadu <sup>1</sup> R. Woracek <sup>1</sup> A. Siriruk <sup>1</sup> F. Kim <sup>1</sup> N. Kardjilov <sup>2</sup> A. Hilger <sup>2</sup>	<sup>1</sup> UTK, US <sup>2</sup> HZB V7 <b>MAT-04-2032</b>

## List of Contributed Experimental Reports

PAGE TITLE TEAM PROPOSAL

### *Cultural Heritage*

<b>165</b>	<b>Cranial osteological correlates of sensory adaptations in mammals with implications for the palaeoecology of extinct species</b>	N. Crumpton <sup>1</sup> N. Kardjilov <sup>2</sup>	<sup>1</sup> Uni Cambridge, UK <sup>2</sup> HZB	X3	<b>BIO-04-2037</b>
<b>166</b>	<b>Evolution of developments in placental mammals</b>	R. Asher <sup>1</sup> L. Hautier <sup>1</sup> N. Kardjilov <sup>2</sup>	<sup>1</sup> Uni Cambridge, UK <sup>2</sup> HZB	X3	<b>BIO-04-1972</b>
<b>167</b>	<b>Neutron tomography imaging of lead roundshot from the Battle of Towton (1461 AD)</b>	E. Godfrey <sup>1</sup> W. Kockelmann <sup>2</sup> O. Ebrahimi <sup>3+4</sup> N. Karakas <sup>3+4</sup> W. Treimer <sup>3+4</sup>	<sup>1</sup> OU, UK <sup>2</sup> ISIS, UK <sup>3</sup> TFH, Berlin <sup>4</sup> HZB	V19	<b>EF</b>

# **Development of Instruments and Methods**



	<b>EXPERIMENTAL REPORT</b>  <b>Neutron Bragg front and back-face scattering from the perfect and deformed Si single crystal excited with acoustic waves</b>	Proposal: PHY-01-2882  Instrument: E6  Local Contact: Andreas Hoser
	Principal Proposer: E. Raitman, LAS Riga, LV Experimental Team: E. Raitman, LAS Riga, LV V. Gavrilov, LAS Riga, LV A. Hoser, HZB T. Hofmann, HZB	Date(s) of Experiment  01.09.2010 – 05.09.2010

Date of report: 31.01.2011

To investigate neutron Bragg's scattering from front- and back-face at perfect and deformed Si single crystal excited with high frequency ultrasound was proposed.

The longitudinal standing acoustic waves with the length  $\lambda_s \approx 10 \mu\text{m}$  create a field of the dynamic stresses inside the crystal and bending device creates the static strains. Combination of both types stresses should lead not to the growth but to the sharp decreasing of front-face scattering and to the increasing of BFS.

Experiments performed by G.Shull [1] have confirmed the correctness of theoretical considerations based on the dynamical theory of neutron scattering in the perfect crystals.

The experiments carried out by us at BENSC E6 facility on the neutron Bragg scattering from the back face of a Ge single crystal excited with longitudinal and transversal acoustic waves present a version of the Shull's experiments, but with "good" neutrons (monochromatic) and a "spoiled" by ultra-sound perfect crystal instead of Shull's "bad" neutrons (a white beam) and perfect crystals.

The main results is shown on the Fig1., a-d. Such an unpredictable Bragg's scattering was observed for the first time and successfully described within frameworks of the modified dynamic theory of neutron scattering [2,3].

The last result hasn't been explained up to now. On our opinion these experiments should be continued.

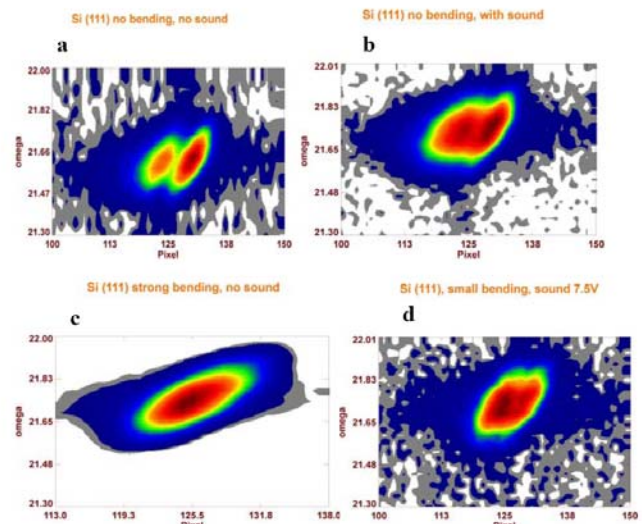



Fig.1 Common view of front- and back face Bragg scattering: a) without sound, no bending. FFS and BFS are clearly seen; b) sound makes reflections not enough resolved; c) FFS and BFS are fused due the strong bending; d) sound in the presence of small bending leads to the two peaks appearance again.

1. C.G.Shull, Phys.Rev.Let. **21**, 1585, (1968)
2. E. Raitman, V. Gavrilov, D. Mjasishev, A. Hoser, N. Stusser, A. Arulraj, NIMB, 268, 2010
3. E.Raitman, V.Gavrilov *et al.* Journ. Surf.Inv.,v.6, N3, 902-907, 2009

#### Acknowledgement:

*This research project has been supported by the European Commission under the 7<sup>th</sup> Framework Programme through "Research Infrastructures" action of the "Capacities" Programme, contract number CP-CSA\_INFRA-2008-1.1.1. Number 226507-NMI*

 <b>NEUTRONS</b>	<b>EXPERIMENTAL REPORT</b>	Proposal: PHY-02-750-EF
	<b>Resolving dispersive mode doublets with the NRSE method</b>	Instrument: <b>V2</b> Local Contact: K. Rule
Principal Proposer: Klaus Habicht, HZB Experimental Team: Klaus Habicht, HZB Felix Groitl, HZB Klaus Kiefer, HZB		Date(s) of Experiment 27.04.2010 – 16.05.2010

Date of report: 17.02.2011

This experiment is part of an extended program aimed at a thorough experimental confirmation of resolution effects in neutron resonance spin-echo (NRSE) type experiments. We have recently generalized the resolution formalism developed earlier [1-3] to include non-satisfied spin echo conditions and arbitrary oriented local gradients of the dispersion surface [4]. In this particular experiment we focused on NRSE measurements on split modes. The artificial split modes were generated by mounting two well orientated niobium crystals in the sample region. The orientation of the local gradient of the dispersion of one crystal was changed by using an attocube module consisting of two goniometers and one rotary table. Split modes generate a modulation in the obtained polarization according to the violated spin echo condition for one mode.

FLEX was operated in a configuration with scattering senses (SM=-1, SS=-1, SA=+1) with an experimental transverse Q-resolution of about  $0.006 \text{ \AA}^{-1}$  FWHM at fixed incident  $k_i = 1.9 \text{ \AA}^{-1}$ . No additional collimators were used besides Mezei cavity polarizers inserted behind the PG monochromator and behind the PG analyzer. Second-order contamination is substantially suppressed by the curved neutron guide. The background TAS parameters and the NRSE parameters were fixed at their nominal values for the (1 1 0.05) excitation which was experimentally found at 1.144 meV at T=66K. The required tilt angles of the RF-flippers were calculated with SERESCAL,  $\theta_1 = -31.95^\circ$ ,  $\theta_2 = +27.62^\circ$  were used. The two niobium crystals were mounted with the [hhk] plane as the scattering plane and kept at T=66 K. The polarization for different spin echo times was measured for both crystals aligned and one crystal tilted in A3 by  $0.4^\circ$  w.r.t. the other crystal (Fig 1). Counting times were 2700 s per point and 11 points covering one period of the echo signal. Additionally elastic NRSE measurements at the (1 1 0) Bragg peak were done with an Lamor diffraction setup for different angles between the crystals w.r.t. A3 (Fig 2).

Fig.1 shows the polarization as a function of the spin echo time tau for an angle of  $0.4^\circ$  w.r.t. A3 between the two crystals. A slight modulation is visible. Fig.2 shows the polarization as a function of the effective frequency in a Lamor diffraction setup for an

angle of  $0.5^\circ$  w.r.t. A3 between the two crystals. A modulation is likewise visible.

The data collected during the course of the experiment will allow a more detailed comparison to our theoretical results than previously possible.

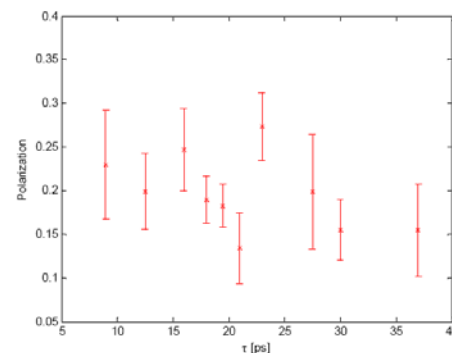


Fig.1: Polarization as a function of spin echo time at (1 1 0.05)  $E=1.144 \text{ meV}$  with an angle of  $0.4^\circ$  between the crystals.

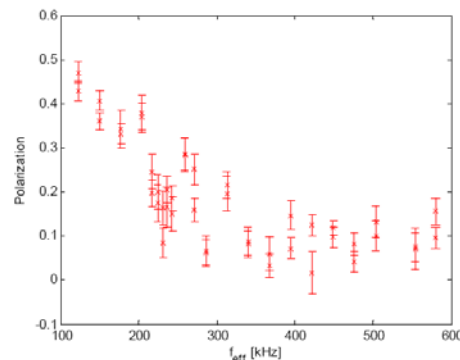



Fig.2: Polarization as a function of the effective frequency at the (1 1 0) Bragg peak with an angle of  $0.5^\circ$  between the crystals in a Lamor diffraction setup.

We acknowledge Klaus Kiefer for appropriation and mounting of the attocube modules.

- [1] K. Habicht, R. Golub, T. Keller, *J. Appl. Cryst.* **36**, 307 (2003).
- [2] K. Habicht, R. Golub, F. Mezei, B. Keimer, T. Keller, *Phys. Rev. B.* **69**, 104301 (2004).
- [3] K. Habicht, T. Keller, R. Golub, *Physica B* **350**, E803-E806 (2004).
- [4] K. Habicht *et al.* submitted to proceedings of the PNSXM 2009 to be published in *J. Phys. J. of Phys. Conf. Series*.

	<b>EXPERIMENTAL REPORT</b>	Proposal: PHY-04-1830
	<b>TISANE Investigations of Microsecond Dynamics in Magnetic Nanomaterials</b>	Instrument: <b>V4</b> Local Contact: U. Keiderling
Principal Proposer: A. Wiedenmann, ILL, F Experimental Team: A. Wiedenmann, ILL, F U. Keiderling, HZB V. Ryukhtin, HZB J. Kohlbrecher, PSI, CH	Date(s) of Experiment  05.05.2010 - 14.05.2010	

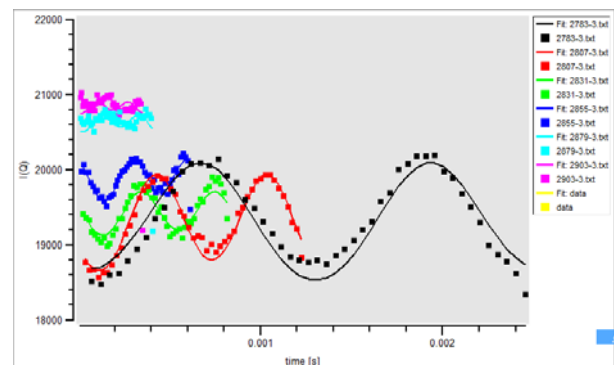
Date of report: 24.02.2011

We have used for the first time the new optimised “TISANE” set-up installed at V4 for stroboscopic investigations of the dynamics of ordering and relaxation processes in Ferrofluids. Locally ordered domains induced by a magnetic field turned out to be of dynamical nature as “living objects” [1]. The goal was to detect any delay between the inducing field and the reorientation of individual particle moments and/or the set-up of inter-particle correlations allowing for a detailed insight in the dynamical processes in sub-ms time range unavailable with conventional SANS.

The main part of the beam time has been used for evaluating the performance of the TISANE technique. A concentrated sample Co-FF sample (MFT3 in L9) has been measured in an ac field up to 0.02T by using a new magnetic coil and power amplifier. SANS data have been recorded at a fixed geometry of  $L_1=17\text{m}$ ,  $L_2=4\text{m}$  using the “white” neutron spectrum when the velocity selector was in off-beam position. The frequencies of the ac-field at the sample varied between 500 Hz and 7000 Hz which resulted in a chopper speed between 360 rpm and 5060 rpm and time periods at the detector  $T_d$  between 2.47 ms and 0.177 ms, respectively.

As part of the commissioning we first evaluated the performance of the TISANE technique: The comparison of time resolved data from measurements with different acquisition times revealed the long-term stability of the phase-locking of the double chopper, sample oscillation and data acquisition for which the different frequencies had to be precisely related by TISANE condition [1]. Second, we evaluated the effective time resolution as a function of frequencies, phases and direction of the chopper rotation, and of the variable size of the incident beam. In Fig 1 we present the time resolved integrated intensity of a radial sector of  $20^\circ$  parallel to the magnetic field measured at different frequencies of the oscillating field between 500 Hz and 3000 Hz together with a fit (solid lines) according to the model function [1] using different time resolutions  $\Delta t_r$ . It turned out that  $\Delta t_r$  scales inversely with the chopper frequency i.e. it is governed by the chopper opening time. In the TISANE mode the relative time resolution should scale as  $\Delta t_r/T_d = DC$ . In fact, the data in Fig. 1 was fitted with a duty cycle of  $DC=20\%$  which is close to the theoretical value of 17% calculated for the

chopper phase and the size of the neutron window in front of the chopper.



**Fig.1:** Integrated intensity of Co-FF in an angle sector of  $20^\circ$  parallel to the oscillating magnetic field at different sample frequencies: 500 Hz (black), 1000Hz (red), 1500 Hz (green), 2000Hz (blue), 3000Hz (light blue) and 4000Hz (pink).

The oscillating response is observed in the whole frequency range but with increasing damping of the contrast as expected when the characteristic relaxation time of the system is approached.[2]

Due to several failures of the sample environment (closed cycle refrigerator and magnetic coil) we were not able to perform most of the proposed experiments such as variation of temperature for different nanomaterial samples.


[1] A. Wiedenmann, U. Keiderling, K. Habicht, M. Russina and R. Gähler, Phys. Rev. Lett. **97**, 057202

[2] A. Wiedenmann et al. submitted to ECNS 2010

## Acknowledgement

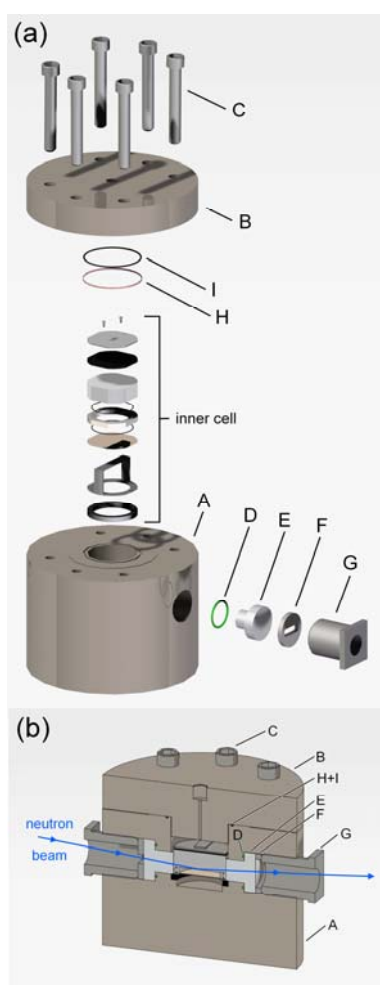
This research project has been supported by the European Commission under the 7<sup>th</sup> Framework Programme through “Research Infrastructures” action of the “Capacities” Programme, contract number CP-CSA\_INFRA-2008-1.1.1. Number 226507-NMI3



 <b>NEUTRONS</b>	<b>EXPERIMENTAL REPORT</b>	Proposal: EF
	<b>High pressure cell for neutron reflectivity measurements up to 2500 bar [1]</b>	Instrument: <b>V6</b> Local Contact: Roland Steitz
Principal Proposer: Experimental Team:	Roland Winter, TU Dortmund, Germany Christoph Jeworrek, TU Dortmund Claus Czeslik, TU Dortmund Roland Steitz, HZB	Date(s) of Experiment 18.01.-21.01.2010 28.09.-02.10.2010

Date of report: 28.01.2011

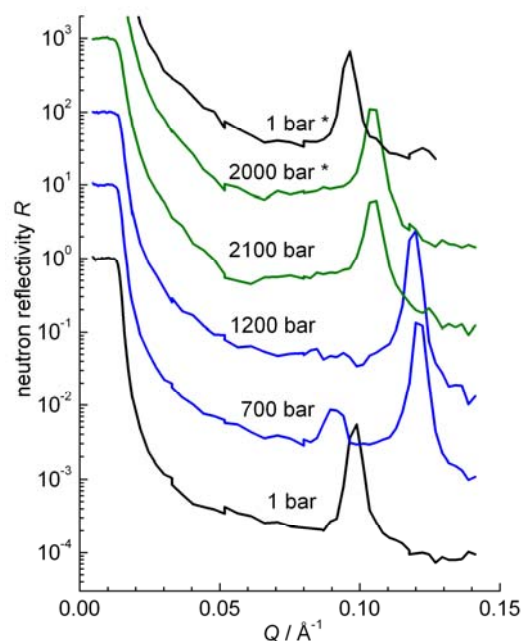
We have designed a new high pressure (HP) cell for neutron reflectivity experiments (Fig. 1). The cell can be used to study solid-liquid interfaces under pressures up to 2500 bar (250 MPa).



**Fig. 1:** High-pressure neutron reflectivity sample cell to study aqueous-solid biointerfaces under pressures up to 2500 bar.

The sample interface is based on a thick silicon block with an area of about 14 cm<sup>2</sup>. This area is in contact with the sample solution which has a volume of only 6 cm<sup>3</sup>. The sample solution is separated from the pressure transmitting medium, water, by a thin flexible polymer membrane. In addition, the HP cell can be


temperature-controlled by a water bath in the range 5 – 75 °C. By using an aluminum alloy as window material, the assembled HP cell provides a neutron transmission as high as 41 %. The maximum angle of incidence that can be used in reflectivity experiments is 7.5°. The large accessible pressure range and the low required volume of the sample solution make this HP cell highly suitable for studying pressure-induced structural changes of interfacial proteins, supported lipid membranes and, in general, biomolecular systems that are available in small quantities, only. To illustrate the performance of the HP cell, we present neutron reflectivity data of a lipid film which undergoes several phase transitions upon pressurization in Fig. 2.



**Fig. 2:** Neutron reflectivity curves of the lipid DOPE, which has been deposited on a silicon wafer. Upon pressurization, the H<sub>II</sub>-, L<sub>α</sub>, and L<sub>β</sub>-phase are formed.

**Reference:**

[1] C. Jeworrek, R. Steitz, C. Czeslik, R. Winter, High pressure cell for neutron reflectivity measurements up to 2500 bar, *Review of Scientific Instruments*, in press.

 <b>HELMHOLTZ ZENTRUM BERLIN</b> für Materialien und Energie  <b>NEUTRONS</b>	<b>EXPERIMENTAL REPORT</b>  <b>Trial for a New SANS Method Using Dark-Field Tomography</b>		Proposal: PHY-04-1946  Instrument: <b>V7</b> Local Contact: N. Kardjilov
	Principal Proposer: K. Taketani, KEK Tsukuba, JP Experimental Team: A. Hilger, HZB N. Kardjilov, HZB I. Manke, HZB M. Strobl, HZB	Date(s) of Experiment  10.05.2010 – 16.05.2010	

Date of report: 31.01.2011

### The aim of the experiment

Small Angle Neutron Scattering (SANS) is a widely used and powerful technique to measure micrometer or sub-micrometer size structures. However, the method assumes that the sample has the same microstructure over its whole volume. To the contrary, neutron dark-field tomography [1] has a possibility to obtain spatial maps of micrometer or sub-micrometer size structures. In order to compare experimental data with a calculated value, it is necessary, as a first step, to measure well-prepared control samples and use them for a comparison with a theoretical model. To achieve this purpose, we measured dark-field images of silica powders.

### Details on the sample and experimental conditions

First, we tried to measure the effects on the dark-field images from the difference of the powder radius. To measure the effects, we prepared five kinds of silica powders, whose radius was 200 nm, 500 nm, 1000 nm, 3000 nm, and 5000 nm. We inserted the different kind of powder of 0.025 g into different aluminum cells. All the inner space of the cells was 10 mm in height, 10 mm in length, and 0.1 mm in thickness.

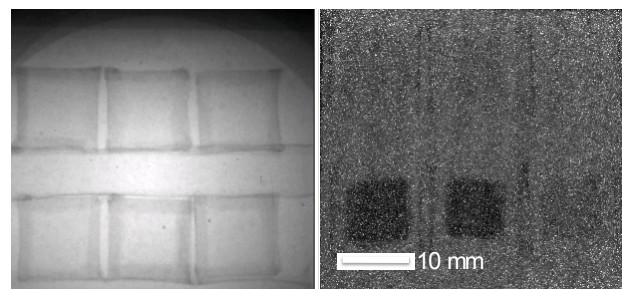
Second, we prepared silica powder samples with a lower number density than the first set of the samples, as these are easier to analyze. We inserted three kinds of silica powders into different cells sold by Hellma Corp. The powder radius of the samples were 200 nm, 500 nm, and 1000 nm and the weight density of the samples were 0.2 g / cm<sup>3</sup>, 0.3 g / cm<sup>3</sup>, and 0.7 g / cm<sup>3</sup>, respectively. For each powder radius, we prepared samples whose thicknesses were 2 mm, 5 mm, and 7 mm.

We used a monochromatic neutron beam whose mean wavelength was 0.4 nm. We irradiated the samples 30 min. with neutrons for each radiographic projection image. By

scanning the position of the source grating, we measured 21 images to construct one dark-field image.

### The general outcome of the experiment

The following figure shows the images obtained by measuring the first set of samples. The left one is the transmission image and the right one is the dark-field image. One of the cells contains no powder (top left), and the others contain powders whose radius was 200 nm (top center), 500 nm (top right), 1000 nm (bottom left), 3000 nm (bottom center), and 5000 nm (bottom right). The result clearly shows that the dark field image changes due to the radius of the powder, though the transmission image does not. We also measured the second set of the samples and observed clear changes of the dark-field images.



### Data analysis

We have already performed a model calculation of the dark field image of one sphere. We are now performing a model calculation of the effects due to the multiple spheres. After completing the calculation, we will compare them with the dark field image of second set of samples.

### References

[1] M. Strobl et al., Phys. Rev. Lett. 101, 123902 (2008)

Principal Proposer: S.-O. Seidel, Beuth Hochschule für Technik Berlin  
 Experimental Team: S.-O. Seidel, Beuth Hochschule für Technik Berlin  
 W. Treimer, Beuth Hochschule für Technik Berlin  
 O. Ebrahimi, Beuth Hochschule für Technik Berlin  
 N. Karakas, Beuth Hochschule für Technik Berlin

Date(s) of Experiment

08.12.2008 - 23.12.2008

Date of report: 31-01.2011

### Introduction

The aim of this work (part I+II) was the development of a software tool for a reconstruction of inner material structures.

First results of the developed software tool, which has been implemented in MATLAB® describe the fundamental characteristics of neutrons and calculate related strong-interaction signals, i.e., absorption, small angle scattering as well as refraction. All data were collected on the Ultra Small Angle Scattering experiment V12.

### Experiment

The V12 USANS set up was used to visualize the two dimensional structure of three different samples inside an aluminium shell. Two similar samples with different dimensions concerning their inner part were tested, investigating their influence on reconstruction.

A monochromatic neutron beam with  $\lambda = 0,476$  nm with an approximate flux density of  $3.5 \cdot 10^3$   $\text{cm}^{-2}\text{s}^{-1}$  was reflected with a silicon crystal from the neutron guide towards the position of the sample. The following analyzer crystal reflects the scattered neutrons to the 2D detector. The cross section of the reflected beam was limited by a slit to 1mm x 30mm.

### Results

In order to continue the work on reconstruction from scattering signals [1] tomography actual measurements were taken where the 2D-detector was used.

The sample in front of a slit (width=1mm), perpendicular to the incident beam, was shifted in 23 steps. This measurement has been carried out with 60 rotation steps over an angular range of 360 deg. With a number of about  $1,4 \cdot 10^3$  files for the whole sample size the programme routine worked automatically, processing the data for reconstruction.

The sample curve in Fig.1 (red) shows the signal for one step at one angle position. The related fit profile (blue) eliminate the parameter respective the interaction, i.e. absorption (see part II).

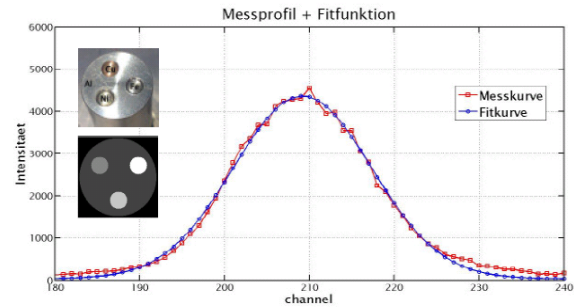


Fig.1 Intensity profile and Fit function for the sample and model depicted in the left corner

The Fig.2 shows the correlation function to define the quality using Gaussian fits.

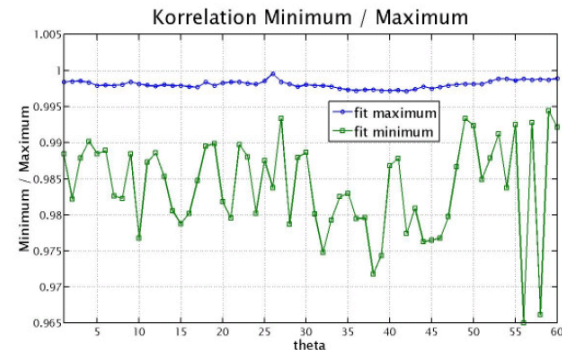


Fig.2 Correlation for deviation of fit function

Last Fig.3 shows the model of Radon transform for absorption compared to the result depending on fit parameter.

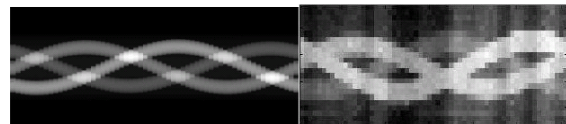


Fig.3 left: Model of Radon transform for absorption, right: Result with Fit parameter

[1] M. Strobl, W. Treimer, A. Hilger, Appl. Phys. Lett. 85 (3) (2004) 488-490

[2] BENS Report - PHY-04-1849-LT (2009)

This work was financed by the BMBF project 05KN7KF1

Principal Proposer: S.-O. Seidel, Beuth Hochschule für Technik Berlin  
 Experimental Team: S.-O. Seidel, Beuth Hochschule für Technik Berlin  
 W. Treimer, Beuth Hochschule für Technik Berlin  
 O. Ebrahimi, Beuth Hochschule für Technik Berlin  
 N. Karakas, Beuth Hochschule für Technik Berlin

Date(s) of Experiment

08.12.2008 - 23.12.2008

Date of report: 31-01.2011

**Introduction**

In principal there are three fit parameters which have to be extracted for the two-dimensional reconstruction. Each fit parameter is related to an interaction, i.e. the attenuation well can be defined by the integrated intensity, the refraction by is given by the centre of gravity of the scattering curve and the ultra small angle scattering signal can be derived from the full width of half maximum (FWHM). Therefore two types of fits, Lorentzian and Gaussian were compared with each other, to get information about the signals which corresponded best to the interactions of neutrons.

The instrument V12 operates with monochromatic neutrons with a wavelength of  $\lambda= 0,476$  nm and has an approximate flux density of  $3.5 \cdot 10^3 \text{ cm}^{-2}\text{s}^{-1}$ . The neutrons coming from the guide and are reflected by a silicon crystal towards the sample position. The analyzer crystal reflects the scattered neutrons to the position-sensitive-detector DENEX-200TN. The neutron sensitive area is uniformly distributed in two dimensional by  $512 \cdot 512$  channels.

**Results**

The possibility of reconstruction primarily depends on the sample geometry and the installation of the sample in the beam. There are many effects which affects the result of reconstruction essentially. For example the chosen slit geometry defines the horizontal spatial resolution and the number of steps, respectively, and the total time of measurements. The detector resolution mainly determines the number of channels. The profiles in Fig.1 – Fig.3 show the interaction and the influence in signal between the empty and scattered beam. The result after reconstruction is shown in the left upper corner for each interaction. The best result was got from attenuation and the refraction. Depending on the software tool, which has evaluated the fit parameter, the two dimensional reconstruction shows details of the inner part sample. This first approximation of reconstruction can be used to improve the

software routine and to get better results in reconstruction of scattered signals.

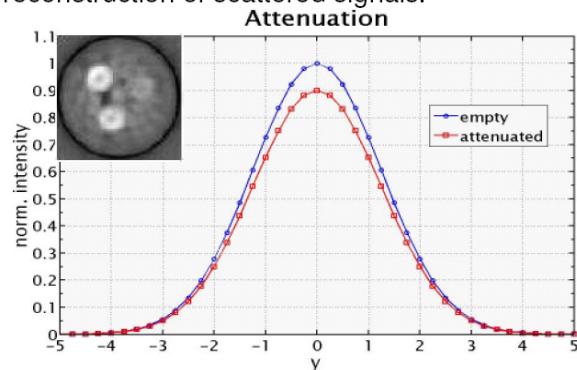


Fig.1 Profile for interaction of attenuation and result of reconstruction in the left upper corner

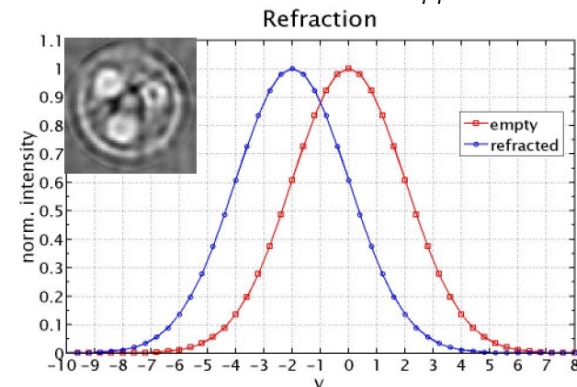


Fig.2 Profile for interaction of refraction and result of reconstruction

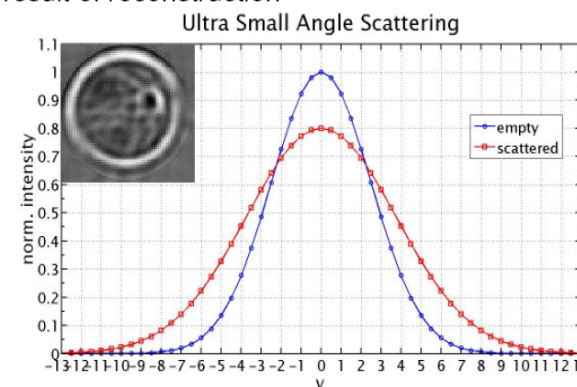



Fig.3 left: Profile for interaction of USANS and result of reconstruction

This work was financed by the BMBF project 05KN7KF1

 <b>NEUTRONS</b>	<b>EXPERIMENTAL REPORT</b>	Proposal: PHY-04-2014
	<b>Spatial distributions of neutrons scattered by vibrating Ge crystals ( Laue geometry)</b>	Instrument: <b>V12a</b> Local Contact: A. Hoser
Principal Proposer: E. Raitmans, LAS Riga, LV Experimental Team: E. Raitmans, LAS Riga, LV V. Gavrilovs, LAS Riga, LV S.-O. Seidel, HZB M. Strobl, HZB		Date(s) of Experiment  20.09.2010 – 02.10.2010

Date of report: 31.01.2011

The dynamical diffraction of neutron in perfect single crystals undergoing to the ultrasonic excitation were studied and the so-called Kato's profiles were observed. As preliminary calculations of the Kato's equation (taking into account ultrasonic excitation) have shown, one can expect for regime of small ultrasound waves amplitudes the fine oscillations in spatial neutron intensities distribution, and sharp increase of intensity in the Bormann triangle center for the high level ultrasonic excitation depending on the ultrasound frequency and samples thickness. The aim of the experiments was to determine how high frequency vibrations introduced into a perfect crystal effect of Kato's profiles in thick crystal. The main results are shown on Figs. 1-3:

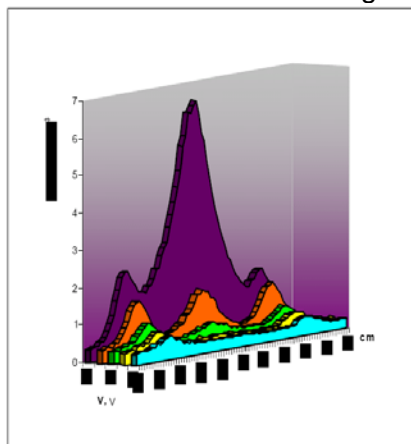


Fig.1 Common view of the ultrasound action on the Kato's profiles

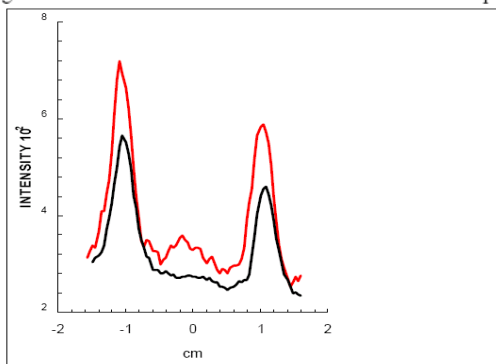


Fig.2 Kato's profiles: (---)–without sound, (---)–  $V_G=0.3$  V. The present of fringes is evident.

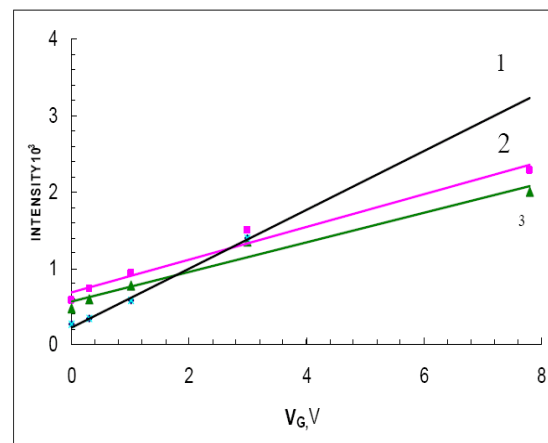



Fig.3. Linear intensities growth depending on the generator voltage: 1-for the center of Kato's profile, 2,3 –the same for the left and right "homs"

It is shown that: i) for relatively small AW amplitudes at least 3-4 "sound" fringes (oscillations) are pronounced and their sizes agrees with theoretical evaluations. The resolutions was not enough but the situation can be improved; ii) the intensities in the center of the Kato's profile sharply increases with AW amplitudes growth and gain factor of 10 was achieved. These results can be explained using many phonon approximation and may be promising for an intensity –to- resolution governed by ultrasound monochromator creating.

#### Acknowledgement:

*This research project has been supported by the European Commission under the 7<sup>th</sup> Framework Programme through "Research Infrastructures" action of the "Capacities" Programme, contract number CP-CSA\_INFRA-2008-1.1.1. Number 226507-NMI*

 <b>NEUTRONS</b>	<b>EXPERIMENTAL REPORT</b>	Proposal: PHY-04-2017-EF
	<b>Energy analysing by magnesium fluoride prisms</b>	Instrument: <b>V14</b> Local Contact: N. Kardjilov
Principal Proposer: R. Bartmann, HZB Experimental Team: J. Schulz, HZB T. Krist, HZB	Date(s) of Experiment 07.08.2010 – 08.08.2010	

Date of report: 24.1.2011

The applicability of magnesium fluoride prism arrays as an energy analysing device was tested at the V14 neutron reflectometer.

The sample consists of a 50x20x2mm<sup>3</sup> single crystal magnesium fluoride block. The upper 0.5mm of the material are cut in the shape of 33 prisms, each with an angle of 45 deg to the basis.

We performed the measurements of the refraction and transmission with a neutron beam with a wavelength of 4.9Å, a beam width of 0.3mm and a divergence of 0.006deg.

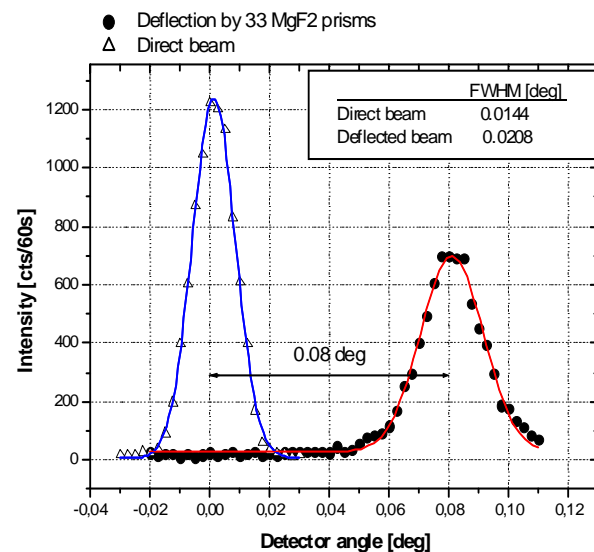
To detect the refracted beam a <sup>3</sup>He Detector with a slit of 0.2mm was placed 2m behind the sample. The angular range contained the interval from -0.02 to 0.12 deg. Fig.1 shows the result of the measurement of the direct and the deflected beam.

For the refracted beam the maximum of intensity was found at 0.08 deg. This experimental result is in good agreement with the theoretical calculation as the discrepancy is only 8%. The beam width increases while passing through the prisms. The beam width after the sample is w=0.021deg which shows an increase of 0,015deg compared to the FWHM of the direct beam.

To measure the transmission through the prism array the distance between sample and detector was reduced to 50cm and the slit was removed. This increased the detector acceptance up to 2deg. It could be shown that 86% of all incoming neutrons were transmitted. This leads to an attenuation coefficient of  $\mu=0.055\text{cm}^{-1}$ , which is about 80% higher than expected. Another transmission measurement was performed with the same experimental setup but with the beam passing through 5cm pure material. In this case the transmission rate leads to an attenuation coefficient of


$\mu=0.03\text{cm}^{-1}$ , which is in perfect coincidence with the expected value<sup>1</sup>.

The increase of the beam width and the high intensity losses while the beam passes through the prism array indicate that the prisms surfaces are very rough and the neutrons are diffusely scattered. This unwanted effect can be reduced by polishing the prisms surfaces and so increase the angular and wavelength resolution of the energy analysing device.



**Fig.1: Deflection of a  $\lambda=0.49\text{nm}$  beam by refraction in comparison with the direct beam**

[1] Barker J.G. et al.. J. Appl. Cryst. 41, 1003-1008 (2008)

 <b>HELMHOLTZ ZENTRUM BERLIN</b> für Materialien und Energie  <b>NEUTRONS</b>	<b>EXPERIMENTAL REPORT</b>  <b>BioRef – testing operational modes</b>		Proposal: EF  Instrument: <b>V18</b>  Local Contact: Markus Strobl
	Principal Proposer: M. Strobl, HZB Experimental Team: M. Kreuzer, Uni Heidelberg R. Steitz, HZB R. Dahint, Uni Heidelberg	Date(s) of Experiment  29.04.2010 - 05.05.2010	

Date of report: Jan. 2011

BioRef is a time-of-flight reflectometer built at the end of the cold neutron guide NL3b and has undergone commissioning in the second half of 2009. It is based on a versatile chopper system, consisting of three disc choppers operated at the same frequency between 20 and 90 Hz. Different frequencies result in different wavelength bands utilized in a measurement. The optical blind mode in which the pulse shaping choppers (1 and 2) are operated allows on the one hand a constant wavelength resolution over the utilized wavelength band, and on the other hand by changing the distance between these two choppers to set this resolution to values between 1% and 5% [1,2].

The corresponding parameters for some potential instrumental settings are given in Tab. 1 while Fig 1 represents measurements made on a NiTi multilayer (single layer thicknesses of app. 100 Å) on a quartz glass substrate in order to test and calibrate the performance of the instrument under these instrumental conditions.

*Acknowledgement: BioRef has been funded by the BMBF, grant No.: 05KN7VH1*

References:

- [1] A.A. van Well, Phys. B 180 & 181 (1992)
- [2] M. Strobl et al. J. Phys. (Conf.Ser.) 251 (2010)

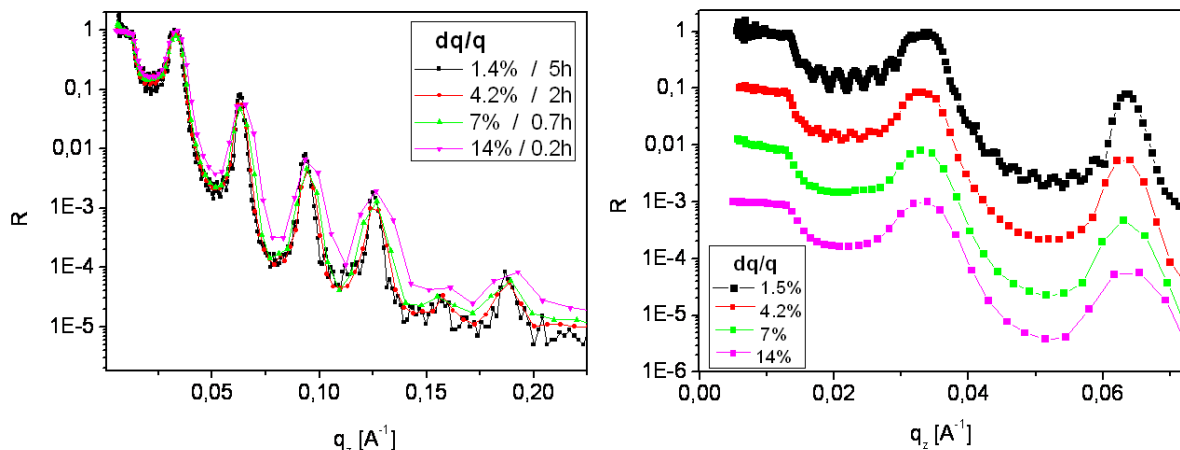



Fig. 1 Measurements of a NiTi multilayer; left: neutron reflectivity recorded with different instrumental resolutions and corresponding exposure times; right: close-up of reflectivity shown on left hand side. Note that reflectivity curves taken at different resolution are shifted along the y-axis by factors of 10 for clarity;

chopper frequency	wavelength band	$\lambda_0$	Nr. ang. sett. to $q \ 0.4 \text{Å}^{-1}$	res. 1.4%		res. 4.2%		res. 7%		res. 14%	
				$z_0$ [mm]	tot. acq.	$z_0$ [mm]	tot. acq.	$z_0$ [mm]	tot. acq.	$z_0$	tot. acq.
90Hz	4Å (3.9 - 7.9Å)	7.9Å	12	80	5h	240	2h	400	0.7h	no	no
45Hz	8Å (3.9 - 11.9Å)	15.8Å	6	80	5h	240	2h	400	0.7h	no	no
25Hz	14.4Å (3.9 - 18.3Å)	28.4Å	3	80	5h	240	2h	400	0.7h	no	no
68Hz	5.2Å (3.9 - 9.1Å)	10.4Å	10	80	5h	240	2h	400	0.7h	no	0.2h

Table 1 Overview of different operation modes of BioRef based on different chopper frequencies utilized. Nr.ang.sett.= number of angular settings; tot. acq.= total acquisition time; res. = resolution, "no" means that no value applies or can be given for a certain setting, grey letters for 68 Hz indicate that this frequency is not routinely used for such measurements, but is represented because it is used for fast low resolution measurements for which SCI is stopped (hence  $z_0$  does not apply) only.

 <b>HELMHOLTZ ZENTRUM BERLIN</b> für Materialien und Energie  <b>NEUTRONS</b>	<b>EXPERIMENTAL REPORT</b>	Proposal: EF
	<b>Visualization of the flux-pinning by polarized neutron radiography</b>	Instrument: <b>V19</b> Local Contact: W. Treimer
Principal Proposer: Experimental Team:	S.-O. Seidel, Beuth Hochschule für Technik Berlin S.-O. Seidel, Beuth Hochschule für Technik Berlin W. Treimer, Beuth Hochschule für Technik Berlin O. Ebrahimi, Beuth Hochschule für Technik Berlin N. Karakas, Beuth Hochschule für Technik Berlin	Date(s) of Experiment  Aug/Sept. 2010

Date of report: 31.01.2011

Due to the high potential and large number of applications of neutron tomography a new instrument dedicated to polarized neutron facility (PONTO) was built and successfully tested at BER II reactor of the Helmholtz Zentrum Berlin. The instrument was tested by imaging magnetic fields in coils, the Meißner effect and by imaging magnetic flux pinning in different lead samples.

To visualize magnetic fields inside of matter, the depolarization of the spin-polarized neutron beam was used. This technique was also applied to study the expelled magnetic field in a polycrystalline lead sample (type-1 superconductor). To visualize these effect, the sample was cooled down below the critical temperature  $T_c = 7.2\text{K}$  to  $T_0=5.5\text{K}$ . Two Helmholtz coils (diameter 200mm) produced a homogenous B-field of 6.3mT at the sample position, which was perpendicular to the neutron spin. In the presence of the external magnetic field of 6.3 mT the sample was cooled down. After the achievement of  $T_0$  the magnetic field was switched off.

For each neutron radiograph a flat field and background image was recorded in order to correct the particular images.

Due to imperfections, dislocations, cracks and grain boundaries inside the polycrystalline lead cylinder, magnetic fields are partially trapped in the superconductor (Fig.2b,c). For  $T > T_c$  or warming up the sample above  $T_c$  flux pinning disappears (Fig.2a).

It must be pointed out that the pinned magnetic field in the sample (and in other as well) was not uniform homogeneous around the rod axis, because one observe a nearly equidistant fringe pattern which cannot be caused by a constant magnetic field having a circular – shaped cross

section. This behaviour could not observed before and preliminary calculations on the interior B-field distribution are in perfect agreement with the experimental results and proved the excellent resolution of this new set up.

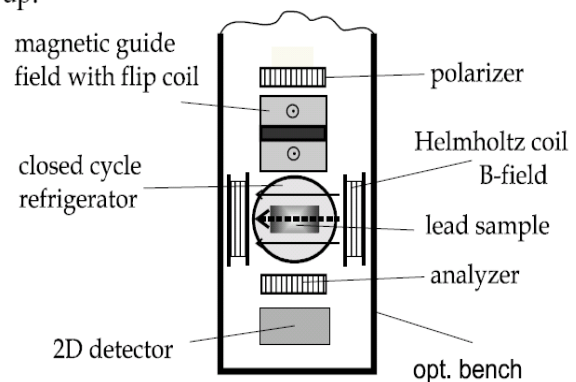


Fig.1: Experimental layout (flux-pinning)

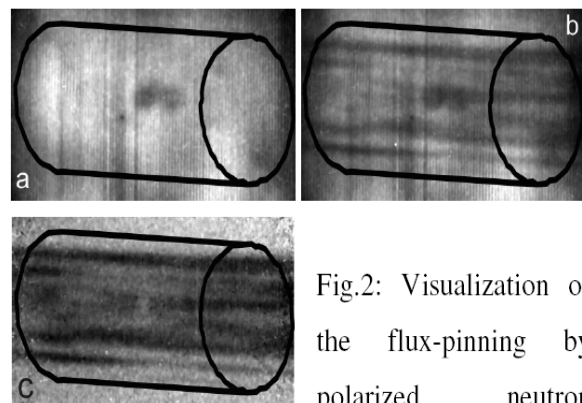


Fig.2: Visualization of the flux-pinning by polarized neutron radiography: a)  $T_0=8,0\text{K}$  ( $T_0>T_c$ ) and b)  $T_0=5,5\text{K}$  ( $T_0<T_c$ ), c) corrected trapped flux at 5,5K, dark area stemmed from the sample holder.

## References

W. Treimer, O. Ebrahimi, An instrument for imaging with polarized neutrons, et al., 9<sup>th</sup> World Conference on Neutron Radiography NIM A, Article in Press, Corrected Proof

This work was part of the BMBF project 5KN7KF1





# Magnetism



Principal Proposer: Bella Lake, HZB  
 Experimental Team: Sandor Toth, HZB  
 Simon Kimber, HZB  
 Dimitri Argyriou, HZB  
 Oliver Pieper, HZB  
 Nazmul Islam, HZB

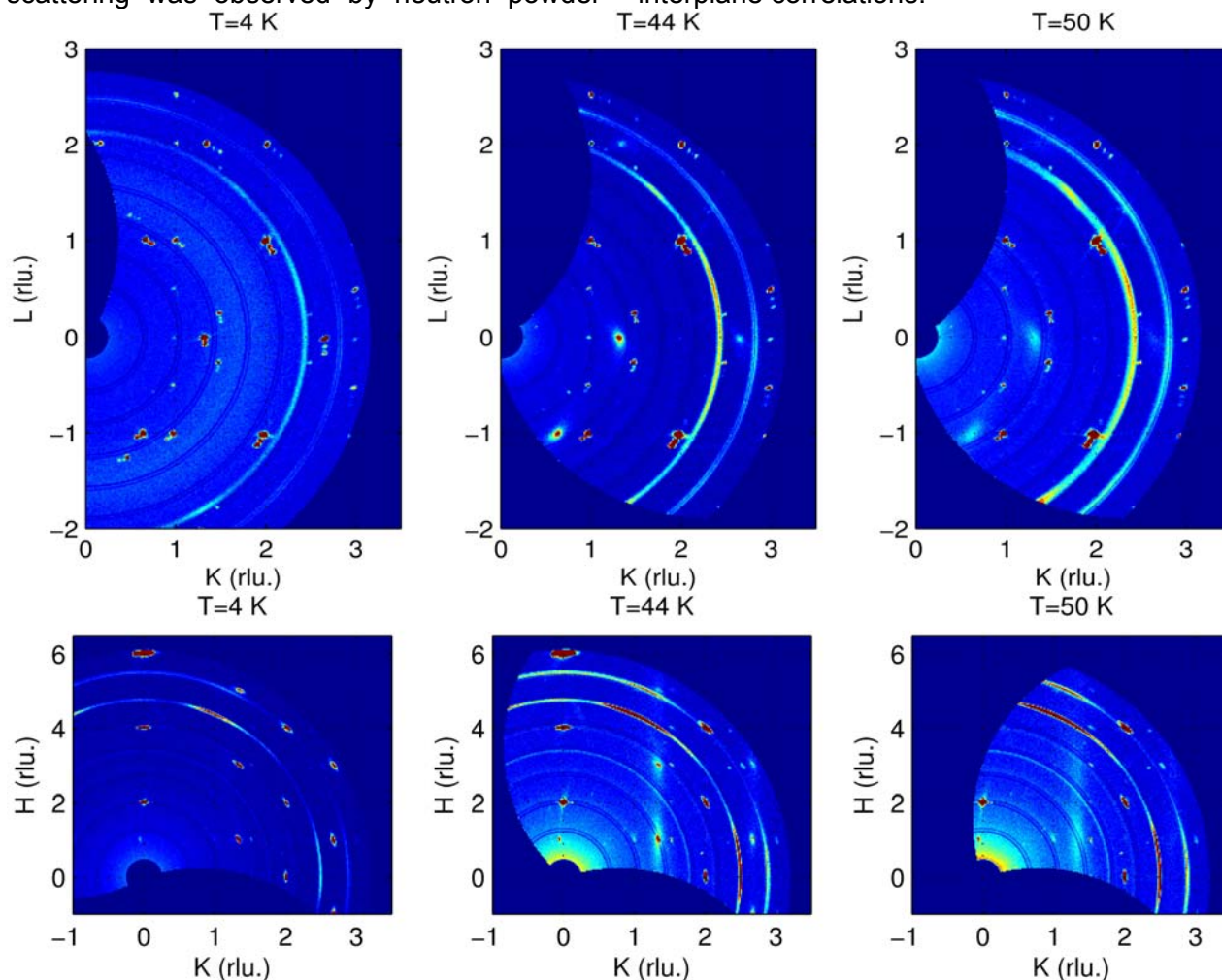
Date(s) of Experiment

26.01.2010 - 31.01.2010

Date of report: 17.02.2011

Alpha-CaCr<sub>2</sub>O<sub>4</sub> is a frustrated triangular lattice antiferromagnet. The crystal structure is orthorhombic *Pmmn* at room temperature [1]. It orders magnetically at  $T_N=43$  K. The slightly distorted triangular layers of magnetic Cr<sup>3+</sup> in the **bc** plane are stacked along **a** axis. Above the Néel temperature, diffuse magnetic scattering was observed by neutron powder


diffraction. We measured this magnetic diffuse scattering on the E2 instrument. Neutron wavelength was fixed to  $\lambda=2.4$  Å using the (0,0,2) reflection of a PG monochromator. Scans were performed at 4 K, 44 K and 50 K. Two sample orientation was used, (1,k,l) to study in-plane correlations and (h,k,0) to study interplane correlations.



Since the crystal has three structural twins, the nuclear peaks of other twins are also present with noninteger reciprocal indices. All plots are summed over the perpendicular direction. On the (1,k,l) plane the strongest magnetic Bragg peaks are (1,1.33,0) and (1,0.66,1). It is clearly

visible that in-plane correlations are still strong at 50 K above the Néel temperature, while the interplane correlations disappear as revealed by the rod like intensity pattern along (h,1.33,0).

[1] H. Pausch *et. al.* Z. Anorg. Allg. Chem. **405**, 113 (1974)

	<b>EXPERIMENTAL REPORT</b>  <b>Magnetic order of Incommensurately Charge-Stripe Ordered La(1.725)Sr(0.275)NiO(4)</b>	Proposal: PHY-01-2702  Instrument: <b>E2</b>  Local Contact: I. Glavatskyi
	Principal Proposer: Paul Freeman, ILL, Grenoble, F Experimental Team: I. Glavatskyi, HZB	Date(s) of Experiment  18.03.2010 – 24.03.2010

Date of report: 21.04.2010

The charge strip ordered system La(2-x)Sr(x)NiO(4) (LSNO) is seen as a model system in which to study charge stripe order due to the static long range order observed in these materials [1]. This makes understanding LSNO ideal for determining the probable nature of charge stripe order in the cuprate superconductors, and its role in high temperature superconductivity[2].

Theories to describe LSNO need to take into account both the magnetism of the ordered Ni spins and the magnetic interactions of the charge stripe electrons themselves. One theory being developed can explain these interactions and the occurrence of a spin reorientation in LSNO[3,4]. This theory predicts magnetic order for the spins of the charge stripe electrons, despite only dynamic correlations being observed[4,5].

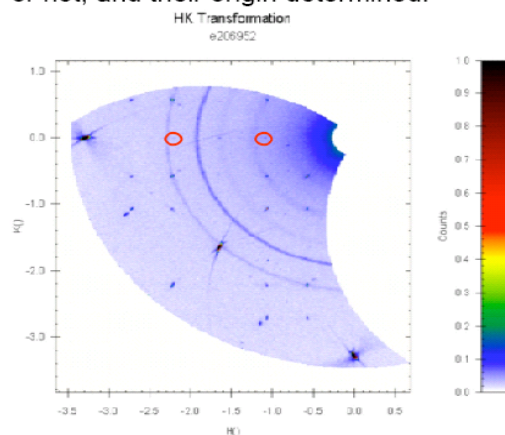
In this experimental investigation we undertook a mapping of reciprocal space using the flatcone technique, to search for the occurrence of magnetic Bragg reflections associated with the spins of the charge stripe electrons. Additionally to this search the wavevectors of third order harmonics were investigated to determine if the charge stripes are centred on Ni or O sites.

Measurements were performed at 4 and 100K mapping out planes of reciprocal space. The scans displayed a rich collection of Bragg reflections from incommensurate spin and charges stripe order aswell as weak second order reflections. These are known reflections, which needed to be indexed to determine if additional Bragg reflections are observed.

In the (hk0) and (hk1) planes we searched for the occurrence of third order harmonics from the ordered Ni spins. This was complicated by the extent of structural Bragg reflections, which created 'x' shaped peaks, which may or may not have instrumental origin. But near structural disallowed (100) positions no third

order harmonics were observed, indicating Ni centred charge stripes.

Additional Bragg reflections were observed, as highlighted in figure1. These reflections indicate order occurring parallel to Ni-O bonds, 45 degrees to the direction of the charge stripes. These peaks that occur at both 4 and 100 K need to be investigated further, before their origin can be determined to be magnetic or not, and their origin determined.



Figure; Elastic scattering from the (hk0) plane of La<sub>1.725</sub>Sr<sub>0.275</sub>NiO<sub>4</sub> measured at 100 K. Red circles outline the newly identified Bragg reflections discovered in this experiment.

*This research project has been supported by the European Commission under the 7<sup>th</sup> Framework Programme through "Research Infrastructures" action of the "Capacities" Programme, contract number CP-CSA\_INFRA-2008-1.1.1. Number 226507-NMI3*


[1] Yoshizawa H., et. al., Phys. Rev. B 61 (2000) R854

[2] Tranquada J.M., et. al., Nature 375 (1995) 561.

[3] Freeman P. G., et. al., Phys. Rev. B 70 (2004) 024413.

[4] Personal communication with Martin Long.

[5] Boothroyd A. T., et. al., Phys. Rev. Lett. 91 (2003) 257201.

 <b>HELMHOLTZ ZENTRUM BERLIN</b> für Materialien und Energie  <b>NEUTRONS</b>	<b>EXPERIMENTAL REPORT</b>  <b>Crystal and magnetic structure evolution of Ni-Mn-In and Ni-Co-Mn-In metamagnetic shape memory alloy</b>	Proposal: PHY-01-2704 Instrument: E2 Local Contact: I. Glavatskyi
	Principal Proposer: Chhayabrita Biswas, Bose Center, Kolkata, India Experimental Team: Sandeep Singh, Bose Center, Kolkata, India I. Glavatskyi, HZB S. Gerischer, HZB	Date(s) of Experiment 10.05.2010 – 16.05.2010

Date of report: 29.07.2010

We have done neutron diffraction ( $\lambda=2.39\text{\AA}$ ) measurement on the  $\text{Ni}_{50}\text{Mn}_{34}\text{In}_{16}$  and  $\text{Ni}_{45.3}\text{Co}_{5.4}\text{Mn}_{36.2}\text{In}_{13.1}$  samples at different temperatures with 0T and 4T field cooling (FC).

The data of  $\text{Ni}_{45.3}\text{Co}_{5.4}\text{Mn}_{36.2}\text{In}_{13.1}$  at 0T was taken using helium cryostat without magnet (OF-2). Whereas the 0T and 4T field and temperature dependent data of  $\text{Ni}_{50}\text{Mn}_{34}\text{In}_{16}$  was taken, using helium cryostat with superconducting magnet (VM5). This same cryostat was also used for 4T field cooling data of  $\text{Ni}_{45.3}\text{Co}_{5.4}\text{Mn}_{36.2}\text{In}_{13.1}$ .

#### $\text{Ni}_{45.3}\text{Co}_{5.4}\text{Mn}_{36.2}\text{In}_{13.1}$

This composition is in the martensitic phase below 325 K. Figure 1 shows the neutron diffraction pattern of  $\text{Ni}_{45.3}\text{Co}_{5.4}\text{Mn}_{36.2}\text{In}_{13.1}$  at 420K and 150K. At 420K it is in the Austenitic phase having  $L2_1$  structure. Some extra peaks of small intensity are present, which might be purely magnetic in nature or due to some other phase. We are doing the analysis to identify these peaks. At 150 K the diffraction pattern is different than 420K, showing the structural transition. Analysis is going on to find out the exact crystal and magnetic structure.

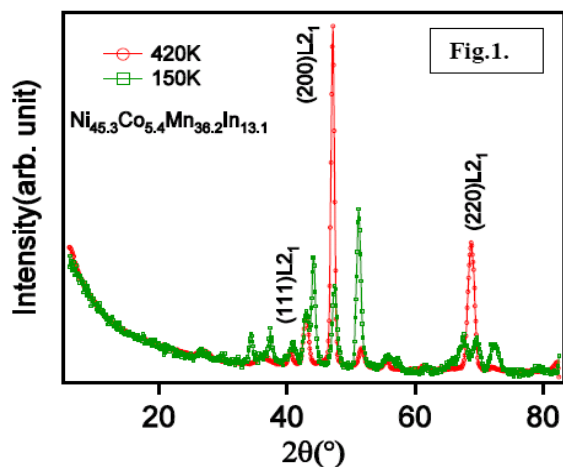
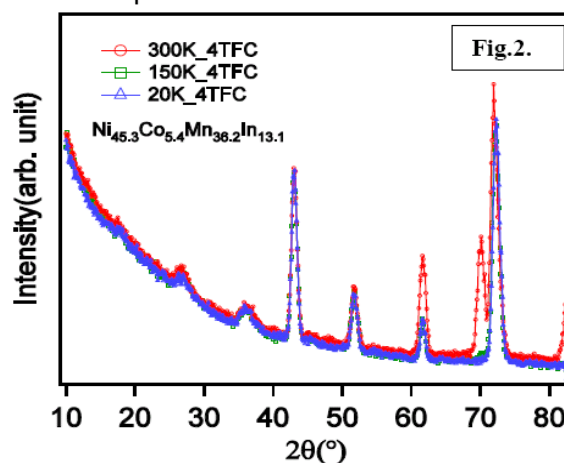



Figure 2 shows the 4T FC data at different temperatures. At 300K sample is in the mixed phase region (austenite and martensite) due to the shift in the transition temperature under application of 4T magnetic field. At 150K and 20K it is in the martensitic phase.



#### $\text{Ni}_{50}\text{Mn}_{34}\text{In}_{16}$

At 300K it is in the austenitic phase and below 230K it goes to the martensitic phase. The diffraction patterns of  $\text{Ni}_{50}\text{Mn}_{34}\text{In}_{16}$  at different temperatures were taken during heating cycle. Unluckily, there are strong peaks found on the pattern due to the Al and Cu present around the sample holder. There is no significant change in the diffraction pattern as a function of temperature. Unfortunately, we could not reach the reverse martensite-austenite transformation temperature due to some problems with VM5 cryomagnet. Also, we lacked the temperature stability during the pattern measurements, due to the cryostat needle valve problems and could not reach the austenite phase. Thus, we need to repeat the experiment for  $\text{Ni}_{50}\text{Mn}_{34}\text{In}_{16}$  alloy.

 <b>HELMHOLTZ ZENTRUM BERLIN</b> für Materialien und Energie  <b>NEUTRONS</b>	<b>EXPERIMENTAL REPORT</b>  <b>Magnetic structure of Tm<sub>2</sub>AlB<sub>6</sub></b>	Proposal: PHY-01-2705 Instrument: <b>E2</b> Local Contact: Illia Glavatskyi
	Principal Proposer: Takao Mori, NIMS, Japan Experimental Team: Takao Mori, NIMS, Japan Konrad Siemensmeyer, HZB Illia Glavatskyi, HZB Sebastian Gerischer, HZB	Date(s) of Experiment  28.06.2010 – 04.07.2010

Date of report: 6.9. 2010

Tm<sub>2</sub>AlB<sub>6</sub> is a new material where the rare earth ions are located in 1D channels formed by the boron network. It undergoes two successive phase transitions at 3.4 and 2.8K. Remarkable is a high field phase stable up to 14 T.

In this experiment we have investigated a powder sample in zero field and in applied field up to 5 Tesla at temperatures between 2K and 150K.

At low temperature - zero field we observe af reflections that indicate (incommensurate) magnetic ordering. For reasons of instrumental resolution the data do not allow a separation of the fundamental peaks. Therefore, currently it is not possible to tell the size of the (large) magnetic unit cell.

In applied magnetic field the diffraction pattern shows distinct changes that indicate a new af structure. Also here, it was not yet possible to determine due to peak overlap.

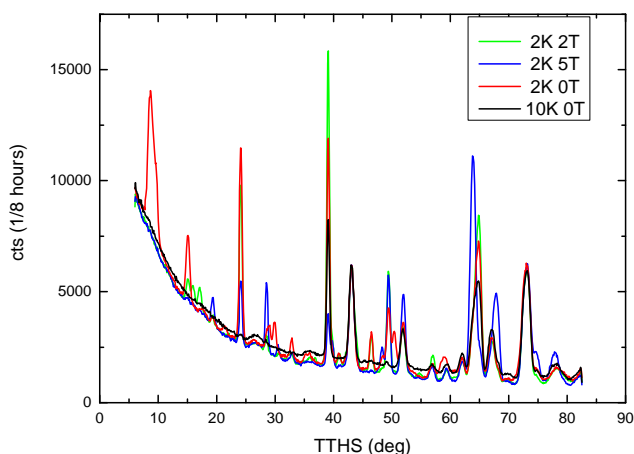


Fig. 1: The figure shows selected diffraction patterns for some field values in the af phase at T=2K. For comparison a high temperature data set at T=10K has been added.

The field dependent data, however, support the existence of a high field phase that was suggested based on specific heat and magnetisation data [1]: At 2K af reflections remain in fields as high as 5T, well within the proposed high field phase.

The comparison of high temperature and low temperature data yields an unexpected result: Fig.2 gives the diffuse signal as obtained from the difference of a powder pattern at 10 K and 50 K in zero field, i.e. well above the Neel temperature. The modulation of the diffuse signal resembles a Bessel function of zeroth order. This type of scattering e.g. would arise from uncorrelated dimers with a distance of ~ 1.8 Å. The nature of this effect remains to be clarified in detail.

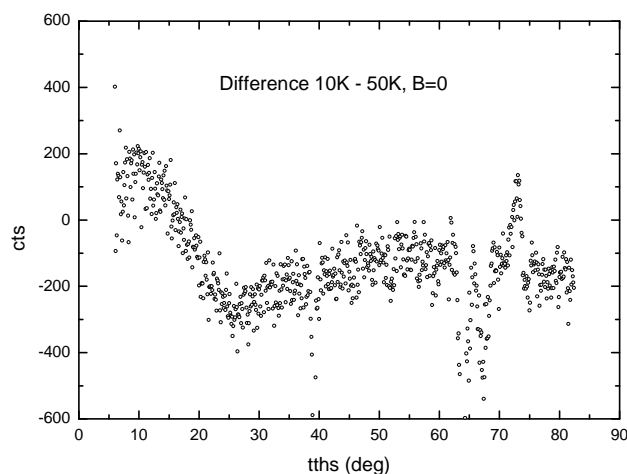



Fig. 2.: Difference of powder pattern at 10K and 50K, B=0 Tesla.

In conclusion, the data support the suggested phase diagram, but higher resolution is needed to determine the magnetic structure.

[1] T. Mori et. al.; J. Appl. Phys. 105, 1, (2009)

 <b>HELMHOLTZ ZENTRUM BERLIN</b> für Materialien und Energie  <b>NEUTRONS</b>	<b>EXPERIMENTAL REPORT</b>  <b>Magnetic Structure of PrB<sub>6</sub></b>	Proposal: PHY-01-2742-EF  Instrument: <b>E2</b>  Local Contact: I. Glavatskyi
	Principal Proposer: M.D. Le, HZB Experimental Team: M.D. Le, HZB K.A. McEwen, UCL H.C. Walker, ESRF I. Glavatskyi, HZB	Date(s) of Experiment  16.06.2010 – 21.06.2010

Date of report: 12.01.2011

Interactions between orbital moments in rare earth compounds which results in the ordering of those moments in low temperature phases, analogous to the magnetic ordering of dipole moments has become a topic of recent interests. CeB<sub>6</sub>, which has the same simple cubic structure as our subject PrB<sub>6</sub>, is known to exhibit quadrupolar order. It was hypothesised that similar quadrupolar interactions serve to stabilise the double- $q$  magnetic structure of PrB<sub>6</sub>. A mean-field analysis of the quadrupolar interactions suggests that there may be additional diffraction peaks not measure by a previous magnetic structure analysis of PrB<sub>6</sub>[1]. We thus performed measurements using the D10 single crystal diffractometer at ILL. No additional peaks as suggested by the mean-field analysis were found in this measurement. However, we found a curious temperature behaviour, which was to be further investigated in this E2 experiment.

PrB<sub>6</sub> has two ordered phases: below 7K, there is an incommensurate (IC) ordering of the magnetic moments, with ordering wavevector  $\mathbf{q}=(\frac{1}{4}-\delta, \frac{1}{4}, \frac{1}{2})$  where  $\delta=0.05$ , which becomes commensurate (C), with  $\mathbf{q}=(\frac{1}{4}, \frac{1}{4}, \frac{1}{2})$ , below 4.2K. We thus expected to see peaks of the type  $\langle \frac{1}{4}, \frac{1}{4}, \frac{1}{2} \rangle$  below 4.2K and  $\langle 0.2, \frac{1}{4}, \frac{1}{2} \rangle$  between 4.2K and 7K only. We observed in the D10 measurements (0.8,0.75,0.5) and (0.75,0.75,0.5) peaks at all temperatures below 7K, albeit with a intensity change at 4.2K.

We thus measured the diffraction pattern at 2K, 3.5K, 5K, 6.5K and 8K in zero field using the area detector on E2 to confirm these anomalous peaks. *The diffraction patterns showed no IC types peaks in the C phase and vice versa.* It thus appears that the D10 measurements may have observed multiple scattering reflections or other artefacts.

In addition to the zero field measurements we also undertook some measurements at 4T in order to confirm the single- $k$  high field structure measured in [1], and to see if there are addition reflections missed in the older study.

Unfortunately, the sample became rotated during the ramp up in field, such the field came to be

approximately parallel to the [001]-direction rather than the [1,-1,0]-direction as originally planned. The scattering plane became the (hk0) rather than the original (hhl) plane, and furthermore was some 12° from horizontal. As this occurred towards the end of the experiment, there was no enough time to remove and realign the sample, but we were able to observe reflections of the type  $\langle 0.25, 0.75, 0 \rangle$  at 2K, and 4T.

The table below shows a list of the measured diffraction peaks and normalised intensities. Refinement of the structure is in progress.

## References

[1]. Burret et al. *J.Phys. Colloque* **8** 459 (1988)

$h$	$k$	$l$	Int	
0.25	0.25	0.5	100	} 2K, 0T
-0.25	-0.25	0.5	33	
-0.25	0.25	0.5	75	
-0.5	0.75	0.75	31	
0.5	0.75	0.75	46	
0.25	0.25	1.5	47	
-0.25	-0.25	1.5	35	
0.25	0.5	0.75	29	
-0.25	0.5	0.75	22	
-0.75	0.5	0.75	41	
0.2	0.25	0.5	100	} 5K, 0T
-0.2	0.25	0.5	70	
-0.2	-0.25	0.5	44	
-0.25	0.2	0.5	68	
0.2	0.5	0.75	22	
-0.2	0.5	0.75	24	
-0.25	0.5	0.8	13	
0.25	0.5	0.8	13	
0.5	0.75	0.8	57	
-0.5	0.75	0.8	34	
-0.75	0.5	0.8	26	
-0.8	0.5	0.75	35	
0.75	0.75	0	100	} 2K, 4T
0.25	0.75	0	34	
-0.25	0.75	0	32	
-0.75	0.75	0	28	
-0.75	-0.25	0	18	
-0.75	0.25	0	16	

Table 1. Reflections and intensities of PrB<sub>6</sub>



Principal Proposer: Oliver Stockert, MPI CPfS Dresden  
 Experimental Team: Oliver Stockert, MPI CPfS Dresden  
 Ariane Haase, MPI CPfS Dresden  
 Jens-Uwe Hoffmann, HZB

Date(s) of Experiment

17.08.2010 – 25.08.2010

Date of report: 01.09.2010

The heavy-fermion compound YbCo<sub>2</sub>Si<sub>2</sub> orders antiferromagnetically below  $T_N = 1.7\text{K}$  and serves as a magnetically ordered reference compound to almost quantum critical YbRh<sub>2</sub>Si<sub>2</sub>. While at lowest temperature the magnetic order in YbCo<sub>2</sub>Si<sub>2</sub> is commensurate with  $\tau = (0.25\ 0.25\ 1)$ , the magnetic structure becomes incommensurate above  $T \approx 0.9\text{K}$  with  $\tau = (0.08\ 0.25\ 1)$ . In a previous experiment on E6 the magnetic order was studied on a YbCo<sub>2</sub>Si<sub>2</sub> single crystal for magnetic fields along  $[1\bar{1}0]$  [1]. The aim of the present experiment was to resolve the issue about the basal plane anisotropy observed in transport measurements [2].

The measurements on E2 were carried out on the same single crystal as used previously on E6 ( $5 \times 4 \times 0.5\text{mm}^3$ ). The sample was mounted in a <sup>3</sup>He cryostat inside a vertical magnet. Data were taken in the temperature range between 0.25 and 3 K and in magnetic fields up to 2.2 T applied along the  $[010]$  direction.

Fig. 1 displays the intensity of the  $(0.75\ 0.25\ 0)$  magnetic peak as a function of magnetic field at lowest temperature  $T = 0.25\text{K}$ . The intensity increases slightly from 0.6 to 0.8 T,

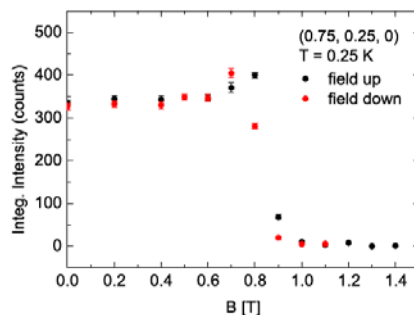


Figure 1: Magnetic field dependence of the integrated intensity of  $(0.75, 0.25, 0)$  in YbCo<sub>2</sub>Si<sub>2</sub> at 0.25 K.

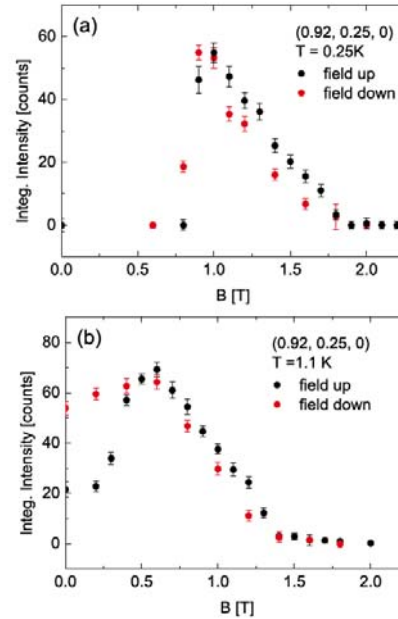


Figure 2: Magnetic field dependence of the integrated intensity of  $(0.92, 0.25, 0)$  at 0.25 K (a) and 1.1 K (b) in YbCo<sub>2</sub>Si<sub>2</sub>.

but vanishes suddenly for  $B > 0.9\text{T}$ . At this first order transition magnetic intensity appears at the incommensurate position  $(0.92\ 0.25\ 0)$  as seen in Fig. 2a. Moreover, for increasing and decreasing magnetic field a hysteresis in the intensity is found which most likely can be attributed to different domain population. Whereas the hysteresis at low temperatures is still small, at  $T = 1.1\text{K}$  a marked hysteresis in the magnetic intensity of the incommensurate peak is visible for ramping up or down the field (cf. Fig. 2b). Here domain repopulation effects play a more important role.

[1] N. Mufti et al., BENS experiment PHY-01-2526

[2] N. Mufti et al., phys. stat. sol. b 247, 743 (2010)

**Magnetic order within subsystem of Cr atoms intercalated into transition metal dichalcogenides**

Instrument: E2

Local Contact:  
Illia Glavatskiy

Principal Proposer: N. Baranov, RAS IMP Ekaterinburg, RU  
Experimental Team: A. Gubkin, RAS IMP Ekaterinburg, RU  
E.M. Sherokalova, USU Ekaterinburg, RU  
N.V Selezneva, USU Ekaterinburg, RU  
I. Glavatskiy, HZB

Date(s) of Experiment

04.08.2010 – 08.08.2010

Date of report: 20.12.2010

The dichalcogenides of transition (T) metals of IV and V groups  $TX_2$  ( $X=S, Se, Te$ ) have a hexagonal crystal structure of the CdI2 type. The triple X-T-X layers in these compounds are bound by weak van der Waals forces. By intercalation of different M atoms between the X-T-X layers a wide class of  $M_xTX_2$  compounds with unusual electronic and magnetic properties can be obtained. The  $M_xTiX_2$  compounds intercalated by 3d transition (M) metals can be considered as an analog of artificial multi-layer structures with magnetic M layers which are separated by non-magnetic layers. In order to answer the question how the type of a  $TX_2$  matrix influences the magnetic order within the subsystems of intercalated Cr ions and to determine the magnetic structures of magnetically ordered compounds of the  $Cr_xTX_2$  type we have performed neutron diffraction measurements on powder samples of  $Cr_{0.33}NbSe_2$  and  $Cr_{0.55}TiTe_2$  compounds at various temperatures using the E2 diffractometer with the neutron wavelength  $\lambda = 2.4 \text{ \AA}$ .

The room temperature powder neutron diffraction (PND) pattern for  $Cr_{0.33}NbSe_2$  (shown in Fig.1) was refined on the basis of  $P63/mcm$  space group with the superstructure  $\sqrt{3}a_0, \sqrt{3}a_0, 2c_0$  caused by the ordered arrangement of Cr ions. The appearance of ferromagnetic contribution to the (002), (100) and (102) Bragg reflections was observed below the Curie temperature  $T_C = 100K$ , which is indicative of ferromagnetic arrangement of Cr magnetic moments ( $\mu_{Cr} \approx 2.7 \mu_B$ ) in  $Cr_{0.33}NbSe_2$  along the  $b$ -axis in the basal plane (see inset in Fig. 1).

The ferromagnetic contribution to the low angle nuclear reflections was also observed below the Curie temperature  $T_C \sim 120 K$  on the PND patterns measured for the intercalated compound  $Cr_{0.65}TiTe_2$  (shown in Fig.2). These data are in agreement with magnetic measurements performed recently for the  $Cr_xTiTe_2$  system [1].

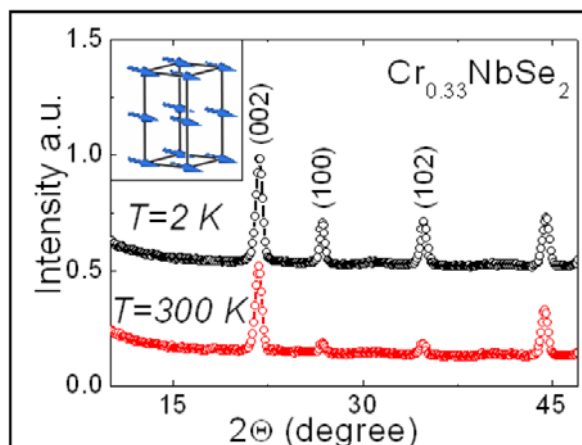


Fig.1. Neutron diffraction patterns for  $Cr_{0.33}NbSe_2$  measured at  $T = 2K$  and  $300K$ .

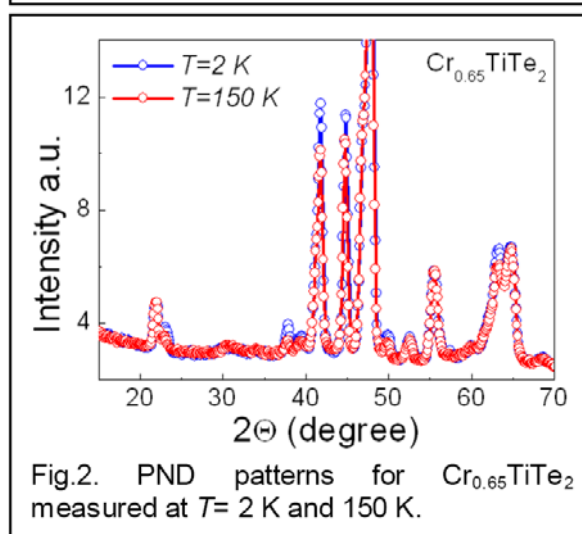


Fig.2. PND patterns for  $Cr_{0.65}TiTe_2$  measured at  $T= 2 K$  and  $150 K$ .

References:

1. N. Baranov et al // J. Phys.: Condens. Matter 21 (2009) 506002.

**Low-Temperature Magnetic Structure of  
Frustrated Antiferromagnet SrYb<sub>2</sub>O<sub>4</sub>**

Instrument: **E4, E6, E9**

Local Contact:  
Kimber, Hoser, Mat'as

Principal Proposer: Diana Lucia Quintero Castro, HZB  
 Experimental Team: Bella Lake, HZB  
 Manfred Reehuis, HZB  
 Nazmul Islam, HZB

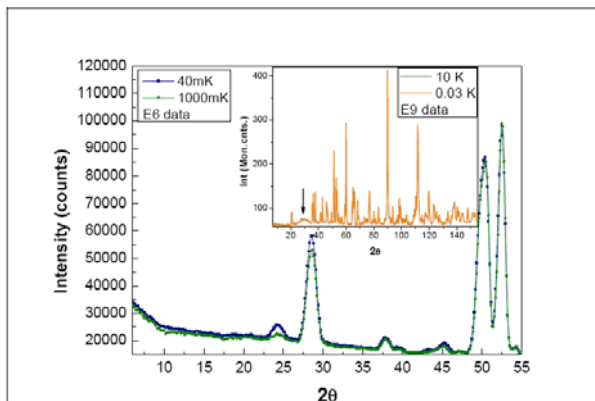
Date(s) of Experiment  
 29.09.2009 – 04.10.2009  
 10.11.2009 – 16.11.2009  
 18.08.2009 – 20.08.2009

Date of report: 02.12.2010

SrYb<sub>2</sub>O<sub>4</sub> is a frustrated, low dimensional antiferromagnet. The magnetic Yb<sup>3+</sup> ions have angular momentum  $S=1/2$ ,  $L=3$  and  $J=7/2$  and form sub-lattices of double chains running parallel to the crystallographic  $c$ -axis. There are two inequivalent although highly similar chains due to the two inequivalent Yb<sup>3+</sup> ions per unit cell. These chains suggest the presence of frustrated first and second neighbour magnetic interactions. Moreover the coupling between the chains is also frustrated and the Yb<sup>3+</sup> ions form a hexagonal structure around the Sr ions.

Powder and single crystal neutron diffraction measurements have been performed on three different diffractometers at HZB in order to determine the crystal and magnetic structure of the compound. The compound orders antiferromagnetically at a temperature of 0.9 K according to heat capacity measurements (see inset figure 2). For all the diffraction experiments we have used a dilution stick to reach temperatures below and above this phase transition.

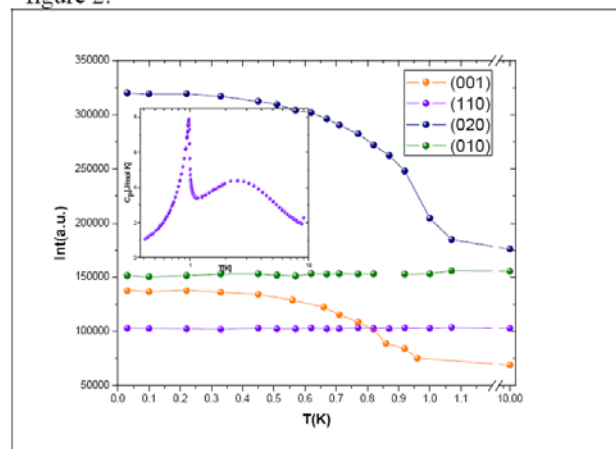
For the experiment on E6 we have used an initial wavelength of 2.4 Å and the sample mass was 12 g. For this experiment we used an aluminium sample container, which consisted in a cylindrical shell of 2 mm thickness. The container was filled with the powder sample, sealed under a He4 atmosphere and filled with He3 to ensure the thermal conductivity. The container was design for inelastic neutron scattering and not for diffraction therefore the Bragg peaks were wider and the resolution was not as good as expected. We took patterns at 40 mK, 200 mK, 400 mK, 600 mK, 800 mK and 1000 mK.



**Fig 1.** Diffraction patterns acquired in E6 (main figure) and E9 (inset). The main figure shows the low 2theta patterns for the lowest and higher temperature.

On E9 we have used a cylindrical Cu sample can and this was fill with the powder sample and a mixture of deuterated ethanol and methanol to ensure the thermal contact. Unfortunately, the diffraction pattern show a bump of incoherent scattering around  $2 \text{ \AA}^{-1}$  due to the alcohol mixture as is showed on the inset in figure 1. The data were collected at two temperatures 0.03 K and 10 K.

For the single crystal neutron diffraction experiment on E4 we have used a initial wavelength of 2.43 Å and we have measured in two scattering planes (0KL) and (HK0). The single crystal was a cylinder of mass 3.2 g mounted in a copper holder. We measured a total 82 reflections and we followed the temperature dependence of the intensity on 4 reflections as showed in figure 2.



**Fig 2.** Temperature dependence of the intensity of four reflections measured in E4. Two of them are pure nuclear reflections (110) and (010). And the other two have magnetic and nuclear component, showing a transition around 0.9 K in agreement with the heat capacity measurement (inset).

The results proved that antiferromagnetic order occurs below 0.9 K with ordering wavevector  $\mathbf{k}=0$ . Both Yb ions order, this differs from the magnetic structure of the isostructural compound SrEr<sub>2</sub>O<sub>4</sub> where the two Er sites are inequivalent [1]. On the single crystal experiment we found intensity on some reflections forbidden for the space group, this suggests a crystal distortion. The data analysis is in progress.

Reference

[1] O.A. Petrenko et al. Phys. Rev. B **78**, 184410 (2008)

Principal Proposer: S. Mat'as, HZB  
Experimental Team: Z. Mitroova, SAS Kosice, SK  
K. Prokes, HZB

Date(s) of Experiment

27.01.2010 – 31.01.2010

Date of report: 30.12.2010

Rare-earth ferricyanides Re[Fe(CN)<sub>6</sub>]<sub>n</sub>H<sub>2</sub>O (n = 4,5), as a member of Prussian blue family [1-4], have been extensively studied for a few decades. Depending on chemical composition and preparation conditions they form tetrahydrate and pentahydrate complexes. The crystal structure of such materials was classified by Hulliger et al. [3] as orthorhombic (nearly pseudo-hexagonal) and hexagonal, respectively.

### Experiment and Results:

The Pr[Fe(CN)<sub>6</sub>]<sub>6</sub> · 4H<sub>2</sub>O was synthesized by mixing of saturated H<sub>2</sub>O solution of K<sub>3</sub>[Fe(CN)<sub>6</sub>] with H<sub>2</sub>O solution of rare earth ions Pr<sup>3+</sup>. The crystal structure of powdered sample was characterized by means of X-ray diffraction. The structure adopts a Cmc<sub>2</sub>m space group. The single crystal Pr[Fe(CN)<sub>6</sub>]<sub>6</sub> · 4H<sub>2</sub>O of size 5 x 5 x 4 mm with room temperature lattice cell parameters: a = 7.496 Å, b = 12.958 Å, c = 13.825 Å, α = β = γ = 90 was mounted so that reflections in a-c scattering plane were accessible. The experiment was carried out at the E4 diffractometer at a wavelength λ = 2.43 Å. The following experimental set up has been

chosen: PG filter - 40' collimation-sample-open-detector.

In this experiment we have explored the contribution to the scattering at high and low temperatures of 0.3 K, 0.4 K and 1.8 K well below and above the transition temperature T<sub>N</sub> indicated by heat capacity measurement (see Fig.1.).

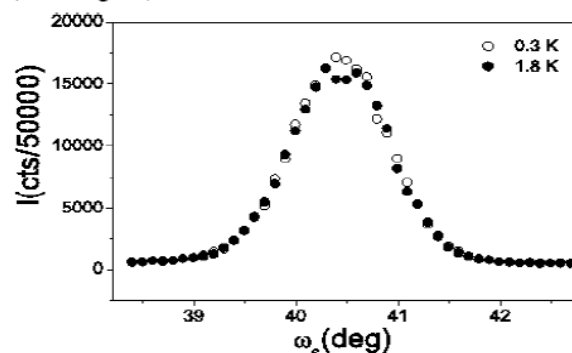


Fig. 2. OMGS scans across (400) reflection positions taken at temperature of 0.3 K and 1.8 K.

Data collected on Pr[Fe(CN)<sub>6</sub>] at the E4 diffractometer show a small increase of the intensities at (004) and (400) nuclear reflections, however, no clear magnetic signal is observed at respective low-2θ reflections that should be more sensitive to magnetism. Lambda like anomalies observed via heat capacity measurements indicate that cooperative effects occur at temperatures of 1.3 K, 0.47 K 0.4 K for Ln = Pr, their origin becomes an open question. Due to the absence of a clear magnetic signal no final statement about the magnetic structure can be made.

### References

- [1] M. T. Hirvonen et al., Phys. Rev. B, Vol. 15, No. 3 (1977) 1445
- [2] Z. Mitroová et al., Czechoslovak J. of Physics, 54: D559, Suppl. D 2004
- [3] F. Hulliger et al., J. of Solid State Chem. Vol. 18 (1976) 283
- [4] F. Hulliger et al., J. of Solid State Chem. Vol. 18 (1976) 1365

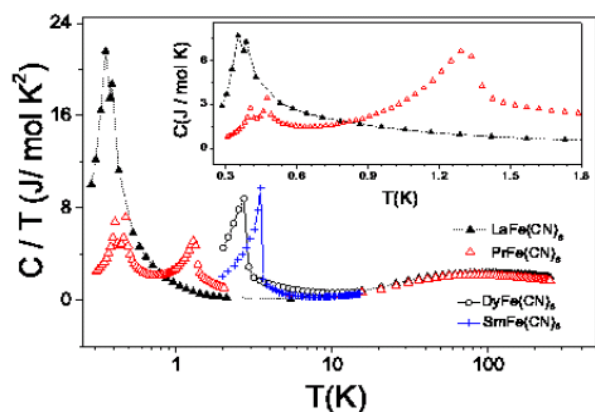



Fig. 1 Low temperature heat capacity data of selected rare-earth ferricyanides Ln[Fe(CN)<sub>6</sub>]<sub>n</sub>H<sub>2</sub>O, Ln=Pr (~1.3 K), La (~0.39 K), Sm (T<sub>N</sub> ~3.5 K [2]), Dy (T<sub>N</sub> ~2.8 K [2]) in semilogarithmic scale. The inset shows lambda like anomalies for Ln=Pr and La in C vs. T plot.

 <b>HELMHOLTZ ZENTRUM BERLIN</b> für Materialien und Energie  <b>NEUTRONS</b>	<b>EXPERIMENTAL REPORT</b>	Proposal: PHY-01-2747-EF
	<b>Investigation of the low temperature and applied field phase diagram in azurite</b>	Instrument: <b>E4</b> Local Contact: K. Prokes
Principal Proposer: K. C. Rule, HZB Experimental Team: Clare Gibson, HZB Alan Tennant, HZB	Date(s) of Experiment  26.05.2010 – 31.05.2010	

Date of report: 20.07.2010

Azurite,  $\text{Cu}_3(\text{CO}_3)_2(\text{OH})_2$ , is a natural-mineral that is also an interesting quantum magnet. Originally thought to be a model system of an  $s=1/2$  Heisenberg antiferromagnetic chain (HAFC), azurite has recently exhibited interesting new features pointing to a complex ground state in zero and low applied magnetic fields. A deeper understanding of these new features provided the motivation for this study in which we scanned the B-T phase diagram for azurite.

Recent neutron scattering results indicated that the Cu-chain direction, propagating along the crystallographic b-axis, shows large changes in intensity at temperatures close to the Neel temperature, 1.86 K. Thus a small cube of azurite (side length  $\sim 5$  mm) was aligned in the  $ab$ -scattering plane. A series of 6 nuclear Bragg reflections were measured as a function of temperature (from 0.045 – 1 K) and magnetic field (0-5 T). These peaks include two of each type:  $H00$  (100, 200),  $0K0$  (020, 040) and  $HK0$  (110, 120).

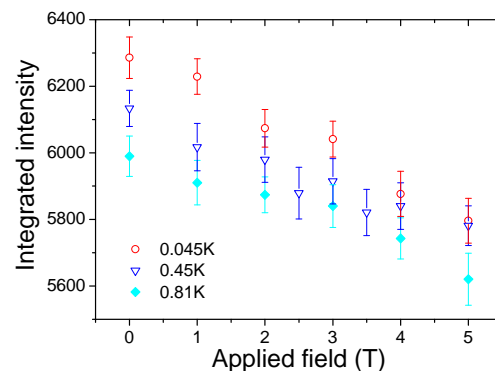
To ensure the highest resolution, all measurements were taken with the longest wavelength for E4, 2.4Å. A dilution insert with the vertical field magnet VM3 was used for this experiment. The magnetic field was applied parallel to the  $c^*$ -axis, that is, perpendicular to the Cu-O chains.

For the reflections 110 and 120 clear temperature dependence was observed in the integrated intensity below 1.86 K. It was also evident that in increasing magnetic fields the overall integrated intensity decreased, as can be seen in figure 1. The 020 and 040 peaks showed less temperature and field dependence whereas the 100 and 200 Bragg reflections remained statistically unchanged with both temperature and applied field.

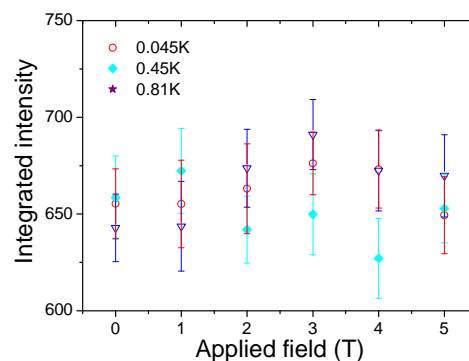
Extinction effects within the single crystal have been suggested as the main cause of the temperature dependent intensities in azurite, but this is the first time that a field dependence has also been observed. This field dependence of the nuclear Bragg reflections points to magnetoelastic

behavior in this material and may indicate frustrated magnetic interactions. With sufficient applied field, the structure and atomic fractional coordinates may vary, however a study based on 4 nuclear Bragg peaks is not detailed enough to confirm this hypothesis.


Integrated intensity of the 110 peak with field and temperature



Integrated intensity of the 100 peak with field and temperature



From the small selection of peaks surveyed, there were no obvious new phases around 3 T and 5 T, nor was there a clear change around 0.5 K, each of which has been seen in other measurements. With only a small selection of Bragg peaks accessible, a full study of reciprocal space could not be performed. We have also focused our attentions on the nuclear Bragg reflections, rather than the magnetic peaks which are very weak and appear outside the  $ab$ -scattering plane, with a propagation vector of  $\mathbf{k} = 1/2, 1/2, 1/2$ . It is currently not possible to observe these reflections using E4 if the applied field is constrained along the  $c^*$  crystallographic axis. A more detailed investigation on a 4-circle diffractometer would be valuable.

 <b>EXPERIMENTAL REPORT</b>		Proposal: PHY-01-2750 Instrument: <b>E4</b> Local Contact: K. Prokes
<b>NEUTRONS</b>	<b>Magnetic ordering of the Er<sup>3+</sup>-ions in ErVO<sub>3</sub></b>	
Principal Proposer:	C. Ulrich, B. Keimer – MPI Stuttgart M. Reehuis, HZB S. Miyasaka, J. Fujioka, Y. Tokura – University of Tokyo, Japan	Date(s) of Experiment
Experimental Team:	M. Reehuis, HZB K. Prokes, HZB S. Mat'as, HZB	20.01.2010 – 27.01.2010

Date of report: 17.06.2010

We have started to investigate intensively the structural and magnetic properties of vanadates  $RVO_3$  ( $R = Y$  or rare-earth element) [1-4]. These compounds exhibit many exciting properties, which can be related to orbital or spin rearrangements. A phase transition from an orthorhombic to a monoclinic structure sets in at  $T_{S1}$ . Below  $T_N$ , in the monoclinic phase, the vanadium moments show antiferromagnetic ordering with the modes  $C_x$ ,  $C_y$  and  $G_z$ , where the z-component is the weakest [2, 3]. Some of the vanadates exhibit an additional structural phase transition at  $T_{S2}$ , which sets in well below  $T_N$ . This transition can only be observed for the vanadates with smaller  $R^{3+}$ -ions ( $R^{3+} = Y^{3+}$ ,  $Dy^{3+}$ ,  $Ho^{3+}$ ,  $Er^{3+}$ ,  $Tm^{3+}$ ,  $Yb^{3+}$ ,  $Lu^{3+}$ ) [3]. Here the crystal structure changes again to the orthorhombic structure, in which the vanadium moments are purely G-type ordered along the z-direction [1-3].

The magnetic order of the V-sublattice was investigated earlier on the E5 instrument [5]. It was shown that the second phase transition ( $T_{S2}$ ) sets in between 55 K and 61 K, well below the Néel temperature  $T_N = 112(1)$  K. In the present single-crystal neutron diffraction study we have investigated the magnetic ordering of the  $Er^{3+}$ -ions in  $ErVO_3$  on the instrument E4 using the neutron wavelength  $\lambda = 2.45$  Å (PG-monochromator). The used cylindrical single-domain crystal of  $ErVO_3$  with the dimensions of  $d = 3$  mm and  $h = 5$  mm was grown by the floating zone technique [1]. In Fig. 1 it can be seen that magnetic intensity appears spontaneously at  $T_N = 2.5(2)$  K. This clearly indicates the onset of a C-type ordering of the Er-moments. For the Er-atoms in the Wyckoff position  $4c$  [(1)  $x, y, \frac{1}{4}$ ; (2)  $-x, -y, \frac{3}{4}$ ; (3)  $\frac{1}{2} - x, \frac{1}{2} + y, \frac{1}{4}$ ; (4)  $\frac{1}{2} + x, \frac{1}{2} - y, \frac{3}{4}$  with  $x = 0.977$  and  $y = 0.072$ ] the basis vectors are defined  $C(+ + - -)$ . From the representation analysis one finds a C-mode in the irreducible representations  $\Gamma_1(-, -, C_2)$ ,  $\Gamma_2(F_x, C_y, -)$  and  $\Gamma_3(C_x, F_y, -)$ .

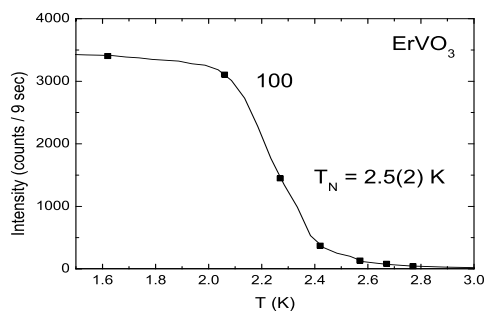


Fig. 1. T-dependence of the magnetic intensity of the Bragg reflection 100 of  $ErVO_3$ .

A strong intensity we also found at the position of the 010, indicating the presence of a C-type ordering along the z-direction. Due to the fact that no magnetic intensity was found on the reflections 200, 020 and 002 the presence of a ferromagnetic component can be excluded. Further the absence of the 001 excludes the presence of a A-type ordering defined as  $A(+ - - -)$ . The refinements of the magnetic structure finally confirmed a pure C-type ordering along the z-direction. At 1.6 K the Er-moment reaches a value  $\mu_z = 8.2(2)$   $\mu_B$ , which is smaller than the theoretical value  $\mu_{eff} = gJ = 9.0$   $\mu_B$ . The magnetic structure  $ErVO_3$  is presented in Fig. 2.

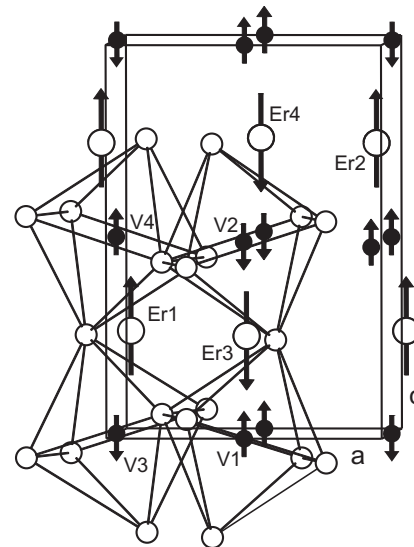


Fig. 2. Magnetic structure of  $ErVO_3$  at 1.6 K. The V-moments show a G-type ordering with a spin sequence  $+ - - +$ , while the Er-moments show a C-type ordering with a spin sequence  $+ + - -$ .

#### References

- [1] S. Miyasaka, Y. Okimoto, M. Iwama, Y. Tokura, Phys. Rev. B **68**, 100406(R) (2003).
- [2] C. Ulrich, G. Khaliullin, J. Sirker, M. Reehuis, M. Ohl, S. Miyasaka, Y. Tokura, B. Keimer, Phys. Rev. Lett. **91**, 257202 (2003).
- [3] M. Reehuis, C. Ulrich, P. Pattison, B. Ouladdiaf, M.C. Rheinstädter, M. Ohl, L.P. Regnault, S. Miyasaka, Y. Tokura, B. Keimer, Phys. Rev. B **73**, 094440 (2006).
- [4] M. Reehuis, C. Ulrich, P. Pattison, S. Miyasaka, Y. Tokura, B. Keimer, Eur. Phys. J. B **64** (2008) 27.
- [5] C. Ulrich, B. Keimer, S. Miyasaka, J. Fujioka, Y. Tokura, M. Reehuis, BENSCE Exp. Rep. 2009, p. 100.

Principal Proposer: Umeo, Kazunori Hiroshima Univ., JP  
 Experimental Team: Prokes, Karel, HZB  
 Onimaru, Takahiro, Hiroshima Univ., JP  
 Kubo, Hirokazu, Hiroshima Univ., JP  
 Takabatake Toshiro, Hiroshima Univ., JP

Date(s) of Experiment

27.04.2010 – 05.05.2010

Date of report: 27.01.2011

The Yb-based intermetallic compound YbAgGe, crystallising in the hexagonal ZrNiAl-type structure, is a candidate of the magnetically frustrated 4f-electron system. This compound undergoes two antiferromagnetic transitions at  $T_{M1} = 0.8$  K and  $T_{M2} = 0.65$  K. The magnetic structures were determined by our neutron diffraction experiments with a single-crystalline sample; the magnetic moments confined in the  $c$  plane make an angle of  $120^\circ$  with each other with  $\mathbf{Q} = (0, 0, \delta)$  ( $\delta = 0.327$ ) at  $T_{M1} \geq T \geq T_{M2}$  and  $\mathbf{Q} = (2/3, 0, 2/3)$  at  $T \leq T_{M2}$ . These  $120^\circ$  magnetic structures strongly suggest the presence of the magnetic frustration. Furthermore, with applying pressures above  $P^* = 1.6$  GPa, the magnetic entropy  $S_m$  at  $T_{M1}$  rises continuously, whereas the Kondo

temperature does not change. These facts strongly suggest that the magnetic structure changes above  $P^*$  by the release of the magnetic frustration. The aim of the present experiment was to detect pressure-induced change of the magnetic structure by means of neutron diffraction.

A single crystal of YbAgGe of 2.8 mm in diameter and 3.8 mm in height was used. The sample was set in the home made piston cylinder-type cell with size of 14 mm in diameter and 40 mm in height, which was placed on a mixing chamber of a dilution refrigerator. Thereby, the  $a^* - c^*$  plane was set on the horizontal scattering plane. The wavelength of neutron beams was 2.43150 Å and the horizontal collimation was Open - Open - S - 40' on E4.

The magnetic field dependence of the profile scans of the magnetic peak at  $\mathbf{Q} = (2/3, 0, 2/3)$  for 1.47 GPa is shown in Fig. 1. The peak at  $(2/3, 0, 2/3)$  disappears above 2.0 T. These results are consistent with the  $B - T$  phase diagram under pressure obtained by our magnetoresistance and magnetization measurements.

Fig. 2 shows the profile scans of the magnetic Bragg peak at  $\mathbf{Q} = (2/3, 0, 2/3)$  observed at  $T = 0.04$  K and  $P = 1.11, 1.47$  and  $1.55$  GPa. With increasing pressures up to 1.55 GPa, the integrated intensity decreases, indicating the change of the magnetic structure at  $P = P^*$  by the suppression of the magnetic frustration.

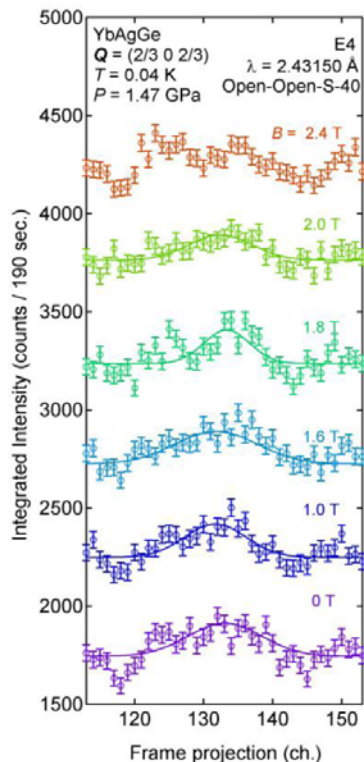


Fig. 1. Profile scans of the magnetic peak at  $\mathbf{Q} = (2/3, 0, 2/3)$  observed at  $T = 0.04$  K and  $P = 1.47$  GPa in various magnetic fields up to 2.6 T. The solid curve shows fitting with the Gaussian function.

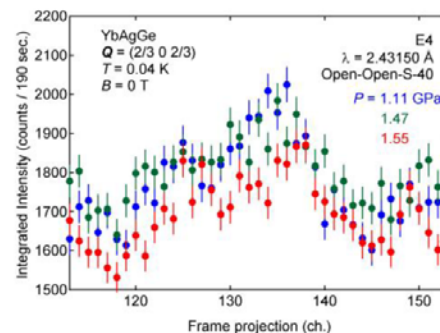


Fig. 2. Profile scans of the magnetic Bragg peak at  $\mathbf{Q} = (2/3, 0, 2/3)$  observed at  $T = 0.04$  K and  $P = 1.11, 1.47$  and  $1.55$  GPa.

 <b>HELMHOLTZ ZENTRUM BERLIN</b> für Materialien und Energie  <b>NEUTRONS</b>	<b>EXPERIMENTAL REPORT</b>  <b>Magnetic structure of magnetoelectric hexaferrites under low field: planar or conical?</b>	Proposal: PHY-01-2752  Instrument: <b>E4</b>  Local Contact: Karel Prokes
	Principal Proposer: Jae-Ho Chung, Korea University, Seoul Experimental Team: Hakbong Lee, Korea University, Seoul Karel Prokes, HZB	Date(s) of Experiment  05.05.2010 – 16.05.2010

Date of report: 13.08.2010

In this proposal experiment, we have measured the field dependent changes in the magnetic structures of magnetoelectric hexaferrite  $\text{Ba}_{0.5}\text{Sr}_{1.5}\text{Zn}_{22}(\text{Fe}_{1-x}\text{Al}_x)_{12}\text{O}_{22}$  ( $x = 0.08$ ). The purpose of the experiment was to understand the spin structures in the phases that exhibit maximum magnetoelectric polarization.

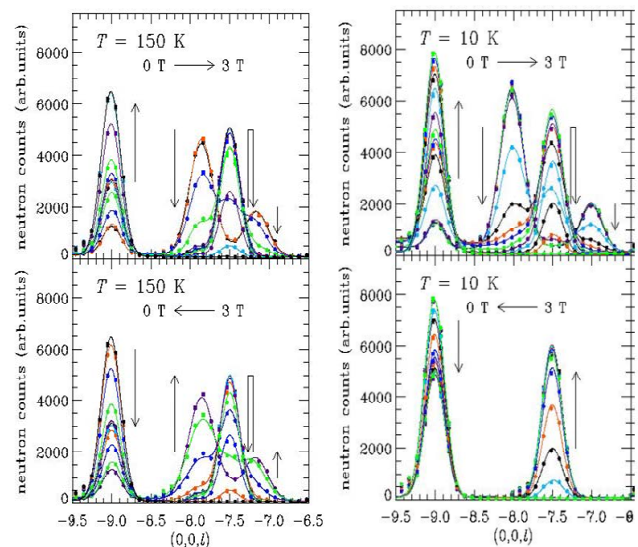
The crystal used in this study is high quality with virtually no twins. Therefore, it is suitable for the quantitative analysis of the magnetic structures. We have aligned the crystal inside a vertical field magnet in such a way that both  $a^*$  and  $c^*$  axes are in the horizontal scattering plane. In this H0L-geometry, one can observe relatively larger number of magnetic peaks than in the HHL-geometry used for twinned crystals. The direction of the applied field, which is perpendicular to the  $c$ -axis, is same as what is required to induce magnetoelectric polarization.

Previously using the data obtained from E5, we have learned that the magnetic structure change from normal longitudinal cones (below 80 K) to alternating longitudinal cones (80 – 180 K). Once the sample was cooled under zero field, we have measured the detailed field dependence at 10 K and at 150 K during either ramping up or down the field. As shown in Figure 1, the field dependent behaviours of the two phases have both similarities and differences. First of all, the incommensurate magnetic peaks disappear quickly under the field at both temperatures. Simultaneously, magnetic peaks at  $(0,0,3/2)$  grow in intensity indicating drastic change in magnetic structures. The observed changes are complete when the field has reached the values where maximum magnetoelectric polarizations have been observed. This result very clearly indicates that the magnetic structure responsible for the magnetoelectric polarization observed in this material is far from conical alignments. We also observed the


field dependent changes of the nuclear magnetic peaks consistently with the enhancement of ferromagnetic components.

Second, we learned that most important difference between the two phases under the field is in their reversibility. Figure 1 shows that the alternating cones at 150 K recover themselves when the field is lowered. In contrast, the normal cones at 10 K are not recovered but all the spin order remains commensurate to the lattice through the field cycling. It suggests that the anisotropy is not fully reduced in this system, and there is a local but stable energy minimum in the plane.

The quantitative Rietveld analysis is under way in order to understand the field dependent evolution of the magnetic structures.





 <b>HELMHOLTZ ZENTRUM BERLIN</b> für Materialien und Energie  <b>NEUTRONS</b>	<b>EXPERIMENTAL REPORT</b>  <b>Evolution of the magnetic order in Yb(Rh<sub>1-x</sub>Co<sub>x</sub>)<sub>2</sub>Si<sub>2</sub></b>	Proposal: PHY-01-2873  Instrument: <b>E4</b>  Local Contact: <b>S. Mat'as</b>
	Principal Proposer: <b>Oliver Stockert, MPI CPFS Dresden</b> Experimental Team: <b>Oliver Stockert, MPI CPFS Dresden</b> <b>A. Haase, MPI CPFS Dresden</b> <b>S. Mat'as, HZB</b>	Date(s) of Experiment  <b>30.07.2010 – 07.08.2010</b>

Date of report: 07.09.2010

The heavy-fermion compound YbCo<sub>2</sub>Si<sub>2</sub> orders antiferromagnetically in an incommensurate structure just below  $T_N = 1.7$  K with  $\tau = (0.08 \ 0.25 \ 1)$ , the magnetic structure becomes commensurate below  $T_L \approx 0.9$  K with  $\tau = (0.25 \ 0.25 \ 1)$ . In contrast, the magnetic order in the isostructural, almost quantum critical heavy-fermion compound YbRh<sub>2</sub>Si<sub>2</sub> is unknown. The aim of a single crystal diffraction experiment on E4 was to study the alloying series Yb(Rh<sub>1-x</sub>Co<sub>x</sub>)<sub>2</sub>Si<sub>2</sub> to follow the magnetic order starting from high Co content samples to crystals with low Co concentration (and finally to pure YbRh<sub>2</sub>Si<sub>2</sub>).

In our measurement we studied two single crystals with Co concentrations  $x = 0.58$  and  $0.27$ . Fig.1 displays scans along  $[100]$  through  $0.25 \ 0.75 \ 0$  in Yb(Rh<sub>0.42</sub>Co<sub>0.58</sub>)<sub>2</sub>Si<sub>2</sub> at different temperatures. A magnetic satellite peak is clearly visible at  $T = 0.26$  K while it is (almost) absent at  $T = 0.8$  K. The magnetic intensity vanishes at  $T_N \approx 0.7$  K as shown in Fig.2. This is in close agreement with thermodynamic measurements on samples with  $x = 0.58$ . Within the ordered state no further phase transition has been detected, especially no incommensurate phase has been found just below  $T_N$  as seen in pure YbCo<sub>2</sub>Si<sub>2</sub>. Instead, the magnetic order for  $x = 0.58$  remains constant commensurate for all temperatures below  $T_N$  with a propagation vector  $\tau = (0.25 \ 0.25 \ 1)$ , i.e., the same value as observed in YbCo<sub>2</sub>Si<sub>2</sub> at lowest temperatures. We also searched for magnetic intensity in Yb(Rh<sub>0.73</sub>Co<sub>0.27</sub>)<sub>2</sub>Si<sub>2</sub>, i.e., the  $x = 0.27$  sample. However, despite careful investigation no magnetic intensity has been detected, neither at the known propagation

vectors of the system,  $(0.25 \ 0.25 \ 1)$  and  $(0.25 \ 0.08 \ 1)$ , nor along high symmetry directions. Therefore, a drastic change of the magnetic structure seems to take place for samples with low Co content. Further experiments on Yb(Rh<sub>1-x</sub>Co<sub>x</sub>)<sub>2</sub>Si<sub>2</sub> crystals with  $x \leq 0.58$  are highly desired to study the marked change in the magnetic ordering.

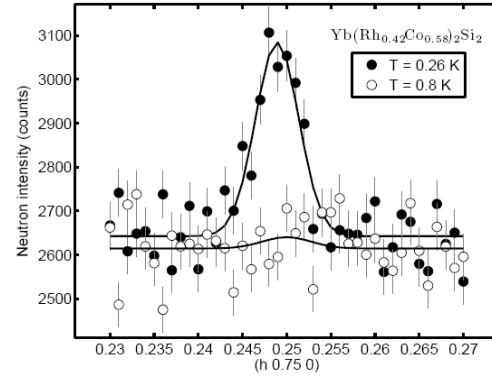


Fig. 1: Scans in reciprocal space through the magnetic  $(0.25 \ 0.75 \ 0)$  peak in Yb(Rh<sub>0.42</sub>Co<sub>0.58</sub>)<sub>2</sub>Si<sub>2</sub> below and above  $T_N$ .

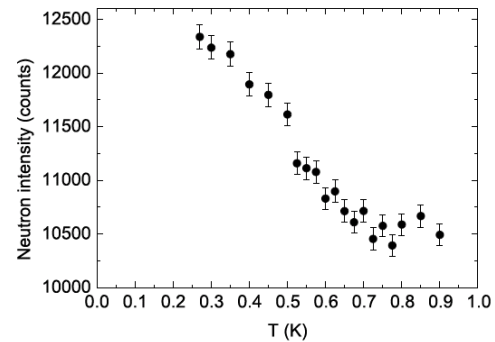



Fig. 2: Intensity of the magnetic  $(0.25 \ 0.75 \ 0)$  peak in Yb(Rh<sub>0.42</sub>Co<sub>0.58</sub>)<sub>2</sub>Si<sub>2</sub> as a function of temperature.

 <b>HELMHOLTZ ZENTRUM BERLIN</b> für Materialien und Energie  <b>NEUTRONS</b>	<b>EXPERIMENTAL REPORT</b>	Proposal: PHY-01-2874  Instrument: <b>E4</b> Local Contact: Karel Prokes
	<b>Effect of uniaxial pressure on helimagnetic structures in Lu<sub>2</sub>Fe<sub>17</sub> and Y<sub>2</sub>Fe<sub>17</sub></b>	Date(s) of Experiment 20.09.2010 – 02.10.2010
Principal Proposer: Experimental Team:	J. Kamarad, ASCR IP Prague, CZ M. Misek, ASCR IP Prague, CZ K. Prokes, HZB S. Mat'as, HZB	

Date of report: 10.01.2011

In the Y<sub>2</sub>Fe<sub>17</sub> and Lu<sub>2</sub>Fe<sub>17</sub> intermetallics, the ferromagnetic ground state has been totally suppressed by high hydrostatic pressures above 800 MPa and 300 MPa, respectively [1,2]. The pressure induced incommensurate helimagnetic structures (IHS) were characterized by a propagation vector (00τ). Recently, a complex dependence of exchange interactions,  $J_{nm}$ , ( $n, m = f, j, k$  and  $g$ ) on distances between Fe-atoms in the inequivalent crystal positions ( $4f$ ,  $12j, 12k$  and  $6g$ ) in Y<sub>2</sub>Fe<sub>17</sub> was presented in ref. [3]. Using these data, a simple model of the exchange interactions in the layered Y<sub>2</sub>Fe<sub>17</sub> and Lu<sub>2</sub>Fe<sub>17</sub> intermetallics was discussed [2]. The negative  $J_{ff}$  interaction is strongly intensified by a decrease of inter-atomic Fe–Fe distance along the crystal  $c$ -axis. Simultaneously, decreasing positive  $J_{jg}$ ,  $J_{gk}$  and  $J_{kk}$  interactions under hydrostatic pressure induce a frustration of the ferromagnetic crystal  $ab$ -planes. The  $J_{ff}$  interaction seems to be dominant for the existence and stabilization of IHS under hydrostatic pressure.

To verify the model and the dominant role of  $J_{ff}$  for suppression of the ferromagnetic ground state and a presence of IHS in Y<sub>2</sub>Fe<sub>17</sub> and Lu<sub>2</sub>Fe<sub>17</sub>, we have studied their magnetization in EMD under uniaxial compression of single crystals in a SQUID magnetometer, with stress  $\sigma \parallel a$  and  $\sigma \parallel c$ , see Fig.1. The observed metamagnetic transitions verify the presence of IHS in Lu<sub>2</sub>Fe<sub>17</sub> at 5 K under hydrostatic pressure and under uniaxial stress  $\sigma \parallel c$  only.

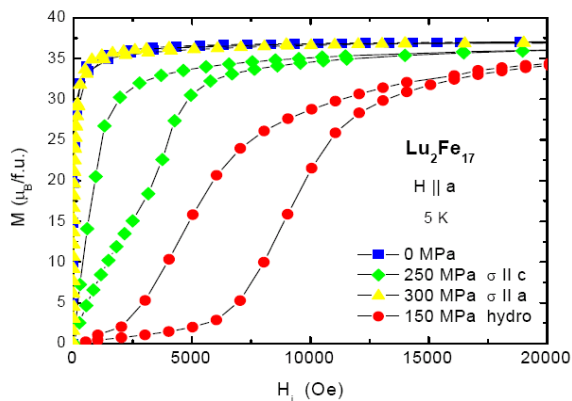


Fig.1: Magnetization of Lu<sub>2</sub>Fe<sub>17</sub> in EMD under pressure.

Using the 2-axis E4 diffractometer with 2D-detector, the VM1 cryo-magnet and the TiAlV

uniaxial ( $\sigma \parallel c$ ) pressure cells, IHS of the Y<sub>2</sub>Fe<sub>17</sub> and Lu<sub>2</sub>Fe<sub>17</sub> single crystals (with  $a$ -axis  $\parallel H \parallel$  axis of E4) were searched in wide pressure, temperature and field ranges by neutron diffraction technique.

The maximum uniaxial stress  $\sigma$  is restricted by the yield stress of the studied intermetallics, i.e.  $\sigma \leq 350$  MPa. Due to this restriction, we have not observed IHS in the Y<sub>2</sub>Fe<sub>17</sub> intermetallics under uniaxial compression.

The magnetic reflections (00τ)<sup>±</sup> around nuclear reflections have been observed in the Lu<sub>2</sub>Fe<sub>17</sub> intermetallics under uniaxial stress  $\sigma \parallel c$ , with stress  $\sigma \geq 100$  MPa. Temperature dependence of values of a propagation vector  $\tau$  determined by neutron diffraction under hydrostatic and uniaxial pressures is presented and compared in Fig.2. Due to a decrease of hydrostatic pressure with decreasing

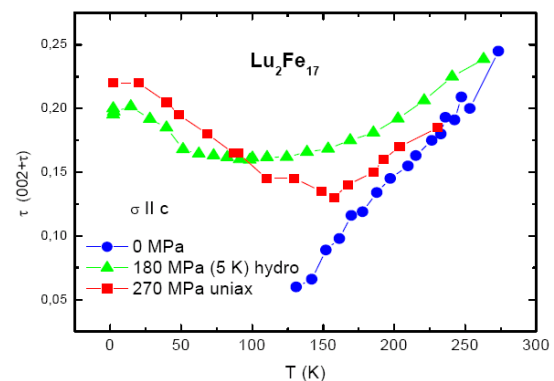



Fig.2: Temperature dependence of propagation vector  $\tau$  of IHS in Lu<sub>2</sub>Fe<sub>17</sub> under hydrostatic and uniaxial pressure

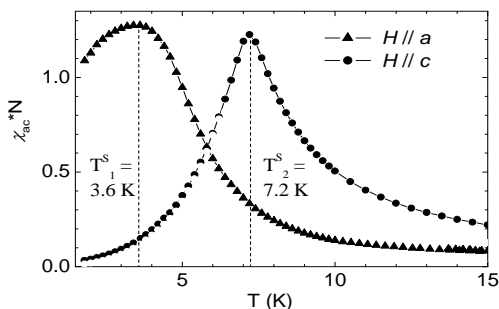
temperature, the effect of uniaxial stress  $\sigma \parallel c$  is more pronounced at low temperatures. Analyses of all the received data, including the effects of external magnetic fields, are running.

*This research project has been supported by the EC 7<sup>th</sup> Framework Programme through the "Research Infrastructures" action, contract: CP-CSA\_INFRA-2008-1.1.1. Number 226507-NMI3*

- [1] O. Prokhnenko et al., Phys. Rev. Lett. **94**, 107201 (2005)
- [2] J. Kamarád et al., J. Mag. Magn. Matter. **310** (2007) 1801
- [3] M.S. Anagnostou, et al., J. Magn. Magn. Mater. **130** (1994) 57

 <b>HELMHOLTZ ZENTRUM BERLIN</b> für Materialien und Energie  <b>NEUTRONS</b>	<b>EXPERIMENTAL REPORT</b>	Proposal: PHY-01-2875 Instrument: <b>E4</b> Local Contact: Karel Prokes
	<b>Magnetic ordering in Tb<sub>0.3</sub>Er<sub>0.7</sub>Ni<sub>5</sub> single crystal with competitive anisotropies</b>	Date(s) of Experiment 25.08.2010 – 30.08.2010
Principal Proposer: Experimental Team:	A. Pirogov, RAS, RU Karel Prokes, HZB Slavomir Mat'as, HZB Pavel Terentev, RAS, RU	Date of report: 17.01.2011

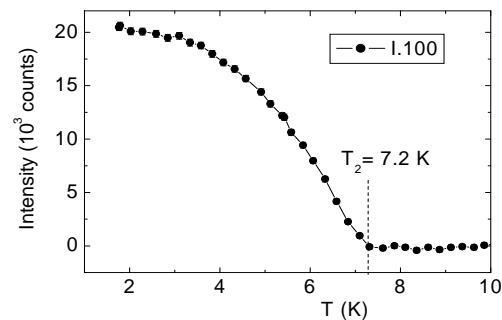
In literature much attention has been paid to systems having competing anisotropies [1]. Two types of such systems have been studied in detail: a random mixture of the “easy axis”–“easy axis” anisotropies (Ising-Ising coupling) and a mixture of the “easy axis”–“easy plane” anisotropies (Ising-XY coupling). We have measured AC-susceptibility, magnetization and heat capacity of hexagonal single - and polycrystalline Tb<sub>x</sub>Er<sub>1-x</sub>Ni<sub>5</sub> compounds in which Tb ions possess the “easy plane” type of magnetic anisotropy, while Er ions exhibit “easy axis” anisotropy, i.e. these compounds are the system with competitive anisotropies of the Ising-XY coupling type [2]. According to AC-susceptibility measurements two ( $T_1^s=3.6$  K and  $T_2^s=7.2$  K) different transition temperatures take place in the Tb<sub>0.3</sub>Er<sub>0.7</sub>Ni<sub>5</sub> single crystal if a magnetic field is oriented along *a*- and *c*-axis, respectively (see Fig.1).



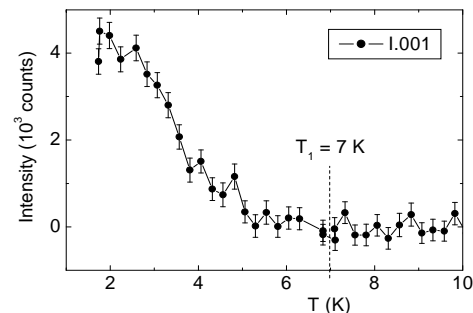
**Fig. 1.:** Temperature dependence of the ac-susceptibility of Tb<sub>0.3</sub>Er<sub>0.7</sub>Ni<sub>5</sub> measured along two principal directions.

In order to determine ordering temperatures of Tb and Er magnetic moments, we have performed neutron diffraction on the Tb<sub>0.3</sub>Er<sub>0.7</sub>Ni<sub>5</sub> single crystal using E4 instrument. (100), (001), (101) and (002) reflections were recorded between 1.8 and 30K. The temperature dependence of the (100) reflection intensity, shown in Fig. 2, contains contribution resulting from the Er and Tb moments, while the (001) reflection (see Fig. 3) is governed by the Tb moments.

From Fig. 2, one can see that a magnetic ordering of Er moments occurs at  $T_2=7.2$  K, which is in good agreement with AC-susceptibility data.



**Fig. 2.:** The temperature dependence of the (100) reflection of the Tb<sub>0.3</sub>Er<sub>0.7</sub>Ni<sub>5</sub> single crystal.




**Fig. 3.:** The temperature dependence of the (001) reflection of the Tb<sub>0.3</sub>Er<sub>0.7</sub>Ni<sub>5</sub> single crystal.

On the contrary, Fig. 3 that presents the temperature dependency of the (001) magnetic reflection intensity, suggests that Tb magnetic moments order at  $T_1=7$  K. This is close to the  $T_2$  temperature and higher than temperature  $T_1^s$ , determined from AC-susceptibility measurements.

Thus, according to neutron diffraction, in the Tb<sub>0.3</sub>Er<sub>0.7</sub>Ni<sub>5</sub> single crystal the temperature of magnetic ordering of XY magnetic moments is close to transition temperature of Ising moments.

## References

- [1] S. Fishman, and A. Aharony, Phys. Rev. B **19** (1979) 3776.
- [2] A. Pirogov et al. Phys. Rev. B **79** (2009) 174412.

 <b>HELMHOLTZ ZENTRUM BERLIN</b> für Materialien und Energie  <b>NEUTRONS</b>	<b>EXPERIMENTAL REPORT</b>  <b>Structural and magnetic properties of</b> <b>Sr<sub>3</sub>Fe<sub>2</sub>O<sub>7-x</sub></b>	Proposal: PHY-01-2784-LT  Instrument: <b>E5</b>  Local Contact: M. Reehuis
	Principal Proposer: M. Reehuis, A. Maljuk, HZB J. Kim, B. Keimer, MPI Stuttgart Experimental Team: M. Reehuis, HZB	Date(s) of Experiment  20.08.2010 - 05.09.2010 16.09.2010 - 26.09.2010

Date of report: 26.10.2010

Complementarily to our neutron-powder diffraction study of Sr<sub>3</sub>Fe<sub>2</sub>O<sub>7-x</sub> (instrument E6) we have carried out single-crystal diffraction experiments on the 4-circle diffractometer E5. In order to investigate the crystal and magnetic structures of this material the neutron wavelengths  $\lambda = 0.89 \text{ \AA}$  (Cu-monochr.) and  $\lambda = 2.38 \text{ \AA}$  (PG-monochr.) were used. We have started to measure a high-quality single crystal of Sr<sub>3</sub>Fe<sub>2</sub>O<sub>7-x</sub> with the dimensions  $4 \times 6 \times 7 \text{ mm}^3$ . This sample was air-annealed, and  $x$  does not fully reach the saturation value  $x = 0$ . In a second step of this experiment we measured the same sample with a strongly reduced O-content (O3-atom) at the Wyckoff position 2a (0,0,0) of the space group  $I4/mmm$ . Therefore this crystal was annealed again under argon for 6 days reaching almost a stoichiometric sample of Sr<sub>3</sub>Fe<sub>2</sub>O<sub>6</sub>. For both samples no forbidden peaks ( $h+k+l = 2n+1$ ) could be observed indicating that the body centering is not violated.

For the air-annealed sample a full data set of 1548 (311 unique) reflections were collected at 10 K. The crystal structure could be successfully refined in the tetragonal space group  $I4/mmm$  resulting in very satisfactory residual  $R_F = 0.028$  ( $wR_F = 0.024$ ). In Table 1 the positional parameters as well as the occupancy of the O3-atom are compared with the values obtained from our neutron powder diffraction study. The refinements of the powder and the single-crystal data results in occupancies of the O3-site  $occ = 0.736(6)$  and  $occ = 0.675(10)$ , respectively. After the Ar-annealing process of the single crystal a large number of Bragg reflections showed a strong splitting. This only allowed us to use a reduced number of 648 (265 unique) observations for the structure refinements. Consequently we were not able to refine the structural parameters of this sample with such a good accuracy as obtained for the air-annealed one. However, the positional parameters of both Ar-annealed samples (the powder and the single-crystal) show a good agreement (Table 1). The O3-sites here only show populations of 2.7(5)% (pow) and 5.4(1.9)% (sk), respectively. Further, in Table 1 it can be seen that an increasing O-content of the O3-site leads to a strong elongation of the bond length  $d_{Fe-O3}$ . For stoichiometric Sr<sub>3</sub>Fe<sub>2</sub>O<sub>7</sub> the three bond lengths were found to be similar:  $d_{Fe-O1} = 1.927(1) \text{ \AA}$ ,  $d_{Fe-O2} = 1.936(4) \text{ \AA}$ ,  $d_{Fe-O3} = 1.958(2) \text{ \AA}$  [1].

For Ar-annealed powder and single-crystal the observed propagation vector is  $\mathbf{k} = (\frac{1}{2}, \frac{1}{2}, 0)$ . Fig. 1 shows that the magnetic intensity of the strong peak  $(\frac{1}{2}, \frac{1}{2}, 3)_M$  disappears at the Néel temperature  $T_N = 367(6) \text{ K}$ . During the powder experiment this magnetic reflection was only measured up to 296 K. But it is interesting to see that the ratios  $F_M^2(2 \text{ K}) / F_M^2(296 \text{ K})$  determined for the powder and the single-crystal are 2.3 and 2.7, respectively. This indicates that the magnetic transition of the powder sample sets in at a similar temperature. But it

has to be mentioned that and increasing O-content probably change  $T_N$ . For the air-annealed single-crystal relatively weak magnetic intensities were found for reflections, which can be generated with the propagation vector  $\mathbf{k} = (\frac{1}{4}, 0, 0)$ . The magnetic intensity disappears at about 110 K. But these reflections show a strong broadening, that may indicate the presence of short-range order. For the air-annealed powder, where the O-content is slightly higher, the magnetic peaks were observed to be stronger. Possibly a full long-range order sets in for Sr<sub>3</sub>Fe<sub>2</sub>O<sub>7-x</sub> with increasing O-content reaching an  $x$ -value closer to zero.

Table 1. Results of the crystal structure refinements of Sr<sub>3</sub>Fe<sub>2</sub>O<sub>7-x</sub> as determined from powder (pow) and single-crystal (sk) diffraction. The O-deficiencies of O3 and the refineable z-parameters of the different atoms are listed. Sr1 and Sr2 are located at the position 2b(0,0, $\frac{1}{2}$ ) and 4e (0,0,z), respectively. At the position 4e one also finds the atoms Fe1 and O2, while O1 and O3 are located at 8g (0, $\frac{1}{2}$ ,z) and 2a (0,0,0), respectively.

Atom	Sr <sub>3</sub> Fe <sub>2</sub> O <sub>7-x</sub> (Ar-annealed)		Sr <sub>3</sub> Fe <sub>2</sub> O <sub>7-x</sub> (air-annealed)	
	z K, pow	z K, sk	z K, pow	z K, sk
Sr1	$\frac{1}{2}$	$\frac{1}{2}$	$\frac{1}{2}$	$\frac{1}{2}$
Sr2	0.31893(8)	0.31886(12)	0.31678(15)	0.31741(4)
Fe	0.10214(6)	0.10192(8)	0.09825(15)	0.09883(3)
O1	0.08479(7)	0.08486(10)	0.09271(14)	0.09173(3)
O2	0.19677(13)	0.19641(15)	0.1939(2)	0.19414(5)
O3	0	0	0	0
$x(O3)$	0.973(5)	0.946(19)	0.264(6)	0.325(10)
$d_{Fe-O1}$	1.9529(3)	1.9519(4)	1.9202(3)	1.9223(1)
$d_{Fe-O2}$	1.875(3)	1.872(3)	1.918(6)	1.9111(12)
$d_{Fe-O3}$	2.0240(12)	2.0196(16)	1.970(3)	1.9817(6)

$a = 3.84481(11)$ ,  $c = 19.8158(7)$  (Ar-annealed)

$a = 3.83403(16)$ ,  $c = 20.0509(10)$  (air-annealed)

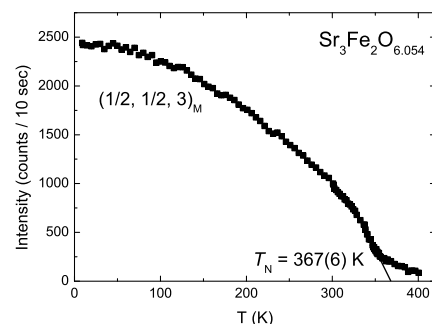



Fig. 1. Temperature dependence of the magnetic reflection  $(\frac{1}{2}, \frac{1}{2}, 3)_M$  Sr<sub>3</sub>Fe<sub>2</sub>O<sub>6.054</sub>.

#### Reference

[1] S.E. Dann, M.T. Weller, D.B. Currie, J. Solid State Chem. **97** (1992) 179.

EXPERIMENTAL REPORT		Proposal: PHY-01-2786-EF
 <b>HELMHOLTZ ZENTRUM BERLIN</b> für Materialien und Energie  <b>NEUTRONS</b>	<b>Magnetic structure determination of the pseudo-triangular antiferromagnet alpha- CaCr<sub>2</sub>O<sub>4</sub></b>	Instrument: <b>E5</b>
		Local Contact: Manfred Reehuis
Principal Proposer: Experimental Team:	Bella Lake, HZB Sandor Toth, HZB Simon Kimber, HZB Dimitri Argyriou, HZB Oliver Pieper, HZB Nazmul Islam, HZB	Date(s) of Experiment  26.01.2010 - 31.01.2010

Date of report: 17.02.2011

Alpha-CaCr<sub>2</sub>O<sub>4</sub> is a frustrated triangular lattice antiferromagnet. The crystal structure is orthorhombic *Pmmn* at room temperature [1]. The slightly distorted triangular layers of magnetic Cr<sup>3+</sup> ions are stacked along the **a** axis. Below  $T_N=43$  K magnetic order develops as revealed by neutron powder diffraction. Although powder diffraction would enable us to refine the magnetic structure, due to data resolution problems, several possible models fit equally well. The ordering wavevector is (0,0.333(5),0) and the angle between neighbouring magnetic moments in the triangular plane is  $\sim 120^\circ$ . The planes are stacked antiferromagnetically. The powder diffraction revealed that the magnetic structure is helical, although the plane of the moments could not be determined exactly. We performed neutron single-crystal diffraction on a large (340 mg) sample using E5 four-circle single-crystal diffractometer to determine unambiguously the low temperature magnetic structure of alpha-CaCr<sub>2</sub>O<sub>4</sub>. A pyrolytic graphite monochromator selected an incident wavelength of  $\lambda=2.36$  Å. A total of 616 magnetic and 423 nuclear Bragg reflections were collected at 6 K for a total counting time of five minutes each. The Racer program was used to integrate the reflections. FullProf software was used to refine the magnetic structure. Our single crystal sample is twinned. Since the three-fold symmetry of the triangular planes is weakly distorted, three structural twins can exist rotated with respect to each other by  $60^\circ$  in the **bc** plane, while sharing the out-of-plane **a** axis. The volume ratio of the twins could be determined from the ratio of non-overlapping nuclear reflections and they turned out to be non-equal, see Table I.

Twin 1	Twin 2 (+60°)	Twin 3 (+120°)
64(2)%	19(2)%	17(3)%

**Table I. Twinning ratio of alpha-CaCr<sub>2</sub>O<sub>4</sub> sample.**

The magnetic structure were refined assuming three different configurations. Spins were restricted to the **ab**, **bc** or **ac** plane.

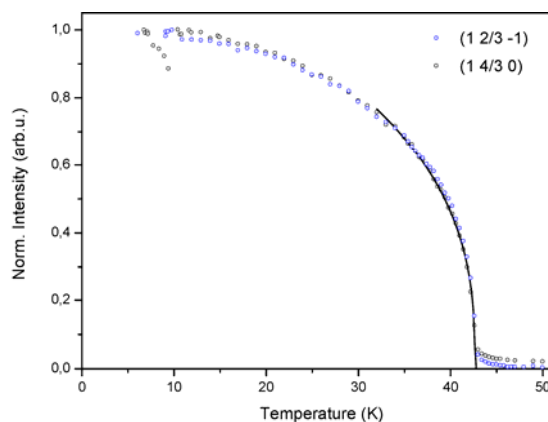
The two best fits are shown in Table II.

	<b>ab</b>	<b>ac</b>
$m_x$	2.34(3)	2.26(2)
$m_y$	2.78(4)	-
$m_z$	-	2.97(3)
$R_F$	0.338	0.321

**Table II Best solutions for the magnetic structure. All moments are in units of  $\mu_B$ .**

The quality of the fit is given by the  $R_F$ -factor values:  $R_F = \frac{\sum |F_{OBS} - F_{CALC}|}{\sum |F_{OBS}|}$ , where  $F_{OBS}$  and  $F_{CALC}$  are the observed and calculated structure factors.

The temperature dependence of two magnetic peaks (1,2/3,-1) and (1,4/3,0) were measured in the temperature range  $6 \leq T \leq 50$  K, see Fig. 1.



**Fig. 1 Temperature dependence of (1,2/3,-1) and (1,4/3,0) magnetic Bragg peaks.**

The intensity is proportional to the square of the magnetisation which is the magnetic order parameter and can be fitted with  $I(T) = C((T - T_N)/T_N)^{2\beta}$ , where  $C$  is an overall constant and  $\beta$  is the critical exponent. The data were fitted between 32 K and 48 K and gave a transition temperature of  $T_N = 42.6(1)$  K and the exponent is  $\beta = 0.1815(9)$  for both peaks. Although the function fits well, according to the theory the phase transition is first order and the value of  $\beta$  is not universal [2].

[1] H. Pausch *et al.*, Z. Anorg. Allg. Chem. **405**, 113 (1974)

[2] V. T. Ngo *et al.*, Phys. Rev. E **78**, 031119 (2008)

***T*-dependence of the magnetic structure of YbVO<sub>3</sub>**

Proposal: PHY-01-2789

Instrument: **E5**

Local Contact:  
M. Reehuis

Principal Proposer: C. Ulrich, ANSTO, Menai, Australia  
M. Reehuis, HZB, Berlin  
B. Keimer, MPI Stuttgart  
J. Fujioka, S. Miyasaka, Y. Tokura – Department of Applied Physics, University of Tokyo, JP

Experimental Team: M. Reehuis, HZB, Berlin

Date(s) of Experiment

08.02.2010 – 20.02.2010

Date of report: 21.04.2010

In the present single-crystal neutron diffraction study we have measured the  $T$ -dependence of magnetic reflections of YbVO<sub>3</sub> on the E5-instrument using the neutron wavelength  $\lambda = 2.38$  Å. For the experiment we have used a cylindrical single crystal of this compound with the dimensions  $d = 3$  mm and  $h = 6$  mm. The structural and magnetic properties of the electrically insulating perovskite CeVO<sub>3</sub> were investigated earlier by single-crystal neutron diffraction [1]. A structural phase transition sets in at  $T_S = 136$  K from an orthorhombic ( $Pbnm$ ) to a monoclinic structure ( $P2_1/b$ ). At  $T_N = 124$  K the magnetic moments of the V-atoms show a pure antiferromagnetic  $C$ -type ordering in the  $ab$ -plane. For YbVO<sub>3</sub> these transitions could be observed from specific heat measurements at  $T_S = 170$  K and  $T_N = 100$  K, respectively [2]. Our neutron-diffraction study of this compound showed that the magnetic transition sets in at  $T_N = 102$  K. Earlier studies showed that the ionic radii of the rare-earth ions  $R^{3+}$  strongly influence the structural and magnetic properties of the vanadates [2-4]. For  $RVO_3$  ( $R = Y, Dy, Ho, Er, Tm, Yb, Lu$ ), where the ionic radii of the  $R^{3+}$ -ions are smaller than  $r(Tb^{3+})$ , a second structural phase transition could be observed. At  $T_{S2}$  the monoclinic phase changes again to the orthorhombic structure with the space group  $Pbnm$ . In the present study of YbVO<sub>3</sub> this second transition could be clearly detected. In Fig. 1 it can be seen that a hysteresis occurs at  $T_{S2}$ . With increasing and decreasing temperature the transition sets in at 63.5(3) K and 60.5(3) K, respectively. The appearance of magnetic intensity below  $T_N$  at the position of the reflections 100, 010, 102 and 012 clearly suggests a  $C$ -type ordering in the  $ab$ -plane. Between  $T_{S2}$  and  $T_N$  weak magnetic intensity could be observed for the 011, indicating an additional  $G$ -type ordering along the  $c$ -axis. The same behavior was found earlier for YVO<sub>3</sub> [3, 4]. Thus, it could be confirmed that a  $G_z$ -component only exists for the vanadates containing smaller  $R^{3+}$ -ions. Below  $T_{S2}$  the antiferromagnetically ordered V-moments induce a progressive magnetic polarization of the Yb-sublattice. It was interesting to see that this polarization was much stronger pronounced in CeVO<sub>3</sub> [1]. In this vanadate the purely  $C$ -type ordered V-moments induces a magnetic ordering with the basis functions  $F_x C_y$  and  $C_x F_y$ . In the present study of YbVO<sub>3</sub> we observed at low temperature magnetic intensity on the 100, 102 and 012, but not on the 010, suggesting that only the  $C_y$ -component is induced. A weak magnetic intensity observed on the 020 indicated the presence of a ferromagnetic  $F_x$ -component. The observation of the modes  $F_x$  and  $C_y$  is surprising, since the vanadium sublattice is purely  $G$ -type ordered along the  $c$ -axis. However, weak changes of magnetic intensities could

also be observed for the reflections 011 and 101 indicating the presence of an additionally induced  $G_z$ -component.

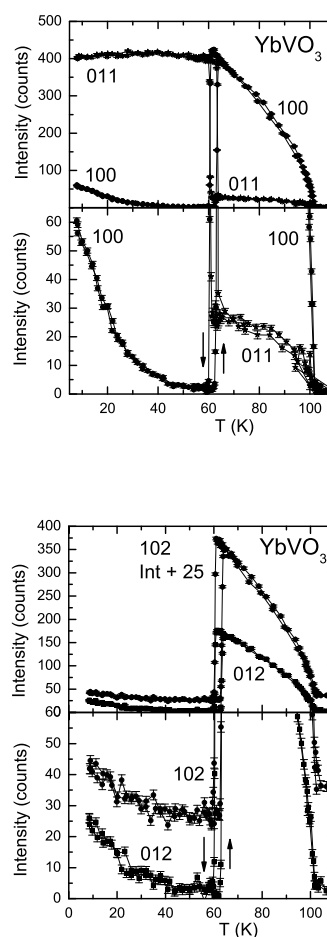



Fig 1.  $T$ -dependence of magnetic Bragg intensities of the reflections 100, 102 and 012 of YbVO<sub>3</sub>.

**References**

- [1] M. Reehuis, C. Ulrich, P. Pattison, M. Miyasaka, Y. Tokura, B. Keimer, Eur. Phys. J. B. **64** (2008) 27.
- [2] S. Miyasaka, Y. Okimoto, M. Iwama, Y. Tokura, Phys. Rev. B. **68** (2003) 100406(R).
- [3] C. Ulrich, G. Khaliullin, J. Sirker, M. Reehuis, M. Ohl, M. Miyasaka, Y. Tokura, B. Keimer, Phys. Rev. Lett. **91** (2003) 257202.
- [4] M. Reehuis, C. Ulrich, P. Pattison, B. Ouladdiaf, M.C. Rheinstädter, M. Ohl, L.P. Regnault, M.2 Miyasaka, Y. Tokura, B. Keimer, Phys. Rev. B. **73** (2006) 094440.

 <b>NEUTRONS</b>	<b>EXPERIMENTAL REPORT</b>	Proposal: PHY-01-2791
	<b>Magnetic structure of magnetoelectric hexaferrites under low field: planar or conical?</b>	Instrument: <b>E5</b> Local Contact: M. Reehuis
Principal Proposer: Experimental Team:	Jae-Ho Chung, Korea University, Seoul, KR Hakbong Lee, Korea University, Seoul, KR Manfred Reehuis, HZB	Date(s) of Experiment  28.04.2010 – 16.05.2010

Date of report: 13.08.2010

In this proposal experiment, we have measured the low-temperature spin structure of the magnetoelectric hexaferrite  $\text{Ba}_{0.5}\text{Sr}_{1.5}\text{Zn}_{22}(\text{Fe}_{1-x}\text{Al}_x)_{12}\text{O}_{22}$  ( $x = 0.08$ ), and its temperature dependence using the E5 four-circle diffractometer. The purpose of the experiment was to verify the existence of the incommensurate longitudinal spin cones proposed for this material, which will then be used for studying the field dependent changes of the magnetic structure.

It is notable that this material is prone to forming stacking-fault-like twins. In such cases, the quantitative analysis of nuclear/magnetic structure becomes all but impossible. We obtained several high quality crystals, some of which are virtually twin-free. Although some measurements were done with a crystal containing twins, the Rietveld refinement was carried out using the data obtained from a twin-free crystal only.

The magnetic order parameters were observed by performing momentum scans along  $Q = (0,0,l)$  and  $(1,0,l)$  at several temperatures, which is summarised in Figure 1. It showed that there are multiple magnetic transitions over the wide temperature ranges. Below 180 K, we observed the incommensurate magnetic ordering wave vectors,  $k_1 = (0,0,\delta)$ , that change substantially as a function of temperature. The changes occurred mostly within 80 - 180 K, below which they remained virtually constant. The scans along  $(1,0,l)$  revealed that there are two different additional commensurate magnetic ordering wave vectors for the two temperature ranges, respectively. The additional magnetic intensities were observed at  $k_2 = (0,0,3/2)$  for 80 - 180 K, whereas the intensity of the nuclear Bragg peaks were enhanced below 80 K indicating  $k_0 = (0,0,0)$ . The combination of the two ordering wave vectors at the lowest temperature range ( $k_1$  &  $k_0$ ) is consistent with the longitudinal conical structure expected for

this material. In contrast, the other combination for 80 - 180 K ( $k_1$  &  $k_2$ ) indicates that the longitudinal cones evolve into “alternating” longitudinal cones along the  $c$ -axis. Both magnetic structures are capable of creating the magnetoelectric polarization as reported by previous works.

We have already performed the Rietveld refinement of the magnetic structure at 10 K using the obtained data. It revealed that the magnetic structure indeed conforms to the longitudinal cones, in which the rotating spiral component lie in the plane and the axial component is perpendicular to it.

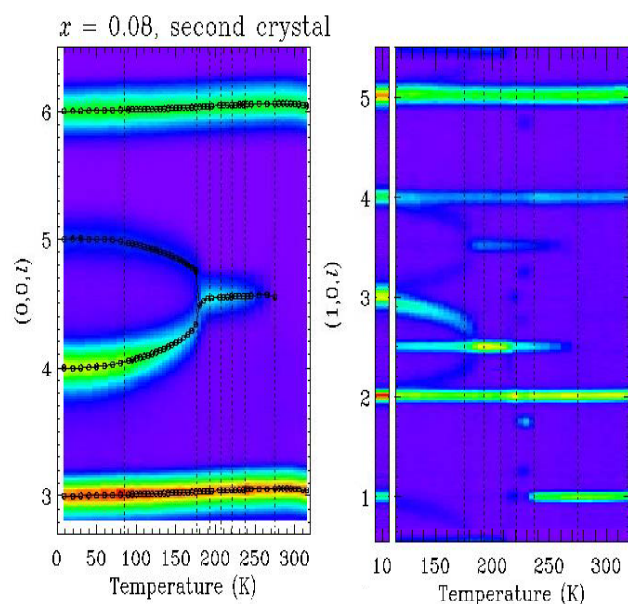



Fig. 1: Summary of the temperature dependence of the order parameter for  $x = 0.08$ . The left and the right panels are measured for  $(0,0,l)$  and  $(1,0,l)$ , respectively.

	<b>EXPERIMENTAL REPORT</b> <b>Investigating the magnetic unit cell doubling in room temperature semiconductor LiMnAs</b>	Proposal: MAT-01-2897 Instrument: <b>E5</b> Local Contact: M. Reehuis
	Principal Proposer: Xavier Marti, CU Prague, CZ Experimental Team: Vaclav Holy, CU Prague, CZ Vit Novak, Academy of Sciences of the Czech Republic Tomas Jungwirth, Academy of Sciences of the Czech Republic Manfred Reehuis, HZB Berlin	Date(s) of Experiment 27.08.2010 – 28.09.2010

Date of report: 10.10.2010

Semiconductors have undoubtedly triggered the technological progress in the past decades. Spintronics has more recently appeared and also strongly contributed. Efforts to synergize both disciplines have been carried out in the past decade based on the pursue for room temperature ferromagnetic semiconductors compatible with the common industrial growth methodologies, but the record magnetic ordering temperature is still well below the room temperature. Although they were mentioned even before the well known III-V compounds (GaAs, InAs, ...), the I-II-V (LiMnAs, for instance) semiconductors have remained unexplored and thin films of these materials have never been grown before. Beyond its semiconducting nature, the most appealing and surprising fact is that I-II-V metallic alloys were reported earlier by Bronger et al. that LiMnAs to be antiferromagnetic [1], but the connection between the concepts "semiconductor" and "antiferromagnet" at room temperature was not settled. Notice that spintronics needs both either ferromagnets or antiferromagnets.

We have recently prepared these films of LiMnAs by MBE growth on standard InAs(001) substrates and demonstrated its semiconducting nature. It remained to be confirmed that the room temperature antiferromagnetic behaviour was persistent in the films.

To this end we decided to carry out the somewhat uncertain experiment of measuring thin films (500 nm thick) by neutron diffraction in reflection geometry. For the experiment we used a PG-monochromator selecting the neutron wavelength  $\lambda = 2.38 \text{ \AA}$ . Our aim was to evidence magnetic intensity on the position of the structurally forbidden reflections (100) and (10<sub>1/2</sub>) of the space group *P4/nmm*. However after almost two days of measurements it was not possible to detect magnetic intensity of the LiMnAs-films under the present conditions. We have prepared a list of possible enhancements to

increase the intensity of the magnetic reflections around 200 times more. We list here the most relevant ones to be applied in the next round of experiments:

- Substitution of the InAs(001) wafer substrates for In-free substrates, such us GaAs. The structural peaks from the substrate counted around 1000 counts on top of the background. Taking into account that there are 2-3 orders of magnitude more substrate than sample in typical conditions we could not expect a measurable signal from the films, most probably due to the high In absorption.

- Polishing mechanically the substrates down to the limit of about 100 microns and stack up a series of 10-20 samples with area of 1 cm<sup>2</sup>. This can be done easily as the wafers pulled out display are typically several cm diameter.


- Improve the alignment of the stacks of samples and crosscheck it by standard X-ray diffraction in reflection geometry on one of the sides of the stack. We could detect a sizable spread of 1 degree in the reflections stemming from the InAs substrate which we used for creation of the UB matrix.

*This research project has been supported by the European Commission under the 7<sup>th</sup> Framework Programme through the Key Action: Strengthening the European Research Infrastructures. Contract n°: CP-CSA\_INFRA-2008-1.1.1 Number 226507-NMI3*

#### Reference

[1] Bronger W., Muller P., Hoppner R., Schuster H.U., Z. anorg. allg. Chem. **539** 176 (1986)



 <b>HELMHOLTZ ZENTRUM BERLIN</b> für Materialien und Energie  <b>NEUTRONS</b>	<b>EXPERIMENTAL REPORT</b>  <b>Structural properties of YbVO<sub>3</sub></b>	Proposal: PHY-01-2899  Instrument: <b>E5</b>  Local Contact: M. Reehuis
	Principal Proposer: C. Ulrich, ANSTO, AU; M. Reehuis, HZB; B. Keimer, MPI Stuttgart J. Fujioka, S. Miyasaka, Y. Tokura – Univ. Tokyo, JP  Experimental Team: M. Reehuis, HZB	Date(s) of Experiment  08.03.2010 – 16.03.2010 19.03.2010 – 01.04.2010

Date of report: 28.12.2010

In the second part of our single-crystal neutron diffraction study we have investigated the structural properties of YbVO<sub>3</sub> on the 4-circle diffractometer E5. For the experiment we have used a cylindrical single crystal of this compound with the dimensions  $d = 3$  mm and  $h = 6$  mm. In order to determine the structural phase transitions we have measured the  $T$ -dependence of purely nuclear reflections of YbVO<sub>3</sub> using the neutron wavelength  $\lambda = 2.38$  Å. Specific heat and magnetization measurements already showed that structural phase transitions set in at  $T_{S1} = 60$  K and  $T_{S2} = 170$  K [1]. Between these temperatures YbVO<sub>3</sub> crystallizes in a monoclinic structure with the space group  $P2_1/b$ , while below  $T_{S1}$  and above  $T_{S2}$  in an orthorhombic structure with  $Pbnm$ . The  $T$ -dependence of the reflections (110) and (202) clearly showed that  $T_{S1}$  sets in at 63.5(3) K and 60.5(3) K with increasing and decreasing temperature. A much stronger hysteresis could be found only recently for the vanadates DyVO<sub>3</sub> and HoVO<sub>3</sub> [2]. The second transition at  $T_{S2}$  is not so strongly pronounced. From  $T_{S1}$  the intensity of the (202) is continuously decreasing up to  $T_{S2}$ . Above this temperature its intensity seems to be unchanged.

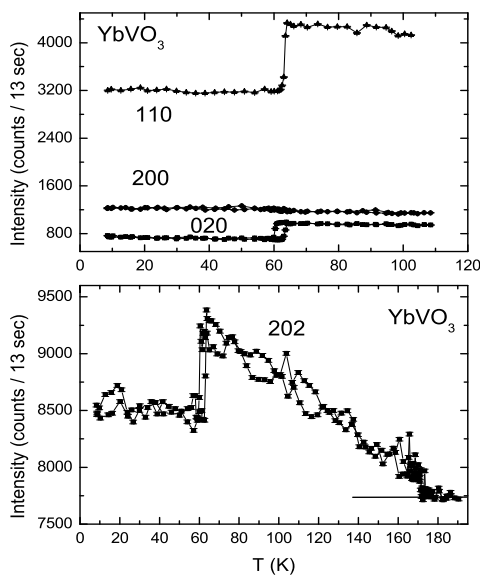


Fig 1.  $T$ -dependence of magnetic Bragg intensities of the reflections 110, 200, 020 and 202 of YbVO<sub>3</sub>.

In order to investigate the orthorhombic crystal structures of YbVO<sub>3</sub> we have collected full data sets at 8 K and 295

K using the shorter neutron wavelength  $\lambda = 0.89$  Å. The results of the refinements are summarized in Table 1.

Table 1. Positional parameters of YbVO<sub>3</sub> as determined from the data sets collected at 8 K and 295 K.

8 K:  $a = 5.2337(5)$  Å,  $b = 5.5618(6)$  Å,  $c = 7.5088(8)$  Å

$Pbnm$	site	$x$	$y$	$z$
Yb	4c	0.97721(6)	0.07248(6)	$\frac{1}{4}$
V	4b	$\frac{1}{2}$	0	0
O1	4c	0.11794(14)	0.45552(13)	$\frac{1}{4}$
O2	8d	0.68396(10)	0.30277(8)	0.05974(6)

$R_F = 0.036$ , 654 (unique) reflections

295 K:  $a = 5.2352(6)$  Å,  $b = 5.5926(7)$  Å,  $c = 7.5537(9)$  Å

$Pbnm$	site	$x$	$y$	$z$
Yb	4c	0.97970(7)	0.07099(7)	$\frac{1}{4}$
V	4b	$\frac{1}{2}$	0	0
O1	4c	0.11775(15)	0.45488(16)	$\frac{1}{4}$
O2	8d	0.68884(9)	0.30509(9)	0.05953(9)

$R_F = 0.038$ , 662 (unique) reflections

From the data set collected at 295 K we have determined the occupancies of the Yb and O-atoms. Due the weak scattering powder of the V-atoms the occupancy of the site 4b could not be determined with good accuracy. However the values  $occ(Yb) = 1.003(6)$ ,  $occ(O1) = 1.004(10)$  and  $occ(O2) = 0.994(7)$  show that the O-positions do not show any significant deficiencies. Further we have determined the interatomic distances between the V- and O-atoms in the VO<sub>6</sub>-octahedra. At 290 K the distances are slightly influenced by the ionic-size effect:  $d_{V-O1} = 2.0023(4)$  Å,  $d_{V-O21} = 2.0110(6)$  Å,  $d_{V-O22} = 2.0226(6)$  Å. At 8 K the *Jahn-Teller*-effect is strongly active. Therefore the bond between V and O21 is strongly elongated [ $d_{V-O21} = 2.0348(5)$  Å], whereas for the other two bonds [ $d_{V-O1} = 1.9915(3)$  Å,  $d_{V-O22} = 1.9909(5)$  Å] the values were found to be practically the same. The same tendency was found recently for YVO<sub>3</sub> [3].

#### References

- [1] S. Miyasaka, Y. Okimoto, M. Iwama, Y. Tokura, Phys. Rev. B. **68** (2003) 100406(R).
- [2] M. Reehuis, C. Ulrich, K. Prokeš, S. Matáš, J. Fujioka, S. Miyasaka, Y. Tokura, B. Keimer, Phys. Rev. B. (in print).
- [3] M. Reehuis, C. Ulrich, P. Pattison, B. Ouladdiaf, M.C. Rheinstädter, M. Ohl, L.P. Regnault, M.2 Miyasaka, Y. Tokura, B. Keimer, Phys. Rev. B. **73** (2006) 094440.

Principal Proposer: Bensch, Wolfgang, CAU Kiel  
 Experimental Team: Arulraj, Anthony, IGCAR Kalpakkam, India  
 Ophey, Jannes, CAU Kiel  
 Dietl, Bastian, CAU Kiel

Date(s) of Experiment  
 17.07.2007-21.07.2007

Date of report: 13.12.2010

While other chromium tellurides are well characterized, there is only little known about the tellurium richest compound  $\text{CrTe}_3$ .<sup>[1,2,3]</sup> The magnetic behaviour was studied with temperature and field dependent measurements, but could not be fully understood. In the experiment the magnetic structure of  $\text{CrTe}_3$  should be investigated. Diffraction patterns were measured at different temperatures and applying different external magnetic fields.

Diffraction pattern were also measured without an external magnetic field at 2, 160, 200, 230, and 280 K. Rietveld refinements were performed showing a pronounced anisotropic contraction of the lattice parameters. The temperature evolution of the cell parameters could be fitted with a 4<sup>th</sup> order polynomial (Fig. 2). Further investigations are under way to explain the unusual magnetic behaviour which may be strongly related with the anisotropic changes of the lattice parameters.

The diffraction patterns obtained at 2, 160, and 170 K with different magnetic fields ( $H = 0, 1,$  and  $4 \text{ T}$ ) exhibit no significant differences (Fig. 1). Hence a long range magnetic behaviour can be excluded.

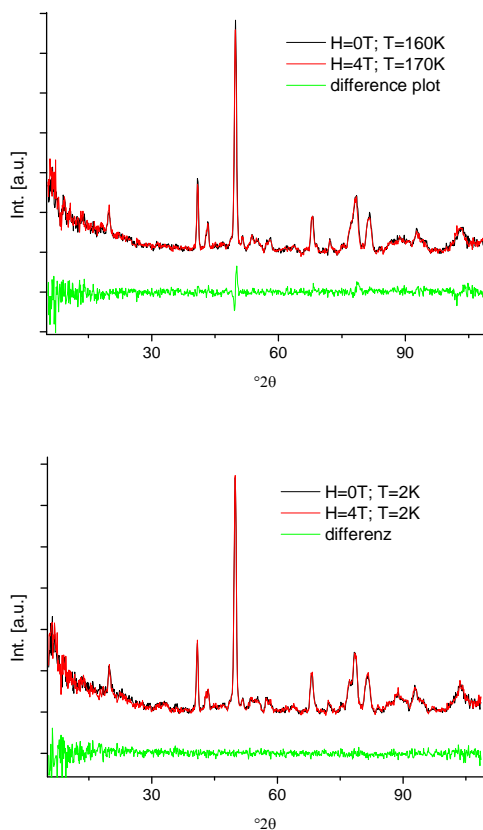


Fig. 1: Examples of diffraction patterns collected at different temperatures/magnetic fields.

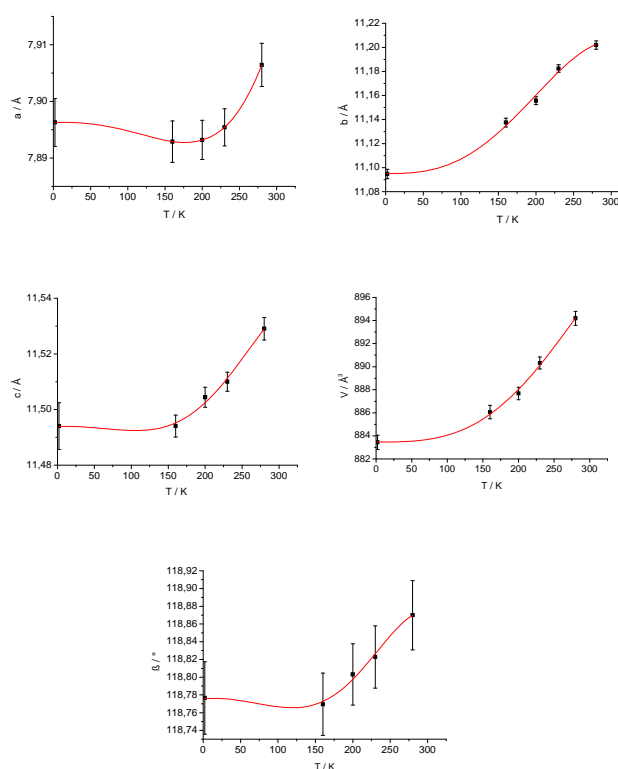



Fig.2: Evolution of the cell parameters.

[1] K. O. Ipser, H. Klepp, *Monatshefte für Chemie* 1979, 110, 499-9501.

[2] K. O. Ipser, H. Klepp, *Angew. Chem.* 1982, 94, 931-932.

[3] J. Rouxell et al., *J. Solid State Chem.* 1998, 96, 169-180.

 <b>NEUTRONS</b>	<b>EXPERIMENTAL REPORT</b>	Proposal: PHY-01-2511
	<b>Determination of magnetic structure of NpPdSn</b>	Instrument: <b>E6</b> Local Contact: T.Hoffman, K.Prokes
Principal Proposer:	K. Gofryk and R. Caciuffo, ITU Karlsruhe and LANL, USA	Date(s) of Experiment
Experimental Team:	J.-Ch. Griveau, ITU Karlsruhe K.Prokes, D. Wallacher, S. Gerischer, T. Hoffman, N. Grimm, HZB	29.09.2010 - 02.10.2010

Date of report: 31.01.2011

A new compound NpPdSn adopting ZrNiAl-type structure was prepared and studied up to now by means of x-ray diffraction and magnetic bulk measurements. NpPdSn orders antiferromagnetically at 19 K and exhibits a Curie-Weiss behaviour with  $\mu_{\text{eff}} = 2.66 \mu_B$  and  $\theta_P = -47$  K. Bulk properties show temperature variations similar to systems with strong electronic correlations with a large negative paramagnetic Curie temperature and an enhanced low-temperature specific heat ( $\gamma \sim 90$  mJ/mol.K<sup>2</sup>). It suggests that NpPdSn may be classified as a new Np-based antiferromagnetic Kondo lattice.

To be able to place NpPdSn in the context of other magnetically ordered Np-containing and AnPdSn (An – 5f element) compounds and to draw



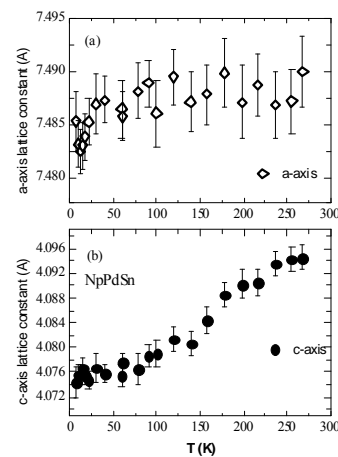
**Fig. 1:** Radiogram of the sample enclosed inside the double-wall certified Al-capsule developed by ITU.

connection between the bulk magnetic properties and the microscopic arrangement of magnetic moments in this system we have suggested to perform neutron powder diffraction experiment using E6 and a specially developed environment that monitors constantly the integrity of the capsule containing the sample (Fig. 1).

Besides the alpha radiation also the pressure and flow inside the closed circuit were monitored and if found outside specified range, alarms in the form of SMS messages was sent. Whether the software works properly, was monitored and reported in the same manner as well. All the system was working well proving that such a type of experiment is at HZB feasible.

During the experiment we have collected two kinds of diffraction patterns. One type, with lower statistics, was during cooling and heating, leading to


the temperature dependencies of the lattice parameters and the other, with high statistics, were collected at two different temperatures to be able to detect magnetic signal.



**Fig. 2:** The temperature dependence of the NpPdSn lattice parameters.

During slow cooling and heating (to avoid thermal shocks and thus minimize the risk of integrity of the sample container) we have collected patterns with the aim to determine the temperature dependence of the lattice constants. Resulting dependencies are shown in Fig. 2. At 30 K, i.e. above the proposed magnetic phase transition temperature and at 5.5-6 K, i.e. well below  $T_N$ , we have collected diffraction patterns for  $\sim 24$  hours each with the aim to detect the magnetic signal. Although such a method lead normally to sensitivity that is enough to detect magnetic moments of the order of  $0.2 \mu_B$  (if leading to magnetic Bragg reflections at positions that do not coincide with the nuclear ones), we were unable to detect any signal that would be of magnetic origin. From the pattern obtained at 30 K, we were able to determine the basic structural parameters.

We can conclude that the experiment, although rather demanding for the preparation and human and technical resources, is feasible and no major difficulties were met. Unfortunately, the determination of the AF structure was not successful, most probably due to high absorption of the Np.

 <b>HELMHOLTZ ZENTRUM BERLIN</b> für Materialien und Energie  <b>NEUTRONS</b>	<b>EXPERIMENTAL REPORT</b>	Proposal: PHY-01-2629
	<b>Evolution of the magnetic structure of YbCo<sub>2</sub>Si<sub>2</sub> in magnetic field</b>	Instrument: <b>E6</b> Local Contact: Andreas Hoser
Principal Proposer: Experimental Team:	Nandang Mufti, Max-Planck-Institut CPfS Dresden Nandang Mufti, Max-Planck-Institut CPfS Dresden Oliver Stockert, Max-Planck-Institut CPfS Dresden Andreas Hoser, HZB	Date(s) of Experiment 20.01.2010 – 25.01.2010

Date of report: 26.02.2010

We recently carried out powder neutron diffraction on YbCo<sub>2</sub>Si<sub>2</sub> using the diffractometer E2 at BENSC [1]. We found out that the magnetic structure of this compound is commensurate with a propagation vector  $k_1 = (\frac{1}{4}, \frac{1}{4}, 1)$  at lowest temperature below  $T_L = 0.9$  K and becomes incommensurate with a propagation vector  $k_2 = (\frac{1}{4}, 0.08, 1)$  at intermediate temperatures between  $T_L$  and  $T_N = 1.7$  K. Moreover, the field dependence in the powder sample indicate that the propagation vector in both phases does not change under magnetic field. The aim of the present experiment was to study the evolution of the magnetic structure of a YbCo<sub>2</sub>Si<sub>2</sub> single crystal with the magnetic fields.

The measurements on E6 were performed on a YbCo<sub>2</sub>Si<sub>2</sub> single crystal of approximate dimensions  $5 \times 4 \times 0.5$  mm<sup>3</sup> ( $m \approx 60$  mg). The sample was mounted on a <sup>3</sup>He insert inside a vertical magnet and allowed measurements in the temperature range between 0.27 and 3 K and in magnetic fields up to 4 T. The magnetic field was applied along the  $[1, -1, 0]$  crystallographic direction.

In figure 1(a) we plot the magnetic field dependence of the integrated intensity of the  $(\frac{1}{4}, \frac{1}{4}, 3)$  magnetic reflection at lowest temperature  $T = 0.27$  K. In measurements up to  $B = 2$  T we observed no change in the peak position indicating that the propagation vector remains unchanged in magnetic field along  $[1, -1, 0]$ . However, the integrated intensity dramatically increases at  $B = 0.5$  T which is the transition from AFM II to AFM IV in the  $B$ - $T$  phase diagram of YbCo<sub>2</sub>Si<sub>2</sub> for  $B//[110]$  [2]. In line with bulk measurements the magnetic intensity vanishes at  $B \approx 1.8$  T. In the intermediate phase at  $T = 1.1$  K the measurements revealed two magnetic reflections in the 2D detector which can be identified as the  $(\frac{1}{4}, 0.08, 3)$  and  $(\frac{1}{4}, -0.08, 3)$  peaks. When magnetic field is applied, we find an increase of the intensity of the  $(\frac{1}{4}, 0.08, 3)$  reflection while simultaneously the intensity of the  $(\frac{1}{4}, -0.08, 3)$  reflection

decreases. This happens at  $B \approx 0.7$  T which is a transition from AFM I to AFM III in the  $B$ - $T$  phase diagram of YbCo<sub>2</sub>Si<sub>2</sub> for  $B//[110]$  [2]. This phenomenon can be understood in terms of a domain population effect. It is also suggested that this mechanism is active in the ground state. To further corroborate the domain population as origin for the observed magnetic transitions, it is highly desired to study the evolution of the magnetic structure in YbCo<sub>2</sub>Si<sub>2</sub> for  $B//[100]$  and  $[001]$  in future experiments.

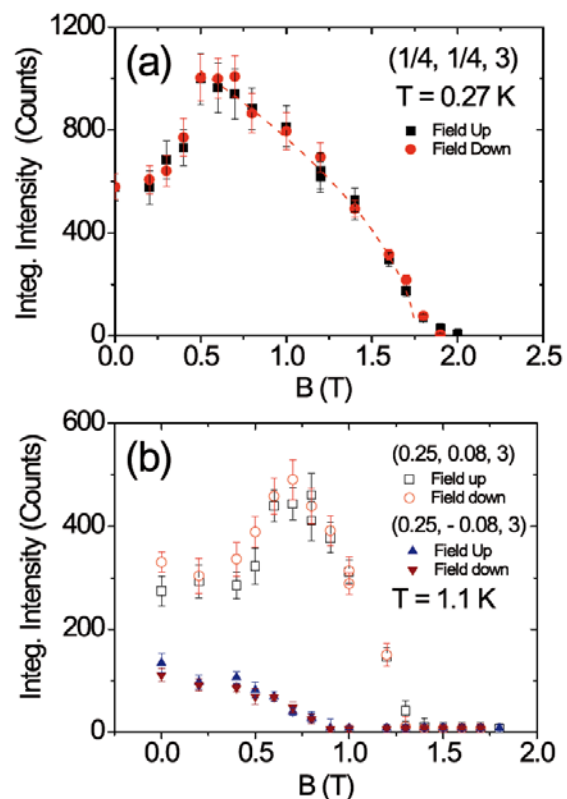



Figure 1 Magnetic field dependence of the integrated intensity of (a)  $(\frac{1}{4}, \frac{1}{4}, 3)$  in the ground state ( $T = 0.27$  K) and (b)  $(\frac{1}{4}, \pm 0.08, 3)$  in the intermediate phase ( $T = 1.1$  K).

1. N. Mufti, et al. BENSC experiment PHY-01-2626.
2. N. Mufti et al., phys. stat. sol. b **247**, 743 (2010).

 <b>HELMHOLTZ ZENTRUM BERLIN</b> für Materialien und Energie  <b>NEUTRONS</b>	<b>EXPERIMENTAL REPORT</b>	Proposal: PHY-01-2758-EF  Instrument: <b>E6</b>  Local Contact: Andreas Hoser
	<b>Magnetic phase transitions in NdIr<sub>2</sub>Si<sub>2</sub></b>	Date(s) of Experiment  17.02.2010 – 20.02.2010
Principal Proposer: M. Mihalik, HZB Experimental Team: A. Hoser, HZB		

Date of report: 01.03.2010

The NdIr<sub>2</sub>Si<sub>2</sub> compound belongs to the family of polymorphic compounds, which can adopt both, ThCr<sub>2</sub>Si<sub>2</sub>- ( $\alpha$ -phase) and CaBe<sub>2</sub>Ge<sub>2</sub>-type ( $\beta$ -phase) crystallographic structure. The  $\beta$ -phase of this compound was found to be paramagnetic down to 2 K, however the  $\alpha$ -phase was found to undergo two phase transitions at  $T_N = 33(1)$  K and  $T_t = 18(2)$  [1]. The ground-state magnetic structure was reported according to the powder neutron diffraction to be the simple AF1 antiferromagnet with magnetic moments aligned along the  $c$ -axis [1]. Surprisingly, Welter et al. [1] does not report the change of the magnetic structure when heating the sample above  $T_t$ . Recently, we have prepared the single crystal of  $\alpha$ -NdIr<sub>2</sub>Si<sub>2</sub> and measured again the basic physical properties. According to our magnetization measurements it is impossible that the magnetic structure does not change at  $T_t$ . This led us to the repetition of the powder neutron diffraction experiment.

The neutron powder experiment was performed on the E6 diffractometer using the standard Orange cryostat. Since Iridium is strong neutron absorber, we have used Vanadium container with inner diameter of 6 mm and Aluminium container with inner diameter of 3.75 mm as a sample holders to correctly describe the absorption of the compound. As a sample we have used the accidental mixture of the  $\alpha$ - (82 %) and  $\beta$ -phase (18 %). Since  $\beta$ -phase is nonmagnetic, this accidental impurity played no significant role in the data analysis. During our experiment we have collected the scans in range  $17^\circ < 2\theta < 107^\circ$  for temperatures 2, 7, 10, 15, 20, 25 and 40 K and then we have placed the first detector to the position  $47.5^\circ$  in  $2\theta$  and made the temperature scans around  $T_t$ .

Our scans around  $T_t$  (Fig. 1) have definitely proved that at  $T_t$  the magnetic structure changes. Our data obtained at  $T < T_t$  confirmed the simple AF1 magnetic structure as previously reported [1]. The magnetic structure at  $T_t < T < T_N$  was successfully described by the longitudinal sine-modulated structure with the magnetic propagation vector  $k = (0\ 0\ 5/6)$  (Fig. 2). This structure is the

same as the high-temperature magnetic structure of  $\alpha$ -PrIr<sub>2</sub>Si<sub>2</sub> [2].

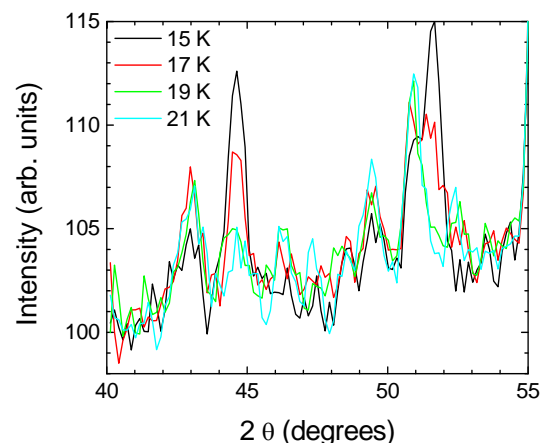


Fig. 1: The temperature scans around  $T_t$ . To simplify the figure only the representative scans are plotted.

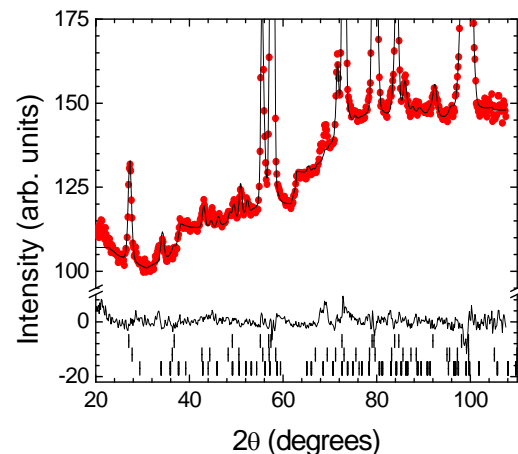



Fig. 2: The refined pattern at  $T = 25$  K where we have plotted the observed data (points), the calculated data (line through points); difference (line below points) and peak positions for (from up to down) nuclear part of  $\alpha$ -phase;  $\beta$ -phase; magnetic part of  $\alpha$ -phase.

#### References:

- [1] R. Welter, et al., J. All. & Comp. 353 (2003) 48.
- [2] M. Mihalik et al. Phys. Rev. B 81, 174431 (2010).

 <b>HELMHOLTZ ZENTRUM BERLIN</b> für Materialien und Energie  <b>NEUTRONS</b>	<b>EXPERIMENTAL REPORT</b>	Proposal: PHY-01-2762
	<b>From 1D to 3D magnetism: spin chain with enhanced interchain coupling</b>	Instrument: <b>E6</b> Local Contact: A. Hoser
Principal Proposer: Experimental Team:	Oliver Stockert, MPI CPfS, Dresden Oliver Stockert, MPI CPfS, Dresden Ariane Haase, MPI CPfS, Dresden Andreas Hoser, HZB	Date(s) of Experiment  16.06.2010 – 19.06.2010

Date of report: 04.01.2011

Strong frustration and pronounced one-dimensionality, as e.g. in  $\text{LiCuVO}_4$  and  $\text{Li}_2\text{ZrCuO}_4$ , leads in a number of copper spin-1/2 chain compounds to spiral magnetic ground states with rather low ordering temperatures. To increase the ordering temperature and to make the material more suitable for applications, one has to introduce strong coupling between the spin chains. This can be achieved in  $\text{Cu}_2\text{OCl}_2$ , where the chains of edge-sharing  $\text{CuO}_4$  squares are aligned along  $[011]$  and  $[01\bar{1}]$ , hence forming a crossing pattern.  $\text{Cu}_2\text{OCl}_2$  undergoes long-range magnetic ordering at  $T_N \approx 70$  K and shows a maximum at 130 K in magnetic susceptibility, which is a signature of short-range spin correlations [1]. To study the magnetic ordering in  $\text{Cu}_2\text{OCl}_2$  we performed a powder neutron diffraction experiment on E6. A sealed sample container was used due to the high sensitivity of  $\text{Cu}_2\text{OCl}_2$  to air moisture. Diffraction patterns were taken at temperatures between 1.5 K and 300 K in a  $2\theta$ -range from 5 to  $60^\circ$  with a wavelength of the neutrons of  $\lambda = 2.4$  Å.

Figure 1 (upper panel) shows the diffraction pattern for 1.5 K, 60 K and 90 K. After subtraction of the data taken at 90 K, i.e. above  $T_N$ , magnetic peaks are clearly visible at scattering angles  $2\theta = 21, 33$  and  $37^\circ$  in the low temperature data (Figure 1, lower panel). A detailed measurement of the temperature dependence of the magnetic intensity was done for the reflection at  $2\theta = 21^\circ$  and is shown in Figure 2. The magnetic intensity vanishes for temperatures higher than 70 K, which is in close agreement with thermodynamic measurements [1]. No simple antiferromagnetic structure can account for the observed magnetic reflections. We are currently considering different incommensurate structures. Single crystal measurements are highly desired to solve the magnetic structure of  $\text{Cu}_2\text{OCl}_2$ .

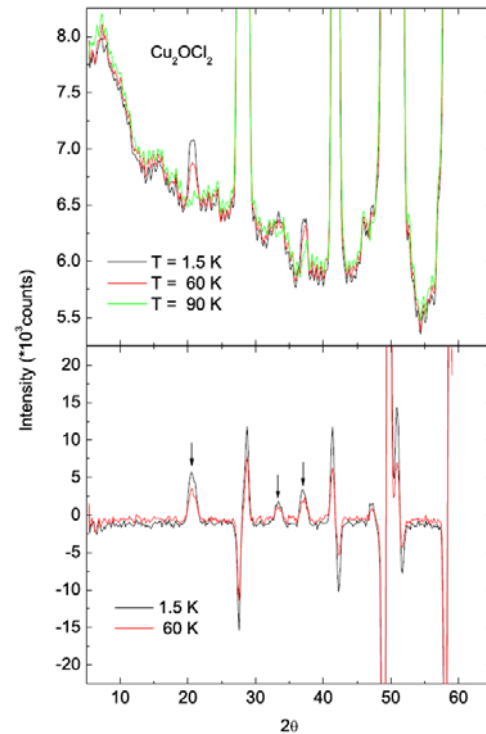


Fig. 1: Diffraction pattern of  $\text{Cu}_2\text{OCl}_2$  at 1.5 K, 60 K and 90 K (upper panel). Data taken at 90 K subtracted from data taken at 1.5 K and 60 K (lower panel).

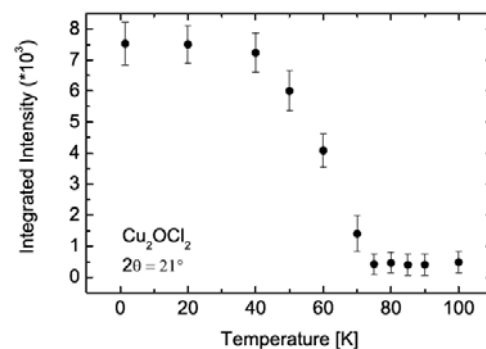



Fig. 2: Temperature dependence of the magnetic intensity in  $\text{Cu}_2\text{OCl}_2$  at  $2\theta = 21^\circ$ .

[1] H. Okabe et al., J. Phys. Soc. Jpn. 75 (2006) 123705.

 <b>HELMHOLTZ ZENTRUM BERLIN</b> für Materialien und Energie  <b>NEUTRONS</b>	<b>EXPERIMENTAL REPORT</b>  <b>Frustrated magnetic structure of Y- substituted CePdAl studied by powder neutron diffraction</b>		Proposal: PHY-01-2764  Instrument: E6  Local Contact: Andreas Hoser
	Principal Proposer: Petr Čermák, CU Prague, CZ Experimental Team: Andreas Hoser, HZB Tommy Hofmann, HZB		

Date of report: 18.06.2010

CePdAl is an antiferromagnetically ordered ( $T_N = 2.7$  K) heavy-fermion compound. The magnetic order is characterized by  $(\frac{1}{2}, 0, 0.35)$  propagation vector and geometrical frustration of  $\frac{1}{3}$  of the Ce moments [1]. We have investigated the influence of Y substitution on the magnetic structure of CePdAl.

Neutron diffraction experiment with polycrystalline samples was performed with  $\lambda = 2.438$  Å. Diffraction patterns for samples with 2 and 6% of Yttrium were measured at 8 K (paramagnetic state) and at 1.3 K, the lowest possible temperature achievable with orange cryostat. Unfortunately the temperature stabilization was not possible, so only way to stabilize temperature was continuous cooling mode. Sample with 10% of Yttrium was measured in  $^3\text{He}$ - $^4\text{He}$  dilution refrigerator in order to reach the temperatures well below  $T_N$ . Diffraction patterns were taken at temperatures 0.4, 1.3 (for comparison) and 8 K.

Refined lattice parameters for all three samples of  $\text{Ce}_{1-x}\text{Y}_x\text{PdAl}$  at 8 K were  $a = 7.175(2)$  Å and  $b = 4.227(1)$  Å for  $x = 0.02$ ,  $a = 7.184(4)$  Å and  $b = 4.226(2)$  Å for  $x = 0.06$  and  $a = 7.202(3)$  Å and  $b = 4.226(3)$  Å for  $x = 0.1$ . Diffraction patterns recorded below  $T_N$  contain additional Bragg reflections arising from scattering on the ordered magnetic moments of Ce atoms. The propagation vector determined from the positions of these magnetic peaks keeps unchanged for all measured concentrations ( $k = (0.5, 0, \tau)$ , with  $\tau = 0.357(2)$  for  $x = 0.02$ ) and is in agreement with the value reported for pure CePdAl [1]. Standard overall magnetic structure refinement was rather difficult, because magnetic reflections are very weak – especially in the sample with  $x = 0.1$ . In general, the magnetic structure reported for CePdAl [1] gives a very good agreement with our measured data. The magnitude of the ordered Ce magnetic moments for  $x = 0.02$  reaches  $1.62(5) \mu_B$  in exact agreement with [1].

We decided to reveal possible changes in magnetic structure following intensities of the

two strongest magnetic peaks  $(\frac{1}{2}, 0, \tau)$  and  $(\frac{1}{2}, -2, \tau)$  – see Fig. 2. Their ratio does not change significantly, indicating unchanged magnetic structure. However, the removal of frustration on  $\frac{1}{3}$  of Ce atoms does not influence significantly this ratio, so possible removing of the frustration with increasing yttrium concentration cannot be excluded.

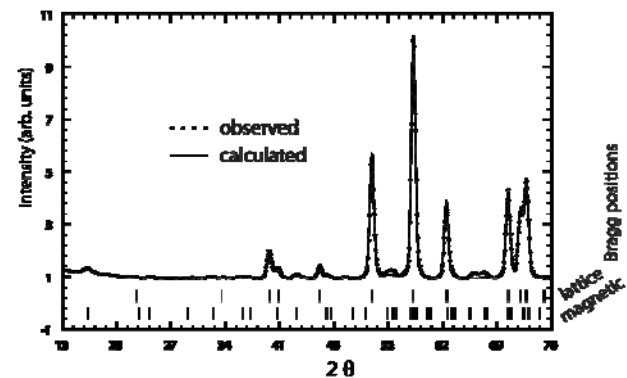


Fig. 1 - Exact refinement of  $\text{Ce}_{0.98}\text{Y}_{0.02}\text{PdAl}$  from Fullprof program. Reflections on  $2\theta=55^\circ$  and around  $2\theta=66^\circ$  are caused by sample can.

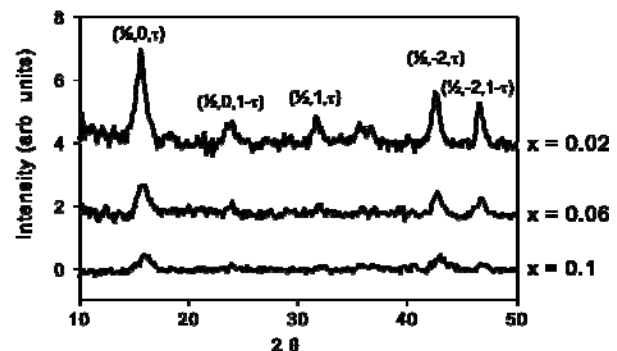


Fig. 2 - differences between ordered and paramagnetic diffraction patterns.

#### References:

[1] A. Dönni et al., J.Phys.: Condens. Matter 8 (1996) 11213.

#### Acknowledgement:

This research project has been supported by the European Commission under the 7<sup>th</sup> Framework Programme through "Research Infrastructures" action of the "Capacities" Programme, contract number CP-CSA\_INFRA-2008-1.1.1. Number 226507-NMI

**Magnetic structure of  $\text{Cs}_3\text{Mn}_2\text{O}_4$**

Proposal: PHY-01-2765

Instrument: **E6**

Local Contact:  
A. Hoser T. Hofmann

Principal Proposer: M. A. Señaris-Rodríguez, Univ. de A Coruña, E  
M. Reehuis, HZB  
M. Jansen, MPI Stuttgart

Experimental Team: M. Reehuis, HZB  
A. Hoser, HZB  
T. Hofmann, HZB  
M.A. Señaris-Rodríguez, Univ. de A Coruña, E

Date(s) of Experiment

04.05.2010 - 07.05.2010

Date of report: 09.06.2010

Recently we have synthesized a new manganese oxide  $\text{Cs}_3\text{Mn}_2\text{O}_4$ , which crystallizes in the monoclinic space group  $P2_1$  (No. 4). In this structure the Mn atoms form unusual Mn-O chains along the  $b$ -axis. Susceptibility measurements indicated the presence of an antiferromagnetic transition at the Néel temperature  $T_N = 12$  K suggesting a magnetic ordering of the Mn-sublattice. In order to investigate the magnetic structure of  $\text{Cs}_3\text{Mn}_2\text{O}_4$  we performed a neutron powder diffraction experiment on the instrument E6 using the neutron wavelength  $\lambda = 2.42$  Å. Powder patterns have been collected in the  $2\theta$ -range between  $6^\circ$  and  $136^\circ$  well below and above the ordering temperature at 2 K and 20 K, respectively. The difference pattern clearly showed the presence of magnetic intensities at the position of nuclear Bragg reflections (Fig. 1). It was interesting to see that strong magnetic intensities were only found for reflections  $hkl$  with  $h = 2n+1$  and  $k, l = 2n$ , respectively. The absence of the reflections 100, 020 and 002 clearly indicates that the magnetic moments of the Mn-atoms are coupled antiferromagnetically in Mn-O chains along the  $b$ -axis (Fig. 2). Rietveld refinements finally showed that the magnetic moments are aligned within the monoclinic  $ac$ -plane with a moment direction almost perpendicular to the  $c$ -axis (Fig. 2). Due to the relatively small number of collected structure factors we were not able to refine the large number of 24 positional parameters of the 8 Mn-atoms in the unit cell with good accuracy. Therefore we used in the refinements the fixed values obtained from the single-crystal x-ray study at room temperature. Further we assumed that the moments of the symmetrically non-equivalent Mn-atoms carry the same magnetic moment.

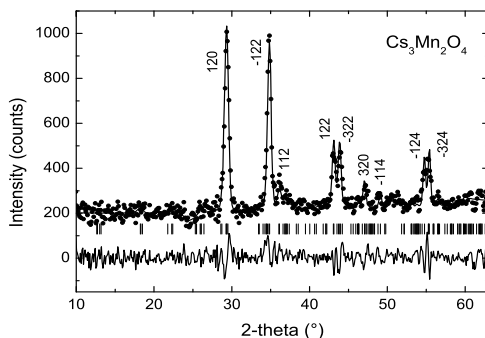


Fig. 1. Magnetic Bragg intensities of  $\text{Cs}_3\text{Mn}_2\text{O}_4$  as obtained from the difference pattern of the data collected at 2 K and 20 K.

In order to determine the temperature dependence of the magnetic moments we have collected several powder patterns from 2 K up to the Néel temperature. The magnetic moments could be determined from the Rietveld refinements. In Fig. 3 it can be seen that the magnetic order vanishes at  $13.5(4)$  K. This temperature is slightly higher than  $T_N = 12$  K obtained from our susceptibility measurements. At 2 K the magnetic moment per Mn-atom reaches a value  $\mu_{\text{exp}} = 2.90(17) \mu_B$ .

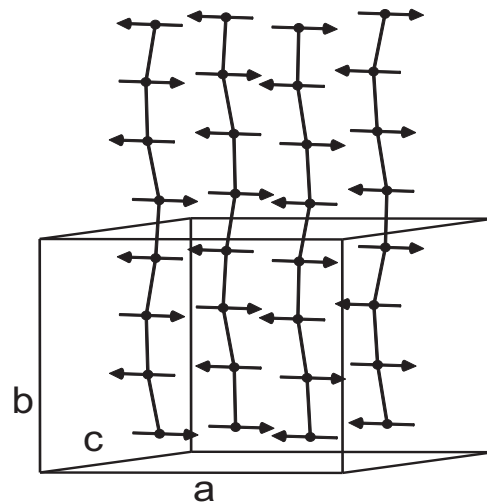


Fig. 2. Antiferromagnetic structure of  $\text{Cs}_3\text{Mn}_2\text{O}_4$ .

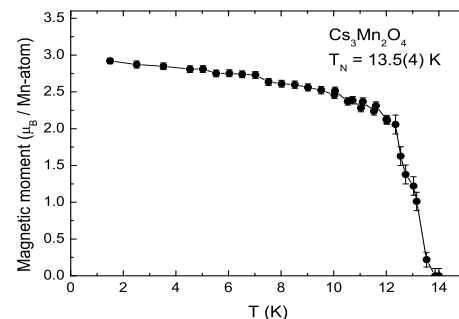



Fig. 3.  $T$ -dependence of the magnetic moment per Mn-atom of  $\text{Cs}_3\text{Mn}_2\text{O}_4$ .

**Acknowledgement:**

This research project has been supported by the European Commission under the 7<sup>th</sup> Framework Programme through "Research Infrastructures" action of the "Capacities" Programme, contract number CP-CSA\_INFRA-2008-1.1.1. Number 226507-NMI



 <b>HELMHOLTZ ZENTRUM BERLIN</b> für Materialien und Energie  <b>NEUTRONS</b>	<b>EXPERIMENTAL REPORT</b>	Proposal: PHY-01-2771
	<b>Temperature dependence of magnetic and crystal structure parameters of NdMn<sub>2-x</sub>Cu<sub>x</sub>Ge<sub>2</sub> and PrMn<sub>2-x</sub>Fe<sub>x</sub>Ge<sub>2</sub> (x = 0.3)</b>	Instrument: <b>E6</b> Local Contact: Andreas Hoser
Principal Proposer: Experimental Team:	Teresa Jaworska-Golab, JU Krakow, PL Stanislaw Baran, JU Krakow, PL Andreas Hoser, HZB Tommy Hofmann, HZB	Date(s) of Experiment  12.05.2010-16.05.2010

Date of report: 27.01.2011

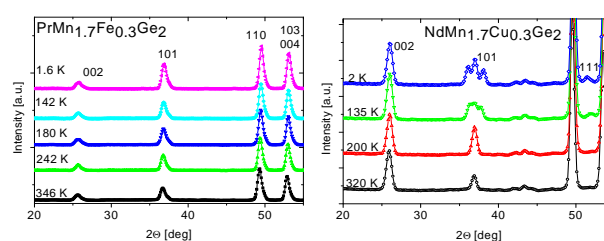
In the tetragonal RMn<sub>2-x</sub>T<sub>x</sub>Ge<sub>2</sub> intermetallics (R-rare earth element, T-transition element, 0 ≤ x ≤ 2) magnetic behavior of the Mn-sublattice and the Mn-Mn spacing are highly correlated. The aim of this proposal was to collect neutron diffraction patterns of two pseudoternary light rare earth germanides (NdMn<sub>1.7</sub>Cu<sub>0.3</sub>Ge<sub>2</sub> and PrMn<sub>1.7</sub>Fe<sub>0.3</sub>Ge<sub>2</sub>) as a function of temperature at ambient pressure to determine the type of magnetic order, its quantitative description (i.e. location, values and orientation of magnetic moments) and the crystal lattice parameters.

According to the aims of our proposal powder neutron diffraction patterns were collected at the E6 diffractometer at ambient pressure in several temperatures between 450 K and 1.6 K chosen on the basis of our preliminary a.c. magnetic susceptibility measurements. For simultaneous refinement of magnetic and structural parameters the Rietveld-type profile refinement program was used (J. Rodriguez-Carvajal, FullProf, Physica B 192(1993)55; <http://www.ill.eu/sites/fullprof>).

The diffraction data confirmed that the studied compounds crystallize in the body-centered tetragonal ThCr<sub>2</sub>Si<sub>2</sub>-type crystal structure (space group I4/mmm) and the transition metal atoms (Mn and Fe/Cu) are randomly distributed at the 4(d) site. A long range magnetic ordering was observed in the Mn-sublattice as well as in the rare earth (Nd or Pr) one (at far lower temperatures) and several order-order magnetic phase transitions were detected.

In PrMn<sub>1.7</sub>Fe<sub>0.3</sub>Ge<sub>2</sub> the magnetic structure in the Mn-sublattice changes from AF1 to Fmc while decreasing temperature. In the case of NdMn<sub>1.7</sub>Cu<sub>0.3</sub>Ge<sub>2</sub> the satellites of the 101 reflection and the 111 reflection itself are well developed below 130 K indicating another sequence of magnetic structures in the Mn-sublattice: AF1, AFmc and Fmc. Then, at lower temperatures, the Pr and Nd magnetic moments order ferromagnetically. The

representative data sets are plotted in **Fig. 1**. The magnetic structures are denoted according to G. Venturini, B. Malaman and E. Ressouche, *J. Alloys Compounds* 240 (1996) 139.



**Fig. 1** The low angle part of the neutron diffraction patterns of NdMn<sub>1.7</sub>Cu<sub>0.3</sub>Ge<sub>2</sub> and PrMn<sub>1.7</sub>Fe<sub>0.3</sub>Ge<sub>2</sub> at selected temperatures.


Some of the results obtained in the course of the reported experiment were presented during the national Silesia-Cracow Seminar on Physics of Condensed Phase (Rychwald, Poland, June 2010; short communication) and at the 17<sup>th</sup> Conference on Solid Compounds of Transition Elements (Annecy, France, September 2010; poster). Further analysis of the data is in progress and the results will be published in scientific journals.

#### Acknowledgements:

*We would like to gratefully acknowledge professional and helpful assistance of the E6 diffractometer team during the experiment and exceptional kindness and helpfulness of all the people at the Helmholtz Zentrum Berlin.*

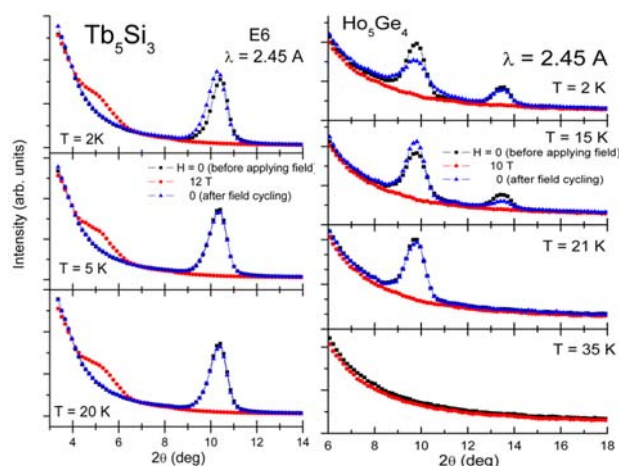
*Financial support of the Ministry of Science and Higher Education in Poland under the grant No. PB 0784/B/H03 is acknowledged.*

*This research project has been supported by the European Commission under the 7<sup>th</sup> Framework Programme through "Research Infrastructures" action of the "Capacities" Programme, contract number CP-CSA\_INFRA-2008-1.1.1. Number 226507-NMI3.*

 <b>HELMHOLTZ ZENTRUM BERLIN</b> für Materialien und Energie  <b>NEUTRONS</b>	<b>EXPERIMENTAL REPORT</b>  <b>Magneto-structural Studies on Intermetallics <math>Tb_5Si_3</math> and <math>Ho_5Ge_4</math> using Neutron Diffraction</b>	Proposal: PHY-01-2774  Instrument: <b>E6</b>  Local Contact: Andreas Hoser
	Principal Proposer: Sudhindra Rayaprol, UGC-DAE CSR, India Experimental Team: Vasudeva Siruguri, UGC-DAE CSR, India E. V. Sampathkumaran, TIFR, India Andreas Hoser, HZB	Date(s) of Experiment  24.06.2010 – 01.07.2010

Date of report: 24.01.2011

$Tb_5Si_3$  crystallizes in the  $Mn_5Si_3$ -type hexagonal structure. The compound orders antiferromagnetically below 69 K and exhibits a field-induced ferromagnetic transition. This transition is distinctly first order at 1.8 K and at a field of 6 Tesla, whereas it appears to become second order near 20 K. We find clear evidence for this observation through neutron diffraction (ND) experiment carried out at several temperatures below and above 69 K and also in the presence of magnetic field.



**Fig. 1** ND patterns for  $Tb_5Si_3$  and  $Ho_5Ge_4$ .

Neutron diffraction studies exhibit the field induced magnetic transition in this compound. Detailed ND experiments were carried out at low temperatures (that is at temperatures, below and close to the magnetic transition temperatures) with and without applying magnetic fields up to 12 Tesla. The results clearly establish the irreversibility effect of magnetic field on the magnetic structure. At 2 K, the magnetic field induces changes in the magnetic structure while the field is ramped up to 12 Tesla. It is interesting to observe that the magnetic structure does not relax back to its original state even after removing the applied field. At 20 K, the magnetic state is restored after the field cycling, strongly indicating that there is magneto-crystalline anisotropy in this compound in a specific temperature range.


The compound  $Ho_5Ge_4$  belongs to the  $R_5T_4$  family of compounds where  $R$  is a rare-earth and  $T$  is a Group 14 element, which are known to exhibit giant magneto-caloric effect (GMCE). The origins for GMCE lie in the magnetostructural transitions (MST) that are exhibited by these compounds.  $Ho_5Ge_4$  was studied in the temperature range 1.8 K to 100 K using neutron diffraction with and without external magnetic field.

The preliminary results of ND experiments showed drastic changes in the magnetic structure under the application of magnetic fields up to 5 Tesla, as evidenced by changes in the intensities of magnetic reflections and appearance of new diffraction lines at high magnetic fields. The results indicate multiple magnetic transitions and coexistence of different types of magnetic ordering.

In order to understand the correlations between magnetism and structure, influenced by conditions of temperature and external magnetic field, ND patterns of  $Ho_5Ge_4$  were recorded at  $T = 2, 15$  and  $21$  K at various applied fields up to 10 T. The results showed drastic changes in the magnetic structure under the application of magnetic fields as evidenced by changes in the intensities of magnetic reflections and appearance of new diffraction lines at high magnetic fields. As a representation of the interesting features observed in the ND patterns of  $Ho_5Ge_4$ , the low angle data of the ND measured at  $T = 2, 15, 21$  and  $35$  K is shown in Fig. 1.

The ND data for both  $Tb_5Si_3$  and  $Ho_5Ge_4$  samples are being currently analyzed, and it is expected to yield interesting results, which will help in explaining the magneto-structural properties exhibited by these two intermetallic compounds.

*Financial support in the form of travel grant was provided by Department of Science and Technology, Government of India to carry out this research project.*

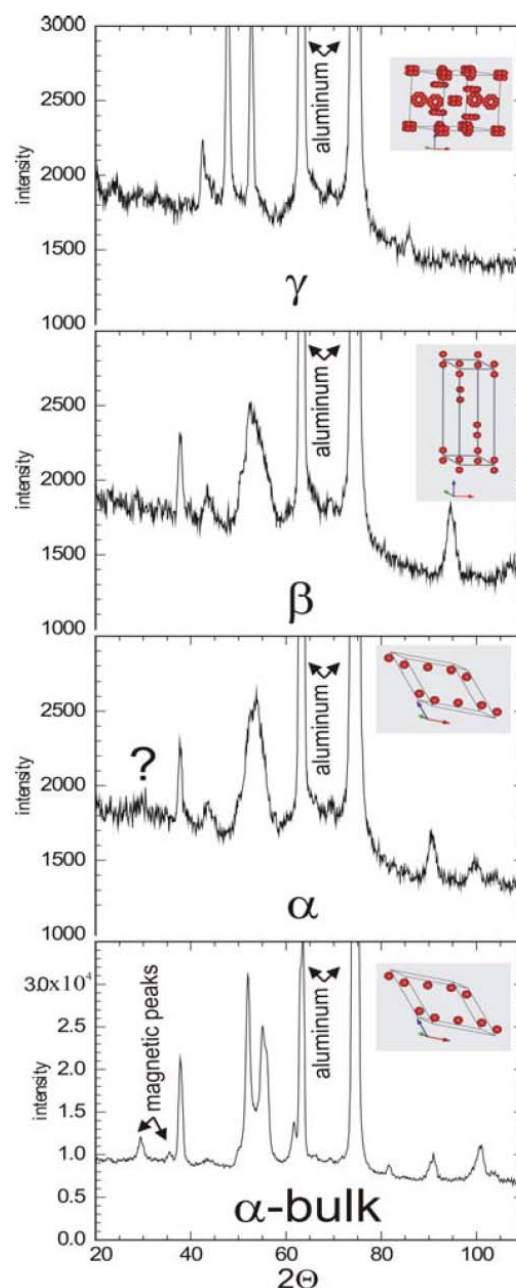
 <p><b>HELMHOLTZ ZENTRUM BERLIN</b> für Materialien und Energie</p> <p><b>NEUTRONS</b></p>	<p><b>EXPERIMENTAL REPORT</b></p> <p><b>Structural and Magnetic Properties of Solid Oxygen Confined into Oriented Mesopores of Anodized Aluminum</b></p>	<p>Proposal: PHY-01-2878-EF</p> <p>Instrument: <b>E6</b></p> <p>Local Contact: T. Hofmann</p>
	<p>Principal Proposer: Tommy Hofmann, HZB</p> <p>Experimental Team: Dirk Wallacher, HZB</p>	<p>07.08.2010 - 08.08.2010</p> <p>16.08.2010 - 23.08.2010</p>

Date of report: 28.01.2011

In course of this experiment we probed the nuclear and magnetic structure of solid oxygen ( $s\text{-O}_2$ ) confined into an array of 30nm wide several micrometer long nanochannels in anodized aluminum (a-Al). Scattering experiments were performed at the thermal powder diffractometer E6 ( $\lambda=2.44\text{\AA}$ ). An elaborate sorption setup was provided by HZB's department for sample environment to fill the porous host with liquid  $\text{O}_2$ . Subsequently it allowed to perform in-situ scattering experiments at the filled host as function of temperature. Scattering data were recorded for various orientations of the pore axes with respect to the incoming neutron beam to elucidate correlations between the growth directions of confined oxygen crystals and the direction of the long pore axes.

The three for bulk known nuclear structures (ref. 1-3) were also found in confined oxygen (Fig. 1). A cubic  $\gamma$ -phase was stable right after solidification at 54K. It transformed at 44K in a rhombohedral  $\beta$ -phase with an ABC stacking sequence along the (001) direction. At 24K, a small monoclinic distortion of the rhombohedral cell led to the known monoclinic  $\alpha$ -structure. Found transition temperatures  $T(\text{liquid}-\gamma)$ ,  $T(\gamma-\beta)$  and  $T(\beta-\alpha)$  in the pores agreed in the margin of error with bulk transition temperatures as expected for 30nm wide pores. In bulk  $\alpha\text{-O}_2$ , the anti-ferromagnetic orientation between spins at (0, 0, 0) positions and spins at (0.5, 0.5, 0) positions causes magnetic (-101) and (100) reflections (Fig. 1). This anti-ferromagnetic structure could not be readily ascertained for confined oxygen (Fig. 1). The search for well defined, preferred orientations of  $\text{O}_2$  crystallites in the pores remained inconclusive.

Future experiments will utilize a-Al with smaller pore diameters (10nm-15nm) to increase the confinement effect on the pore condensate. It might also be wise to improve the signal to noise ratio in the scattering experiment to find possible magnetic reflections from confined oxygen.



**Figure 1:**  $\gamma$ -,  $\beta$ -,  $\alpha$ -  $\text{O}_2$  in a-Al at 50K, 35K and 2K,  $\alpha\text{-O}_2$  as bulk at 2K

References

- 1) R. Ackermann et al., Europhys. Lett. 64 p. 260 (2003)
- 2) P. W. Stephens et al., Phys. Rev. B 28 p. 452 (1983)
- 3) G. C. DeFotis, J. Chem. Phys. 71 p. 5336 (1979)

Principal Proposer: S. Baran, JU Krakow, PL  
 Experimental Team: A. Gil, Jan Długosz University, Częstochowa, PL  
 Andreas Hoser, HZB  
 Tommy Hofmann, HZB

Date(s) of Experiment

25.09.2010 – 28.09.2010

Date of report: 26.01.2011

## Experiment

Two powder samples of ternary intermetallics: TmCu<sub>4</sub>Ge<sub>4</sub> and TmCu<sub>4</sub>Sn<sub>4</sub> were investigated by means of neutron diffraction within the temperature range from 1.5 to 5 K on the E6 diffractometer. The incident neutron wavelength was 2.45 Å.

## Results

TmCu<sub>4</sub>Ge<sub>4</sub> crystallizes in the orthorhombic Gd<sub>3</sub>Cu<sub>4</sub>Ge<sub>4</sub>-type crystal structure (space group *Immm*) whereas TmCu<sub>4</sub>Sn<sub>4</sub> crystallizes in a distorted variant of the abovementioned crystal structure (monoclinic space group *C2/m*).

The analysis of the experimental data revealed the presence of an antiferromagnetic order below 2.8 K in both compounds. In TmCu<sub>4</sub>Ge<sub>4</sub> the magnetic unit cell is doubled when compared to the crystal one and the propagation vector is  $\mathbf{k} = [0, \frac{1}{2}, 0]$ . A larger magnetic unit cell was found in TmCu<sub>4</sub>Sn<sub>4</sub> - the propagation vector describing this magnetic phase is equal to  $\mathbf{k} = [\frac{1}{2}, \frac{1}{2}, 0]$  (for simplicity the orthorhombic description is used for both the germanide and the stannide).

Below 2.1 K in TmCu<sub>4</sub>Ge<sub>4</sub> and 1.8 K in TmCu<sub>4</sub>Sn<sub>4</sub> another incommensurate antiferromagnetic order develops (see Fig. 1). This magnetic phase is related to  $\mathbf{k} = [\frac{1}{4}, 0, k_z]$  where  $k_z$  is close to 0.49 in the germanide and 0.47 in the stannide. Both the magnetic transitions were confirmed by heat capacity measurements (see Fig. 2).

## Acknowledgement

This research project has been supported by the European Commission under the 7<sup>th</sup> Framework Programme through "Research Infrastructures" action of the "Capacities" Programme, contract number CP-CSA\_INFRA-2008-1.1.1. Number 226507-NMI3

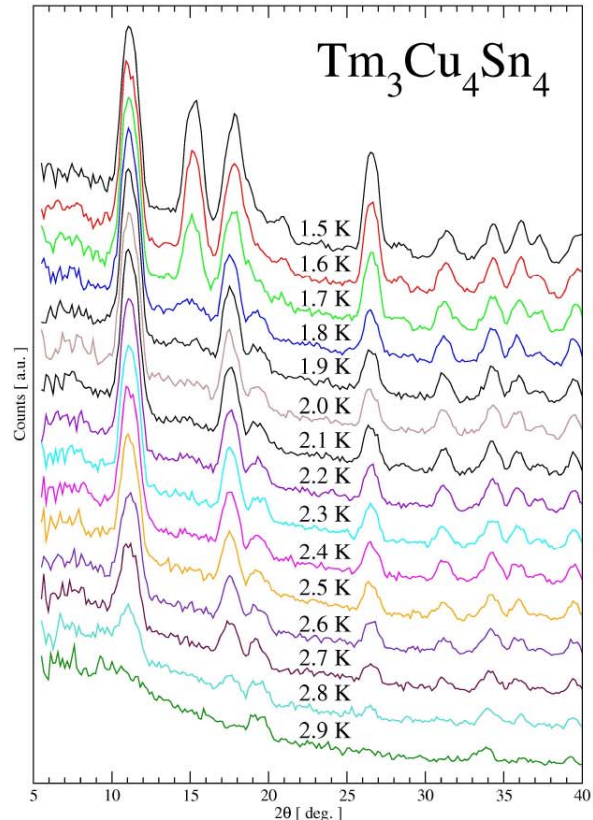


Fig. 1. Temperature evolution of TmCu<sub>4</sub>Sn<sub>4</sub> neutron diffraction pattern.

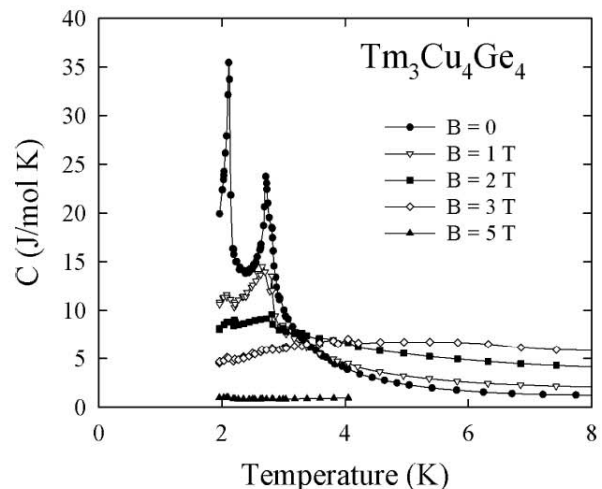


Fig. 2. Temperature dependence of TmCu<sub>4</sub>Ge<sub>4</sub> heat capacity.

 <b>HELMHOLTZ ZENTRUM BERLIN</b> für Materialien und Energie  <b>NEUTRONS</b>	<b>EXPERIMENTAL REPORT</b>  <b>Magnetic structure of hexagonal HoMn<sub>2</sub>D<sub>4.5</sub> deuteride</b>	Proposal: PHY-01-2888  Instrument: <b>E6</b> Local Contact: Andreas Hoser
	Principal Proposer: Andrzej Budziak, PAS IFJ Krakow, PL Experimental Team: Andrzej Budziak, PAS IFJ Krakow, PL Lukasz Gondek, AGH-UST, Krakow, PL Andreas Hoser, HZB	Date(s) of Experiment  23.08.2010 – 26.08.2010

Date of report: 14.01.2011

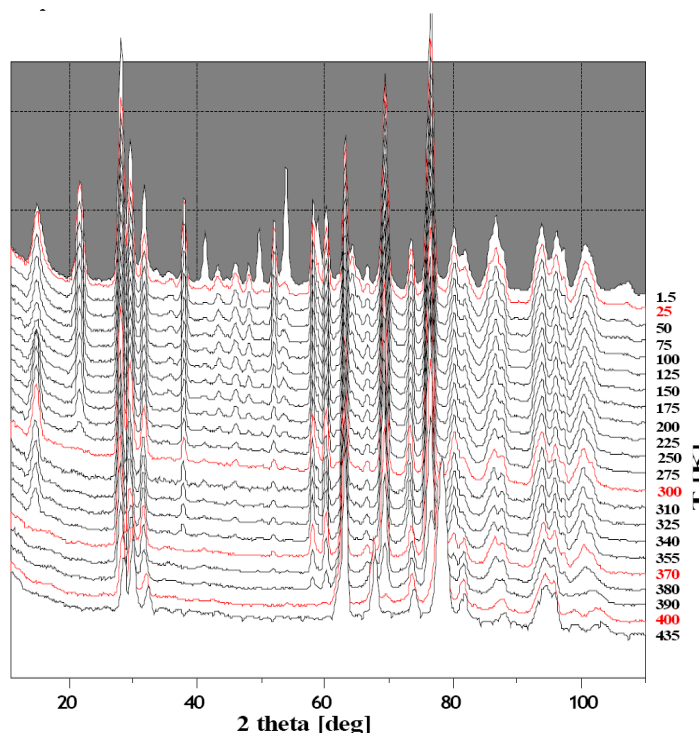
The deuteride of the Laves phase type intermetallic compound HoMn<sub>2</sub>D<sub>4.5</sub> has been prepared using the standard melting technique and deuteration process (pressure ~ 3 bar). The pure HoMn<sub>2</sub> compound crystallizes in the cubic C15 or in the hexagonal C14 structure, depending on the heat treatment.

which is probably due to the ordering of the hydrogen/deuterium sublattice and a weak structural transformation from the rhombohedral phase (*Cmcm*) to the hexagonal one (*P6<sub>3</sub>/mmc*) in contrast to what XRD measurements implied.

The ND result presented here was obtained for the C14 structure (sg: *P6<sub>3</sub>/mmc*). Temperature scans of the x-ray diffraction patterns show that for the HoMn<sub>2</sub>D<sub>4.5</sub> deuteride the hexagonal (C14) structure persists in the wide temperature range 80-360K.

The magnetic ordering temperature of the pure HoMn<sub>2</sub> is ~24 K. The aim of the project was to get insight into the magnetic structure and ordering process of hydrogen (deuterium), as well as to confirm the nuclear structure (2-360K).


The enclosed figure depicts the ND patterns of the HoMn<sub>2</sub>D<sub>4.5</sub> deuteride in the temperature range from 1.5 to 435 K. Four characteristic temperatures (25, 300, 370 and 400 K) are apparent above which some of the diffraction lines either disappear or significantly reduce their intensities.



More accurate measurements repeated below 25 K showed a transformation at ~7.4 K which can be related to magnetic ordering temperature of the Ho sublattice. Temperatures 300 and 370 K mark either the ordering or the reorientations of the magnetic moments in the two Mn sublattices.

*This research project has been supported by the European Commission under the 7<sup>th</sup> Framework Programme through "Research Infrastructures" action of the "Capacities" Programme, contract number CPCS\_A\_INFRA-2008-1.1.1. Number 226507- NMI3.*

Moreover, above 370 K the paramagnetic phase of the sample is observed. It is consistent with magnetic measurements and the general tendency of increasing the magnetic ordering temperature with increasing hydrogen concentration, which was observed for other RMn<sub>2</sub>H<sub>x</sub> hydrides (R: rare earth). At 400 K the last transformation is observed

 <b>HELMHOLTZ ZENTRUM BERLIN</b> für Materialien und Energie  <b>NEUTRONS</b>	<b>EXPERIMENTAL REPORT</b>	Proposal: PHY-01-2889
	<b>Sublattice Magnetization in RbMnF<sub>3</sub></b>	Instrument: <b>E6</b> Local Contact: A. Hoser
Principal Proposer: Jeffrey Klein, Univ. Pennsylvania (UPenn), USA Experimental Team: Ulrich Köbler, FZ Jülich Andreas Hoser, HZB	Date(s) of Experiment 03.08.2010 – 06.08.2010	

Date of report: 28.01.2011

RbMnF<sub>3</sub> has long been considered [1] to be an ideal realization of a cubic Heisenberg antiferromagnet because of its minute energy gap ( $T_G$ ). Conventional spin-wave theory [SWT] predicts that the sublattice magnetization [SLM] of an antiferromagnet with a negligibly small gap follows a simple  $T^2$  power-law. But no stringent test of the temperature dependence of the SLM in RbMnF<sub>3</sub> has been possible because of intrinsic problems with NMR in RbMnF<sub>3</sub>. Two other recently proposed semi-empirical schemes [2, 3] also predict power-law dependences of the SLMs at low temperatures, but with different exponents, and not just for compounds with  $T_G \sim 0$ . Koebler *et al.* [2] predict that for 3D half-integral isotropic-spin systems, a  $T^2$  fall-off should obtain all the way up to  $\sim 85\%$   $T_N$ . In the scheme of Bykovetz [3], however, there are three possible power-law temperature fall-offs,  $T^{2.29}$ ,  $T^{2.67}$ , and  $T^4$ , for  $T \leq 0.50T_c$ . Early measurements by Seiden and Teaney [4] led them to claim that the SLM of RbMnF<sub>3</sub> follows a  $T^3$  fall-off for  $T \leq 25$ K. We proposed neutron scattering (NS) measurements to differentiate between these different predictions/observations.

Measurements were made on a large single crystal and on a powdered sample from a piece of the crystal. Extinction effects were unfortunately too great in the single crystal. Two runs on the powdered sample, a lower-temperature run (1.5K to  $\sim 70$ K), and a critical region run (70K to 88K) were completed.

At temperatures below  $\sim 25$ K, the scatter in our data is too large to give a stringent limit on the exponent of the power-law. However, the data do exclude the purported AFMR and NMR observation of  $T^3$  behavior reported in Ref [4]. Graphical analysis shows that within the scatter of the data, the  $T^2$  behavior expected in SWT is not inconsistent with our data for  $T \leq 28$ K. A least-squares fit of the data for  $T \leq 25$ K does give an exponent of  $\approx 2$ , but with an uncertainty  $\pm 0.4$ . A fit to the entire "lower-temperature" data, i.e., for  $T \leq 71$ K ( $\sim 0.85T_N$ ), yields an exponent of  $2.47 \pm 0.01$  (see Fig. 1). Koebler would allow an exponent of 2.5 for RbMnF<sub>3</sub> only if the crystal structure is distorted from cubic.

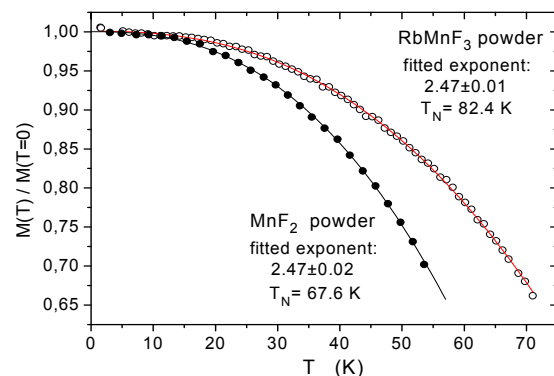
However, previous measurements showing virtually no magnetostriction [5] or quadrupole splitting [6] make this possibility unlikely.

A  $T^{2.5}$  behavior was observed previously in neutron measurements [2] on MnF<sub>2</sub> (Fig. 1). However, precision NMR measurements [7] showed that for  $20\text{K} \leq T \leq 43\text{K}$ , the exponent was precisely 2.29, as predicted by Bykovetz [3].

Fitting our NS data in the higher precision region,  $22\text{K} \leq T \leq 50\text{K}$ , gives an exponent of  $2.24 \pm 0.08$ : consistent with an exponent of 2.29, and with the behaviour observed in MnF<sub>2</sub>.

In summary, our NS measurements shed some light on the low-temperature behaviour of RbMnF<sub>3</sub>, but do not, as yet, definitively discriminate between the alternative theories.

We propose to do measurements with a bigger sample or longer run times in order to decrease the statistical errors and permit a more stringent determination of the power law(s).



## References

- [1] T. Teaney, et al, Phys. Rev. Lett., 9 (1962) 212.
- [2] U. Köbler, A. Hoser : *Renormalization Group Theory-Impact on Experimental Magnetism*, (Springer-Verlag, Berlin, Heidelberg 2010).
- [3] N.Bykovetz, J. Appl. Phys. 55 (1984) 2062.
- [4] P.E.Seiden, Phys. Lett. 28A (1968) 239.
- [5] D.T. Teaney, et al., J. Appl. Phys. 37 (1966) 1122.
- [6] A. Heeger, D. Teaney, J. Appl. Phys. 35 (1964) 846.
- [7] Shyam Das (unpublished); see also NMR by M. Kawakami in Koebler, et.al., Physica B 307 (2001) 175.

	<b>EXPERIMENTAL REPORT</b> <b>Neutron diffraction studies of the crystal and magnetic structure of Pr<sub>0.5</sub>Sr<sub>x</sub>La<sub>1-x</sub>CoO<sub>3</sub></b>	Proposal: PHY-01-2598 Instrument: <b>E9</b> Local Contact: Simon Kimber
	Principal Proposer: Vadim Sikolenko, ETH Zürich and PSI, CH Experimental Team: Vadim Sikolenko, ETH Zürich and PSI, CH Vadim Efimov, JINR Dubna, RU	Date(s) of Experiment 15.10.2009 – 20.10.2009

Date of report: 10.02.2010

Cobaltite oxides with perovskite-like structure have attracted a considerable interest of many researchers because of their specific properties making them promising materials for chemical reactors catalysis, gas separation membranes and many other applications. An especially interesting feature observed for these materials is an ordering of oxygen vacancies which can drastically change the physical properties of such compounds in comparison with stoichiometric ones. The oxygen deficient layered double perovskites  $\text{La}_{1-x}\text{Sr}(\text{Ba})_x\text{CoO}_{3-d}$  and  $\text{RBaCo}_2\text{O}_{5+d}$  (where R = rare earth element) are being increasingly studied because of their interesting magnetic and transport properties. In particular, the materials with  $d = 0.5$  exhibit a paramagnetic, ferromagnetic and antiferromagnetic transitions, which are related to an interplay between spin, charge and orbital degrees of freedom of the cobalt ions. In  $\text{RBaCo}_2\text{O}_{5.5}$  only  $\text{Co}^{3+}$  ions are present, which are sited in ideally alternating octahedral  $\text{CoO}_6$  and pyramidal  $\text{CoO}_5$  environments. Depending on the ratio of the crystal field and the intra-atomic exchange energies,  $\text{Co}^{3+}$  ions can be stabilized either in low-spin (LS) state, intermediate-spin (IS) state or high-spin (HS) state. The IS state of  $\text{Co}^{3+}$  leads to a Jahn-Teller (JT) distortion of the oxygen octahedra in the structure. Substitution  $\text{La}^{3+}$  by  $\text{Sr}^{2+}$  ( $\text{Ba}^{2+}$ ) leads to changing of Co-O bond length as well as formation of tetravalent  $\text{Co}^{4+}$ . Most researchers interpretate magnetism by double exchange between  $\text{Co}^{3+}$  and  $\text{Co}^{4+}$  as in the case with manganites or by superexchange  $\text{Co}^{3+}\text{LS}-\text{Co}^{4+}\text{HS}$  anions through oxygen cation. Substituting  $\text{La}^{3+}$  by  $\text{Pr}^{3+}$  with lower ion radius and  $\text{Sr}^{2+}$  by  $\text{Ba}^{2+}$  with higher ion radius we can change spin state of  $\text{Co}^{3+}$ , keeping constant  $\text{Co}^{4+}$  content.

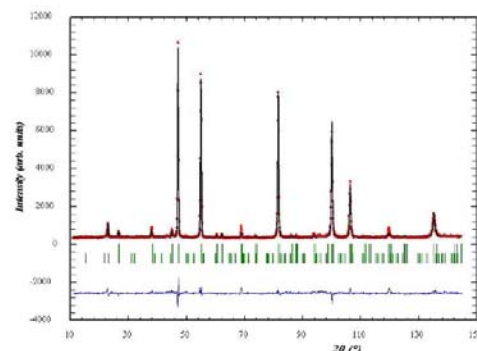



Fig.1. Rietveld refinement of diffraction pattern, collected at the E9 at 2K. Space group R-3c, AF with moments in a-b plane.

Our previous studies showed that Pr doping leads to symmetry reduction from rhombohedral to monoclinic, whereas Sr doping leads to symmetry rise to cubic. Here we have found that by simultaneously doping with Pr and Sr crystal symmetry remain rhombohedral, but the magnetic structure is FM at the temperature region 100 – 170 K and at low temperature changes to AF with magnetic moments in a-b plane (see Fig.1), The refined values of  $\text{Co}^{3+}$  magnetic moments indicate a mixed high-low spin state, that could be the result from a competition between positive and negative exchange interactions.

#### Acknowledgement

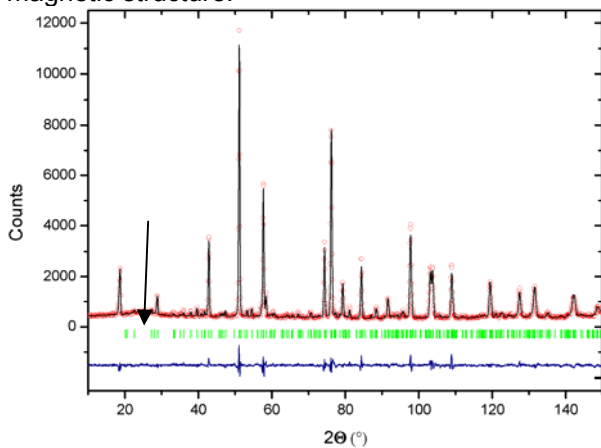
*This research project has been supported by the European Commission under the 7th Framework Programme through the Key Action: Strengthening the European Research Area, Research Infrastructures. Contract n° 226507 (NMI3)*

*This project has been also partly supported by RFBR, project 08-09-90053-Bel\_a.*

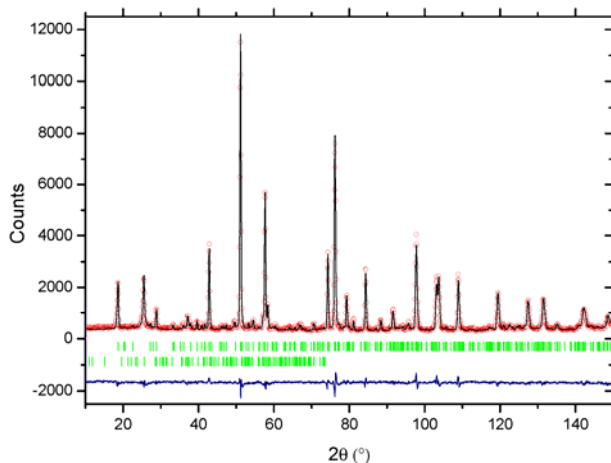
 <b>EXPERIMENTAL REPORT</b>		Proposal: PHY-01-2605-DT
<b>Magnetic transitions in a frustrated triangular lattice compound Ca<sub>0.5</sub>CrO<sub>2</sub></b>		Instrument: <b>E9</b>
		Local Contact: Simon Kimber
Principal Proposer: Experimental Team:	Sandor Toth, HZB Bella Lake, HZB Simon Kimber, HZB	Date(s) of Experiment  14.08.2009 - 18.08.2009

Date of report: 18.02.2011

Alpha-Ca<sub>0.5</sub>CrO<sub>2</sub> is a frustrated triangular lattice antiferromagnet. The crystal structure is orthorhombic *Pmmn* at room temperature [1]. It orders magnetically at  $T_N=43$  K. We performed neutron diffraction on a powder sample at 2.1 K and 50 K using  $\lambda=1.799$  Å wavelength neutrons selected by a Ge monochromator. Using the data we refined the low temperature nuclear and magnetic structure.



**Figure 1 Refined diffraction pattern T=50 K**



**Figure 2 Refined diffraction pattern T=2.1 K**

From the 50 K data (Fig. 1), we refined the nuclear structure, using the data of [1] as a starting point. The refined atomic positions are shown in Table 1. The lattice parameters are:

a	11.0579(2) Å
b	5.8239(2) Å
c	5.0553(1) Å

The nuclear Bragg factor is  $R_B=0.049$ . The refined parameters are close to the previously published numbers.

Atom	Site	x	y	z
Ca(1)	2a	3/4	3/4	0.3495(15)
Ca(2)	2b	1/3	3/4	0.0367(13)
Cr(1)	4d	1/2	1/2	1/2
Cr(2)	4f	0.4930(7)	1/4	0.0041(13)
O(1)	4f	0.4005(4)	1/4	0.3396(8)
O(2)	4f	0.5846	1/4	0.6766
O(3)	8g	0.6013(2)	0.4970(7)	0.1624(8)

**Table I Refined atomic positions at T=50 K**

On the low temperature scan new peaks appear at incommensurate positions, evidence of long range magnetic order. The strongest is at  $2\theta\sim 30^\circ$ , where a broad bump could be observed at 50 K (see Fig. 1 arrow), the evidence of short range magnetic correlations above  $T_N$ . The magnetic structure were refined using the FullProf [2] software. The ordering wavevector is  $(0, 0.333(5), 0)$ , and the phase between the two inequivalent Cr is  $120^\circ$ . With these restrictions there are several different possible structures. The spins can be collinear but this structure can not be distinguished from the equivalent helical structure by powder diffraction. For the structures with the smallest R-value, see Table II.

	a-b	a-c
$m_x$	2.16(10)	2.30(8)
$m_y$	2.41(12)	-
$m_z$	-	2.41(11)
$R_B$	0.081	0.083

**Table II Best solutions for the magnetic structure. All moments are in units of  $\mu_B$ .**


The possible magnetic structures are helical in the a-b or a-c plane. The sinusoidal structures can be excluded because the maximum moment length would exceed the spin only  $gS\sim 3\mu_B$  value.

To unambiguously determine the plane of the magnetic moments, higher resolution data or single crystal measurements are necessary.

[1] H. Pausch *et. al.* Z. Anorg. Allg. Chem. **405**, 113 (1974)

[2] J. Rodriguez-Carvajal, Physica B **192**, 55 (1993)



 <b>HELMHOLTZ ZENTRUM BERLIN</b> für Materialien und Energie  <b>NEUTRONS</b>	<b>EXPERIMENTAL REPORT</b>	Proposal: PHY-01-2726
	<b>Neutron diffraction studies Y<sub>2</sub>Co<sub>2</sub>O<sub>5+δ</sub> doped with Fe</b>	Instrument: <b>E9</b> Local Contact: Paul Henry
Principal Proposer: Experimental Team:	Vadim Sikolenko, ETH Zürich and PSI, CH Vadim Sikolenko, ETH Zürich and PSI, CH Vadim Efimov, JINR Dubna, RU	Date(s) of Experiment  20.06.2010 – 25.06.2010

Date of report: 14.11.2010

The Y<sub>0.44</sub>Sr<sub>1.56</sub>Sr(Co<sub>1-x</sub>Fe<sub>x</sub>)<sub>2</sub>O<sub>5+δ</sub> (x = 0 and 0.12) system has been studied using neutron diffraction technique, magnetization and elastic properties measurements.

Undoped sample exhibits superstructure

with  $2\sqrt{2}a_p \times 2\sqrt{2}a_p \times 4a_p$  metrics in tetragonal space group *I4/mmm* and structural phase transition at T = 360 K. Magnetic ordering starts to develop below 360 K. Spontaneous magnetization shows anomalous behavior and reaches maximal value nearly room temperature. A magnetic structure of the both compounds has been described assuming G-type antiferromagnetic ordering. There are two different magnetic moment values for Co ions in CoO<sub>6</sub> and CoO<sub>4.5</sub> layers. Magnetic moments in CoO<sub>4.5</sub> layers are larger than those for octahedrons. The refined values of magnetic moments indicate a mixed low–high spin state of Co<sup>3+</sup> for the both layers. There is no evidence for any change of the magnetic structure type with temperature lowering despite the anomalous magnetization behaviour. Iron doping (x = 0.12) leads to a suppression of the small ferromagnetic component,

disappearance of the  $2\sqrt{2}a_p \times 2\sqrt{2}a_p \times 4a_p$  metrics, and strong increase of the average magnetic moment for Co<sub>4.5</sub> layer. It is suggested that the ferromagnetic component in the undoped samples is a result of non-collinearity of the magnetic moments within CoO<sub>4.5</sub> layers.

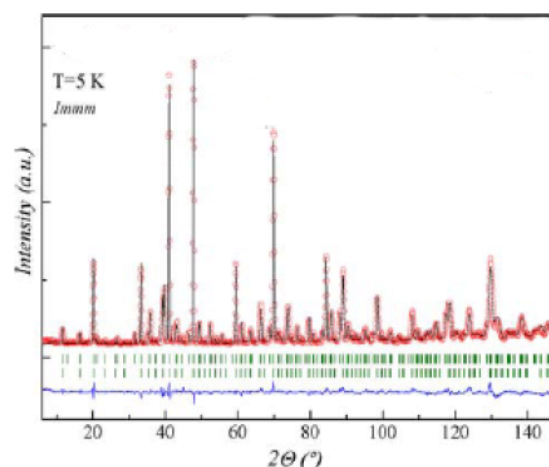


Fig.1 Neutron powder diffraction pattern of the Fe-doped compound at T = 5 K. Experimental data, results of Rietveld refining and their difference are shown. Vertical lines show Bragg peak position for crystal and magnetic (G-type antiferromagnetic) structures.

 <b>HELMHOLTZ ZENTRUM BERLIN</b> für Materialien und Energie  <b>NEUTRONS</b>	<b>EXPERIMENTAL REPORT</b>  <b>Neutron diffraction study of the crystal and magnetic structure transformation in Pr<sub>0.5</sub>A<sub>0.5</sub>FeO<sub>3-d</sub> perovskite</b>	Proposal: PHY-01-2732 Instrument: <b>E9</b> Local Contact: Paul Henry
	Principal Proposer: Victor Kabanov, IJS Ljubljana, Slovenia Experimental Team: Vadim Sikolenko, PSI, CH Vadim Efimov, JINR Dubna, RU	Date(s) of Experiment  15.06.2010 – 20.06.2010

Date of report: 05.03.2011

Perovskite compounds of the type  $Re_{1-x}A_xBO_3$  (Re is rare earth, A is Ba, Ca or Sr and B is Fe, Mn, Co or Ni), are of considerable importance due to their interesting electronic, magnetic and catalytic properties. Depending on their compositions, they show a variety of magnetic and electronic phenomena, including ferromagnetic, antiferromagnetic, charge and orbital ordering.

Among substituted cobaltites a compound  $Pr_{0.5}Sr_{0.5}CoO_3$  is an extraordinary case. This solid solution possesses two-phase transitions at  $T_A \sim 120K$  and  $220K$ . A substitution Co ions by Fe ones causes a modification of phase transition at these  $T_A$

The E9 neutron diffraction data confirm a stabilization of orthorhombic phase sp.gr. Imma. (see Fig. 1).

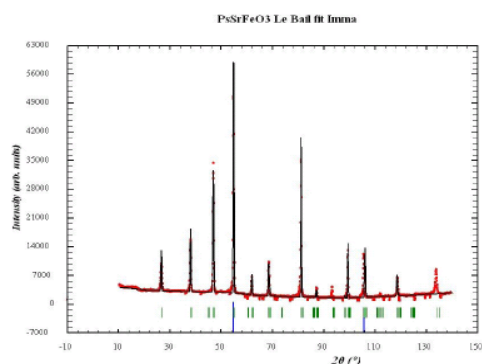


Fig.1 Refinement of the  $Pr_{0.5}Sr_{0.5}FeO_3$  sample at the room temperature. Experimental points and calculated profile is shown.

The Pr/Sr – O bond length have been calculated below and above the transition temperature. The variation in the bond length was appreciably more expressed as compared with that for B-sublattice ions. Bond length deviation from mean value for the apical anions has a small magnitude like for B-O length in

rare-earth sublattice causes a modification in the B – O bond length and thus in the  $FeO_6$  octahedra parameters.

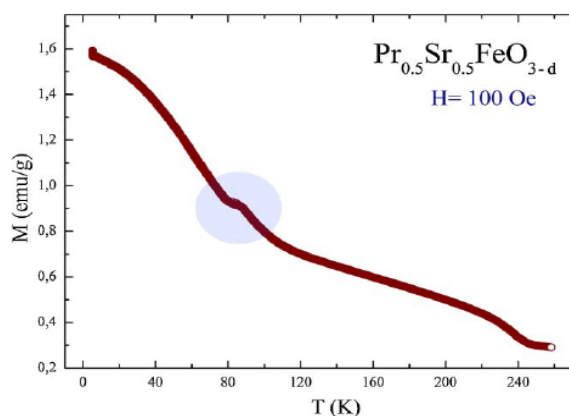


Fig.2. Temperature dependence of magnetization for the  $Pr_{0.5}Sr_{0.5}CoO_3$  measured in field cooling mode. Circle shows the peculiarity at the  $T \sim 80K$ .

Tilting of  $FeO_6$  octahedra modifies magnetic moment alignment and leads to appearance of the magnetic peculiarity (See Fig.2)

#### Acknowledgment

This research project has been supported by the European Commission under the 7<sup>th</sup> Framework Programme through "Research Infrastructures" action of the "Capacities" Programme, contract number CP-CSA\_INFRA-2008-1.1.1. Number 226507-NMI3

Principal Proposer: M. Señaris-Rodríguez, Univ. de A Coruña, ES  
M. Reehuis, HZB  
M. Jansen, MPI Stuttgart, Germany

Experimental Team: M. Reehuis, HZB  
A. Hoser, HZB

Date(s) of Experiment

16.08.2010 – 20.08.2010

Date of report: 17.11.2010

The new manganese oxide  $\text{Cs}_3\text{Mn}_2\text{O}_4$  crystallizes in the monoclinic space group  $P2_1$  (No. 4). In this structure the Mn atoms form unusual Mn-O chains along the monoclinic  $b$ -axis. From our first neutron powder diffraction experiment on E6 we found that the Mn moments are coupled antiferromagnetically with a moment direction perpendicular to  $b$  [1]. Magnetization measurements at 2.5 K showed a metamagnetic transition with two steps (Fig. 1). Starting from zero-field the first step occurs immediately with increasing field followed by a second step at about 0.8 T. No further transitions were observable up to 7 T. The magnetization of the intermediate phase reaches about 1/3 of that observed at higher field.

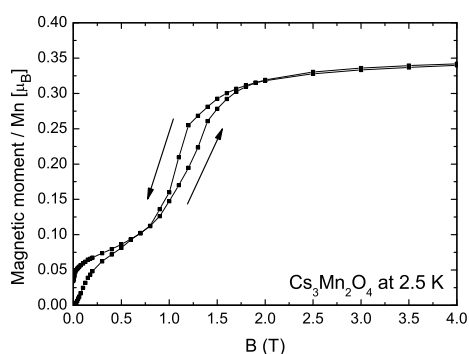


Fig. 1. Field-dependence of the magnetic moment per Mn-atom of  $\text{Cs}_3\text{Mn}_2\text{O}_4$ .

In order to investigate the change of the magnetic structure of  $\text{Cs}_3\text{Mn}_2\text{O}_4$  with increasing field we carried out a neutron powder diffraction experiment on the instrument E9 using the neutron wavelength  $\lambda = 2.795 \text{ \AA}$  (PG-monochromator). Powder patterns at different magnetic fields have been collected at 2 K in the  $2\theta$ -range between  $6^\circ$  and  $139^\circ$ . In agreement with our E6-experiment the same type of magnetic reflections  $hkl$  with  $h = 2n+1$  and  $k, l = 2n$  could be observed. Rietveld refinements of the E9-data confirmed the anti-ferromagnetic structure of  $\text{Cs}_3\text{Mn}_2\text{O}_4$ . The experimental magnetic moments of the Mn-atoms in zero-field were found to be the same:  $\mu_{\text{exp}} = 2.90(17) \mu_B$  (E6),  $\mu_{\text{exp}} = 2.86(3) \mu_B$  (E9).

At 2.5 T, where the high-field magnetic phase is well established, the magnetic reflections observed at zero-field are completely vanished (Fig. 2). On the other hand strong magnetic reflections could be observed with  $h, k, l = 2n$ . Strong magnetic intensity appeared on the position of 020 suggesting a ferromagnetic alignment of the Mn-moments in the monoclinic  $ac$ -plane. Further the data analysis showed that the magnetic order within the Mn-O-chains, pointing along  $b$ , remains unchanged. Therefore, with increasing magnetic field only a change occurs from an antiferro- to a ferromagnetic interchain coupling along the  $a$ -axis (Fig. 3). In

the powder patterns collected at 0.75 T and 1.5 T no other new sets of magnetic reflections could be observed (Fig. 2). In this range, where one may expect an intermediate magnetic phase, the magnetic reflections of the zero- and the high-field phases are more or less observable. In fact, it is interesting to see that the magnetization measurements show a weak ferromagnetism that could not be detected from neutron powder diffraction. Possibly an additional ferromagnetic component is induced along the  $b$ -axis.

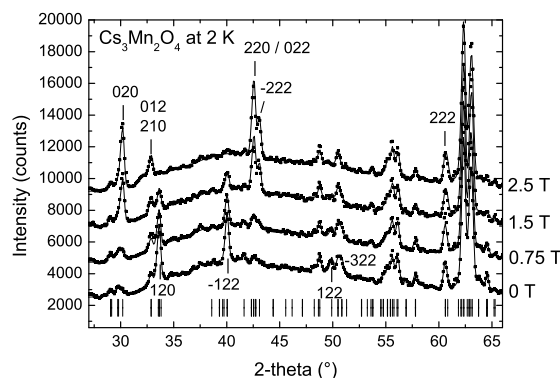


Fig. 2. Neutron powder patterns of  $\text{Cs}_3\text{Mn}_2\text{O}_4$  at 2 K and magnetic flux densities between 0 and 2.5 T.

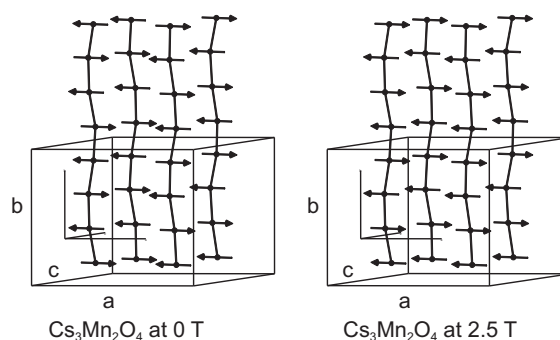



Fig. 2. Antiferromagnetic structures of  $\text{Cs}_3\text{Mn}_2\text{O}_4$  at 2 K.

#### Reference

[1] M.A. Señaris-Rodríguez, M. Reehuis, M. Jansen, A. Hoser, T. Hofman, BENS Experimental Reports 2010.

#### Acknowledgement:

This research project has been supported by the European Commission under the 7<sup>th</sup> Framework Programme through "Research Infrastructures" action of the "Capacities" Programme, contract number CP-CSA\_INFRA-2008-1.1.1. Number 226507-NMI

 <b>HELMHOLTZ ZENTRUM BERLIN</b> für Materialien und Energie  <b>NEUTRONS</b>	<b>EXPERIMENTAL REPORT</b>  <b>Magnetic excitation Spectrum of the distorted triangular antiferromagnet alpha- CaCr2O4</b>	Proposal: PHY-02-736-EF  Instrument: <b>V2</b>  Local Contact: K. Rule
	Principal Proposer: Bella Lake, HZB Experimental Team: Sandor Toth, HZB Bella Lake, HZB Kirrily Rule, HZB	Date(s) of Experiment  27.10.2009 – 02.11.2009

Date of report: 15.01.2011

This internal beamtime was intended for  $\text{InV}_2\text{O}_5$ . Because samples could not be grown  $\alpha\text{-CaCr}_2\text{O}_4$  was measured instead.

$\alpha\text{-CaCr}_2\text{O}_4$  is a distorted quasi 2D Heisenberg triangular lattice antiferromagnet. The crystal structure is orthorhombic ( $Pmmn$ ). The  $\text{Cr}^{3+}$   $S=3/2$  magnetic ions are arranged into triangular layers that form the **b-c** plane and which are stacked antiferromagnetically along the **a** axis. The crystal orders magnetically below  $T_N=41$  K with a magnetic ordering wavevector of  $\mathbf{k}=(0 \ 2/3 \ 0)$ . Strong direct exchange interactions which are both isotropic and antiferromagnetic are expected between the magnetic ions within the **b-c** while antiferromagnetic superexchange interactions are expected along **a** which are much weaker due to the longer interplane Cr-Cr distance. This system is interesting because of its potential for frustration, non-collinear magnetic ordering and strong magnon-magnon interactions.

We measured a single crystal sample ( $m=340$  mg), at the base temperature of 2K well below the Neel temperature using the FLEX triple axis spectrometer. The sample was oriented with  $(h,k,0)$  as the horizontal scattering plane and the spectrometer was used in *W* configuration for optimum resolution with the final wavelength fixed and collimation of  $(60^\circ)$  before the sample. Most of the data were collected with final wavevector  $k_F=1.55 \text{ \AA}^{-1}$ , which gave a vanadium width of  $0.2 \text{ meV}$  FWHM. To check certain linewidths we used  $k_F=1.2 \text{ \AA}^{-1}$ , where the energy resolution was  $0.1 \text{ meV}$  FWHM. In the low resolution mode, the maximum possible energy transfer was  $11 \text{ meV}$ .

In accordance with expectations, a steep dispersion is observed along  $(1 \ k \ 0)$  due to the strong exchange interactions within the plane. (see figure 1). The top of the dispersion is much higher than the instrumental limit. Assuming a undistorted triangular antiferromagnet, the in-plane spin-spin coupling is estimated to be  $23 \pm 3 \text{ meV}$  by

fitting the expression  $E=J|\sin(2\pi Q)|$  to the dispersion along  $(1 \ k \ 0)$ .

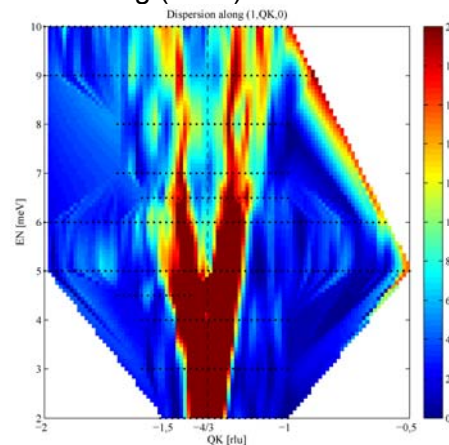


Fig. 1. Dispersion along  $(1 \ k \ 0)$ .

We also measured the spin wave dispersion along the  $(h \ -1.33 \ 0)$  direction, in order to probe the interplanar interactions (see Fig. 2). The measured linewidths are resolution limited and the top of the dispersion is around  $4 \text{ meV}$ . A small energy gap of  $0.5 \text{ meV}$  was observed at  $(1 \ -1.33 \ 0)$  above the magnetic Bragg-peak.

Data analysis is underway to determine the exchange interactions and the nature of the excitations.

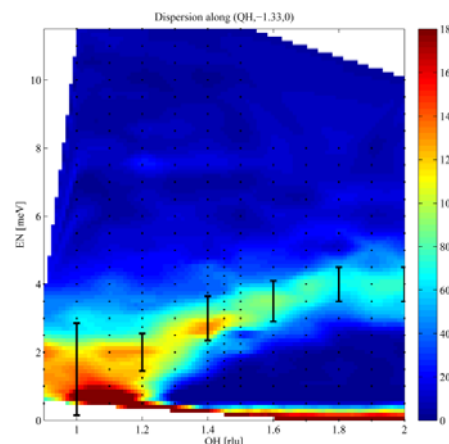


Fig. 2. Spinwave dispersion along **a**, error bars are simulated instrumental resolution where the broadening due to the strong dispersion in the *b-c* plane has been taken into account.

Principal Proposer: Diana Quintero Castro, HZB  
Experimental Team: Bella Lake, HZB  
Nazmul Islam, HZB

Date(s) of Experiment

09.02.2010 - 10.02.2010  
09.03.2010 - 15.03.2010

Date of report: 07.02.2011

SrYb<sub>2</sub>O<sub>4</sub> is a frustrated, low dimensional antiferromagnet. The magnetic Yb<sup>3+</sup> ions have angular momentum  $S=1/2$ ,  $L=3$  and  $J=7/2$  and form sub-lattices of double chains running parallel to the crystallographic  $c$ -axis. There are two inequivalent although highly similar chains due to the two inequivalent Yb<sup>3+</sup> ions per unit cell [1]. Heat capacity measurements show a long range antiferromagnetic order below 0.9 K ( $k=(0,0,0)$ ) and a shottky anomaly centred at 2.5 K. This anomaly could be explain as diffuse magnetic scattering, having a total magnetic entropy of  $\ln 2$  per Yb, which is expected as the magnetic entropy of the doublet degenerate ground state.

We have used the cold triple axis spectrometer FLEX-V2 at BERII, in order of investigate the energy and wavevector dependence of this low energy excitation. For our investigations we used one single crystal of SrYb<sub>2</sub>O<sub>4</sub> of length 1.5 cm, diameter 5 mm and mass 3.197 g. A Cuper crystal holder was used ensuring the thermal conductivity at dilution temperatures. FLEX was operated in the W configuration (+ - +). The collimation settings were 60'-60'. Most of the measurements were performed with a fixed final wavevector  $k_f=1.12 \text{ \AA}^{-1}$ . The expected resolution was 0.05meV. Using a dilution stick a temperature of about  $50 \pm 20 \text{ mK}$  was reached. A Be filter was used in order to cut lambda half contamination. In particular, this filter was useful to proof the nuclear space group (Pnam), which was unclear before. We performed wavevector scans through specific key Bragg reflections (see Fig 1).

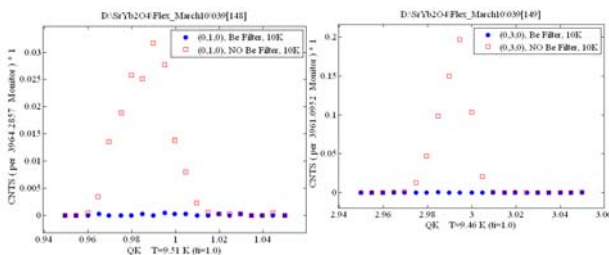


Fig 1a. (0,1,0), forbidden in Pnam.  
Fig 1b.(0,3,0), forbidden in Pnam.

The magnetic excitations were measured by performing energy scans at constant wavevector in the QK-QL plane . Figures 2 and 3 show the excitations along (0,2,L) and (0,K,0). Each point was measured in average for 8min. We found a band of magnetic excitations with a gap of 0.25meV. It seems to be a lot of diffuse scattering (up to 1meV) 1meV even though the

measurement was performed below the Neél temperature in the antiferromagnetic ordered state.

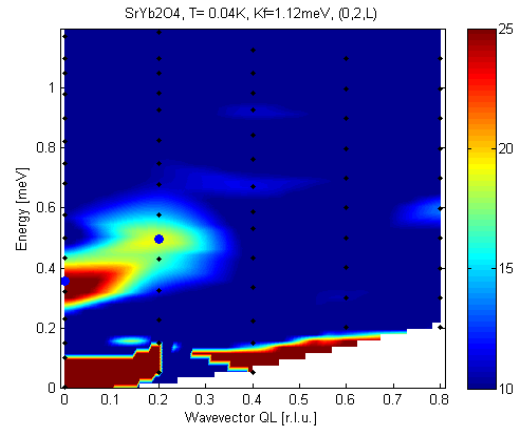


Fig 2. Data from V2. Scans along (0,2,L) plotting together in a colorplot. Being the color the number of counts for a monitor of monitor=2400000. The temperature is: 0.04K.

The intensity of the excitations is very weak plus it seems to be modulated. All of these makes difficult to point out the bandwidth of the excitations and the number of modes.

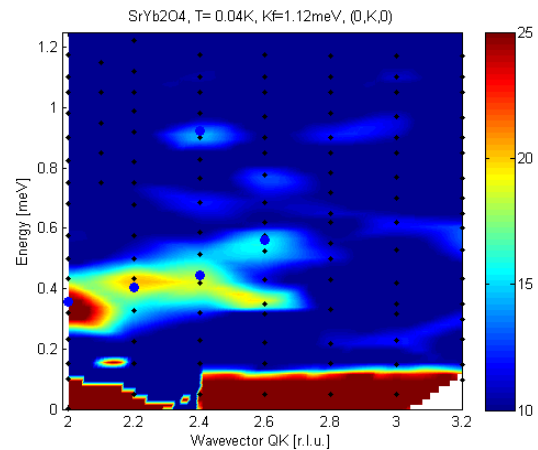


Fig 2. Data from V2. Scans along (0,K,0) plotting together in a colorplot. Being the color the number of counts for a monitor of monitor=2400000. The temperature is: 0.04K.

Experiments using a bigger neutron flux will be necessary in order to analyze the magnetic excitations in this material.

[1] D. Quintero-Castro, experimental report PHY-01-2595-EF

Principal Proposer:

N. Nikseresht, EPFL, Lausanne, CH  
H. Roennow, EPFL, Lausanne, CH

Experimental Team:

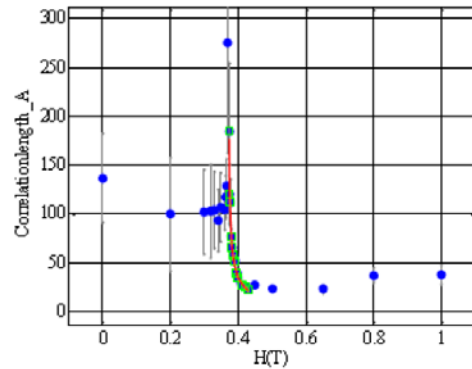
N. Nikseresht, EPFL, Lausanne, CH  
N. Tsyulin, EPFL, Lausanne, CH  
K. Rule, HZB

Date(s) of Experiment

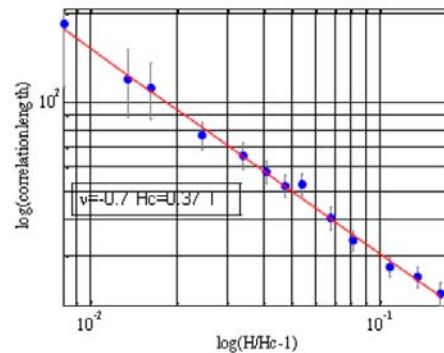
19.03.2010 – 01.04.2010

Date of report: 31.01.2011

LiErF4 is a dipolar coupled planar antiferromagnet with an ordering temperature of  $T_N=375$  mK, which shows a quantum phase transition at a critical field  $H_c=4$  kOe applied along the crystallographic c-axis [1,2,3]. Our studies of critical exponents for order parameter and specific heat measurements, mostly at HZB through E4 and V2, showed that the thermal transition falls in the 2D XY/ $h_4$  universality class, while the quantum phase transition is 3D. Exploiting large perfect crystals, negligible incoherent scattering and the large rare-earth moment, LiErF4 represent an ideal model system, where criticality and scaling relations can be explored in great detail. On V2 we studied the critical scattering in the vicinity of  $T_N$  and  $H_c$ , with the ambition of extracting exponents for the correlation length as fct. of resp.  $T$  and  $H$ , and for the spatial correlation function at the critical points. With careful track of samples' thermalisation and enough wide scans, we could obtain very accurate and interesting results. The extracted critical exponent of correlation length for QPT is in agreement with 3D class. However, there is no exact value reported so far for the 2D XY system with strong field anisotropy. Hence, some theoretical investigation is essential for subtle interpretation of physics.



Correlation length versus Field

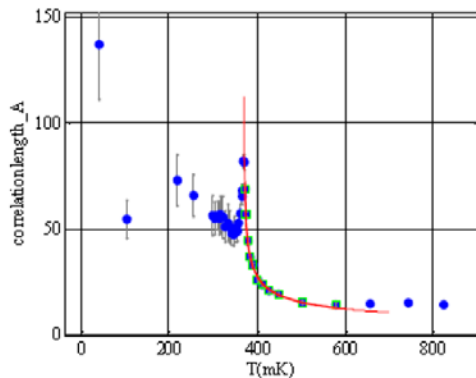


Power law fit to the obtained correlation length ( $H > H_c$ )

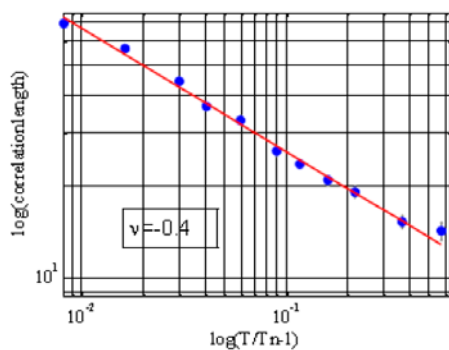
[1] [http://infoscience.epfl.ch/record/144121/files/Thesis\\_CKraemer.pdf](http://infoscience.epfl.ch/record/144121/files/Thesis_CKraemer.pdf). [2] C. Kraemer et al., in preparation for Nature Physics. [3] C. Kraemer et al., in preparation for PRL.

### Acknowledgement:


*This research project has been supported by the European Commission under the 7<sup>th</sup> Framework Programme through "Research Infrastructures" action of the "Capacities" Programme, contract number CPCSA\_INFRA-2008-1.1.1. Number 226507- NMI3*



Correlation length versus T



Power law fit to the obtained correlation length ( $T > T_N$ )

	<b>EXPERIMENTAL REPORT</b>  <b>Spin Excitations and Bose-Einstein Condensation in the random bond spin ladder material <math>(C_5D_{12}N)_2CuBr_4(1-x)Cl_{4x}</math></b>	Proposal: PHY-02-754  Instrument: <b>V2</b>  Local Contact: Klaus Habicht
	Principal Proposer: Christian Ruegg, UCL, UK Experimental Team: Simon Ward, UCL, UK	Date(s) of Experiment  26.05.2010 – 03.06.2010

Date of report: 29.01.2011

The metal-organic material  $(C_5H_{12}N)_2CuBr_4$  is an exceptional realisation of a quantum spin ladder. We proposed to investigate the influence of bond randomness on the spin Luttinger-liquid and BEC physics observed in this material and search for a Bose glass phase, by a combined neutron spectroscopy and diffraction study performed on Cl-substituted  $(C_5D_{12}N)_2CuBr_4(1-x)Cl_{4x}$  on FLEX/V2.

$(C_5D_{12}N)_2CuBr_4(1-x)Cl_{4x}$  based compounds have superexchange spin-spin couplings  $J_r$  and  $J_l$ , which correspond to ladder rungs and legs. In the pure Br case ( $x=0$ ) these have values of 12.8K and 3.2K respectively. On application of magnetic field the sample starts to become magnetised at a quantum critical point (QCP)  $H_c = 6.9T$  and reaches magnetic saturation at another QCP  $H_s$  which has a value of 14T [1]. Between  $H_c$  and  $H_s$  the system is in a Luttinger-liquid (LL) phase described by a 1D conductor where second order interactions are described by Bosonic interactions. When the temperature is reduced to the order of inter-ladder coupling ( $J' \sim 25mK$ ) the system transitions from LL to 3D-XY ordered and is controlled the critical exponent  $\beta$ . This critical exponent allows the system to be described as a Bose Einstein Condensation (BEC) of magnons.

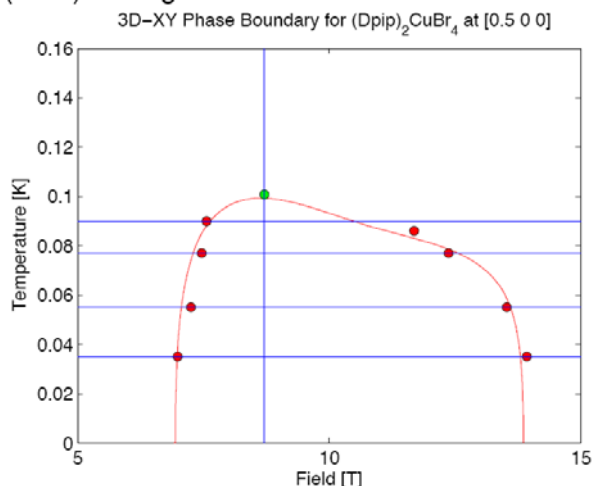


Figure 1:  $H_c$  and  $H_s$  (Red points) and  $T_c$  (Green Points) on theoretical expectation (Red line)

The temperature and field dependence of the magnetic order  $m_{XY}(B, T)$  of  $(C_5D_{12}N)_2CuBr_4$  was studied in order to provide confirmation of theoretical limits of  $H_c$ ,  $H_s$  and  $T_c$ . The resulting critical fields and temperatures are summarised in Figure 1 and notably  $T_c$  was found to be in excellent agreement with [2].

This shows exemplar confirmation to theoretical expectations [2], which has only been possible thanks to the exacting standards of the sample environment team. The critical exponent  $\beta$  has also been extracted and found to be  $\beta=1/3$  as expected.


A doping concentration of 10% ( $x=0.1$ ) was chosen to examine the effect of bond randomness as it was expected not lead to a completely disordered system. However at 35mK magnetic order could not be found, which suggests that even at  $x=0.1$  there is sufficient bond disorder to prevent order from forming, or that order occurs at temperatures lower than 35mK.

$(C_5D_{12}N)_2CuCl_4$  has ladder interactions  $J_l = 1.13K$ ,  $J_r = 3.52K$  [3] and was also studied. Inter-ladder couplings are expected to be roughly half of those of the Br case leading to an expected  $T_c \approx 50mK$ . Due to problems maintaining constant temperature in the presence of a magnetic field, temperatures lower than 50mK between  $H_c$  and  $H_s$  were not obtained.

In conclusion the effect of bond disorder on 3D-XY ordering could not be studied in this experiment however it has provided excellent reinforcement of theoretical expectations of  $(C_5H_{12}N)_2CuBr_4$ .

[1] B.C. Watson et al., Phys. Rev. Lett. 86, 5168 (2001). [2] B. Thielemann, Ch. Rüegg et al., Phys. Rev. Lett. 102, 107204 (2009). [3] T. Tajiri et al., JMMM 272-276, 1070 (2004).

*This research project has been supported by the European Commission under the 7<sup>th</sup> Framework Programme through "Research Infrastructures" action of the "Capacities" Programme, contract number CP-CSA\_INFRA-2008-1.1.1. Number 226507-NMI3*

 <b>HELMHOLTZ ZENTRUM BERLIN</b> für Materialien und Energie  <b>NEUTRONS</b>	<b>EXPERIMENTAL REPORT</b>  <b>Magnetic field dependence of Luttinger Parameter for a spin chain</b>	Proposal: PHY-02-771  Instrument: <b>V2</b>  Local Contact: K. Rule, D. Le
	Principal Proposer: Dan Hübner, ETH Zürich Experimental Team: Duc Le, HZB Kirrily Rule, HZB	Date(s) of Experiment  19.08.2010 – 29.08.2010

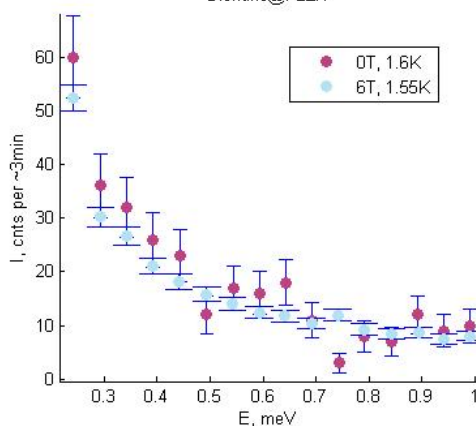
Date of report: 21.01.2011

In current experiment we test experimentally a fundamental scaling law for one-dimensional fermion systems with gapless linear spectrum - Luttinger liquids. We measure dynamic structure factor at zone centre as a function of magnetic field and temperature and fit the theoretical prediction with 2 free parameters - scaling constant and Luttinger parameter  $K$ . For 1D Heisenberg model in magnetic field  $K$  changes from  $K=0.5$  in zero field to  $K=1$  at saturation. In magnetic fields dynamic structure factor retains universality but acquires different values for projections parallel and perpendicular to magnetic field. Horizontal field geometry was chosen to measure explicitly  $S^{xx}(\pi, E, T)$  component and to avoid difficulties of deconvoluting it from  $S^{zz}$  which shifts to incommensurate wavevectors in magnetic field.

Current experiment consisted of measuring inelastic scans at  $q_L = \pi$  at 1.6K in 0T field and comparing the results to measurements at several temperatures (0.09K, 0.5K, 1.55K, 2.45K, 5K) in 6T fields to deduce change in Luttinger parameter  $K$ . Background was measured at exactly the same  $Q$  and  $E$  values but at 20K where magnetic dynamic structure factor is negligible. Figure 1 shows typical inelastic scans over the spinon continuum at  $q_L = \pi$  in zero field (bad statistics) and in 6T field.

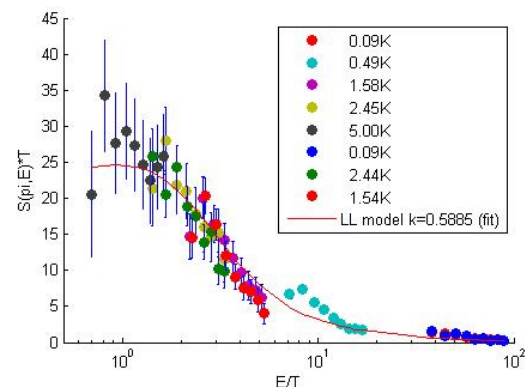
Figure 1

Dioxane@FLEX



The background subtracted data measured in 6T field was plotted in  $E/T \sim S^*T$  axis to deduce the Luttinger parameter from the scaling law, see Fig. 2. We note that this fitting procedure is very sensitive to background subtraction since we are measuring weakly scattering spinon continuum and therefore the result should be considered preliminary until additional supporting measurements will be carried out.


Figure 2



The smooth run of current experiment on V2 with horizontal field magnet HM-3 was hindered by the following problems: a) power supply failure on one of the stepper motor encoders (6 hours), b) nonoperational He level meter on HM3 cryomagnet, which resulted in magnet quench (6 hours), c) software error reading motor encoder angle motor A1 (8 hours), which resulted in readjustment of the instrument and necessitated new background collection (24 hours).

*This research project has been supported by the European Commission under the 7<sup>th</sup> Framework Programme through "Research Infrastructures" action of the "Capacities" Programme, contract number CP-CSA\_INFRA-2008-1.1.1. Number 226507-NMI3*



 <b>HELMHOLTZ ZENTRUM BERLIN</b> für Materialien und Energie  <b>NEUTRONS</b>	<b>EXPERIMENTAL REPORT</b>	Proposal: PHY-03-661-EF
	<b>Magnetic Excitations of the Quantum Spin-Chain Compounds <math>\beta</math>-CuNb<sub>2</sub>O<sub>6</sub></b>	Instrument: <b>V3</b> Local Contact: M. Russina/Z. Izaola
Principal Proposer: Bella Lake, HZB Experimental Team: Oliver Pieper, HZB Nazmul Islam, HZB	Date(s) of Experiment  21.12.2009 - 23.12.2009	

Date of report: 24.01.2011

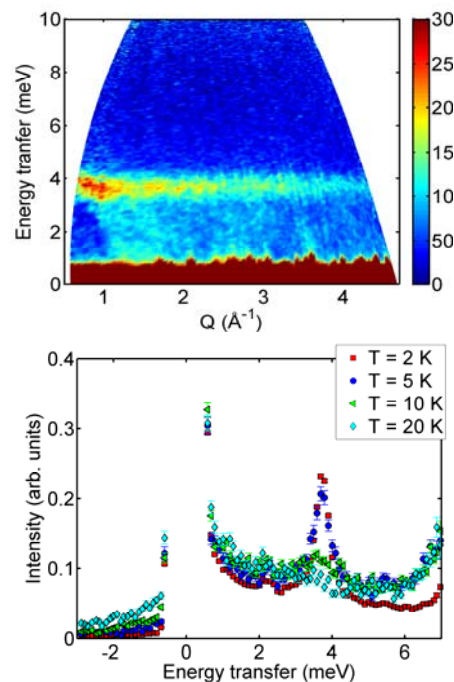
Inelastic neutron scattering investigations have been performed on powder samples of the spin- $\frac{1}{2}$  compound  $\beta$ -CuNb<sub>2</sub>O<sub>6</sub> using the time-of-flight spectrometer NEAT/V3.

$\beta$ -CuNb<sub>2</sub>O<sub>6</sub> crystallizes in orthorhombic spacegroup (Pbcn) and the Cu<sup>2+</sup> ions which possess spin-1/2 give rise to the magnetism. The material consists of zigzag chains of edge-sharing CuO<sub>6</sub> octahedra suggesting that there are one-dimensional interactions between the Cu<sup>2+</sup>-ions in the chain direction [1]. Furthermore, weak interchain coupling leads to antiferromagnetic long range order below  $T \approx 7$  K [2].

In order to study the magnetic excitation spectra of the system, we performed measurements using neutrons with incident wavelengths ranging from 1.9-5.9 Å. Measurements took place at base temperature ( $T=2$  K) and up to  $T=20$  K.

Below the magnetic ordering temperature the magnetic excitation spectrum is dominated by an almost flat feature at  $E \approx 3.9$  meV with some additional spectral weight at lower energies [Fig. 1 (top)]. The peculiar flat shape of the magnetic excitations can be explained by the high density of states in the vicinity of the magnetic zone boundaries, where the spin wave dispersion has its maximum. However, the particularly strong intensity of this  $E \approx 3.9$  meV feature also indicates that there are strong and approximately equal spin-spin correlations along more than one direction, suggesting that the system is most probably 2D in nature.


The spin wave character of the spectra is further underlined by its temperature dependence. In Fig. 1 (bottom) the Q-integrated intensity is displayed as a function of the energy transfer, which shows the smooth disappearance of the 3.9 meV feature above the Néel-temperature.



**Figure 1:** (Top) Energy-wavevector colormap of  $\beta$ -CuNb<sub>2</sub>O<sub>6</sub> ( $\lambda=2.5$  Å,  $T=2$  K), (bottom) Q-integrated spectra for various temperatures.

Data analysis for this material is on-going and additional measurements on single crystals of  $\beta$ -CuNb<sub>2</sub>O<sub>6</sub> are also planned in order to map out the spin wave dispersion along all crystallographic directions and therefore to shed light on the true dimensionality of that system.

- [1] M.G.B. Drew et al J. Mater Chem 3 889 (1993)  
 [2] K. Kodama et al.; J. Phys. Soc. Japan **67**, 57 (1998)

 <p><b>HELMHOLTZ ZENTRUM BERLIN</b> für Materialien und Energie</p> <p><b>NEUTRONS</b></p>	<p><b>EXPERIMENTAL REPORT</b></p> <p><b>Magnetic Excitations of the Quantum Spin-Chain Compounds <math>\beta</math>-CuNb<sub>2</sub>O<sub>6</sub></b></p>	<p>Proposal: PHY-03-686</p> <p>Instrument: <b>V3</b></p> <p>Local Contact: M. Russina/Z. Izaola</p>
	<p>Principal Proposer: Bella Lake, HZB</p> <p>Experimental Team: Oliver Pieper, HZB Nazmul Islam, HZB</p>	<p>Date(s) of Experiment</p> <p>21.12.2009 - 23.12.2009</p>

Date of report: 24.01.2011

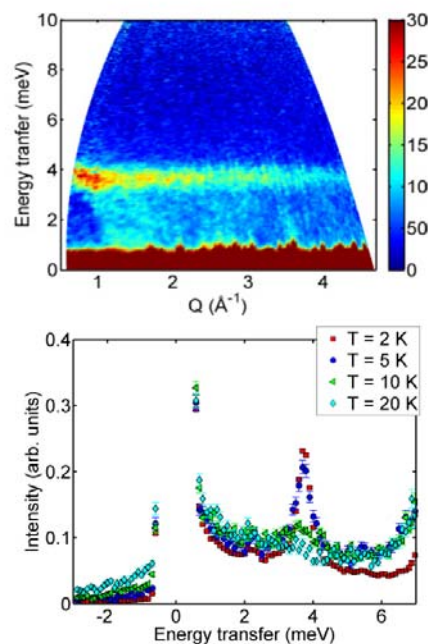
Inelastic neutron scattering investigations have been performed on powder samples of the spin- $\frac{1}{2}$  compound  $\beta$ -CuNb<sub>2</sub>O<sub>6</sub> using the time-of-flight spectrometer NEAT/V3.

$\beta$ -CuNb<sub>2</sub>O<sub>6</sub> crystallizes in orthorhombic space group (Pbcn) and the Cu<sup>2+</sup> ions which possess spin-1/2 give rise to the magnetism. The material consists of zigzag chains of edge-sharing CuO<sub>6</sub> octahedra suggesting that there are one-dimensional interactions between the Cu<sup>2+</sup>-ions along the chain direction [1]. Furthermore, weak interchain coupling leads to antiferromagnetic long range order below T $\approx$ 7 K [2].

In order to study the magnetic excitation spectra of the system, we performed measurements using neutrons with incident wavelengths ranging from 1.9-5.9 Å. Measurements took place at base temperature (T=2 K) and up to T=20 K.

Below the magnetic ordering temperature the magnetic excitation spectrum is dominated by an almost flat feature at E $\approx$ 3.9 meV with some additional spectral weight at lower energies [Fig. 1 (top)]. The peculiar flat shape of the magnetic excitations can be explained by the high density of states in the vicinity of the magnetic zone boundaries, where the spin wave dispersion has its maximum. However, the particularly strong intensity of this E $\approx$ 3.9 meV feature also indicates that there are strong and approximately equal spin-spin correlations along more than one direction, suggesting that the system is most probably 2D in nature.

The spin wave character of the spectra is further underlined by its temperature dependence. In Fig. 1 (bottom) the Q-integrated intensity is displayed as a function of the energy transfer, which shows the smooth disappearance of the 3.9 meV feature above the Néel-temperature.



**Figure 1:** (Top) Energy-wavevector colormap of  $\beta$ -CuNb<sub>2</sub>O<sub>6</sub> ( $\lambda=2.5$  Å, T=2 K), (bottom) Q-integrated spectra for various temperatures.

Data analysis for this material is on-going and additional measurements on single crystals of  $\beta$ -CuNb<sub>2</sub>O<sub>6</sub> are also planned in order to map out the spin wave dispersion along all crystallographic directions and therefore to shed light on the true dimensionality of that system.

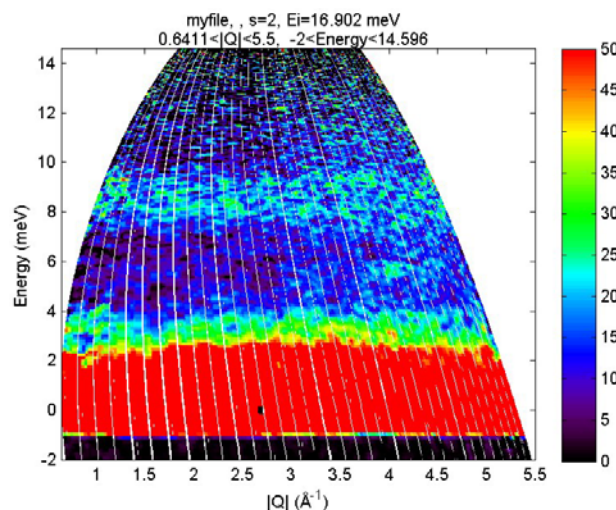
- [1] M.G.B. Drew et al J. Mater Chem 3 889 (1993)  
[2] K. Kodama et al.; J. Phys. Soc. Japan **67**, 57 (1998)

 <b>HELMHOLTZ ZENTRUM BERLIN</b> für Materialien und Energie  <b>NEUTRONS</b>	<b>EXPERIMENTAL REPORT</b>	Proposal: PHY-03-712-EF
	<b>Structural and magnetic properties of ortho-Sr<sub>2</sub>VO<sub>4</sub></b>	Instrument: <b>V3</b> Local Contact: N. Tsapatsaris
Principal Proposer: Bella Lake, HZB Experimental Team: Joachim Deisenhofer, Uni Augsburg Sandor Toth, HZB Enrico Giannini, University of Geneva, CH	Date(s) of Experiment 20.09.2010 - 29.09.2010	

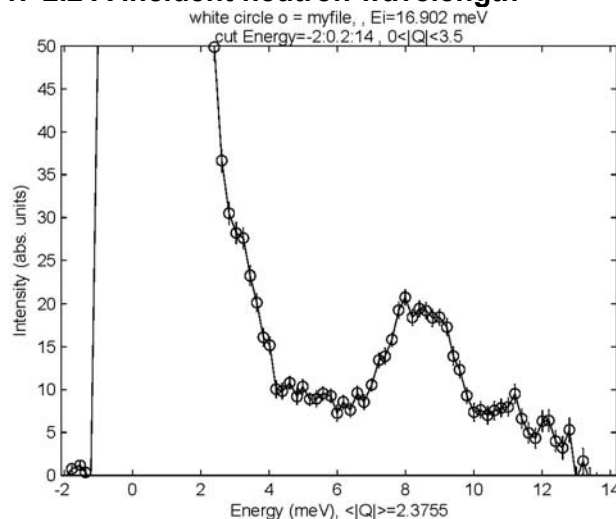
Date of report: 17.02.2011

Ortho-Sr<sub>2</sub>VO<sub>4</sub> is a new magnetic material. The V<sup>4+</sup> ions have a single electron in the d-shell which result spin-1/2, and gives rise to the magnetic properties. The structure of Sr<sub>2</sub>VO<sub>4</sub> has been investigated using neutron and x-ray powder diffraction [1]. The data reveal that the symmetry is orthorhombic with space group Pna2<sub>1</sub> and show that the V<sup>4+</sup> ions lie within a distorted tetrahedral environment. The low temperature magnetic ground state is probably a singlet due to dimerisation as, revealed by DC magnetic susceptibility measurements. The data was fitted to the Bleaney-Bowers expression for a spin-1/2 dimer system and an intradimer exchange of  $J=52 \text{ K} \sim 4.5 \text{ meV}$  was extracted. The nature of the dimer bond is however unknown, the structure reveals no obvious features such as direct pairing of the VO<sub>4</sub> tetrahedra via V-O-V bonds, instead long-distance superexchange bonds of the form V-O-O-V and V-O-Sr-O-V must be involved.

We investigated the magnetic excitations of Sr<sub>2</sub>VO<sub>4</sub>. The powder sample had a mass of  $m=6.763 \text{ g}$ . The sample holder was an aluminium can, inner diameter 16 mm, 1 mm thick. Different incident neutron wavelengths were used to look for the magnetic excitations (1.9 Å, 2.2 Å, 3.0 Å, 4.0 Å, 4.75 Å). Sample temperature was controlled by an orange cryostat, it was in the range  $1.6 \leq T \leq 5 \text{ K}$  throughout the experiment. The only inelastic intensity was found around 9 meV, see Fig. 1. The mode is broad in energy and the intensity is slowly decreasing with increasing Q, proving its magnetic origin. The center of the mode is at 8.5 meV, see Fig. 2. The most probable explanation of the data is that we are seeing the excitation of the spin-1/2 dimers. We failed to extract any additional information (e.g. dimer size) from the Q dependence of the mode intensity due to the low signal to noise ratio.




**Fig. 1. Inelastic spectra measured with  $\lambda=2.2 \text{ \AA}$  incident neutron wavelength**



**Fig. 2. Cut along energy, intensity integrated between  $0 \leq Q \leq 3.5 \text{ \AA}^{-1}$**

[1] W. Gong *et al.*, J. solid State Phys. **94**, 213 (1991)

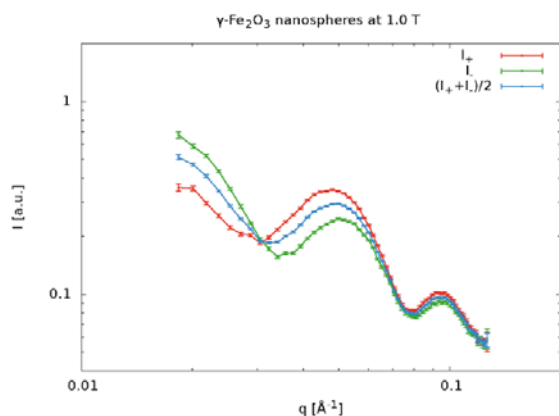
 <b>EXPERIMENTAL REPORT</b>		Proposal: PHY-04-1651
<b>Polarized SANS measurements on <math>\gamma</math>-Fe<sub>2</sub>O<sub>3</sub> nanoparticles</b>		Instrument: <b>V4</b> Local Contact: Uwe Keiderling
Principal Proposer: Experimental Team:	Sabrina Disch, FZ Jülich Elisabeth Josten, FZ Jülich Peter Busch, FZ Jülich Subhankar Bedanta, FZ Jülich Uwe Keiderling, HZB	Date(s) of Experiment  20.01.2010 - 25.01.2010

Date of report: 17.01.2011

Small angle neutron scattering with polarized neutrons was performed on diluted iron oxide nanoparticles in d-toluene. The size of the particles was between 4 and 25 nm in diameter with a size distribution of less than 5% [1].

Flipping ratio measurements have been performed on all samples under different magnetic fields applied perpendicular to the incoming beam. Due to a possible effect of ageing, the organic ligand shell of the particles may have been partially decomposed, leading to agglomeration. Therefore only the 12 nm nanoparticles showed a reasonable scattering intensity that allowed us to deduce the magnetic scattering.

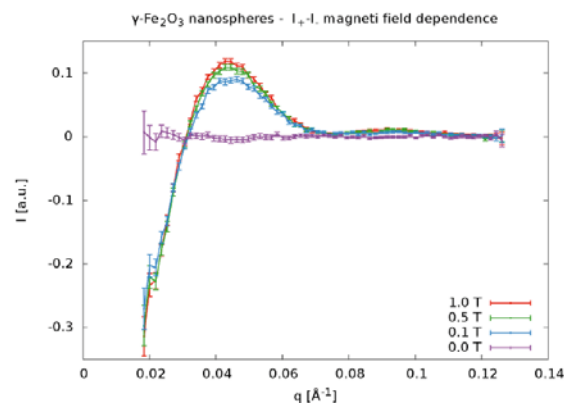
Here we show the result of the scattering from nanoparticles of 12 nm size:



**Figure 1:** Polarized SANS from 12nm nanospheres at 1 T.


Fig. 1 shows the radially integrated scattering intensity at 1 T in the channels with spin-up ( $I_+$ ), spin-down ( $I_-$ ) and the average of both. The upturn for lower  $q$  shows that even for the best sample, we got some agglomeration.

The second plot (fig. 2) shows the field dependence from the difference of spin-up and spin-down scattering. Obviously there is no preferential direction of the magnetic moments without field and it saturates between 0.5 and 1 T. The magnetic contrast increases in higher fields, as is expected for superparamagnetic particles.



**Figure 2:** Field dependent magnetic scattering from 12nm nanospheres.

[1] Park, J.; An, K.; Hwang, Y.; Park, J.; Noh, H.; Kim, J.; Park, J.; Hwang, N.; Hyeon, T. *Nat. Mater.* **2004**, 3, 891–895

 <p><b>HELMHOLTZ ZENTRUM BERLIN</b> für Materialien und Energie</p> <p><b>NEUTRONS</b></p>	<p><b>EXPERIMENTAL REPORT</b></p> <p><b>Search for the FFLO phase in a heavy-fermion superconductor CeCoIn<sub>5</sub></b></p>	<p>Proposal: PHY-04-1672/ PHY-04-1673/PHY-04-1841</p> <p>Instrument: <b>V4</b></p> <p>Local Contact: Uwe Keiderling</p>
<p>Principal Proposer: Experimental Team:</p>	<p>H. Furukawa, OU Tokyo, JP S. Kawamura, OU Tokyo, JP P. Das, University of Notre Dame, USA A. Cameron, University of Birmingham, UK E. M. Forgan, University of Birmingham, UK U. Keiderling, HZB S. Gerischer, HZB</p>	<p>Date(s) of Experiment</p> <p>16.08.2010 – 25.08.2010</p>

Date of report: 25.01.2011

Novel superconductivity in the heavy-fermion compound CeCoIn<sub>5</sub> with  $T_c = 2.3$  K has been studied extensively. In particular, various experimental results have suggested that the “FFLO state” appears in the low- $T$  and high- $H$  corner of the  $H$ - $T$  phase diagram [1]. Small angle neutron scattering (SANS) is a unique technique to verify such an exotic state, but no experimental evidence has yet been established. On the other hand, this technique has succeeded in detecting the anomalous electronic state of the quasi particles in the vortex cores [2,3]. During the present beamtime, to extend our understanding, we began measurements of the dependence of the flux line lattice (FLL) structure on field direction in CeCoIn<sub>5</sub>.

The measurements were carried out on V4. Neutrons with wavelength of 5 Å were used, with PSD and collimation set at 8 and 12 m respectively from the sample. A <sup>3</sup>He-<sup>4</sup>He dilution refrigerator was used to cool the sample down to 50 mK inside a vertical-field magnet. Two single crystal mosaics of CeCoIn<sub>5</sub> were prepared on an Al plate so that the  $c$ -axis and one of the [100] or [110] axes were in the horizontal plane. The total mass of each mosaic was about 0.65g (Fig.1).

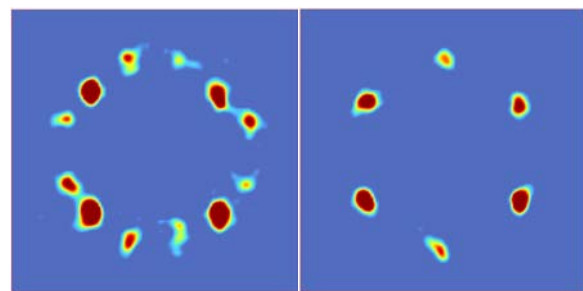
We had some trouble with unpredictable magnetic field trips - which were caused by a time-varying resistance of the leads inside the cryomagnet. We also found that the cryostat tilt motor would not drive at fields above 5T. We ascribed this to magnetisation of the motor, but simple attempts to shield the motor were insufficient, and we had to limit our tilt scans to below 4.5T. Further, we found that the sample stick was not exactly at the centre of the sample rotation. However despite these difficulties we could collect beautiful data.

Figure 2 shows typical scattering patterns measured at 4.5 T and 50 mK, with the field applied at two different angles to the  $c$ -axis. The data reveal a FLL phase transition between these two directions.

There was not enough time to perform the FLL structure measurements with the field rotated towards the [110] direction. We expect to propose a continuation experiment on V4.



**Fig. 1** Photo of the sample mosaic. CeCoIn<sub>5</sub> with [110] axis vertical (left), with [100] axis vertical (centre) and an Nb crystal for initial alignment of the field with the neutron beam. All samples were mounted on one plate and we changed between them by changing height of the dilution stick in the magnet.



**Fig. 2** FLL patterns at  $H = 4.5$  T and  $T = 50$  mK. The field was rotated by 15deg. (left) and 30 deg. (right) from the  $c$ -axis towards the [100] direction. The data were smoothed, and the centre area was masked.

#### References

- [1] For example: K. Kumagai *et al.*, *Phys. Rev. Lett.* **97**, 227002 (2006).
- [2] A. D. Bianchi *et al.*, *Science* **319**, 177-180 (2008).
- [3] S. Ohira-Kawamura *et al.*, *J. Phys. Soc. Jpn* **77**, 023702 (2008).

Principal Proposer: E. Moskvina, RAS PNPI Gatchina, RU  
 Experimental Team: S. Grigoriev, RAS PNPI Gatchina, RU  
 V. Piyadov, RAS PNPI Gatchina, RU  
 S. Wellert, HZB

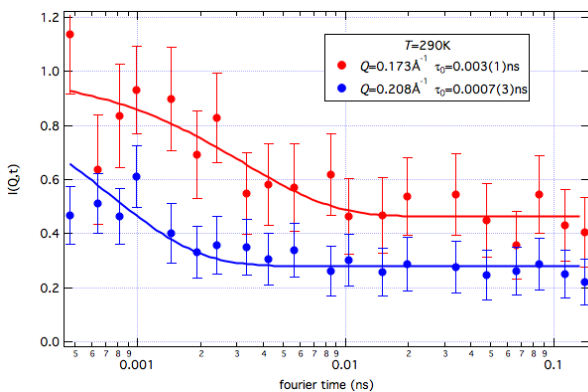
Date(s) of Experiment

9.11.2009 – 17.11.2009

Date of report: 24.06.2010

The YMn<sub>6</sub>Sn<sub>6</sub> is a compound crystallized in hexagonal HfFe<sub>6</sub>Ge<sub>6</sub>-type structure (space group P6/mmm) [1]. The lattice has an intrinsically layered structure, where Mn atoms are organized in a so-called “kagome” lattice within the *ab* planes, which are stacked along the *c* axis with Y and Sn<sub>3</sub> atomic planes between them. The Mn-Mn interplane distance through Sn<sub>3</sub> atomic plane is slightly larger than that through Y atomic plane. Below the Neel temperature  $T_N=333\text{K}$  the YMn<sub>6</sub>Sn<sub>6</sub> compound has an incommensurate periodic structure [2]. It is believed that spins are ordered in the helix along the *c* axis similar to a simple planar helimagnet with period 3.76nm [3].

The aim of this experiment was use paramagnetic neutron spin echo (NSE) to investigate the critical dynamics in this compound for different temperature (*T*) and the momentum transfer (*Q*).

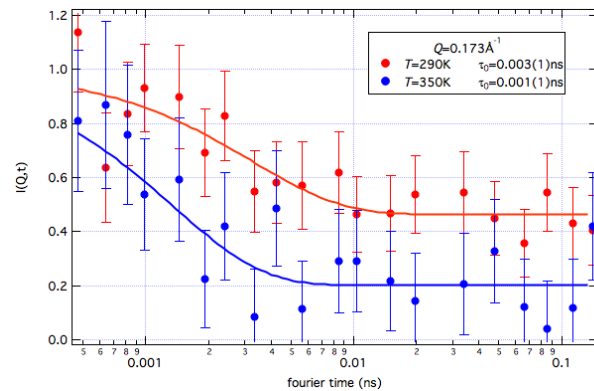


**Figure 1: Normalized scattering function for two different *Q* at  $T=290\text{K}$ .**

The experiments were performed at the wavelength of 2.5Å with relative dispersion  $\Delta\lambda/\lambda \approx 0.15$ .

The intermediate scattering function  $I(Q, t)$  was measured at different temperatures in the critical region near  $T_N$  and for different scattering vectors *Q* in the vicinity of Bragg reflexion.


Figure 1 shows the time dependence of the relaxation rate at the temperature  $T=290\text{K}$  below  $T_N$  for two different *Q*, while at the Figure 2 two isotherms are shown for  $Q = 0.173\text{Å}^{-1}$ .



**Figure 2: Normalized scattering function for two different *T* at  $Q=0.173\text{Å}^{-1}$ .**

The straight lines on both figures are respectively the best fits with exponential decay.

The preliminary data look very promising. As it's clearly seen from these pictures, there are both *T* and *Q* dependencies of the relaxation rate  $\Gamma_0 \sim \tau_0^{-1}$ . The background at higher *t* is higher for lower temperatures (compare two blue lines) due to the raising of the magnetic elastic contamination to the echo signal.

	<b>EXPERIMENTAL REPORT</b>  <b>Magnetization reversal in exchange coupled system with a field perpendicular to the cooling field and the sample plane</b>	Proposal: PHY-04-1956-EF  Instrument: <b>V6</b>  Local Contact: A. Teichert
	Principal Proposer: Amitesh Paul, HZB Experimental Team: Amitesh Paul, HZB	Date(s) of Experiment  17.11.2009 – 25.11.2009

Date of report: 31.05.2010

We have investigated the impact of out-of-plane ferromagnetic (FM) anisotropy, where antiferromagnetic (AF) anisotropy is along the film-plane, as we probe the in-plane magnetization in an IrMn/CoFe exchange coupled system.

To introduce a unidirectional anisotropy perpendicular to the film plane, we make use of a special experimental set-up using the electromagnet at the sample position of V6 reflectometer. A heating chamber was introduced between the pole pieces of the magnet as the sample stage was heated to around 500° C. This was followed by cooling the sample to room temperature (RT) in presence of 4.0 kOe of magnetic field ( $H_{FC}$ ). The arrangement has been shown in Fig. 1.

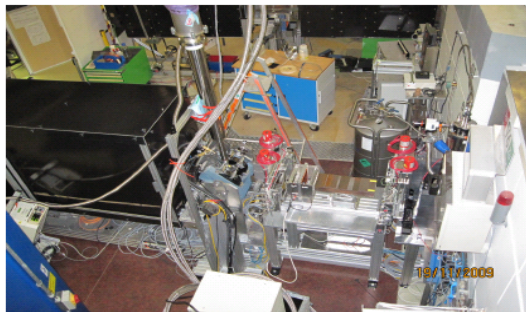


Fig.1. Experimental arrangement at V6 for cooling/heating the sample perpendicular to the film-plane.

Since neutron scattering signal is insensitive to the magnetization component parallel to the scattering vector (surface normal), in case of a non-collinear coupling, the magnetization can be measured along a direction different from the FM easy axis. Neutron scattering with polarization analysis can discriminate between the longitudinal (NSF) and transverse (SF) components of magnetization. All measurements were done at RT.

In Fig. 2, we show the polarized specular reflectivity intensity at a fixed Q value (corresponding to the highest intensity) for a variation of applied field ( $H_a$ ) values

perpendicular to the cooling field direction for the 1<sup>st</sup> half of the 1<sup>st</sup> field cycle and along the decreasing branch of the hysteresis loop (sign of  $H_{FC}$  opposite to that of  $H_a$ ). The arrow mark on the cartoon of the sample in Fig 2 indicates the direction of easy axis before the application of the cooling field.

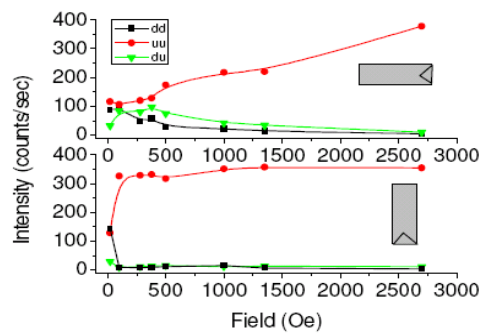


Fig.2. The polarized neutron scattered intensity at  $Q=0.02 \text{ \AA}^{-1}$  are plotted with field during field cycling of the 1<sup>st</sup> half of the 1<sup>st</sup> field cycle.

Next we show the reflectivity patterns in Fig. 3 along the direction of easy axis (perpendicular to the original easy axis) after the application of the cooling field. The measurements indicate a change of FM easy axis, though it fails to introduce a unidirectional anisotropy.

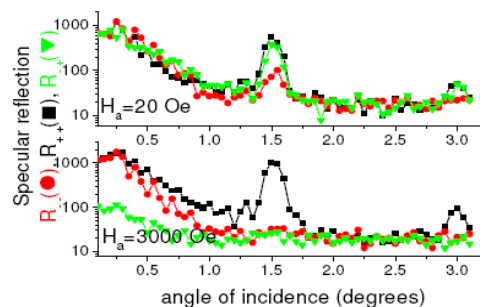



Fig.3. The polarized neutron scattered intensity with angle of incidence plotted with field during field cycling of the 1<sup>st</sup> half of the 1<sup>st</sup> field cycle.

	<b>EXPERIMENTAL REPORT</b>	Proposal: PHY-04-1959-EF
	<b>PNR study of the magnetization reversal mechanism of the implanted Ni/NiO system</b>	Instrument: <b>V6</b> Local Contact: Anke Teichert
Principal Proposer: Experimental Team:	J. Demeter, KU Leuven, B J. Demeter, KU Leuven, B E. Menéndez, KU Leuven, B A. Teichert, HZB & KU Leuven, B	Date(s) of Experiment  26.04.2010 – 04.05.2010

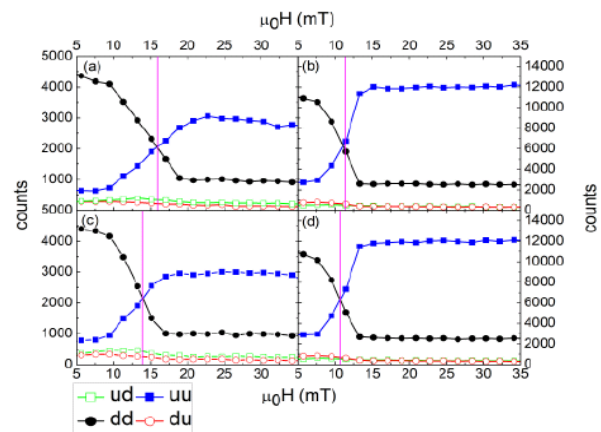
Date of report: 06.01.2011

Exchange Bias (EB), being the interfacial coupling between a ferromagnet and an antiferromagnet, has been studied primarily in the Co/CoO bilayer system.<sup>1</sup> Recently, it has been shown that EB can also be induced by the use of implantation of O ions into Co thin films. Remarkable for this system is that the magnetization reversal mechanism is radically different than in the classical Co/CoO EB bilayer system. This has been revealed by Polarized Neutron Reflectometry (PNR) *magnetic field scans*, performed on the V6 reflectometer.<sup>2</sup> This new approach to form EB has been extended to the Ni/NiO system: EB can also be induced by implanting O ions into Ni thin films. It is known from literature that EB in Ni/NiO bilayers is weaker than in the Co/CoO bilayer system. This is also observed in the implanted system. In the present experiment we aimed at studying the influence of this weaker EB coupling on the magnetization reversal mechanism of the implanted Ni/NiO system.

The measured sample consisted of a 100 nm thick Ni layer grown on a MgO(100)-substrate and capped with a Au layer to prevent from natural surface oxidation. Consecutively, the sample was implanted with a fluence of  $1.5 \times 10^{17}$  O-ions/cm<sup>2</sup>. Vibrating Sample Magnetometry measurements revealed clear EB and training properties. During the PNR measurements, the EB state was achieved by cooling the sample down to a temperature of 10 K in a field of 400 mT. In this state PNR magnetic field scans are performed for the different branches of the hysteresis loop, so the different magnetization reversals (see figure for the different branches: (a) virgin descending, (b) virgin ascending, (c) trained descending, (d) trained ascending). Magnetic field scans consist of measuring the PNR signal at a specific angle while varying the magnetic field.

The analysis of the measurements reveals a number of considerable differences with the implanted Co/CoO counterpart. Firstly, the EB


shift is much smaller than for the implanted Co/CoO system. Secondly, in the descending branches the dd signal is smaller than the uu signal after the coercive field, a phenomenon not observed in the implanted Co/CoO system. Moreover, a structure could be found in the *spin flip signal*. This can possibly be explained by the formation of closure-domains in the film, where the signal reflects the formation and annihilation of these domains. In conclusion, it has been shown that the weaker EB in Ni/NiO has a strong influence on the magnetization reversal mechanism.



- [1] J. Nogués, *et al.*, J Mag. Magn. Mat. **192**, 203 (1999)  
 [2] J. Demeter, *et al.*, Appl. Phys. Lett. **96**, 132503 (2010)

*In Cooperation Agreement between KU Leuven and HZ Berlin*



	<b>EXPERIMENTAL REPORT</b>  <b>PNR study of the proximity effect in a Nb/Fe/Nb superconductor/ferromagnet multilayer</b>	Proposal: PHY-04-1960-LT  Instrument: <b>V6</b>  Local Contact: Anke Teichert
	Principal Proposer: J. Demeter, KU Leuven, B Experimental Team: J. Demeter, KU Leuven, B S. Couet, KU Leuven, B A. Teichert, HZB & KU Leuven	Date(s) of Experiment  14.06.2010 – 21.06.2010

Date of report: 15.01.2011

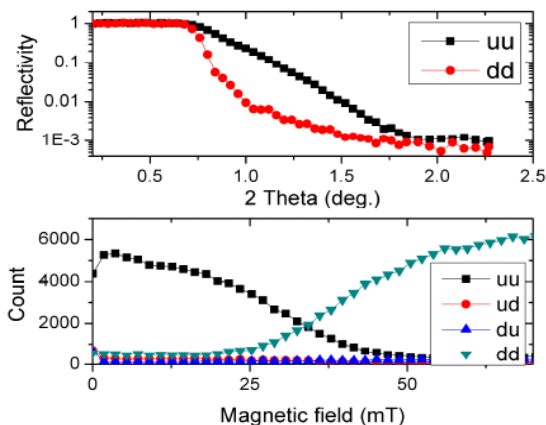
The aim of this experiment was to study the magnetization depth profile in a ferromagnet/superconductor bilayer by polarized neutron reflectometry. The focus of the experiment was to study how the superconductor's magnetization is disturbed by the contact to the adjacent ferromagnet, but also to study the reverse effect, i.e. the influence of the superconductor on the magnetic state of the ferromagnet. This latter point is in principle much easier to monitor by PNR since the induced splitting in spin up and spin down reflected intensity is large due to the large net magnetization of the ferromagnet.

The measurements were performed on a MBE grown Nb(60nm)/Fe(10nm) bilayer, deposited on a MgO(100) substrate. The superconducting properties of the film were characterized in advance and showed a  $T_c$  of 8.3 K, which is very good for such Nb films. The experiment was carried out in a standard orange cryostat installed for the occasion on the V6 instrument. In order to monitor the superconducting phase transition, four in-line electrical contacts were made on the sample surface. The drop of resistance to  $0 \Omega$  allowed us to clearly observe the superconducting phase transition. This enabled a precise selection of the temperatures at which the PNR experiments had to be carried out.


First we recorded specular reflectivity curves at 15K (above  $T_c$ ), 3.5 K and 1.7 K (base temperature) with an applied magnetic field. The goal was to resolve the change in the magnetization profile of the superconducting film below  $T_c$ . As expected however, the change in splitting is very small. Precise fitting of the data will be required to extract information. In particular, it seems unrealistic to obtain the detail of the magnetization depth profile very near to the ferromagnet. Still the data can be used as an investigation of how to design such an experiment and to find out what statistical quality is required for this purpose.

In a second stage, we focused on performing magnetic field scans at various temperatures

and at different angles. We restricted our region of interest to the crossing point of the spin up and spin down reflected intensities. This point gives a measure of the coercive field of the Fe layer. Indeed, this information cannot be accessed below  $T_c$  with conventional magnetometry measurements, due to the strong diamagnetic response of the superconductor. We performed such scans at different angles for each temperatures to increase the reliability of our measurement. What we see is that for very low temperature, a small shift of the crossing appears. However, this happens at a different magnetic field for the spectra recorded at an angle very close to the critical edge. We are still in the process of modelling these effects, but we believe this new approach can yield very valuable insight into the interactions appearing at ferromagnet/superconductor interfaces.



*In Cooperation Agreement between KU Leuven and HZ Berlin*

 <p><b>HELMHOLTZ ZENTRUM BERLIN</b> für Materialien und Energie</p> <p><b>NEUTRONS</b></p>	<p><b>EXPERIMENTAL REPORT</b></p> <p><b>Inverse proximity effects at the superconductor-ferromagnet interface revealed by polarized neutron</b></p>	<p>Proposal: PHY-04-1705</p> <p>Instrument: <b>V6</b></p> <p>Local Contact: A. Teichert</p>
<p>Principal Proposer: Experimental Team:</p>	<p>Y. Khaydukov, FLNP JINR, RU B. Nagy, RMKI KFKI, HU R. Steitz, HZB A. Paul, HZB D. Wallacher, HZB</p>	<p>Date(s) of Experiment</p> <p>18.05.2009 – 24.05.2009</p>

Date of report: 31.01.2011

### Experimental description

Sample – 8104B, nominal structure  
Cu(33nm)/V(40nm)/57Fe(1nm)/MgO  
Instrument – V6,  
Sample plane – horizontal  
Polarizer – magnetic mirror, polarization > 95%  
Analyzer – stack of mirrors, polarization >90%  
Detector – 2D PSD, area 190x190 mm<sup>2</sup>  
Neutron wavelength – 4.66 Å.  
Cryostat:  
Closed cycle cryostat, minimum temperature  
1.4K. Approximate time for cooling down to  
minimum and warming up to room temperature  
is 8-10 hours.

### Short diary of the experiment

#### May 18

11.00 – Start of the cryostat installation  
17.55 – The cryostat has been installed.  
Search for the neutron reflection  
21.45 – Reflected beam has been found, start  
of the measurement of reflectivity curves in (+  
+) and (- -) in the region  $\theta_1 = 0.01^\circ \div 2^\circ$  at  
magnetic field  $H = 1$  kOe (current - 25 amps )  
applied parallel to the surface.

#### May 19

14.00. Scan has been finished. Specular beam  
is blocked at small incident angles(< 0.02°)  
was observed  
Beam stop has been moved out. Measurement  
has been repeated at small angles only.  
18.00. Cryostat with the sample has been  
rotated 90° along the axis perpendicular to  
beam path. Magnetic field of 2 kOe (50 Amps)  
has been applied for 1 min and then released.  
Cryostat rotated back. Check for the presence  
of reflected beam - measuring of reflectivity  
curves in guide field  $20 \pm 0.5$ Gs.  
23.30. Measurement finished. Resolution is not  
enough for waveguide features ( dip at (+ +)  
and (- -) and peak at (+ -) and (- +)). Adjusting  
S1 slit width's to increase resolution

#### May 20

01 15 Cooling's started. After cooling to helium  
temperature sample stick has been  
deformed and reflection has been lost.

Repeat procedure of reflection adjustment at  
small temperatures

#### May 21

11.15 At T=30K cryostat 90° rotated,  
magnetized for 2 min in field of ~ 1kOe, then  
released and rotated back.  
16.00. Started measuring of (+ +) and (- +)  
reflectivity curves around the resonant peak ( $\theta$   
 $\approx 0.2^\circ$ ) at temperatures 1.4K – 3.8K (step 0.2K  
and 4.0K – 6K (step 0.5K)

#### May 22

Re-measure of T = 1.9K, T=2.4K and T =2.8K  
Before it, temperature has been set to T =30K  
and remagnetizing procedure has been done.

#### May 23 – May 24.

The measurements of reflectivity curves at T =  
1.6K, T = 2.6K and T = 4.5K. Last point later  
has been changed to T = 8K due to  
temperature jump.


Reflectivities has been measured at (+ +), (+ -  
) and (- -) channels.

### Main results

a) Reflectivity curves at T=1.6K, T=2.6K has  
been measured in big Q region. Shift of  
oscillations at spin asymmetry at change of  
temperature from T =1.6K and T =2.6K has  
been proven. Unfortunately reflectivity at T >  
T<sub>c</sub> has not been finished due to reactor cycle  
end.

b) Temperature evolution of the spin flip  
resonance peak has been investigated.  
Previous result at ADAM reflectometer has  
been proven.

In addition, temperature evolution of diffuse  
scattering has been collected. However no  
significant change of it has been detected.

	<b>EXPERIMENTAL REPORT</b>  <b>PNR and AMR measurement along the easy axis of a Co/CoO exchange bias system</b>	Proposal: PHY-04-2045-LT  Instrument: <b>V6</b>  Local Contact: Anke Teichert
	Principal Proposer: J. Demeter, KU Leuven, B Experimental Team: J. Demeter, KU Leuven, B E. Menéndez, KU Leuven, B A. Teichert, HZB & KU Leuven, B Klaus Kiefer, HZB	Date(s) of Experiment  02.08.2010 – 08.08.2010

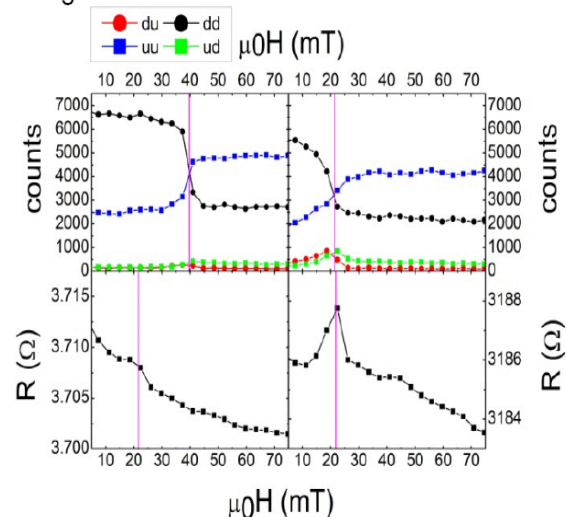
Date of report: 05.01.2011

During experiment PHY-04-1894-LT a new method was developed in which Polarized Neutron Reflectometry (PNR) is combined with Anisotropic Magnetoresistance (AMR) measurements.<sup>1</sup> Both PNR<sup>2</sup> and AMR<sup>3</sup> have been used extensively in the past to study the magnetization reversal mechanism in exchange bias (EB) systems. This proof-of-principle experiment was performed on a Co/CoO bilayer, a model system for the exchange bias effect. The sample that was measured exhibits a strong magnetocrystalline anisotropy and it is expected that the magnetization reversal mechanism is strongly dependent on the crystallographic direction. This previous experiment was performed along the *magnetic hard direction*. In the present experiment the measurements are repeated on the same sample, but now along the *magnetic easy direction*. Moreover, the present experiment acts as a first full scale experiment benefiting from the developments made during the previous experiment.

The sample measured during this experiment, was exactly the same as the one measured during the previous experiment. It consisted of a 50 nm Co layer with a 45 nm Cu seed layer grown by MBE on a Si(100) substrate. The Co layer was subsequently oxidised in a reduced oxygen atmosphere to form a 3 nm thick CoO layer at the surface. Structural and magnetic characterization confirmed the epitaxial growth and the corresponding magnetocrystalline anisotropy. The sample environment consisted of a closed-cycle cryostat capable of cooling down to 10 K and adapted to house the AMR measurement device.

First, a series of *specular reflectivity measurements* were performed at specific magnetic fields. From these measurements the structural and magnetic depth profile can be revealed by means of simulation. These simulations yield essentially the same depth profile as along the hard axis. Subsequently, *magnetic field scans* were performed, by

measuring the reflectivity at a well-chosen angle, while varying the magnetic field. During these measurements the AMR was recorded simultaneously. Shown below are the virgin descending and virgin ascending branch, with in the upper panels the PNR measurements and in the lower panels the AMR measurements. Remarkable in these measurements is the change in *non spin flip* signal after the coercive field and the particular shape of the AMR signal. Moreover, the peak position of the respective AMR and PNR measurements is not coinciding, which was the case for the measurement along the hard axis. This indicates that a different reversal mechanism is present along the easy axis than along the hard axis.




[1] J. Demeter, *et. al.*, accepted by Rev. Sci. Instrum.

[2] F. Radu, *et. al.*, Phys. Rev. B **67**, 134409 (2003)

[3] S. Brems, *et. al.*, Phys. Rev. Lett. **95**, 157202 (2005)

*In Cooperation Agreement between KU Leuven and HZ Berlin*

 <b>HELMHOLTZ ZENTRUM BERLIN</b> für Materialien und Energie  <b>NEUTRONS</b>	<b>EXPERIMENTAL REPORT</b>	Proposal: PHY-01-2926-EF
	<b>Investigation of vortex lattices by means of TOF-SANS</b>	Instrument: <b>V15</b> Local Contact: O. Prokhnenko
Principal Proposer: V. Ryukhtin, HZB Experimental Team: O. Prokhnenko, HZB W.D. Stein, HZB U. Keiderling, HZB	Date(s) of Experiment 27.08.2010 - 07.09.2010	

Date of report: 24.01.2011

Small angle neutron scattering (SANS) technique allows the direct measurement of flux line lattices (FLL) structure in type-II superconductors (SC). It leads to very weak SANS signal since spots intensity decaying with  $1/(\lambda_L)^4$ . Thus, so far there is only one publication of FLL observation in iron-pnictides – hole overdoped  $KFe_2As_2$  [1].

Decision to measure flux lines using EXED (V15) was taken after successful testing of SANS option with AgBE [2] powder (see Fig). It was important to check this possibility before long interruption of BER-II operation. Information collected during this experimental attempt should be useful for instrumental improvement of V15.

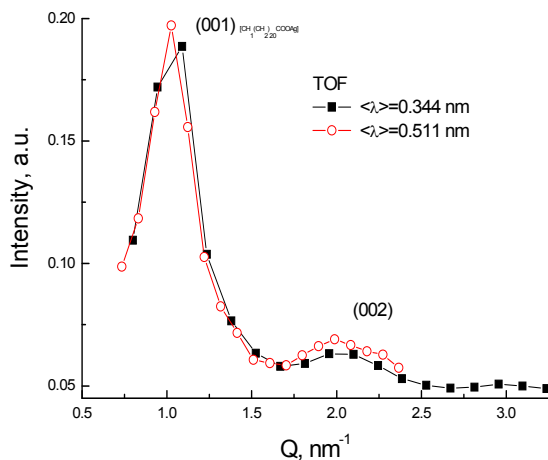


Fig. Radially averaged SANS spectra of AgBE measured at EXED (V15). Two curves represent different TOF bands.

Main problem for such scattering geometry is occurrence of reflections from parabolic neutron guide which was located between collimating cadmium slits. Spatial positions of reflections at second collimating aperture were hardly predictable and changing with wavelength. Decreasing of first cadmium aperture led to partial disappearing of these parasitic reflecting but also to increasing of background (both neutron and gamma) and decreasing of useful intensity. That is why FLL were not detected during this test measurement.

As output of this experiment the following technical improvements are suggested:

1. Construction of separated collimator with two-by-four adjustable blades. It can be completely identical to present guide sections but without guides. This collimator can use existing vacuum pumps. PE + Boron shielding should be necessary.
2. Building of larger Helium container which will make possible to move detector banks further from the sample (~ 4.5 m). This container has to be equipped by automatic system of gas pressure compensation.  $B_4C$  shielding is highly recommended for suppression of background.
3. Manufacturing and installing of cadmium beamstop system. Since number of possible SANS configurations is limited to 2-4, for each combination of sample-detector should correspond to one defined size beamstop. Optionally, it can be motorized in order to remove it from the beam without touching of helium chamber in front of the detector.
4. Optional introducing attenuator for making incident beam weaker without changing spectra. It could be cadmium plate with many drilled holes. However, it should be tested where is better place for it because of possible gamma background.
5. Sample changer with temperature controlling (like LAUDA) would be option for carrying out of routine SANS measurements with many samples.

Besides these things it is still open questions of choosing of software for SANS data treatment at EXED.

[1] H. Kawano-Furukawa *et al.*, (Submitted, (2010)), arXiv:1005.4468v2.

[2] R. Gilles *et al.*, Materials Science Forum Vols. 321-321 (2000) pp. 264-269.

Principal Proposer: W. Treimer, Beuth Hochschule für Technik & HZB  
O. Ebrahimi, Beuth Hochschule für Technik  
N. Karakas, Beuth Hochschule für Technik  
S.-O. Seidel, HZB

Experimental Team: O. Ebrahimi, Beuth Hochschule für Technik  
N. Karakas, Beuth Hochschule für Technik  
S.-O. Seidel, HZB  
W. Treimer, Beuth Hochschule für Technik & HZB

Date(s) of Experiment

25.06.2010 – 11.07.2010

Date of report: 31.01.2011

Due to their magnetic moments  $\mu$  neutrons interact very sensitive with magnetic fields and magnetic matter. In the presence of an external magnetic field the potential energy of spin up and spin down states are different thus neutrons are polarized by means of total reflection into spin up and spin down neutrons having different angles of reflection. The analysis of the spin orientation is done by the same method. Therefore, any interaction of neutrons with matter that influences the spin can be attributed to the magnetism in the sample, only. In order to visualize the expulsion of the magnetic field in a lead sample the beam divergence was reduced with two soller-collimators horizontally to  $0.1^\circ$  yielding a  $L/D_h = 570$  and vertically to  $< 0.2^\circ$  yielding a  $L/D_v = 300$ . The collimated beam in front of the polarizer had a size of  $30 \times 30 \text{ mm}^2$ . A bender-type spin polarizer close behind the soller-collimators unit sorted out the spin down neutrons. The distance between polarizer and analyzer was equipped with magnetic guide fields [app. 5mT], to avoid the depolarization of the beam (Fig.1).

The characteristics of the superconductivity are resistanceless current flow through the superconductor, Meissner effect and flux-pinning. To observe the Meissner effect we chose lead as an easy sample to work with.

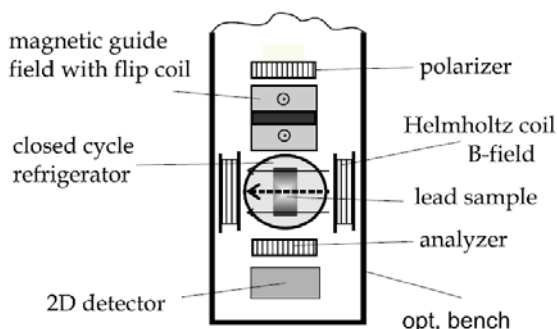


Fig. 1: Experimental layout (Meissner-effect)

Lead is a type-I superconductor, therefore after reaching the critical temperature of  $T_c = 7.192 \text{ K}$  the superconductivity arises for this material immediately. However, the Meissner effect depends on the critical temperature  $T_c$  as well on the external critical magnetic field  $B_c$  as

$$B_c(T) = B_c(0) \left[ 1 - \left( \frac{T}{T_c} \right)^2 \right]$$

$T$  = temperature [K],  $T_c$ : critical temperature,  $B_c(0)$  = critical magnetic field at  $0^\circ \text{ K}$ ; for lead  $B_c(0) = 80.3 \text{ mT}$ . For fields above the critical magnetic field  $B_c$  the Meissner effect breaks down, and the external field can penetrate the sample. Then the superconductor is not able any more to block the external magnetic field to enter the superconductor. For these measurements different lead samples (single crystals and poly-crystals) were investigated. An example of these measurements is shown in Fig. 2.

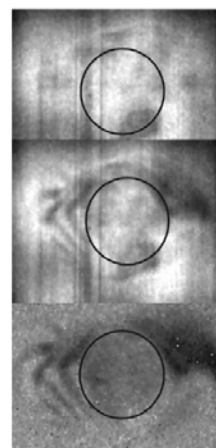



Fig.2 (left, from top to bottom): Visualization of the Meissner effect; top: image of the lead sample at  $T = 8 \text{ K}$ , b:  $T = 5.5 \text{ K}$ , c: flat and dark field corrected image; black circle shows the shape of the lead cylinder with a diameter of 12mm, the exposure time was 3h.

The results show the excellent spatial resolution less than  $250 \mu\text{m}$  for polarized neutrons with 'PONTO' which affords investigations of magnetic fields inside different lead samples in the Meissner-phase and magnetic flux trapping.

This work was part of the BMBF project 05KN7KF1

# Structure



 <b>HELMHOLTZ ZENTRUM BERLIN</b> für Materialien und Energie  <b>NEUTRONS</b>	<b>EXPERIMENTAL REPORT</b>  <b>Temperature evolution of nano-twinned martensitic structure in Ni<sub>1.99</sub>Mn<sub>1.14</sub>Ga<sub>0.87</sub> single crystal</b>	Proposal: PHY-01-2841 Instrument: E2 Local Contact: I. Glavatskyi
	Principal Proposer: N. Glavatska, Institute for Metal Physics, UA Experimental Team: N. Glavatska, Institute for Metal Physics, UA I. Glavatskyi, HZB	Date(s) of Experiment 22.09.2010 - 28.09.2010

Date of report: 20.01.2011

The evolution of nano-twinning and stacking fault structure within the single martensitic phase of the multiferroic Ni<sub>2.01</sub>Mn<sub>1.12</sub>Ga<sub>0.87</sub> single crystal during temperature ramp from 5K to 295K was studied.

**Experiment:** Ni-Mn-Ga single crystals were studied with E2 diffractometer at  $\lambda=1.2$  and  $2.4\text{\AA}$  at  $30'$  collimation. Measurements were performed during heating cycles with and without magnetic field, using the VM-3 magnet. The single crystalline specimen was initially cooled down over the martensite transformation point, in the  $H=0.5T$  magnetic field, to achieve the single variant (non-twinned) martensite.

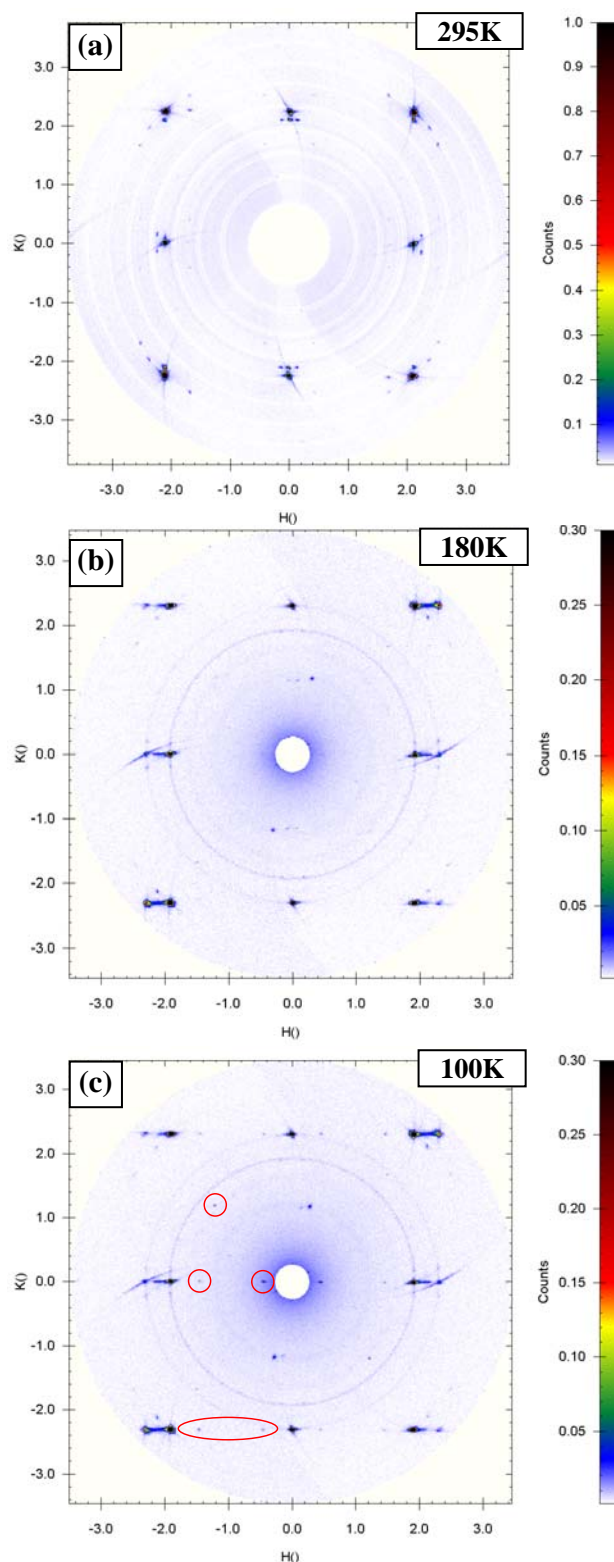
**Results:** As seen from the diffraction pattern taken of the  $(h0l)$  plane (Fig.1a), the specimen is of a single martensite phase with some residual twinning, less than 5%, according to peak intensity ratio.

During temperature ramp inside of the martensitic phase of the single crystalline specimen, the diffraction pattern of the  $(101)$  plane changed drastically. Namely, after cooling from 295K to 180K (Fig.1b), the main diffraction peaks split in the direction along  $[h00]$  in a manner similar to further twinning, which might be attributed only to the self-accommodation of the single martensite phase to the strong anisotropic change of the lattice parameters. Though, besides that splitting, which is the very new feature by itself, the strong diffuse scattering rods appear between those split peaks. The nature of such diffuse stripes is yet unclear, but we speculate that it is due to very high density of the stacking faults or nanotwins, produced on the martensite self-accommodation, as it is known that the material possess an extremely low energy of the stacking faults. Some additional satellite peaks appear near  $(002)$  reflection.


On further cooling down to 100K we observe, for the first time the appearance of the purely magnetic reflections (Fig.1c, marked with red). Those we preliminary associate to the AFM order appearance, due to change of the Mn-Mn exchange with further anisotropic thermal lattice distortion, ending with mixed FM+AFM order coexistence.

It was found that magnetic field, up to 10kOe does not influence the observed behavior. Higher field led to the specimen fault off the holder.

**Fig.1.** Thermal evolution of the  $(101)$ -reciprocal plane diffraction pattern.





 <b>HELMHOLTZ ZENTRUM BERLIN</b> für Materialien und Energie  <b>NEUTRONS</b>	<b>EXPERIMENTAL REPORT</b>	Proposal: PHY-01-2603 PHY-01-2491
	<b>Structure evolution of AgI in a restricted geometry</b>	Instrument: <b>E2, E9</b> Local Contact: M. Tovar, I. Glavatskyy
Principal Proposer: A. Naberezhnov, Ioffe Institute, Russia Experimental Team: D. Kurdyukov, Ioffe Institute, Russia M. Tovar HZB I. Glavatskyy HZB	Date(s) of Experiment 23.11.2009 - 29.11.2009 21.09.2009 - 23.09.2009	

Date of report: 31.01.2011

Model super ionic material AgI embedded into nanocavities of artificial opals demonstrates the very unusual dielectric properties approaching the melting point. The microscopic origin of this anomaly is absolutely unclear. We have studied the temperature evolution of structure of AgI embedded into two types of porous matrices: artificial opals (regular 3D nets of pores with average pore diameter 25 nm) and porous glasses with a random net of interconnected dendrite-type 7 nm nanochannels. Under ambient conditions, bulk silver iodide exists as a mixture of  $\beta$  (with hexagonal structure of the wurtzite type) and  $\gamma$  (face-centered cubic structure of the zinc blend type) phases [1]. In our experiments we have used three types of samples: the opals filled from melt and from water solution and porous glasses filled from AgI water solution. The total volume amounts of the salt were about 23% in opals and ~6% in porous glasses. In Fig.1 the lineshapes and widths of elastic peaks for the bulk AgI (black squares) and AgI within opals embedded from melted state (red circles) and from water solution (blue triangles) are presented.

The principle results are:

1 – At room temperature the crystal structure of all samples correspond to the structure of bulk AgI, but the ratios of intensities of different peaks differ essentially from observed for the bulk materials.

2 – Using the broadening of elastic peaks due to size effect we have estimated the sizes of AgI nanoparticles within opals. They are  $21 \pm 2$  nm for filling from solution and  $41 \pm 4$  for filling from melted state. For AgI within porous glasses the nanoparticle size does not exceed 20 nm.

3 – The temperature hysteresis of phase transition (PT) in the superionic state increases to lower temperatures at decreasing of nanoparticles size. It is equal to ~30 K for AgI within opals and 75 K for AgI within porous glasses.  $T_C$  of this PT did not depend on nanoparticle sizes.

Unfortunately the small amount of AgI within glasses and large absorption cross section of Ag did not permit us to study the structure evolution of AgI within glasses in details and we are going to do it using combined synchrotron radiation and neutron scattering data.

[1] G. Burley J. Chem. Phys. 38, 2807 (1963)

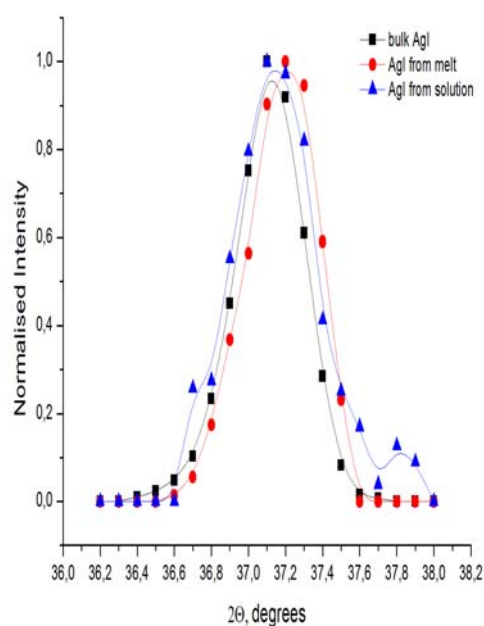


Fig.1 Lineshapes and widths of elastic peaks for the bulk AgI (black squares) and AgI within opals embedded from melted state (red circles) and from water solution (blue triangles).

Rare-earth cyanides RE[Fe(CN)<sub>6</sub>]*n*H<sub>2</sub>O; RE = rare earth atom; form a large group of rare earth materials with interesting electronic and magnetic properties at low temperatures. In the middle of 80-ties, crystal structures and magnetic ground states of rare-earth ferricyanides were classified by Hulliger et al. The Pr[Fe(CN)<sub>6</sub>]*n*H<sub>2</sub>O system has been classified as an antiferromagnet with the ordering temperature  $T_N$  approximately ~ 1 K. The phase transition as shown in the figure 1 is indicated by the sharp lambda anomaly in the heat capacity data ( Fig.1 ), moreover, bulk measurements conducted at higher tempe-

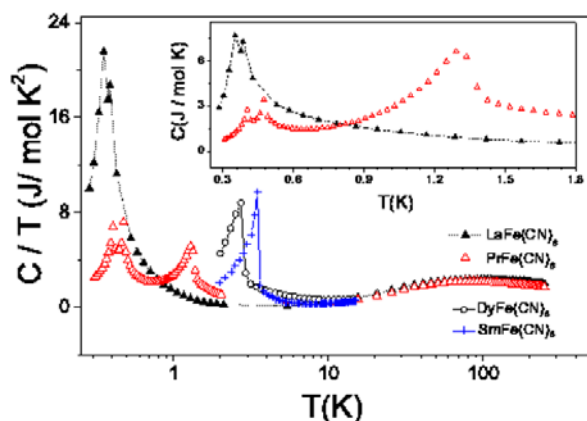


Fig . 1 Low temperature heat capacity data of selected rare-earth ferricyanides Ln[Fe(CN)<sub>6</sub>]*x*H<sub>2</sub>O, Ln=Pr (~1.3 K), La (~0.39 K), Sm ( $T_N$  ~3.5 K), Dy ( $T_N$  ~2.8 K ) in semilogarithmic scale. The inset shows lambda like anomalies for Ln=Pr and La in C vs. T plot.

ratures indicated development of magnetic correlations in the system at about 12 K (a maximum in AC susceptibility and in zero-field-cooling magnetization curves).

Despite extensive studies performed on Pr[Fe(CN)<sub>6</sub>]*4*H<sub>2</sub>O system and indications from different experiments performed by means of NMR spectroscopy, bulk magnetization, DC- and AC- susceptibility measurements, no significantly relevant magnetic signal in the elastic neutron experiment has been found. Neither single crystal nor powder experiment

showed any magnetic signal within a chosen statistic down to lowest temperature of 0.028 K. To complete our feasibility test we performed also the neutron elastic powder experiment on K<sub>3</sub>Fe(CN)<sub>6</sub> powdered sample. According published information the system undergoes a magnetic transition to the order state at about 128 mK.

Powder K<sub>3</sub>Fe(CN)<sub>6</sub> sample of 1.4 g weight was filled into copper container together with deuterated ethanol-methanol mixture in order to establish a reasonable thermal contact and so enable the heat exchange between the cold finger attached to the copper cell and powder sample inside the cell. The low temperature and high temperature patterns are displayed the figure 2. No difference in measured intensities were found.

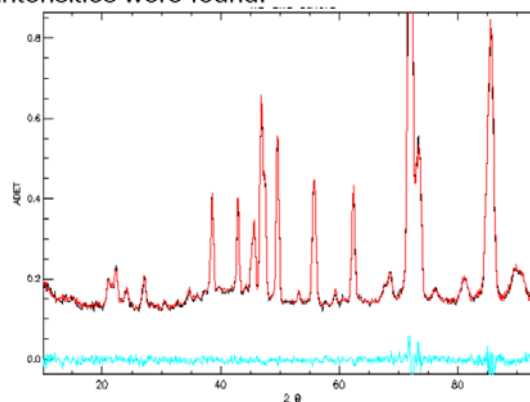



Fig. 2. Neutron diffraction pattern taken at low temperature  $T= 0.028$  K and high temperature of 0.86 K for K<sub>3</sub>Fe(CN)<sub>6</sub> *n*H<sub>2</sub>O powdered sample.

This negative result underlines facts as:

(i) difficulty of cooling down to 0.03 K in case of powders and (ii) problems of signal to background ratio typical for such small magnetic moment (of size 0.3  $\mu_B$ ) and not quite high neutron beam flux of order 10<sup>6</sup> cm<sup>2</sup>/s at sample position. One can conclude that for successful experiment several conditions are required to fulfil : the high flux at the sample position, large amount of powder and/or respective a big single crystal.

 <b>HELMHOLTZ ZENTRUM BERLIN</b> für Materialien und Energie  <b>NEUTRONS</b>	<b>EXPERIMENTAL REPORT</b>	Proposal: PHY-01-2727 PHY-01-2788
	<b>The annealing process and high temperature phase transition of UCoGe</b>	Instrument: <b>E5, E9</b> Local Contact: M. Reehuis, M. Tovar
Principal Proposer: J. Pospisil, CU Prague, CZ Experimental Team: K. Prokes, HZB M. Reehuis, HZB M. Tovar, HZB M. Kratochvilova, CU Prague, CZ	Date(s) of Experiment  25.05.2010 - 30.05.2010 16.09.2010 - 20.09.2010	

Date of report: 10.01.2011

The opinion on the magnetic ordering of UCoGe lived through enormous progress. Buschow et al. [1] presented UCoGe with nonmagnetic ground state down to the temperature 1.2 K. According to recent findings UCoGe is a ferromagnet with  $T_C \approx 3$  K and in addition superconductor with temperature of superconducting transition around  $T_{sc} \approx 0.7$  K [2]. Ferromagnetism and robust superconductivity of UCoGe were reported only on the well-annealed samples, whereas as-cast samples exhibited poorly developed FM and SC [3]. The unusual coexistence of SC and FM is apparently dependent on the sample state and annealing process [3,4,5].

UCoGe crystallizes in the orthorhombic structure. Two possible space arrangements of atoms come into consideration – the TiNiSi-type structure that belongs to the Pnma space group and CeCu<sub>2</sub>-type structure (Imma).

We speculated that different as-cast and annealed sample behaviours is connected with TiNiSi-CeCu<sub>2</sub> crystal structure transformation at high temperature. The main subjects of the proposal were therefore verification of the UCoGe crystal structure (TiNiSi or CeCu<sub>2</sub> structure type) and study of the possible structure change during annealing process. The work was performed on the single crystal diffractometer E5 and powder diffractometer E9.

The single crystal neutron diffraction confirmed TiNiSi structure type (annealed crystal) at room temperature with almost negligible atoms mixture between Co and Ge-sites. We found lattice parameters  $a = 6.8303$  Å,  $b = 4.1791$  Å and  $c = 7.2169$  Å. The fractional coordinates are listed in Table 1.

	x/a	x/b	x/c
U	0.01000	0.25000	0.20719
Ge	0.80369	0.25000	0.58720
Co	0.21140	0.25000	0.58287

Tab. 1. Fractional positions of the atoms in UCoGe.

The systematic extinction of reflections according to the rule  $h + k + l = 2n$  for body-centred lattice in the case Imma space group was studied during heating of polycrystalline UCoGe sample from room temperature to 1150°C on E9.

We focused mainly on angle area in the range  $2\theta = 25^\circ - 45^\circ$  where demonstrable extinction of the (111), (102), (201) and (210) reflections can be observed (see Fig. 1).

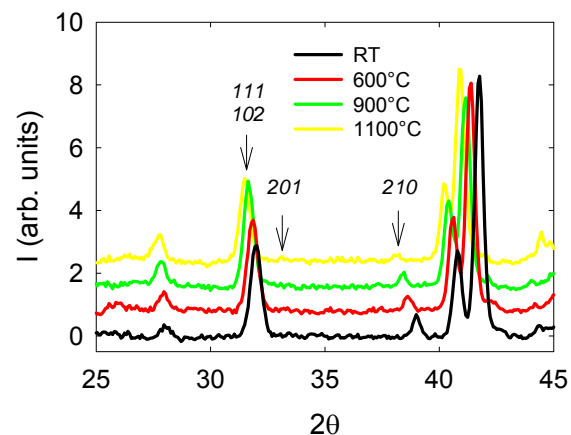


Fig 1: Temperature evolution of the neutron diffraction pattern of UCoGe. The arrows mark reflections, which should become extinct when Pnma-Imma transformation occurs.

If UCoGe structure had changed from Pnma to Imma during the temperature increase the selected reflections should have started to become extinct. Nevertheless, all the mentioned reflections were conserved during the heating process. Thus, UCoGe keeps clearly the TiNiSi-type structure. Only shift of reflections to lower angles appeared as a result of the expansion of unit cell (Fig. 1). The unit cell volume expanded by 5%, uniformly along all three crystallographic main axes.

#### References

- [1] K. H. J. Buschow, et al., Journal of Applied Physics, **9** (1990) 5215-5217
- [2] N. T. Huy, et al., PRL **99** (2007) 067006
- [3] N. T. Huy, et al., PRL **100** (2008) 077002
- [4] N. T. Huy, et al., JMMM **321** (2009) 2691–2693
- [5] J. Poltiero Vajpravova, PRB **82** (2010) 180517(R)

#### Acknowledgement:

This research project has been supported by the European Commission under the 7<sup>th</sup> Framework Programme through “Research Infrastructures” action of the “Capacities” Programme, contract number CP-CSA\_INFRA-2008-1.1.1. Number 226507-NMI

Principal Proposer: Bella Lake, HZB  
 Experimental Team: Diana Lucia Quintero Castro, HZB  
 Manfred Reehuis, HZB  
 Nazmul Islam, HZB

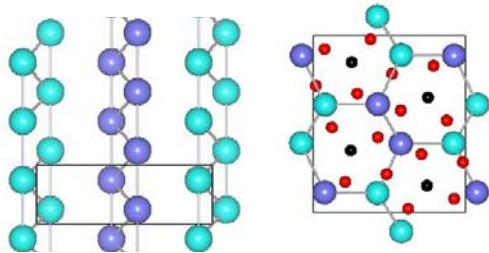
Date(s) of Experiment

19.01.2010 – 26.01.2010

Date of report: 18.03.2011

This beamtime was originally intended for measurement of the magnetic structure of  $\beta$ -CuNb<sub>2</sub>O<sub>6</sub>, however the cryostat on E5 can achieve a minimum temperature of 6K which is only just below the ordering temperature for  $\beta$ -CuNb<sub>2</sub>O<sub>6</sub> of  $T_N=7$ K. Beamtime was subsequently received for  $\beta$ -CuNb<sub>2</sub>O<sub>6</sub> on D10 at the ILL where it is possible to cool to 2K and therefore the E5 beamtime was used for a completely different measurement – the investigation of the crystal structure of SrYb<sub>2</sub>O<sub>4</sub>.

SrYb<sub>2</sub>O<sub>4</sub> is a frustrated, low dimensional antiferromagnet. The magnetic Yb<sup>3+</sup> ions have angular momentum  $S=1/2$ ,  $L=3$  and  $J=7/2$  and form sub-lattices of double chains running parallel to the crystallographic  $c$ -axis. There are two inequivalent although highly similar chains due to the two inequivalent Yb<sup>3+</sup> ions per unit cell. These chains suggest the presence of frustrated first and second neighbor magnetic interactions. Moreover the coupling between the chains is also frustrated and the Yb<sup>3+</sup> ions form a hexagonal structure around the Sr ions. See figure 1.

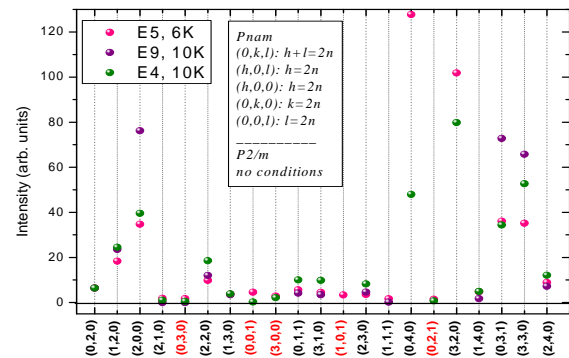


**Fig 1.** Structure of SrYb<sub>2</sub>O<sub>4</sub> pale blue and lilac represent the two inequivalent Yb sites, red – O, black – Sr. The left panel show the double chains running along  $c$ . The right panel shows the 'hexagonal' structure perpendicular to  $c$ .

This compound orders antiferromagnetically at a temperature of 0.9 K according to heat capacity measurements. Powder and single crystal neutron diffraction measurements have been performed on the E6, E9 and E4 diffractometers at HZB in order to determine the crystal and magnetic structure. For all the diffraction experiments we have used a dilution stick to reach temperatures below and above this phase transition.

The measurement on E4 revealed some new structural peaks at positions forbidden by the  $Pnam$  space group previously reported for SrYb<sub>2</sub>O<sub>4</sub> [1]. These peaks were present at room temperature as well as base temperature. In order to investigate this further we used the E5 4-circle single crystal diffractometer. The single

crystal sample was a cylinder of mass 1.29 g mounted in an Aluminium holder. A closed cycle cryostat was used to cool the sample and measurements took place at 6K. We measured a total 2399 reflections. 4 layers of Er filters (1mm thickness each) were used to suppress second order scattering. In figure 2 the intensity of some of the bragg reflections measured in E4, E5 and E9 are shown. Forbidden reflections are labelled in red.



**Fig 2.** Relative intensity for some bragg reflections measured in three different instruments (E5, E9 and E4). Red labels represent forbidden reflections for the  $Pnam$  space group. Insert shows the reflection conditions for both space groups  $Pnam$  and  $P2/m$ .

Measurements were performed both with and without the Er filters to check to what extent the forbidden peaks consisted to second order scattering. Results are listed in table 1. The results suggest that the space group is  $P2/m$ .


**Table 1.** Intensity comparison using Er filter and without it. E5, 6K.

(h,k,l)	Intensity (Er filter)	Intensity (without filter)
(0,0,-2), allowed	6878.62	7000.46
(0,0,-1)	65.99	236.6
(10,0,-1), allowed	7073.63	18745.03
(5,0,-0.5)	3.35	49.99

Subsequently measurements of the forbidden peaks were performed on the V2 cold triple axis spectrometer where a Be filter was used to suppress the second order scattering. The peaks were found to be completely absent when the filter was used suggesting that the peaks are entirely due to second order scattering and that the crystal structure is in fact  $Pnam$  after all [2].

**Reference:**

- [1] H. Karunadasa *et al.* *Phys. Rev. B* 71, 144414 (2005)
- [2] Experimental report: PHY-02-751-EF

 <b>NEUTRONS</b>	<b>EXPERIMENTAL REPORT</b>		Proposal: MAT-01-2894
	<b>Single-crystal neutron diffraction study of LiCuVO<sub>4</sub></b>		Instrument: <b>E5</b> Local Contact: M. Reehuis
Principal Proposer:	H. Schier, R. K. Kremer, C. Kallfaß, Max-Planck-Institut Stuttgart		Date(s) of Experiment
Experimental Team:	M. Reehuis, HZB		14.06.2010 - 27.06.2010

Date of report: 29.12.2010

The effect of the defect structure of lithium cations in distorted cubic spinell structure of LiCuVO<sub>4</sub> has not been investigated in detail up to now. In order to understand the exiting magnetic properties of this material at low temperatures, it is important to establish how the Li-cations are distributed as a function of temperature in LiCuVO<sub>4</sub>. In 1992 the structure of LiCuVO<sub>4</sub> was determined from X-ray powder diffraction data using the Rietveld method. Here it was shown that LiCuVO<sub>4</sub> is a member of the huge group of cubic spinels showing a one-dimensional cooperative *Jahn-Teller* ordering [1]. Further it shows interesting magnetic properties as long-range antiferromagnetic ordering ( $T_N = 2.5$  K) and multiferroic behaviour in the Néel phase [2, 3].

In order to determine the Li-positions in LiCuVO<sub>4</sub> with good accuracy we performed a single-crystal neutron diffraction experiment at 10 K on the 4-circle diffractometer E5. This instrument uses a Cu-monochromator selecting the neutron wavelength  $\lambda = 0.896$  Å. Our data analysis showed that LiCuVO<sub>4</sub> crystallizes in the orthorhombic structure with the space group *Imma*, which is in agreement with the result given in Ref. [1]. The V-, O1- and O2-atoms were found to be at the Wyckoff positions  $4e(0, \frac{1}{4}, z)$ ,  $8h(0, y, z)$  and  $8i(x, \frac{1}{4}, z)$ , respectively. A difference Fourier analysis clearly showed that the Li-atoms are located at the position  $4d(\frac{1}{4}, \frac{1}{4}, \frac{3}{4})$ . No other interstitial sites could be detected for the Li-atoms. For the refinement of the crystal structure, using the programme *Xtal* [4], we used 1463 (485 unique) structure factors. This allowed us to refine the overall scale factor, the extinction parameter, 5 positional and 16 anisotropic thermal parameters with good accuracy resulting in a satisfactory residual  $R_F = 0.043$  ( $wR_F = 0.029$ ). The results of the refinements are summarized in Tables 1 and 2. Due to the fact that the neutron scattering power of vanadium is much weaker than for the other atoms the isotropic thermal parameter as well as the occupancy of the V-atom was not allowed to vary during the refinements. But the refinement of the z-parameter was successful. In comparison with the other atoms the standard deviation of z(V) is strongly enlarged. Further we have determined the occupancies of the Li- and O-atoms. The sites of Cu and V were assumed to be fully occupied. For the Li-site a deficiency of about 15 % could be detected. The

occupancies of the O1- and O2-atoms are found to be slightly smaller than  $occ = 1$ .

**Table 1:** Results of the refinements of the single-crystal neutron diffraction data of LiCuVO<sub>4</sub>. The occupancies of the Cu- and V-sites were not allowed to vary.


<i>Imma</i>	X	y	z	occ
Li	$\frac{1}{4}$	$\frac{1}{4}$	$\frac{3}{4}$	0.85(2)
Cu	0	0	0	1.000
V	0	$\frac{1}{4}$	0.3856(15)	1.000
O1	0	0.01595(11)	0.27360(7)	0.966(7)
O2	0.23555(10)	$\frac{1}{4}$	0.99849(10)	0.987(6)

**Table 2:** Anisotropic thermal parameters of LiCuVO<sub>4</sub> as obtained from the refinements. The thermal parameters  $U_{ij}$  (given in 100 Å<sup>2</sup>) are in the form  $\exp[-2\pi^2(U_{11}h^2a^{*2} + \dots + 2U_{13}hla^*c^*)]$ . For symmetry reasons the values  $U_{12}$  of all the atoms,  $U_{13}$  of Cu and O1, as well as  $U_{23}$  of Li and O2 are equal to zero for the space group *Imma*. The isotropic thermal parameter of V was fixed.

<i>Imma</i>	$U_{11}$	$U_{22}$	$U_{33}$	$U_{13}$	$U_{23}$
Li	0.74(15)	1.02(15)	0.62(17)	0.38(10)	0
Cu	0.21(2)	0.18(2)	0.45(3)	0	-0.03(2)
V	0.25	0.25	0.25		
O1	0.35(2)	0.34(3)	0.44(3)	0	-0.07(2)
O2	0.27(2)	0.39(2)	0.43(3)	-0.03(2)	0

## References

- [1] R. Kanno, Y. Kawamoto, Y. Takeda, M. Hasegawa, O. Yamamoto, N. Kinomura, J. Solid State Chem. **96** (1992) 397.
- [2] B.J. Gibson, R. K. Kremer, A.V. Prokofiev, W. Assmus, G.J. McIntyre, Physica B **350** (2004) e253.
- [3] M. Enderle, C. Mukherjee, B. Fåk, R.K. Kremer, et al., Europhys. Lett. **70** (2005) 237.
- [4] S. R. Hall, G. S. D. King, J. M. Stewart, Eds., *Xtal3.4 User's Manual*. University of Australia: Lamb, Perth (1995).

 <b>NEUTRONS</b>	<b>EXPERIMENTAL REPORT</b>	Proposal: PHY-01-2759-EF
	<b>Polymorphism of REIr<sub>2</sub>Si<sub>2</sub>: LT-HT and HT-LT structure transformations</b>	Instrument: <b>E6</b> Local Contact: A. Hoser, T. Hofmann
Principal Proposer: M. Mihalik, HZB Experimental Team: A. Hoser, HZB T. Hofmann, HZB X. Martí, CU Prague, CZ	Date(s) of Experiment 25.03.2010 – 29.03.2010	

Date of report: 07.06.2010

The  $REIr_2Si_2$  ( $RE = Ce, Pr, Nd$ ) compounds belong to the family of polymorphic compounds, which can adopt both,  $ThCr_2Si_2$ - ( $\alpha$ -phase) and  $CaBe_2Ge_2$ -type ( $\beta$ -phase) crystallographic structure. The  $\alpha$ -phase is stable at low temperatures and the  $\beta$ -phase is stable at higher temperatures; nevertheless  $\beta$ -phase can be stabilized at room temperatures by rapid cooling of the melt. Since both phases exhibit interesting different physical properties, which are driven directly by the crystal structure, the question about detailed study of the phase transformation between the two phases arose.

The experiment was held on the E6 diffractometer using the bulk samples of  $REIr_2Si_2$  ( $RE = Ce, Pr, Nd$ ) and the tantalum container as a holder. During the experiment we have positioned the two detectors of E6 to the position  $51.5^\circ$  and  $76.5^\circ$  and collected data both, for the heating and the cooling of the sample. At the room temperature and the highest-possible temperature (around 1400 °C) we have collected pattern for  $19.5^\circ < 2\theta < 132.5^\circ$ , too. Due to very strong texture of the samples we have processed the data by Le Bail refinement using the program *FullProf*.

In all three compounds we have found and verified that there is only one, step-like transition from the  $\alpha$ -phase to the  $\beta$ -phase on the heating at  $T_{heat} = 960(10), 1135(5),$  and  $1100(20)$  K for the  $CeIr_2Si_2, PrIr_2Si_2$  and  $NdIr_2Si_2$ . On the cooling curve we have found the transition from the  $\beta$ -phase to the  $\alpha$ -phase at  $T_{cool} = 650(10), 880(5), 900(5)$  K for  $CeIr_2Si_2, PrIr_2Si_2$  and  $NdIr_2Si_2$ . These transitions are connected with the change of the crystal symmetry and abrupt change of the lattice parameters (Fig. 1), but very small change in the volume of the unit cell (Fig. 2). All these phase transformations occur at the same temperature, at which we have observed the anomalies in the thermal expansion. We have observed neither intermediate phase, nor continuous shift of the diffraction peaks around  $T_{heat}$  and  $T_{cool}$  which points

really to the pure first order phase transitions in these compounds.

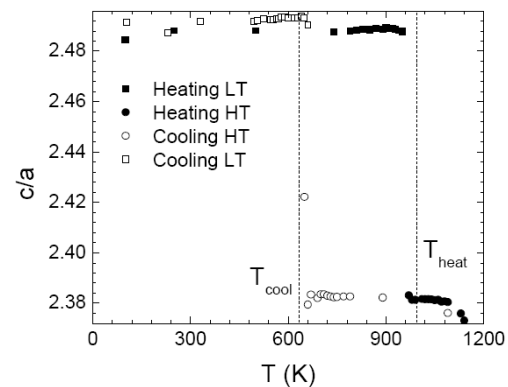


Fig. 1: The  $c/a$  ratio of  $CeIr_2Si_2$ . The dashed lines represent the position of the anomalies as determined from the thermal expansion experiment.

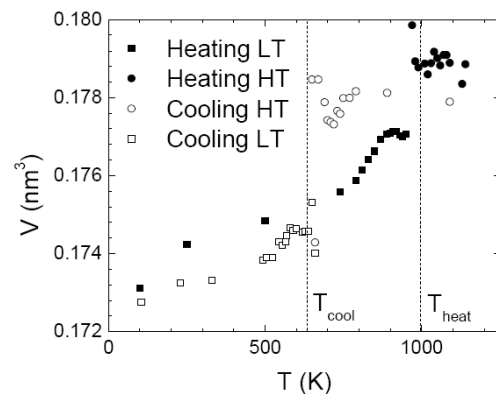



Fig. 2: The temperature evolution of the volume of  $CeIr_2Si_2$  across the structural phase transition. The dashed lines represent the position of the anomalies found by the thermal expansion experiment.

 <b>HELMHOLTZ ZENTRUM BERLIN</b> für Materialien und Energie  <b>NEUTRONS</b>	<b>EXPERIMENTAL REPORT</b>  <b>Solidified Deuterium in Silicon Nanochannels</b>	Proposal: PHY-01-2761-EF  Instrument: <b>E6</b>  Local Contact: Tommy Hofmann
	Principal Proposer: Dirk Wallacher, HZB Experimental Team: Tommy Hofmann, HZB	Date(s) of Experiment  27.05.2010 - 02.06.2010

Date of report: 27.01.2011

In the course of the experiment we studied the structure of deuterium confined in 10nm wide and several micrometer long channels of anodized, crystalline silicon plates (a-Si). The well defined alignment of the channels along the surface normal, a (100)-direction of the Si crystals, was utilized to search for textural growth of solid D<sub>2</sub> in confinement. Powder diffractometer E6 ( $\lambda=2.44\text{\AA}$ ) was employed to perform the scattering experiments. HZB's department for sample environment provided an elaborate sorption setup to fill a-Si with liquid D<sub>2</sub> in a controlled manner for in-situ scattering experiments. Scattering data were recorded as function of scattering angle  $2\Theta$ , orientation  $\omega$  of the pore axis with respect to the incoming neutron beam and temperature.

Found D<sub>2</sub> Bragg peaks ( $\circ$ ) could be assigned to the (111), (002), (220), (113) and (222) peaks of a fcc structure with  $a=5.1\text{\AA}$ . Particular strong fcc peaks were persistently found in direct vicinity to respective Si peaks ( $\times$ ). The existence of discrete Bragg peaks illustrates a strong correlation between orientation of D<sub>2</sub> crystallites in the pores and orientation of the Si matrix. As Fig.2 representatively shows for the (002) reflection, each fcc peak can be found with varying intensity for a multitude of orientations  $\omega$ , implying the existence of several differently orientated fcc-domains. The largest domain however, as an analysis of peak intensities suggests is almost perfectly aligned with the cubic structure of the surrounding Si matrix.

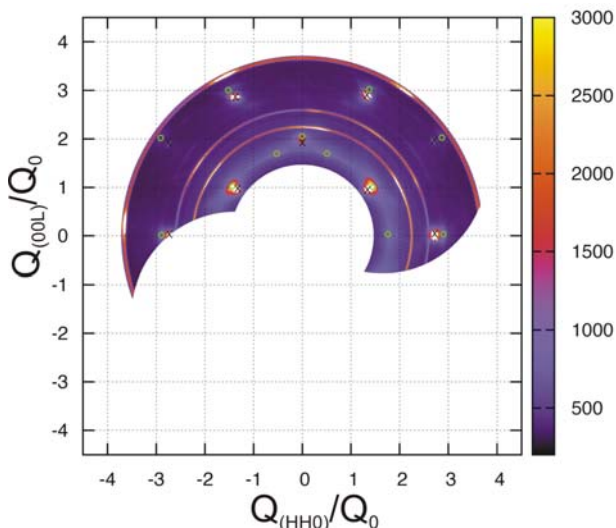


Figure 1: Intensity in the (-110) plane

Fig.1 exhibits scattering intensity in a plane that coincides with the (-110) plane of the Si matrix.  $2\Theta$  and  $\omega$  were converted in wave vector transfers  $Q$  along the pore axis ((001)-direction) and perpendicular to the pore axis ((110)-direction). A colour code scales intensities. Recorded at 7K for completely filled pores, the intensity distribution manifests scattering from the polycrystalline Al sample cell (3 Debye-Scherrer rings), the single crystalline a-Si and from solid D<sub>2</sub> in the pores.

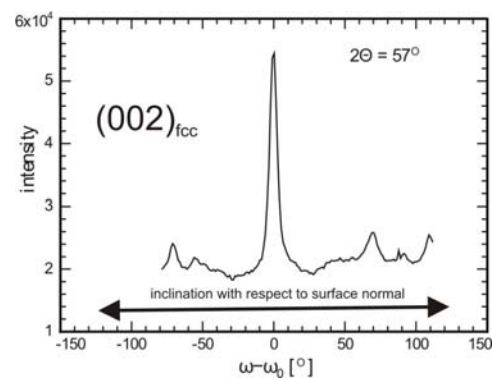



Figure 2 : Rocking scan for the (002) reflection

The existence of fcc-D<sub>2</sub> in the pores is surprising. In bulk the used D<sub>2</sub> solidifies in a hcp structure and remains hcp at all temperatures of the solid phase. But rather than introducing the same hcp structure in the pores, the cubic structure of the silicon matrix seems to be imposed on the porecondensate. The surrounding shifts the energy balance in favour of a face centred cubic structure. The existence of few well oriented D<sub>2</sub>-domains points towards future challenges. D<sub>2</sub> in a-Si seems to be a perfect candidate to study phonons in nano-confinement. Further its surrounding affected structure might be a perfect candidate for ab-initio calculations.

 <b>HELMHOLTZ ZENTRUM BERLIN</b> für Materialien und Energie  <b>NEUTRONS</b>	<b>EXPERIMENTAL REPORT</b>  <b>Structure and thermal decomposition of LiZn<sub>2</sub>(BD<sub>4</sub>)<sub>5</sub></b>	Proposal: MAT-01-2763  Instrument: <b>E6</b>  Local Contact: Andreas Hoser
	Principal Proposer: Arndt Remhof, EMPA Experimental Team: Arndt Remhof, EMPA Oliver Friedrichs, EMPA Dirk Wallacher, HZB	Date(s) of Experiment  09.03.2010 – 17.03.2010

Date of report: 27.03.2010

Complex borohydrides are currently investigated as potential future energy carriers. Much research has been performed on the synthesis of these compounds and their sorption behaviour [1]. However, the mechanism of formation and decomposition is not understood in detail. Boranes, and in particular diborane has been identified as an important intermediate in the formation and decomposition of tetrahydroborates [2]. Recently, a novel series of borohydride based materials, such as LiZn<sub>2</sub>(BH<sub>4</sub>)<sub>5</sub>, NaZn<sub>2</sub>(BH<sub>4</sub>)<sub>5</sub>, NaZn<sub>2</sub>(BH<sub>4</sub>)<sub>3</sub> have been discovered [3]. These materials have high hydrogen contents (~10 mass%) and low decomposition temperatures (<150°C). Unlike the more stable borohydrides, which decompose by hydrogen release at temperatures above 400°C, the novel materials release apart from the hydrogen a reasonable amount of diborane during decomposition.

In the present experiment we studied the structure and thermal decomposition of LiZn<sub>2</sub>(BH<sub>4</sub>)<sub>5</sub> by in-situ neutron powder diffraction. Therefore, we investigated a ball milled mixture of Li<sup>11</sup>BD<sub>4</sub> and ZnCl<sub>2</sub>, corresponding to a molar ratio of 5/2. This mixture is known to release B<sub>2</sub>D<sub>6</sub> upon thermal decomposition [2,3]. During the milling, we expect the formation of LiZn<sub>2</sub>(BD<sub>4</sub>)<sub>5</sub> and ZnCl<sub>2</sub> according to:

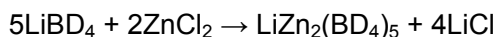


Figure 1 (top curve) shows a neutron powder diffractogram of the as milled sample. All observed reflections could be assigned to LiZn<sub>2</sub>(BD<sub>4</sub>)<sub>5</sub>, LiCl and to the sample container (Al). No traces of remaining LiBD<sub>4</sub> or ZnCl<sub>2</sub> were observed in the diffraction pattern.

Heating the sample to 85°C leads to a decay of the LiZn<sub>2</sub>(BD<sub>4</sub>)<sub>5</sub> reflections and the appearance of new reflections, which can be assigned to elemental zinc. Due to their identical symmetry the similar lattice parameters, the reflections of Al and LiD almost coincide.

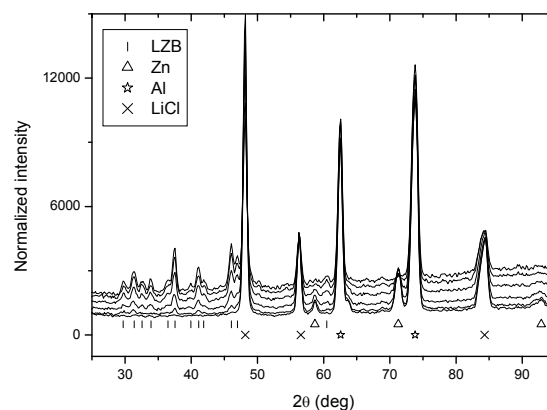
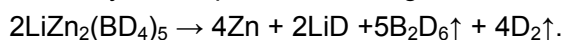


Figure 1: Temporal evolution of the neutron powder diffraction pattern of a ball milled mixture of LiBD<sub>4</sub> and ZnCl<sub>2</sub>.

Therefore, LiD is difficult to distinguish from Al in the present experiment. Figure 1 displays the series of diffraction pattern. Each individual diffractogram was recorded within one hour; the time lag between two depicted measurements equals five hours.

From the solid reaction products and applying Occam's razor, we assume that LiZn<sub>2</sub>(BD<sub>4</sub>)<sub>5</sub> thermally decomposes according to:



The occurrence of higher boranes or of amorphous phases, however, cannot be excluded.


#### References:

- [1] A. Züttel, et al., Scripta Mat., 56 823 (2007); and references therein.
- [2] O. Friedrichs et al., Chem.-Eur. J., 15 5531 (2009).
- [3] D. Ravnsbæk, et al., Angew. Chem.-Int. Edit. 48 6659 (2009).

#### Acknowledgement:

This research project has been supported by the European Commission under the 7<sup>th</sup> Framework Programme through "Research Infrastructures" action of the "Capacities" Programme, contract number CP-CSA\_INFRA-2008-1.1.1. Number 226507-NMI



 <b>NEUTRONS</b>	<b>EXPERIMENTAL REPORT</b>	Proposal: MAT-01-2880
	<b>In situ neutron diffraction investigation on the support effect of V<sub>2</sub>O<sub>5</sub> containing catalyst systems</b>	Instrument: <b>E6</b> Local Contact: Andreas Hoser
Principal Proposer: A. Berthold, TU Berlin Experimental Team: O. Görke, TU Berlin A. Hoser, HZB Berlin Tommy Hofmann, HZB Dirk Wallacher, HZB		Date(s) of Experiment 16.09.2010 - 20.09.2010

Date of report: 22.12.2010

Neutron diffraction experiments were carried out in order to study the defect formation and lattice relaxation of several catalysts as well as to extract information about oxygen vacancy development under catalytic feedgas conditions (ODP). Support material was  $\alpha$ -Al<sub>2</sub>O<sub>3</sub>, Y-Al<sub>2</sub>O<sub>3</sub>, ZrO<sub>2</sub> and TiO<sub>2</sub> (anatase). All measurements were executed under catalytic gas mixture (N<sub>2</sub>:O<sub>2</sub>:C<sub>3</sub>H<sub>8</sub> = 4:1:4) during heating. Starting with pure oxidizing conditions the sample temperature was increased stepwise by 50°C up 500°C. Then atmosphere was switched to catalytic conditions. Thus it was possible to ensure a defined gas environment with changing oxygen partial pressure.

The sets of powder diffraction patterns were recorded at each temperature and atmosphere step.

Our preliminary analysis performed by means of Fullprof program revealed a steep change of lattice parameter of the active component V<sub>2</sub>O<sub>5</sub> as a consequence of atmosphere exchange.

In Fig. 1 the corresponding neutron diffraction patterns are presented.

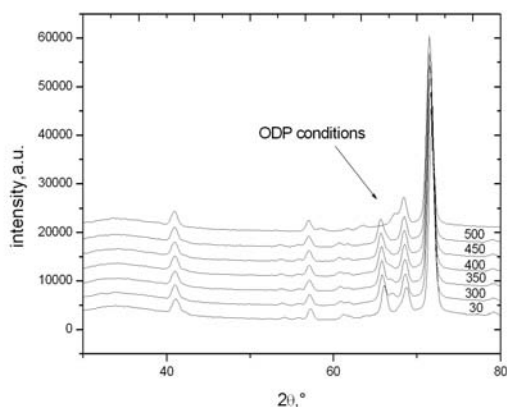


Fig.1: Set of diffraction patterns for sample  $\alpha$ -Al<sub>2</sub>O<sub>3</sub>-V<sub>2</sub>O<sub>5</sub>

Regarding the development of lattice parameters of the active component there is a considerable expansion and contraction respectively of the b- and c-axis. Results are displayed in Fig.2.

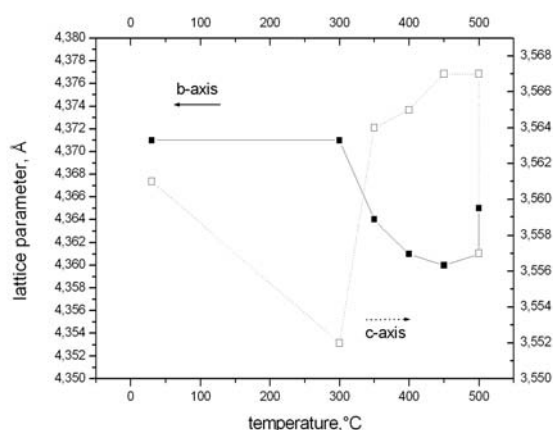


Fig.2: Development of the lattice parameters of b- and c-axis of V<sub>2</sub>O<sub>5</sub> during heating under oxidizing conditions and after switching to catalytic atmosphere (second points at 500°C). Analysis of the commented results are still in progress.

Contrary to expectations there is no formation of V<sub>2</sub>O<sub>3</sub> as proposed for the catalytic reaction but rather a generation of V<sub>4</sub>O<sub>7</sub> and V<sub>9</sub>O<sub>17</sub>. Unfortunately the mixture of anatase (TiO<sub>2</sub>) and V<sub>2</sub>O<sub>5</sub> contains just one independent reflex for V<sub>2</sub>O<sub>5</sub> of additionally small intensity, thus no structural refinement analysis could be applied. For these kind of questions further experiments with higher resolution are necessary.

Principal Proposer: M. Reehuis, A. Maljuk, HZB  
J. Kim, B. Keimer, MPI Stuttgart  
Experimental Team: M. Reehuis, HZB  
A. Hoser, HZB  
T. Hofmann, HZB

Date(s) of Experiment

31.03.2010 - 01.04.2010  
30.04.2010 - 03.05.2010

Date of report: 18.08.2010

Strontium ferrites with the composition  $\text{Sr}_3\text{Fe}_2\text{O}_{7-x}$  ( $0 \leq x \leq 1$ ) crystallize in the tetragonal space group  $I4/mmm$  [1]. For  $\text{Sr}_3\text{Fe}_2\text{O}_7$  ( $x = 0$ ) the onset of charge disproportionation of the iron ions ( $2\text{Fe}^{4+} \leftrightarrow \text{Fe}^{3+} + \text{Fe}^{5+}$ ) was observed at 343(10) K [2]. Therefore two different iron sites should be found in the crystal structure of  $\text{Sr}_3\text{Fe}_2\text{O}_7$ . But in  $I4/mmm$  the iron atoms are located at only one Wyckoff position  $4e$  (0,0,z). Therefore a lower crystal structure symmetry should be expected below the critical transition. At the Néel temperature  $T_N = 120(2)$  K the iron atoms show antiferromagnetic ordering [2]. The magnetic structure, which is possibly incommensurate, could not be determined so far. For  $\text{Sr}_3\text{Fe}_2\text{O}_6$  ( $x = 1$ ) the site of the O3-atom (at  $2a$  of  $I4/mmm$ ) is not populated. In this compound the iron moments show a commensurate structure with a propagation vector  $\mathbf{k} = (\frac{1}{2}, \frac{1}{2}, 0)$  [3]. Interestingly the magnetic transition occurs at the relatively high Néel temperature  $T_N = 550$  K [3].

In order to investigate in detail the crystal and magnetic structures in the system  $\text{Sr}_3\text{Fe}_2\text{O}_{7-x}$  we have started to carry out powder-diffraction studies of two samples of  $\text{Sr}_3\text{Fe}_2\text{O}_{7-x}$  with  $x \approx 1$  (argon-annealed) and  $x \approx 0$  (air-annealed). Neutron powder-diffraction patterns were recorded on the instrument E6 between 2 K and 300 K using the neutron wavelength  $\lambda = 2.45$  Å (PG-monochromator). From the powder data we were not able to find a lower symmetric crystal structure. This may show our single-crystal experiment, which will be carried out on the instrument E5. However the crystal structure could be successfully refined in the tetragonal space group  $I4/mmm$  resulting in very satisfactory  $R_F$ -values between 0.013 and 0.021. In Table 1 it can be seen that the positional parameters as well as the occupancy of the O3-atom could be determined with good accuracy.

Table 1. Results of the Rietveld refinements of  $\text{Sr}_3\text{Fe}_2\text{O}_{6.027}$  and  $\text{Sr}_3\text{Fe}_2\text{O}_{6.736}$ . In the space group  $I4/mmm$  Sr1 and Sr2 are located at the position  $2b(0,0,\frac{1}{2})$  and  $4e(0,0,z)$ , respectively. At the position  $4e$  one also finds the atoms Fe1 and O2, while O1 and O3 are located at  $8g(0,\frac{1}{2},z)$  and  $2a(0,0,0)$ , respectively. In the Table only the fixed and refinable z-co-ordinates are listed.

	$\text{Sr}_3\text{Fe}_2\text{O}_{6.027(5)}$		$\text{Sr}_3\text{Fe}_2\text{O}_{6.736(6)}$	
	z (2 K)	z (295 K)	z (2 K)	z (160 K)
Sr1	$\frac{1}{2}$	$\frac{1}{2}$	$\frac{1}{2}$	$\frac{1}{2}$
Sr2	0.31893(8)	0.31872(8)	0.31678(15)	0.31676(11)
Fe	0.10214(6)	0.10218(7)	0.09825(15)	0.09810(12)
O1	0.08479(7)	0.08503(7)	0.09271(14)	0.09230(10)
O2	0.19677(13)	0.19674(13)	0.1939(2)	0.1939(2)
O3	0	0	0	0

The magnetic structure of  $\text{Sr}_3\text{Fe}_2\text{O}_{6.027}$  was investigated from the powder pattern collected at 2 K (Fig. 1). Magnetic intensity was found at the positions of the commensurate reflections  $(\frac{1}{2}, \frac{1}{2}, \ell)_M$  with  $\ell = \text{even or odd}$ . These reflections can be generated by the rule

$(hkl)_M = (hkl)_N \pm \mathbf{k}$ . The propagation vector  $\mathbf{k} = (\frac{1}{2}, \frac{1}{2}, 0)$  allows to define a magnetic unit cell of the dimension  $a\sqrt{2} \times a\sqrt{2} \times c$ , where the  $ab$ -plane is doubled corresponding to the crystallographic unit cell. The same magnetic cell was found earlier for  $\text{Sr}_3\text{Fe}_2\text{O}_{7-x}$  with  $x = 1.0$  and  $x = 0.79$  [3,4]. No magnetic intensity could be found at the position  $(\frac{1}{2}, \frac{1}{2}, 0)_M$  indicating an antiparallel coupling of the iron moments at  $(0,0,z)$  and  $(0,0,-z)$ . Further the iron moments form spin sequences  $+-+ \dots$  along the  $x$ - and  $y$ -directions of the chemical unit cell. Our Rietveld refinements of  $\text{Sr}_3\text{Fe}_2\text{O}_{6.027}$  showed that the magnetic moments of the iron atoms are aligned predominantly in the basal plane forming an angle to the  $c$ -axis of  $64.0(7)^\circ$ . This is in contrast to the results of Ref. 4, where a moment direction parallel to the  $c$ -axis was claimed. The experimental magnetic moment per Fe-atom is  $\mu_{\text{exp}} = 3.59(13) \mu_B$ . The powder pattern of the oxygen-rich sample  $\text{Sr}_3\text{Fe}_2\text{O}_{6.736}$  showed magnetic intensities at the diffraction angles  $9.7^\circ$ ,  $29.2^\circ$  and  $46.7^\circ$ , respectively. The relatively broad reflections could not be indexed. Further details of the magnetic ordering are given in the report of our single-crystal neutron diffraction study.

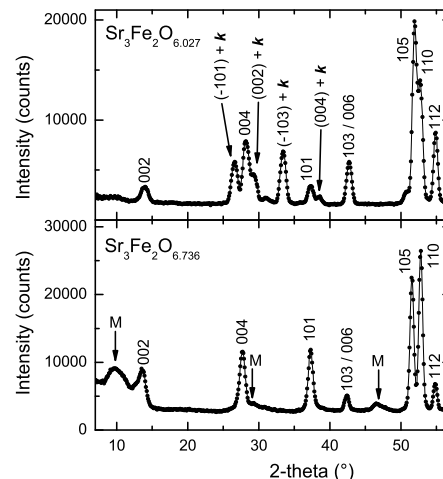



Fig. 1. Neutron powder patterns of  $\text{Sr}_3\text{Fe}_2\text{O}_{6.027}$  and  $\text{Sr}_3\text{Fe}_2\text{O}_{6.736}$  collected at 2 K.

## References

- [1] S.E. Dann, M.T. Weller, D.B. Currie, J. Solid State Chem. **97** (1992) 179.
- [2] K. Kuzushita, S. Morimoto, S. Nasu, S. Nakamura, J. Phys. Soc. Jpn. **69** (2000) 2767.
- [3] S.E. Dann, M.T. Weller, D.B. Currie, M.F. Thomas, A.D. Al-Rawwas, J. Mater. Chem. **3** (1993) 1231.
- [4] K. Mori, T. Kamiyama, H. Kobayashi, T. Arima, K. Ohoyama, S. Ikeda, Appl. Phys. A **74** [Suppl.] S914.

 <b>HELMHOLTZ ZENTRUM BERLIN</b> für Materialien und Energie  <b>NEUTRONS</b>	<b>EXPERIMENTAL REPORT</b>  <b>Order and disorder in kesterite (Cu<sub>2</sub>ZnSnS<sub>4</sub>)</b>	Proposal: PHY-01-2520  Instrument: <b>E9</b>  Local Contact: M. Tovar, F. Yokaichiya
	Principal Proposer: Susan Schorr, FU Berlin Experimental Team: Susan Schorr, FU Berlin Michael Tovar, HZB	Date(s) of Experiment  02.06.2009 – 04.06.2009

Date of report: 7. 9. 2010

The multinary chalcogenide Cu<sub>2</sub>ZnSnS<sub>4</sub> (kesterite) has newly attracted attention as possible photovoltaic material [1]. It crystallizes in the kesterite type structure (s.g.  $I\bar{4}$ ) which is described in literature [2] as an ordered distribution of the cations Cu<sup>+</sup> and Zn<sup>2+</sup>. In doing so one Cu occupies the 2a (0,0,0) position, while Zn and the remaining Cu are ordered at 2d (0,  $\frac{1}{4}$ ,  $\frac{3}{4}$ ) and 2c (0,  $\frac{1}{2}$ ,  $\frac{1}{4}$ ).

Because the elements Cu and Zn are neighbours in the periodic table, the cations Cu<sup>+</sup> and Zn<sup>2+</sup> have the same number of electrons (28), thus they have equal atomic form factors. Hence both cations are not distinguishable by conventional X-ray diffraction. Neutron powder diffraction is a powerful method to investigate structures containing electronic similar elements, as the neutron scattering length of Cu and Zn ( $b_{\text{Cu}}=7.718(4)$  fm,  $b_{\text{Zn}}=5.680(5)$  fm) is different.

In earlier investigations Cu<sub>2</sub>ZnSnS<sub>4</sub> powder samples synthesized by solid state reaction of the elements at 750°C were used. The Rietveld analysis of neutron diffraction data obtained before [3, 4] have revealed a disorder of Cu and Zn on the positions 2c (0,  $\frac{1}{2}$ ,  $\frac{1}{4}$ ) and 2d (0,  $\frac{1}{4}$ ,  $\frac{3}{4}$ ). The degree of disorder depends on the cooling rate (see figure 1): the quenched sample shows a random distribution of Cu and Zn on the 2c and 2d positions, whereas in the sample with controlled cooling (750°C to room temperature with 1K/h) the distribution has changed to (0.7Cu + 0.3Zn) on 2c and (0.3Cu + 0.7Zn) on 2d. Thus it was concluded, that the cation order in kesterite is influenced by the sample synthesis routine (temperature, rates).

For this work a new sample was prepared using a different synthesis. The stoichiometric mixture of the elements was heated above the melting point of Cu<sub>2</sub>ZnSnS<sub>4</sub>. The temperature was hold for a certain time to guarantee a complete mixing of all constituents, followed by a controlled cooling to room temperature. It should be noted, that during this cooling the

structural phase transition temperature was crossed. It was shown [5], that above 885°C a cubic high temperature phase of kesterite (sphalerite type structure) exists.

The average neutron scattering length of the cation sites of the kesterite type structure ( $\bar{b}_{2a}, \bar{b}_{2c}, \bar{b}_{2d}$ ) were calculated according to the algorithm described in [6]. Figure 1 shows, that also in the kesterite sample grown by a different method Cu<sup>+</sup> and Zn<sup>2+</sup> are disordered on the positions 2c and 2d.

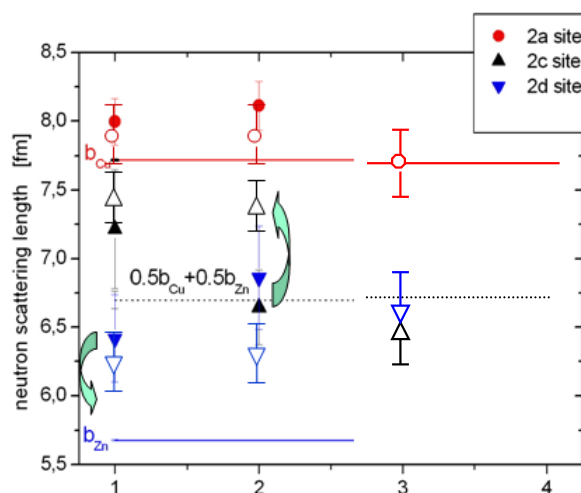



Figure 1: Average neutron scattering length of the cation sites 2a, 2c and 2d of the investigated Cu<sub>2</sub>ZnSnS<sub>4</sub> samples. Horizontal lines mark the neutron scattering length of copper, zinc and a mixture of 0.5Cu+0.5Zn. Closed symbols: quenched sample [3]

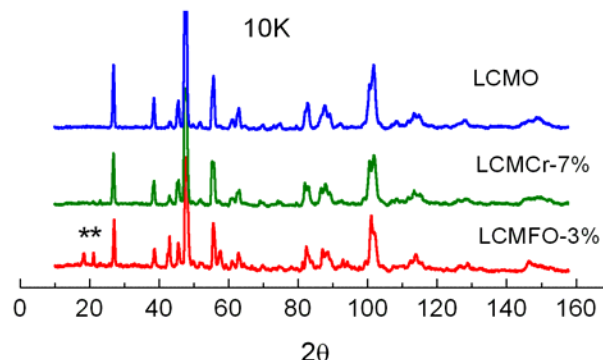
Open symbols (1 and 2): 1 K/h cooling rate [4]  
 Open symbols (3): this work

- [1] H. Katagiri et al., *Appl. Phys. Express* **1**, 041201, (2008).
- [2] S.R. Hall et al., *Can. Mineral.*, **16**, 131 – 137(1978).
- [3] S. Schorr, H.-J. Hoebler, M. Tovar, *Europ. J. Mineral.* **19**, 65 (2007).
- [4] S. Schorr, M. Tovar, *BENSC Experimental Report* (2006).
- [5] S. Schorr, G. Gonzalez-Aviles, *Phys. Stat. Sol. C* (2008)
- [6] Schorr, S., et al., *X-Ray and Neutron Diffraction on Materials for Thin Film Solar Cells in Advanced Characterization Techniques for Thin Film Solar cells.*, eds. D. Abou-Ras, T. Kirchhartz and U. Rau. 2011, Wiley VCH.

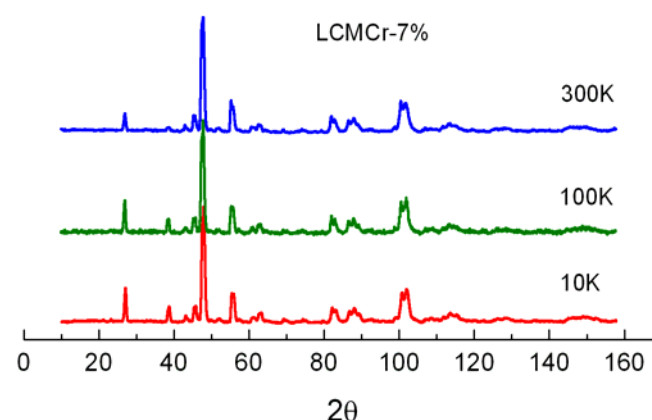
 <b>HELMHOLTZ ZENTRUM BERLIN</b> für Materialien und Energie  <b>NEUTRONS</b>	<b>EXPERIMENTAL REPORT</b>	Proposal: PHY-01-2532
	<b>Potential Neutron Powder Diffraction in La<sub>2/3</sub>Ca<sub>1/3</sub>A<sub>x</sub>Mn(1-x)O<sub>3</sub> with A=Cr(x=0.07 and 0.08), Fe(x=0.03)</b>	Instrument: <b>E9</b> Local Contact: Fabiano Yokaichiya
Principal Proposer: Experimental Team:	Oscar Arnache, Universidad de Antioquia, Co Diana Lucia Quintero, HZB Doris Giratá, Universidad de Antioquia, Co	Date(s) of Experiment  11.05.2009 – 18.05.2009

The doping effects by Fe/Cr in Mn site in La<sub>2/3</sub>Ca<sub>1/3</sub>MnO<sub>3</sub> (LCMO) manganites powder have shown that the magnetotransport properties change, where the magnetization, Curie temperature and metal-insulator transition decrease as a function of the increment of Fe/Cr concentration [1]. Regarding to the effects of the Fe/Cr ion in these manganites, there are many interesting questions about whether the interactions of Fe/Cr and Mn, which can be explained by the model of double exchange (DE), or whether this interaction is less effective due to the change of the crystal field when we introduced doping, if there are Cr super-lattices for any doping concentration, or if there are AF coupling between these ions [2]. According to the magnetotransport properties studies we do know that Cr (x = 0.07 and 0.08) and Fe (x=0.03) concentrations are critical in the physical behavior. In order to obtain information and elucidate the effect of the Fe/Cr ions substitution in LCMO, we performed powdered neutron diffraction at different temperatures in the FM and PM regime. The expected achievements of this experiment are to gain insights on the nuclear and magnetic structures for these compounds. Base on this we are able to draw conclusions on the possible formation of AF clusters and the competition between FM region due to the introduction of Fe<sup>3+</sup> ions, which are not involved in the DE. And with respect to Cr doped LCMO, we could be able to discuss the implication of the super-double interchange for the FM bounds Cr<sup>3+</sup>-O-Mn<sup>3+</sup> in these samples. For this purpose, measurements were performed using E9 instrument in the reactor BER II, with a wavelength of 1.79Å. Neutron diffraction patterns (NPD) were acquired in a scattering angle's range 10° ≤ 2θ ≤ 150°, at T = 10, 100 and 300K for LCMO and LCMCr-7% compounds; at T = 10K for LCMCr-8% compound; and at T = 10, 25, 50, 75, 100 and 300K for LCMFO-3%. Fig. 1 shows NPD patterns recorded at 10K for doped and Fe/Cr undoped samples. Two additional Bragg peaks

Date of report: 29.01.2011  
 at low angular range (~18 – 21°) were found in the LCMFO-3% compound, attributed probably any long-range-ordered magnetic phase (AF) or magnetic inhomogeneity due to a phase separation occurred during the cooling process of the sample preparation or impurities in the synthesis. This result is quite interesting and will be discussed in detail after a Rietveld refinement. The temperature dependence of the NPD patterns of LCMCr-7% is depicted in Fig. 2. In all temperature range no impurities were observed.




**Fig. 1.** Plot of the NPD data of LCMO, LCMCr-7% and LCMFO-3% at 10K.



**Fig. 2.** Plot of the NPD data of LCMCr-7% at 10, 100 and 300K.

- [1] F. Rivadulla. *Phys. Rev B*, 62, 9, 2000.  
 [2] K. H Ahn. *Phys. Rev. B* 54, 15299 (1996).

 <b>HELMHOLTZ ZENTRUM BERLIN</b> für Materialien und Energie  <b>NEUTRONS</b>	<b>EXPERIMENTAL REPORT</b>  <b>Structural investigation of the kesterites</b> <b><math>\text{Cu}_2\text{ZnSn}(\text{S}_{1-x}\text{Se}_x)_4</math></b>	Proposal: PHY-01-2596  Instrument: <b>E9</b>  Local Contact: M. Tovar
	Principal Proposer: Susan Schorr, FU Berlin Experimental Team: Susan Schorr, FU Berlin Michael Berkes, FU Berlin Michael Tovar, HZB	Date(s) of Experiment  24.09.2010 – 29.09.2010

Date of report: 7. 9. 2010

In the last years the quaternary semiconducting compound  $\text{Cu}_2\text{ZnSnS}_4$  (kesterite) has attracted attention due to its suitability as absorber material in thin film solar cells [1]. Recently a thin film solar cell with  $\text{Cu}_2\text{ZnSn}(\text{S},\text{Se})_4$  as absorber material reached 9.66 % efficiency [2].

The structure of both compounds consists of a *ccp* array of sulfur atoms, with metal atoms occupying one half of the tetrahedral voids. The structure of  $\text{Cu}_2\text{ZnSnS}_4$  was described as kesterite type structure [3] (space group  $I\bar{4}$ ) with an ordered distribution of Cu and Zn. Neutron diffraction experiments on  $\text{Cu}_2\text{ZnSnS}_4$  have shown, that a Cu/Zn disorder on the positions 2c ( $0, \frac{1}{2}, \frac{1}{4}$ ) and 2d ( $0, \frac{1}{4}, \frac{3}{4}$ ) exists [4, 5]. On the other hand,  $\text{Cu}_2\text{ZnSnSe}_4$  crystallizes in the stannite type structure (space group  $I\bar{4}2m$ ) [6].

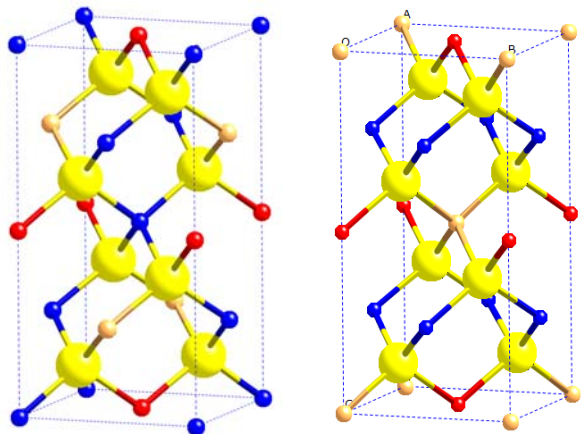


Figure 1: Structure of  $\text{Cu}_2\text{ZnSnS}_4$  (left) and  $\text{Cu}_2\text{ZnSnSe}_4$  (right). The main difference is the Cu/Zn distribution (Cu-blue, Zn-orange, Sn-red). Big spheres are sulfur and selenium, respectively

The main goal of the experiment was to clarify the structure of  $\text{Cu}_2\text{ZnSnSe}_4$ . The investigation described in literature [6] is based on X-ray diffraction data only, disregarding the problem of the electronic similarity of the elements Cu and Zn. They are neighbouring elements in the periodic table,  $\text{Cu}^+$  and  $\text{Zn}^{2+}$  have the same number of electrons and therefore, nearly similar atomic scattering factors in X-ray diffraction. Otherwise the coherent neutron scattering length of Cu and Zn is different. Thus structural analysis by Rietveld refinement of neutron diffraction data

allows the separation of isoelectrical ions like it is the case for  $\text{Cu}^+$  and  $\text{Zn}^{2+}$ .

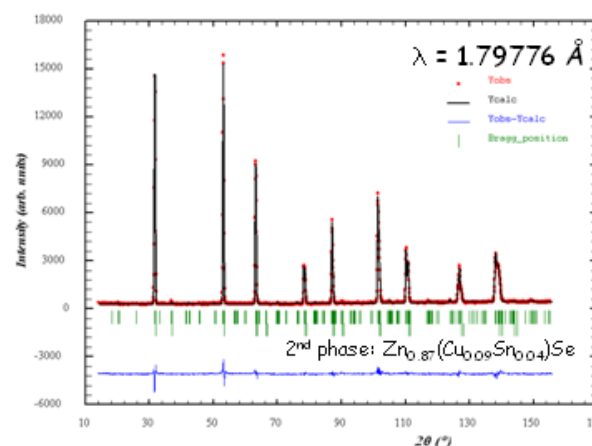



Figure 2: Rietveld analysis of neutron diffraction data obtained for  $\text{Cu}_2\text{ZnSnS}_4$  ( $R_{\text{Bragg}}=3.54$ ) using the kesterite type structure as model in the refinement.

The average neutron scattering length of the cation sites of the kesterite type structure ( $\bar{b}_{2a}, \bar{b}_{2c}, \bar{b}_{2d}$ ) were calculated according to the algorithm described in [7]. The resulting cation occupancy concerning copper and zinc is as follows (Sn occupies the 2b position):

2a: Cu / 2c:  $0.30\text{Zn}+0.70\text{Cu}$  / 2d:  $0.25\text{Cu}+0.75\text{Zn}$ .

Thus we have shown that  $\text{Cu}_2\text{ZnSnSe}_4$  crystallizes in the kesterite type structure with a Cu/Zn disorder similar to  $\text{Cu}_2\text{ZnSnS}_4$ .

- [1] H. Katagiri et al., *Appl. Phys. Express* **1**, 041201, (2008).
- [2] A. Todorov et al., *Adv. Material* **22**, E156, (2010).
- [3] S. R. Hall et al., *Can. Mineral.* **16** 131 (1978).
- [4] S. Schorr et al., *Europ. J. Mineral.* **19** 65 (2007).
- [5] S. Schorr et al., *BENSC Experimental Report* (2006).
- [6] I. D. Oleksyuk et al., *J. Alloys Comp.* **340** 141 (2002).
- [7] S. Schorr et al., X-Ray and Neutron Diffraction on Materials for Thin Film Solar Cells in *Advanced Characterization Techniques for Thin Film Solar cells.*, eds. D. Abou-Ras, T. Kirchhartz, U. Rau. 2011, Wiley.

 <b>EXPERIMENTAL REPORT</b>		Proposal: MAT-01-2723 Instrument: <b>E9</b> Local Contact: Michael Tovar
<b>NEUTRONS</b>	<b>Investigations in the phase system Li-Zr-Y-Mg-O</b>	
Principal Proposer: Ulla Simon, TU Berlin Experimental Team: Michael Tovar, HZB Dirk Wallacher, HZB Nico Holst, HZB Oliver Görke, TU Berlin		Date(s) of Experiment  05.07.2010 – 11.07.2010

Date of report: 29.01.2011

Li promoted MgO catalysts are intensely investigated catalysts for oxidative coupling of methane (OCM) [1,2]. However, substantial deactivation of Li/MgO catalysts during catalytic performance was reported [2]. Doping with transition metal ions was found to stabilize the catalytic activity temporarily [3].

Neutron diffraction experiments were carried out in order to study the defect formation and lattice relaxation of several Li- and transition metal doped MgO catalysts. Thus, samples were under investigation at RT as well as at 750 °C under varying atmospheres including simulated OCM conditions.

Two possible defect models for Li doping are given in Kröger-Vinck notation [4] and are shown schematically in Fig. 1. First, a substitutional replacement of Li on the Mg site may be considered which would cause anionic defects (Model1). Alternatively the oxygen site could be filled, which then would cause interstitial Li ions (Model2).

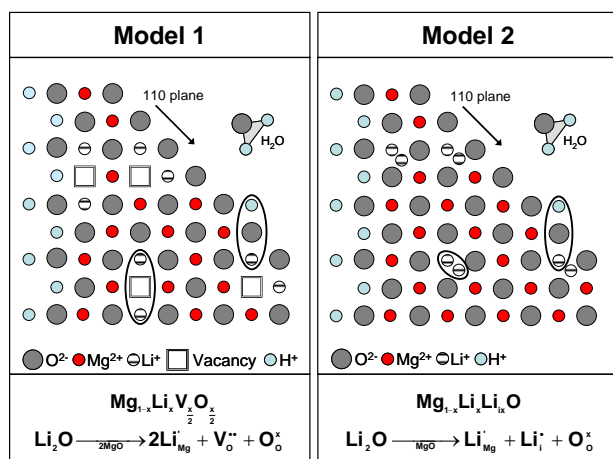


Fig. 1. Defect models for Li-MgO solid solutions. Model1: Substitutional replacement; Model2: Interstitial Li<sup>+</sup> ion.

Neutron diffraction patterns at RT indicate a reduction in lattice parameter from 4.2066±1 to 4.2048±1 Å for MgO due to the Li doping. Thus, the formation of oxygen vacancies (Model1) seems to be the determining process of Li doping. This assumption is supported by the similar ionic radii of Li and Mg.

A drastically increase in lattice parameter to 4.2532±2 and 4.2720±3 Å was observed, due to a

further doping of Li/MgO with Zr and Y/Zr respectively (Fig. 2). Thus, Li and Zr seem to occupy cation lattice sites. Surprisingly a secondary MgO phase showing smaller lattice parameters of 4.2125±4 was observed for both Zr and Y/Zr doped Li/MgO.

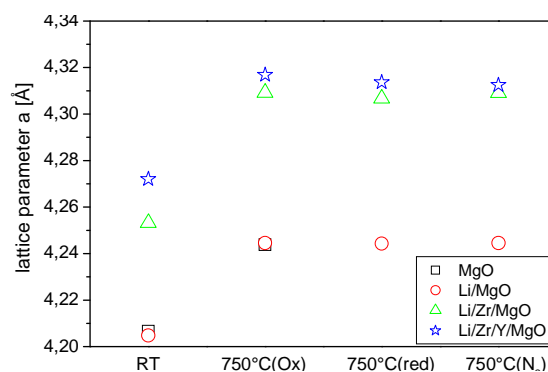


Fig. 2. Development of the lattice parameters of Li/Zr/Y doped MgO samples for RT and 750°C under varying atmospheres.

Increasing the temperature to 750°C under static syn. air flow (750°C(Ox)) leads to a strong growth of lattice parameter for all samples (Fig. 2). Switching to simulated OCM conditions induced a minimal decrease in lattice parameter.

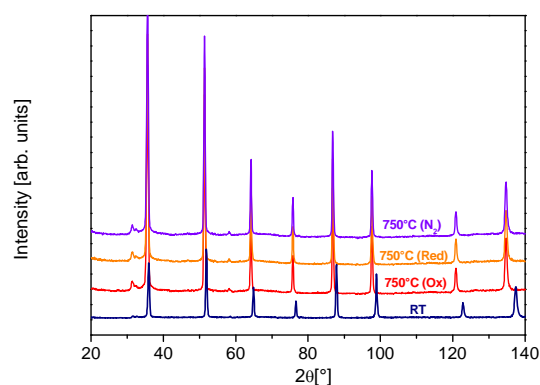



Fig. 3. Set of diffraction patterns for Li/MgO samples

The neutron measurements show the benefit of complex sample environment in catalytic research. By varying temperature and gas atmosphere we could elucidate the characteristics of the catalyst and confirm a working model. The report represents only part of the data, analysis is still in progress.

- [1] T. Ito *et al.*, J. Am. Chem. Soc. 107 (1985) 5062-5068.
- [2] C. Mirodatos *et al.*, Stud. Surf. Sci. Catal. 34 (1987) 183-195.
- [3] G. C. Hoogendam *et al.*, Catal. Today 21 (1994) 333-340.
- [4] F. A. Kröger, North-Holland, Amsterdam 1964.

 <b>EXPERIMENTAL REPORT</b>		Proposal: PHY-01-2734
<b>Neutron diffraction studies on Nd<sub>7</sub>Rh<sub>3</sub></b>		Instrument: <b>E9</b>
		Local Contact: Paul Henry
Principal Proposer:	Sudhindra Rayaprol, UGC-DAE CSR, Mumbai, India	Date(s) of Experiment
Experimental Team:	Vasudeva Siruguri, UGC-DAE CSR, Mumbai, India E. V. Sampathkumaran, TIFR, Mumbai, India Andreas Hoser, HZB Paul Henry, HZB	01.07.2010 – 03.07.2010

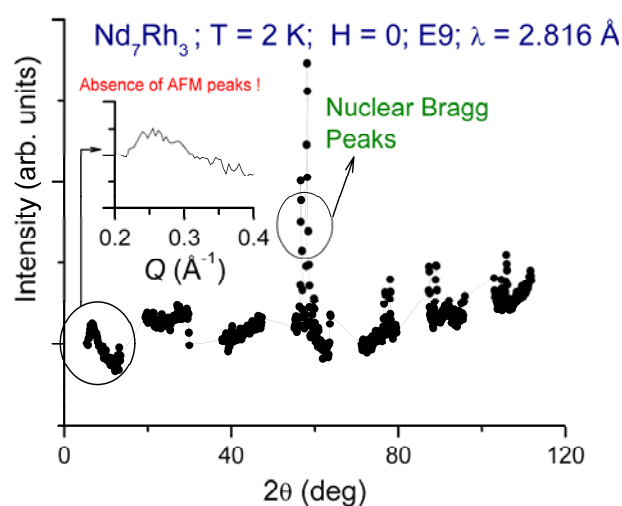
Date of report: 20.01.2011

The phenomena of electronic phase separation are observed across the first order metal-insulator transition in systems exhibiting *giant magnetoresistance* because of change in temperature or magnetic field, resulting in percolative conduction. Magnetic and transport measurements on Nd<sub>7</sub>Rh<sub>3</sub> exhibit field-induced first-order-phase-transition (FOPT). In order to explore the phenomenon of FOPT in Nd<sub>7</sub>Rh<sub>3</sub> at microscopic level, we had initially carried out magneto-thermal neutron diffraction (ND) experiments using neutrons at wavelength ( $\lambda$ ) of 2.451 Å on E6.

Initially, the ND experiments were carried out on polycrystalline powder sample of Nd<sub>7</sub>Rh<sub>3</sub> at temperatures between 1.5 and 50 K and under external magnetic field (1.5 Tesla). The position of the AFM peak for Nd<sub>7</sub>Rh<sub>3</sub> estimated from its isostructural compounds was expected at  $Q = 0.26 \text{ \AA}^{-1}$ . It was observed from the analysis of the initial ND experiments carried out on E6 that the magnetic structure of Nd<sub>7</sub>Rh<sub>3</sub> is different from its isostructural counterparts like Nd<sub>7</sub>Ni<sub>3</sub> or Er<sub>7</sub>Rh<sub>3</sub>. In sharp contrast to the observations made in magnetization measurements in bulk/single crystal samples as well as in ND patterns of its isostructural counterparts, no peaks attributable to antiferromagnetic ordering could be seen down to 2 K. The absence of the AFM peak in the ND patterns recorded earlier could be attributed to the fact that it is either too weak to be observed due to the strong interference from the direct beam or has shifted to a much lower Q-value.

To address the issue of low-angle AFM peak, the ND experiments on polycrystalline sample of Nd<sub>7</sub>Rh<sub>3</sub> were carried out on E9 with higher resolution and longer wavelength. To overcome the limitations of Q-range observed in our previous experiments, we carried out neutron diffraction experiments at Q values smaller than  $0.3 \text{ \AA}^{-1}$  using a wavelength of 2.816 Å.

For measuring the data on E9, the TTHS was fixed at  $-16^\circ$  and data was recorded in 8 detectors. In the Fig. 1, the ND pattern of Nd<sub>7</sub>Rh<sub>3</sub> recorded at  $T = 2 \text{ K}$ , in  $H = 0$  is shown.




**Fig. 1** ND pattern for Nd<sub>7</sub>Rh<sub>3</sub> recorded at  $T = 2 \text{ K}$  in  $H = 0$ .

In the main panel of the figure, the raw data is plotted after proper calibration. The pattern could be refined for nuclear (crystalline) structure. No additional peaks attributable to antiferromagnetic ordering were observed. To highlight this point, the low angle diffraction data is plotted as a function of  $Q$  as inset. The anomaly observed around  $0.25 \text{ \AA}^{-1}$  is most likely arising due to direct beam effects and not because of the sample, as this could not be attributed to any magnetic structure.

Detailed diffraction studies are planned to elucidate the magnetic structure and to explain the field-induced FOPT in Nd<sub>7</sub>Rh<sub>3</sub>.

*Financial support in the form of travel grant was provided by Department of Science and Technology, Government of India to carry out this research project.*

	<b>EXPERIMENTAL REPORT</b>  <b>Determination of metal atom site distribution in complex transition metal chalcogenides</b>	Proposal: CHE-01-2852  Instrument: <b>E9</b>  Local Contact: Paul Henry
	Principal Proposer: W. Bensch, CAU Kiel Experimental Team: Kathrin Gerwien, CAU Kiel Paul Henry, HZB Michael Tovar, HZB	Date(s) of Experiment  01.10.2010 – 02.10.2010

Date of report: 26.01.2011

#### Experimental section:

Chromium and vanadium cannot be unambiguously distinguished using X-ray Rietveld refinements. The occupancies of the V and Cr atoms on the four independent crystallographic sites in the crystal structures of  $\text{Cr}_2\text{V}_3\text{Se}_8$  and  $\text{CrV}_4\text{Se}_8$  should be determined by neutron diffraction experiments. The metal atom distribution must be known to understand the physical properties and to compare the properties and metal atom distribution obtained for the isostructural  $\text{Cr}_{5-y}\text{Ti}_y\text{Se}_8$  series [1].

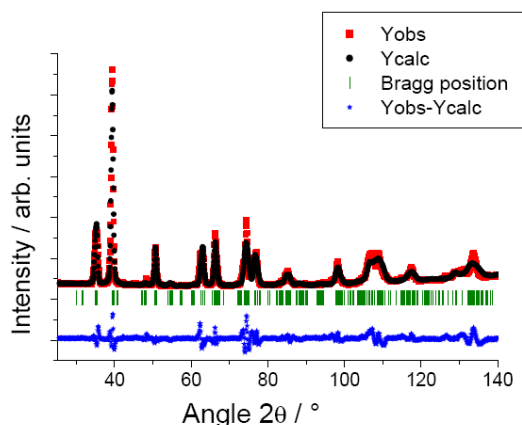


Fig. 1: Rietveld refinement of the pattern of  $\text{CrV}_4\text{Se}_8$

The crystal structure can be derived from the NiAs type structure by ordered removal of metal atoms from every second metal atom layer. In the resulting structure the metal atoms occupy different sites: M1 and M4 are partially, M2 and M3 are fully occupied.

To determine the Cr/V distribution over the different sites several models were considered and subsequently tested.

Best results were obtained  $\text{CrV}_4\text{Se}_8$  with Cr being located on sites M1 and M3 (Fig. 1). The refined composition is  $\text{Cr}_{1.05(5)}\text{V}_{3.80(5)}\text{Se}_8$  being close to the 5:8 ratio for M:Se.

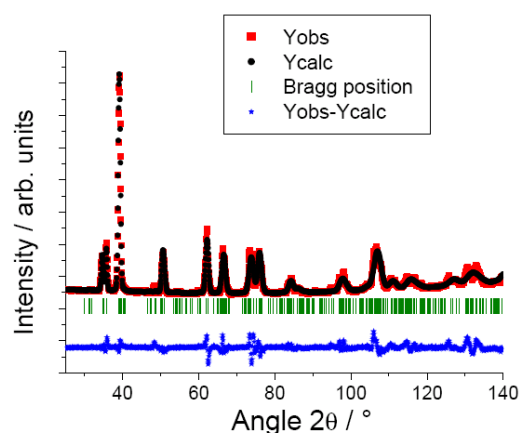


Fig. 2: Rietveld refinement of the pattern of  $\text{Cr}_2\text{V}_3\text{Se}_8$

For the Cr-richer compound  $\text{Cr}_2\text{V}_3\text{Se}_8$  the Cr atoms occupy all metal atom sites (Fig. 2) yielding the final composition  $\text{Cr}_{1.97(5)}\text{V}_{2.62(5)}\text{Se}_8$ . The metal atom content is slightly too low and further efforts are under way to improve the results.

- [1] J. Wontcheu, W. Kockelmann, Z.L. Huang, W. Schnelle, W. Bensch, *Solid State Sci.* 9, 6, 2007, 506-514.



 <b>HELMHOLTZ ZENTRUM BERLIN</b> für Materialien und Energie  <b>NEUTRONS</b>	<b>EXPERIMENTAL REPORT</b>	Proposal: PHY-01-2863
	<b>Isothermal structural transition in Bi1-xLaxFeO3 system</b>	Instrument: <b>E9</b> Local Contact: Michael Tovar
Principal Proposer: Experimental Team:	Alexey Kuzmin, Univ. of Latvia, Riga, LV Vadim Sikolenko, ETH Zürich and PSI, CH Vadim Efimov, JINR Dubna, RU	Date(s) of Experiment  22.09.2010 – 27.09.2010

Date of report: 18.11.2010

Neutron powder diffraction experiment of the Bi<sub>1-x</sub>LaxFeO<sub>3</sub> with the different 0.15 < x < 0.25 have been performed at the new upgraded E9 instrument. The sample with x = 0.18 at room temperature can be described as antiferroelectric *Pbam* with additional *R3c*. A fraction of the rhombohedral phase rises to 10.5 %, 24 %, and 53 % with increasing the temperature to 240, 340, and 420 °C, respectively, thus demonstrating of gradual antipolar to polar structural transformation upon a thermal excitation. At 700 °C, the compound possesses a single-phase orthorhombic *Pnma* structure. Comparison of the fractional coordinates of the A-site atoms obtained at 20 °C and 420 °C indicate that antiferroelectric displacements are strongly suppressed with increasing temperature.

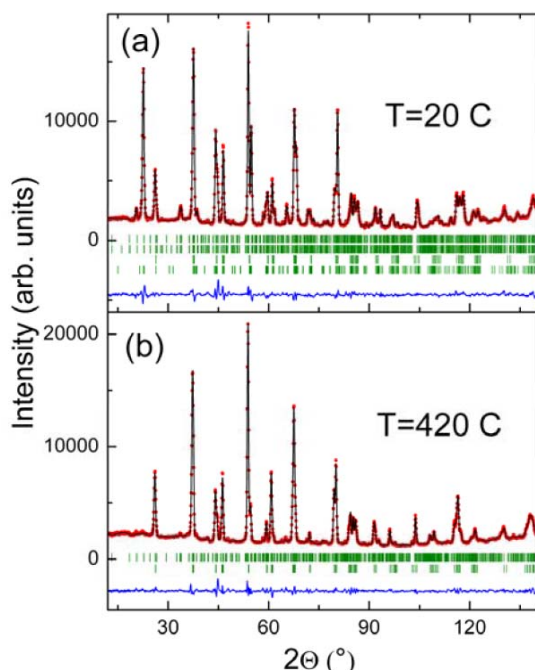



Figure 1. Observed (circles), calculated (solid line) and difference patterns resulting from the Rietveld analysis of the neutron powder diffraction data of x=0.185 sample obtained at 960 °C. Bragg reflections are indicated by tick marks

The x = 0.25 sample can be refined in the frame of *Pbam* below 470 °C, unsolved low intensity peaks may indicate an incommensurate structure, which can be described as a first approximation by a *Pbam* model with commensurate subcell. Upon cooling the following sequence transitions is realized: paraelectric orthorhombic *Pnma*; polar rhombohedral *R3c* and antipolar *Pbam*. Both isothermal and thermal phase behavior can be understood assuming that the energetic barrier between polar rhombohedral and antipolar orthorhombic phases is large whereas thermodynamic potentials (Gibbs free energy) are very close. So these phases can coexist or exist as unique in very wide temperature range. The isothermal transition between them occurs via mechanism of inhomogeneous nucleation which strongly affected temperature. Than the temperature larger than the effectively occurs transition due to increasing mobility of the defects. At larger temperature the polar phase is more stable than the antipolar one, so the inverse isothermal transition takes place. One can suggest that the large energetic barrier between two phases is associated with low mobility of the lanthanum ions due to relatively small polarizability. The rhombohedral polar phase becomes completely unstable at x>0.2 where a modified type of the antipolar structure is observed.

#### Acknowledgement

This research project has been supported by the European Commission under the 7<sup>th</sup> Framework Programme through the Key Action: Strengthening the European Research Area, Research Infrastructures. Contract n°: **226507** (NMI3)

This project has been also partly supported by RFBR, project 10-02-90053-Bel\_a.

 <b>HELMHOLTZ ZENTRUM BERLIN</b> für Materialien und Energie  <b>NEUTRONS</b>	<b>EXPERIMENTAL REPORT</b>	Proposal: PHY-03-692 Instrument: <b>V3</b> Local Contact: Z. Izaola
	<b>Crystal electric field in PrT<sub>2</sub>Ge<sub>2</sub> (T = Ni, Rh) compounds</b>	Date(s) of Experiment 25.06.2010 - 01.07.2010
Principal Proposer: Experimental Team:	L. Gondek, AGH-UST, Krakow, PL L. Gondek, AGH-UST, Krakow, PL J. Czub, AGH-UST, Krakow, PL Z. Izaola, HZB	

Date of report: 14.01.2011

The performed experiment aimed at determination of crystal field (CF) levels distribution in group of praseodymium samples of RT<sub>2</sub>Ge<sub>2</sub> family. Namely PrNi<sub>2</sub>Ge<sub>2</sub>, PrRh<sub>2</sub>Ge<sub>2</sub>, samples were investigated. This project is a continuation of our previous studies (PHY-03-670).

In case of praseodymium-based compounds the CF ground state is formed by intrinsically non-magnetic singlet. However, if magnetic interactions are of the order of splitting between ground and first excited CF level the long-range magnetic ordering may occur.

The experiment was performed using two wavelengths: 2.15 and 3.20 Å in order to get better insight into low-energetically excitations, which are crucial for magnetic properties of those compounds. Measurements done below the ordering temperature of the Pr lattices of 25 K (T=Ni) and 50 K (T = Rh) gave us some information of the influence of the molecular field on crystal field levels splitting scheme. This information is very important for understanding a role of the ground state for establishing of magnetic ordering. On the other hand, measurements done above the ordering temperature let us to determine the overall crystal field levels splitting scheme and corresponding values of the crystal field parameters.

In Fig. 1 INS spectra of PrNi<sub>2</sub>Ge<sub>2</sub> are presented. It is clearly noticeable that at energy loss part of the spectra there is an asymmetry. This can be connected to the structure of the lowest lying crystal field levels. A significant change when comparing spectra recorded at 3 K and 50 K is related to molecular field effects. Please note that ordering temperature of this compound is about 25 K.

Similar behaviour was evidenced for PrRh<sub>2</sub>Ge<sub>2</sub>. Therefore, a significant influence of magnetic ordering on crystal field levels splitting was confirmed.

Upon rising the temperature some features arises on the energy gain side of spectra. This is related to deexcitation of the thermally populated higher crystal field levels.

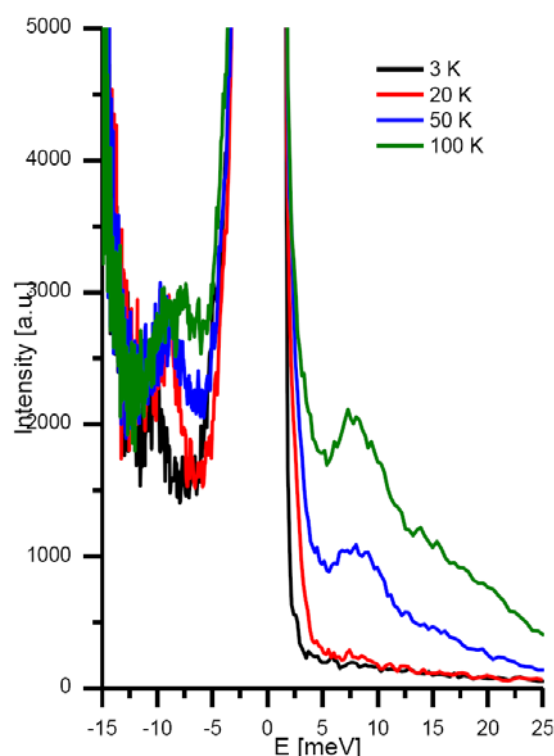



Fig. 1 INS raw data for PrNi<sub>2</sub>Ge<sub>2</sub> (2.15 Å).

*This research project has been supported by the European Commission under the 7<sup>th</sup> Framework Programme through "Research Infrastructures" action of the "Capacities" Programme, contract number CP-CSA\_INFRA-2008-1.1.1. Number 226507-NMI3.*

 <b>NEUTRONS</b>	<b>EXPERIMENTAL REPORT</b>	Proposal: PHY-03-717
	<b>Changes of crystal field upon deuteration of RPdIn compounds</b>	Instrument: <b>V3</b> Local Contact: N. Tsapatsaris
Principal Proposer: Experimental Team:	L. Gondek, AGH-UST, Krakow, PL L. Gondek, AGH-UST, Krakow, PL J. Czub, AGH-UST, Krakow, PL N. Tsapatsaris, HZB	Date(s) of Experiment  16.08.2010 -23.08.2010

Date of report: 14.01.2011

The proposed experiment was a continuation of PHY-03-589 and PHY-03-552 projects concerning investigation of the crystal field (CEF) levels splitting in RPdIn (R = Ce, Pr, Nd) compounds [1]. The performed experiment aimed at determining of the changes of the crystal field levels schemes upon introducing deuterium into the crystal structure of CePdIn, PrPdIn and NdPdIn compounds.

Influence of the hydrogen on magnetic properties of rare-earth intermetallics is well established. Surprisingly enough no studies on crystal field change upon hydrogenation of RPdIn compounds were reported.

The changes of the crystal field parameters are of a twofold nature. It seems that primary role is being played by a geometrical change of the rare earth ions surroundings due to expansion of the lattice constants. On the other hand, an introducing hydrogen nuclei into a crystal lattice changes significantly electric charge distribution. The latter must be considered as well, as the crystal field parameters are dependent on charge of ligands.

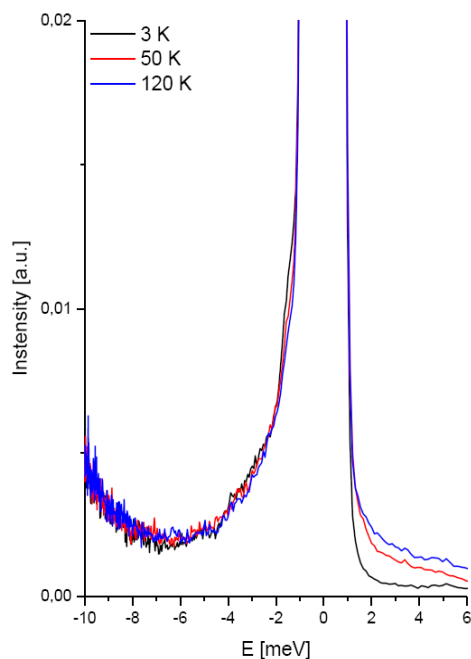


Fig. 1 INS spectra for PrPdInD (2.5Å).

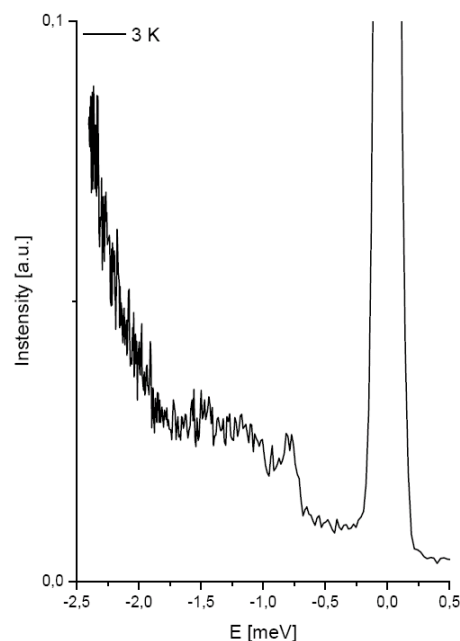


Fig. 2 INS spectra for PrPdInD (5.2 Å)


In Figs. 1 and 2 INS spectra collected for RPdInD sample with different wavelengths of incident neutrons are shown. As apparent from Fig. 2 a low energy excitation at about 0.75 meV is visible. This may be related to transition between the ground and first excited crystal field state. This value is significantly lower than for RPdIn sample (1.2 meV) [1]. Similar results were collected for NdPdInD compound, where some noticeable changes upon hydriding were evidenced as well.

[1] L. Gondek, J. Czub, A. Szytuła, Z. Izaola, E. Kenner, Sol. State. Commun. 140 (2009) 1596

*This research project has been supported by the European Commission under the 7<sup>th</sup> Framework Programme through "Research Infrastructures" action of the "Capacities" Programme, contract number CP-CSA\_INFRA-2008-1.1.1. Number 226507-NMI3.*

# **Biology & Soft Matter**



	<b>EXPERIMENTAL REPORT</b>	Proposal: BIO-01-2661
	<b>Molecular actions of arginine, glucose and arginine-glucose MRP on DMPC bilayer</b>	Instrument: V1 Local Contact: Thomas Hauß
Principal Proposer: Experimental Team:	Jeremy Bradshaw, University of Edinburgh, UK Lijing Ke, The University of Edinburgh, UK Farid Sa'adedin, The University of Edinburgh, UK Thomas Hauß, HZB, Germany	Date(s) of Experiment 14.09.2009-28.09.2009

Date of report: 01.04.2010

As an alkaline amino acid and abundant components in antiviral herb *radix Isatidis*, arginine is an active reactant in the Maillard reaction. MRPs of arginine and glucose was prepared to mimic MRPs derived from the plant. We therefore wish to continue our study of TCM ingredients by collecting lamellar neutron diffraction data from arginine, glucose and arginine-glucose MRPs. Both components are readily available in deuterated forms.

In previous neutron diffraction studies, the distributions of three TCM components have been studied on stacked bilayers of dioleoyl-phosphatidylcholine (DOPC). In this study, we measured lamellar diffraction data on V1 from stacks of DMPC bilayers containing different concentrations of deuterated and non-deuterated Arg-Glc MRPs, arginine and glucose. Three different relative humidities were used at 8%  $^2\text{H}_2\text{O}$  (the isotopic composition at which water is 'invisible' to neutrons) and one relative humidity at 25%  $^2\text{H}_2\text{O}$ . These data would help to locate the different components relative to the membrane and would reveal any disruption of the membrane (bilayer thinning, water penetration etc.) brought about binding. The differences in the distribution of arginine, glucose and Arg-Glc MRPs were identified.

The neutron diffraction patterns of subjects were achieved by subtracting from that of pure DMPC. Data analysis is continuing, but the primary findings are that distributions of Arg-Glc MRPs on DMPC bilayer are very similar to those on DOPC bilayer, which reflects a truth that the two lipids share the same headgroup. Arginine and glucose distribute across the hydrophilic region of bilayer, from *N*-methyls, the phosphate, to the ester carbonyls. They might account for part of the scattering intensity of Arg-Glc MRPs at hydrophilic backbone and headgroup of lipid bilayer. But none of them penetrated into the hydrophobic hydrocarbon chains of lipids, which is in agreement with the fact that arginine and glucose are both hydrophilic reagents. Arg-Glc MRPs penetrated to

the hydrophobic core of bilayer and expanded the *d*-repeat of DMPC bilayers slightly. The water distribution on DMPC bilayers containing these components finely supports the observation above.

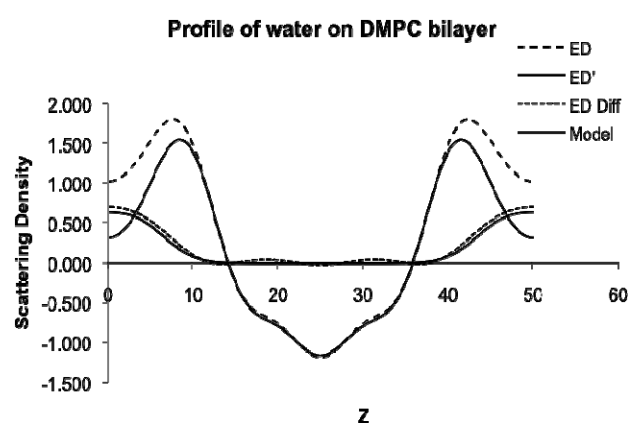


Figure 1. Water distribution across DMPC bilayers

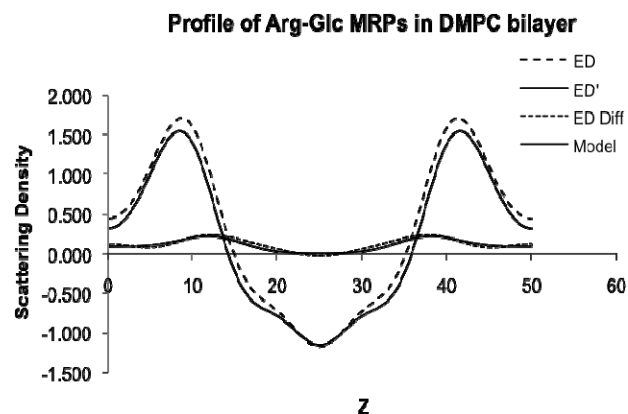


Figure 2. Distribution of Arg-Glc MRPs across DMPC bilayers

*This research project has been supported by the European Commission under the 6<sup>th</sup> Framework Programme through the Key Action: Strengthening the European Research Infrastructures.*

*Contract n°: RII3-CT-2003-505925 (NMI 3).*

 <b>HELMHOLTZ ZENTRUM BERLIN</b> für Materialien und Energie  <b>NEUTRONS</b>	<b>EXPERIMENTAL REPORT</b>  <b>Membrane disruption by NK-2</b>	Proposal: BIO-01-2799  Instrument: <b>V1</b>  Local Contact: Thomas Hauß
	Principal Proposer: Regine Willumeit, GKSS Geesthacht Experimental Team: Angieszka Rzeszutek, GKSS Geesthacht Maksym Golub, GKSS Geesthacht	Date(s) of Experiment  14.06.2010 – 04.07.2010

Date of report: 16.12.2010

The aim of this project was to clarify the position of the antimicrobial peptide NK-2 with respect to POPE and POPG model membranes. It should give the missing link to the full understanding of the mode of action between the peptide and its target membrane.

NK-2 is a selective and active antimicrobial peptide which shows significant membrane activity. Those peptides are relatively small and build up by 20 - 30 amino acid residues. Usually they are amphipatic molecules. Contrary to classical antibiotics which effect is based upon the interaction with bacterial enzymes, peptide antibiotics destroy the bacterial membrane purely by physical interaction. Enzymes are not needed in this case. This physical mechanism of destruction makes peptide antibiotics especially interesting for drug design.

To obtain information about the depth of penetration of the amino acid chain into the model membranes isotopically labelled peptide (deuterated leucine at position 3 and 23) was studied by neutron diffraction. The peptides NK2-[L3D] and NK2-[L23D] (concentration 50:1 lipid:peptide ratio) were measured in interaction with the lipids POPE or POPG by contrast variation (three contrasts: 8, 20 and 50% D<sub>2</sub>O). The experiment was performed under 98% relative humidity during the measurements. As reference only the lipids and the lipids with protonated peptide were measured. The expected small differences in intensities between the labelled and unlabelled samples was measured with small statistical error.

According to the standard procedure of data analysis on V1 scattering length density (SLD) profiles were calculated from 5 peaks of diffraction intensities.

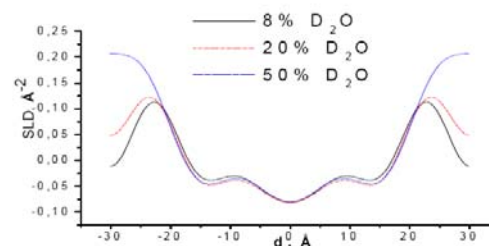


Fig. 1 Example of the SLD profiles of POPE lipids with protonated NK-2 peptide at three contrasts.

The comparison of the SLD profiles of the labelled and unlabelled peptide gives the possibility to clarify the position of deuterated amino acids. The first preliminary result shows that the amino acid leucine at the position 3 can intercalate into the membrane by approximately 10 Å. This can explain why the peptide strongly induces the formation of an inverse hexagonal structure as observed by SAXS [1]

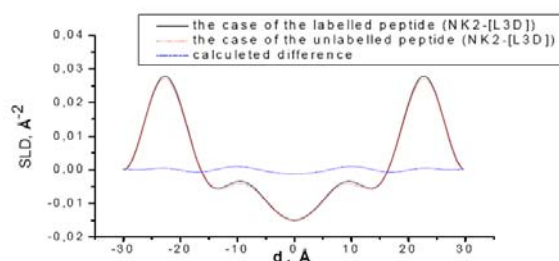



Fig. 2 SLD profiles of POPE lipids with NK2-[L3D] (labelled and unlabelled) at 8% D<sub>2</sub>O with calculated difference between the profiles.

Reference:

- 1) Willumeit, R., Kumpugdee, M., Funari, S.S (2005) Structural Rearrangement as Reason for Bacterial Membrane Destruction by the Peptide Antibiotic NK-2. BBA 1669, 125-134.

 <b>EXPERIMENTAL REPORT</b>		Proposal: BIO-01-2801
<b>Investigation of the effects of penetration enhancers on the lipid assembly in stratum corneum lipid model membranes</b>		Instrument: <b>V1</b>
		Local Contact: A. Buchsteiner, T. Hauß
Principal Proposer:	T. Engelbrecht, MLU Halle/Saale	Date(s) of Experiment
Experimental Team:	B. Dobner, MLU Halle/Saale R. Neubert, MLU Halle/Saale A. Buchsteiner, HZB T. Hauß, HZB	03.05.2010 – 16.05.2010

Date of report: 05.01.2011

The unique lamellar lipid matrix of the stratum corneum (SC) is known to represent the main protecting barrier of the mammalian skin, preventing uncontrolled water loss as well as penetration of substances, for example drugs. For topical drug administration it is therefore necessary to overcome that barrier.

*Penetration enhancers* are known to improve the skin penetration of several substances. To learn more about their mode of action, the present study aimed at the characterization of the influence of lipophilic penetration enhancers like *oleic acid* (OA) and *isopropyl myristate* (IPM, a wax) on the bilayer structure of highly oriented multilamellar SC model membranes. For exact localization of the enhancer molecules inside the bilayers of the studied SC models, we added specifically deuterated oleic acid molecules (OA-9,10-*d*2, see Fig. 1) to the SC lipids.

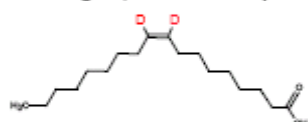


Fig. 1:  
Chemical structure  
of OA-9,10-*d*2

The sample compositions used are displayed in Table 1.

Basic composition: CER[AP]/CHOL/PA/ChS 55/25/15/5 m/m		
Sample 1	Sample 2	Sample 3
+10% OA(m/m)	+10% OA- <i>d</i> 2(m/m)	Basic comp.

Table 1: Presentation of the sample composition

For both samples a one-phase system was detected, the calculated *d*-spacings are in the same range:  $44.6 \pm 0.03 \text{ \AA}$  for sample 1 and  $44.4 \pm 0.08 \text{ \AA}$  for sample 2. No phase separations were found. Comparison with the *d*-spacing of the basic system (sample 3) without OA revealed only a slight difference

which is within the experimental error ( $d=44.7 \pm 0.03 \text{ \AA}$ ).

Benefitting from the possibility to distinguish between hydrogen and its isotope deuterium, we could evaluate the exact position of the deuterium labels represented by the deuterium density distribution function. That allowed us to localize the oleic acid molecules inside the membrane bilayers (see Fig. 2). For that purpose, the neutron scattering length density (SLD) profiles  $\rho_s(x)$  were calculated for both the "non-deuterated" sample 1 (red) and the "deuterated" sample 2 (blue). The difference profile calculated according to:

$$\rho_s(x)_{DEUT} - \rho_s(x)_{PROT}$$

(black dot-dash) and the concluded position of OA-9,10-*d*2 are presented in Fig. 2:

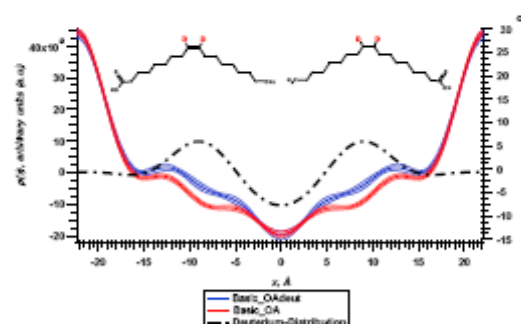



Fig. 2: Presentation of the results of the experiment

Our findings indicate a complete incorporation of the enhancer molecules into the multilayers of oriented SC lipid model membranes and provide new knowledge about the impact of penetration enhancers on the SC barrier.



 <b>EXPERIMENTAL REPORT</b>		Proposal: BIO-01-2904
<b>Effects of oleic acid on the lipid assembly in stratum corneum lipid model membranes based on asymmetric ceramides</b>		Instrument: <b>V1</b>
		Local Contact: A. Buchsteiner, T. Hauß
Principal Proposer:	T. Engelbrecht, MLU Halle	Date(s) of Experiment  20.09.2010 - 02.10.2010
Experimental Team:	B. Dobner, MLU Halle R. Neubert, MLU Halle W. Buchsteiner, HZB Th. Hauß, HZB	

Date of report: 06.01.2011

Stratum corneum (SC) lipid model membranes have been shown to be an appropriate approach for structural investigation of the assembly of the SC lipids by means of neutron diffraction. The results can provide new insights into the lamellar organization of the skin barrier, the SC.

In our former experiment BIO-01-2801, we started to evaluate the influence of lipophilic penetration enhancers on the SC lipid bilayers of oriented model membranes. The results indicated a complete incorporation of *oleic acid* (OA, a lipophilic penetration enhancer) into the model membrane multilayers, no phase separation was detectable. In the present study we focused on further elucidation of OA-containing SC model membranes. We chose a ternary model system based on “asymmetric” ceramide (CER) species comprising a different alkyl chain length of amide-bound fatty acid and sphingosine base, like CER[NP]-C24. It features a C24 fatty acid amide-bound to a C18 phytosphingosine base; the chemical structure is presented in Fig. 1.

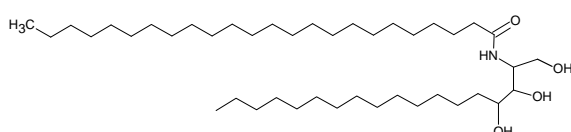


Fig. 1: chemical structure of CER[NP]-C24.

The samples investigated in BIO-01-2904 and their compositions are displayed in Table 1:

CER[NP]-C24, cholesterol, tetracosanoic acid (equimolar ratio)			
Sa. 1	Sa. 2	Sa. 3	Sa. 4
+ 10% OA	+ 10% OA-9,10-d2	+15% OA	+ 15% OA-9,10-d2

Table 1: compositions of the samples studied in BIO-01-2904 (OA ratio given as m/m).

Fig. 2 shows the neutron diffraction patterns recorded for the samples 1, 2 and 4. The following results can be taken from Fig. 2:

- i. Detection of higher diffraction orders  $h$  (1-6) suggests the formation of quite well ordered multilamellar systems.
- ii. Phase separations are visible.
- iii. For the case of sample 4 comprising a higher amount of OA (15 % m/m), an additional lamellar phase (black arrows) appears.

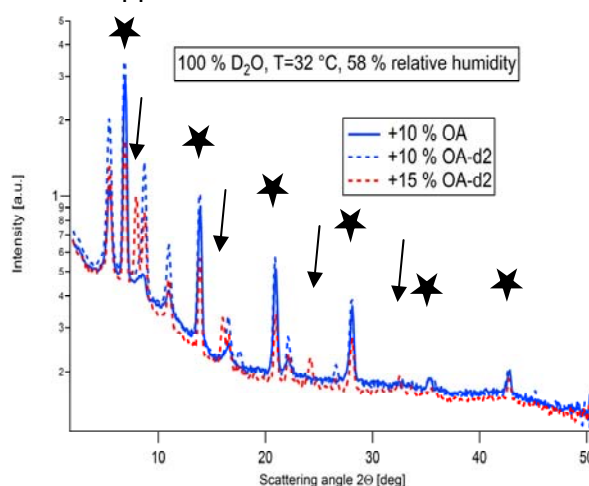



Fig. 2: diffraction patterns recorded for sample 1 (blue solid), sample 2 (blue dashed) and sample 4 (red dashed). Measurement parameters are added.

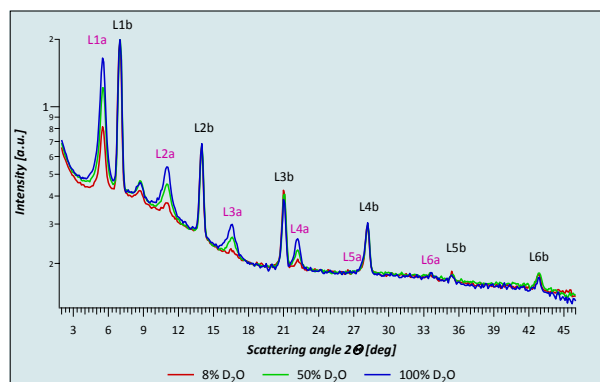
First results obtained by Fourier Transformation show that the lamellar phase assigned with the asterisk (★) shows almost no intensity change during  $D_2O$  contrast variation. We conclude that phase to be very dense, rigid and poorly hydrated. Therefore the determination of the signs of the structure factors will be sophisticated. For the second phase, contrast variation for phasing is suitable, therefore the neutron scattering length density profiles  $\rho_s(x)$  will reveal whether the D-label is located in that phase. The newly arising phase (arrows) could maybe formed by OA which extracts other bilayer components to form a new phase. The four diffraction orders detectable allow for calculation of  $\rho_s(x)$  to reveal the presence of **OA-9,10-d2**. That fact is to be evaluated, work is in progress.

 <b>NEUTRONS</b>	<b>EXPERIMENTAL REPORT</b>	Proposal: BIO-01-2905
	<b>Molecular Structure of the Stratum corneum Lipid Membrane: A New Theoretical Model for the Lipid matrix</b>	Instrument: <b>V1</b> Local Contact: Thomas Hauß
Principal Proposer: Experimental Team:	Annett Schröter, MLU Halle-Wittenberg Annett Schröter, MLU Halle-Wittenberg T. Engelbrecht, MLU Halle-Wittenberg R.H.H. Neubert, MLU Halle-Wittenberg Thomas Hauß, HZB	Date(s) of Experiment  02.08.2010 – 08.08.2010

Date of report: 17.01.2011

Recently, a new model concerning the structural assembly of the Stratum corneum (SC) lipid matrix was presented by Norlén, the so-called “Asymmetry model” [1]. This model is based on the assumption that the short-chain ceramides (CER) such as CER[NP], CER[AP] are present in the fully extended conformation, whereby the chains of the CER molecules are directed in opposite directions (see right side). The CER molecules thereby create alternating bilayers with a repeating unit of 4.5 nm and 6.5 nm, respectively.

On the basis of the Asymmetry model neutron diffraction experiments have been carried out on a simplified SC lipid model membrane composed of the asymmetric CER[NP] with tetracosanoic acid bound to the phytosphingosine backbone (CER[NP]-C24), cholesterol (CHOL) and tetracosanoic acid (TA) in an equimolar ratio.

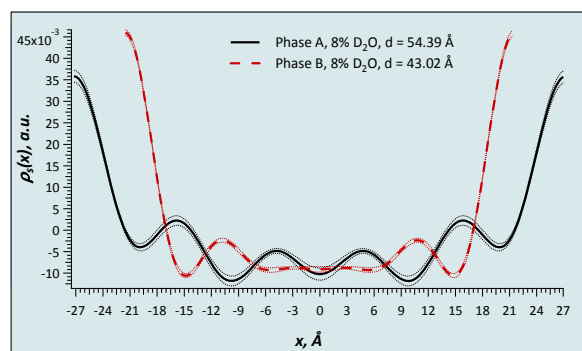


**Fig. 1** Neutron diffraction pattern of the SC lipid mixture. The measurements were carried out at 58% RH, 32°C and 8, 50 and 100% D<sub>2</sub>O, respectively.

The diffraction pattern revealed a two phase system (see Fig. 1). Phase A displayed a membrane thickness of  $(54.4 \pm 0.1)$  Å, while for phase B a repeat distance of  $(43.0 \pm 0.05)$  Å was evaluated.

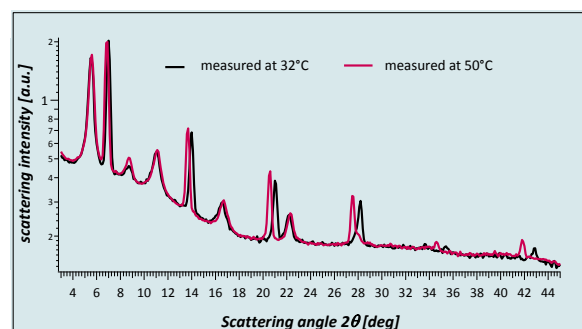
The presence of two lamellar phases indicates that asymmetric CER[NP]-C24 exhibits the fully extended or splayed conformation as proposed by Norlén [1].

The calculation of neutron scattering length density (NSLD) profiles revealed only slight differences in the centre of the membrane. Phase B shows a less pronounced minimum in the centre of the membrane, which indicates that the lipids are partly interdigitated in this phase (see Fig. 2).



**Fig. 2** Comparison of the NSLD profiles of the two phases measured at 32°C, 58% RH and 8% D<sub>2</sub>O.


The increase of the temperature to 50°C caused an interesting effect: while phase A displayed no change in the membrane repeat distance upon temperature increase, a slight *increase* in the membrane thickness of  $\Delta d = 1.1$  Å to 44.1 Å was observed for phase B (see Fig. 3). This is atypical for lipid membranes, as normally a decrease is observed due to partial chain melting of the lipids at higher temperature and with the resulting increase in membrane disorder.



**Fig. 3** Comparison of the diffraction pattern of the SC lipid membrane measured first at 32°C (black) and afterwards heated to 50°C (red). Both experiments were carried out at 58% RH and 100% D<sub>2</sub>O.

#### References:

- [1] Norlén. 2010, unpublished results, personal communication

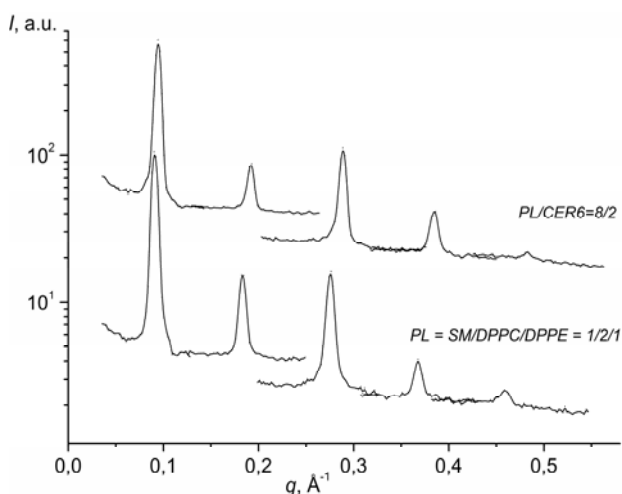
 <b>EXPERIMENTAL REPORT</b>		Proposal: BIO-01-2908
<b>Structure of the model oral epithelial membranes based on ceramide-6</b>		Instrument: <b>V1</b>
Principal Proposer: N. Ryabova, JINR, Dubna, Russia Experimental Team: S. Sheverev, JINR, Dubna, Russia A. Buchsteiner, HZB T. Hauß, HZB		Local Contact: Alexandra Buchsteiner
		Date(s) of Experiment 26.08.2010 – 05.09.2010

Date of report: 25.01.2011

The epithelium covering the oral cavity (*oral stratum corneum*, OSC) provides a protective barrier for underlying tissue, but it is not so distinct like in the case of the epidermal *stratum corneum* (ESC). The OSC lipid matrix consists mainly of the phospholipids (PL), cholesterol (Ch), fatty acids (FA), cholesterol sulphate (ChS), triglycerides and short-chain ceramides (CER). Although the lipid composition of the OSC is well defined the physical studies of the nanostructure of rare OSC-lipid bilayers are lacking [1] and their role in formation of the barrier function is still unclear.

The oriented model phospholipids membrane PL=SM<sub>bovine brain</sub>/DPPC/DPPE, PL-membrane with ceramide-6 (CER6) PL/CER6, and the multicomponent membrane CER6/Ch/FA/ChS/PL, simulated a native OSC-lipid matrix, have been measured at 20°C, 58% RH and 37°C, 98% RH (close to physiological conditions of the oral epithelium).

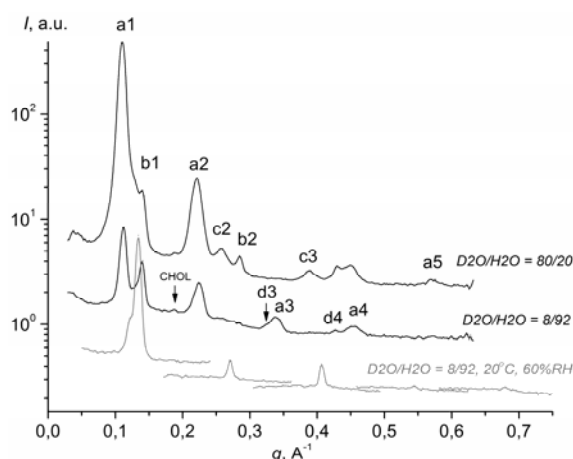
Figure 1 demonstrates the spectra from a one-lamellar phase system of the PL and PL/CER6 mixtures. CER6 at 20 mol% decreases the lamellar repeat distance  $d$  and the bilayer thickness  $d_B$  in comparison with the pure PL-membrane at the same conditions (see Table 1). This result about CER6 influence on the bilayer thickness is opposite to the previously obtained results for the DPPC/CER6 binary mixtures [2].



**Fig. 1:** Neutron diffraction patterns of the PL and PL/CER6 membranes at contrast  $D_2O/H_2O$  of 8/92, 37°C and 98% RH.

**Table 1:** Structure parameters of the partly hydrated PL-membranes.

	$d \pm \Delta d$ [Å]	$d_B \pm \Delta d_B$ [Å]	$d_W \pm \Delta d_W$ [Å]
<u>PL = SM/DPPC/DPPE = 1/2/1</u>			
20°C, 58%RH	$62.63 \pm 0.05$	$53.80 \pm 0.08$	$8.83 \pm 0.10$
37°C, 98%RH	$69.0 \pm 1.1$	$56.4 \pm 0.6$	$12.6 \pm 1.3$
<u>PL/CER6 = 8/2</u>			
20°C, 58%RH	$60.77 \pm 0.04$	$52.91 \pm 0.10$	$7.86 \pm 0.09$
37°C, 98%RH	$65.1 \pm 0.3$	$54.3 \pm 0.2$	$10.9 \pm 0.4$




**Fig. 2:** Diffraction patterns of the membrane CER6/Chol/FFA/ChS/PL = 28/23/15/8/26 (w/w) at 20°C, 58% RH,  $D_2O/H_2O$  = 8/92 (gray line) and at 37°C, 98% RH,  $D_2O/H_2O$  = 8/92, and 80/20 (black lines). Numbers indicate the diffraction orders for different phases.

Several structure phases coexist in the membrane CER6/Chol/FFA/ChS/PL (Fig. 2). The main phase "a" ( $d_{98\%RH} \sim 55$  Å) and the phase "d" ( $d_{98\%RH} \sim 58$  Å) are likely phospholipids-enriched phases. The structure of the low swelling phase "b" ( $d_{58\%RH} \sim 44$  Å,  $d_{98\%RH} \sim 46$  Å) at 58% RH is similar to that of the ESC-model membrane [3].

*This research project has been supported by JINR-grant for young scientists (2010). The financial support from HZB is gratefully acknowledged.*

#### References:

- [1]. P.W. Werzt, B. van den Bergh. Chemistry and Physics of Lipids 91 (1998) 85-96.
- [2]. M. Kiselev et al. BENS experimental reports 2006. P. 119.
- [3]. M. Kiselev et al. Eur. Biophys. J. 34 (2005) 1030-1040.

 <b>HELMHOLTZ ZENTRUM BERLIN</b> für Materialien und Energie  <b>NEUTRONS</b>	<b>EXPERIMENTAL REPORT</b>	Proposal: BIO-03-715
	<b>Does specific protein mutation affect the myelin membrane dynamics?</b>	Instrument: <b>V3</b> Local Contact: M. Russina
Principal Proposer: J. Peters, ILL Grenoble, F Experimental Team: W. Knoll, ILL Grenoble, F N. Tsapatsaris, HZB	Date(s) of Experiment 25.09.2010 – 02.10.2010	

Date of report: 19.01.2011

The project deals with myelin, a multi lamellar tightly packed membrane surrounding selected nerve axons in the vertebrate central (CNS) and peripheral nervous systems (PNS), which is essential for the proper functioning of the vertebral nervous system. Myelin is destroyed by autoimmune diseases, such as multiple sclerosis (MS), which affects the CNS, and the Guillain-Barré syndrome, which acts on the PNS. In addition, inherited neuropathies are linked to mutations involving myelin molecules. Biochemically, the main components of myelin are lipids (75-80%) and proteins (20-25%) [1]. Although the subset of the myelin-specific proteins is well defined [2], relatively little is known about their influence on the membrane dynamics, *i.e.* myelin stability. Myelin basic protein (MBP) is the second-most abundant protein of the myelin sheath [3]. It represents 35% of total myelin protein in the CNS [1] and exists *in vivo* as a series of charge isomers (MBP-C1 to MBP-C8) [4]. While C1 is the least modified form and corresponds to the wild type protein, C8 mimics the form seen, for example, in MS [5].

The experiments were performed on NEAT from September 25th to October 2nd 2010. The purpose was to investigate the role of the protein mutant MBP-C8 on the membrane dynamics to better understand the structure and dynamics of healthy and disease-affected myelin.

Due to difficulties during the sample preparation of the membrane with proteins, the planning was changed. Membranes without proteins, but with protein-buffer were prepared to determine if the required protein-buffer (essential for the survival of the proteins) influences the membrane dynamics. This information is also needed for the experiment BIO-03-669 performed on NEAT in December 2009 on reconstituted membranes made of mixed DOPS+DOPC lipids with and without MBP-C1 as well as with the myelin protein P2.

Neutron scattering experiments on artificial membranes made of DOPS+DOPC lipids with and protein-buffer (HEPES) were carried out on NEAT. The energy resolution was 220 $\mu$ eV and the wavelength 5.1Å. The following deuterated membranes spread on silica wafers were investigated:

- 1) 100mg DOPS + DOPC (1:1 ratio)
- 2) 100mg DOPS + DOPC (1:1 ratio) + 1.88mg HEPES-buffer (amount in the last samples measured on NEAT)
- 3) 50mg DOPS + DOPC (1:1 ratio) + 1.88mg HEPES-buffer (double amount in the last samples measured on NEAT)

The samples were measured at 230K and 300K (below and above the phase transition temperature of the lipids) oriented at 45 and 135 degrees with respect to the incoming beam.

At both temperatures (see figure 1) there is no difference visible between the different samples. Thus we can conclude that the protein-buffer does not influence the dynamics of the membrane.

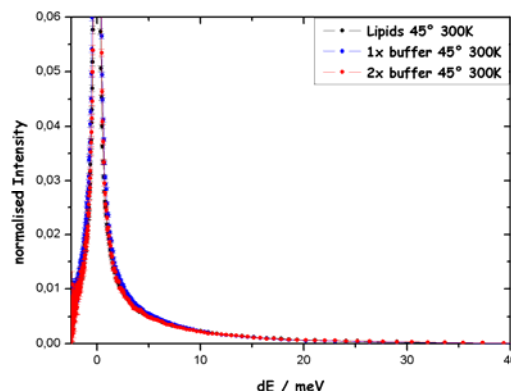



Figure 1: Quasielastic spectra of all samples integrated over the whole accessible Q-range and normalised to vanadium at 300K. The samples were oriented at 45 degrees with respect to the incoming beam. There is no difference between the lipids in presence or absence of the buffer both for a 45-degree-orientation and a 135-degree-orientation.

#### References

- [1] Brady, et al., 1981, Biophys. J. 34, 345-350.
- [2] Greenfield, et al., 1973, J. Neurochem. 20(4): 1207-1216.
- [3] Bates, et al., 2000, Protein Expression and Purification 20, 285-299.
- [4] Moscarello, et al., 1994, J. Clin. Invest. 94, 146-154.
- [5] Beniac, et al., 1999, Mol. Cell. Biol. Res. Commun. 1 : 48-51.

#### Acknowledgement:

This research project has been supported by the European Commission under the 7<sup>th</sup> Framework Programme through "Research Infrastructures" action of the "Capacities" Programme, contract number CP-CSA\_INFRA-2008-1.1.1. Number 226507-NMI

 <b>NEUTRONS</b>	<b>EXPERIMENTAL REPORT</b>	Proposal: CHE-04-1555 Instrument: <b>V4</b> Local Contact: Uwe Keiderling
	<b>SANS study of temperature-stable colloidal structures in mixtures of Ionic Liquids</b>	Date(s) of Experiment 21.06.2010 -24.06.2010
Principal Proposer: Experimental Team:	Oliver Zech, Uni Regensburg Agnes Harrar, Uni Regensburg Doris Rengstl, Uni Regensburg Uwe Keiderling, HZB	

Date of report: 04.01.2011

In this study we focused on the surfactant behaviour of a long-chain imidazolium-based ionic liquid (IL)  $[C_{16}mim][Cl]$  exhibiting amphiphilic properties in the IL ethylammonium nitrate (EAN) as solvent. Recently, we demonstrated that surfactant-like ILs (SLILs) can form colloidal structures in room temperature ionic liquids that act as solvent.<sup>1</sup>

Prior SAXS experiments at 150 °C obtained at the MPI Golm proved that colloidal structures are present not exclusively at ambient temperature but also at elevated temperatures well above 100 °C. However, the results indicated that neutron scattering might be the more suited method for investigations on the present system.

First SANS experiments (Proposal CHE-04-1462) were performed at ambient temperature in order to receive detailed information about the nature of the colloidal structures present. The experiments carried out in the framework of proposal CHE-04-1555 represent a continuation of the previous study. The aggregation behaviour of the most auspicious SLIL  $[C_{16}mim][Cl]$  was investigated as a function of temperature and surfactant concentration.

Solutions of  $[C_{16}mim][Cl]$  in EAN with different concentrations (4 wt% surfactant IL, 6 wt% surfactant IL, 8 wt% surfactant IL, 12 wt% surfactant IL) were measured at four temperatures (50 °C, 75 °C, 100 °C, and 150 °C).

The obtained scattering patterns are depicted for 8 wt%, 10 wt%, and 12 wt% surfactant in Figure 1, Figure 2, and Figure 3, respectively. Several observations can be made so far: colloidal structures seem indeed to be present up to at least 150 °C; with increasing surfactant concentration as well as with decreasing temperature the correlation peak is more pronounced. Data evaluation will start in the near future.

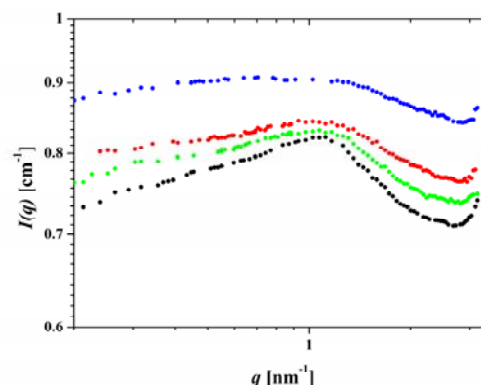


Figure 1: Scattering pattern for a solution of 8 wt%  $[C_{16}mim][Cl]$  in EAN. Green: 150 °C, red: 100 °C, blue: 75 °C, black: 50 °C.

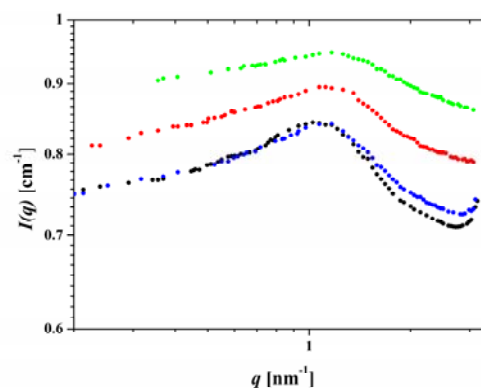


Figure 2: Scattering pattern for a solution of 10 wt%  $[C_{16}mim][Cl]$  in EAN. Green: 150 °C, red: 100 °C, blue: 75 °C, black: 50 °C.

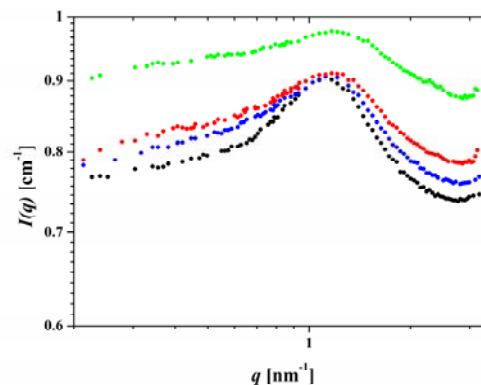



Figure 3: Scattering pattern for a solution of 12 wt%  $[C_{16}mim][Cl]$  in EAN. Green: 150 °C, red: 100 °C, blue: 75 °C, black: 50 °C.

- Thomaier, S.; Kunz, W., Aggregates in mixtures of ionic liquids. *J. Mol. Liq.* **2007**, *130* (1-3), 104-107.

 <b>HELMHOLTZ ZENTRUM BERLIN</b> für Materialien und Energie  <b>NEUTRONS</b>	<b>EXPERIMENTAL REPORT</b>  <b>Protein Interactions in Solution Containing Concentrated Electrolytes Studied by SANS</b>	Proposal: PHY-04-1652  Instrument: <b>V4</b>  Local Contact: Uwe Keiderling
	Principal Proposer: Frank Schreiber, Uni Tübingen Experimental Team: Fajun Zhang, Uni Tübingen Marcell Wolf, Uni Tübingen Andrea Sauter, Uni Tübingen Uwe Keiderling, HZB	Date(s) of Experiment  27.05.2010 – 31.05.2010

Date of report: 14.09.2010

Protein interactions and phase behavior in solution containing concentrated electrolytes are crucial in understanding the mechanism of protein crystallization or the ion specificity [1-3]. For example, salt induced precipitation has been extensively used as an initial step for protein purification. However, protein solubility is not well understood, and selecting the optimum conditions to precipitate a target protein is difficult because the solubility is governed by many factors including pH, surface hydrophobicity, surface charge distribution, salt type and concentration [1-3].

In this beamtime, we have performed SANS measurements on protein interactions in aqueous solutions containing concentrated electrolytes. The aim is to explore the Hofmeister effects on the protein stability in solution in the molecular level. We have performed SANS measurements on a model protein system (ovalbumin from hen egg white) in the presence of concentrated salting-in electrolytes (NaSCN). In Fig.1, we show the preliminary scattering profiles of ovalbumin (OVA) solutions with NaSCN in high concentrations (1.0 and 2.0 M). Due to the strong screening effect of the concentrated salt solutions, the forward intensity can be used to determine the second virial coefficient ( $A_2$ ), which describes the overall interactions in protein solution. We have also measured protein solutions (lysozyme, BLG and OVA) at two temperatures (10 and 20°C) Further data analysis of the effect of the salt type on protein hydration by fitting the full  $Q$  range and determining  $A_2$  will be carried out imminently. Together with model fitting on the whole  $Q$  range, the effective protein interactions under the experimental conditions can be evaluated.

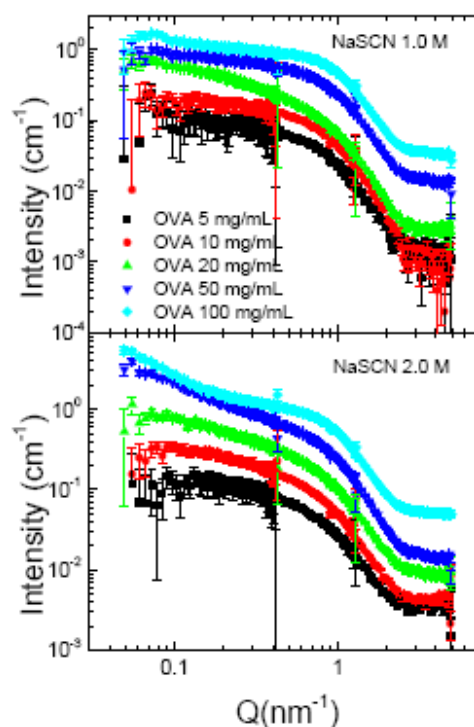


Fig. 1 Example of SANS data from OVA solutions with concentrated NaSCN. The whole  $Q$ -range data were merged from 3 sample-to-detector distance measurements.

[1] Curtis, R. A.; Blanch, H. W.; Prausnitz, J. M. *J. Phys. Chem. B* **2001**, *105*, 2445.

[2] Durbin, S. D.; Feher, G. *Annu. Rev. Phys. Chem.* **1996**, *47*, 171

[3] D. I. Sevrgun et al. *PNAS* **1998**, *95*, 2267.

	<b>EXPERIMENTAL REPORT</b>	Proposal: BIO-04-1835
	<b>Self-assembly and gelation mechanism of ionic complementary peptides</b>	Instrument: <b>V4</b> Local Contact: S. Prevost
Principal Proposer: Experimental Team:	A. Saiani, University of Manchester, UK J.-B. Guilbaud, University of Manchester, UK D. Adams, University of Manchester, UK S. Prevost, HZB	Date(s) of Experiment  31.05.2010 – 03.06.2010

Date of report: 04.06.2010

### Introduction:

Molecular self-assembly is a powerful tool for the preparation of molecular materials with a wide variety of properties. This is illustrated by the abundance of self-assembled proteins and polysaccharides encountered in Nature. Considerable advances have been made in the use of oligo-peptides and nucleic acids as building blocks for the production of novel biomaterials. Peptides are particularly promising as building blocks for a number of reasons. The natural amino acid pool consists of 20 members with different physical properties (polar, non-polar, acid, basic and aromatic), which can be combined in endless different ways leading to a vast number of building blocks with different physical properties. However, the understanding of the molecular interactions and the paradigms that control self assembly in these materials is still limited. The understanding of the self-assembling and gelation phenomena in short peptides is of interest for the creation of new biomaterials with tailored properties as well as for the understanding of protein fibrillogenesis which is known to be at the origin of a number of diseases including Alzheimer and Parkinson.

### Experiments performed:

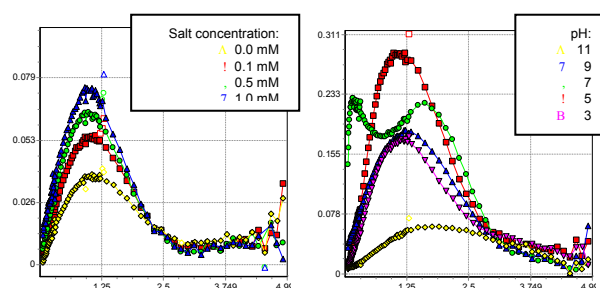
During this experimental session we have investigated via SANS the self assembling of four octapeptides: FEFEFKFK, VEVEVKVK, VKVEVKVK and FEFEFKFG at different concentration and different pH and/or salt content. We also investigated the denaturation and subsequent gelation of  $\beta$ -Lactoglobulin, a small whey protein, at different concentration in the presence of DTT.

Three samples to detector distances were used with a fixed wavelength of 0.455 nm covering a q-range of 0.06 to 4.90 nm<sup>-1</sup>.

### Preliminary analysis:

The normalization and extraction of the data was performed on site using BerSANS with the assistance of the local contact. The scattering profiles obtained for FEFEFKFK at fixed concentration and pH but with increasing salt content all have a similar shape on a Krakty

representation ( $q^2 I(q)$  vs.  $q$ ) and an increase in the scattered intensity with increasing salt concentration is observed indicating a larger degree of self-assembly. The bell shape of the curves is reminiscent rod-like structure in agreement with TEM results. A rod-like model will be used to fit the results allowing the extraction of geometric parameters.



**Fig 1:** Krakty representation of the intensity scattered by FEFEFKFK (10 mg mL<sup>-1</sup>) with increasing salt concentration (left) and by VEVEVKVK (40 mg mL<sup>-1</sup>) at different pH (right).

Variation in scattered intensities and scattering profiles are observed for VEVEVKVK at different pH suggesting changes in the self-assembly. TEM imaging will be undertaken to investigate the morphology of this system and appropriate models will be used to fit the scattering data in order to determine structural parameters. Similar systematic analysis will be performed for the results obtained for the peptides FEFEFKFG and VKVEVKVK.

Finally the experiments on the denaturation of  $\beta$ -Lactoglobulin show interesting results, in particular the presence of structural peaks. A thorough interpretation will be carried out to understand the origin of such feature and relate it to the mechanism of denaturation and gelation process.

### Acknowledgement:

*This research project has been supported by the European Commission under the 7<sup>th</sup> Framework Programme through "Research Infrastructures" action of the "Capacities" Programme, contract number CP-CSA\_INFRA-2008-1.1.1. Number 226507-MI3*

Principal Proposer:  
Experimental Team:

Aristides Bakandritsos, University of Patras, GR  
 Aristides Papagiannopoulos, NHRF, Athens, GR  
 Stergios Pispas, NHRF, Athens, GR  
 Konstadinos Avgoustakis, University of Patras, GR  
 Vasyl Ryukhtin, HZB  
 Theodor Steriotis, NCSR "Demokritos", GR  
 Frank Winnefeld, EMPA, Zurich, CH

Date(s) of Experiment

05.07.2010 – 08.07.2010

Date of report: 24.01.2011

Hybrid hydrophilic colloids based on iron oxide magnetic nanoparticles functionalized with copolymers of methylpoly(ethyleneglycol-methacrylate) and methacrylic acid sodium salt were synthesized and characterized with polarized small angle neutron scattering (SANSPOL). Such colloids will be utilized as carriers for cationic drugs for magnetically targeted therapy. The aim of the SANSPOL experiments was to collect information on their size and internal organization in their dilute suspensions (0.15 % w/v or 0.03 v/v in magnetic material), as well as the effects of drug loading on the above characteristics.

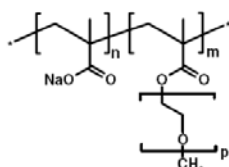


Figure 1. Unit ratio of  $n:m = 6:1$ ; number of EO units in the PEO side chains  $p = 102$ .

The best fitting of the SANSPOL scattering profile of the colloids in neat water (Figure 2) was obtained using a sphere model based on a core and two shells of lower scattering length densities. The core radius was estimated at 4.3 nm, while the first shell has a thickness of 5 nm and the second shell (the outer layer), which is composed of 90 % v/v water, has a thickness of 10 nm. That is, the diameter of the hybrid colloid based on this model is estimated at 38.6 nm. The output from dynamic light scattering (DLS) results was 41 nm hydrodynamic diameter. This value was obtained in two different instruments one in University of Patras (Malvern) and one in NHRF (ALV). SANSPOL and DLS (despite that the measurement was performed in neat  $H_2O$  in the former case) gave practically the same results regarding the particle diameter. The slightly smaller value from SANSPOL should be attributed to the very high water content at the outer parts of the PEO polymer shell.

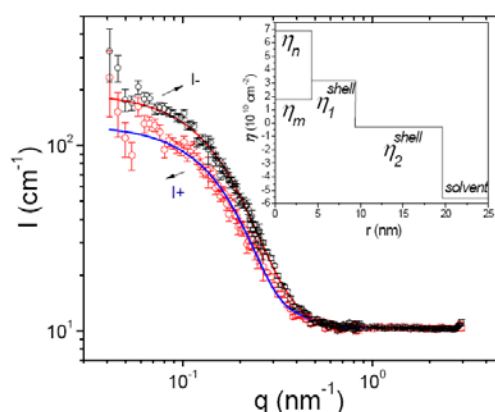


Figure 2. SANSPOL scattering intensity from the hybrid colloids and the best fit (solid line). Inset: scattering length density profile.

Therefore the colloids could be roughly described with the model shown in Figure 3. In addition, the obtained parameters from fitting regarding the SLD of the core ( $\eta = 6.93 \cdot 10^{10} \text{ cm}^{-2}$ ) coincide very well with the theoretical SLD of magnetite. The relatively high SLD of the 5 nm layer ( $\eta = 3.21 \cdot 10^{10} \text{ cm}^{-2}$ ) is attributed to the  $-\text{COONa}$  segments that reside near the surface of the inorganic core. The outer layer of PEO with a very low SLD ( $-2.96 \cdot 10^{10} \text{ cm}^{-2}$ ) is indicative of its high hydration after comparing it to the theoretical value of  $0.64 \cdot 10^{10} \text{ cm}^{-2}$ . Currently, ongoing analysis is focused on evaluating data from drug loaded colloids.

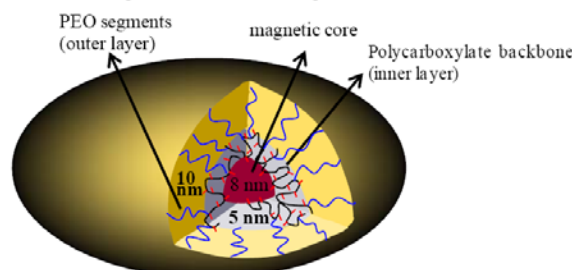



Figure 3. Approximate model describing the structure of the studied colloids based on the SANS fitting results.

*This research project has been partially supported by the European Commission under the 7<sup>th</sup> Framework Programme through "Research Infrastructures" action of the "Capacities" Programme, contract number CP-CSA\_INFRA-2008-1.1.1. Number 226507-NMI3.*



 <b>HELMHOLTZ ZENTRUM BERLIN</b> für Materialien und Energie  <b>NEUTRONS</b>	<b>EXPERIMENTAL REPORT</b>	Proposal: PHY-03-703  Instrument: <b>V5</b>  Local Contact: S. Wellert
	<b>Rotational and translational self-diffusion of benzene molecules on graphite</b>	Date(s) of Experiment  07.05.2010 – 29.05.2010
Principal Proposer: Experimental Team:	Peter Fouquet, ILL, Grenoble, F Irene Calvo-Almazan, ILL, Grenoble, F Stefan Wellert, HZB Beate Bruening, HZB	

Date of report: 31.01.2011

#### Objectives:

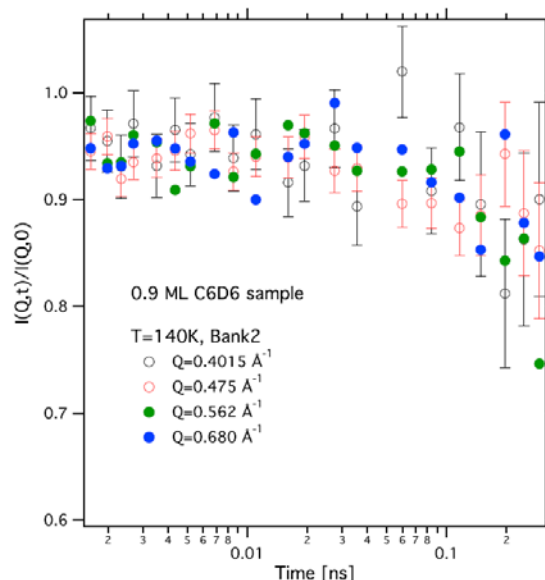
The understanding of molecule diffusion in porous media is crucial for many areas of chemical engineering and science such as separation technology, catalysis, the glass transition and fuel cells. With recent neutron and helium scattering experiments we have made important progress in the analysis of surface diffusion of one of the key model molecules (benzene) on basal plane graphite.

The aim of the proposed experiment was to contribute to a complete microscopic description of the translational and rotational diffusion in this system via neutron spin echo measurements on benzene/graphite in the high  $Q$  range and including incoherent scattering.

#### Experimental Results:


We have measured neutron spin echo (NSE) spectra on V5 (SPAN) from two samples (0.5 monolayer (ML) film of C<sub>6</sub>H<sub>6</sub> and 0.9 ML film of C<sub>6</sub>D<sub>6</sub>, both adsorbed on exfoliated graphite) using two neutron beam wavelengths of 3 Å and 4.5 Å, respectively. The resolution function in all cases was measured at 1.5 K. Dynamics were recorded at 140 K and 200 K, respectively. The high momentum transfer range available with SPAN was exploited by recording spectra in parallel at low angles (long range diffusion) and in the vicinity of the structure factor peak related to the carbon-carbon distances. The 0.5 ML C<sub>6</sub>H<sub>6</sub>-graphite sample (incoherent scattering) did not show evidence for dynamical signal within the - rather large - experimental error bar. We should note that during the entire experiment, we had problems with the stability of the instrument, which was problematic for this particular experiment as counting times were long – in the order of 1-2 days per spectrum. The 0.9 ML C<sub>6</sub>D<sub>6</sub>-graphite sample (coherent scattering) showed indication of dynamics within the expected time range and (for the 4.5 Å beam) also with the expected signal

strength. The number of molecules participating in long-range diffusion increased strongly when heating from 140 to 200 K. The data for the deuterated sample are very promising, but we were not able to finalize the data taking yet as SPAN power supplies failed at the end of the experiment 2 days lost. Exemplary data is shown in the Figure below.



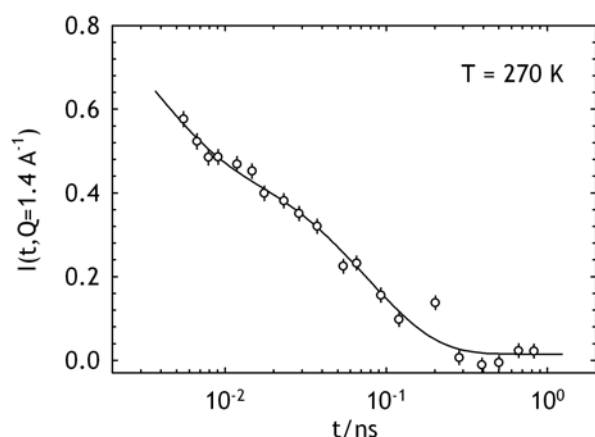
#### Acknowledgement:

*This research project has been supported by the European Commission under the 7<sup>th</sup> Framework Programme through "Research Infrastructures" action of the "Capacities" Programme, contract number CP-CSA\_INFRA-2008-1.1.1. Number 226507-NMI*

 <b>HELMHOLTZ ZENTRUM BERLIN</b> für Materialien und Energie  <b>NEUTRONS</b>	<b>EXPERIMENTAL REPORT</b>  <b>How does supercooled water diffuse?</b>	Proposal: PHY-03-704  Instrument: <b>V5</b>  Local Contact: S. Wellert
	Principal Proposer: G. Schiro, Univ. Palermo (UNIPA), I Experimental Team: M. Cammarata, Stanford University, USA G. Schiro, Univ. Palermo (UNIPA), I A. Cupane, Univ. Palermo (UNIPA), I M. Levantino, Univ. Palermo (UNIPA), I	Date(s) of Experiment  19.03.2010 – 31.03.2010

Date of report: 12.01.2011

Aim of this experiment was to investigate the  $(Q,t)$ -dependence of the intermediate scattering function for water confined in silica hydrogels at different temperatures from 200 K to room temperature. In particular, exploiting the unique  $Q$ -range available at SPAN, we expected to obtain experimental evidence for jump-like translational diffusion of confined water in the supercooled regime, as suggested by our previous neutron scattering data in the energy domain, and to clarify the diffusive character of rotational motions.



**Figure 1.** Intermediate scattering function at  $T=270$  K for the momentum transfer  $Q=1.4 \text{ \AA}^{-1}$  measured in a sample of water confined in the pores of a silica hydrogel.


The measurements have been taken at two different temperatures, 250 K and 270 K. We used the incident wavelength  $\lambda=4.5 \text{ \AA}$  in order to obtain a resolution of 100 neV and to explore a  $Q$ -range of  $0.4 - 3 \text{ \AA}^{-1}$ . Two different configurations of detector banks have been used to obtain the suitable  $Q$ -range. We measured an incoherent contribution of about 85% over the total signal, essentially due to the water hydrogen atoms contained in the silica matrix. This enabled us to assume that we probed the diffusion dynamics of water molecules. An unexpected  $Q$ -dependence of the ratio between incoherent and coherent signals has been observed. This set an upper limit to the explorable  $Q$ -range and calls for further investigations. An

acceptable signal-to-noise ratio has been achieved by acquiring four scans per configuration. This limited the number of different temperatures explored during the beam time with respect to the planned ones.

In Figure 1 we report an example of the intermediate scattering function at  $T=270$  K for the momentum transfer  $Q=1.4 \text{ \AA}^{-1}$ . The data show that a bimodal decay in the correlation function occurs, thus suggesting the presence of two relaxation processes in confined water. A detailed analysis of the collected data and their interpretation is in progress.

#### Acknowledgement:

*This research project has been supported by the European Commission under the 7<sup>th</sup> Framework Programme through "Research Infrastructures" action of the "Capacities" Programme, contract number CP-CSA\_INFRA-2008-1.1.1. Number 226507-NMI*

	<b>EXPERIMENTAL REPORT</b> <b>Effect of cholesterol on the collective bilayer undulations of phospholipid model membranes: Linking curvature and lateral compression modes</b>	Proposal: PHY-03-721-IT Instrument: <b>V5</b> Local Contact: B. Brüning
	Principal Proposer: Peter Falus, ILL, Grenoble, F Experimental Team: Beate Brüning, HZB Ralf Stehle, Uni Bayreuth Catherine Pappas, TU Delft, NL	Date(s) of Experiment 20.09.2010 – 02.10.2010

Date of report: 04.10.2010

The low wavelength wide-angle neutron spin-echo spectrometer SPAN has only recently been incorporated into the newly formed Soft Matter and Functional Materials group at HZB. Therefore, the reported experiment was dedicated to the adaption of the instrument to a new soft matter applications. Today, most soft matter applications require high  $q$ -resolutions particularly in the small-angle regime, as well as the use of the higher wavelengths the instrument was designed for. Therefore, a significant part of the experiment was spent with the tuning of our two presently largest wavelengths of 6.5 Angs. and 8.0 Angs. in the small-angle regime (first of three detector banks).

The higher wavelengths are generally more difficult to tune due to losses in signal intensity (on SPAN on the order of a factor of six compared to peak intensity). In comparison to previous tuning attempts, we worked with a new configuration of Fresnel coils at the incoming beam and on the detector banks. These coils are corrective elements in the spin-echo setup, which compensate for inhomogeneities in the magnetic field integral. The previous setup consisted of three Fresnel coils in each of the respective detector banks, of which two are now merged in a manner, such that the effect of the Fresnel coil on the incoming and outgoing side of the beam is mirrored. In order to gain optimum signal intensity, the two coils on the small-angle detector bank were fine-tuned with respect to each other by using a combinatory algorithm.

Apart from the adaption of Fresnel coils, the first detector bank was mechanically height adjusted. The combined path height of incoming and outgoing beam was adjusted through a correction field. Additionally, the main field compensation coils were fine-tuned, shifters, which allow further separate height adjustment of incoming and outgoing beam were built in and adjusted.


Further, a newly designed soft matter sample environment was tested. In this environment, a centrosymmetric liquid sample cell suited to cover the broad angular range available on the instrument is inserted into a set of water flooded temperature blocks connected to a Julabo bath. The whole environment is sealed with an aluminium lid, and can easily be adapted to include other sample cells, or simultaneous humidity control with salt solutions. In the future, the control of the water bath will be implemented into the instrument steering software, in order to ensure a higher user friendliness and synchronicity with the experiment.

First test measurements were then taken on different soft matter samples at both wavelengths, including uni-lamellar phospholipid vesicles (ULV's), as well as microemulsions. For the lipid vesicles, a dominant D<sub>2</sub>O background contribution was observed at 6.5 Angs. At the higher wavelength of 8 Angs. a separation of the two dynamic contributions was more feasible. The results can be compared with the ones recently obtained in overlapping  $(q,t)$ -ranges on the long-wavelength spin-echo spectrometer IN15 (ILL, Grenoble, France).

In summary, the SPAN instrument was adapted to soft matter research on several levels: the available wavelength range was significantly broadened from previously up to 4.5 Angs, to now up to 8.0 Angs. A new room temperature sample environment was implemented. First data sets were taken at the two newly implemented wavelengths of 6.5 Angs. and 8.0 Angs.

**Acknowledgement:**

*This research project has been supported by the European Commission under the 7<sup>th</sup> Framework Programme through "Research Infrastructures" action of the "Capacities" Programme, contract number CP-CSA\_INFRA-2008-1.1.1. Number 226507-NMI*

 <b>HELMHOLTZ ZENTRUM BERLIN</b> für Materialien und Energie  <b>NEUTRONS</b>	<b>EXPERIMENTAL REPORT</b>  <b>Binding and diffusion of Glutamate on PAH and PSS terminated polyelectrolyte multilayers</b>	Proposal: PHY-04-1952-EF  Instrument: V6  Local Contact: R. Steitz
	Principal Proposer: Amitesh Paul, HZB Experimental Team: Neelima Paul, HZB Martin Kreuzer, HZB	Date(s) of Experiment  04.05.2010 – 11.05.2010

Date of report: 25.05.2010

In this experiment, we wanted to test the binding of the polarized aminoacid L-Glutamate on a positively charged Si/PEI/(PSS/PAH)<sub>8</sub> surface and on a negatively charged Si/PEI/ (PSS/PAH)<sub>8</sub> PSS surface. We also wanted to compare the binding of Glutamate on a positively charged Si/PEI/(PSS/PAH)<sub>8</sub> surface and on a positively charged Si/PEI/ (PSS/PAH)<sub>12</sub> surface. This comparison would reveal if glutamate binds just to the surface or diffuses in the PEM. Further on, we wanted to test the possibility of separating out the entropic contribution from the electrostatic contribution of the binding by heating the sample to 38 °C.

As the thickness of glutamate layer deposited on the surface was expected to be small, we thought it useful to investigate with indexed-matched water (IMW) technique too. Here, we adjusted the ratio of D<sub>2</sub>O and H<sub>2</sub>O solvent in the liquid cell. For a certain ratio, Kiessig fringes due to PEMs disappeared as their contrast is dependent on the mole fraction of deuterium in the solvent (due to a considerable amount of solvent adsorption by the PEM layer). After introduction of glutamate in the solvent, Kiessig oscillations reappeared and are a result of the adsorbed glutamate layer. The observable Kiessig oscillations correspond to a Glutamate thickness of about 50 Å as indicated in Fig. 1.

To confirm this result, we took the reflectivity curves before and after the incubation of the Si/PEI/(PSS/PAH)<sub>8</sub> surface in Glutamate solution. The shift in the Kiessig oscillations in Fig. 2 show a additional layer of about 44 Å after incubation. We observed that after heating the sample to 38 °C, the thickness reduced to 39 Å. We could observe no significant increase in the thickness of glutamate layer in case of thicker PEM layers like Si/PEI/ (PSS/PAH)<sub>12</sub> which points to the fact that glutamate molecules bind to the

surface only and do not diffuse into the PEM layer.

In the control experiment on negatively charged samples, the reflectivity curves before and after the incubation of the Si/PEI/(PSS/PAH)<sub>8</sub> PSS surface in Glutamate solution show no shift in the Kiessig oscillations. This implies that there is no adsorption of Glutamate on the negatively charged surface.

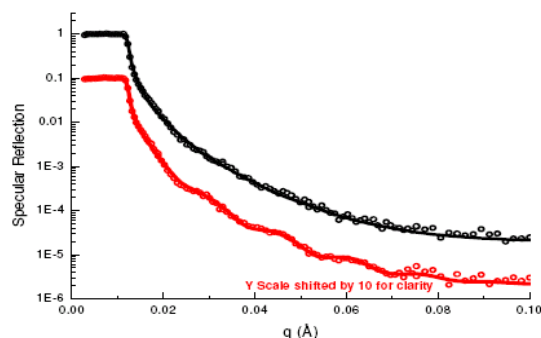


Fig.1. Reflectivity curves from a NR experiment on Si/PEI/(d-PSS/PAH)<sub>8</sub>/IMW (black squares) and Si/PEI/(d-PSS/PAH)<sub>8</sub>/GLU/IMW (red squares). The Kiessig oscillations were retrieved after incubation of the substrate with a diluted solution of Glutamate in IMW ( $4.9 \times 10^{-6} \text{ Å}^{-2}$ )

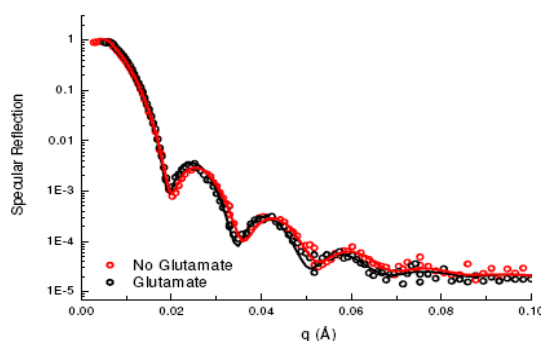



Fig.2. Reflectivity curves and their fits from a NR experiment on Si/PEI/(d-PSS/PAH)<sub>8</sub>/50%D+50%H<sub>2</sub>O (red circles) and Si/PEI/(d-PSS/PAH)<sub>8</sub>/GLU/50%D+50%H<sub>2</sub>O (black circles). The Kiessig oscillations shifted to lower q values after incubation of the substrate with a diluted solution of Glutamate.

 <b>HELMHOLTZ ZENTRUM BERLIN</b> für Materialien und Energie  <b>NEUTRONS</b>	<b>EXPERIMENTAL REPORT</b>  <b>Functional interfaces under load (hydrostatic pressure)</b>	Proposal: PHY-04-1953-EF  Instrument: <b>V6</b>  Local Contact: Roland Steitz
	Principal Proposer: Roland Steitz, HZB Experimental Team: Matthias Reinhardt, HZB Martin Kreuzer, Ruprecht-Karls-Universität Heidelberg	Date(s) of Experiment  08.02.2010 - 15.02.2010

Date of report: 02.03.2010

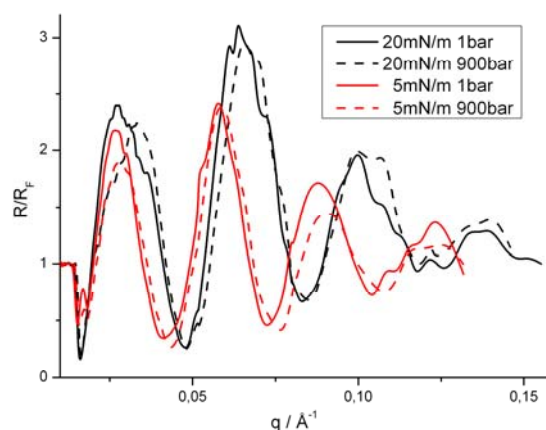
High pressure is an important feature of certain natural membrane environment as for instance marine biotopes. In that case pressure induced unfolding and denaturation of proteins is of utmost importance. Polymer brushes anchored at the interface of a solid support and an aqueous solution provide a soft cushion for adsorbed proteins without changing their functionality and thus offer a possibility to study pressure induced effects on proteins by neutron reflectivity.

Here, we report the first steps towards assembly and characterization of a model system for such investigations. Two samples with different polymer brush graft density were prepared by transferring the precursor Langmuir layers, i.e. the free floating monolayers of poly(styrene)-b-poly(acrylic-acid) ( $PS_N$ - $PAA_M$ ) on silicon wafers (blocks) pre-coated with deuterated polystyrene (dPS) via Langmuir-Schäfer technique. Transfer from the air-water interface of a Langmuir trough to solid support were conducted at two different graft densities that were controlled by adjusting movable barriers to surface pressures of 20 mN/m (graft density  $\approx 0.35$  molecules/ $nm^2$ ) and 5 mN/m ( $\approx 0.15$   $nm^{-2}$ ). Thereafter assembled brush samples on solid support were tempered for 15 minutes at 110 °C against air.

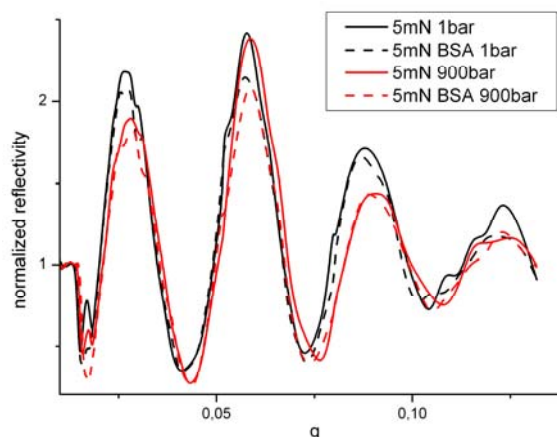
Both samples were re-incubated with water and investigated by neutron reflectometry at V6 against liquid  $D_2O$  at 1, 900 bar and again 1 bar hydrostatic pressure in the Heidelberg high pressure cell. Variations in the measured reflectivity curves indicate structural changes of the brushes at elevated pressure (Figure 1). The changes are fully reversible given that the second measurement at 1 bar shows no difference as compared to the first measurement at 1 bar.

After the pressure experiment against pure  $D_2O$  the brush sample prepared at higher graft density, i.e. at 20 mN/m transfer pressure, was exposed to a 0.1 mg/mL solution of  $\beta$ -lactoglobulin ( $\beta$ -LG) in  $D_2O$ . We did not see any substantial changes in reflectivity at 1 bar


and also not at 900 bar when compared to the respective reference system. We conclude that  $\beta$ -LG does not adsorb to the brush at supplied conditions. The same study was conducted for the brush sample prepared at the 5 mN/m transfer pressure and a solution of bovine serum albumine (BSA). In that case the adsorbed BSA modified the scattering length density of the brush and resulted in a slightly changed reflectivity curve for 1 and also 900 bar (figure 2). A detailed analysis of the data is currently under way.



**Figure 1:** Neutron reflectivity curves of Si/dPS/PS-PAA against  $D_2O$  for different hydrostatic pressure and graft density, expressed as transfer pressure  $\Pi$  in mN/m. Reflectivity curves are normalized to that of a smooth Si/ $D_2O$  interface.



**Figure 2:** Neutron reflectivity curves of Si/dPS/PS-PAA (5 mN/m surface pressure;  $\approx 0.15$   $nm^{-2}$  graft density) against  $D_2O$  with and without 0.1 mg/ml BSA at 1 bar and 900 bar hydrostatic pressure. The reflectivity curves are normalized to the Fresnel reflectivity of the plain Si/ $D_2O$  interface.

 <b>NEUTRONS</b>	<b>EXPERIMENTAL REPORT</b>	Proposal: BIO-04-1958-EF
	<b>Temperature Dependent Unbinding of Lipid Multilayers</b>	Instrument: <b>V6</b> Local Contact: Roland Steitz
Principal Proposer:	Martin Kreuzer, Ruprecht-Karls-Universität Heidelberg	Date(s) of Experiment
Experimental Team:	Reiner Dahint, Ruprecht-Karls-Universität Heidelberg Roland Steitz, HZB	23.06.2010 - 30.06.2010

Date of report: 31.01.2011

The combination of suitable implant surfaces with lipid coverage is most promising for forthcoming implant modifications. To that end, one of the fundamental requirements is the reliable preparation of stable lipid coatings in physiological environment. For the very reason, we assessed the stability of supported lipid multilayers. The measurements were performed in a temperature controlled liquid cell against excess  $D_2O$ . The lipid coating was realized by spin coating a solution of 10, 20 or 30 mg/ml DMPC in chloroform on three different disc-shaped silicon substrates A, B and C. This procedure yielded highly oriented lipid multilayers with different total numbers of lipid bilayers on substrates A, B, C. All multilayers produced well pronounced Bragg peaks in the neutron reflectivity measurements at around  $0.1 \text{ \AA}^{-1}$ . After incubating the samples in  $D_2O$  at  $21^\circ\text{C}$ , each sample was measured from  $23^\circ\text{C}$  to  $28^\circ\text{C}$  in  $0.5^\circ$  steps, while at each temperature the Bragg peak position(s) of the lipid multilayers were measured two times. Figure 1 shows the results for sample C. Right after incubation at  $21^\circ\text{C}$  a single Bragg peak is visible which is due to the gel like  $L_\beta$  phase of the lipid coating. Between  $23^\circ\text{C}$  and  $25^\circ\text{C}$  the single Bragg peak, also for samples A and B, evolved into two peaks. Two lipid membrane states can be identified this way on the basis of a Gaussian decomposition: the  $L_\beta$  phase and the liquid like  $L_\alpha$  phase. Figure 2 displays the d-spacings of the lipid membranes of sample C calculated from the Bragg peak positions. Above  $25^\circ\text{C}$ , again, only one Bragg peak is visible, indicating a dominating  $L_\alpha$  phase. Figure 3 shows the integrated area of the Bragg peaks, which is a measure of layer ordering and total number of layers. All three samples showed an increase in Bragg peak area between  $21^\circ\text{C}$  and  $24^\circ\text{C}$ , which is due to a better alignment of the lipid layers. Between  $24.5^\circ\text{C}$  and  $25.5^\circ\text{C}$  samples show an abrupt decrease in intensity, presumably indicating the occurrence of a  $P_\beta'$  state. Above  $25.5^\circ\text{C}$  there is a continuous decay of intensity in the  $L_\alpha$  phase. The latter indicates the onset of the lipid layers detachment from silicon support. Measurements up to a temperature of  $60^\circ\text{C}$  revealed that only one lipid membrane remains on the substrate. Further analysis is on its way.

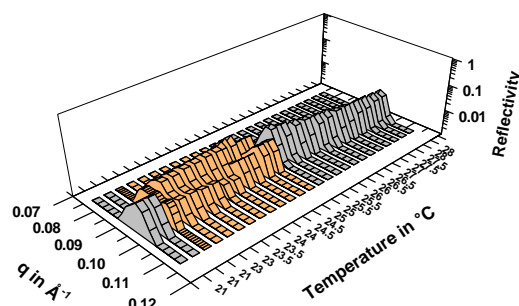


Figure 1

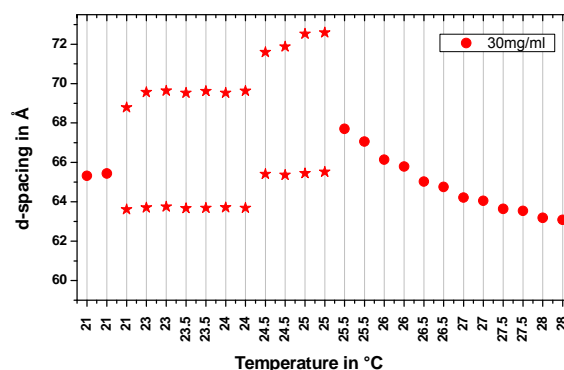


Figure 2

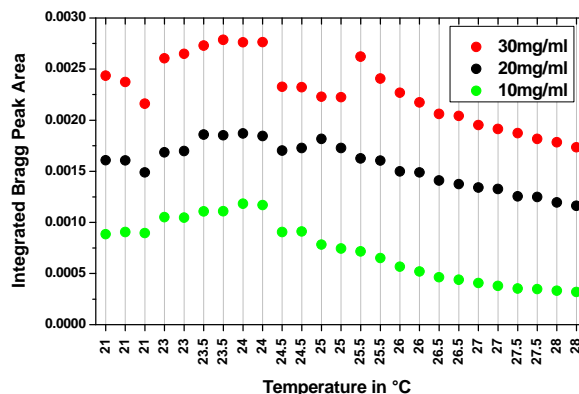



Figure 3

*This research project has been funded by the BMBF under grant number 05KN7VH1. Additional financial support was received from HZB.*

 <b>EXPERIMENTAL REPORT</b>		Proposal: MAT-04-1962
<b>Measurements of solvent distribution in swollen lamella-forming block copolymer films</b>		Instrument: <b>V6</b>
		Local Contact: R. Köhler
Principal Proposer:	Larisa Tsarkova, Uni Bayreuth	Date(s) of Experiment
Experimental Team:	Ralf Köhler, HZB Rumen Krastev, Uni Tübingen NMI	14.02.2010 – 21.02.2010

Date of report: 31.01.2011

Recently was shown that the macroscopic swelling behaviour of nanostructured block copolymer films exhibits a clear film thickness-dependence [1]. As was proposed by Steiner et al [2], the chain conformation and the degree of the chains entanglements in spin-coated films significantly deviates from that in bulk. The aim of the present neutron reflectivity (NR) study was to quantify the solvent distribution in swollen block copolymer films as a function of the film thickness and potentially to get insight into the degree of conformational heterogeneity in spin-coated polymer films.

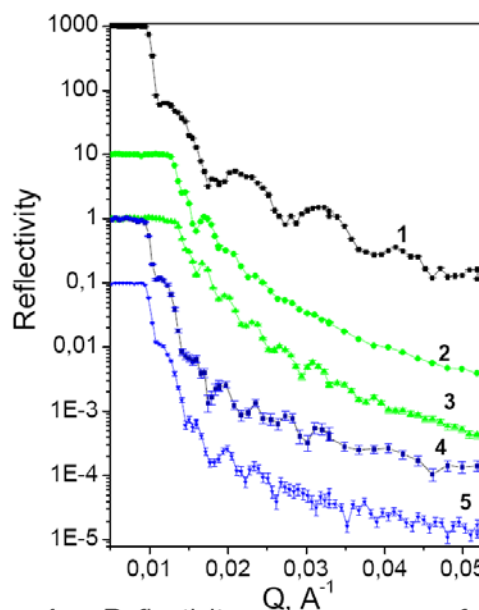
Films from polystyrene(PS)-*b*-poly(2 vinylpyridine(P2V)) (SV) with the thickness ~30 nm and ~50 nm have been prepared by spin-coating from perdeuterated chloroform (CDCl<sub>3</sub>) solutions. Silicon wafers with the sizes (3 x 3) cm<sup>2</sup> have been used as substrates. The specular reflectivity from the films was measured in the Q-range up to 0.07 Å<sup>-1</sup> in dry N<sub>2</sub>, then in the presence of perdeuterated toluene (D8-toluene), and after drying in N<sub>2</sub> in the presence of unlabelled toluene vapour. The organic solvent was filled in the reservoir inside the chamber (as in reference [3]). The flow of dry N<sub>2</sub> was let through the chamber for 10 min to build up the equilibrium solvent vapour pressure, and then the chamber was sealed for the duration of the NR measurement. The microphase separated structure in the studied SV films has been additionally analysed with the scanning force microscopy (SFM).

Fig. 1 shows the reflectivity curves of a solvent-free and of swollen lamella-forming SV films. In the dry state (curve 1), the interference fringes primarily arose from the total film thickness because of the weak scattering from the PS/P2VP interfaces. For an equilibrated swollen film (curve 3) the sharp fringes at low Q<sub>z</sub> (Q<sub>z</sub><0.05 Å<sup>-1</sup>) primarily correspond to the thickness of the selectively swollen P2V and PS lamella sheets.

The performed experiments gave strong indications that block copolymer films are

suitable models to study the confinement effects in polymer films. The following outlines are important for the further development of the research:

- i) For quantitative conclusions regarding the solvent uptake and related solvent density distribution across the film, the swelling experiments have to be done under controlled "partial vapour pressure" conditions within the chamber.
- ii) The intrinsic topographical "roughness" of the equilibrated block copolymer films (known as terrace formation) does not prevent to accumulate the signal of sufficient intensity.



**Fig. 1:** Reflectivity  $Q, \text{\AA}^{-1}$  curves of a 30 nm-thick SV film in a dry state (1), and of the same film after 1 hour (2 and 4) and after 8 hours (3 and 5) of exposure to D8-toluene vapor and to unlabeled toluene vapor, respectively. The reflectivity curves are vertically offset for clarity.

#### References

- [1] Tsarkova, L.; Sevink, G.J.A.; Krausch G. *Adv. Polym. Sci.* 2010, **227**, 33-73.
- [2] Barbero, D. R.; Steiner, U. *Phys. Rev. Lett.* 2009, **102**, 248303.
- [3] Köhler, R.; Dönch, I.; Ott, P., et al, *Langmuir* 2009, **25**, 11576-11585.

Principal Proposer: C. A. Helm, EMAU Greifswald  
 Experimental Team: O. Soltwedel, EMAU Greifswald  
 P. Nestler, EMAU Greifswald  
 C. A. Helm, EMAU Greifswald  
 Ralf Köhler, MPI Kolloid- und Grenzflächenforschung

Date(s) of Experiment

11.05.2010 – 16.05.2010  
 30.06.2010 – 05.07.2010

Date of report: 20.08.2010

Polyelectrolyte multilayers (PEMs) are composed of alternating layers of oppositely charged polyelectrolytes (PEs) (synthetic PEs or biomolecules), which are generally built up based on the layer-by-layer technique [1]. PEMs have stimulated great interests from both academic researchers and industries due to their potential applications, such as membrane, encapsulation, and matrix materials for enzymes and proteins in sensor applications. The linear, layer-by-layer, growth mode of PEMs is an inherently nonequilibrium process, yielding nonequilibrium structure. In the adsorption process itself, individual molecules attach to the surface of a growing PEM via many ion pairing contacts. Large scale rearrangements within PEMs may be induced by changing the interactions between PEs by immersing the PEM into solutions of ionic strength above preparation conditions because some monomers form no longer ion pairs with other monomers but with their monovalent counterions [2].

In our experiments, each PEM consists of a protonated and a deuterated block,  $p_9d_5$ , similar to [3] (cf. Fig. 1). This film architecture was selected to obtain as few independent parameters as possible, specifically the thickness and the scattering length density of each block, as well as the internal roughness between the blocks [4]. For this architecture, the thickness of the protonated block (9 polycation/polyanion bilayers) is the same as for the deuterated block (5 bilayers).

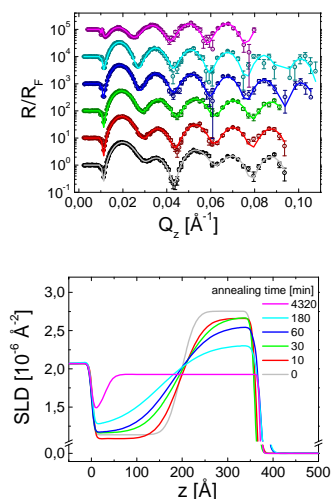


Fig. 1: Normalized neutron reflectivity curves (top) and corresponding SLD profiles (bottom) of a PEI/PSS/(PDADMA/PSS)<sub>6</sub>/(PDADMA/PSS-d)<sub>5</sub> film, measured at 0% r.h. (preparation conditions: 0.1 M NaCl, T = 20°C). After preparation, the PEMs are immersed for the time indicated in the bottom part into 1 M NaCl solution at 20°C, and dried. For clarity, the reflectivity curves are shifted relative to each other by one order of magnitude. Actually, the measurements are from 3 different PEMs (always the same preparation conditions, and identical reflectivity curves immediately after preparation).

Polydiallyl-dimethyl ammonium (PDADMA,  $M_w = 35$  kDa) is used as polycation, due to its widespread use [1], polystyrene

sulfonate (PSS,  $M_w = 76$  kDa) is the polyanion. The first polycation layer is branched polyethylene imine (PEI). Deposition conditions are standard for PDADMA/PSS films (0.1 M NaCl, 20°C).

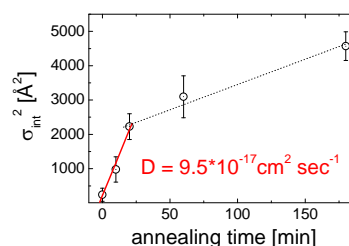


Fig. 2: Square of internal roughness,  $\sigma_{\text{int}}^2$ , of PEI/PSS/(PDADMA/PSS)<sub>6</sub>/(PDADMA/PSS-d)<sub>5</sub> films vs. immersion time in 1 M NaCl solution.  $\sigma_{\text{int}}$  is deduced from the measurements shown in Fig. 1, the diffusion constant  $D$  from annealing times below 30 min.

After preparation, the film is first characterized by neutron reflectivity (0% r.h. adjusted with P<sub>2</sub>O<sub>5</sub>) as shown in Fig. 1. Then the PEM is immersed for different times in 1 M NaCl solution at 20°C, washed in pure water, dried and characterized again. From the scattering length density profiles (cf. Fig. 1) the width of the internal interface is found to increase, indicating interdiffusion. For immersion times below 30 min, the rearrangement can be described as a 1-dimensional diffusion between infinite reservoirs [4]. Comparing coefficients, one obtains – (with  $\sigma_{\text{int}}$  as internal roughness,  $D$  as diffusion coefficient and  $t$  as time), and obtains  $D = 9.5 \cdot 10^{-17} \text{ cm}^2 \text{ s}^{-1}$  (cf. Fig. 2). This diffusion constant is of the same order of magnitude as values for similar systems [5]. For immersion times larger than 30 min, the SLD next to the air (the substrate) are no longer those of the pure deuterated (protonated) block, but decreased (increased), indicating mixing of the PEs. The internal roughness  $\sigma_{\text{int}}$  increases more slowly with time, due to back diffusion of the PEs. After 72 h (4320 min) the mixing is complete, the protonated and the deuterated block can no longer be distinguished. The SLD is the arithmetic mean. However, close to the substrate, the SLD remains decreased in a 30 Å thick layer. This decrease is attributed to the branched PEI together with the 1<sup>st</sup> PSS layer, which are immobile, or have a very low mobility beyond our resolution. Actually, this immobility is a good thing, since it provides stability for the PEM.

#### Literature

- G. Decher, *Science* **277** (1997) 1232; M. Schönhoff, *Journal of Physics: Condens. Matter* **15** (2003), 1781; R. v. Klitzing, *PCCP* **8** (2006), 5012
- S.T. Dubas; J.B. Schlenoff, *Langmuir* **17** (2001) 7725; B. Qiao; J.J. Cerda, C. Holm, *Macromolecules* **43** (2010) ASAP
- O. Ivanova, O. Soltwedel, M. Gopinadhan, R. Köhler, R. Steitz, C.A. Helm, *Macromolecules* **41** (2008) 7179
- O. Soltwedel, O. Ivanova, P. Nestler, M. Müller, R. Köhler, C.A. Helm, *Macromolecules* **43** (2010) ASAP.
- H. Jooma, J.B. Schlenoff, *Macromolecules* **38** (2005) 3473



	<b>EXPERIMENTAL REPORT</b>  <b>Critical and multilayer adsorption from alkane + perfluoroalkane mixtures to chemically modified silicon substrates</b>	Proposal: PHY-04-1968  Instrument: <b>V6</b>  Local Contact: Anke Teichert
	Principal Proposer: A. Zarbakhsh, QM UCL, UK Experimental Team: John Webster, RAL ISIS, UK Roland Steitz, HZB Anke Teichert, HZB	Date(s) of Experiment  25.05.2010 – 01.06.2010

Date of report: 31.01.2011

## Introduction

Hydrocarbon-fluorocarbon interactions are of great practical importance in applications such as non-stick coatings, anti-graffiti paint, specialised lubricants and surfactants as well as being of significant academic interest. Important adsorption behaviour occurs close to the liquid-liquid coexistence curve of a binary liquid mixture. As coexistence is approached along a path of constant composition a thick film of the preferentially adsorbed component builds up. The thickness  $l$  of this multilayer film is expected to grow as  $l \sim |T - T_0|^{-1/3}$ , where  $T_0$  is the coexistence temperature. A special situation arises when the critical solution temperature  $T_c$  is approached. In this region the behaviour of the system is governed by composition fluctuations in the bulk. The adsorbed-film thickness scales with the bulk correlation length  $\xi$ , and varies as  $l \sim \xi \sim |T - T_c|^{-0.305}$ . However, despite the similarity in the film thickness divergence, the analytical behaviour of the composition profiles is different in the two regimes. The power-law dependence of critical adsorption is well established, and  $\phi(z) - \phi(\text{bulk}) \sim z^{-0.52}$ , where  $\phi$  is the volume fraction composition and  $z$  is the coordinate normal to the interface. We have in the past examined the nature of both critical and multilayer adsorption profiles.

## Experimental

The aim of our experiment was to explore how the critical adsorption profiles and the multilayer adsorption profiles differ along a path of non-critical composition. In this study we explored the adsorption of liquid mixtures of n-hexane-perfluoro-n-hexane on a C18 alkylated silicon substrate in addition to a bare Si for comparison. The experiment was designed to approach the phase boundary between  $\phi(\text{Hexane}) = 0.08$  and  $0.12$  and to measure the reflectivity profiles as a function of composition for several temperatures to establish the exact location of any prewetting line and the phase boundary itself. In this way, we hope to

establish the nature of the adsorption profiles in this non-critical region of the phase diagram.

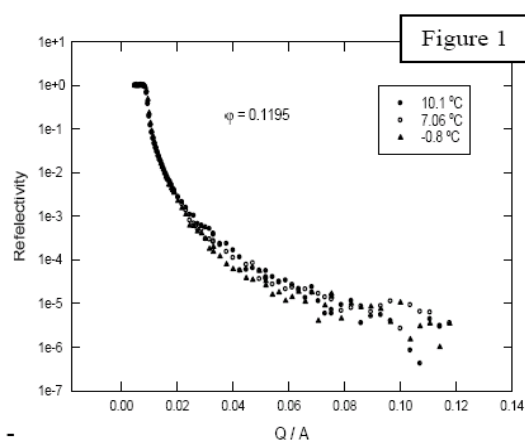
Typical data obtained for the C18 substrate are shown in Figure 1. The C18 alkylated silicon was

first characterised for a series of contrast namely Hexane and perfluoro-n-hexane. The results obtained were consistent with our previous work (8 Å oxide layer followed by an 18Å C18 layer). Adsorptions from the mixture of hexane-perfluoro-n-hexane were carried out at 9 different temperatures for both these substrates.

## Result and discussion

The data are currently being analysed using a decay model. The fits so far suggested that there is a comparatively thin (14Å) film of mainly n-hexane on the surface as expected. The generality of the dilute tail of the adsorption profile and the thickness of adsorbed films to the thickness of the coupled film will be determined when the data obtained are fully analyzed.

The result so far suggest there seems to be no dependence of the data on the precise nature of the surface, within error. There is an absence of any trend with alkyl chain length, for example. The decay of composition profiles is exponential and at low temperature also exponential rather than a power law, as has been reported.



## Acknowledgement:

This research project has been supported by the European Commission under the 7<sup>th</sup> Framework Programme through "Research Infrastructures" action of the "Capacities" Programme, contract number CP-CSA\_INFRA-2008-1.1.1. Number 226507-NMI

Principal Proposer: C. A. Helm, EMAU Greifswald  
Experimental Team: O. Soltwedel, EMAU Greifswald  
P. Nestler, EMAU Greifswald  
R. Köhler, MPI Kolloid- und Grenzflächenforschung

Date(s) of Experiment

18.03.2009 – 23.03.2009  
14.07.2009 – 20.07.2009

Date of report: 30.08.2010

Polyelectrolyte multilayers (PEMs) are composed of alternating layers of oppositely charged polyelectrolytes (PEs) (synthetic PEs or biomolecules), which are generally built up based on the layer-by-layer technique [1]. The linear, layer-by-layer, growth mode of PEMs is an inherently non-equilibrium process, yielding nonequilibrium structure. In the adsorption process itself, individual molecules attach to the surface of a growing PEM via many ion pairing contacts. We found recently that the internal roughness  $\sigma_{\text{int}}$  is smallest next to the film/air interface and increases with the number of bilayers away from the film/air interface [2]. This suggests that each deposition step promotes the interdiffusion of the supporting layers. Many questions remain to be answered: (i) if the driving force of interdiffusion is stress-relaxation only, then at a defined distance away from the film-air interface stress-relaxation should be finished, either because equilibrium is achieved or because further movement is ruled out due to large energetic penalties; (ii) on increase of the salt concentration  $c$  during preparation the polycation/polyanion bilayer thickness  $d_{\text{BL}}$  increases and the influence on  $\sigma_{\text{int}}$  needs to be quantified; (iii) the diffusion constant  $D$  of polymers decreases with molecular weight  $M_w$ . Yet, if  $M_w$  of the oppositely charged PE is changed, then the effects of the changed obstacles in the path of the diffusing PE are not clear.

In our experiments, each PEM consists of a protonated and a deuterated block,  $p_{N-n}d_n$ , similar to [2,3] (cf. Fig. 1). This film architecture is selected since the scattering length density (SLD) depends only on few independent parameters: the thickness and the SLD of each block, as well as the internal roughness  $\sigma_{\text{int}}$  [2,3].

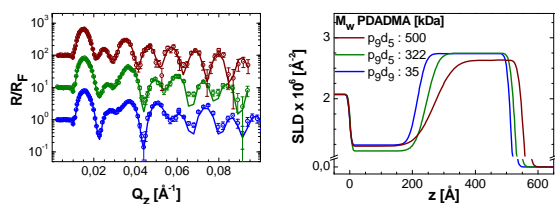


Fig. 1: Normalized neutron reflectivity curves (left) and corresponding SLD profiles (right) of a PEI/PSS/(PDADMA/PSS)<sub>n</sub> / (PDADMA/PSS-d)<sub>x</sub> film, measured at 0% r.h. Varied is the PDADMA molecular weight  $M_w$ , as indicated (PEMs prepared @ 0.1 M NaCl). With decreasing  $M_w$  the thickness per bilayer  $d_{\text{BL}}$  decreases. For clarity, the reflectivity curves are shifted relative to each other by one order of magnitude.

Polydiallyl-dimethyl ammonium (PDADMA,  $M_w = 35, 322, 500$  kDa) is used as polycation, due to its widespread use [1], polystyrene sulfonate (PSS,  $M_w = 76$  kDa; deuterated PSS-d,  $M_w = 75$  kDa) is the polyanion. The first polycation layer is branched polyethylene imine (PEI). Deposition temperature is 20°C. Typical neutron reflectivity curves are shown in Fig. 1, the Kiessig oscillations are modulated by beats due to the different blocks.

Fig. 2 shows the internal roughness  $\sigma_{\text{int}}$ , if the salt concentration  $c$  is varied ( $M_w(\text{PDADMA}) = 500$  kDa). A defined number bilayers below the film-air interface, the internal

roughness  $\sigma_{\text{int,max}}$  is constant.  $\sigma_{\text{int,max}}$  is the same for large  $c$  (0.1, 0.3 M). This suggests that an equilibrium value of the PSS conformation is achieved (note that the ratio  $\sigma_{\text{int,max}}/d_{\text{BL}}$  is not a constant as found for PAH/PSS [1], but has a maximum at 0.1 M). At low  $c$  (0.03 M),  $\sigma_{\text{int,max}}$  is smaller. Clearly, many stable monomer/monomer ion pairs typical for low  $c$  [4] limit the PSS diffusion.

Obviously, the number of deposition cycles  $k$  required for saturation depends on  $c$ . Seven bilayers are necessary for  $c = 0.1$  M; yet for  $c = 0.03$  M or  $c = 0.3$  M less than five bilayers suffice. (1) Comparing  $c = 0.1$  M and  $c = 0.3$  M, fewer cycles are necessary to reach  $\sigma_{\text{int,max}}$  if  $c$  is larger, due to the increased PE mobility (fewer ion pairs between monomers and more ion pairs between monomers and their counterions [4], up to now the diffusion constant is determined only for  $c = 0.1$  M, according to  $\sigma_{\text{int}}^2 = 2Dt$  [2]). (2) At low  $c$  (0.03 M), the PSS diffusion is hindered, little stress-relaxation occurs and a stable PSS conformation is achieved after a few deposition cycles.

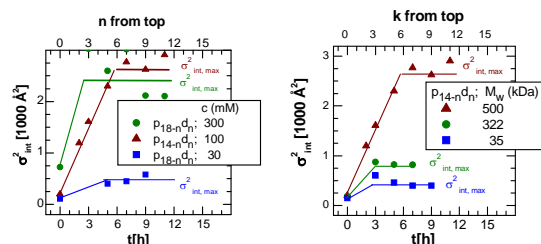



Fig. 2: Square of internal roughness,  $\sigma_{\text{int}}^2$ , of PEI/PSS/(PDADMA/PSS)<sub>N-w</sub> / (PDADMA/PSS-d)<sub>n</sub> films vs. the immersion time in the deposition solution (or vs. the position of the investigated interface, i.e.  $n$  bilayers below the film-air interface). Films were prepared from different NaCl concentration  $c$  (left, with  $M_w = 500$  kDa for PDADMA) or from different PDADMA polymer weight (right, with 100 mM NaCl).  $\sigma_{\text{int}}$  is determined from the reflectivity curves similar to those shown in Fig. 1.

Additionally, Fig. 2 shows  $\sigma_{\text{int}}$  and  $\sigma_{\text{int,max}}$  if at constant preparation conditions (0.1 M NaCl) the weight of PDADMA is varied.  $\sigma_{\text{int,max}}$  decreases with  $M_w$ . Furthermore, the ratio  $\sigma_{\text{int,max}}/d_{\text{BL}}$  is not a constant, but decreases with  $M_w$ . This suggests that lightweight polycations encumber the PSS diffusion. The effect is similar to a film deposited at a smaller ion concentration, even though the reasons are different.

#### Literature

- G. Decher, *Science* **277** (1997) 1232; M. Schönhoff, *Journal of Physics: Condens. Matter* **15** (2003), 1781; R. v. Klitzing, *PCCP* **8** (2006), 5012
- O. Soltwedel, O. Ivanova, P. Nestler, M. Müller, R. Köhler, C.A. Helm, *Macromolecules* **43** (2010) ASAP.
- O. Ivanova, O. Soltwedel, M. Gopinadhan, R. Köhler, R. Steitz, C.A. Helm, *Macromolecules* **41** (2008) 7179
- B. Qiao; J.J. Cerda, C. Holm, *Macromolecules* **43** (2010) ASAP

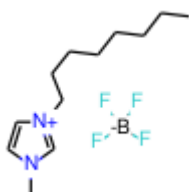
 <b>NEUTRONS</b>	<b>EXPERIMENTAL REPORT</b>	Proposal: PHY-04-2042-LT PHY-04-1954-LT
	<b>Structure of ionic liquids in thin films and at solid interfaces</b>	Instrument: <b>V6</b> Local Contact: Ralf Köhler
Principal Proposer: Experimental Team:	Ralf Köhler, MPI of Colloids and Interfaces, Potsdam Rumen Krastev, NMI Uni Tübingen José Restolho, IST Lisbon, PT Benilde Saramago, IST Lisbon, PT	Date(s) of Experiment 27.01.2010 – 31.01.2010 23.08.2010 – 29.08.2010

Date of report: 31.Jan.11

Ionic Liquids (IL) are salts which are in liquid state at room temperature. IL typically consist of a relatively small inorganic ion and a awkwardly shaped organic counterion. The resulting steric hindrance prevents the liquid from crystallisation.

IL are promising candidates for application on many technical fields: As solvents, for heterogeneous catalysis, in electro-chemistry and micro-electromechanics, and as lubricants. For all of these applications the ordering and wetting behaviour of the IL at the solid/liquid interface plays an important role. Despite the interest on those interfaces, the research in this area is still scarce and, sometimes, controversial.

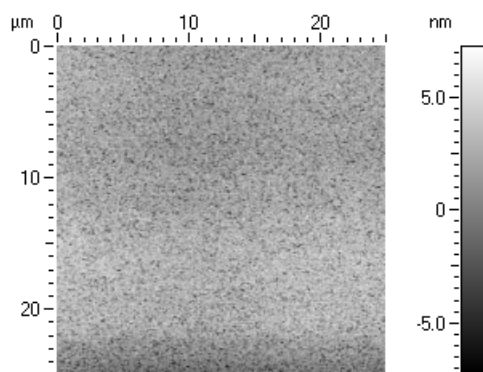
In the present work we characterize wetting films of 1-methyl-3-octylimidazolium tetrafluoroborate ([omim][BF<sub>4</sub>]), a room temperature ionic liquid which exhibits surfactant properties due to the relatively long side chain on the imidazolium ring. The wetting films were obtained by spin coating from ethanol solutions on metal-coated silicon substrates (Al, Cr, Ag).



To study possible ordering, especially layering effects, at the interface, we use hydrogenated [omim] and two [omim]-derivatives which have 50% or 90% deuterium-enrichment in the molecular ring structure. This would allow for the detection of a separation of hydrogen-rich chains and deuterium-rich rings in the contact zone to the solid interface.

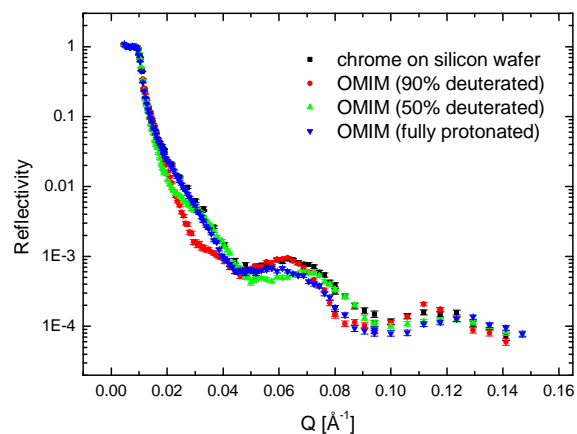
Preliminary Atomic Force Microscopy (AFM), and X-ray (XRR) measurements allowed for estimation of the preparative conditions for homogeneous IL films on metal-coated silicon substrates (Fig. 1).

Neutron reflectivity experiments at the instrument V6 in the HZB Berlin show that homogeneous layers of the differently labelled



**Figure 1: AFM image of a homogeneously wetting IL film (concentration 1mg/ml) at a Al/Si substrate**

[omim]-derivatives exhibit distinctly deviating reflectivity curves although the films are of comparable thickness (Fig. 2).



**Figure 2: Neutron reflectometry curves of wetting layers of differently labelled IL's on Cr/Si substrate**

This finding gives strong hint for a layered structure/ordering of the IL perpendicular to the interface. Future work shall help to generalise these first results to films of different thicknesses. Additionally the structure of the IL at the liquid/air interface shall be investigated.

Principal Proposer: Christiane A. Helm, Uni Greifswald  
 Experimental Team: Olaf Soltwedel, Uni Greifswald  
 Peter Nestler, Uni Greifswald  
 Ralf Köhler, HZB and Stranski Lab, Berlin

Date(s) of Experiment

30.8.2010 - 05.9.2010

Date of report: 31.01.2011

Polyelectrolyte multilayers (PEMs) are composed of alternating layers of oppositely charged polyelectrolytes (PEs) (synthetic PEs or biomolecules), which are prepared by the layer-by-layer technique [1]. The linear, layer-by-layer, growth mode of PEMs is an inherently nonequilibrium process, yielding nonequilibrium structure. In the adsorption process itself, individual molecules attach to the surface of a growing PEM via many ion pairing contacts. We found recently that the internal roughness  $\sigma_{\text{int}}$  is smallest next to the film/air interface and increases with the number of bilayers away from the film/air interface [2]. This suggests that each deposition step promotes the interdiffusion of the supporting layers. Many questions remain to be answered: (i) if the driving force of interdiffusion is stress-relaxation only, then after the deposition of a defined distance away from the film-air interface stress-relaxation should be finished, either because equilibrium is achieved or because further movement is ruled out due to large energetic penalties; (ii) on increase of the salt concentration  $c$  in the deposition solution, the electrostatic interactions are shielded, both in range and in amplitude. This leads to reduced electrostatic polycation/polyanion binding, and should increase the polyelectrolyte diffusion constant  $D$ ; [2] (iii) furthermore,  $D$  should decrease with polymer molecular weight  $M_w$ .

In our experiments, each PEM consists of a protonated and a deuterated block,  $p_{N-n}d_n$ , similar to [3,4] (cf. Fig. 1). The number of bilayers  $N$  is kept constant; the position of the interface between the blocks is varied systematically. This film architecture is selected since the scattering length density (SLD) profile depends only on few independent parameters: the thickness and the SLD of each block, as well as the internal roughness  $\sigma_{\text{int}}$  [3,4].

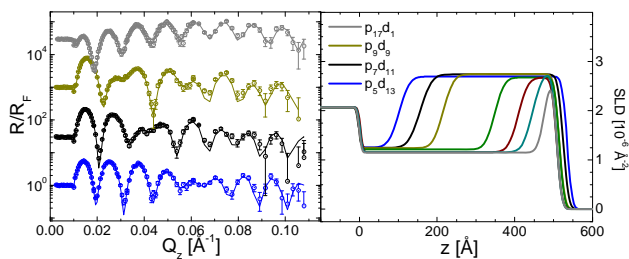


Fig. 1: Normalized neutron reflectivity curves (left) and corresponding SLD profiles (right; additional profiles are given) of a PEI/PSS/(PDADMA/PSS)<sub>18-n</sub>/(PDADMA/PSS-d)<sub>n</sub> film, measured at 0% r.h. (PEMs prepared @ 0.1 M NaCl,  $M_w$  of PDADMA is 35 kDa). For clarity, the reflectivity curves are shifted relative to each other.

Polydiallyl-dimethyl ammonium (PDADMA,  $M_w = 35, 322, 500$  kDa) is used as polycation, due to its widespread use [1], polystyrene sulfonate (PSS,  $M_w = 76$  kDa; deuterated PSS-d,  $M_w = 75$  kDa) is the polyanion. The first polycation layer is branched polyethylene imine (PEI). Deposition temperature is 20°C. Typical neutron reflectivity curves

are shown in Fig. 1, the Kiessig oscillations are modulated by beats due to the different blocks. The internal roughness is smallest next to the film/air interface and increases with the number of bilayers away from the film/air interface until an equilibrium value is reached. For PDADMA/PSS films prepared at constant  $c$ , the highest value of  $\sigma_{\text{int,max}}$  is found for the largest PDADMA  $M_w$ . Furthermore, the largest diffusion constant, as well as the longest duration of the diffusion process, is found for the highest  $M_w$ . ( $D$  is calculated according to  $\sigma_{\text{int}}^2 = 2 D t$  [2], with  $t$  the deposition time). Since these observations cannot be explained with the theory of polymers in solution, the driving force of diffusion is thought to be stress relaxation during deposition.

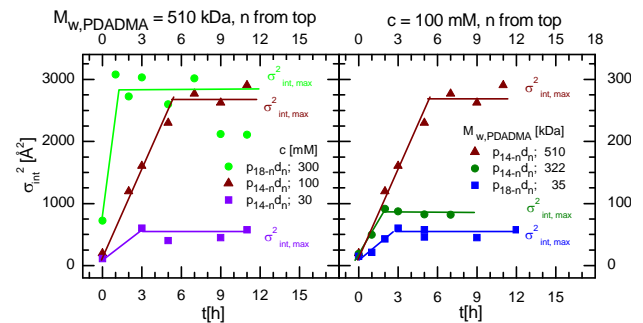


Fig. 2: Square of internal roughness,  $\sigma_{\text{int}}^2$ , of PEI/PSS/(PDADMA/PSS)<sub>18-n</sub>/(PDADMA/PSS-d)<sub>n</sub> films vs. the immersion time in the deposition solution (or vs. the position of the investigated interface, i.e.  $n$  bilayers below the film-air interface). Films are prepared from different NaCl concentration  $c$  (left,  $M_w = 500$  kDa for PDADMA) or from different PDADMA polymer weight (right, @  $c = 0.1$  M NaCl).  $\sigma_{\text{int}}$  is deduced from reflectivity curves akin to those shown in Fig. 1.

If the salt concentration  $c$  is varied (PDADMA: 500 kDa), similar features are observed: Close to the film/air interface,  $\sigma_{\text{int}}$  is small and increases towards an equilibrium value deep down in the film. Furthermore,  $\sigma_{\text{int,max}}$  increases with  $c$ , and appears to approach an equilibrium value for large  $c$  (0.1, 0.3 M). At low  $c$  (0.03 M),  $\sigma_{\text{int,max}}$  is smaller. Also, the number of deposition cycles required for saturation depends on  $c$ . Seven bilayers are necessary for  $c = 0.1$  M; yet for  $c = 0.3$  M less than one bilayer is sufficient. Indeed, the diffusion constant increases with  $c$  by about a factor of 5. At low  $c$  (0.03 M), the PSS diffusion is hindered, little stress-relaxation occurs and the PSS conformation is stable after a few deposition cycles.

#### Literature

- G. Decher, *Science* **277** (1997) 1232; M. Schönhoff, *Journal of Physics: Condens. Matter* **15** (2003), 1781; R. v. Klitzing, *PCCP* **8** (2006), 5012
- B. Qiao; J.J. Cerda, C. Holm, *Macromolecules* **43** (2010) 7828
- O. Soltwedel, O. Ivanova, P. Nestler, M. Müller, R. Köhler, C.A. Helm, *Macromolecules* **43** (2010) 7288.
- O. Ivanova, O. Soltwedel, M. Gopinadhan, R. Köhler, R. Steitz, C.A. Helm, *Macromolecules* **41** (2008) 7179

**Water Distribution in Electrochemically Swellable Polyelectrolyte Multilayers**

Instrument: **V6**

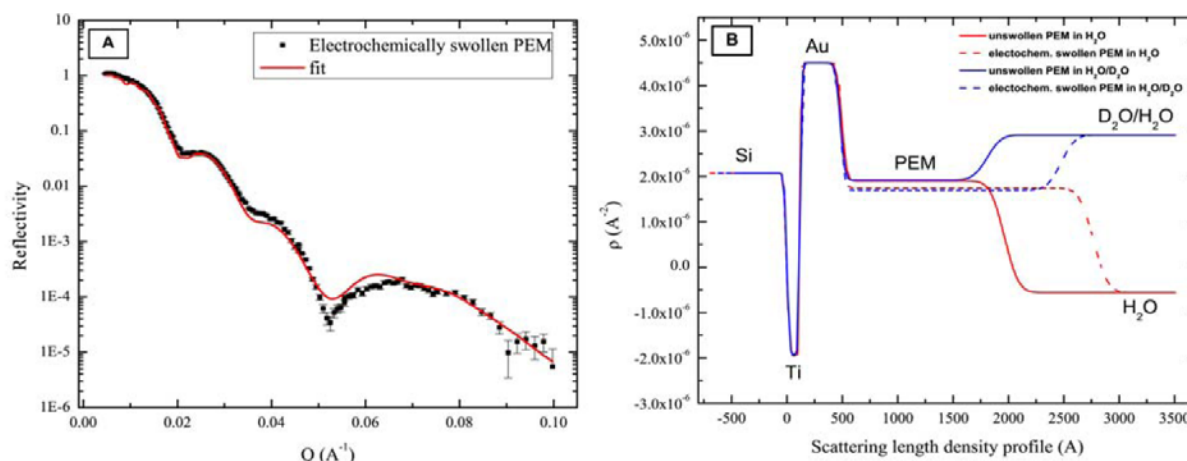
Local Contact:  
R. Köhler

Principal Proposer: Raphael Zahn, ETH Zürich  
Experimental Team: Ralf Köhler, HZB Berlin  
Katrin Bickel, KIT Karlsruhe  
János Vörös, ETH Zürich  
Tomaso Zambelli, ETH Zürich

Date(s) of Experiment

16.08.2010 – 23.08.2010

Date of report: 26.01.2011



**Fig. 1.:** (A) Reflectivity curve and fit for an electrochemically swollen PEM in  $D_2O/H_2O$  (50%/50% v/v) solution containing 300 mM NaCl. (B) Scattering length profiles for unswollen and electrochemically swollen PEMs in  $H_2O$  and  $D_2O/H_2O$  (50%/50% v/v) solutions (300 mM NaCl).

### Experiments and Results

We investigated the water distribution in electrochemically swelling polyelectrolyte multilayers (PEMs) which consist of Poly-L-Glutamic Acid (PGA) and Poly-(Allylamine Hydrochloride) (PAH) and contain Ferrocyanide (FC) ions as electrochemically active species. The PEMs (PGA/PAH<sub>8</sub> with FC) were prepared prior to the Neutron Reflectivity (NR) experiment by dip-emersion of a gold-coated silicon waver into polyelectrolyte solution of fixed ionic strength (100 mM KCl) and pH (7.4). Prior to the NR experiments the PEMs were exposed to two different ionic strengths (100 mM and 300 mM of KCl). For every equilibrated sample two NR experiments were carried out: (1) The PEMs were measured in the “unswollen” state, i.e. without applying any potential. (2) To measure the “swollen” state of the PEM a low potential (~ 300 mV) was applied. This positive potential leads to an oxidation of the FC and a subsequent swelling of the multilayer through uptake of water and counter ions. Two series of the swelling experiments were carried out, one set in  $H_2O$ , the other one in a  $H_2O/D_2O$  mixture (50%/50% v/v). From the fits of the obtained reflectivity curves the scattering densities and the thicknesses for the unswollen and the swollen PEMs were


extracted (see Fig. 1). A swelling of 4% was detected in the low ionic strength solvent, while the swelling was approx. 40% for the high ionic strength. Comparing the calculated scattering densities in  $H_2O$  and in  $H_2O/D_2O$  to the ones obtained from the fits to the experimental data, we can explain this increased swelling by an increased uptake of  $H_2O$  (or  $H_2O/D_2O$ ) to the PEM. From these calculations we can exclude an increased uptake of salt ions as cause for the higher swelling. The calculated scattering density for this possibility is in disagreement with experimental data.

### Difficulties

Due to the use of a Ti adhesion layer an unfavorable scattering density profile was obtained with limited sensitivity in the region of the adsorbed PEM (see Fig. 2B). We suggest the use of a Cr adhesion layer for future experiments.

### Acknowledgements

This research project has been supported by the ETH Zurich (Research Grant ETH-17 08-1) and by the European Commission under the 7<sup>th</sup> Framework Programme through “Research Infrastructures” action of the “Capacities” Programme, contract number CP-CSA\_INFRA-2008-1.1.1. Number 226507-NMI3.

 <b>HELMHOLTZ ZENTRUM BERLIN</b> für Materialien und Energie  <b>NEUTRONS</b>	<b>EXPERIMENTAL REPORT</b>  <b>Neutron reflectivity from Silicon/EVA interface</b>	Proposal: PHY-04-1898  Instrument: <b>V6</b>  Local Contact: Roland Steitz
	Principal Proposer: B. Röder, HU Berlin Experimental Team: S. Jungwirth, HU Berlin R. Steitz, HZB R. Köhler, HZB	Date(s) of Experiment  19.10.2009 – 26.10.2009

Date of report: 15.09.2010

Here we report on our neutron reflectivity measurements on ethylene-vinyl-acetate (EVA)/Silicon interface carried out in October 2009.

EVA is an encapsulating polymer most widely used for photovoltaic modules. The behaviour of this material in contact with Si under different humidity conditions is in the focus of actual reliability investigations worldwide.

For our experiments we used the neutron reflectometer V6 at Helmholtz Zentrum Berlin with an aluminium humidity chamber at a temperature of about 52°C (see Fig. 1). We also used a setup measuring the reflectivity of the sample against liquid D<sub>2</sub>O.

The samples were made of EVA laminated onto a silicon block. We investigated samples from two different charges, one fabricated in June 2009 (sample 0 and sample 4) and the other one fabricated in October 2009 (sample 2 and sample 3). Sample 3 has been stored in D<sub>2</sub>O for about 18 days before the measurement.

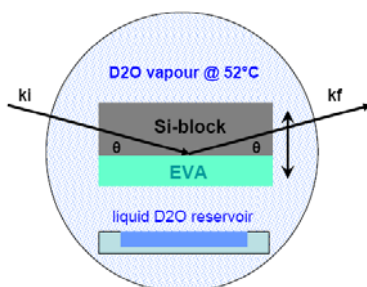


Fig. 1: Experimental setup. The sample is hosted in a humidity chamber made from aluminium. The closed chamber is water-tempered at 52°C and supplies a liquid D<sub>2</sub>O reservoir of ca. 10 ml for installation of saturated D<sub>2</sub>O vapour atmosphere.

The measured data show that the reflectivity is higher for samples placed in a saturated D<sub>2</sub>O atmosphere than in dry air. The sample measured against liquid D<sub>2</sub>O has the highest reflectivity of all samples. Sample 3 which has been stored in a saturated D<sub>2</sub>O atmosphere for 18 days before the measurement has reflectivity values between those of a sample measured against liquid D<sub>2</sub>O and those of a sample which has not been pre-treated with D<sub>2</sub>O vapour before measurement (see Fig. 2). This indicates that the D<sub>2</sub>O vapour diffusion into the

polymer is a slow process which takes a couple of days to achieve maximum D<sub>2</sub>O concentration in the polymer.

The height scans of the June 09 and October 09 samples show significant differences. It seems that the October samples are made of three layers with different neutron absorption (see Fig. 3). At the moment it is not clear how this structure could be formed. Therefore continuous measurements have to be made.

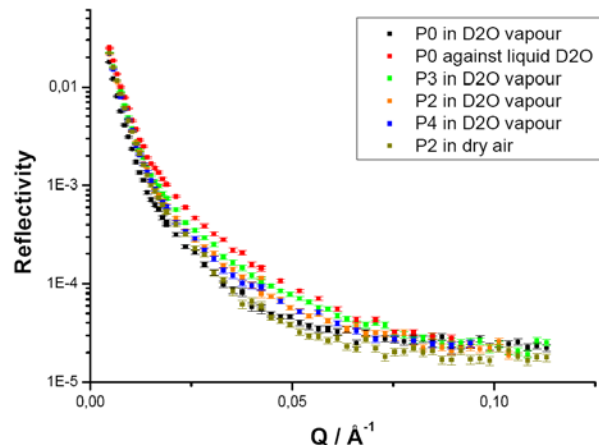


Fig. 2: Neutron reflectivity from silicon/EVA interface in air and D<sub>2</sub>O at 52°C

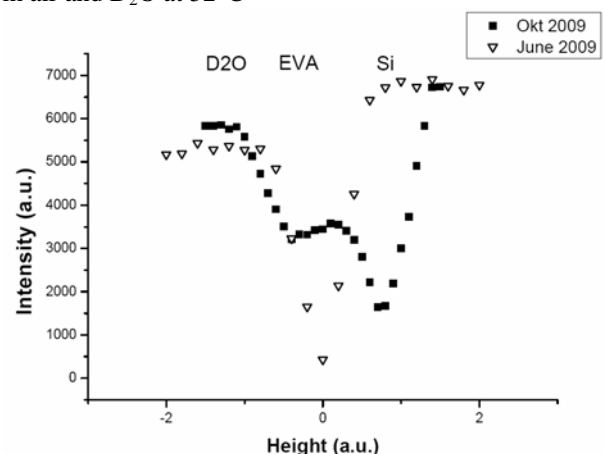


Fig. 3: Height scan of an EVA/Si sample

Principal Proposer: C. A. Helm, EMAU Greifswald  
Experimental Team: O. Ivanova, EMAU Greifswald  
O. Soltwedel, EMAU Greifswald  
P. Nestler, EMAU Greifswald  
M. Meyer, EMAU Greifswald

Date(s) of Experiment

24.09.2009 – 28.09.2009  
25.11.2009 – 29.11.2009

Date of report: 26.02.2010

Polyelectrolyte multilayers (PEM) are formed by sequential adsorption of oppositely charged polyelectrolytes from aqueous solutions [1]. The thickness of the first PEMs described in the literature increases linearly with the number of deposition cycles [1], later exponential growth was found [2]. The difference is attributed to diffusion. Nondiffusing polyelectrolytes (i.e., most synthetic, strong polyelectrolytes) cannot diffuse, resulting in spatially organized structures wherein each deposited species is only able to interact with neighboring layers in close proximity (usually two to three layers). However, diffusing polyelectrolytes (i.e., many polypeptides and polysaccharides) are assumed to be able to rapidly diffuse throughout PEMs architectures during assembly, resulting in exponential film growth and poorly organized, blended structures. To verify and eventually quantify this concept, intralayer diffusion needs to be measured. We start with PEMs showing linear growth.

Each PEM consists of a protonated and a deuterated block,  $p_{14-n}d_n$ , similar to [3] (cf. Fig. 1). This film architecture was selected to obtain as few independent parameters as possible, specifically the thickness and the scattering length density of each block, as well as the internal roughness between the blocks. [4]

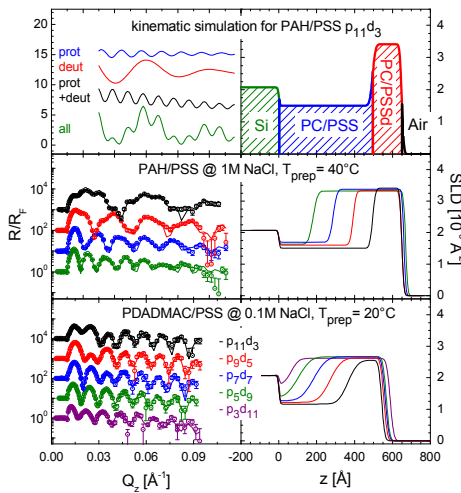


Fig. 1. Normalized neutron reflectivity curves (left) and corresponding scattering length density profiles (right). Top: Concept of film architecture: The calculated reflectivity (green) is a superposition of the interference fringes of the protonated block  $p_{14-n}$  (14-n polycation/PSS bilayers, blue), the deuterated block  $d_n$  (n polycation/PSS-d bilayers, red) and the total film  $p_{14-n}d_n$  (black). Centre and Bottom: Experiments on PAH/PSS and PDADMAC/PSS at 0% r.h. For clarity, the reflectivity curves are shifted relative to each other.

Poly (diallyl-dimethyl ammoniumchloride) (PDADMAC) is used as one polycation, since it is very popular strong polyelectrolyte, especially for biological applications [1]. The other polycation is poly(allyl amine) (PAH). Poly(sty-

rene sulfonate) (PSS) is always the polyanion. The deposition conditions are standard for PDADMAC/PSS (0.1 M NaCl, 20°C); they were adjusted for a similar film thickness for PAH/PSS (1 M NaCl, 40°C).

From the scattering length density profiles (cf. Fig. 1) the internal structure is found to monitor the growth of the PEM (cf. Fig. 2). However, the first five bilayers are thinner than the average bilayer in the PEM core. The deviation is more pronounced for PDADMAC/PSS; for that film the terminating three bilayers are thicker than in the core.

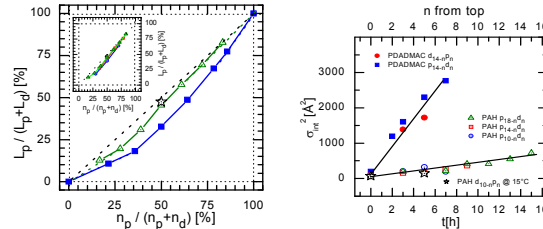



Fig. 2. Left: Thickness of the protonated block  $L_p$  normalized with respect to the total film thickness  $L_p + L_n$  for PAH/PSS ( $p_{18-n}d_n$ , green) and PAH/PSS ( $p_{14-n}d_n$ , blue) as function of number of deposited bilayers  $n_p$  normalized by total number of bilayers,  $n_p + n_d$ . Right: Square of internal roughness,  $\sigma_{int}^2$ , vs. number of bilayers separating the internal interface from the film/air interface, or vs. time the film stayed in various deposition solutions. Deposition conditions as in Fig. 1, if not indicated otherwise.

Counting from the top, the internal roughness increases with the number of deposited bilayers (cf. Fig. 2). For PAH/PSS, it grows from 10 to 25 Å, the latter number is measured 15 bilayers beneath the film/air interface. The corresponding numbers for PDADMAC/PSS are 14 Å, up to 55 Å, measured seven bilayers beneath the top (9 or 11 bilayers down  $\square_{int}^2$  cannot be determined reliably, cf. Fig. 1). Obviously, each deposition step promotes intralayer diffusion. Mathematically, it is a 1-dimensional diffusion [5], with an error function as solution. Similarly, in the kinematic model the internal interface of the SLD profile is described by an error function [1]. Comparing coefficients, one obtains  $\square_{int}^2 = 2 D t$  (with  $D$  as diffusion coefficient and  $t$  as time). We assume that layer interdiffusion takes place during the deposition process only (30 min for each layer). Then, the diffusion coefficient is for PAH/PSS ( $5.3 \cdot 10^{-20} \text{ cm}^2 \text{ s}^{-1}$ ) two orders of magnitude smaller than for PDADMAC/PSS ( $7.8 \cdot 10^{-18} \text{ cm}^2 \text{ s}^{-1}$ ).

#### Literature

- G. Decher. *Science* **277** (1997) 1232; Schönhoff, M., *Journal of Physics: Condens. Matter* **15** (2003), 1781; Klitzing, R.v., *PCCP*, **8** (2006), 5012
- Ladam, G., P. Schaad, J.C. Voegel, P. Schaaf, G. Decher, and F. Cuisinier. *Langmuir* **16** (2000) 1249
- O. Ivanova, O. Soltwedel, M. Gopinadhan, R. Köhler, R. Steitz, C.A. Helm, *Macromolecules* **41** (2008) 7179
- O. Soltwedel, O. Ivanova, P. Nestler, M. Müller, R. Köhler, CA. Helm, *JACS*, *subm.*
- J. Crank, *Mathematics of Diffusion*, Wiley, New York, 1992

 <b>HELMHOLTZ ZENTRUM BERLIN</b> für Materialien und Energie  <b>NEUTRONS</b>	<b>EXPERIMENTAL REPORT</b>  <b>Evaluation of systematic Hofmeister effects on protein adsorption</b>	Proposal: CHE-04-1963  Instrument: <b>V6</b>  Local Contact: Roland Steitz
	Principal Proposer: Claus Czeslik, TU Dortmund, Germany Experimental Team: Florian Evers, TU Dortmund Metin Tolan, TU Dortmund Roland Steitz, HZB Christoph Jeworrek, TU Dortmund	Date(s) of Experiment  25.03.2010 - 01.04.2010

Date of report: 28.01.2011

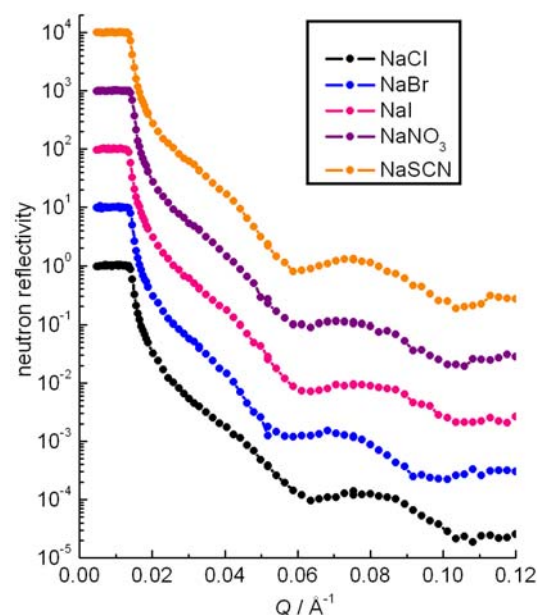
We have found recently by using neutron reflectometry that both kosmotropic and chaotropic cosolvents lower the degree of protein adsorption at aqueous-solid interfaces [1-3]. This effect has been observed for non-ionic cosolvents, such as urea, glycerol and other osmolytes, and ionic cosolvents, such as  $(\text{NH}_4)_2\text{SO}_4$  and  $\text{Ca}(\text{SCN})_2$ . Since kosmotropic and chaotropic agents interact with dissolved protein molecules in a rather different way, their influence on adsorbed proteins needs further investigation.

In 1888, Hofmeister described a ranking of ions according to their effectiveness in precipitating hen egg-white proteins [4]. This Hofmeister series has also been found to rule the conformational stability of native proteins in aqueous solution. In the case of anions, the following order is often reported:  $\text{SO}_4^{2-} > \text{F}^- > \text{CH}_3\text{COO}^- > \text{Cl}^- > \text{Br}^- > \text{I}^- > \text{ClO}_4^- > \text{SCN}^-$ . From the left to the right of this series, ions stabilize (kosmotropic) and destabilize (chaotropic) native protein molecules.

The results outlined above suggest that kosmotropic salts reduce the degree of protein adsorption by disfavoring a conformational adaption and a dehydration of the protein molecules at a hydrophobic surface. On the other hand, chaotropic salts shield hydrophobic interactions between the protein molecules and the substrate surface by saturating hydrophobic patches on the protein surface. The data obtained so far do not support the idea of a single Hofmeister effect ranging from kosmotropic to chaotropic ions.

However, in the current project, we aimed at analyzing chaotropic ions separately, in order to investigate, if there might be a systematic behaviour of Hofmeister ions within the chaotropic part, only. To achieve this goal, we have spin-coated silicon wafers with a thin film of perdeuterated poly(styrene), dPS. The adsorption of the model protein RNase from  $\text{D}_2\text{O}$  solution onto this surface has been quantified by applying neutron reflectometry. A hydro-

phobic dPS surface has been used in order to rule out any direct electrostatic protein-interface interactions, which may also be modulated by the ionic strength. Furthermore, dPS and  $\text{D}_2\text{O}$  have almost the same neutron scattering length density, which greatly enhances the neutron sensitivity for adsorbed proteins. Selected data, as obtained in the experiments, are shown in Fig. 1. They will be analyzed with a layer model, in order to obtain structural information about the protein adsorbates that were formed in the presence of various salts.




**Fig. 1:** Neutron reflectivity data of RNase that has been adsorbed at a hydrophobic poly(styrene) film in the presence of various salts selected from the Hofmeister series.

#### References:

- [1] J. Koo, T. Gutberlet, C. Czeslik, Control of protein interfacial affinity by nonionic cosolvents, *J. Phys. Chem. B* **112** (2008) 6292-6295.
- [2] F. Evers, R. Steitz, M. Tolan, C. Czeslik, Analysis of Hofmeister effects on the density profile of protein adsorbates – a neutron reflectivity study, *J. Phys. Chem. B* **113** (2009) 8462-8465.
- [3] F. Evers, R. Steitz, M. Tolan, C. Czeslik, Reduced protein adsorption by osmolytes, *Langmuir*, submitted.
- [4] F. Hofmeister, *Arch. Pharmacol.* **24** (1988) 247.



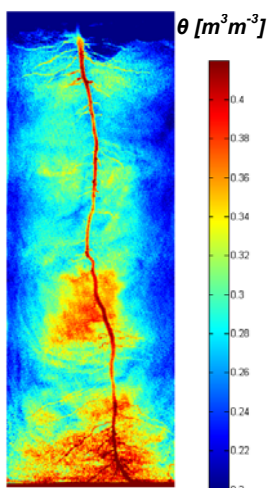
	<b>EXPERIMENTAL REPORT</b>  <b>Visualisation of plant root structure and water uptake from soil using neutron radiography and D<sub>2</sub>O</b>	Proposal: BIO-04-1944 Instrument: <b>V7</b> Local Contact: N. Kardjilov
Principal Proposer: Experimental Team:	S.E. Oswald, Uni Potsdam U. Matsushima, Iwate University, JP A. Carminati, UFZ Leipzig N. Rudolph, Uni Potsdam A. B. Moradi, UFZ Leipzig H.G. Esser, Uni Potsdam A. Hilger, HZB N. Kardjilov, HZB	Date(s) of Experiment  12.03.2010 - 15.03.2010

Date of report: 31/12/2010

Root-induced water dynamics have a strong impact on soil water balance. Nevertheless, due to technical limitations there is still a lack of knowledge concerning root water uptake dynamics.

By neutron radiography it is possible to visualize in situ water movements in soil at high temporal and spatial resolution. Using heavy water (D<sub>2</sub>O) as a tracer, water fluxes from soils to roots and within the root system can be detected.

In our experiment we used 3 glass containers (30 x 10 x 1 cm<sup>3</sup>) filled with an artificial quartz-sand-mixture and planted with a white lupin (*lupinus albus* L.) or a blue lupin (*lupinus angustifolius* L.). After a growing period of 20 days we cut the stem of one blue lupin in order to interrupt transpiration. Then, we infiltrated D<sub>2</sub>O into all the samples by a peristaltic pump. The slabs with the blue lupins were rewetted from the bottom by 20g of D<sub>2</sub>O (data not shown), whereas the one with the white lupin was infiltrated from the top by adding 30g of D<sub>2</sub>O. During and after each infiltration procedure, a neutron radiography time-series was taken. In vertical direction we took up to 5 pictures to get an impression of the entire sample (field of view at CONRAD: 10 x 10 cm) considering a homogeneous illumination.



**Figure 1:** Image mosaic from 5 neutron radiographies. Stitched picture shows water content in the vicinity of a blue lupin root.

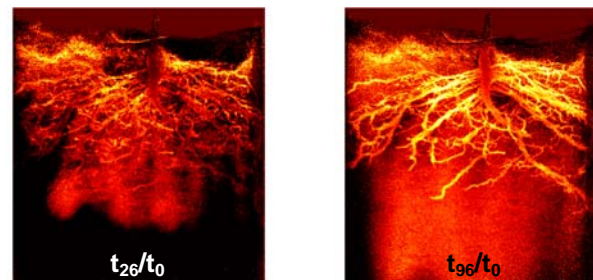
considering a homogeneous illumination. The images were corrected for flat field, zingers, spectral effect, and CCD dark current by the IDL tool QNI (Quantitative Neutron Imaging). This program is based on Monte Carlo simulations of neutron transport and Point Scattered Functions.

The images were corrected for flat field, zingers, spectral effect, and CCD dark current by the IDL tool QNI (Quantitative Neutron Imaging). This program is based on Monte Carlo simulations of neutron transport and Point Scattered Functions.

The 5 images were stuck together vertically by applying the ImageJ plugin “TrakEM2” (Figure 1). Figure 2 shows our main observations:

- D<sub>2</sub>O entered the roots of non-transpiring plants (data not shown) and of transpiring plants within the first few minutes of infiltration.
- D<sub>2</sub>O first entered young, fine roots. Later it also went into higher order, older roots.
- D<sub>2</sub>O moved in the laterals towards the main root. It also flowed upwards towards the soil surface in the tap root of transpiring plants.


Since D<sub>2</sub>O also entered into the roots of the non-transpiring plant, we suppose that water flux from soil to roots was (mainly) driven by diffusion where water advance within the root-system



**Figure 2:** Quotient of time series radiography of D<sub>2</sub>O infiltration into soil with white lupin. D<sub>2</sub>O enters faster into fine roots. Transport within the root is visible. Dark is H<sub>2</sub>O, bright is D<sub>2</sub>O. t<sub>26</sub>=20min, t<sub>96</sub>=73min.

should be driven by convection. Varying flow velocity into different root sections seems to be related to decreasing root permeability at increasing root age.

Further experiments are required to verify our hypotheses. Local injection of D<sub>2</sub>O would help to distinguish advection from diffusion processes and to improve understanding about the specific contribution on water uptake by different root sections.

	<b>EXPERIMENTAL REPORT</b>  <b>Combining neutron radiography and fluorescence imaging to simultaneously record dynamics of oxygen, pH and water</b>	Proposal: BIO-04-2024  Instrument: <b>V7</b>  Local Contact: Dr. N. Kardjilov
	Principal Proposer: Nicole Rudolph, Uni Potsdam Experimental Team: Ahmad B. Moradi, UFZ Leipzig Sascha E. Oswald, Uni Potsdam Nikolay Kardjilov, HZB Andre Hilger, HZB	Date(s) of Experiment  21.08.2010 – 26.08.2010

Date of report: 31.01.2011

We have established and optimized a quantitative approach for studying plant roots and soil materials with neutron radiography. The results show that the interaction between roots and soil are very dynamic and heterogeneous. Furthermore, we developed a fluorescence imaging set-up to monitor the dynamics of oxygen around the roots. The combination of both imaging techniques provides the possibility to study the dynamics of oxygen and water content at the same time at the complex soil-plant interface.

In our experiments we used 2 glass containers of 15x15x1.5 cm<sup>3</sup> filled with an artificial quartz-sand mixture planted with white lupine (*lupinus albus L.*). A clay layer separated the lower and the upper part of the container. Additionally we used 4 glass containers of 10x10x1 cm<sup>3</sup> filled again with the quartz-sand mixture. We grew two blue lupines (*lupinus angustifolius L.*) and two white lupines. The sensor foils for oxygen were attached to the vertical inner-side of the container. We also used a foil sensitive for pH, for the first time. This foil allowed only a qualitative impression of locations where pH changes took place.

After a growing period of two weeks we imaged the root growth, water content and oxygen distribution. The two 15x15x1,5 cm<sup>3</sup> containers were radiographed with 9 single images because of the small field of view at CONRAD to ensure homogeneous illumination.

The images were corrected for flat field, zingers, spectral effects, and CCD dark current via applying the software QNI (Quantitative Neutron Imaging) by Hassanein (2006). The images were stitched together by applying the ImageJ plugin "TrakEM2". Water content ( $\theta$ ) was calculated from the corrected and stitched images according to Carminati (2007).

The combination of both methods works well. We are able to simultaneously record the dynamics of oxygen and water content with the perspective to add pH detection. This combined set up results in two characteristic features. Firstly, the radiographs

show the roots and the root development and, secondly, we are able to directly link the root activity to the pattern of oxygen and pH.

Concerning the distribution of oxygen we were able to visualize that oxygen depletion zones are spatially correlated to the location of roots. With respect to pH we visualized locations of acidification for a living plant. Furthermore, we observed a spatial variation along the root axes: young roots showed a strong acidification of their rhizosphere whereas older roots show an alkalization of their vicinity. Secondly, the radiographs visualized the water content distribution with a high spatial and temporal resolution. With reference to oxygen distribution we visualize that high water contents limits the oxygen diffusion and resulted in oxygen depletion zones (Fig.1).

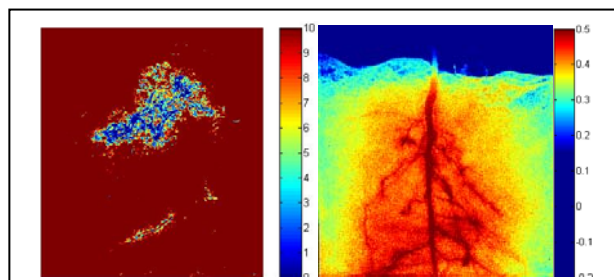


Figure 1: Calculated oxygen (left) and water content (right) distribution in a homogeneously filled container

Due to ongoing transpiration activities of the plants the water content decreased and allowed for better oxygen re-supply via the gas phase. Concerning pH we observed a direct link between water content and the acidifying effect, presumably from root exudates. High water content seemed to dilute the root exudates whereas for drier soil the acidification of the rhizosphere was stronger.

In conclusion, we established the experimental set up and now further investigations are possible to quantitatively understand the mechanisms involved.

 <b>HELMHOLTZ ZENTRUM BERLIN</b> für Materialien und Energie  <b>NEUTRONS</b>	<b>EXPERIMENTAL REPORT</b>  <b>Structure of DNA films</b>	Proposal: MAT-04-2041-EF  Instrument: <b>V18</b> Local Contact: Marcus Strobl
	Principal Proposer: Alisa Becker, Helmholtz-Zentrum Berlin Experimental Team: Martin Kreuzer, Ruprecht-Karls-Universität Heidelberg Markus Strobl, Helmholtz-Zentrum Berlin Roland Steitz, Helmholtz-Zentrum Berlin Matthias Reinhardt, Helmholtz-Zentrum Berlin	Date(s) of Experiment  30.08.2010 – 04.09.2010

Date of report: 31.01.11

DNA is a valuable tool for the bottom-up assembly of nanostructured materials. Neutron reflectometry was used to examine thin DNA films during the layer-by-layer assembly method. The structure of DNA films, specifically their thickness, density and roughness, were the parameters of interest for neutron reflectometry.

A DNA film was assembled by alternate adsorption of DNA sequences onto a precursor layer of positively charged poly(ethyleneimine) (PEI). The well characterised homopolymeric DNA sequences of PolyA<sub>15</sub>PolyG<sub>15</sub> and PolyC<sub>15</sub>PolyT<sub>15</sub> in a D<sub>2</sub>O sodium citrate buffer with 0.5 M NaCl were used in the first instance. The initial PEI layer was successfully adsorbed as observed in the neutron reflectometry curve (Figure 1, black line). After 4 layers and 10 layer of DNA had been adsorbed the reflectometry was measured again. An increase in roughness was observed but no increase in the film thickness (Figure 1, red and green lines). DNA films are known to be highly hydrated and not very dense. To increase the contrast of the film, it was reassembled in a higher salt concentration, 2 M NaCl. Again, the PEI precursor layer was observed (Figure 1, cyan line) but no increase in thickness when the DNA layers were assembled (Figure 1, magenta line).

To understand if the DNA films are assembling or not, a standard polyelectrolyte multilayer (PEM) film was assembled as a precursor layer. Characteristic Kiessig oscillations were seen in the reflectometry signal (Figure 2, black line). After assembling DNA on the surface of the PEM film, the reflectometry signal was dampened (Figure 2, red line). This indicates increased roughness, showing that some DNA is assembling on the film. However it is not in a uniform thin film of sufficient contrast for neutron reflectometry. Thus, DNA films are not structured similarly to other layer-by-layer assembled PEM films.

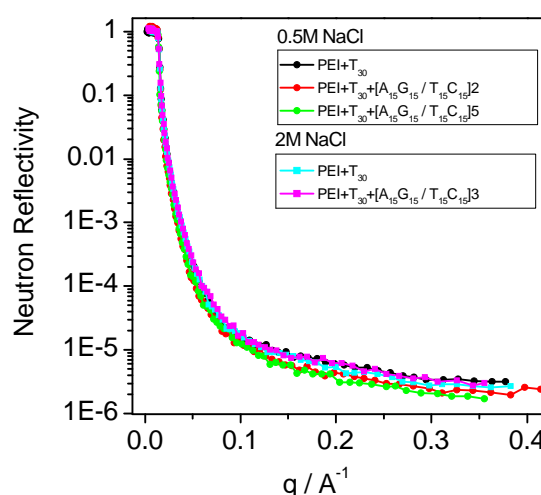


Figure 1. Reflectivity of polymer precursor films and DNA films against a solution of 10 mM Sodium Citrate buffer in D<sub>2</sub>O with varying salt concentration.

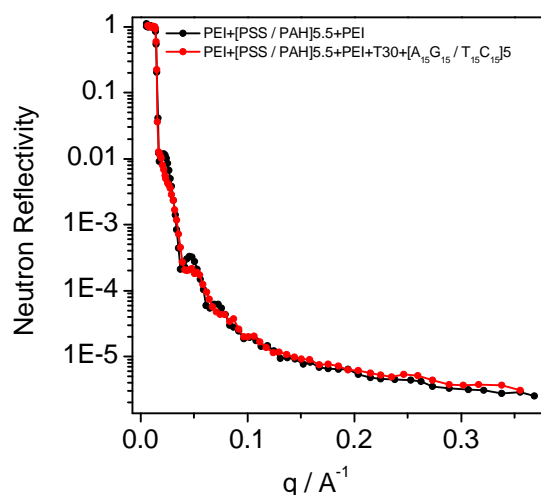



Figure 2. Reflectivity of polymer precursor films and DNA films against a solution of 10 mM Sodium Citrate buffer in D<sub>2</sub>O with 2 M NaCl.

*This research project has been supported by the German Ministry for Education and Science (BMBF) through Contract n°: 05KN7VH1. Additional financial support was received from HZB.*

 <b>HELMHOLTZ ZENTRUM BERLIN</b> für Materialien und Energie  <b>NEUTRONS</b>	<b>EXPERIMENTAL REPORT</b>  <b>Phase transition of the lipid molecule DMPC in a combined Neutron Reflectivity and FTIR experiment</b>		Proposal: EF  Instrument: <b>V18</b> Local Contact: Markus Strobl
	Principal Proposer: Martin Kreuzer, Ruprecht-Karls-Universität Heidelberg Experimental Team: Markus Strobl, Helmholtz-Zentrum Berlin Roland Steitz, Helmholtz-Zentrum Berlin Reiner Dahint, Ruprecht-Karls-Universität Heidelberg	Date(s) of Experiment  14.05.2010 - 16.05.2010	

Date of report: 17.01.2011

DMPC lipids (1,2-dimyristoyl-*sn*-glycero-3-phospho-choline) are well known to undergo a phase transition from their gel-like  $L_{\beta}'$  ( $P_{\beta}'$ ) state to their liquid-like  $L_{\alpha}$  state between 21.5°C and 24.5°C as reported in literature. This phase transition is held responsible for lamellae (layer) thickness variations measured by neutron reflectivity around the phase transition temperature,  $T_M$ . However, although underlining the correlation, reported phase transition temperatures for bulk systems as measured by different techniques seem to disagree slightly concerning the value of  $T_M$ . Consequently, temperature dependent combined neutron reflectivity (NR) and attenuated total reflection Fourier transformed infrared spectroscopy (ATR-FTIR) measurements (Figure 1) were performed around the main phase transition of a silicon supported lipid multilayer system against excess  $D_2O$  in the respective temperature range from 20 to 30 °C in order to directly correlate the response of the lipid multilayer as seen by both techniques (Figure 2). The neutron reflectivity measurements were performed with an instrumental resolution of 7% concerning the scattering vector component  $q_z$  probed in specular reflectivity mode resulting in a measurement time of about 40 minutes per scattering curve. [1]

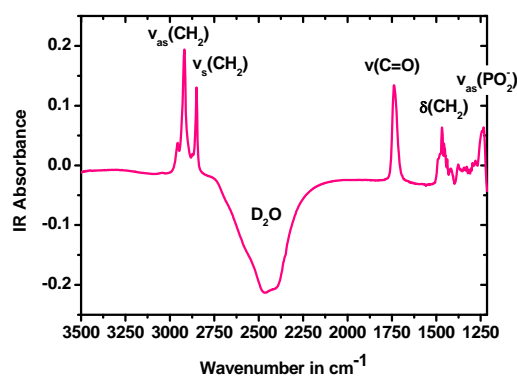


Figure 1: ATR-FTIR absorbance spectrum of a silicon supported DMPC multilayer against excess  $D_2O$ .

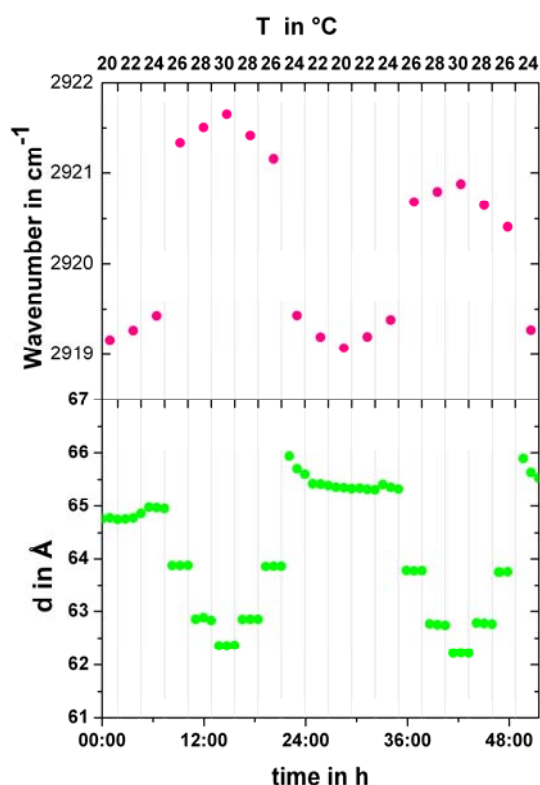



Figure 2: Results of a temperature dependent series focusing on the asymmetric vibrational mode of the  $CH_2$  groups in the IR spectrum (top) and the individual lipid layer thickness achieved from the simultaneous neutron reflectivity measurements (bottom).

The two techniques simultaneously applied on the same sample reveal the same main transition temperature. But, there are obvious differences in the way the phases are approached as seen by NR and ATR-FTIR. Detailed analysis of the data is under way.

[1] M. Strobl, R. Steitz, R. Dahint, M. Kreuzer, A. Nawara, F. Mezei, M. Rose, M. Grunze, Journal of Physics: Conference Series 251 (2010) 012059

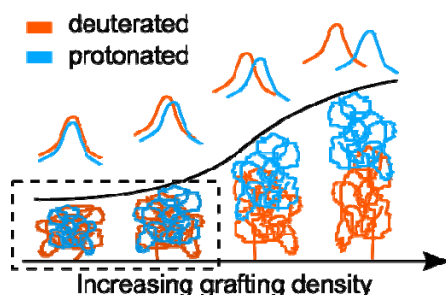
*The presented work has been supported by the Federal Ministry of Education, Research and Technology (BMBF) of Germany (Contract No. 05KN7VH1).*

 <b>NEUTRONS</b>	<b>EXPERIMENTAL REPORT</b>	Proposal: EF
	<b>Instrument test: Grafted PMMA film in the low-grafting-density-regime</b>	Instrument: <b>V18</b> Local Contact: M. Strobl
Principal Proposer: B. Stühn, TU Darmstadt Experimental Team: Martin Müller, TU Darmstadt Markus Appel, TU Darmstadt Andreas Weber, TU Darmstadt Markus Strobl, Matthias Reinhardt, HZB	Date(s) of Experiment  02.08.2010 – 07.08.2010	

Date of report: 20.01.2011

We are interested in conformations of grafted polymers on flat surfaces. Depending on grafting densities 3 general regimes are predicted: Low grafting density with less than  $\sigma=0.2$  chains per  $\text{nm}^2$  building separated mushroom-like structures and high grafting density with about 1 chain per  $\text{nm}^2$  consisting of stretched brushes. Both regimes are connected by an intermediate density region.

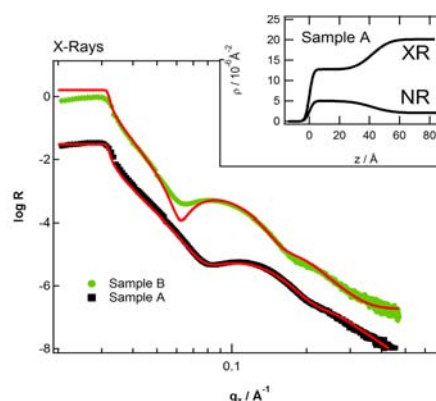
As a first step we investigated ATRP grafted d-PMMA (10.000-40.000 g/mol) on silicon wafers with low grafting densities  $\sigma < 0.2 \text{ nm}^{-2}$ . The d-PMMA contained a protonated block located either at the beginning or the end of the chain. Going from low to high grafting densities one expects a change in conformation as depicted in fig. 1 [1]. The density distributions of p- and d-PMMA separate along the z-axis when increasing the grafting density. In contrast to a SLD bilayer structure of stretched brushes with d-p-PMMA-blockcopolymers the mushroom conformation leads to a single layer of average SLD.



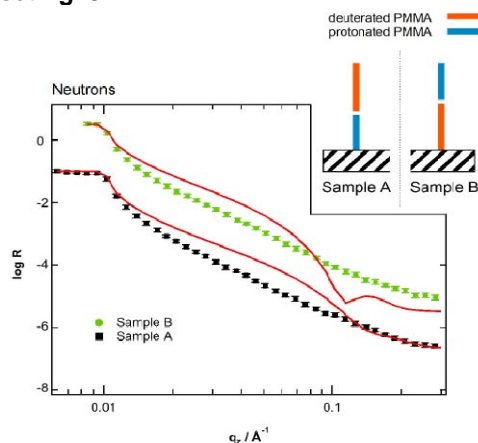
**Fig. 1 – Sketch of conformation development from low to high grafting density. The marked area shows the experimental densities.**

Preliminary experiments with X-Ray reflectivity showed well defined PMMA layers of 4-7 nm thickness. In neutron reflectivity we expected to see a single layer of corresponding thickness and average neutron SLD (see inset fig. 2). The red curve in fig. 3 show single layer reflectivity of calculated SLDs and parameters determined by X-Rays (fig. 2) compared with neutron data measured at V18. Unfortunately the mismatch between the scattering data and the model is unresolved to the present state. In the beam time

20 samples of different block lengths and labelling were measured. The analysis is still in progress.



**Fig. 2 – X-Ray spectra of d-p-PMMA single layers on silicon. Sample A and sample B differ in different ordering of polymerization onto silicon, see inset fig. 3.**



**Fig. 3 – Neutron spectra of d-p-PMMA single layers on silicon. The red line is a prediction of calculated SLDs, see text. The inset is a sketch of the order of polymerization of selected samples.**

Future experiments would contribute to compatible results in X-Rays and neutrons. We thank the HZB for the possibility to perform test measurements at V18.

[1] Brittain, W.J., Minko, S., J. POLYM. SCI. PART A: POLYM. CHEM.: VOL. 45 3505, (2007)

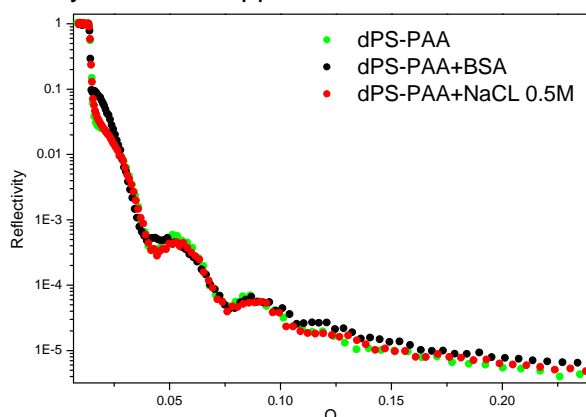
*The presented work has been supported by the Federal Ministry of Education, Research and Technology (BMBF) of Germany (Contract No. 05KN7VH1).*

 <b>HELMHOLTZ ZENTRUM BERLIN</b> für Materialien und Energie  <b>NEUTRONS</b>	<b>EXPERIMENTAL REPORT</b>  <b>Protein adsorption to charged polymer brushes</b>	Proposal: EF  Instrument: <b>V18</b>  Local Contact: Markus Strobl
	Principal Proposer: Roland Steitz, HZB Experimental Team: Matthias Reinhardt, HZB Martin Kreuzer, Uni Heidelberg Markus Strobl, HZB	Date(s) of Experiment 29.06.2010 – 07.07.2010 20.08.2010 - 22.08.2010

Date of report: 24.01.2011

Polymer brushes provide a soft interface for proteins, potentially without changing their functionality. Protein adsorption processes to such brushes at the solid-liquid interface can easily be followed by neutron reflectivity. Here, we report on a cross-check of preparation of a polyacrylic acid (PAA) brush on disc shaped Si Wafers ( $\varnothing$  6cm) and the achievement of additional contrast information on samples also investigated at AMOR/PSI.

For the preparation of a polymer brush on Si substrate we used deuterated polystyrene ( $M=5500$ ) – polyacrylic acid ( $M=16000$ ) block copolymer (dPS-PAA) and the Langmuir-Schäfer technique. In a first step the pre-cleaned Si wafer was spin-coated with a 20-30nm thick layer of deuterated polystyrene (dPS). A floating monolayer of the dPS-PAA block copolymer was then prepared on the surface of a Langmuir film balance. This monolayer was transferred to the pre-coated Si wafer at adjusted grafting density. Subsequent annealing of the sample firmly coupled dPS-anchor layer to dPS coating. This way, we achieved PAA brushes with thick dPS interlayers on Si-support.

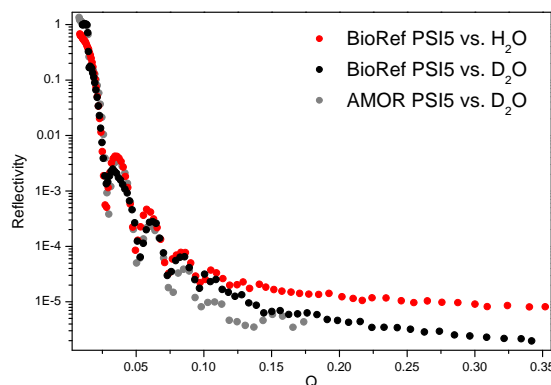


**Figure 1:** BSA adsorption/desorption at a charged PAA brush

The sample measured at BioRef was prepared at a grafting density of 0.1 polymers per  $\text{nm}^2$ . Figure 1 shows the neutron reflectivity measurements at the solid-liquid interface against  $\text{D}_2\text{O}$ ,  $\text{D}_2\text{O}$  + BSA (0.5 mg/ml) and

$\text{D}_2\text{O}$  + 0.5M NaCl in that order. There is a pronounced change in the reflectivity upon adsorption of BSA and upon addition of NaCl to the liquid phase. Protein adsorption to the like charged PAA brush (no NaCl) is known to be entropy driven with a concomitant release of counter ions from the protein into the bulk solution ( $\Delta S > 0$ ). At high salt concentration of the liquid phase  $\Delta S \sim 0$  and hence there is no net driving force of adsorption of screened BSA to the screened brush.


The second part of the experiment at BioRef was conducted after our measurements at AMOR/PSI. Here, we tried to achieve additional information on the SLD of the dPS layer and did a contrast variation measurement for a sample (PSI5) with a grafting density of  $0.2 \text{ nm}^{-2}$ . Figure 2 shows the neutron reflectivity measured vs.  $\text{H}_2\text{O}$  at BioRef and vs.  $\text{D}_2\text{O}$  at BioRef and AMOR/PSI.



**Figure 2:** contrast variation measurements

For the measurement vs.  $\text{H}_2\text{O}$  the SLD of the PAA brush matches that of  $\text{H}_2\text{O}$  and only the dPS layer should contribute to the reflectivity. The SLD of the dPS layer would thus easily be fitted. Figure 2 shows that the PAA-brush survives intermediate rest time in dried state and can be re-activated to full length by re-incubating in aqueous environment.

*BioRef is supported by the Federal Ministry of Education, Research and Technology (BMBF) of Germany (Contract No. 05KN7VH1).*

 <p><b>HELMHOLTZ ZENTRUM BERLIN</b> für Materialien und Energie</p> <p><b>NEUTRONS</b></p>	<p><b>EXPERIMENTAL REPORT</b></p> <p><b>Interaction of lipid multilayers with the polysaccharide hyaluronic acid</b></p>	<p>Proposal: EF</p> <p>Instrument: <b>V18</b></p> <p>Local Contact: Markus Strobl</p>
<p>Principal Proposer:</p> <p>Experimental Team:</p>	<p>Martin Kreuzer, Ruprecht-Karls-Universität Heidelberg</p> <p>Markus Strobl, Helmholtz-Zentrum Berlin Roland Steitz, Helmholtz-Zentrum Berlin Reiner Dahint, Ruprecht-Karls-Universität Heidelberg</p>	<p>Date(s) of Experiment</p> <p>14.06.2010 - 18.06.2010</p>

Date of report: 17.01.2011

The interaction of the lipid molecule DMPC (1,2-dimyristoyl-*sn*-glycero-3-phosphocholine) with the natural polysaccharide hyaluronic acid (HA) was studied in a combined experiment using neutron reflectivity (NR) and attenuated total reflection Fourier transformed infrared spectroscopy (ATR-FTIR) simultaneously. The neutron reflectivity measurements were performed with an instrumental resolution of 7% with respect to the scattering vector component  $q_z$  probed in specular reflectivity. This mode resulted in a measurement time of about 40 minutes per scattering curve. A lipid multilayer was prepared on a silicon ATR crystal by paint brush technique. After incubation of the sample in a solution of 3mg/ml HA in  $D_2O$  the film was tempered within a temperature range from 20°C to 50°C for 12 days. This yielded a highly orientated stack of lipid multilayers with a repeat distance  $d$  of 162Å (Figure 1, black circles).

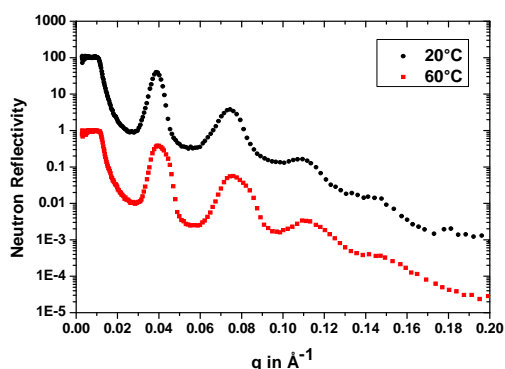


Figure 1

Subsequently the film was heated from 20°C to 30°C and cooled down again to 20°C with 0.5°C steps, followed by a temperature scan to 32°C with a step width of 2°C. By analyzing the first Bragg peak position and its amplitude it was possible to follow a swelling and shrinking behavior of the multilayer (Figure 2). Interestingly the infrared spectra showed that the swelling occurred in the liquid-like  $L_\alpha$  state of the lipid molecules, which is in contradiction

to results measured earlier against a solution of pure  $D_2O$  (not shown). Finally the film was heated up to 60°C (Figure 1, red squares). Further analysis is currently under way.

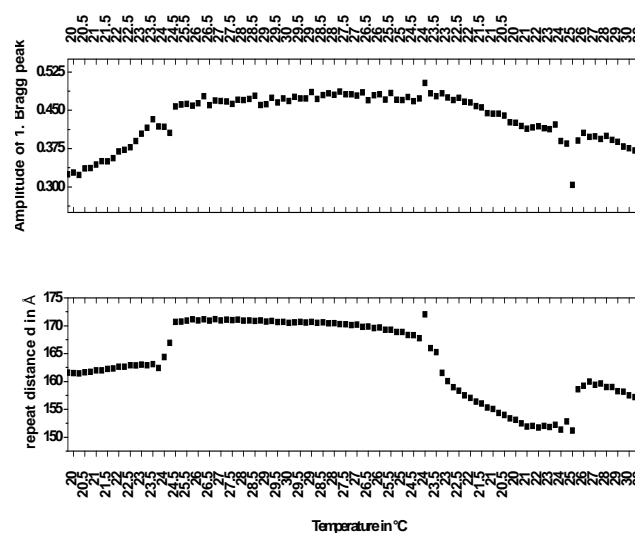



Figure 2: Analysis of first order Bragg peak of a DMPC multilayer, incubated in a solution of HA in  $D_2O$ . The temperature of the system was cycled between 20°C – 30°C – 20°C – 32°C.

*The presented work has been supported by the Federal Ministry of Education, Research and Technology (BMBF) of Germany (Contract No. 05KN7VH1).*

 <b>NEUTRONS</b>	<b>EXPERIMENTAL REPORT</b>	Proposal: EF
	<b>Origins of swelling of a lipid multilayer system induced by the polysaccharide HA</b>	Instrument: <b>V18</b> Local Contact: Markus Strobl
Principal Proposer:	Martin Kreuzer, Ruprecht-Karls-Universität Heidelberg	Date(s) of Experiment
Experimental Team:	Markus Strobl, Helmholtz-Zentrum Berlin Matthias Reinhardt, Helmholtz-Zentrum Berlin Roland Steitz, Helmholtz-Zentrum Berlin Reiner Dahint, Ruprecht-Karls-Universität Heidelberg	30.03.2010 - 01.04.2010

Date of report: 18.01.2011

Recent neutron reflectometry measurements against excess  $D_2O$  showed, that an oligolamellar DMPC lipid (1,2-dimyristoyl-*sn*-glycero-3-phosphocholine) bilayers coating detaches almost completely from its solid support at  $38^\circ C$  in its chain-disordered  $L_\alpha$  state. Up to now the mechanism of detachment of the oligolamellar DMPC stack at  $38^\circ C$  is unclear. On the contrary, oligolamellar lipid bilayers remain stable on a substrate at  $38^\circ C$ , when incubated with a solution of  $D_2O$  with negatively charged hyaluronic acid (HA): In an independent experiment, carried out at the V6 reflectometer at HZB (Exp. Nr. BIO-04-1893-EF), an oligolamellar lipid bilayers stack was measured against a solution of 3mg/mL HA in  $D_2O$ . The sample was investigated shortly after incubating at  $21^\circ C$  and after raising sample temperature to  $38^\circ C$  (**Figure 1**, gray circles). The oligolamellar lipid layer remained stable on the substrate and an immense swelling occurred with a repeat distance  $d$  of 276 Å. So far the origins of these effects are unknown.

The experiment we report here was focused on the interaction of a synthetic charged polymer with the oligolamellar lipid bilayers system to verify electrostatic interactions between charged molecules and the zwitter ionic head group of DMPC. As a reference system an oligolamellar DMPC lipid bilayers stack was measured against a solution of pure  $D_2O$ . For a whole reflectivity profile the sample was measured at four different angles to cover a  $q$ -range from  $0.01 \text{ \AA}^{-1}$  to  $0.18 \text{ \AA}^{-1}$ . **Figure 2** shows the detector image measured at  $1.9^\circ$ , with the full reflectivity profile in the inset. The Bragg peak at  $0.096 \text{ \AA}^{-1}$  corresponds to a repeat distance of 65 Å, which is in good agreement with literature for that system. A freshly prepared silicon substrate, covered with a lipid multilayer, was then incubated in a solution of the negatively charged polymer PSS in  $D_2O$ . A first neutron reflectivity measurement was recorded 7 hours after incubation at  $21^\circ C$  (**Figure 1**, black circles). As opposed to the measurement against pure  $D_2O$  a

swelling effect is already visible: The first Bragg peak at  $0.029 \text{ \AA}^{-1}$  corresponds to a repeat distance of 276 Å. 21hours after raising temperature to  $38^\circ C$  the Bragg peaks are even more pronounced (**Figure 1**, red circles).

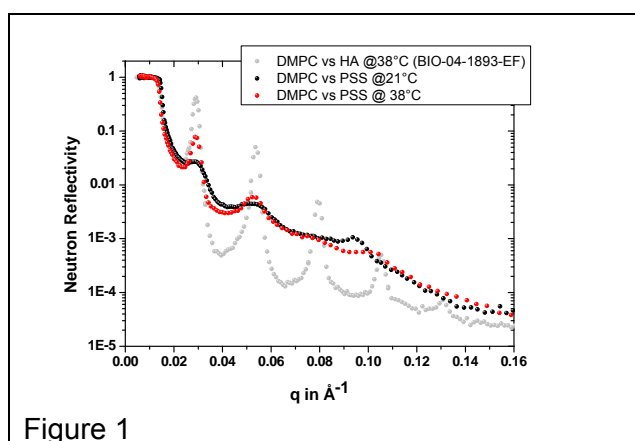


Figure 1

This basic analysis shows, that PSS also incorporates in the lipid layer system, even resulting in a similar repeat distance as in the case of incorporated HA. Further analysis of the data is on its way.

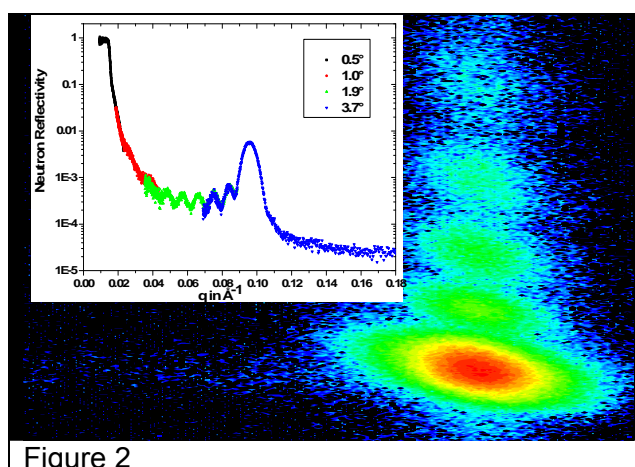



Figure 2

*The presented work has been supported by the Federal Ministry of Education, Research and Technology (BMBF) of Germany (Contract No. 05KN7VH1).*



 <p>HELMHOLTZ ZENTRUM BERLIN für Materialien und Energie</p> <p>NEUTRONS</p>	<p><b>EXPERIMENTAL REPORT</b></p> <p><b>Lateral phase separation in oriented bilayers made from an unsaturated, a saturated and a hybrid lipid at fixed humidity</b></p>	<p>Proposal: EF</p> <p>Instrument: <b>V18</b></p> <p>Local Contact: Markus Strobl</p>
<p>Principal Proposer: Experimental Team:</p>	<p>Chris Garvey, ANSTO, Lucas Heights, Australia Gary Bryant, RMIT University, Melbourne, Australia Taavi Hunt, RMIT University, Melbourne, Australia Martin Kreuzer, Ruprecht-Karls-Universität Heidelberg Markus Strobl, Ruprecht-Karls-Universität Heidelberg</p>	<p>Date(s) of Experiment</p> <p>24.09.2010 - 02.10.2010</p>

Date of report: 24.01.2011

Mixtures of saturated and unsaturated lipids are thought to undergo phase separation due to energetic cost of hydrophobic packing. It has been proposed that the literature uncertainty in the size of domains may be due to experimental observations in the various intermediate stages of total phase separation of saturated and unsaturated lipid and that the addition of a lipid containing both saturated and unsaturated tails may stabilize domains in well defined sizes by lowering the interfacial free energy between the unsaturated and saturated hydrophobic phases. The presence of hybrid lipids in reasonable quantities in natural systems gives physiological relevance to these observations. In this case we examine a model system of a deuterated saturated lipid Dipalmitoylphosphatidylcholine (DPPC), with a phase transition temperature of 41°C, hydrogenated hybrid lipid 1-palmitoyl-2-oleoyl-sn-glycero-3-phosphocholine (POPC) and a hydrogenated unsaturated lipid dioleoylphosphatidylcholine (DOPC). Deuteration has been used to add contrast for the neutron scattering measurement. Here we investigate the possibilities of using this model system for experimental studies of lipids rafts.

**Experimental Method:** Oriented bilayers were produced by spraying chloroform solution containing a lipid ratio of 1:2:2 (POPC: DOPC: d16-DPPC) on a silicon substrate with an airbrush, the chloroform removed by vacuum and then hydrated to equilibrium in an atmosphere of 75% relative humidity (RH – produced by a saturated aqueous solution of NaCl). The system was then cycled between 30°C and 55°C, with neutron reflectivity (Figure 1) and infrared spectroscopy (Figure 2) measurements at each temperature after equilibration of Bragg peak position, producing reproducible Bragg reflections. The instrumental resolution was set to 7% concerning the scattering vector component  $q_z$  probed in specular reflectivity mode. Using a position sensitive detector, we could also record the off-specular reflectivity,

which might give additional information about phase separation in the plane parallel to the silicon surface. This data is currently under evaluation. However, the phase transition visible in the shift of the  $\text{CH}_2$  vibrational modes of the infrared data, results in an additional Bragg peak series at 0.14 Å and 0.28 Å visible in the specular neutron reflectivity profiles. A phase separation in the z-direction of the multilayer system could be verified this way.

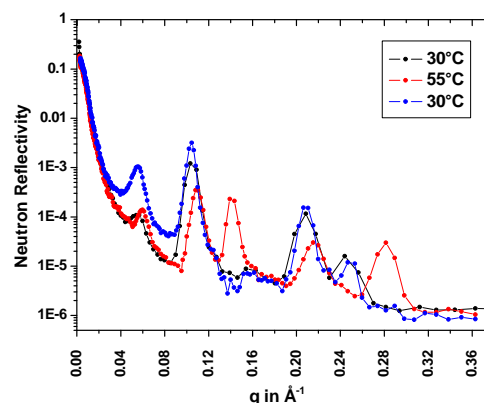


Figure 1: Specular neutron reflectivity profiles.

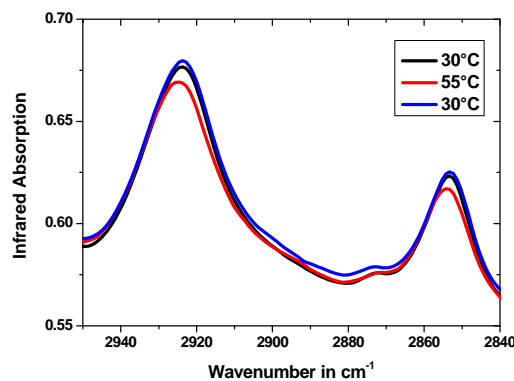


Figure 2: Infrared spectroscopy spectra

*The presented work has been supported by the Federal Ministry of Education, Research and Technology (BMBF) of Germany (Contract No. 05KN7VH1).*

# **Material Science**



Principal Proposer: I. Glavatskyi, HZB  
 Experimental Team: G. Firstov, Institute for Metal Physics, Kiev,  
 Ukraine  
 D. Wallacher, HZB

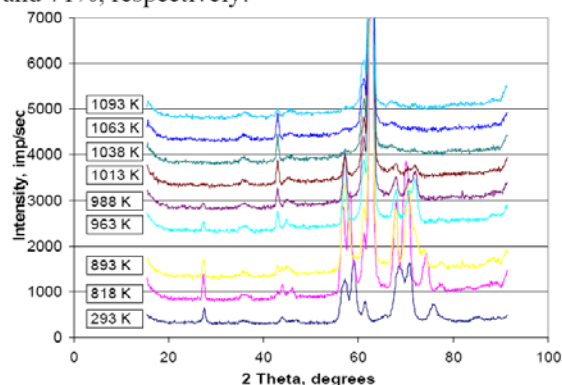
Date(s) of Experiment

08.03.2010 – 13.03.2010

Date of report: 10.06.2010

Two fine-grained non-textured polycrystalline specimens of  $Zr_2CuNi$  and  $Zr_2CoNi$  were studied as the function of temperature using the 2.4Å and 1.21Å wavelength at 30' collimation, with the temperature span of 15-50K on heating and cooling cycles through the martensitic transformation.

**$Zr_2CuNi$ :** A complex pattern at 293K, after Rietveld refinement, appeared to be a result of the mixture of two monoclinic phases: **1** – of the  $P2_1/m$  space group with  $B19'$  type of structure (3.336Å, 4.193Å, 5.235Å,  $\beta=103.1^\circ$ ); **2** -  $Cm$  space group (6.234 Å, 8.973 Å, 5.301 Å,  $\beta=103.8^\circ$ ). The volume fractions for  $B19'$  and  $Cm$  phases are 29% and 71%, respectively.

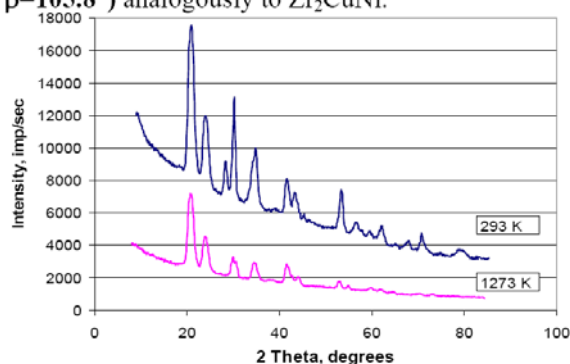


**Fig.1.** Evolution of the neutron diffraction patterns on heating of the  $Zr_2CuNi$  intermetallic compound.

Indeed, the pattern taken at 818 K shows the appearance of the austenitic peak just above 60 degrees and at expense of the  $B19'$  martensite, while the  $Cm$  phase appeared to be more stable, starting to diminish in intensities at higher temperatures. At 1063K the transformation to the austenite is completed but some peaks, nonmartensitic peaks remained. Moreover, taking into account  $Zr_2CuNi$  stoichiometry, it was unclear whether the austenite is a Heusler phase or is it of a  $B2$  type of structure. Quantitative Rietveld refinement for the phase analysis has shown that at 1063 K after reverse martensitic transformation completion the  $B2$  austenite phase undergoes decomposition with the precipitation of the  $Cu_{10}Zr_7$  phase and the whole material volume is occupied by 33% of  $Cu_{10}Zr_7$  phase and 77% of  $B2$  austenite.

**$Zr_2CoNi$ :** Room temperature (293K) neutron diffraction data (Fig.2) shows that at normal

conditions the entire volume is occupied with two monoclinic phases: one belongs to the  $P2_1/m$  space group and possesses  $B19'$  type of structure (3.274 Å, 4.05 Å, 5.34 Å,  $\beta=106.1^\circ$ ) and another belongs to  $Cm$  space group (6.439 Å, 8.461 Å, 5.362 Å,  $\beta=105.8^\circ$ ) analogously to  $Zr_2CuNi$ .




**Fig.2.** Evolution of the neutron diffraction patterns on heating of the  $Zr_2CoNi$  compound ( $\lambda=1.21\text{\AA}$ ).

In this case the volume fractions for  $B19'$  and  $Cm$  phases are 90% and 10%, respectively, which is significantly different from the  $Zr_2CuNi$ . In-situ heating with several scans at different temperatures did not reveal much change in the crystal structure of the phases observed except for the lattice parameters temperature dependence. It turns out that 1273K was not enough for the reverse martensitic transformation (no peaks from austenite phase appeared), which is also quite a surprise.

### Conclusions

1. NPD studies of the crystal structure of  $Zr_2CuNi$  and  $Zr_2CoNi$  intermetallic compounds revealed that in both cases the whole material volume at room temperature is occupied by two monoclinic martensitic phases belonging to  $P2_1/m$  ( $B19'$ ) and  $Cm$  space groups.
2. In the case of  $Zr_2CuNi$  the major martensitic phase is  $Cm$  (71% volume), while in the case of  $Zr_2CoNi$  the major phase is  $B19'$  (90% volume).
3. In-situ neutron diffraction studies on heating up to 1273K did not reveal any transformation for the case of  $Zr_2CoNi$ ; heating to 1093K revealed the reverse martensitic transformation in  $Zr_2CuNi$  with the primary disappearance of  $B19'$  martensite. Subsequent decomposition of the  $B2$  austenitic phase results in the formation of about 30% of  $Cu_{10}Zr_7$  phase.

 <b>HELMHOLTZ ZENTRUM BERLIN</b> für Materialien und Energie  <b>NEUTRONS</b>	<b>EXPERIMENTAL REPORT</b>  <b>Residual stress states in case hardened discs for the validation of simulation results</b>	Proposal: MAT-01-2496  Instrument: <b>E3</b>  Local Contact: Robert C. Wimpory
	Principal Proposer: Jeremy Epp, Uni Bremen Experimental Team: Thomas Hirsch, Uni Bremen Robert C. Wimpory, HZB Jeremy Epp, Uni Bremen	Date(s) of Experiment  09.06.2009 - 16.06.2009 19.07.2009 - 21.07.2009

Date of report: 10.12.2010

In the present study, the residual stress state of a low pressure case hardened and quenched disc from steel grade AISI 5210 (EN 20MnCr5) has been investigated by means of neutron and laboratory X-ray diffraction methods. These discs served as a simplified model for gear components. The measured results were compared to simulation results.

The case hardening was accomplished by low pressure carburization. Each batch consisted of eight disks hanging in a single layer. Carburization was carried out at 940 °C in a C<sub>2</sub>H<sub>2</sub>-atmosphere. The batch was gas quenched with 10 bar nitrogen after holding for 20 minutes at 840 °C. The case hardening depth was adjusted to 0.8 mm. The microstructure after quenching consisted of martensite and retained austenite in the carburized layer and martensite/bainite and retained austenite in the core.

For the X-ray diffraction measurements of the surface layer (up to 1.5 mm in depth) measurements of residual stress tensors were realized as the microstructure in the surface layer is composed of two phases (martensite and austenite). Moreover, in this type of material a triaxial residual stress state with  $\sigma_{33} \neq 0$  should be considered. For this, equations predicting changes of stress free lattice spacings as a function of the carbon content have been used.

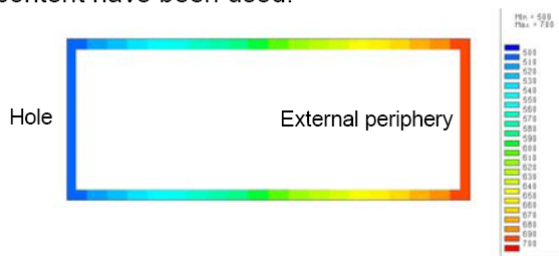


Figure 1: Distribution of the heat transfer coefficients on the half disc

For comparison, simulations of the case hardening process were made. For these simulations the commercial FEM-software package Sysweld® was used. Heterogeneities

in the heat transfer coefficients were used because of the gas quenching oriented from top to bottom. Values were between 500 and 700 W/m<sup>2</sup>K distributed as shown in Figure 1.

Neutron diffraction measurements were evaluated using  $d_0$  from cube measurements and with  $d_0$  calculated from a condition of axial force balance in the whole cross section. The results calculated with  $d_0$  from a condition of a force balance are about 50 MPa than those calculated with  $d_0$  from the cubes.

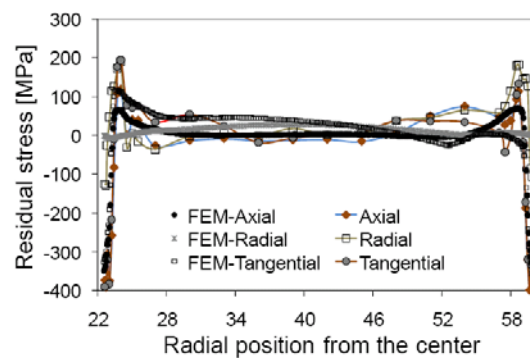



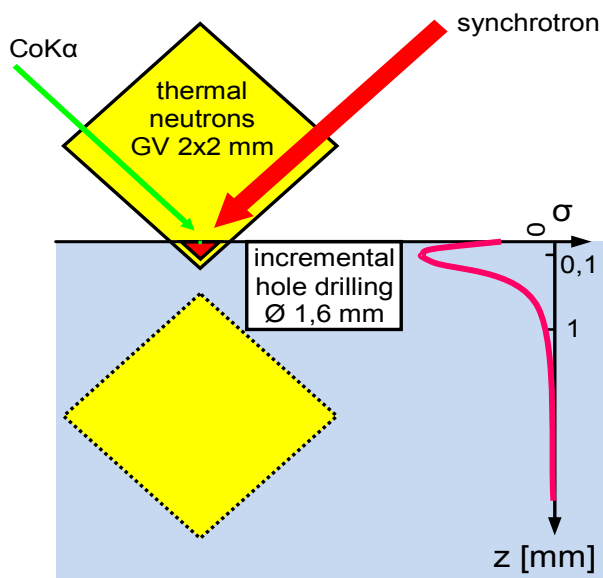
Figure 2: Residual stress distribution measured along the radius compared to simulation results

The comparison of the experimental results (obtained with  $d_0$  from the force balance criterion) with the simulation is given in figure 2. Simulation and experimental results show a satisfying overall agreement in the residual stress distribution but discrepancies are still present. In order to improve the simulation results, 3-dimensional simulations with enhanced streaming simulation of the gas quenching process will be employed.

 <b>NEUTRONS</b>	<b>EXPERIMENTAL REPORT</b>  <b>Complementary surface measurements (using synchrotron, neutron and hole drilling methods)</b>	Proposal: MAT-01-2809-EF  Instrument: <b>E3</b>  Local Contact: Robert C. Wimpory
	Principal Proposer: Robert C. Wimpory, HZB Experimental Team: Tillman Fuß, HZB Christoph Genzel, HZB Manuela Klaus, HZB	Date(s) of Experiment 14.09.2009 - 21.09.2009 28.09.2009 – 01-10.2009 03.10.2009 – 04.10.2009

Date of report: 21.01.2011

Complementary surface measurements (using synchrotron, neutron and hole drilling methods) have been made on specimens with strong surface strain gradients, in this case a shot-peened specimen. By none of these methods is it possible to cover the complete depth range and thus it is demonstrated that the combined application of surface sensitive X-ray methods and neutron diffraction used normally for bulk stress analysis allows for the study of residual stress gradients generated by mechanical surface treatment. Furthermore, it is shown that the hole drilling method can bridge the information gap between X-ray and neutron diffraction. Figure 1 shows the relative 'gauge volumes' over which the measurements are made.

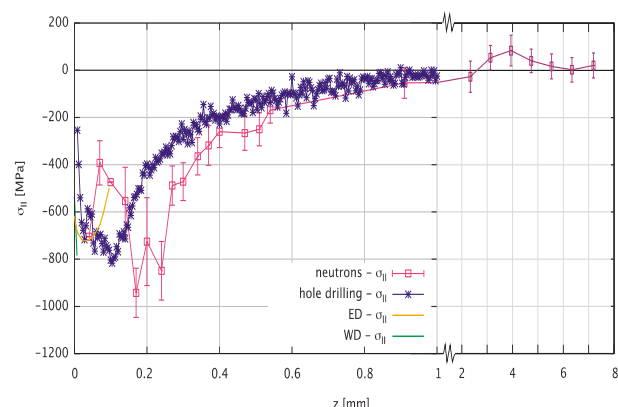


**Fig. 1:** Schematic view of the dimensions probed by the different methods for residual stress depth profiling used in this paper.

E3 is equipped with a perfectly bent Si(400) crystal monochromator, which has the ability to suppress the so-called surface effect [1] even when the gauge volume is not completely submerged in the material. For the through surface strain scanning investigations the

{211} ferrite reflection was analyzed. To increase the diffracted intensity, a 2 x 2 x 20 mm<sup>3</sup> 'match stick' gauge volume was used.

Although the different techniques differ considerably with respect to the information depth, it can be seen that the individual curves and depth profiles form a 'master plot' revealing a long-range residual stress gradient with a compressive stress maximum below the surface. The maximum accessible information depth that could be analyzed in the present case with photons is about 100 μm. The information depth covered with neutron diffraction lies between about 50 μm and 7 mm, but from Fig. 2 it becomes apparent that the region below about 250 μm contains less reliable results indicated by the large error bars. With the incremental hole drilling method, on the other hand, we were able to close the gap in the information depth between the photon and neutron diffraction in the intermediate region between the nearest surface region and the bulk of the material, respectively.



**Fig. 2:** Comparison of the results obtained by all methods used in the present study for residual stress depth profiling.

[1] M. Vrana, P. Mikula: Mat. Sci. Forum 490 – 491 (2005) 234.

Principal Proposer: Markus Chmielus, HZB  
 Experimental Team: Robert C. Wimpory, HZB  
 Rainer Schneider, Beuth Hochschule, Berlin  
 Peter Müllner, Boise State University, USA  
 David C. Dunand, Northwestern University, USA

Date(s) of Experiment

08.03.2010 – 16.03.2010

Date of report: 05.01.2011

Recently, we have shown that a polycrystalline Ni-Mn-Ga magnetic shape-memory alloy (MSMA), when containing two populations of pore sizes, shows very high magnetic-field-induced strain (MFIS) of up to 8.7% [1,2]. Here, the amount, orientation and martensite structure of the grains of the MSMA sample that showed 8.7% was investigated.

The sample was mounted onto an Euler cradle and rotated around its longest axis by 180° for ten different  $\chi$  angles from 0° to 90°. The diffractograms of each  $\chi$  step were analysed (see Fig.1 for an exert of four  $\chi$  steps) and the clearly identified grains were plotted in a  $\chi$ - $\Omega$  orientation map (Fig. 2).

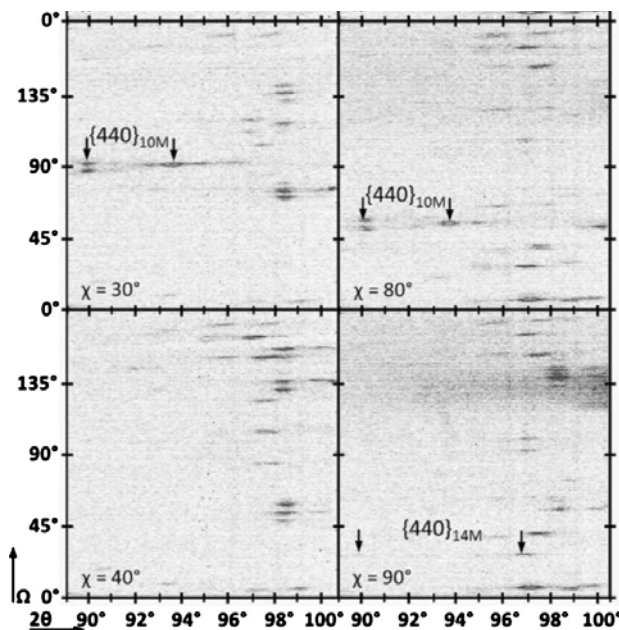


Figure 1: Excerpt of the neutron diffractograms of the foam sample for four  $\chi$  steps [3].

The diffractograms revealed six large, clearly identifiable grains - four with 10M and two with 14M structure with lattice parameters of the pseudo-tetragonal and pseudo-orthorhombic unit cells of  $a_{14M} = 6.11(3)$  Å,  $b_{14M} = 5.79(3)$  Å, and  $c_{14M} = 5.51(3)$  Å, and  $a_{10M} = b_{10M} = 5.91(2)$  Å and  $c_{10M} = 5.58(2)$  Å comparable to single crystalline 10M and 10M Ni-Mn-Ga MSMA.

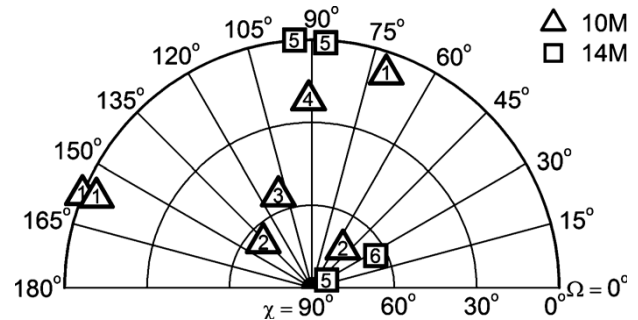


Figure 2:  $\chi$ - $\Omega$  orientation map showing the six identified 10M and 14M grains, labelled 1–6. Repeated labels are due to symmetry or twinning [3].

Two fundamental structure reflections i.e., reflection 2 at  $\chi = 73^\circ$ ,  $\Omega = 51^\circ$  and reflection 4 at  $\chi = 22^\circ$ ,  $\Omega = 90^\circ$  span over a large  $\chi$  range of 9° and 12°, respectively, while the other reflection span only over a 2° – 4° range. Integrating the (404) reflections of the six clearly identified grains and comparing their intensity with the sum of all six (404) reflections, grain 2 (10M) had the largest volume fraction of 38%. Grain 3 (10M) followed with 20%, grain 5 (14M) with 19%, grain 1 (10M) with 10%, grain 4 (10M) with 8%, and grain 6 (14M) with 5%.

The neutron diffraction experiments were accompanied by in situ magnetomechanical experiments and magnetization measurements at Boise State University and x-ray microtomography at the HZB (see MAT-04-1928-EF) [3].

This work was supported by the German Research Foundation (DFG) through priority program SPP 1239, National Science Foundation Division of Materials Research Grant Nos. DMR-0804984 (BSU) and DMR-0805064 (NU).

**References:**

- [1] M. Chmielus et al. Nature Mater. **8**, 863 (2009)
- [2] P. Müllner et al. Mater. Sci. Forum **635**, 119 (2010)
- [3] M. Chmielus et al. J. Appl. Phys. **108**, 123526 (2010)

Principal Proposer: Jeremy Epp, Uni Bremen  
 Experimental Team: Thomas Hirsch, Uni Bremen  
 Robert C. Wimpory, HZB  
 Jeremy Epp, Uni Bremen

Date(s) of Experiment

26.08.2010 – 03.09.2010

Date of report: 27.01.2011

Compared to previous measurements of discs with same dimensions, the investigated gear presents a different behavior in terms of residual stress distribution as well as Full Width at Half Maximum (FWHM) along the radius. FWHM are indicators for the residual stresses of 3<sup>rd</sup> kind which in this case characterize the microstructure.

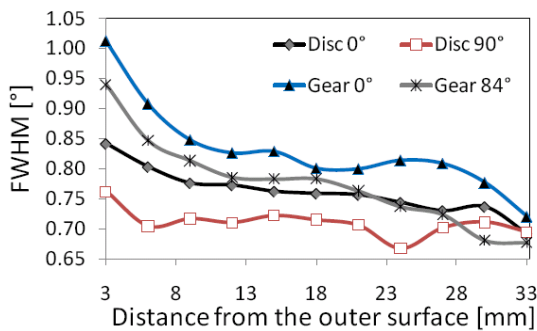


Fig. 1: FWHM Distribution measured along the radius of a disc and a gear at 0° and 90° (84°)

The distributions of FWHM in Fig.1 show that in the case of a disc, the distribution at 0° present a decreasing value while at 90°, almost no change of the FWHM occurs. This is due to the streaming direction during gas quenching, as the discs are hanging with their 0° mark at the top. As the 90° line is perpendicular to the streaming direction, no gradient is present. For the gear, gradients along the radius are present in the 0° as well as in the 84° direction (84° was measured instead of 90° in order to measure the head of a tooth). This proves that a different microstructure distribution is present in the case of gears compared to discs.

Measurements of a shaft were also done. The residual stress distribution along one single line over the diameter could be measured. A comparison of the measured residual stress distribution over the diameter and simulation data is given in Fig. 2. It can be seen, that the simulated residual stresses in the near surface area present a similar behavior as the

measured one. However, in the center (-5 to +5 mm), large discrepancies are found.

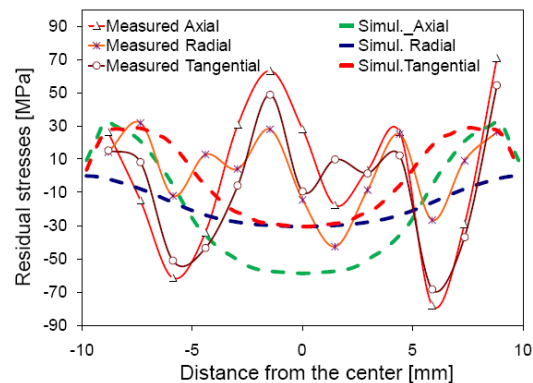


Fig. 2: Measured and simulated residual stress distribution along the diameter of a shaft

In previous investigations, it was found that the shafts present a particular microstructure distribution over the cross section. This is illustrated in Fig. 3, where a “square” appears after etching. Strong elements segregations are present that can be correlated to that “square”. This might induce differences in phase transformation behavior between surface and core. As this was not taken into account in the simulation, it could be the reason for the different distributions.

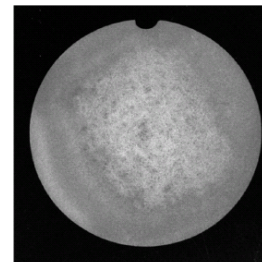


Fig. 3: Microstructure of the cross section of a shaft after etching



Principal Proposer: Thomas Nitschke-Pagel, Uni Braunschweig  
Experimental Team: Thomas Nitschke-Pagel, Uni Braunschweig  
Robert C. Wimpory, HZB

Date(s) of Experiment

25.05.2010 – 05.06.2010

Date of report: 27.01.2011

### Introduction:

Although many theories about the amount and the effect of tensile residual stresses in longitudinal stiffeners with fillet welds have been developed the knowledge about the real residual stress conditions is rather poor because only few experimental results with regard to the residual stresses respectively to their stability under certain loads are available.

### Experiment and results

Through thickness measurements of the spatial residual stress distributions (RS) around the top side of welds with longitudinal stiffeners have been carried out on E3 diffractometer and where combined with surface measurement performed by means of X-ray diffraction. The samples were 300x75x10 mm<sup>3</sup>-plates (AISI 304 stainless steel) with 75 mm long stiffeners which had been

concentrated on the neighbourhood of the weld seam and on the surface region. Over the entire cross section a smooth RS distribution without remarkable peaks is generated. Loads up to the yield strength of the base material do not affect the RS condition significantly. If the load exceeds the yield strength the plastifications occur in deeper layers. However the consequence is an increase of the near surface RS. As such effects are not yet considered in calculation models the results give an important contribution to understand the usual discrepancies between experimental

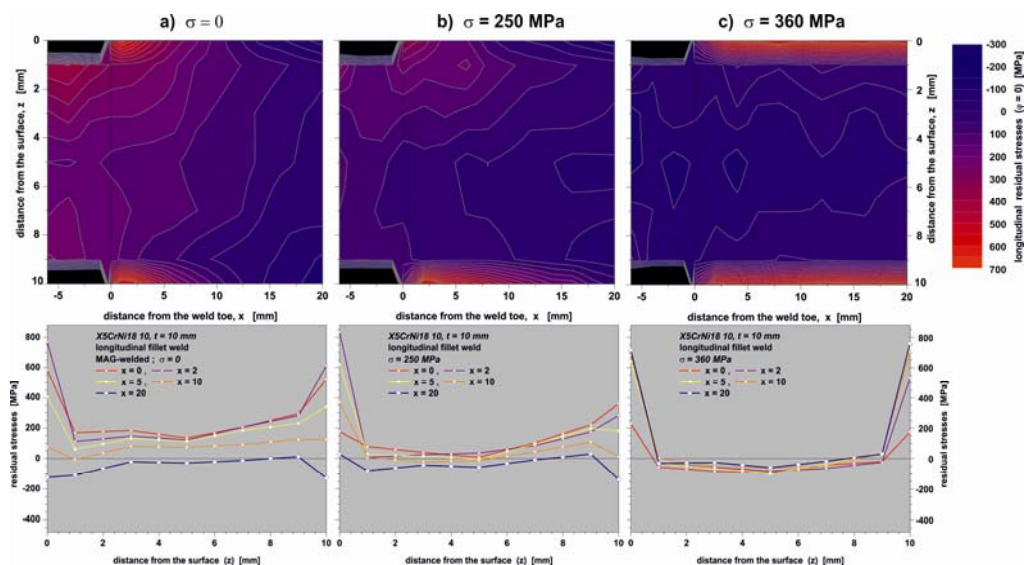


Fig.1: Through thickness distributions of the longitudinal RS in plates with longitudinal stiffeners (AISI 304) in the as-welded state (a) and after different static loads (b and c).

GMA-welded symmetrically on both sides. The residual stresses were measured in the centre line starting from the weld toe up to the base material, starting 1 mm below the surface and ending 1mm below the opposite surface. The resolution was 2x2x2mm<sup>3</sup>.

The experimental results have shown, that due to plastic deformations generated by the thermal strains during welding a local surface hardening effect enables tensile residual stresses much higher than the yield strength of the base material. The high tensile RS are

and calculative results. Further experiments are desirable in order to develop realistic models for the calculation of welding RS.

Principal Proposer: Adele Carradò IPCMS, Strasbourg, F  
Experimental Team: Thilo Pirling ILL, Grenoble, F  
Robert C. Wimpory, HZB

Date(s) of Experiment

25.04.2010 - 05.05.2010

Date of report: 14.07.2010

In this proposal we aimed to characterise the triaxial residual stress field generated by extrusion and brought to final dimension by successive drawing through a die in steel precision drawn tubes. Steel tube was not available and so we measured a copper one (variation of eccentricity). We will measure steel tube at a later date. This experiment is technologically important, as residual strains are known to affect the fatigue performance in ways that are unpredictable on the basis of hole-drilling and surface x-ray residual stress measurements.

Information on the 3-dimensional stress field in precision drawn tubes have significant value, and provides a basis for the quantifying of residual stresses induced in engineering samples of commercial and scientific importance.

The tube investigated was produced by extrusion, drawn twice in a cold drawing process and stress annealed before being cold drawn without plug under controlled laboratory conditions to its final dimension (final outer diameter of 40 mm) under variation of eccentricity. The geometry of the tube was measured before and after drawing. The parameters for fabrication of the investigated tube are given in the table below (Table 1).

Outer Ø (mm)		Av. thickness (mm)		Δ thickness (mm) Δt	Ovality O (%)	Eccentricity E (%)		
d <sub>A0</sub>	d <sub>A1</sub>	t <sub>ave0</sub>	t <sub>ave1</sub>			Before	After	
Before	After	Before	After	Before	After	Before	After	
48.0	40.0	4.2	4.37	0.8	0.54	<.05	7.2	5.6

Table 1: Geometrical data of tube investigated.

This neutron diffraction experiment was performed on E3. The wavelength used was 0.14865 nm. Scans were performed in the minimum and maximum thicknesses. For each point measured (min and max), 9 to 11 scans (900 s) have been done over wall thickness to obtain representative radial, longitudinal, transverse stress and strain profiles. Gauge volume has been selected to 2 x 2 x 2 mm<sup>3</sup>. The elastic constants used were 116 GPa for the Young's modulus and 0.36 for the Poisson ratio.

Figure 1 shows the residual stress distribution across the thickness in the area of maximum thickness. It can be seen that the radial stress component has the expected small level (> -100 MPa) around zero at the inside to slightly compressive state at outside. The axial component shows the strongest change in stress over thickness starting on the inside with strong compression (-350 MPa) and with broad

plateau (approx. 200 MPa). The hoop component changes from compression at the inner surface (-200 MPa) in the outer region, increasing pressure level to centre and then changing to tension to the outside (100 MPa). The positions directly at the surfaces were corrected by boundary effects. The comparison between thickest and thinnest wall (max. and min.) shows no significant difference without a small shifting in the position of zero stress. *These data have not been corrected for the surface effect.*

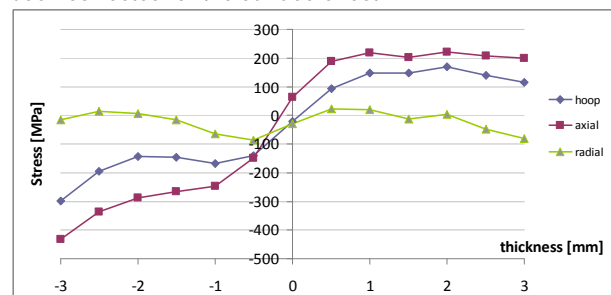


Figure 1: Profile of residual stress in minimum wall thickness (position "-3" internal surface of the tube)

Taken in conjunction with FEM simulation data clear insight into drawing process can be extracted. *This work is currently underway.* Future work (involving further neutron diffraction experiments) will focus on drawn versus pilgrim processes to better understand the influence of the process on the residual stress field.

This understanding will allow for the selection of process parameters that allow optimizing the residual stress field. This whole area of "process and stress engineering" is of technological significance to advancing performance in many technology applications limited by residual stress and structural integrity interactions. The obtained residual stress data will help to validate our FE model predictions of this process, and ultimately the work will lead to a better understanding of drawing processes in general. The results will be disseminated via the normal academic routes, and will form part of the PHD thesis of one of the experiment investigators.

**Acknowledgement:**

*This research project has been supported by the European Commission under the 7th Framework Programme through the 'Research Infrastructures' action of the 'Capacities' Programme, Contract No: CP-CSA\_INFRA-2008-1.1.1 Number 226507-NMI3".*

Principal Proposer: Kamran Nikbin, ICL, UK  
Experimental Team: Robert C. Wimpory, HZB  
Catrin M. Davies, ICL, UK  
Sefika Elvin Eren, ICL, UK

Date(s) of Experiment

19.07.2010 - 26.07.2010  
02.08.2010 - 08.08.2010

Date of report: 05.02.2011

The purpose of the experiment is to identify the role of residual stresses on the fatigue behaviour of CO<sub>2</sub> laser beam welded (LBW), crenulated plates. Fatigue life extension is achieved by the retardation of a growing crack under cyclic loading is achieved by the crenulations i.e. thickness variations or ribs on one side & surface of the welded components. Residual stresses must be quantified to determine the crack tip driving force parameters.

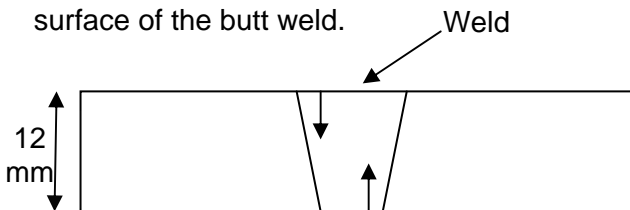
The plates are manufactured from sheets of steels designated RQT701, which is a quench and tempered structural steel combining high strength with excellent forming and welding performance. After laser beam welding crenulations are subsequently machined onto one side of the plate.

**Table 1 - Typical composition of RQT 701 (wt%).**

C	Si	Mn	S	P	Cr	Mo
0.14	0.40	1.35	0.003	0.012	0.01	0.12
Nb	Ti	V	Ni	Cu	B	Al
0.035	0.025	0.05	0.01	0.01	0.002	0.035

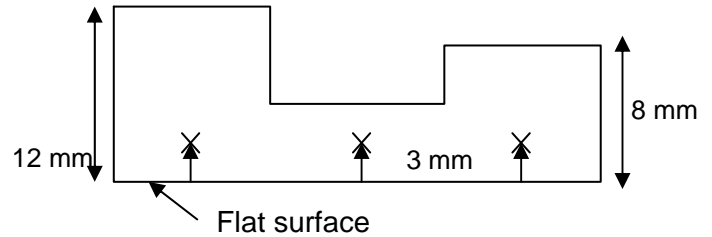
The possible effect of crenulations on the residual stress profiles were established through comparison of measurements on LBW plain reference plate, and a crenulated plate.

On the plain, 12mm thick reference panel the residual stress measurements were conducted along two lines. The location of the first line is 3 mm above the root of the weld whereas the location of the second is 3 mm below the top surface of the butt weld.

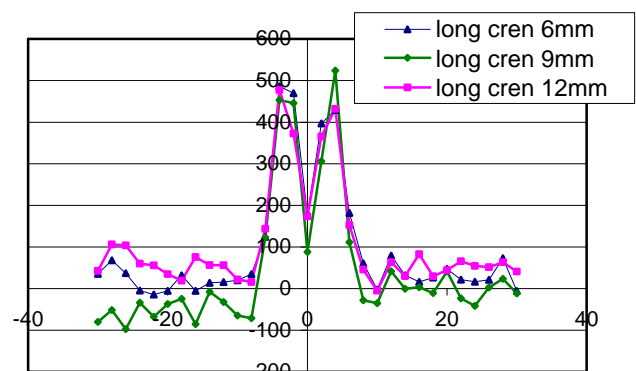
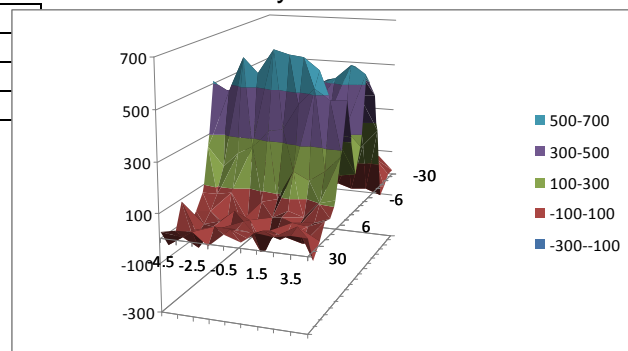



On one surface of the crenulated specimen, the thickness was machined as 6mm, 8mm and 12mm. Three measurements were

conducted and all the measurements were conducted 3 mm above the flat surface.



In the figure below, results of residual stress measurements in longitudinal direction are presented. No difference was observed between plain and crenulated panels of higher strength steel (S690QL) butt-joint welds. That means, an introduction of crenulations via machining does not cause any change of the original residual stress distribution of the panels. Therefore, it can already be concluded that all observed differences in the mechanical performance between reference and crenulated panels should be attributed to the crenulation effect only.



 <b>NEUTRONS</b>	<b>EXPERIMENTAL REPORT</b>  <b>The Effect of Residual Stress Distribution on Creep Cracking Behaviour of Weld 316H Stainless Steel</b>	Proposal: MAT-01-2819  Instrument: <b>E3</b>  Local Contact: Robert C. Wimpory
	Principal Proposer: N.P. O'Dowd, University of Limerick, IE Experimental Team: H. N. Yazdani, University of Limerick, IE Robert C. Wimpory, HZB C.M. Davies, Imperial College London, UK	Date(s) of Experiment  17.06.2010 – 22.06.2010

Date of report: 25.01.2011

### Objectives:

Fracture prediction of structures manufactured from high strength engineering steels is a high priority. In this work residual stress (RS) effects on creep crack initiation and growth are studied. In order to quantify the RS magnitude and RS relaxation, measurements are performed along the crack direction in pre-stressed components. The aim of this experiment was to quantify the residual stresses in 316H austenitic steel and their relaxation due to creep on compact tension, C(T), specimens.

### Achievements / difficulties:

Four C(T) specimens extracted from a 316H austenitic steel, pre-loaded in compression and the first two pre-compressed C(T)s, A1B1 and A1B2 (25mm thickness), were measured (Fig. 1). Pre-tensioned C(T) specimens from 347 were also measured after creep and the results were compared to the previous results. Results showed a significant relaxation in normal stress values ahead the notch tip after creep (Fig. 2).

Measurements were taken at 30 points ahead of the notch along the crack path with a measuring time of approximately 30 minutes per point. Residual stress profile along the crack direction follows the predictions previously performed by finite-element (FE) analysis (see Fig. 1). The reasonable agreement between the FE analysis and ND measurements was achieved except for a disparity near the notch.

More investigations are being performed at the University of Limerick and Imperial College London. These measurements along with those from FE will be investigated for further analysis after creep testing.

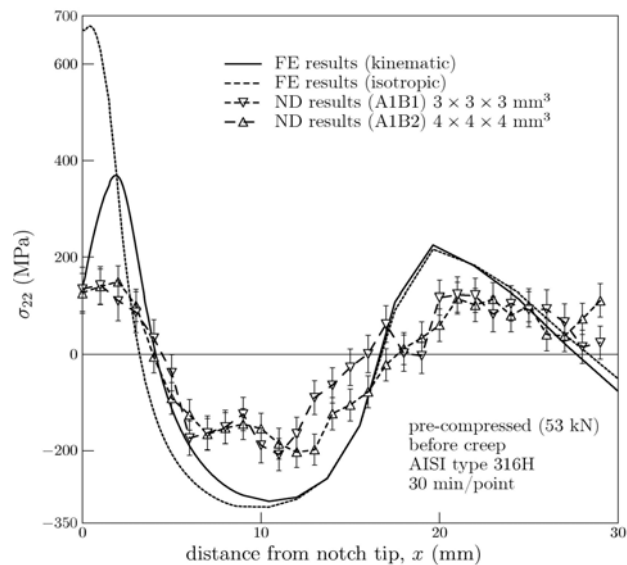


Figure 1: Measured stress vs. distance from tip (pre-compressed by 53kN)

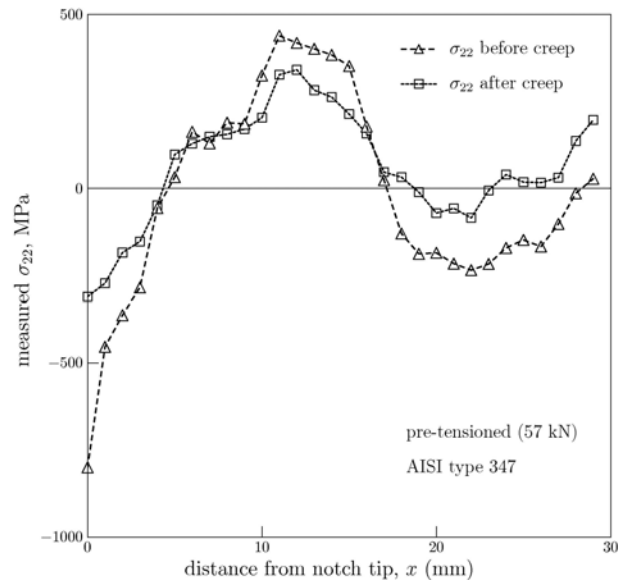


Figure 2: Comparison of measured normal stress vs. distance from tip

### Acknowledgement:

*This research project has been supported by the European Commission under the 7<sup>th</sup> Framework Programme through "Research Infrastructures" action of the "Capacities" Programme, contract number CP-CSA\_INFRA-2008-1.1.1. Number 226507-NMI3*

Principal Proposer: A. da S. Rocha, UFRGS, Porto Alegre, Brazil  
 Experimental Team: A. da S. Rocha, Rafael Nunes and Juliana Dagnese, UFRGS, Brazil  
 Thomas Hirsch, IWT  
 Robert C. Wimpory, HZB

Date(s) of Experiment

06.05.2010 – 16.05.2010

Date of report: 05.06.2010

**Introduction:**

In this work a combined straightening and bar drawing process to produce AISI 1045 round bars from coils of a hot-rolled material are investigated. The generation of residual stresses is seen as one of the main causes of distortion of these bars. Furthermore residual stresses are also responsible for a possible distortion in any further manufacturing step of this material. These results support an undergoing Ph. D. thesis and a Master degree dissertation executed in cooperation between UFRGS-Brazil and IWT-Germany.

**Experimental Description:**

The processed material is an AISI 1045 steel. The combined process starts with the as hot rolled material with a nominal diameter of 21.64 mm. The final products are round bars with nominal dimensions of 20.25 mm of diameter and 6 m of length. Samples were taken after each step of the process, as follows: Horizontal and vertical pre-straightening; Sand blasting; Drawing with 15° and 20°; Cutting, polishing and straightening with crossed rolls "PERC" with 16° and 18°.

A gauge volume of 2 x 2 x 2 mm has been used to optimize the use of the beam time. For the determination of the reference d0 value a cube of size 3 x 3 x 3 mm was prepared and measured at the actual measurement set-up used in the experiment.

**Results:**

The following four figures present the results. Figure 1 gives the residual stresses in a cross section of the bar. If the d0-value is taken as a mean value of all measurements compressive residual stresses of 0 to 150 MPa in axial and hoop direction are measured near the surface. In the center of the bar the axial residual stresses decrease to compressive stresses of -250 MPa. Hoop and radial stresses increase to tensile stresses of about 100MPa. Radial stresses remain quite low over the whole cross section. Figure 2 gives an image of the significant change of the axial residual stress state near the end of

the bar. The values of the middle plane of the bar are taken from figure 1. The decrease of the axial residual stresses at the end of the cylindrical bar rearranges hoop and radial residual stresses to high tensile values. It is assumed that this behavior will contribute to distortions of the bar during the following surface heat treatments.

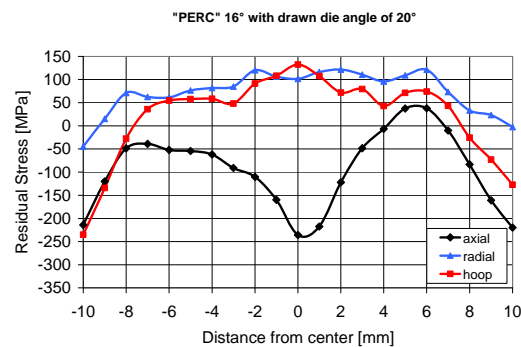


Figure 1: Axial, hoop and radial residual stresses plotted against the distance from the central axis of the bar (PERC 16° in combination of drawing with a die angle of 20°).

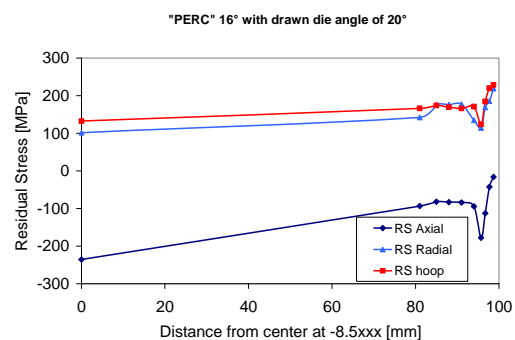



Figure 2: Axial, hoop and radial residual stresses plotted against the distance from the central plane of the bar (PERC 16° in combination of drawn with a die angle of 20°).

**Consequences:**

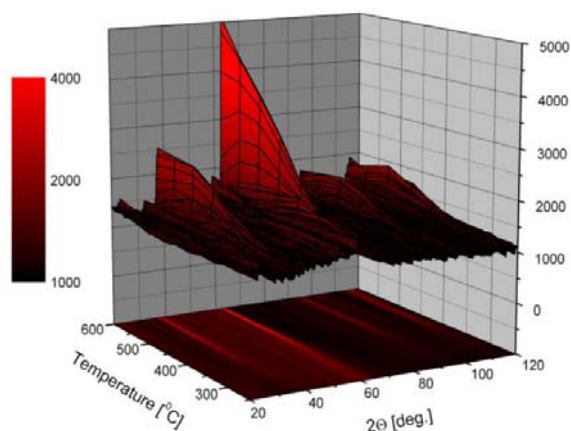
The results will be published in the near future. The next experiments will be extended to other steps of the shaft manufacturing route including induction hardening and machining of the cylinders.

 <b>NEUTRONS</b>	<b>EXPERIMENTAL REPORT</b>  <b>Structural characterisation of Ti-Zr-Ni nanoalloys and its deuterides</b>	Proposal: MAT-01-2884  Instrument: <b>E6</b>  Local Contact: Andreas Hoser
	Principal Proposer: L. Gondek, AGH-UST, Krakow, PL Experimental Team: L. Gondek, AGH-UST, Krakow, PL A. Zywczyk, AGH-UST, Krakow, PL Andreas Hoser, HZB	Date(s) of Experiment  26.08.2010 – 31.08.2011

Date of report: 14.01.2011

Mechanically alloyed Ti<sub>45</sub>Zr<sub>38</sub>Ni<sub>17</sub> composition (from pure elements) becomes amorphous after about 40 h of milling. Thermal treatment of the amorphous alloy it transforms into the icosahedral (i-phase) structure, in which Ti and Zr atoms possess very good chemical affinity for hydrogen absorption. The main goals of the proposed experiment were: studying the transition from amorphous into quasicrystal phase, that occurs at about 800 K; checking possibility of further structural transformations at higher temperatures and evidencing of releasing deuterium from the deuterided samples.

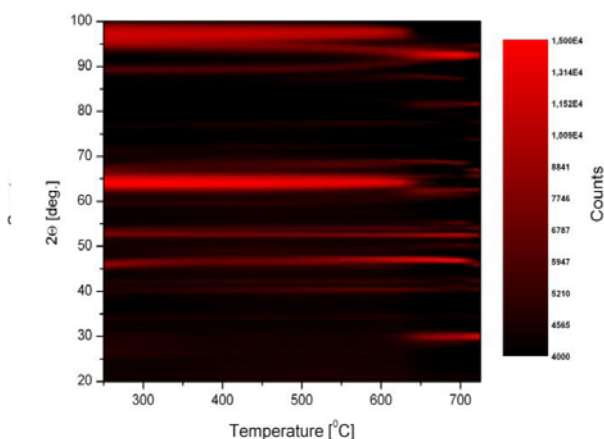
Graph 1 shows the transformation of primarily amorphous Ti<sub>45</sub>Zr<sub>38</sub>Ni<sub>17</sub> material into quasicrystalline phase (this process starts at about 350°C). At temperature of 600°C additional transformation takes place (small additional reflections between 80-100 deg. of 2θ). Our preliminary data processing hints at transition into some cubic structure. This findings are in a perfect agreement with known DSC data.



Graph. 1

Releasing of the deuterium from the amorphous and quasicrystalline deuterides was successfully observed as well. In both cases releasing of the deuterium takes place at temperature connected to transition between quasicrystalline and cubic phase. This holds for amorphous deuteride as well. Namely, deuterided amorphous material becomes deuterided quasicrystal, than above 600°C it undergoes transition into cubic phase accompanied with releasing of hydrogen. The releasing of the deuterium from the quasicrystalline sample can be spotted as the diffraction maximas shifts towards higher angles (lower d-spacings) at graph 2. At about 600°C all deuterium is released and above that temperature cubic phase is formed.

*This research project has been supported by the European Commission under the 7<sup>th</sup> Framework Programme through "Research Infrastructures" action of the "Capacities" Programme, contract number CP-CSA\_INFRA-2008-1.1.1. Number 226507-NMI3.*



Graph. 2

Principal Proposer: Michael Schöbel, TU Wien, AT  
Experimental Team: Johannes Jonke, TU Wien, AT  
Peter Degischer, TU Wien, AT

Date(s) of Experiment

05.07.2010 – 11.07.2010

Date of report: 31.01.2011

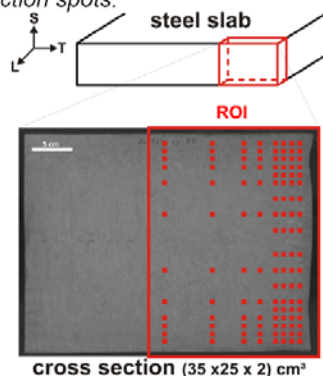
## Motivation

Residual stresses in continuously cast steel slabs are by far unknown. During casting liquid metal is poured through a nozzle into a channel. Cooling, rolling and bending of the partially solidified slab produces a complex stress situation of thermally, deformation and transformation induced stresses. Location, magnitude and origin of these stresses have to be determined to understand the heterogeneous material condition.

## Experiment

For stress mapping in S/T-direction in the slab, a sample of  $T \times S \times L = 35 \times 27 \times 2 \text{ cm}^3$  was cut.

Figure 1: Sample cut from a steel slab and point grid of the set diffraction spots.



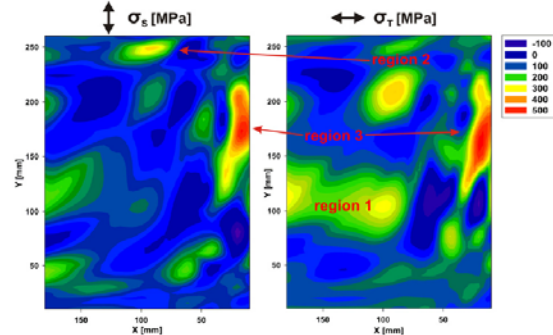
A scan grid was laid over the sample as shown in Fig. 1. Diffraction was made in the middle of the 2 cm in thickness using a big gauge volume of  $6 \times 6 \times 6 \text{ mm}^3$ . The Fe  $\{2\ 1\ 1\}$  peak at  $78.83^\circ$  ( $\lambda = 1.486 \text{ \AA}$ ) was acquired in 5 min in each spot / direction. Multiplicity of Fe  $\{2\ 1\ 1\}$  and the big gauge volume increased the grain statistics sufficiently for strain analysis. All three directions were scanned for stress calculation. Expected relaxation in L-direction from cutting was neglected.

## Results

The stress maps in S/T-direction (Fig. 2, S left, T right) show some small high tensile stress islands compensated by large low compressive regions. Three significant areas can be distinguished. Region 1 is located in

the lower middle of the slab with tensile stresses up to  $\sim 300 \text{ MPa}$  in T-direction only. Region 2 is located in the upper half with up to  $\sim 450 \text{ MPa}$ . In S-direction  $\sim 2 \text{ cm}$  from the surface and T-direction  $\sim 5 \text{ cm}$ , the highest tensile stress island in both directions is located in the surface near region 3 on the right. Stresses reach up to  $\sim 600 \text{ MPa}$  tension.

Figure 2: Results from stress mapping in S- and T-direction of the slab.



## Discussion

The steel slab shows a combination of surface near stresses induced by severe deformation and inner stresses originating from thermal gradients during cooling. The slab gets compacted from the side reducing the surface-near deformation. This compression produces tension by stress inversion after plastification in these areas resulting in region 1. A combination of cooling and bending generates tension observed in region 2 with spatial deviation between S and T direction. T-stress in region 1 originates from shrinkage during cooling with the solidification front moving from the cooled surface into the still molten centre.

## Conclusions

Tensile stresses in steel slabs are produced by mechanical as well as thermal loads during casting. Deformation on the surface leads to crack inducing tensile regions. Stress islands in the centre are produced by thermal gradients during cooling. The origin of anisotropic stress regions has to be clarified by further investigated in the third (L-) dimension.

*This research project has been supported by the European Commission under the 7<sup>th</sup> Framework Programme through "Research Infrastructures" action of the "Capacities" Programme, contract number CP-CSA\_INFRA-2008-1.1.1. Number 226507-NMI*

The overall aim of this work is to determine the effects of prior creep damage on fatigue crack growth and fracture toughness in 316H stainless steel and to propose simplified methods for including these effects in fatigue crack growth and fracture assessments. High temperature components often undergo creep-fatigue loading conditions and defect assessments need to consider the potential effects of prior creep damage on subsequent fatigue crack growth (FCG) and fracture behaviour. Local creep damage (where the damage is confined to a small region local to the crack tip) is introduced in a fracture specimen by interrupting a creep crack growth (CCG) test after a small amount of crack extension has taken place. FCG or fracture toughness testing is then performed in these locally creep damaged fracture specimens at room temperature.

During the interrupted CCG the specimen is loaded in tension at 550°C and subsequently unloaded after a small amount of crack extension. The process of loading and unloading may lead to a significant compressive residual stress field being generated at the crack tip, which may subsequently affect the fracture toughness and FCG results. Neutron diffraction measurements were therefore performed on 2 interrupted CCG test specimens, denoted 2-5 and 2-6 to quantify the extent of residual stress in these compact tension fracture specimens. The 311 peak was measured, as recommended for this steel. Due to the relatively large grain size of this material a gauge volume of  $3 \times 3 \times 3 \text{ mm}^3$  was used.

Specimens 2-5 and 2-6 were both 50 mm in width and had initial crack lengths of 17.5 mm, however specimen 2-5 was of total thickness of 18 mm (net thickness 14.4 mm) whereas specimen 2-6 was 25 mm in thickness (net thickness 17.5 mm). During the CCG tests, the load applied to each specimen resulted in an initial stress intensity factor,  $K$ , of  $35 \text{ MPa}\sqrt{\text{m}}$  in 2-5 and  $25 \text{ MPa}\sqrt{\text{m}}$  in 2-6. The residual stress results from both specimens are shown in Figure 1. In Fig. 1(a) the final crack tip location is indicated as it has since been fatigue cracked open. It can be clearly seen that a compressive peak of around -100 MPa is indicated at the crack tip and a peak of 250 MPa in the 2 direction i.e. normal to crack plane. Significant stresses of around 150 MPa are

also seen in the 3 (through thickness) and 1 (in crack plane) direction. Similar results are seen in specimen 2-6, however the peak values may be lower due to the lower final  $K$  experienced at the interruption of this CCG test. These results are an important indication that residual stresses may need to be considered in the subsequent FCG analyses. Finite element analyses are being performed to complement and validate these findings.

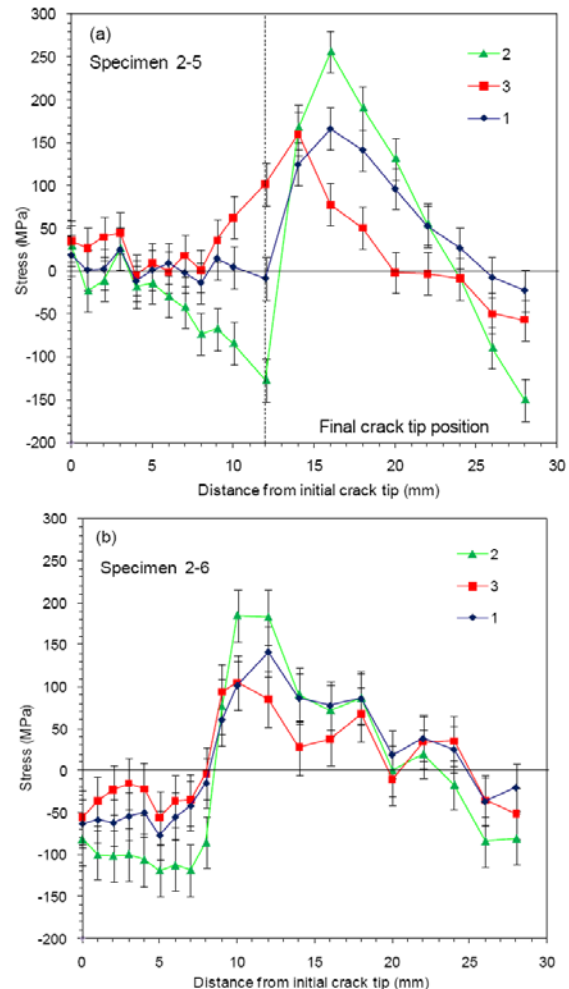



Figure 1: Residual stress results for (a) specimen 2-5 and (b) specimen 2-6

**Acknowledgement:**

This research project has been supported by the European Commission under the 7<sup>th</sup> Framework Programme through "Research Infrastructures" action of the "Capacities" Programme, contract number CP-CSA\_INFRA-2008-1.1.1. Number 226507-NMI



	<b>EXPERIMENTAL REPORT</b>  <b>Testing fundamental understandings of evolution of lattice strains under in-situ multi-axial loading</b>	Proposal: MAT-01-2923  Instrument: E3  Local Contact: Robert C. Wimpory
	Principal Proposer: R. Woracek, Univ. Tennessee (UTK), USA Experimental Team: R. Woracek, Univ. Tennessee (UTK), USA D. Penumadu, Univ. Tennessee (UTK), USA J. Bunn, Univ. Tennessee (UTK), USA Robert C. Wimpory, HZB N. Kardjilov, HZB	Date(s) of Experiment  16.02.2010 - 20.02.2010 22.03.2010 - 01.04.2010

Date of report: 20.01.2011

## Introduction

The Residual Stress Analysis and Texture Diffractometer (E3) at HZB was used for two main purposes within this experiment:

- Mapping of elastic strain response for a flat Fe BCC sample under in-situ tensile loading as a reference/benchmark measurement for comparison to Transmission Bragg Edge Imaging which was performed at CoNRAD (V7; Proposal MAT-04-1781)
- Investigation of in-situ torsional loading (case of pure shear) to a round steel (Fe BCC) bar with the goal to determine shear strain response on a granular level

The results obtained for a) are essential for the joint HZB-UTK project of developing and exploring possibilities to perform Bragg Edge Imaging at a reactor source with which strains/stresses of large areas or complete samples could be visualized. The results of b) should be seen as a first step to develop an experimental technique to measure shear strains by neutron diffraction. Better understanding of shear is very important for many engineering problems, since most parts fail in shear or a combination of loading conditions rather than pure tension.

## Experiment and results

For the in-situ experiments a load frame has been used (developed by the proposers at the University of Tennessee in collaboration with HZB; Fig. 1a) that is both portable and high capacity. The frame capacity is 50kN in tension and 12Nm in torsion. For a) three locations along the specimen axis have been investigated for 2 hkl's (211 and 220 while for 200 statistics were not good enough) in a simple tensile loading experiment (Fig. 1b inset) at 13 stress states (elastic and plastic). For each point, strain was measured in axial, in-plane and out-of-plane direction. Elastic moduli for both planes were determined as 220GPa and agree with published literature. Furthermore the results verified the

correctness of data obtained at CoNRAD within 100 microstrains resolution (Fig. 1b). Moreover several locations of the tensile sample could be mapped successfully (Fig. 2) and determined strains and stresses agree with FE modeling. Part b) of the experiment was used to probe strain in different directions and locations while loading the sample in torsion (elastic range only). For most locations in the sample no significant amount of d-spacing change could be measured in neither radial nor hoop direction. However, a novel approach developed by the proposers showed a response of d-spacing change related to applied torque. Ongoing research, based on these valuable 'preliminary' results, at NRSF2 (ORNL) currently further explores this approach.

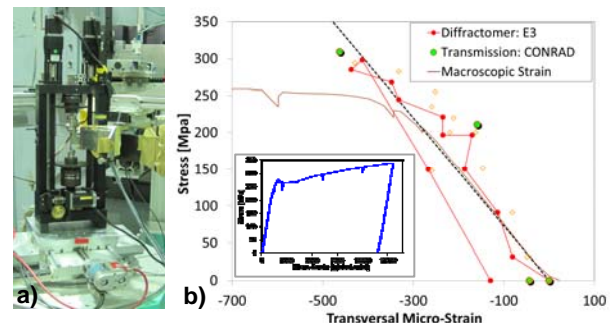


Fig. 1: a) Experimental Setup b) Example results for 220 out-of-plane (Inset: Stress-Strain from Loading System)

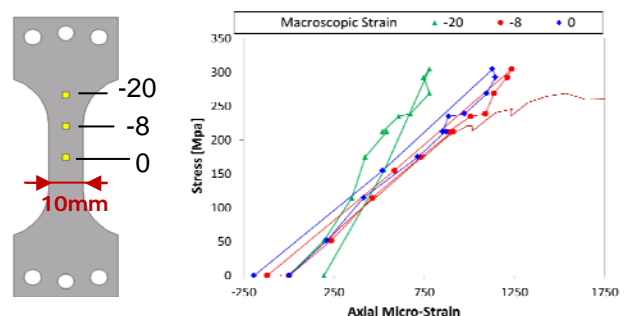

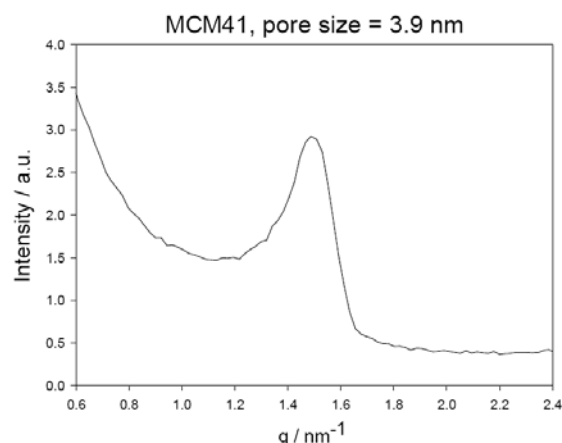


Fig.2: a) Locations of measured d-spacing on tensile sample b) Example results for 3 locations for 220 (axial direction)

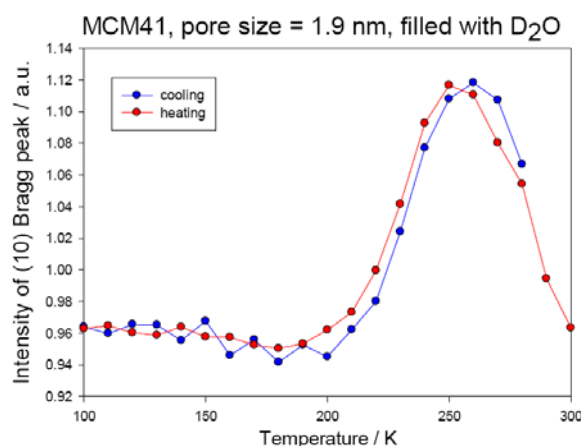
 <b>HELMHOLTZ ZENTRUM BERLIN</b> für Materialien und Energie  <b>NEUTRONS</b>	<b>EXPERIMENTAL REPORT</b>  <b>Freezing and melting of water in confinement</b>	Proposal: PHY-01-2803 Instrument: <b>V1</b> Local Contact: Th. Hauß
	Principal Proposer: Oskar Paris, MU Leoben, AT Experimental Team: Maxim Erko, MU Leoben, AT Thomas Hauß, HZB	Date(s) of Experiment  22.03.2010 – 01.04.2010

Date of report: 31.01.2011

The aim of the present experiment was to continue the investigation of the temperature dependent changes of the scattering signal from water confined in MCM-41 mesoporous materials using in-situ SANS at V1 instrument at BER II neutron reactor. In particular, the temperature-induced density change of confined water was studied. An exemplary SANS pattern of the well defined hexagonal pore structure of MCM-41 porous material is shown in Figure 1. Our recent in-situ synchrotron SAXS measurements at BESSY II show a strong change of the scattering intensity of the (10) Bragg peak at water phase transition temperature. The temperature-induced strong change of the scattering intensity is even observed for water confined in pores of 2 nm size where it is assumed not to freeze at all. Therefore the measured intensity change is expected to be due to water density change during a transformation from a liquid to an amorphous state. To confirm this observation in current experiment we used two water mixtures in order to perform contrast variation between the silica pore matrix of MCM-41 and the fluid inside the pores. The first water mixture was pure D<sub>2</sub>O with a higher neutron scattering length density than that for silica (SiO<sub>2</sub>). The other water mixture contained 21.4 % D<sub>2</sub>O and 78.6 % H<sub>2</sub>O resulting in a smaller neutron scattering length density than that for silica. The idea is to monitor the temperature-induced change of water density, which should lead to a different change in the neutron scattering contrast for the two water mixtures. We performed measurements on two different MCM-41 porous materials with pore diameters of 2 nm and 3.9 nm filled with water up to the filling factor  $f$  close to but not higher than  $f = 1$  to avoid ice nucleation outside the pores. We used the in-situ DEGAS system developed at the Helmholtz Zentrum Berlin to fill the mesoporous material in a controlled way. For each sample and water mixture a cooling and a heating cycle between 300 K and 100 K have been performed. Figure 2 illustrates first results for the density of confined water. A shallow minimum around 200 K is observed in agreement with earlier investigations.




**Figure 1: SANS pattern of MCM41 with (10) Bragg peak resulting from the two-dimensional hexagonal mesopore lattice**



**Figure 2: Integrated scattering intensity of the (10) Bragg peak for one cooling and one heating cycle**

#### Acknowledgement:

*This research project has been supported by the European Commission under the 7<sup>th</sup> Framework Programme through "Research Infrastructures" action of the "Capacities" Programme, contract number CP-CSA\_INFRA-2008-1.1.1. Number 226507-NMI*

 <b>HELMHOLTZ ZENTRUM BERLIN</b> für Materialien und Energie  <b>NEUTRONS</b>	<b>EXPERIMENTAL REPORT</b>  <b>Carbon dioxide adsorption to montmorillonite clay and nanoporous silica</b>	Proposal: PHY-01-2804  Instrument: V1  Local Contact: Thomas Hauß
	Principal Proposer: Gernot Rother, ORNL, USA Experimental Team: Dirk Wallacher, HZB Nico Grimm, HZB	Date(s) of Experiment  28.04.2010 – 03.05. 2010

Date of report: 26.01.2011

In order to find ways to mitigate the effects of rising carbon dioxide levels in the atmosphere the feasibility of carbon sequestration into subsurface reservoirs is investigated. We study two questions using both experimental and computer simulation techniques: a) How does supercritical (sc) CO<sub>2</sub> accommodate in small pores under carbon sequestration conditions? b) How does CO<sub>2</sub> interact with clays and shales?

Clay formations may serve as caprocks for subsurface CO<sub>2</sub>, but the impact of CO<sub>2</sub> on clay long-term stability and integrity is unknown. We have performed neutron scattering/diffraction measurements of CO<sub>2</sub> adsorption to proxy materials for reservoir rocks (porous silica) and caprocks (Na-montmorillonite) for different conditions of fluid density and temperature. Experiments were performed at the membrane diffractometer, which covers the length scale of the clay interlayer spacing.

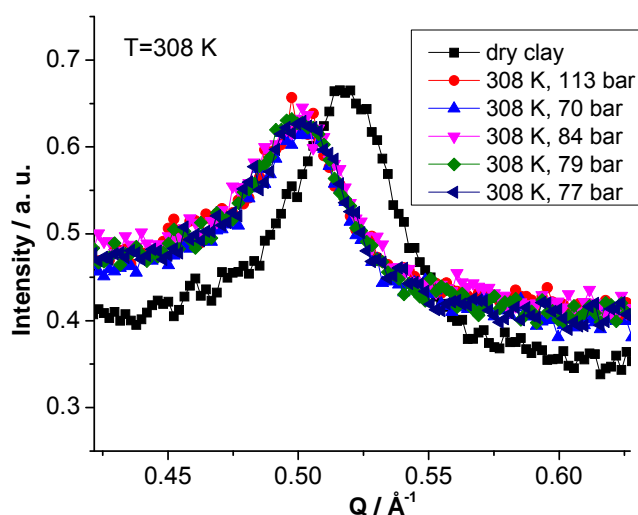
A pressure cell (shown mounted at the V1 in Figure 1) was built for this experiment.

Data were corrected for the empty cell scattering.

Measurements were performed at 290-340 K and pressures of 0-200 bar. A neutron scattering curve was collected in about 2.5 hours; scans covered the range  $0 \leq Q/\text{\AA}^{-1} \leq 0.7$ . Figure 2 shows the results obtained for dry Na-montmorillonite clay at 308 K.



**Figure 1:** Al-Pressure cell (0-200 bar) mounted at the V1 instrument. The inner diameter of the cell is 4 mm.



**Figure 2:** Interlayer spacing peak position for Na-montmorillonite clay interacting with sc CO<sub>2</sub> at different pressures.

It was found that the interlayer spacing widened upon CO<sub>2</sub> addition, going from 1.215 nm for dry clay to 1.259 nm for CO<sub>2</sub> saturated clay. Interestingly, the shift in peak position is independent from both the CO<sub>2</sub> pressure (see Figure 2) and temperature (not shown here).

We also performed gravimetric high-pressure sorption experiments on this system, using the Rubotherm apparatus in the DEGAS labs at the Helmholtz Center Berlin. Combined neutron and sorption data analysis is underway.

#### Acknowledgement:

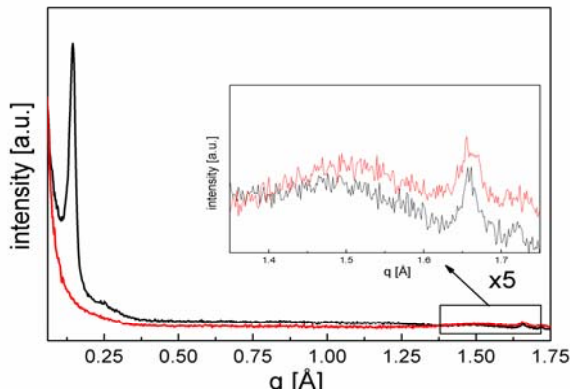
Research by GR was sponsored by the Division of Chemical Sciences, Geosciences, and Biosciences, Office of Basic Energy Sciences (OBES), U.S. Department of Energy. Oak Ridge National Laboratory (ORNL) is managed by UT-Battelle, LLC for the U.S. Department of Energy under Contract No. DE-AC05-00OR22725.

 <b>NEUTRONS</b>	<b>EXPERIMENTAL REPORT</b> <b>Investigation of pristine and SO<sub>3</sub>H modified benzene PMO by SANS with in situ nitrogen adsorption</b>	Proposal: MAT-01-2906 Instrument: V1 Local Contact: Astrid Brand
	Principal Proposer: Michael Wark, Leibniz University Hannover Experimental Team: Michael Wark, Leibniz University Hannover Monir Sharifi, Leibniz University Hannover Dirk Wallacher, HZB Thomas Hauß, HZB	Date(s) of Experiment 16.08.2010 – 26.08.2010

Date of report: 30.01.2011

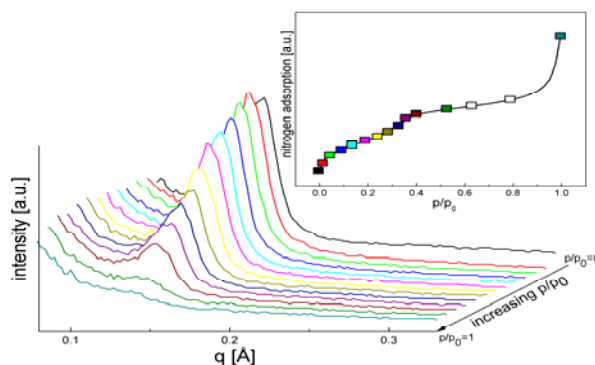
During our last stay at BENSCH in August 2010 we investigated periodic mesoporous organosilica (PMO) materials with SANS experiments combined with in situ N<sub>2</sub> adsorption at 77 K in order to get detailed information regarding contrast matching behavior, crystal-like ordering of the organic bridges R within the pore walls as well as change of the scattering length density (SLD) by surface functionalization.

We found that by complete pore filling with nitrogen the reflection of pristine benzene-PMO at  $q=0.14 \text{ \AA}^{-1}$ , representing the long range order of the mesopores and thus in general the contrast of wall and pore, disappears completely while the reflections at  $q=1.44 \text{ \AA}^{-1}$  and  $q=1.66 \text{ \AA}^{-1}$  remain almost unchanged (Fig.1). This proves the molecular-scale periodicity as well as the SLDs of inorganic-organic benzene-PMO and of N<sub>2</sub> in the condensed state being equal.



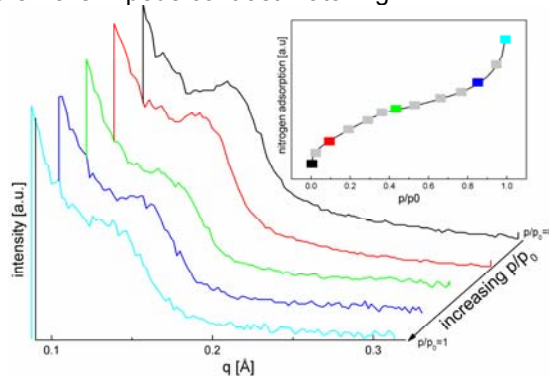
**Fig.1:** Neutron scattering of benzene-PMO at vacuum (black) and with filled nitrogen (red).

Furthermore benzene-PMO materials were functionalized by tethering SO<sub>3</sub>H acid groups to the surface Si groups using mercaptopropyltrimethoxy silane (MPMS) and oxidizing the thiol group in a subsequent step. With progressing N<sub>2</sub> adsorption the sample exhibits analogue results to pristine benzene-PMO (Fig.2), as the intensity of the main signal at  $q \approx 0.14 \text{ \AA}^{-1}$  decreases at low adsorption levels. Once capillary condensation appears at relative pressures of  $p/p_0 \geq 0.22$  a faster decrease and finally a complete matching of the neutron scattering reflection of the main signal is obtained. However a comparable SLD of both materials pristine and for SO<sub>3</sub>H functionalized benzene-PMO was expected since a very low functionalization degree was achieved (0.67 mmol<sub>SO<sub>3</sub>H</sub>/g).



**Fig.2:** SANS patterns for SO<sub>3</sub>H-benzene-PMO grafted on Si groups in dependence of pore filling with nitrogen.

However benzene-PMO functionalized with SO<sub>3</sub>H-groups at the silica groups as well as the benzene rings (1.61 mmol<sub>SO<sub>3</sub>H</sub>/g) behaves differently (Fig.3). Nitrogen adsorption at relative pressure  $p/p_0 > 0.4$  and finally completely filling of the mesopores does not show any changes in the SANS patterns, the signal intensity remains almost constant. This indicates that for a high degree of functionalization with homogenous distribution of the functional groups the SLDs of SO<sub>3</sub>H-modified benzene-PMO walls and that of adsorbed N<sub>2</sub> become different. Hence the modified pore walls impede contrast matching.



**Fig. 3:** SANS patterns for SO<sub>3</sub>H-benzene-PMO grafted on Si groups and benzene rings in dependence of pore filling with nitrogen.

These findings, which confirm earlier results on modified Si-MCM-41, were already reported in a talk on the „BENSCH User’s Meeting of BESSY II and BER II” in Berlin Adlershof (December 2010). A further report (poster) will be given at the „23. Deutsche Zeolith-Tagung” in Erlangen (March 2011). A publication is in preparation.

 <b>NEUTRONS</b>	<b>EXPERIMENTAL REPORT</b>	Proposal: PHY-03-632
	<b>Temperature evolution of dynamics of lead nanoparticles</b>	Instrument: <b>V3</b> Local Contact: Margarita Russina
Principal Proposer: Experimental Team:	A. Naberezhnov, RAS Ioffe PTI St. Petersburg., RU P. Parshin, NRC KI Moscow, RU Y. Kibalin, RAS PNPI Gatchina, RU M. Russina, HZB	Date(s) of Experiment 30.06.2009 - 07.07.2009 16.02.2010 - 20.02.2010

Date of report: 31.01.2011

Lead demonstrates the strong nonlinearity at growth of temperature and large thermal lattice expansion. On the other hand it is shown that the physical properties and structure of confined materials change drastically. In particular in confined sodium nitrite the amplitudes of thermal motions above the ferroelectric phase transition increase in 6-8 times [1]. Our diffraction measurements have indicated an absence of a softening of atomic vibrations due to thermal expansion (Grüneisen effect) in the lead embedded into porous glasses with average pores diameter 7 nm. The characteristic size of nanoparticles was practically constant ( $\sim 15$  nm) up to 550 K. We have measured the temperature evolution of vibration density of states (VDOS) of the bulk material and lead within porous glass at RT and at 588 K, i.e. in a vicinity of melting point, where the growth of nanoparticle size was observed in diffraction experiment. For the wavelength  $5.5 \text{ \AA}$  there is no Bragg scattering neither by lead nor by aluminum, the material of the sample cell, in the available range of the scattering angles. In Fig. 1 the experimental spectra for the bulk at 304 K (curve 1) and at 588 K (curve 2) are presented. It is necessary to underline that the “softening” of VDOS spectrum is absolutely visible. In Fig. 2 the experimental spectra for lead in a restricted geometry are presented, curve 1 – at 304 K, curve 2 – at 588 K. These spectra are the sum of scattering on confined lead, silica matrix and sample environment. The growth of intensity at small energies (250 – 300 channels) is due to scattering on porous glasses. So to compare the results for the bulk and confined materials we have obtained the direct experimental evidence

of hardening of phonon spectra in lead embedded into porous glasses with average pore diameter 5 nm.

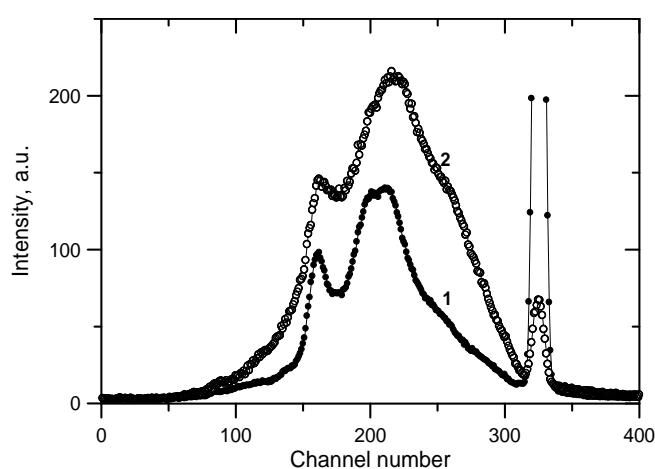


Fig. 1

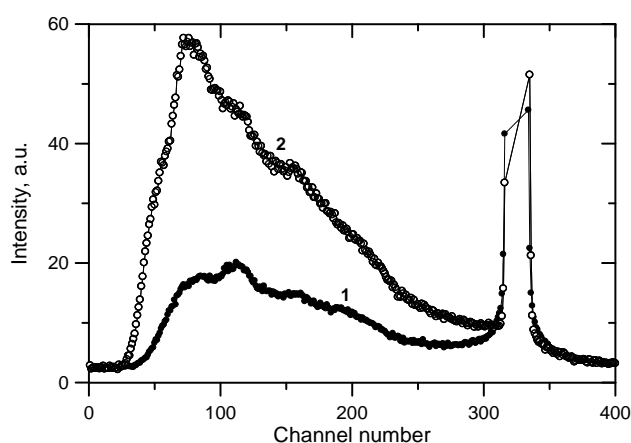


Fig. 2

- 1 A. Naberezhnov, A. Fokin, Yu. Kumzerov, A. Sotnikov, S. Vakhrushev, and B. Dorner, *Eur. Phys. J. E* **12**, s21-s24 (2003)
- 2 I.V. Golosovsky, R.G. Delaplane, A.A. Naberezhnov, Y.A. Kumzerov, *Phys. Rev.* **B69**, 132301-1 – 132301-4 (2004)

Principal Proposer: Laurence Aldridge, ANSTO, AU  
Experimental Team: Heloisa Nunes Bordallo, HZB  
Will Gates, Monash University, AU  
Remco Havenith, Univ. Groningen, NL

Date(s) of Experiment

25.05.2010 – 03.06.2010  
23.08.2010 – 25.08.2010

Date of report: 31.01.2011

Water retention controls smectite swelling underpinning the ability of clays to act as barriers for hazardous waste sites. As relative humidity (RH) changes so does the volume of the clay. Therefore the control and definition of the clay-water interaction is of considerable industrial interest.

Water in clay can be broadly separated into three categories:

- interparticle (or external) water
- water in the clay interlayer and in the cation hydration shell
- interlayer water outside the cation shell.

The aim of this experiment was to use the spectrometer NEAT,  $\lambda = 5.1\text{\AA}$  and  $\Delta E = 98\mu\text{eV}$ , to compare water in these three states in selected montmorillonite clays. The results obtained here have been published in [1], where we show that by analysing the QENS part of the spectra we were able to elucidate the cation interaction with interlayer water as a function of interlayer cation (Na or Ca), layer charge (by carefully preparing our clay samples) and water content in the interlayer (by controlling the RH using various salts or by simple oven drying the at  $110^\circ\text{C}$ ).

In addition, we were able to carefully monitor differences between the behaviour of water loss in the Ca and Na exchanged SAz clays as a function of time. To obtain such information, we performed a *leaking sample holder* experiment where the clay water loss was monitored while measuring the time of flight signal for a period of 24 hours. To obtain the desired information spectra were recorded continuously and saved each hour, and then each one-hour spectrum was binned to one single Q. The QE signal was analysed using a resolution function plus a single Lorentzian curve. From the loss of the total intensity it was possible to estimate the amount of water left in the clay plotted against both the half width of the quasi-elastic line (Figure 1 upper) and the quasi-elastic fraction (which is the ratio of the area of the single Lorentzian to the total area – Figure 1 lower). Such procedures indeed

allowed us to separate different populations of mobile water in the clays as well as distinguish the effect of interlayer cation.

Finally, we conclude that neutron scattering does have the capability to distinguish between three types of water in clays [1,2].

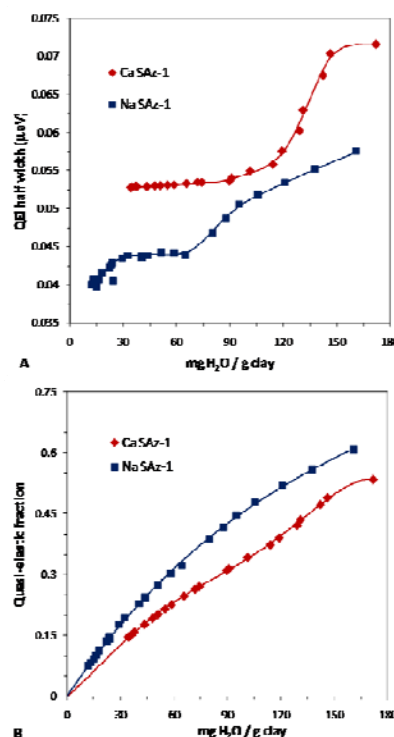


Figure 1 (Upper) Half-width of the QE peak as function of water content (Lower) QE fraction of water as function of water content.

- (1) Bordallo, H.N., Gates, W.P., Aldridge, L.P., Churchman, G.J., and Izaola, Z. (2010) Water-Cation interaction in Na or Ca saturated smectite SZa-1 interpreted by Neutron Scattering. ACMS 2010 - Australian Clay Minerals Society Conference, Brisbane, Australia.
- (2) Bordallo, H.N., Aldridge, L.P., Churchman, G.J., Gates, W.P., Telling, M.T.F., Kiefer, K., Fouquet, P., Seydel, T., and Kimber, S.A.J. (2008) Quasi-Elastic Neutron Scattering Studies on Clay Interlayer-Space Highlighting the Effect of the Cation in Confined Water Dynamics. The Journal of Physical Chemistry C 112(36), 13982 -13991

Principal Proposer: H. Fritzsche, NRC-CNBC, Chalk River, CA  
 Experimental Team: C. Harrower, NRC-NINT, Edmonton, CA  
 E. Poirier, NRC-CNBC, Chalk River, CA  
 H. Fritzsche, NRC-CNBC, Chalk River, CA  
 A. Teichert, HZB  
 R. Steitz, HZB  
 D. Wallacher, HZB  
 N. Grimm, HZB

Date(s) of Experiment

10.03.2010 – 15.03.2010  
19.03.2010 – 25.03.2010

Date of report: 26.01.2011

Using neutron reflectometry, we studied the deuterium absorption in Mg<sub>70</sub>Al<sub>30</sub> thin films capped with Ta/Pd, Ni/Pd, and Ti/Pd catalyst bilayers. The measurements were performed at room temperature in a pressure range from 0 – 1 bar. The modelling of the measured reflectivity curves provided the deuterium profile in the layers at different stages of the absorption process. The absorption mechanism observed was found to involve spillover of atomic deuterium from the catalyst layer to the Mg alloy phase, followed by the deuteration of the Mg alloy. Complete deuteration of the Mg alloy occurs in a pressure range between 100 and 500 mbar, dependent on the type of bilayer catalyst. The use of a Ti/Pd bilayer catalyst yielded the best results in terms of both, storage density and kinetic properties.

The thin films were prepared by sputtering. First, a 5 nm thick Ta layer was deposited onto a Si(100) wafer and without interruption the MgAl alloy was co-sputtered followed by a 5 nm Ta (or Ni or Ti) and 5 nm Pd layer.

Reflectivity curves and SLD profiles of the Mg<sub>70</sub>Al<sub>30</sub>/Ti/Pd sample are presented in Fig. 1 for increasing D<sub>2</sub> pressures. Fig. 1a shows the results obtained on the as-prepared Mg<sub>70</sub>Al<sub>30</sub>/Ti/Pd sample. The SLD values were found, as for previous samples, in agreement with expected ones from tabulated data. The dip in the SLD profile observable around 5 nm is due to the negative coherent scattering length of titanium. Following deuterium introduction over the 1 - 20 mbar range, (Fig. 1b-c), the sample absorbs deuterium mainly in the top Ti/Pd bilayer. Significant absorption is observed in the Mg<sub>70</sub>Al<sub>30</sub> layer around 100 mbar (Fig. 1d) where the SLD reaches  $5.3 \times 10^{-4} \text{ nm}^{-2}$  or D/M=1.3. This ratio is reached after about 7.5 h at this pressure, a time comparable to the Ta/Pd- catalyzed material at the same pressure. Further increase of the

pressure lead to incremental changes in the SLD, the latter ultimately reaches about  $5.5 \times 10^{-4} \text{ nm}^{-2}$  or D/M=1.32 at 1 bar. The whole Mg<sub>70</sub>Al<sub>30</sub> layer has ultimately expanded by about 23%, i.e. from 54 nm (as-prepared) to 66 nm.

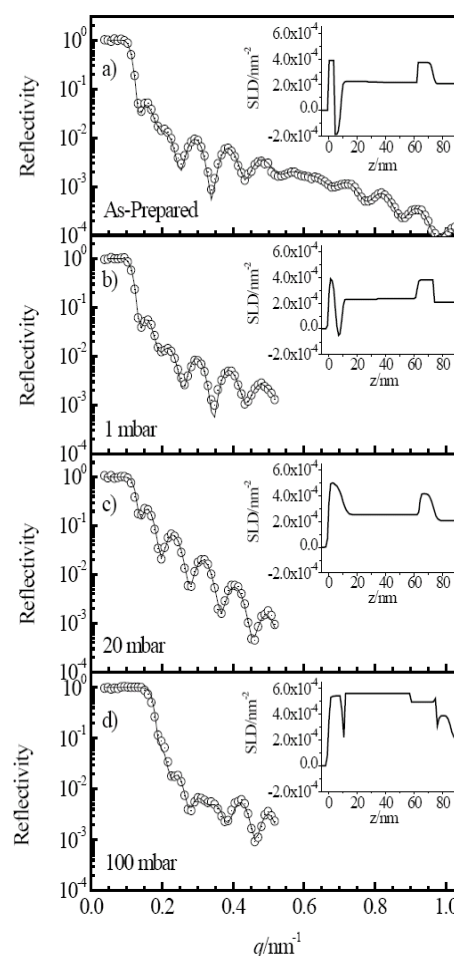



Fig. 1: Neutron reflectivity curves and corresponding SLD profiles on the Ta/Mg<sub>70</sub>Al<sub>30</sub>/Ti/Pd sample: (a) as prepared, and at D<sub>2</sub> pressures of: (b) 1 mbar, (c) 20 mbar, (d) 100 mbar.

	<b>EXPERIMENTAL REPORT</b>	Proposal: MAT-04-1928-EF
	<b>Martensite Structure, Grain Orientation and Cracks in Polycrystalline Ni-Mn-Ga Foams</b>	Instrument: <b>V7</b> Local Contact: A. Hilger
Principal Proposer: Experimental Team:	Markus Chmielus, HZB Andreas Paulke, HZB Rainer Schneider, Beuth Hochschule, Berlin Peter Müllner, Boise State University, USA David C. Dunand, Northwestern University, Evanston, USA	Date(s) of Experiment  04.03.2010 - 05.03.2010

Date of report: 05.01.2011

Recently, we have shown that a polycrystalline Ni–Mn–Ga magnetic shape-memory alloy (MSMA), when containing two populations of pore sizes, shows very high magnetic-field-induced strain (MFIS) of up to 8.7% [1,2]. During this proposal time, x-ray microcomputer tomography was used to determine the pore and crack distribution of dual pore size Ni-Mn-Ga MSMA foam.

For this experiment, the x-ray radiation was generated by a microfocus tube (Hamamatsu, L8121-03) with a spot size of 7  $\mu\text{m}$  and detected by a flat panel detector (Hamamatsu, C7942SK-05). The scanner was set to an acceleration voltage of 100 keV and a current of 95  $\mu\text{A}$ . The out coming beam was filtered by a 1 mm thick Aluminum plate. The magnification ratio was preset to 7.1 with an effective pixel size of 7.1  $\mu\text{m}$  for the sample.

The x-ray tomography scans (Fig. 1) revealed a fairly homogenous distribution of both pore sizes throughout the entire sample. The center portion of the sample had a somewhat reduced number of large pores. Additionally, the cross section at  $x \approx 2/3 t_x$  and  $x \approx t_x$  (where  $t_x$  is the thickness of the sample) showed small cracks in the bottom right regions and at  $x \approx t_x$  also at the top edge of the sample. These cracks spanned between large pores and can also be seen between some small pores that are located between large pores (black arrows in Fig. 1).

The x-ray microcomputer tomography experiments were accompanied by in situ magnetomechanical experiments and magnetization measurements at Boise State University and neutron diffraction experiments at the HZB (see MAT-01-2810-EF) [3].

Combining the results of all experiments it was concluded that the small pores in a dual pore

foam are inhibiting the crack growth and, thus, improve the performance and high cycle life of polycrystalline MSMA foams.

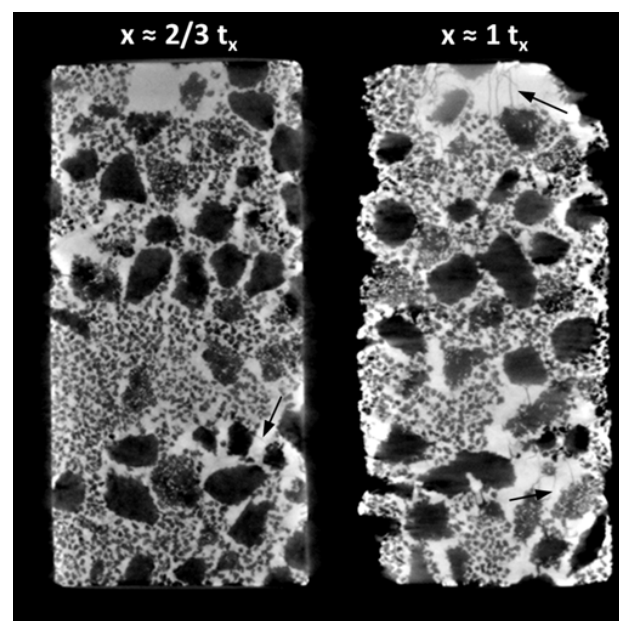



Figure 1: Exemplary x-ray tomography slices of the foam sample in the y-z plane along the x axis (parallel to the shortest dimension of the sample).  $t_x$  is the thickness of the sample in the x direction. Arrows indicate cracks [3].

This work was supported by the German Research Foundation (DFG) through priority program SPP 1239, National Science Foundation Division of Materials Research Grant Nos. DMR-0804984 (BSU) and DMR-0805064 (NU).

#### References:

- [1] M. Chmielus et al. Nature Mater. **8**, 863 (2009)
- [2] P. Müllner et al. Mater. Sci. Forum **635**, 119 (2010)
- [3] M. Chmielus et al. J. Appl. Phys. **108**, 123526 (2010)



 <b>HELMHOLTZ ZENTRUM BERLIN</b> für Materialien und Energie  <b>NEUTRONS</b>	<b>EXPERIMENTAL REPORT</b>  <b>Hydrogen distribution in cylindrical-like hydrogen-metal based storage tanks by neutron imaging</b>	Proposal: MAT-04-1942  Instrument: <b>V7</b>  Local Contact: N. Kardjilov
	Principal Proposer: L. Gondek, AGH-UST, Krakow, PL Experimental Team: L. Gondek, AGH-UST, Krakow, PL J. Czub, AGH-UST, Krakow, PL N. Kardjilov, HZB	Date(s) of Experiment  01.07.2010 – 04.07.2010

Date of report: 14.01.2011

The proposed research project was aimed at optimization of efficiency of metal-hydrogen based storage system. Although the active material itself exhibits certain capability of hydrogen absorption under laboratory conditions, the effectiveness achieved in the ready to use storage tank is limited by many factors. Among the most important limiting factors one may count spatial distribution inside the tank that may prevent hydrogen from penetration into full volume of the material.

For purposes of this experiment a set of cylindrical aluminum containers of inner diameters of 3, 4, 5, 6, 7 mm were prepared. The containers, filled by  $\text{LaNi}_{5-x}\text{Al}_x$  were connected to specially build Sievert's apparatus. This set up enabled studying containers being under constant pressure or constant concentration of introduced hydrogen.

Neutron imaging techniques are very convenient for studying distribution of hydrogen within solid state active materials enclosed in metallic vessels. Extremely high cross section for incoherent scattering of hydrogen enables tracking even small quantities of it. On the other hand, it provides excellent contrast in comparison to simple metals and alloys.

In Fig. 1 radiographic picture of the containers used for experiments are presented. The containers are under 4 bar of hydrogen pressure. The darkest 4 parts of the picture represents active material with absorbed hydrogen inside.

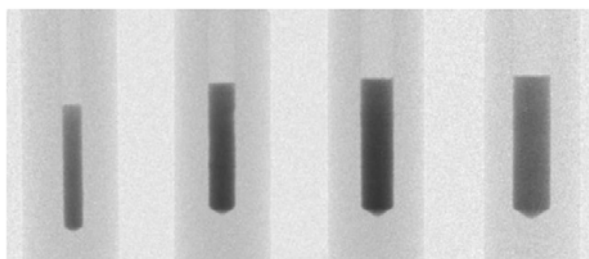


Fig. 1 Radiogram of investigated containers under hydrogen loading.

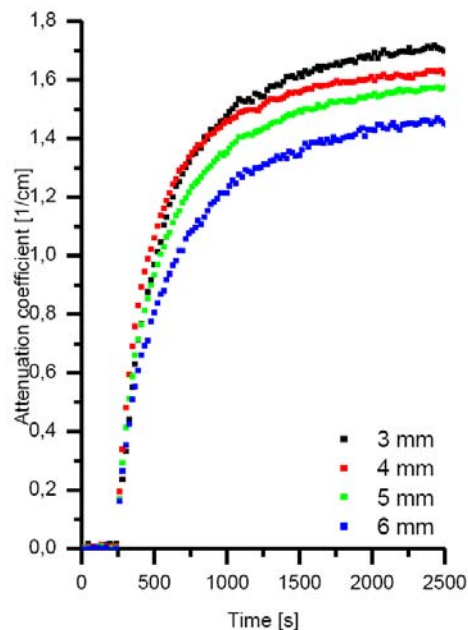



Fig. 2 attenuation coefficient versus time for each of investigated container at 4 bar of hydrogen pressure.

As one can notice, hydrogen uptake speed is related to inner diameter of the container (see Fig. 2). From preliminary data treatment, it was concluded that the speed is reciprocally proportional to the inner diameter of the container. Moreover, for thick containers the concentration of hydrogen is smallest comparing to the thinner ones.

*This research project has been supported by the European Commission under the 7<sup>th</sup> Framework Programme through "Research Infrastructures" action of the "Capacities" Programme, contract number CP-CSA\_INFRA-2008-1.1.1. Number 226507-NMI3.*

	<b>EXPERIMENTAL REPORT</b>  <b>Cold Neutron Imaging of a Humified PEM Fuel Cell Membrane</b>	Proposal: MAT-04-1947  Instrument: <b>V7</b>  Local Contact: N. Kardjilov
	Principal Proposer: D. Penumadu, University of Tennessee, USA Experimental Team: J. Bunn, University of Tennessee, USA R. Woracek, University of Tennessee, USA S. Williams, HZB A. Hilger, HZB	Date(s) of Experiment  14.06.2010 – 19.06.2010

Date of report: 28.01.2011

## Introduction

The ConRAD instrument at HZB was used along with a custom system developed water uptake measurement system for PEM at the University of Tennessee to measure small amounts of water uptake in a hydrogen fuel cell membrane under various relative humidity conditions. This system eliminates many components of an active fuel cell so that very accurate measurements can be made on water content changes in a PEM. Water management in a fuel cell is extremely important to efficient operation. Many imaging experiments are performed on an entire fuel cell system. Experiments normally measure the water generated during operation of this whole system. However, these results are high convoluted and location of water through thickness of the assembly is difficult to ascertain. These experiments are an attempt to de-couple the results and measure the water uptake of the membrane alone. The results of these measurements are very important in experimentally verifying if the modelling parameters currently used are valid and can also serve as a new characterization technique for novel fuel cell membranes for rating them using neutron imaging.

## Experiment and Results

A custom system has to control a flow of nitrogen at a desired relative humidity. Our measurement system can deliver N<sub>2</sub> at relative humidity ranging from 10%-100% using dew point control. The system also controls the temperature of the relative humidity cell. The relative humidity cell is precisely designed to have six independent channels with ribs between them (Fig 1). These areas of raised ribs ensure that no condensation can be on the surface of the membrane and moisture shown must be water uptake in the membrane. Experiments were conducted initially at 67% RH with the relative humidity cell being held at 80C.

Neutron radiographs taken every at exposures of 40 seconds after the flow of humidified gas began. Very small thicknesses of water are observed in the results. Median Images are shown in Fig 2. The water thickness sensitivity observed (Fig 3) at ConRAD is the smallest seen in a neutron image of a fuel cell membrane to the author's knowledge. This will have a large impact because this level of sensitivity is very interesting to fuel cell modelling community. A detailed analysis of the data is ongoing and a publication is being drafted currently.

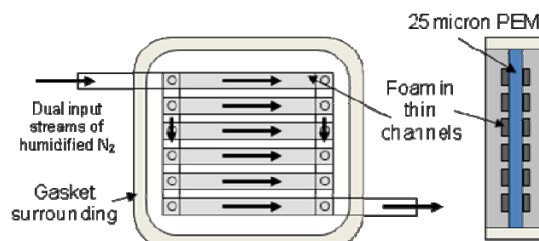


Fig. 1 – Relative humidity cell

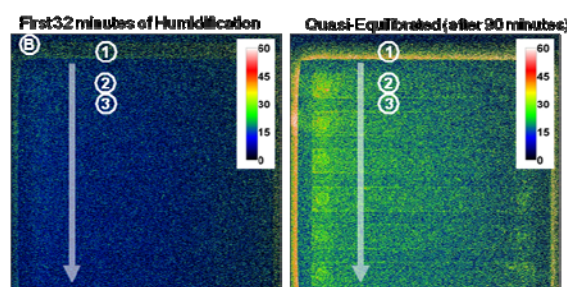


Fig. 2 Radiographs of the RH cell after a) 32 minutes of humidification and b) equilibration after 90 minutes.

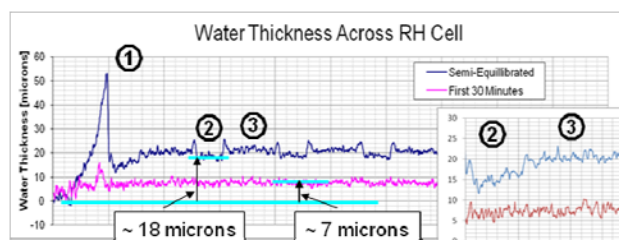



Fig. 3 Water thickness seen across the RH cells as shown in Fig. 2.

 <b>NEUTRONS</b>	<b>EXPERIMENTAL REPORT</b>  <b>Multimodality of Partially Saturated Sand from High Resolution Neutron and X-ray Tomography</b>	Proposal: MAT-04-1947  Instrument: <b>V7</b>  Local Contact: N. Kardjilov
	Principal Proposer: D. Penumadu, University of Tennessee, USA Experimental Team: F. Kim, University of Tennessee, USA N. Kardjilov, HZB M. Dawson, HZB A. Hilger, HZB	Date(s) of Experiment  14.06.2010 – 19.06.2010

Date of report: 21.01.2011

### Introduction

Partially saturated sand samples were imaged at the CONRAD instrument and the X-ray micro CT machine at HZB. Partially saturated sand is a 3-phase material composed of silica, air, and water phases. The structural distribution and orientation of the solid silica phase governs the deformation behavior of soil mass. Additionally, the distribution of water phase in the pore space adds cohesive force between sand grains. Thus, the quantification of the phase distribution is an important step to understand the shear strength of granular materials. The approach of using multimodality of neutron and X-ray imaging was used due to the difficulty of segmenting all 3 phases with a single modality. In neutron images, the water phase shows a high contrast from other phases, and in X-ray images, the silica phase is shown very well. The high resolution setup was used to visualize sample at the grain level.

### Experiments and results

Three partially saturated samples were tested both with high resolution neutron and X-ray imaging systems: Ottawa sand with water, Q-Rok sand with water, and Ottawa sand with heavy water. Ottawa sand has a rounded shape and Q-Rok sand has an angular shape as shown in Fig. 1. Both sands have average diameter of 800  $\mu\text{m}$ . The dry sands were mixed with the liquid (water or heavy water) to make the gravitational water content to 12%. The wet sand was placed in an aluminium sample holder with 3 compacted layers as shown in the radiography of Fig. 2.

The high resolution (13.7  $\mu\text{m}$  voxel size) setup of CONRAD instrument was used to take neutron tomography of each sample. The X-ray micro CT machine was used to take high resolution X-ray tomography (11.2  $\mu\text{m}$  voxel size).

The result of neutron and X-ray tomography results for Ottawa sand with water and Q-Rok sand with water samples are shown in Fig. 3. The modality was compared at approximately the same location for each sand sample with

reconstructed slices. The bright area of neutron data clearly shows the location of water and the X-ray data provides the location of silica phases. Image registration algorithms will be applied to the neutron and X-ray data sets, and the complementary information from the two modalities will be combined in the future analysis.

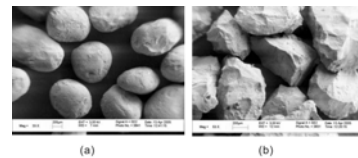


Fig. 1: Ottawa (a) sand and Q-Rok sand (b)

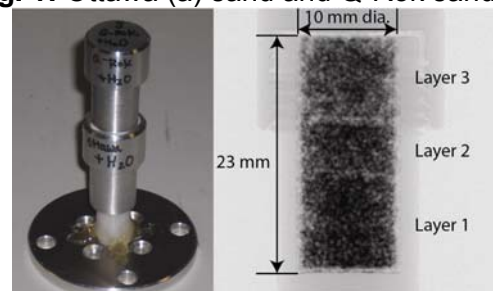
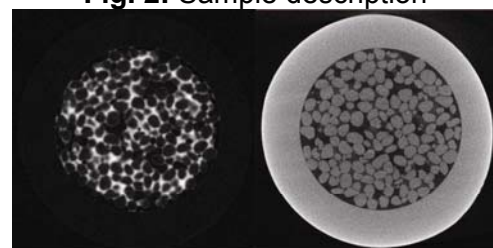
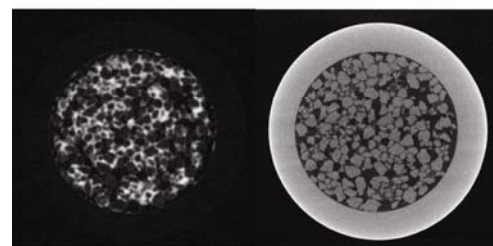


Fig. 2: Sample description




Ottawa Sand with Water



Q-Rok Sand with Water

Fig. 3: Multimodality of neutron (left) and X-ray (right) tomography data

 <b>HELMHOLTZ ZENTRUM BERLIN</b> für Materialien und Energie  <b>NEUTRONS</b>	<b>EXPERIMENTAL REPORT</b>  <b>Carbon Fiber Polymer Composites and Environmental Degradation Using Neutron Tomography</b>	Proposal: MAT-04-2032  Instrument: <b>V7</b>  Local Contact: N. Kardjilov
	Principal Proposer: D. Penumadu, University of Tennessee, USA Experimental Team: R. Woracek, University of Tennessee, USA A. Siriruk, University of Tennessee, USA F. Kim, University of Tennessee, USA A. Hilger, HZB N. Kardjilov, HZB	Date(s) of Experiment  27.08.2010 – 02.09.2010

Date of report: 31.01.2011

## Introduction

The CoNRAD instrument at HZB was used to investigate carbon fiber reinforced vinyl ester resin polymeric composite samples under various mechanical loading conditions. This material can serve as facing for sandwich structures, which are utilized in boat/ship and aircraft structures and are therefore subjected to environmental degradation by (sea) water. Experiments conducted at HZB can help to understand the structural properties and why this material shows significant degradation in cyclic fatigue and fracture behavior when saturated with water compared to dry condition. It is suspected that water conglomerates in voids, micro-capillary pores at the interface between carbon fiber bundles and resin matrix, and/or within the free volume of the polymer matrix and incompressibility of water leads to premature failure of bonding between fiber and matrix material.

## Experiment and results

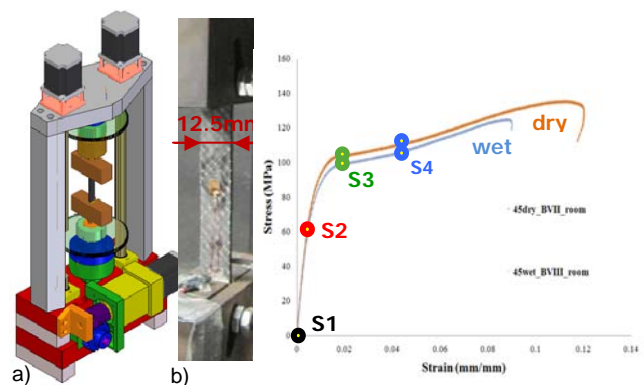
An automated mechanical loading system has been developed by the proposers especially for the use in combination with the CoNRAD instrument. The loading system (Fig. 1) has a capability of 50kN axial force and 12Nm torque, while the sample can also be rotated 360 degrees under load (tomography mode). Two different types of samples ( $\pm 45^\circ$  and  $0^\circ/90^\circ$  matrix layout) have been investigated in two conditions:

- Dry
- After saturation with salt water (over 12 month)

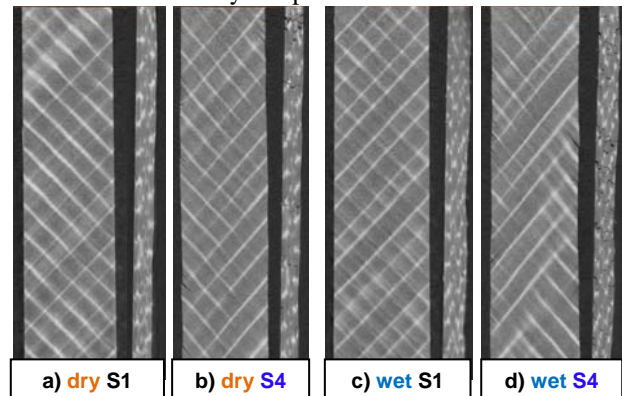
Neutron tomography was performed for all samples (4 samples total: CF  $\pm 45^\circ$  dry and wet; CF  $0^\circ/90^\circ$  dry and wet) at 4 stress levels:

- Unstressed (S1)
- 90% of elastic range (S2)
- After yield (S3)
- After significant amount of yield (S4)

Tomographic/Radiographic images show individual fiber bundles within the sample volume and how they are embedded in the resin matrix. After applying mechanical stress, fractured fiber bundles and cracks in the resin can be observed. Initial analysis shows that dry samples fail concentrated in one/few locations while wet samples show failure and separation mechanisms in many locations throughout the sample, which indicates that water has penetrated and weakened the matrix. However a more detailed analysis of the data is currently being undertaken and combined with additional tomographs obtained using the X-ray micro-CT instrument at HZB.



**Fig. 1:** a) Portable Loading system b) Specimen with rosette strain gauge in grips c) recorded Stress-Strain curve for wet and dry sample




**Fig. 2:** Tomographic reconstructions of  $\pm 45^\circ$  specimen (side and front view from inside the sample) for: a) dry S1 b) dry S4 c) wet S1 d) wet S4



# Cultural Heritage



	<b>EXPERIMENTAL REPORT</b>	Proposal: BIO-04-2037
	<b>Cranial osteological correlates of sensory adaptations in mammals with implications for the palaeoecology of extinct species</b>	Instrument: X3 Local Contact: N. Kardjilov
Principal Proposer: Experimental Team:	N. Crumpton, University of Cambridge, UK N. Crumpton, University of Cambridge, UK N. Kardjilov, HZB	Date(s) of Experiment  01.12.2010 – 07.12.2010

Date of report: 07.02.2011

BIO-04-2037 consisted of a sample of 54 mammal skulls being micro-CT scanned at the X3 resource. This was facilitated by the efforts of Nikolay Kardjilov, resulting in a large number of data generated during a relatively short 7-day period. The taxa sampled included a range of faunivorous mammals representative of the Lipotyphla families (Erinaceidae, Soricidae and Solenodontidae) including species of Talpidae (semiaquatic and terrestrial). The investigation was designed in order for us to discover whether evidence of tactile sensitivity were recorded in bony structures of the skull. One principle site of importance was the mandibular canal through which the third partition of the trigeminal nerve is transmitted. This has recently received interest in the literature due to the presence of a hypertrophied canal in a fossil mammal now interpreted to be an electroreceptive monotreme. An aim of this investigation is to review the mandibular canal in extant mammals in order to ascertain whether such claims are appropriate (e.g. hypertrophied canals are unusual in mammals). This would have been very difficult to study without the use of a good quality micro-CT scanner as in HZB. However, see figure 1 for an example of the ease with which this information can be taken from the data. Preliminary results show a hypertrophied canal may not just be associated with electrosensitivity. Other anatomy closer to the braincase difficult to sample without micro-CT data have corroborated this result.

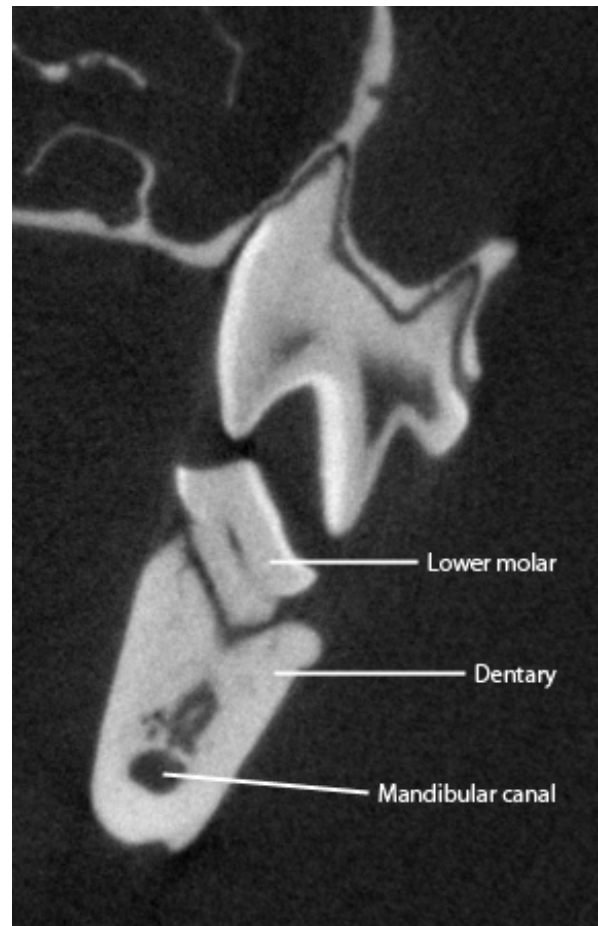


Figure 1. Coronal slice of *Scapanus orarius*.

Figure 2. illustrates the excellent results of our inner-ear study generated from the HZB scans. The resolution of these data is far superior to anything possible at other institutions we enquired at. Initial results have indicated a correlation between properties of the semicircular canals and agility in the animals sampled including a marked difference between semi-aquatic and terrestrial species. New software is being applied to the anatomies in order to investigate what role phylogeny plays in inner ear morphology.

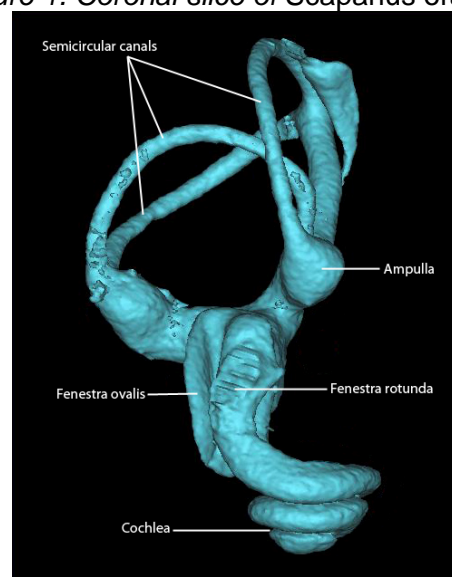



Figure 2. Reconstructed inner ear of *S. orarius*.

Additionally, simple descriptive work will lead to further papers due to the unusual morphology of the inner ears found in the Talpid species sampled. No major problems were found with the equipment and all our data appear to be extremely high quality.



 <p><b>HELMHOLTZ ZENTRUM BERLIN</b> für Materialien und Energie</p> <p><b>NEUTRONS</b></p>	<p><b>EXPERIMENTAL REPORT</b></p> <p><b>Evolution of development in placental mammals</b></p>	<p>Proposal: BIO-04-1972</p> <p>Instrument: <b>X3</b></p> <p>Local Contact: N. Kardjilov</p>
<p>Principal Proposer: Experimental Team:</p>	<p>R. Asher, Univ. Cambridge, UK L. Hautier, Univ. Cambridge, UK N. Kardjilov, HZB</p>	<p>Date(s) of Experiment</p> <p>25.01.2010 – 31.01.2010 22.03.2010 – 03.04.2010</p>


Date of report: 21.01.2011

Dr. Lionel Hautier spent three weeks at the Helmholtz Zentrum Berlin from 25 to 30 January 2010 and then from 22 March to 2 April 2010. The aim of this study was to scan fetuses of placental mammals. We used standard sampling protocols plus non-invasive microCT to recognize developmental anatomy. We wanted to collect data on the sequences of skeletal ossification, soft tissue formation, dental eruption, and frequency of adult and juvenile vertebral anomalies such as cervical ribs and hemivertebrae throughout mammalian orders, with a particular focus on Afrotheria and Xenarthra.

Our project integrates the disciplines of embryology, systematics, palaeontology and genetics. Such integration is essential to understanding developmental morphology, which comprises one of the most fundamental targets of selection that, over time, results in the generation of major evolutionary patterns. Such patterns can be illuminated by projects such as ours that form non-traditional combinations of biological and earth-historical disciplines, which fall inbetween the remits of research councils such as BBSRC (focusing on living diversity and molecular biology) and NERC (earth history and environment). Only EU support could give us the opportunity to have access freely to several weeks of beam time that would be totally inconceivable otherwise.

The Helmholtz Zentrum Berlin gave us access to a large time of beam time that allowed us have at our disposal dense samples of growth series of afrotherian and xenarthran genera. Nikolay Kardjilov and his collaborators were very helpful and

their knowledge about microtomography very precious. The Helmholtz Zentrum Berlin offered us the perfect conditions for working by combining a talented staff, a freedom of action, and great amount of beam time.

 <b>HELMHOLTZ ZENTRUM BERLIN</b> für Materialien und Energie  <b>NEUTRONS</b>	<b>EXPERIMENTAL REPORT</b>  <b>Neutron tomographic imaging of lead roundshot from the Battle of Towton (1461 AD)</b>	Proposal: EF  Instrument: <b>V19</b>  Local Contact: O. Ebrahimi
	Principal Proposer: E. Godfrey, Open University, Milton Keynes, UK Experimental Team: W. Kockelmann, ISIS, Rutherford Appleton Lab. UK O. Ebrahimi, Beuth Hochschule für Technik & HZB N. Karakas, Beuth Hochschule für Technik & HZB W. Treimer, Beuth Hochschule für Technik & HZB	Date(s) of Experiment  26.09.2010 – 02.10.2010

Date of report: 30.01.2011

Two lead roundshot have been recovered during archaeological field survey at the Towton battlefield site, by Tim Sutherland and Simon Richardson of the Towton Battlefield Archaeological Survey Project. Sutherland and Richardson have provided the artefacts for non-destructive characterisation.

The Battle of Towton (1461 AD) was fought near Tadcaster in Yorkshire during the War of the Roses, and is remembered as the bloodiest battle ever fought before or since in England, due to the very high number of casualties suffered on both sides. Following the discovery of a mass grave-pit in 1996, Towton was the subject of a television documentary and popular publication [1]. There is continuing interest in Towton, partly due to the new finds and partly due to activities surrounding the upcoming 550<sup>th</sup> anniversary of the battle in 2011.

At the time of Towton in the mid-fifteenth century AD, gunpowder weapons were just being introduced to the battlefield. The two lead shot from Towton are the earliest identified remains of munitions from a British battlefield. Around 250 welded wrought iron arrowheads have been recovered from the site of Towton, compared with just the two examples of lead shot; a clear indication that the armies were mainly dependent on bow-and-arrow, along with the other iron hand-weapons (e.g. sword, spear, pike, axe). Gunpowder weapons appear to have been used experimentally in this battle. Some twenty-five years later, by the end of the War of the Roses, at the Battle of Bosworth (1485), lead munitions are represented in much higher proportion, and by the time of the English Civil War in the 17<sup>th</sup> century, artillery had fully replaced the bow and arrow on the battlefield. We have studied the two Towton roundshot objects by neutron imaging, using discrete neutron wavelengths of 3.9 and 4.2 Å. Full tomographies were collected at 3.9 Å, with a spatial resolution of 120 µm and with 400 angular steps for the 30 mm diameter shot.

The collection time per step was 300 seconds. A replica 30mm roundshot sample of solid Pb was studied for comparison.

Neutron radiographs of the objects are shown in Fig. 1 and Fig. 2. The data on the 30mm Towton roundshot show an off-centre positioned iron block cast inside the lead shot. The darker features within the lead areas are presumed to relate to the crystallographic texture. Most of the features visible in the neutron radiograph of the solid lead Towton 25mm shot (Fig. 2) also appear to relate to the lead microstructure. It is a notable result (1) that imaging with one wavelength reveals microstructural features, (2) that these structures are present at all in these objects, as in theory lead re-crystallises at just above room temperature. It appears that there are in fact a variety of texture features present, which could be related to the manufacture and use of the munition. The reconstruction of the 3D images, characterisation of the iron block, and quantification of the texture by neutron diffraction measurements will help interpreting the data.

[1] V. Fiorato, A. Boylston, C. Knusel eds., *Blood Red Roses*, Oxbow Books, Oxford, 2000.

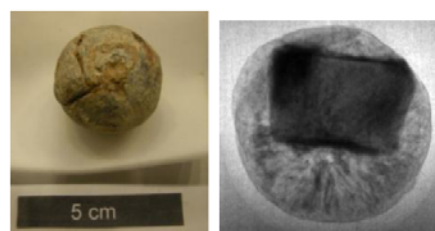


Fig. 1. Towton 30mm lead-iron shot (left) with neutron radiograph (right)

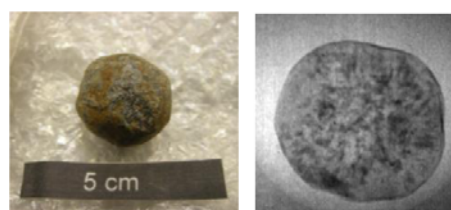


Fig. 2. Towton 25mm lead shot (left) with neutron radiograph (right)



# **Part II**

## **List of Publications**

<b>Theses</b>	<b>171</b>
<b>Publications</b>	<b>172</b>
<b>Author Index</b>	<b>181</b>



## Theses 2010

### Examina

#### PhD theses

2010

---

*Aoun, B.*

**Liquides ioniques : structure et dynamique**  
CNRS Orléans, France (2010)

---

*Chmielus, M.*

**Composition, Structure and Magneto-Mechanical Properties of Ni-Mn-Ga Magnetic Shape-Memory Alloys**  
Technische Universität Berlin, Germany (2010)

---

*Landsgesell, S.*

**Emerging Magneto-Electric Properties in Orthorhombic Nd<sub>1-x</sub>YxMnO<sub>3</sub>**  
Technische Universität Berlin, Germany (2010)

---

*Lijing, K.*

**Mechanism of anti-influenza virus activity of Maillard reaction products derived from Isatis roots**  
The University of Edinburgh, United Kingdom (2010)

---

*Nunes, R.M.*

**Investigação de Distorções de Forma e Empenamentos e suas Causas em uma Rota de Fabricação de Hastes de Amortecedores Automotivos**  
UFRGS - Universidade Federal do Rio Grande do Sul (2010)

---

*Pefoute Takom, E.W.*

**Vers une meilleure compréhension du stockage de l'Hydrogène dans les clathrate hydrates : Analyse de leur dynamique par simulation numérique par dynamique moléculaire et par diffusion quasiélastique de neutrons**  
Université de Bordeaux - l'École doctorale des sciences chimiques, France (2010)

---

*Pieper, O.*

**Neutron Scattering Investigations of Zero- and One-dimensional Quantum Magnets**  
Technische Universität Berlin, Germany (2010)

---

*Ryabova, N.Y.*

**Structure and hydration of model lipid membrane based on ceramide-6. Neutron diffraction investigations in real time**  
Joint Institute for Nuclear Research, Russian Federation (2010)

---

#### Diploma

2010

---

*Cermák, P.*

**Magnetic properties of Ce compounds studied by specific heat**  
Charles University in Prague, Czech Republic (2010)

---

*Fischer, J.*

**Study of the Vibrational and Structural Properties of the Sulfur-based Amino Acid L-Methionine**  
Universitat Kassel, Germany, (2010)

---

*Matys, M.*

**Investigation of chosen R<sub>3</sub>Cu<sub>4</sub>Sn<sub>4</sub>**  
AGH Univeristy of Scince and Technology, Poland (2010)

---

## Publications 2010

### 2005 (supplement)

---

*Czeslik, C.; Hazlete, T.; Gratton, E.; Steitz, R.; von Grunberg, H.; Ballauff, M.*  
**Effect of salt on the immobilization of proteins at polyelectrolyte brushes**  
 Biophysical Journal **89** (2005), 387A - 388A

---

### 2007 (supplement)

---

*Schorr, S.; Wagner, G.; Tovar, M.; Sheptyakov, D.*  
**Structure and Microstructure of Zn<sub>2x</sub>(CuBIII)<sub>1-x</sub>X<sub>2</sub> semiconductors (BIII=Ga,In; X=S,Se,Te)**  
 Mater. Res. Soc. Symp. Proc. **1012** (2007), 1012-Y03-0

---

*Zagorodniy K.; Shivanyuk V.; Toebbens D.; Danilkin S.; Gavriljuk V.*  
**Hydrogen-caused phase transformations, relaxation and hysteretic phenomena in fcc alloys Fe<sub>55</sub>Cr<sub>25</sub>Ni<sub>20</sub> and Fe<sub>50</sub>Ni<sub>50</sub>**  
 Scripta Materialia **50** (2007), 1467 - 1470

---

### 2008 (supplement)

---

*Brückel, T.; Kentzinger, E.; Mattauch, S.; Paul, A.; Rücker, U.; Voigt, J.*  
**A deeper look into magnetic nanostructures using advanced scattering methods**  
 Pramana : Journal of Physics, **71** (2008) 5, 895

---

### 2009 (supplement)

---

*Kamel, S.; Wimpory, R.C.; Hofmann, M.*  
**The Effects of Constraint and Compressive or Tensile Residual Stresses on Brittle Fracture**  
 ASME Conference Proceedings Vol. **5** (2009), 305 - 313

---

*Lehmann, S.; Fuertes Marrón, D.; Tovar, M.; Tomm, Y.; Wolf, Ch.; Schorr, S.; Schedel-Niedrig, Th.; Arushanov, E.; Lux-Steiner, C.M.*  
**A structural study on the CuGaSe<sub>2</sub>-related copper-poor materials CuGa<sub>3</sub>Se<sub>5</sub> and CuGa<sub>5</sub>Se<sub>8</sub>: thin-film vs. bulk material**  
 Physical Status Solidi A **206** (2009), 1009 - 1112

---

*Paul, A.; Mattauch, S.*  
**Microscopic origin of training in exchange bias system**  
 Applied Physics Letter, **95**, 092502 (2009)

---

*Repper, J.; Hofmann, M.; Kremaszky, C.; Wimpory, R.C.; Petry, W.; Werner, E.*  
**Micro stress accumulation in multiphase superalloys**  
 Powder Diffraction **24** [Suppl. 1] (2009), S65-S67

---

*Saensunon, B.; Stewart, G.A.; Gubbens, P.C.M.; Hutchison, W.D.; Buchsteiner, A.*  
**The crystal field interaction at the rare earth site in ErNiAl<sub>4</sub>**  
 Journal of Physics: Condensed Matter **21** (2009), 124215

---

*Smith, M.C.; Smith, A.C.; Wimpory, R.C.; Ohms, C.; Nadri, B.; Bouchard, P.J.*  
**Optimising Residual Stress Measurements and Predictions in a Welded Benchmark Specimen: A Review of Phase 2 of the NeT Task Group 1 Single Bead on Plate Round Robin**  
 Pressure Vessels and Piping Conference (2009), 277 - 301

---

## 2010

---

*Agamalian, M.; Carpenter, J.M.; Treimer, W.*

**Remarkable precision of the 90-year-old dynamic diffraction theories of Darwin and Ewald**

Journal of Applied Crystallography **43** (2010), 900 - 906

---

*Aoun, B.; Gonzalez, M.A.; Ollivier, J.; Russina, M.; Izaola, Z.; Price, D.L.; Saboungi, M.L.*

**Translational and Reorientational Dynamics of an Imidazolium-Based Ionic Liquid**

Journal of Physical Chemistry Letters **1** (2010), 2503 - 2507

---

*Baran, S.; Arulraj, A.; Kaczorowski, D.; Penc, B.; Szytula, A.*

**Magnetic ordering and magnetic properties of ErAuxNi<sub>1-x</sub>In (0 ≤ x ≤ 1) solid solution**

Intermetallics **18** (2010), 42 - 46

---

*Baran, S.; Gondek, L.; Szytula, A.; Kaczorowski, D.; Pikul, A.; Penc, B.; Piekarczyk, P.; Hoser, A.; Gerischer, S.*

**Low temperature thermodynamical properties of ErCu<sub>2</sub>Si<sub>2</sub>**

Journal of Magnetism and Magnetic Materials **322** (2010), 12 - 18

---

*Baran, S.; Kaczorowski, D.; Arulraj, A.; Penc, B.; Szytula, A.*

**Magnetic structure and thermodynamic properties of TmPtIn**

Journal of Magnetism and Magnetic Materials **322** (2010), 2177 - 2183

---

*Behne, D.; Alber, D.; Kyriakopoulos, A.*

**Long-term selenium supplementation of humans: Selenium status and relationships between selenium concentrations in skeletal muscle and indicator materials**

Journal of Trace Elements in Medicine and Biology **24** (2010), 99 - 105

---

*Belo, E.A.; Lima Jr., J.A.; Freire, P.T.C.; Melo, F.E.A.; Mendes Filho, J.; Bordallo, H.N.; Polian, A.*

**High-pressure Raman spectra of racemate dl-alanine crystals**

Vibrational Spectroscopy **54** (2010), 107 - 111

---

*Beskrovny A.I.; Vasilovskii, S.G.; Vakhrushev, S.B.; Kurdyukov, D.A.; Zvorykina, O.I.; Naberezhnov, A.A.; Okuneva, N.M.; Tovar, M.; Rysiakiewicz-Pasek, E.; Jagus, P.*

**Temperature Dependences of the Order Parameter for Sodium Nitrite Embedded into Porous Glasses and Opals**

Physics of the Solid State **52** (2010), 1092 - 1097

---

*Burmistrova, A.; Steitz, R.; von Klitzing, R.*

**Temperature Response of PNIPAM Derivatives at Planar Surfaces: Comparison between Polyelectrolyte Multilayers and Adsorbed Microgels**

ChemPhysChem **11** (2010), 3571 - 3579

---

*Chmielus, M.; Rolfs, K.; Wimpory, R.C.; Reimers, W.; Müllner, P.; Schneider, R.*

**Effects of surface roughness and training on the twinning stress of Ni-Mn-Ga single crystals**

Acta Materialia **58** (2010), 3952

---

*Chmielus, M.; Witherspoon, C.; Wimpory, R.C.; Paulke, A.; Hilger, A.; Zhang, X.; Dunand, D.C.; Müllner, P.*

**Magnetic-field-induced recovery strain in polycrystalline Ni-Mn-Ga foam**

Journal of Applied Physics **108** (2010), 123526

---

*Davies, C.M.; Wimpory, R.C.; Paradowska, A.M.; Nikbin, K.M.*

**Residual Stress Measurements in Large Scale Component Sections**

Materials Science Forum **652** (2010), 321 - 326

---

*Denker, A.; Peltz, U.*

**Gemäldeuntersuchungen mit hochenergetischen Protonen**

Metalla (Sonderheft **3**: Archäometrie und Denkmalpflege 2010) (2010), 68 - 70

---



---

*Ebrahimi, O.; Treimer, W.; Strobl, M.; Feye-Treimer, U.; Beul, N.; Jericha, E.; Seidel, S.O.;*

**Ultra small angle scattering versus refraction**

Journal of Physics: Conference Series **251** (2010) 012072 doi:10.1088/1742-6596/251/1/012072

---

*Epp, J.; Hirsch, T.; Hunkel, M.; Wimpory, R.C.*

**Combined neutron and X-ray diffraction analysis for the characterization of a case hardened disc**

Materials Science Forum **652** (2010), 37 - 43

---

*Erko, M.; Wallacher, D.; Brandt, A.; Paris, O.*

**In-situ small-angle neutron scattering study of pore filling and pore emptying in ordered mesoporous silica**

Journal of Applied Crystallography **43** (2010), 1 - 7

---

*Evers, F.; Reichhart, C.; Steitz, R.; Tolan, M.; Czeslik, C.*

**Probing adsorption and aggregation of insulin at a poly(acrylic acid) brush**

Physical Chemistry Chemical Physics **12** (2010), 4375 - 4382

---

*Evers, F.; Steitz, R.; Tolan, M.; Czeslik, C.*

**Analysis of Hofmeister Effects on Protein Adsorption at Aqueous-Solid Interfaces**

Biophysical Journal **98** (2010), 45a

---

*Exius, I.; Schmidt, K.P.; Lake, B.; Tennant, D.A.; Uhrig, G.S.*

**Vertex corrections in the dynamic structure factor in spin ladders**

Physical Review B **82**, 214410 (2010)

---

*Farajian, M.; Wimpory, R.C.; Nitschke-Pagel, Th.*

**Relaxation and Stability of Welding Residual Stresses in High Strength Steel under Mechanical Loading**

Steel Research International **81** (2010), 1137 - 1143

---

*Feyerherm, R.; Dudzik, E.; Prokhnenko, O.; Argyriou, D.N.*

**Rare earth magnetism and ferroelectricity in RMnO<sub>3</sub>**

Journal of Physics: Conference Series **200** (2010), 012032/1 - 4

---

*Freund, A.K.; Gsell, S.; Fischer, M.; Schreck, M.; Andersen, K.H.; Courtois, P.; Borchert, G.; Skoulatos, M.*

**Diamond single crystals for neutron instrumentation: First experimental results**

Nuclear Instruments And Methods A (2010), doi:10.1016/j.nima.2010.05.043

---

*Friedrichs, O.; Kim, J. W.; Remhof, A.; Wallacher, D.; Hoser, A.; Cho, Y.W.; Oh, K.H.; Züttel, A.*

**Core shell structure for solid gas synthesis of LiBD<sub>4</sub>**

Physical Chemistry Chemical Physics **12** (2010), 4600 - 4603

---

*Frontzek, M.; Tang, F.; Link, P.; Schneidewind, A.; Mignot, J.M.; Hoffman, J.U.; Loewenhaupt, M.*

**A Generic Phase Diagram for R<sub>2</sub>PdSi<sub>3</sub> (R = Heavy Rare Earth)?**

Journal of Physics: Conference Series **251** (2010), 012026/1 - 4

---

*Getzschmann, J.; Senkovska, I.; Wallacher, D.; Tovar, M.; Fairen-Jimenez, D.; Düren, T.; Van Baten, J.M.; Krishna, R.; Kaskel, S.*

**Methane storage mechanism in the metal-organic framework Cu<sub>3</sub>(btc)<sub>2</sub>: An in situ neutron diffraction study**

Microporous and Mesoporous Materials **136** (2010), 50 - 58

---

*Gondek, L.; Penc, B.; Kaczorowski, D.; Baran, S.; Hoser, A.; Gerischer, S.; Szytula, A.*

**Magnetic and thermodynamic properties of NdT<sub>2</sub>Ge<sub>2</sub> (T=Pd, Ag) compounds**

Journal of Solid State Chemistry **183** (2010), 789 - 794

---

*Gondek, L.; Przewoznik, J.; Kapusta, Cz.; Czub, J.; Kozlak, K.; Szytula, A.; Prokhnenko, O.; Piekarczyk, P.*

**Magnetic properties of Nd<sub>3</sub>Ag<sub>4</sub>Ge<sub>4</sub>**

Intermetallics **18** (2010), 1211 - 1215

---

---

*Groitzl, F.; Kiefer, K.; Habicht, K.*

**A resolution model for mode multiplets probed with neutron resonance spin-echo spectroscopy**

Physica B (2010), doi:10.1016/j.physb.2010.11.048

---

*Gubkin, A.F.; Podlesnyak, A.; Baranov, N.V.*

**Single-crystal neutron diffraction study of the magnetic structure of Er<sub>3</sub>Co**

Physical Review B: Condensed Matter **82** (2010), 012403

---

*Hautier, L.; Weisbecker, V.; Sánchez-Villagra, M.R.; Goswami, A.; Asher, R.J.*

**Skeletal development in sloths and the evolution of mammalian vertebral patterning**

Proceedings of the National Academy of Sciences **107** (2010), 18903 - 18908

---

*Ianeselli, L.; Zhang, F.; Skoda, M. W. A.; Jacobs, R. M. J.; Martin, R. A.; Callow, S.; Prevost, S.; Schreiber, F.*

**Protein-protein interactions in ovalbumin solutions studied by small-angle scattering: effect of ionic strength and the chemical nature of cations**

Journal of Physical Chemistry B **114** (2010), 3776 - 3783

---

*Islam N.; Pieper O.; Lake B.; Siemensmeyer, K.*

**Unconventional Growth Mechanism in Optical Traveling Solvent Floating Zone Growth of Large β-CuNb<sub>2</sub>O<sub>6</sub> Single Crystals.**

Crystal Growth and Design, **11** (2010/11) pp 154–157

---

*Islam N.; Quintero-Castro D.; Lake B.; Siemensmeyer K.; Kiefer K.; Skourski Y.; Herrmannsdorfer, T.*

**Optical Floating-Zone Growth of Large Single Crystal of Spin Half Dimer Sr<sub>3</sub>Cr<sub>2</sub>O<sub>8</sub>.**

Crystal Growth and Design **10** 465-468 (2010)

---

*Islam, N.; Quintero-Castro, D.; Lake, B.; Siemensmeyer, K.; Kiefer, K.; Skourski, Y.; Herrmannsdorfer, T.*

**Optical Floating-Zone Growth of Large Single Crystal of Spin Half Dimer Sr<sub>3</sub>Cr<sub>2</sub>O<sub>8</sub>**

Crystal Growth and Design **10** (2010), 465 - 468

---

*Izaola, Z.; Russina, M.*

**Virtual design of the neutron guide for the TOF spectrometer NEAT**

Journal of Physics: Conference Series **251** (2010), 012064/1 - 4

---

*Jornet-Somoza, J.; Deumal, M.; Robb, M.A.; Landee, C.P.; Turnbull, M.M.; Feyerherm, R.; Novoa, J.J.*

**First-Principles Bottom-Up Study of 1D to 3D Magnetic Transformation in the Copper Pyrazine Dinitrate S = Antiferromagnetic Crystal**

Inorganic Chemistry **49** (2010), 1750 - 1760

---

*Kamel, S.; Wimpory, R.C.; Hofmann, M.; Nikbin K.M.; O'Dowd, N.P.*

**Predicting the effect of compressive and tensile residual stresses in fracture mechanics specimens**

Advanced Materials Research **89-91** (2010), 275 - 280

---

*Karpinsky, D.V.; Troyanchuk, I.O.; Chobot, G.M.; Efimov, V.V.; Prokhnenko, O.; Sikolenko, V.*

**Magnetic peculiarity and crystal structure of Pr<sub>0.5</sub>Sr<sub>0.5</sub>Co<sub>1-x</sub>FexO<sub>3</sub>**

Physica Status Solidi (B) Volume **247**, Issue 2, (2010) 411–415

---

*Khaydukov, Y.N.; Aksenov, V.L.; Nikitenko, Y.V.; Zhernenkov, K.N.; Nagy, B.; Teichert, A.; Steitz, R.; Bottyan, L.*

**Magnetic proximity effects in V/Fe superconductor/ferromagnet single bilayer revealed by waveguide-enhanced polarized neutron reflectometry**

Journal of Superconductivity and Novel Magnetism, Volume **24**, (2010) 961-968

---

*Klages, M.; Krüger, P.; Haußmann, J.; Markötter, H.; Arlt, T.; Hartnig, C.; Kardjilov, N.; Banhart, J.; Manke, I.; Scholta, J.*

**Untersuchung des Einflusses von GDL-Eigenschaften auf den Wasserhaushalt mittels Neutronenradiografie = Investigation of the influence of GDL properties on the water balance by means of neutron radiography**

MP Materials Testing **52** (2010), 718 - 724

---

---

*Krist, Th.; Pappas, C.; Teichert, A.; Fehr, C.; Clemens, D.; Steichele, E.; Mezei, F.*

**New polarizing guide for neutron wavelengths above 2.5 Å;**

Journal of Physics: Conference Series **251** (2010), 012081/1 - 4

---

*Lee, S.W.; Kim, K.-Y.; Kwon, O.Y.; Kardjilov, N.; Dawson, M.; Hilger, A.; Manke, I.*

**Observation of Magnetic Domains in Insulation-Coated Electrical Steels by Neutron Dark-Field Imaging**

Applied Physics Express **3** (2010), 106602/1 - 3

---

*Manke, I.; Hartnig, C.; Kardjilov, N.; Riesemeier, H.; Goebbels, J.; Kuhn, R.; Krüger, P.; Banhart, J.*

**In situ Synchrotron X-ray Radiography Investigations of Water Transport in PEM Fuel Cells**

Fuel Cells **10** (2010), 26 - 34

---

*Manke, I.; Kardjilov, N.; Schäfer, R.; Hilger, A.; Strobl, M.; Dawson, M.; Grünzweig, C.; Behr, G.; Hentschel, M.; David, C.; Kupsch, A.; Lange, A.; Banhart, J.*

**Three-dimensional imaging of magnetic domains**

Nature Communications **1** (2010), 125/1 - 6

---

*Martelli, P.; Remhof, A.; Borgschulte, A.; Mauron, P.; Wallacher, D.; Kemner, E.; Russina, M.; Pendolino, F.; Züttel, A.*

**BH<sub>4</sub> - Self-Diffusion in Liquid LiBH<sub>4</sub>**

Journal of Physical Chemistry A **114** (2010), 10117 - 10121

---

*Matas, S.; Dudzik, E.; Feyerherm, R.; Gerischer, S.; Klemke, S.; Prokes, K.; Orendacova, A.*

**Neutron diffraction study on the two-dimensional Ising system KEr(MoO<sub>4</sub>)<sub>2</sub>**

Physical Review B **82** (2010), 184427/1 - 8

---

*Motohashi Y.; Ryukhtin V.; Sakuma T.; Saroun J.*

**Influence of Flat Cavity Formation on Stress vs. Strain and Strain-Rate Relations of Superplastic Deformation in 3Y-TZP**

Materials Transactions **51** (2010), 567 - 573

---

*Nakajima, T.; Mitsuda, S.; Kanetsuki, S.; Yamano, M.; Iwamoto, S.; Yoshida, Y.; Mitamura, H.; Sawai, Y.; Tokunaga, M.; Kindo, K.; Prokes, K.; Podlesnyak, A.*

**Anisotropic magnetic field responses of ferroelectric polarization in the trigonal multiferroic CuFe<sub>1-x</sub>Al<sub>x</sub>O<sub>2</sub> (x=0.015)**

Physical Review B **81** (2010), 014422/1 - 10

---

*Ohms, C.; Wimpory, R.C.; Neov, D.*

**Residual stress measurement by neutron diffraction in a single bead on plate weld - Influence of instrument and measurement settings on the scatter of the results**

Materials Science Forum **638-642** (2010), 2452 - 2457

---

*Ohms, C.; Wimpory, R.C.; Neov, D.; Hofmann, M.; Turski, M.; Haigh, R.; Fitzpatrick, M.; Edwards, L.*

**Residual Stress Measurements in a Three-Bead Slot Weld in a 20 mm Carbon Steel Plate**

American Society of Mechanical Engineers (2010) 469 - 479

---

*Painter, T.A.; Adkins, T.; Bai, H.Y.; Bird, M.D.; Bole, S.; Cantrell, K.; Chen, J.P.; Dixon, I.R.; Ehmler, H.; Gavrilin, A.; Han, K.; Lu, J.; Smeibidl, P.; Walsh, R.; Weijers, H.W.; Xu, T.; Zhai, Y.H.*

**Recent Progress of the Series-Connected Hybrid Magnet Projects**

IEEE Transactions on Applied Superconductivity **20** (2010), 692 - 695

---

*Park, J.T.; Inosov, D.S.; Yaresko, A.; Graser, S.; Sun, D.L.; Bourges, Ph.; Sidis, Y.; Li, Y.; Kim, J.-H.; Haug, D.; Ivanov, A.; Hradil, K.; Schneidewind, A.; Link, P.; Faulhaber, E.; Glavatskyi, I.; Lin, C. T.; Keimer, B.; Hinkov, V.*

**Symmetry of spin excitation spectra in the tetragonal paramagnetic and superconducting phases of 122-ferropnictides**

Physical Review B: Condensed Matter **82** (2010), 134503

---

---

*Paul, A.*

**Manipulation of uncompensated moments in trained exchange bias system**

Applied Physics Letters **97** (2010), 129901

---

*Paul, A.*

**Manipulation of uncompensated moments in trained exchange bias system**

Applied Physics Letters (2010), 032505

---

*Penc, B.; Baran, S.; Kaczorowski, D.; Hoser, A.; Szytula, A.*

**Magnetic structure of ErCu<sub>2</sub>Ge<sub>2</sub>**

Journal of Alloys and Compounds **503** (2010), L18 - L20

---

*Peterson, V.K.; Kearley, G.J.; Wu, Y.; Kepert, C.J.; Ramirez-Cuesta, A.J.; Kemner, E.; Kepert, C.J.*

**Local Vibrational Mechanism for Negative Thermal Expansion: A Combined Neutron Scattering and First-Principles Study**

Angewandte Chemie International Edition Engl. **49** (2010), 585 - 588

---

*Quintero-Castro, D.; Lake, B.; Wheeler E.; Islam A.; Guidi T.; Rule, K.; Izaola, Z.; Russina, M.; Kiefer, K.; Skourski, Y.; Herrmannsdörfer, T.*

**Magnetic excitations of the gapped quantum spin dimer antiferromagnet Sr<sub>3</sub>Cr<sub>2</sub>O<sub>8</sub>**

Physical Review B: Condensed Matter **81** (2010), 014415

---

*Ritzoulis, C.; Strobl, M.; Panayiotou, C.; Choinka, G.; Tsiptsias, C.; Vasiliadou, C.; Vasilakos, V.; Beckmann, F.; Herzen, J.; Donath, T.*

**Ultra-small angle neutron scattering and X-ray tomography studies of caseinate hydroxyapatite microporous materials**

Materials Chemistry and Physics **123** (2010), 77 - 82

---

*Robinson, J.S.; Hossain, S.; Truman, C.E.; Paradowska, A.M.; Hughes, D.J.; Wimpory, R.C.; Fox, M.E.*

**Residual stress in 7449 aluminium alloy forgings**

Materials Science and Engineering A **527** (2010), 2603 - 2612

---

*Rolfs, K.; Chmielus, M.; Wimpory, R.C.; Mecklenburg, A.; Müllner, P.; Schneider, R.*

**Double twinning in Ni-Mn-Ga-Co**

Acta Materialia **58** (2010), 2646 - 2651

---

*Rolfs, K.; Wimpory, R.C.; Petry, W.; Schneider, R.*

**Effect of alloying Ni-Mn-Ga with Cobalt on thermal and structural properties**

Journal of Physics: Conference Series **251** (2010), 012046/1 - 4

---

*Ryabova, N.Y.; Kiselev, M.A.; Dante, S.; Hauß, Th.; Balagurov A.M.*

**Investigation of stratum corneum lipid model membranes with free fatty acid composition by neutron diffraction**

European Biophysics Journal **39** (2010), 1167 - 1176

---

*Ryabova, N.Y.; Kiselev, M.A.; Dante, S.; Hauß, Th.; Balagurov, A.M.*

**Investigation of stratum corneum lipid model membranes with free fatty acid composition by neutron diffraction**

European Biophysics Journal Volume **39**, Number 8, (2010) 1167-1176

---

*Saensunon, B.; Stewart, G.A.; Gubbens, P.C.M.; Hutchison, W.D.; Buchsteiner, A.*

**Corrigendum: The crystal field interaction at the rare earth site in ErNiAl<sub>4</sub>**

Journal of Physics: Condensed Matter **22** (2010), 029801 -

---

*Smeibidl, P.; Tennant, A.; Ehmler, H.; Bird, M.*

**Neutron Scattering at Highest Magnetic Fields at the Helmholtz Centre Berlin**

Journal of Low Temperature Physics **159** (2010), 402 - 405

---

*Sobolev, O.; Favre, F.; Kemner E.; Russina M.; Beuneu, B.; Cuello, G.J.; Charlet, L.*

**Water-clay surface interaction: A neutron scattering study**

Chemical Physics **374** (2010), 55 - 61

---

*Stephan, C.; Schorr, S.; Schock, H.W.*

**New Structural Investigations in the Cu<sub>2</sub>Se(S)-In<sub>2</sub>Se(S)(3)/ Cu<sub>2</sub>Se(S)-Ga<sub>2</sub>Se(S)(3) Phase Diagram**

Mater. Res. Soc. Symp. Proc. Vol. **1165** (2010), 411 - 417

---

---

*Strobl, M.; Steitz, R.; Kreuzer M.; Nawara, A.; Mezei, F.; Rose, M.; Grunze, M.; Dahint, R.*  
**BioRef - a time-of-flight neutron reflectometer combined with in-situ infrared spectroscopy at the Helmholtz Centre Berlin**

Journal of Physics: Conference Series **251** (2010), 012059/1 - 4

---

*Strunz, P.; Mukherji, D.; Šaroun, J.; Keiderling, U.; Rösler, J.*

**Pore structure characterization and in-situ diffusion measurement in nanoporous membrane using SANS**

Journal of Physics: Conference Series **247** (2010), 012023

---

*Szławska, M.; Kaczorowski, D.; Reehuis, M.*

**Experimental study of magnetic ordering in single-crystalline U<sub>2</sub>NiSi<sub>3</sub>**

Physical Review B **81** (2010), 094423/1 - 5

---

*Szytula, A.; Baran, S.; Gondek, L.; Arulraj, A.; Penc, B.; Stusser, N.*

**Magnetic properties of hexagonal RTIn rare-earth intermetallics with frustration**

Acta Physica Polonica A **117** (2010), 590-

---

*Szytula, A.; Kaczorowski, D.; Baran, S.; Penc, B.; Gil, A.; Hoser, A.*

**Magnetic ordering and low-temperature thermodynamic properties of ErFe<sub>2</sub>Ge<sub>2</sub>**

Journal of Magnetism and Magnetic Materials **322** (2010), 2973 - 2977

---

*Szytula, A.; Kaczorowski, D.; Gondek, L.; Pikul, A.; Arulraj, A.; Balanda, M.; Baran, S.; Penc, B.*

**Magnetic ordering in PrT<sub>2</sub>Ge<sub>2</sub> (T = Ni, Ru and Rh) compounds**

Intermetallics **18** (2010), 1766 - 1771

---

*Tang, F.; Link, P.; Frontzek, M.; Mignot, J.-M.; Hoffmann, J.-U.; Löser, W.; Loewenhaupt, M.*

**Neutron diffraction study of magnetic structures in single crystal Ho<sub>2</sub>PdSi<sub>3</sub> in magnetic fields up to 5 T**

Journal of Physics: Conference Series **251** (2010), 012017/1 - 4

---

*Tang, F.; Link, P.; Frontzek, M.; Schneidewind, A.; Löser, W.; Loewenhaupt, M.*

**Magnetic excitations of Er<sub>2</sub>PdSi<sub>3</sub> studied by inelastic neutron scattering in fields up to 12 T**

Journal of Physics: Conference Series **251** (2010), 012004/1 - 4

---

*Ting, V.P.; Henry, P.F.; Kohlmann, H.; Wilson, C.C.; Weller, M.T.*

**Structural isotope effects in metal hydrides and deuterides**

Physical Chemistry Chemical Physics **12** (2010), 2083 - 2088

---

*Ting, V.P.; Schmidtman, M.; Henry, P.F.; Dann, S.E.; Crisp, J.L.; Wilson, C.C.; Weller, M.T.*

**The kinetics of bulk hydration of the disaccharides alpha-lactose and trehalose by in situ neutron powder diffraction**

Medchemcomm **1** (2010), 345 - 348

---

*Treimer, W.; Seidel, S.-O., Ebrahimi, O.*

**Neutron tomography using a crystal monochromator**

Nuclear Instruments and Methods in Physics Research A **621** (2010) 502-505

---

*van Hejkamp, L.F.; de Schepper, I.M.; Strobl, M; Tromp, R.H.; Heringa, J.R.; Bouwman, W.G.*

**Milk gelation studied with Small Angle Neutron Scattering techniques and Monte Carlo simulations**

Journal of Physical Chemistry A **114** (2010), 2412 - 2426

---

*Vogtt, K.; Jeworrek, C.; Garamus, V. M.; Winter, R.*

**Microdomains in Lipid Vesicles: Structure and Distribution Assessed by Small-Angle Neutron Scattering**

Journal of Physical Chemistry B **114** (2010), 5643 - 5648

---

*Wagh, A.; Abbas, S.; Treimer, W.*

**First Sub-arcsecond Collimation of Monochromatic Neutrons**

Journal of Physics: Conference Series **251** (2010) 012074 doi:10.1088/1742-6596/251/1/012074

---

---

*Wang, L.; Davies, C.M.; Wimpory, R.C.; Xie, L.Y.; Nikbin K.M.*

**Measurement and simulation of temperature and residual stress distributions from friction stir welding AA2024 Al alloy**

Materials at High Temperature **27** (2010), 167 - 178

---

*Wang, M.Y.; Luo, H.Q.; Zhao, J.; Zhang, C.L.; Wang, M.; Marty, K.; Chi, S.X.; Lynn, J.W.; Schneidewind, A.; Li, S.L.; Dai, P.C.*

**Electron-doping evolution of the low-energy spin excitations in the iron arsenide superconductor BaFe<sub>2-x</sub>Ni<sub>x</sub>As<sub>2</sub>**

Physical Review B **81** (2010), 174524

---

*Wehrenfennig, C.; Meier, D.; Lottermoser, Th.; Lonkai, Th.; Hoffmann, J.-U.; Aliouane, N.; Argyriou, D. N.; Fiebig, M.*

**Incompatible magnetic order in multiferroic hexagonal DyMnO<sub>3</sub>**

Physical Review B: Condensed Matter **82** (2010), 100414-1 - 100414-4

---

*Wellert, S.; Altmann, H.J.; Richardt, A.; Lapp, A.; Falus, P.; Farago, B.; Hellweg, T.*

**Dynamics of the interfacial film in bicontinuous microemulsions based on a partly ionic surfactant mixture: A neutron spin-echo study**

European Physical Journal E **33** (2010), 243 – 250

---

*Witte, U.; Schedler, R.; Stockert, O.; Loewenhaupt, M.*

**The Investigation of the Crystalline Electric Field of CeCu<sub>2</sub> and CeCu<sub>6</sub>**

Journal of Low Temperature Physics, (2010) DOI: 10.1007/s10909-007-9302-4

---

*Zrnik, J.; Strunz, P.; Maldini, M.; Davydov, V.*

**SANS investigation of gamma prime precipitate morphology evolution in creep exposed single crystal Ni base superalloy**

Materials Science Forum **636-637** (2010), 1475 - 1482

---



# AUTHOR INDEX

Author	Page	Author	Page
<b>A</b>			
Adams, D.	108	Das, P.	66
Aldridge, L.	155	Davies, C.M.	144, 145, 148
Appel, M.	130	Dawson, M.	160
Argyriou, D.	17, 34	Degischer, P.	147
Arnache, O.	89	Deisenhofer, J.	64
Arulraj, A.	39	Demeter, J.	69, 70, 72
Asher, R.	166	Dietl, B.	39
Avgoustakis, K.	109	Disch, S.	65
<b>B</b>			
Bakandritsos, A.	109	Dobner, B.	101, 102
Baran, S.	46, 49	Dunand, D.C.	140, 157
Baranov, N.	23	<b>E</b>	
Bartmann, R.	11	Ebrahimi, O.	8, 9, 13, 74, 167
Becker, A.	128	Efimov, V.	52, 54, 55, 94
Bedanta, S.	65	Engelbrecht, T.	101, 102, 103
Bensch, W.	39, 93	Epp, J.	138, 141
Berkes, M.	90	Eren, S.E.	144
Berthold, A.	86	Erko, M.	151
Bickel, K.	122	Esser, H.G.	126
Biswas, Ch.	19	Evers, F.	125
Bradshaw, J.	99	<b>F</b>	
Brüning, B.	110, 112	Falus, P.	112
Bryant, G.	134	Firstov, G.	137
Buchsteiner, A.	101, 102, 104	Forgan, E.M.	66
Budziak, A.	50	Fouquet, P.	110
Bunn, J.	149, 159	Freeman, P.	18
Busch, P.	65	Friedrichs, O.	85
<b>C</b>			
Caciuffo, R.	40	Fritsche, H.	156
Calvo-Almazan, I.	110	Fujioka, J.	27, 35, 38
Cameron, A.	66	Furukawa, H.	66
Cammarata, M.	111	Fuß, T.	139
Carminati, A.	126	<b>G</b>	
Carrado, A.	143	Garvey, Ch.	134
Cermak, P.	44	Gates, W.	155
Chmielus, M.	140, 157	Gavrilovs, V.	3, 10
Chung, J.-H.	29, 36	Genzel, Ch.	139
Couet, S.	70	Gerischer, S.	19, 20, 40, 66
Crumpton, N.	165	Gerwien, K.	93
Cupane, A.	111	Giannini, E.	64
Czeslik, C.	6, 125	Gibson, C.	26
Czub, J.	95, 96, 158	Gil, A.	49
<b>D</b>			
Da Silva Rocha, A.	146	Girata, D.	89
Dagnese, J.	146	Glavatska, N.	77
Dahint, R.	12, 115, 129, 132, 133	Glavatskyi, I.	18, 19, 20, 21, 23, 77, 78, 137
		Godfrey, E.	167
		Gofryk, K.	40
		Golub, M.	100
		Gondek, L.	50, 95, 96,
			150, 158
		Görke, O.	86, 91
		Grigoriev, S.	67
		Grimm, N.	40, 152, 156
		Griveau, J.-Ch.	40
		Groißl, F.	4
		Gubkin, A.	23
		Guilbaud, J.-B.	108
		<b>H</b>	
		Haase, A.	22, 30, 43
		Habicht, K.	4
		Harrar, A.	106
		Harrower, C.	156
		Hauß, Th.	99, 101, 102, 103, 104, 151, 153
		Hautier, L.	166
		Havenith, R.	155
		Helm, C.A.	117, 119, 121, 124
		Henry, P.	92, 93
		Hilger, A.	7, 126, 127, 159, 160, 161
		Hirsch, Th.	138, 141, 146
		Hoffmann, J.-U.	22
		Hofmann, T.	3, 40, 44, 45, 46, 48, 49, 83, 84, 86, 87
		Holst, N.	91
		Holy, V.	37
		Hoser, A.	3, 41, 42, 43, 44, 45, 46, 47, 49, 50, 51, 56, 83, 86, 87, 92, 150
		Hunt, T.	134
		Hüvonen, D.	61
		<b>I</b>	
		Islam, N.	17, 24, 34, 58, 62, 63, 81
		Ivanova, O.	124
		Izaola, Z.	95
		<b>J</b>	
		Jansen, M.	45, 56
		Jaworska-Golab, T.	46
		Jeworrek, Ch.	6, 125
		Jonke, J.	147
		Josten, E.	65
		Jungwirth, T.	37, 123
		<b>K</b>	
		Kabanov, V.	55
		Kallfaß, C.	82



# AUTHOR INDEX

Author	Page	Author	Page
Kamarad, J.	31	McEwen, K.A.	21
Karakas, N.	8, 9, 13, 74, 167	Mehmanparast, A.N.	148
Kardjilov, N.	7, 126, 127, 149, 158, 160, 161, 165, 166	Menendez, E.	69, 72
Kawamura, S.	66	Meyer, M.	124
Ke, L.	99	Mihalik, M.	42, 83
Keiderling, U.	5, 65, 66, 73, 106, 107	Misek, M.	31
Keimer, B.	27, 33, 35, 38, 87	Mitroova, Z.	25, 79
Khaydukov, Y.	71	Miyasaka, S.	27, 35, 38
Kibalin, Y.	154	Moradi, A.B.	126, 127
Kiefer, K.	4, 72	Mori, T.	20
Kim, F.	160, 161	Moskvin, E.	67
Kim, J.	33, 87	Mufti, N.	41
Kimber, S.	17, 34, 53	Müller, M.	130
Klaus, M.	139	Müllner, P.	140, 157
Klein, J.	51		
Knoll, W.	105	<b>N</b>	
Köbler, U.	51	Naberezhnov, A.	78, 154
Kockelmann, W.	167	Nagy, B.	71
Kohlbrecher, J.	5	Nestler, P.	117, 119, 121, 124
Köhler, R.	116, 117, 119, 120, 121, 122, 123	Neubert, R.	101, 102, 103
Krastev, R.	116, 120	Nikbin, K.	144, 148
Kratochvilova, M.	80	Nikseresht, N.	59
Kremer, R.K.	82	Nitschke-Pagel, Th.	142
Kreuzer, M.	12, 113, 114, 115, 128, 129, 131, 132, 133, 134	Novak, V.	37
Krist, T.	11	Nunes Bordallo, H.	155
Kubo, H.	28	Nunes, R.	146
Kurdyukov, D.	78		
Kuzmin, A.	94	<b>O</b>	
<b>L</b>		O'Dowd, N.P.	145
Lake, B.	17, 24, 34, 53, 57, 58, 62, 63, 64, 81	Onimaru, T.	28
Le, M.D.	21, 61	Ophey, J.	39
Lee, H.	29, 36	Oswald, S.E.	126, 127
Levantino, M.	111		
<b>M</b>		<b>P</b>	
Maljuk, A.	33, 87	Papagiannopoulos, A.	109
Manke, I.	7	Pappas, C.	112
Marti, X.	37, 83	Paris, O.	151
Mat'as, S.	25, 27, 30, 31, 32, 79	Parshin, P.	154
Matsushima, U.	126	Paul, A.	68, 71, 113
		Paul, N.	113
		Paulke, A.	157
		Penumadu, D.	149, 159, 160, 161
		Peters, J.	105
		Pieper, O.	17, 34, 62, 63
		Pirling, Th.	143
		Pirogov, A.	32
		Pispas, S.	109
		Piyadov, V.	67
		Poirier, E.	156
		Pospisil, J.	80
		Prevost, S.	108
		Prokes, K.	25, 27, 28, 29, 31, 32, 40, 80
		Prokhnenko, O.	73
		<b>Q</b>	
		Quintero Castro, D.L.	24, 58, 81, 89
		<b>R</b>	
		Raitman, E.	3, 10
		Rayaprol, S.	47, 92
		Reehuis, M.	24, 27, 33, 35, 36, 37, 38, 45, 56, 80, 81, 82, 87
		Reinhardt, M.	114, 128, 130, 131, 133
		Remhof, A.	85
		Rengstl, D.	106
		Restolho, J.	120
		Röder, B.	123
		Ronnow, H.	59
		Rother, G.	152
		Rudolph, N.	126, 127
		Ruegg, Ch.	60
		Rule, K.	26, 57, 59, 61
		Russina, M.	154
		Ryabova, N.	104
		Ryukhtin, V.	5, 73, 109
		Rzeszutek, A.	100
		<b>S</b>	
		Schreiber, F.	107
		Sa'adedin, F.	99
		Saiani, A.	108
		Sampathkumaran, E.V.	47, 92
		Saramago, B.	120
		Sauter, A.	107
		Schier, H.	82
		Schiro, G.	111
		Schneider, R.	140, 157
		Schöbel, M.	147
		Schorr, S.	88, 90
		Schröter, A.	103
		Schulz, J.	11
		Seidel, S.-O.	8, 9, 10, 13, 74
		Selezneva, N.V.	23
		Señaris-Rodríguez, M.A.	45, 56

# AUTHOR INDEX

Author	Page	Author	Page
Sharifi, M.	153	<b>U</b>	
Sherokalova, E.M.	23	Ulrich, C.	27, 35, 38
Sheverev, S.	104	Umeo, K.	28
Siemensmeyer, K.	20	<b>V</b>	
Sikolenko, V.	52, 54, 55, 94	Vörös, J.	122
Simon, U.	91	<b>W</b>	
Singh, S.	19	Walker, H.C.	21
Siriruk, A.	161	Wallacher, D.	40, 48, 71, 84, 85, 86, 91, 137, 152, 153, 156
Siruguri, V.	47, 92	Ward, S.	60
Soltwedel, O.	117, 119, 121, 124	Wark, M.	153
Stehle, R.	112	Weber, A.	130
Stein, W.D.	73	Webster, J.	118
Steitz, R.	6, 12, 71, 114, 115, 118, 123, 125, 128, 129, 131, 132, 133, 156	Wellert, S.	67, 110
Steriotis, Th.	109	Wiedenmann, A.	5
Stockert, O.	22, 30, 41, 43	Williams, S.	159
Strobl, M.	7, 10, 12, 128, 129, 130, 131, 132, 133, 134	Willumeit, R.	100
Stühn, B.	130	Wimporoy, R.C.	138, 139, 140, 141, 142, 143, 144, 145, 146, 149
<b>T</b>		Winnefeld, F.	109
Takabatake, T.	28	Winter, R.	6
Taketani, K.	7	Wolf, M.	107
Teichert, A.	69, 70, 72, 118, 156	Woracek, R.	149, 159, 161
Tennant, A.	26	<b>Y</b>	
Terentev, P.	32	Yazdani, H.N.	145
Tokura, Y.	27, 35, 38	<b>Z</b>	
Tolan, M.	125	Zahn, R.	122
Toth, S.	17, 34, 53, 57, 64	Zambelli, T.	122
Tovar, M.	78, 80, 88, 90, 91, 93	Zarbakhsh, A.	118
Treimer, W.	8, 9, 13, 74, 167	Zech, O.	106
Tsapatsaris, N.	96, 105	Zhang, F.	107
Tsarkova, L.	116	Zywczak, A.	150
Tsyulin, N.	59		